

# Appendix I

Vaisocherova, H., H. Sipova, I. Visova, M. Bockova, T. Springer, M. Laura Ermini,  
X. Song, Z. Krejčík, L. Chrastinová, O. Pastva, K. Pimková, M. Dostalová  
Merkerová, J. E. Dyr, J. Homola

**Rapid and sensitive detection of multiple microRNAs in cell lysate  
by low-fouling surface plasmon resonance biosensor.**

*Biosensors and Bioelectronics* **70** (2015): 226-231



ELSEVIER

Contents lists available at ScienceDirect

## Biosensors and Bioelectronics

journal homepage: [www.elsevier.com/locate/bios](http://www.elsevier.com/locate/bios)

# Rapid and sensitive detection of multiple microRNAs in cell lysate by low-fouling surface plasmon resonance biosensor



Hana Vaisocherová<sup>a</sup>, Hana Šípová<sup>a</sup>, Ivana Víšová<sup>a</sup>, Markéta Bocková<sup>a</sup>, Tomáš Špringer<sup>a</sup>, Maria Laura Ermini<sup>a</sup>, Xue Song<sup>a</sup>, Zdeněk Krejčík<sup>b</sup>, Leona Chrastinová<sup>b</sup>, Ondřej Pastva<sup>b</sup>, Kristýna Pimková<sup>a,b</sup>, Michaela Dostálová Merkerová<sup>b</sup>, Jan E. Dyr<sup>b</sup>, Jiří Homola<sup>a,\*</sup>

<sup>a</sup> Institute of Photonics and Electronics, Academy of Sciences of the Czech Republic, Chaberská 57, 18251 Prague, Czech Republic

<sup>b</sup> Institute of Hematology and Blood Transfusion, U Nemocnice 1, 12820 Prague, Czech Republic

## ARTICLE INFO

## Article history:

Received 5 December 2014

Received in revised form

5 March 2015

Accepted 16 March 2015

Available online 17 March 2015

## Keywords:

Low-fouling surface chemistry

DNA array

microRNA

Polymer brushes

Surface plasmon resonance imaging

Erythrocyte lysate

## ABSTRACT

We report an ultra-low fouling surface plasmon resonance imaging (SPRi) biosensor for the rapid simultaneous detection of multiple miRNAs in erythrocyte lysate (EL) at subpicomolar levels without need of RNA extraction. The SPRi chips were coated with ultra-low fouling functionalizable poly(carboxybetaine acrylamide) (pCBAA) brushes having optimized thicknesses and directly functionalized with amino-modified oligonucleotide probes. We have characterized the effect of the brush thickness on the probe loading capacity: a loading capacity of  $\sim 9.8 \times 10^{12}$  probes/cm<sup>2</sup> was achieved for pCBAA having a thickness of  $\sim 40$  nm. The probe-functionalized sensor also exhibited a high resistance to fouling from  $\sim 90\%$  EL samples ( $< 2$  ng/cm<sup>2</sup>). A two-step detection assay was employed for multiplexed miRNA detection in EL. Specifically, the assay consisted of (i) a sandwich-type hybridization of the probe-functionalized pCBAA with target miRNA in EL (bound to biotinylated oligonucleotides) and (ii) the capture of streptavidin-functionalized gold nanoparticles to the aforementioned biotinylated probes. We have demonstrated that this approach enables the detection of miRNAs in EL at concentrations as low as 0.5 pM. Finally, we have confirmed the detection of four endogenous miRNAs representing a set of potential miRNA biomarkers of myelodysplastic syndrome (MDS) in clinical EL samples (miR-16, miR-181, miR-34a, and miR-125b). The results revealed significantly higher levels of miR-16 in all the clinical EL samples compared to the other measured miRNAs.

© 2015 Elsevier B.V. All rights reserved.

## 1. Introduction

Mature microribonucleic acids (miRNAs) are  $\sim 19$ – $24$  nucleotide long noncoding RNAs that regulate gene expression in living cells by mediating targeted hydrolysis and translation inhibition of messenger RNAs (He and Hannon, 2004). The miRNAs present in erythrocyte lysate (EL) play an important role in erythropoiesis and final mRNA degradation (Farh et al., 2005; Felli et al., 2005; Georgantas et al., 2007). Although the complex mechanism of miRNA-induced regulation of gene expression is still not fully understood, numerous intracellular and circulating miRNAs have been linked to disease outcomes and prognosis (lorio et al., 2005; Lu et al., 2005). Moreover, there has been increasing evidence over the last five years suggesting that changes in miRNA levels in bodily fluids and tissues are closely associated with the pathogenesis of most human malignancies, including myelodysplastic

syndrome (MDS) or cardiovascular disease (Erdogan et al., 2011; Ikeda et al., 2007; Iorio et al., 2005; Lu et al., 2005; Wang et al., 2009).

Accordingly, miRNAs represent an attractive target as potential disease biomarkers. Although methods for the detection of nucleic acids are well established, there remain great challenges for the accurate and reliable quantification of miRNAs in bodily fluids. These challenges include miRNAs having short sequences, low concentrations of target miRNAs in analyzed samples, and interferences from complex sample matrices (Engels and Hutvagner, 2006; Gao et al., 2014).

Conventional methods for the detection of miRNA include quantitative reverse-transcription real-time polymerase chain reaction (RT-qPCR), microarrays, and northern blotting (Benes and Castoldi, 2010; Lagos-Quintana et al., 2002; Thomson et al., 2004; Wark et al., 2008). Unlike semi-quantitative northern blotting-based approaches (Kuchar et al., 2014; Valoczi et al., 2004), RT-qPCR can cover a broad dynamic range of miRNA concentrations with a relatively high sensitivity. Unfortunately, this method is rather time consuming and requires expensive and complex

\* Corresponding author.

E-mail address: [homola@ufe.cz](mailto:homola@ufe.cz) (J. Homola).

equipment. Furthermore, because highly purified samples are required, the extraction of miRNA from complex biological samples is necessary. Due to the lack of standardized protocols for miRNA extraction, this extraction step may lead to increases in variability and decreases in accuracy (McAlexander et al., 2013; Turchinovich et al., 2012). Microarrays enable parallelized detection of multiple miRNAs (Thomson et al., 2004); however, the complexity of miRNA labeling, insufficient sensitivity, long hybridization times, or challenges for standardization limit the routine use of microarrays in centralized laboratories (Liu et al., 2004).

Several biosensing methods have been proposed as alternative methods to detect miRNAs. These biosensors include those based on (photo)electrochemistry (Dong et al., 2012; Gao et al., 2013; Ge et al., 2014; Kilic et al., 2012; Li et al., 2014; Yin et al., 2014, 2012; Zhu et al., 2014), electrochemiluminescence (Cheng et al., 2014; Liu et al., 2014), fluorescence quenching (Dong et al., 2014; Guo et al., 2014; Ryoo et al., 2013), and surface plasmon resonance (SPR) (Sipova et al., 2010; Zhang et al., 2013). The majority of these studies involve the detection of miRNA either in buffer, diluted complex bodily fluids, or in aqueous solutions of reconstituted RNA extracts (Dong et al., 2014; Wen et al., 2013; Yin et al., 2014). Only a few of these studies involve the detection of miRNA directly in a complex biological sample (without the sample pre-treatment miRNA extraction step). For instance, Yin et al. reported the ultra-sensitive detection of miR-21 in diluted human serum (LOD of 100 aM for miR-21 detection in a buffer) using an electrochemical biosensor; however, this technique had rather long detection time (> 4 h) (Yin et al., 2012). In addition, Ryoo et al. recently reported a fluorescence label-based optical sensor that utilized peptide nucleic acid (PNA) and nano-sized graphene oxide. The sensor was capable of multiplexed detection of miRNAs at picomolar levels in living cells (Ryoo et al., 2013).

In this work, we present a label-free optical biosensor based on surface plasmon resonance imaging (SPRi) that allows for rapid (< 1 h) and multiplexed detection of miRNAs in EL samples without the need for miRNA extraction or pre-amplification. The sensor employs carboxy-functional ultra-low fouling polymer brushes with amino-modified probes for a two-step assay, which utilizes sandwich-type hybridization in EL in addition to signal amplification by streptavidin-functionalized gold nanoparticles (S-AuNPs). We explore the effects of the brush thickness on the surface loading capacity and the resistance to fouling from EL. We targeted four miRNAs (miR-16, miR-181, miR-34a, and miR-125b) that represent potential myelodysplastic syndrome (MDS) biomarkers (McAlexander et al., 2013; Peng and Gao, 2011; Rhyasen and Starczynowski, 2012). After establishing a set of calibration curves for these miRNAs spiked in EL, we screened three clinical EL samples for the levels of native endogenous miRNAs.

## 2. Materials and methods

### 2.1. Reagents and erythrocyte lysate samples

The list of reagents used in this work and procedure of preparation of erythrocyte lysate samples is provided in the [Supplementary material](#). Spherical gold nanoparticles (AuNPs) with a diameter of 35 nm were prepared by the reduction of HAuCl<sub>4</sub> with sodium citrate (Bastus et al., 2011). Bare AuNPs were modified with carboxyl-terminated alkanethiols and then streptavidin was covalently bound to the surface of AuNPs by amine coupling chemistry (see [Supplementary material](#)).

### 2.2. SPR sensors

Two SPR systems developed at the Institute of Photonics and

Electronics (Prague, Czech Republic) were used in this study. A high-resolution SPR imaging (SPRi) system with polarization contrast and internal referencing (Piliarik et al., 2010) combined with dispersionless microfluidics (Springer et al., 2010) was used in the detection experiments. This system enables the simultaneous analysis of biomolecular interactions in 30 individual flow-through sensing spots by using two separate flow-cells with perpendicularly oriented flow chambers. The first (six-channel) flow-cell was used for surface functionalization, while the second (with six perpendicularly oriented channels) was used for the detection (see also [Supplementary material](#)). A four-channel spectroscopic SPR sensor (Homola et al., 2002; Vaisocherova et al., 2014) was used for the optimization of surface functionalization, fouling studies, and assay control experiments. Both SPR sensors were equipped with a temperature controller, enabling SPR measurements in a temperature interval of 5–40 °C with a baseline stability of 0.01 °C. In order to compensate for the effect of decreasing SPR sensitivity with increasing layer thickness (Homola, 2008), the SPR sensor response obtained from both sensors was calibrated using previously described procedures (Piliarik et al., 2010; Vaisocherova et al., 2014). A typical value of the correction factor for bare polymer brush thickness was 1.29 for a 30 nm thick pCBAA (RI=1.401 RIU at 750 nm for wet surface (Vaisocherova et al., 2014)). For the SPR sensors used in this study and a resonant wavelength of about 750 nm, a 1 mRIU SPRi sensor response corresponds to a ~5.9 nm response of the spectroscopic SPR sensor (Piliarik et al., 2010). In terms of surface coverage, a SPRi sensor response of 1 mRIU corresponds to a change in the surface coverage of ~100 ng/cm<sup>2</sup> (Homola, 2006; Vaisocherova et al., 2007).

### 2.3. SPR sensor measurements

The poly(carboxybetaine acrylamide) (pCBAA) coatings were prepared by atom transfer radical polymerization (ATRP) according to a previously described procedure (Vaisocherova et al., 2008). These procedures were carried out under optimized conditions in order to obtain coatings with a wet thickness in the range of 13–45 nm ([Supplementary material](#)). The thickness of wet brushes was measured by means of the spectroscopic SPR sensor via a previously described procedure (Vaisocherova et al., 2014).

The pCBAA surface functionalization was performed using a flow-through regime without extra spotting. The procedure consisted of three steps: (1) activation of the functional carboxyl groups by the NHS/EDC method adjusted to the physical-chemical properties of pCBAA (Vaisocherova et al., 2014), (2) covalent attachment of amino-modified oligonucleotide probes (probe<sub>1</sub> in [Fig. 2](#)), and (3) deactivation of any residual reactive groups. The optimized procedure for surface functionalization is provided in [Supplementary material](#).

In the spiked miRNA detection experiments, the sample with miRNA was mixed with biotin-terminated probes (probe<sub>2</sub>) having a complementary base sequence to the target miRNAs and flowed along the probe<sub>1</sub>-functionalized pCBAA surface at 15 °C for 10 min (step I. in [Fig. 2](#)). This step resulted in the formation of stable miRNA\*probe<sub>1</sub>-probe<sub>2</sub> complexes on the pCBAA-coated sensor surface. In the second step of the assay, the sensor response to miRNA was enhanced with S-AuNPs. The S-AuNPs were flowed along the surface for 25 min at 15 °C and bound to probe<sub>2</sub> via the streptavidin-biotin interaction (step II. in [Fig. 2](#)).

In order to obtain the calibration curves, we carried out the detection of four miRNA spiked samples (miR-16, miR-34a, miR-181, and miR-125b) in EL or PBS at target concentrations of 0.1 pM, 0.5 pM, 1 pM, 100 pM, and 500 pM. Specifically, the undiluted EL sample taken from a healthy individual was spiked with aliquots of EDTA (5 mM), NaCl (150 mM), the biotin-terminated probes to

respective targets (probe<sub>2</sub>, BdmRNA, 0.5 μM), and miRNA targets in a concentration range of 0.1–500 pM. Samples were then heated to 50 °C and cooled down slowly to room temperature while gently mixing, after which SDS (0.5%) was added to each EL sample. It should be noted that after addition of all the reagents, the original solute concentration of each EL sample was not lower than 87% of the original value. At least two different miRNAs were detected simultaneously in a single sample using a single chip (Fig. S-3 in Supplementary material). These samples were flowed along surfaces functionalized with the corresponding probe<sub>1</sub> at 15 °C for 10 min, followed by the injection of S-AuNPs with OD 0.1 in PBS with BSA (200 μg/ml) for 25 min at 15 °C. An EL sample without miRNAs or BdmRNAs (blank sample) was injected in a single channel to check the levels of non-specific S-AuNP binding (reference channel). To help control the surface homogeneity and deactivation after the activation/deactivation surface treatment, one additional control spot in each detection channel without immobilized probes within the same surface was identified using the SPRi software (see also Fig. S-3 in Supplementary material). The signals from the reference channels were subtracted from detection channels to compensate for potential flow disturbance, temperature fluctuations, sample composition variations, or non-specific binding. The change in sensor response to S-AuNPs binding was determined for each sample from the start (0 min) to end time (35 min after washing with PBS). The linear range of sensor detection was determined for each miRNA. The potential y-axis offsets corresponding to the presence of native endogenous miRNA in analyzed samples were subtracted. The limit of detection (LOD) was calculated based on the measurement of three blank EL samples by using “blank + 3 × SD” approach.

The effect of brush thickness on fouling from EL obtained from a healthy individual was measured at 25 °C for 15 min by flowing the EL sample over the Ndmir-16-functionalized pCBAA surfaces (with wet thickness of 20–40 nm, probe surface coverages were kept constant ( $\sim 5.0 \times 10^{12}$  probe/cm<sup>2</sup>). The fouling characteristics were determined after washing the surface with PBS buffer for 10 min.

Screening of clinical EL samples, i.e., a sample obtained from a healthy individual (Normal-1) and two samples from patients diagnosed with MDS (MDS-1, MDS-2) was carried out using the SPRi instrument and the procedure described above (except for an injection of any samples spiked with miRNAs). The sensor response to S-AuNPs was converted to a concentration scale using previously determined sensor calibration curves. Validation of the method was performed using a reverse measurement of miR-16 in a control sample of a miRNA extracted from EL (MDS-3).

### 3. Results

#### 3.1. Functionalization of SPR chips with pCBAA and amino-modified probes

The pCBAA surface functionalization was optimized in order to achieve a maximum loading capacity of immobilized probes while maintaining a surface resistance to fouling from EL, see Supplementary material.

In order to assess the effect of polymer brush thickness on the surface loading capacity, we prepared a series of pCBAA coatings with thicknesses in the range of 13–40 nm. The amino-modified probes for the detection of miR-16 were immobilized to the pCBAA layer using the optimized immobilization procedure. The results are shown in Fig. 1A. It can be seen that the loading capacity increased with increasing brush thickness, yielding a maximum capacity of  $(9.8 \pm 0.6) \times 10^{12}$  probes/cm<sup>2</sup> for a pCBAA layer having a thickness of  $\sim 40$  nm. The limited controllability of grafting

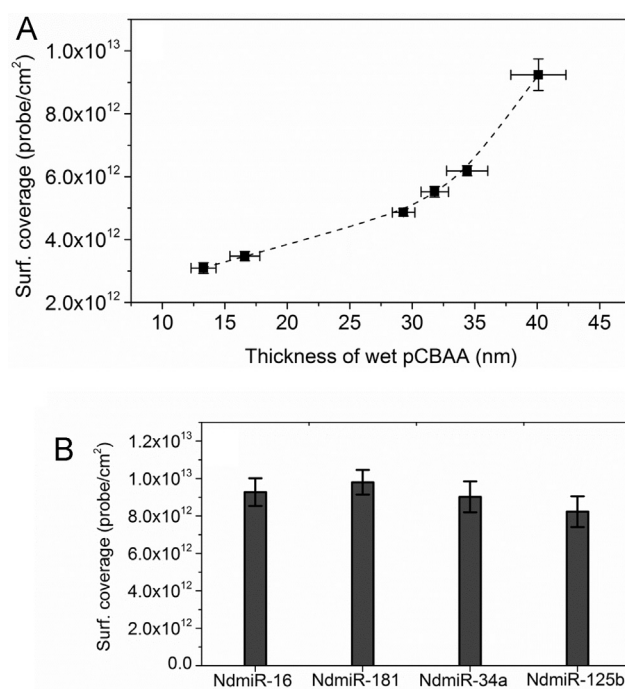


**Fig. 1.** (A) Effect of pCBAA wet thickness on probe immobilization levels measured by the SPR sensor. Data were averaged from at least three individual sensing channels functionalized with either Ndmir-16 or Ndmir-181. (B) Immobilization levels obtained for different amino-modified probes (Ndmir-16, Ndmir-181, Ndmir-34a, and Ndmir-125b) immobilized to pCBAA surfaces with a wet thickness of  $\sim 40$  nm. Each data point was averaged from up to 18 sensing channels using 3 individual sensor chips.

pCBAA layers by ATRP (Rodriguez-Emmenegger et al., 2012) did not allow the preparation of reproducible pCBAA layers thicker than 40 nm; therefore, these were not included in this study. In this work, we assume that there exists a comparable pCBAA grafting density for brush thicknesses in the range of 19–40 nm (Vaisocherova et al., 2014).

The immobilization levels for all of the amino-modified probes used herein for pCBAA coatings with a maximum wet thickness of  $\sim 40$  nm were comparable, ranging from  $8.3 \times 10^{12}$  probe/cm<sup>2</sup> to  $9.8 \times 10^{12}$  probe/cm<sup>2</sup> (Fig. 1B). A high chip-to-chip reproducibility ( $> 90\%$ ) of probe surface density on pCBAA (with a wet thickness of  $\sim 40$  nm) was achieved for each probe. These probe immobilization levels are higher than those ( $1\text{--}5 \times 10^{12}$  probe/cm<sup>2</sup>) obtained using standard low-fouling oligo(ethylene glycol)-based mixed alkanethiolate self-assembled monolayers (OEG-based AT-SAMs) functionalized with probes using the streptavidin–biotin interaction (Lahiri et al., 1999; Sipova and Homola, 2013; Vaisocherova et al., 2008). This finding is in agreement with the assumption that pCBAA brushes form 3D-like structures in solution, with good accessibility of reactive groups for probe coupling within the whole brush structure. Good accessibility of any reactive carboxyls within the hydrophilic pCBAA layer is facilitated by a high flexibility of the pCBAA brushes in aqueous solution (Vaisocherova et al., 2014).

#### 3.2. Characterization of SPR biosensor for miRNA detection

A schematic representation of the two-step assay employed herein for the detection of miRNAs is shown in Fig. 2. The amino-modified probes (probe<sub>1</sub>) were immobilized onto pCBAA-coated gold surfaces using the optimized procedure, where the pCBAA layer had a thickness of 35–42 nm. The SPR signal enhancement used in this miRNA assay is provided by S-AuNPs, whose adsorption within a close proximity to the gold planar surface generates a

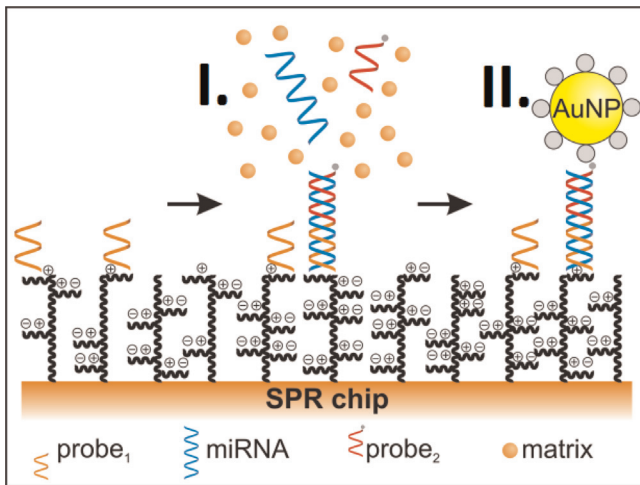


**Fig. 2.** Scheme of two-step assay employed for miRNA detection in erythrocyte lysate (EL) samples: First, the undiluted EL samples spiked with both biotinylated probes ( $probe_2$ ) and miRNAs were flowed along the  $probe_1$ -functionalized pCBA (step I). Streptavidin-coated gold nanoparticles (S-AuNPs) were then injected to bind to  $probe_2$  in order to enhance the sensor response to miRNA detection (step II).

substantial increase in local refractive index. The used S-AuNPs provided an enhancement of approximately  $800 \times$  with respect to the sensor response for the detection of miRNA at a concentration of 2 nM, which is in good agreement with the amplification factor of S-AuNPs previously reported in literature (Springer et al., 2014).

In order to calibrate the sensor for the multiplexed detection of four miRNAs in EL, an EL sample (> 87%) was spiked with miRNAs of various concentrations in the range of 0.1–500 pM. Fig. 3A shows a representative reference-compensated sensor response to S-AuNPs binding to  $probe_1$  covered pCBA surface with miR-181\* $probe_2$  captured from the EL sample spiked with miR-181. Calibration curves for all the miRNAs are shown in Fig. 3B. We observed a minimum influence of the lysate matrix on the biosensor performance (Fig. S-5). The LODs determined from these calibration curves were 0.35 pM, 0.39 pM, 0.50 pM, and 0.95 pM for miR-16, miR-181, miR-34a, and miR-125b, respectively. The observed differences in the LOD may be attributed to differences in each nucleotide sequence that can affect the complex stability. This could be further improved by decreasing the sensor operating temperature to < 15 °C to enhance the oligonucleotide hybridization. Taking into account the sample volume that was analyzed (~300  $\mu$ l), the LODs correspond to a total amount of miRNA in the range of hundreds of attomoles. Such LODs achieved are comparable to those recently obtained using the electrochemical and lateral-flow biosensors employed for single miRNA detection in miRNA buffered extracts and serum (Gao et al., 2013; Ren et al., 2013).

Control experiments were performed in order to characterize the sensor selectivity to miRNA sequences (see Supplementary material). No cross-reactivity between the oligonucleotides used in this study was observed under given experimental conditions.

In order to compare the SPR results with standard RT-qPCR method, total RNA was extracted from a EL sample and analyzed by both methods for the presence of native endogenous miR-16. The concentration of miR-16 determined by SPRi was  $3.1 \pm 1.0$  pM and is in a very good agreement with the value obtained by RT-qPCR ( $4.0 \pm 0.5$  pM).

### 3.3. Screening of clinical erythrocyte lysate samples for the levels of native miRNAs

The SPRi biosensor was used for the detection of endogenous

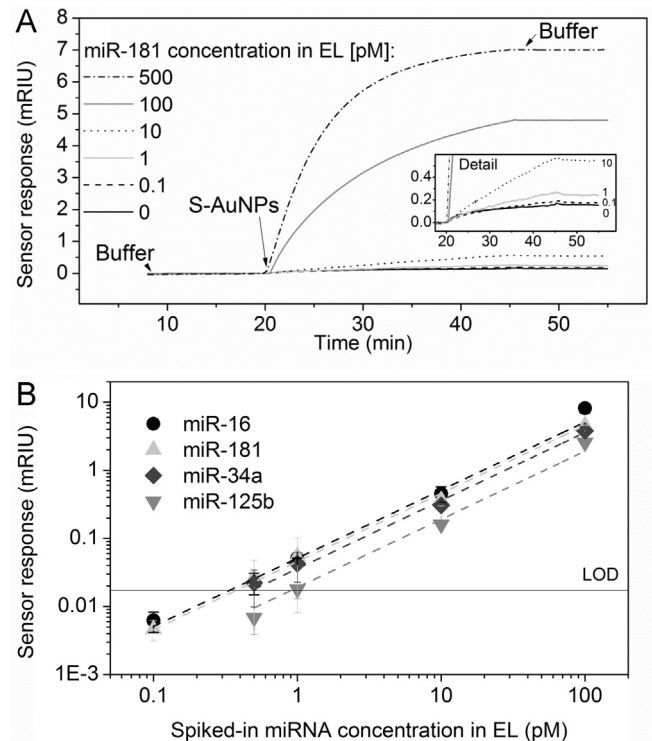


**Fig. 3.** (A) Representative SPRi data corresponding to S-AuNPs binding to miR-181\*NdmiR-181\*BdmiR-181 complexes immobilized on pCBA. (B) Calibration curves for miR-16, miR-181, miR-34a, and miR-125b spiked into normal EL samples.

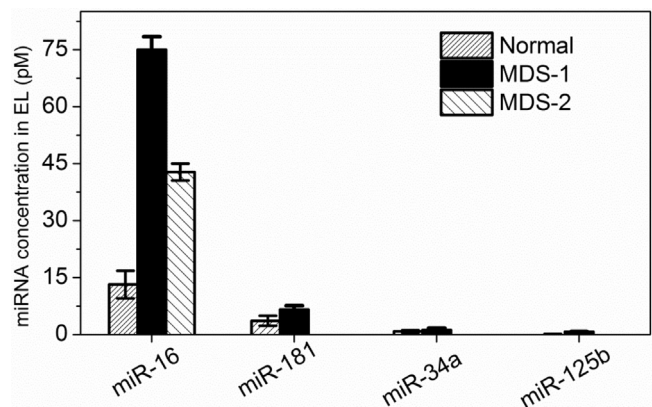


**Fig. 4.** Screening of clinical EL samples (Normal-1, MDS-1, and MDS-2) for miR-16, miR-181, miR-34a, and miR-125b using the SPRi biosensor. The results were averaged from at least 6 spots using 2 different SPR chips. The results from SPRi measurements were converted to concentrations using the previously established calibration curves.

levels of miR-16, miR-181, miR-34a, and miR-125b in EL samples (Normal-1, MDS-1, MDS-2), see Fig. 4 and Table S-3. The results from SPRi measurements were converted to concentrations using the previously established calibration curves, determined for each individual miRNA detection in EL sample. In all of the EL samples, miR-16 was found in significantly higher concentrations (at a concentration range of ~10–100 pM) compared to other miRNAs tested. This finding agrees well with studies reporting relatively high levels of miR-16 in blood serum (Bastus et al., 2011) and over-expression in malignant B-cells of leukemia patients (Cimmino et al., 2005). Our results indicate an over-expression of miR-16 in EL samples of MDS patients. These trends were also observed by the RT-qPCR method (see Table S-3) after total RNA extraction

from the tested samples, although discrepancies in the measured miRNA levels in biological samples by means of RT-qPCR due to RNA extraction can be expected (McAlexander et al., 2013; Turchinovich et al., 2012).

#### 4. Conclusions

We developed a label-free optical biosensor based on SPRi technology for rapid multiplexed detection of miRNAs in real-world erythrocyte lysate (EL) samples with high sensitivity and without the need for RNA extraction. To the best of our knowledge, this is the first work demonstrating the use of an optical label-free biosensor for multiplexed detection of miRNAs in cell lysate. The biosensor utilizes ultra-low fouling carboxy-functional poly(carboxybetaine acrylamide) (pCBAA) coatings and functionalized gold nanoparticles to enhance the sensor response. Using two-step assay, microRNAs were detected in EL in ~45 min at concentrations as low as sub-pM. As the presented SPRi method can detect miRNA directly with no extra EL sample preparation, it may provide more accurate results with respect to methods relying on RNA extraction. We used this biosensor to screen three clinical EL samples for the levels of four miRNAs; we found a higher concentration of miR-16 in EL samples compared to the other three miRNAs tested. These results demonstrate the potential of this SPRi biosensor for the parallelized detection of miRNA in clinical samples. The results indicate that SPR biosensors can ultimately combine the key advantages of current established methods, i.e. the high sensitivity of RT-qPCR and the parallelized detection ability of microarrays.

#### Acknowledgments

This research was supported by Praemium Academiae of the Academy of Sciences of the Czech Republic, the Czech Science Foundation (contract #P205/12/G118), and the Ministry of Health of the Czech Republic (contract # NT13847-4).

#### Appendix A. Supplementary material

Supplementary data associated with this article can be found in the online version at <http://dx.doi.org/10.1016/j.bios.2015.03.038>.

#### References

- Bastus, N.G., Comenge, J., Puentes, V., 2011. Kinetically controlled seeded growth synthesis of citrate-stabilized gold nanoparticles of up to 200 nm: size focusing versus Ostwald ripening. *Langmuir* 27 (17), 11098–11105.
- Benes, V., Castoldi, M., 2010. Expression profiling of microRNA using real-time quantitative PCR, how to use it and what is available. *Methods* 50 (4), 244–249.
- Cheng, Y., Lei, J.P., Chen, Y.L., Ju, H.X., 2014. Highly selective detection of microRNA based on distance-dependent electrochemiluminescence resonance energy transfer between CdTe nanocrystals and Au nanoclusters. *Biosens. Bioelectron.* 51, 431–436.
- Cimmino, A., Calin, G.A., Fabbri, M., Iorio, M.V., Ferracin, M., Shimizu, M., Wojcik, S. E., Aqeilan, R.I., Zupo, S., Dono, M., Rassenti, L., Alder, H., Volinia, S., Liu, C.G., Kipps, T.J., Negrini, M., Croce, C.M., 2005. miR-15 and miR-16 induce apoptosis by targeting BCL2. *Proc. Natl. Acad. Sci. USA* 102 (39), 13944–13949.
- Dong, H.F., Hao, K.H., Tian, Y.P., Jin, S., Lu, H.T., Zhou, S.F., Zhang, X.J., 2014. Label-free and ultrasensitive microRNA detection based on novel molecular beacon binding readout and target recycling amplification. *Biosens. Bioelectron.* 53, 377–383.
- Dong, H.F., Jin, S., Ju, H.X., Hao, K.H., Xu, L.P., Lu, H.T., Zhang, X.J., 2012. Trace and label-free microRNA detection using oligonucleotide encapsulated silver nanoclusters as probes. *Anal. Chem.* 84 (20), 8670–8674.
- Engels, B.M., Hutvagner, G., 2006. Principles and effects of microRNA-mediated post-transcriptional gene regulation. *Oncogene* 25 (46), 6163–6169.
- Erdogan, B., Facey, C., Qualtieri, J., Tedesco, J., Rinker, E., Isett, R.B., Tobias, J., Baldwin, D.A., Thompson, J.E., Carroll, M., Kim, A.S., 2011. Diagnostic microRNAs in myelodysplastic syndrome. *Exp. Hematol.* 39 (9), 915–926, e912.
- Farh, K.K., Grimson, A., Jan, C., Lewis, B.P., Johnston, W.K., Lim, L.P., Burge, C.B., Bartel, D.P., 2005. The widespread impact of mammalian microRNAs on mRNA repression and evolution. *Science* 310 (5755), 1817–1821.
- Felli, N., Fontana, L., Pelosi, E., Botta, R., Bonci, D., Facchiano, F., Luzzi, F., Lulli, V., Morsilli, O., Santoro, S., Valtieri, M., Calin, G.A., Liu, C.G., Sorrentino, A., Croce, C. M., Peschle, C., 2005. MicroRNAs 221 and 222 inhibit normal erythropoiesis and erythroleukemic cell growth via kit receptor down-modulation. *Proc. Natl. Acad. Sci. USA* 102 (50), 18081–18086.
- Gao, X.F., Xu, H., Baloda, M., Gurung, A.S., Xu, L.P., Wang, T., Zhang, X.J., Liu, G.D., 2014. Visual detection of microRNA with lateral flow nucleic acid biosensor. *Biosens. Bioelectron.* 54, 578–584.
- Gao, Z.Q., Deng, H.M., Shen, W., Ren, Y.Q., 2013. A label-free biosensor for electrochemical detection of femtomolar microRNAs. *Anal. Chem.* 85 (3), 1624–1630.
- Ge, Z.L., Lin, M.H., Wang, P., Pei, H., Yan, J., Shou, J.Y., Huang, Q., He, D.N., Fan, C.H., Zuo, X.L., 2014. Hybridization chain reaction amplification of microRNA detection with a tetrahedral dna nanostructure-based electrochemical biosensor. *Anal. Chem.* 86 (4), 2124–2130.
- Georgantas 3rd, R.W., Hildreth, R., Morisot, S., Alder, J., Liu, C.G., Heimfeld, S., Calin, G.A., Croce, C.M., Civin, C.I., 2007. CD34+ hematopoietic stem-progenitor cell microRNA expression and function: a circuit diagram of differentiation control. *Proc. Natl. Acad. Sci. USA* 104 (8), 2750–2755.
- Guo, S., Yang, F., Zhang, Y.L., Ning, Y., Yao, Q.F., Zhang, G.J., 2014. Amplified fluorescence sensing of miRNA by combination of graphene oxide with duplex-specific nuclease. *Anal. Methods* 6 (11), 3598–3603.
- He, L., Hannon, G.J., 2004. MicroRNAs: small RNAs with a big role in gene regulation. *Nat. Rev. Genet.* 5 (7), 522–531.
- Homola, J., 2006. *Surface Plasmon Resonance Based Sensors*. Springer-Verlag.
- Homola, J., 2008. Surface plasmon resonance sensors for detection of chemical and biological species. *Chem. Rev.* 108 (2), 462–493.
- Homola, J., Dostalek, J., Chen, S.F., Rasooly, A., Jiang, S.Y., Yee, S.S., 2002. Spectral surface plasmon resonance biosensor for detection of staphylococcal enterotoxin B in milk. *Int. J. Food Microbiol.* 75 (1–2), 61–69.
- Ikedo, S., Kong, S.W., Lu, J., Bisping, E., Zhang, H., Allen, P.D., Golub, T.R., Pieske, B., Pu, W.T., 2007. Altered microRNA expression in human heart disease. *Physiol. Genomics* 31 (3), 367–373.
- Iorio, M.V., Ferracin, M., Liu, C.G., Veronese, A., Spizzo, R., Sabbioni, S., Magri, E., Pedriali, M., Fabbri, M., Campiglio, M., Menard, S., Palazzo, J.P., Rosenberg, A., Musiani, P., Volinia, S., Nenci, I., Calin, G.A., Querzoli, P., Negrini, M., Croce, C.M., 2005. MicroRNA gene expression deregulation in human breast cancer. *Cancer Res.* 65 (16), 7065–7070.
- Kilic, T., Topkaya, S.N., Ariksoysal, D.O., Ozsoz, M., Ballar, P., Erac, Y., Gozen, O., 2012. Electrochemical based detection of microRNA, mir21 in breast cancer cells. *Biosens. Bioelectron.* 38 (1), 195–201.
- Kuchar, M., Vankova, L., Petrokova, H., Cerny, J., Osicka, R., Pelak, O., Sipova, H., Schneider, B., Homola, J., Sebo, P., Kalina, T., Maly, P., 2014. Human interleukin-23 receptor antagonists derived from an albumin-binding domain scaffold inhibit IL-23-dependent ex vivo expansion of IL-17-producing T-cells. *Proteins—Struct. Funct. Bioinform.* 82 (6), 975–989.
- Lagos-Quintana, M., Rauhut, R., Yalcin, A., Meyer, J., Lendeckel, W., Tuschl, T., 2002. Identification of tissue-specific microRNAs from mouse. *Curr. Biol.* 12 (9), 735–739.
- Lahiri, J., Isaacs, L., Tien, J., Whitesides, G.M., 1999. A strategy for the generation of surfaces presenting ligands for studies of binding based on an active ester as a common reactive intermediate: a surface plasmon resonance study. *Anal. Chem.* 71 (4), 777–790.
- Li, F.Y., Peng, J., Wang, J.J., Tang, H., Tan, L., Xie, Q.J., Yao, S.Z., 2014. Carbon nanotube-based label-free electrochemical biosensor for sensitive detection of miRNA-24. *Biosens. Bioelectron.* 54, 158–164.
- Liu, C.G., Calin, G.A., Meloon, B., Gamlie, N., Sevignani, C., Ferracin, M., Dumitru, C. D., Shimizu, M., Zupo, S., Dono, M., Alder, H., Bullrich, F., Negrini, M., Croce, C.M., 2004. An oligonucleotide microchip for genome-wide microRNA profiling in human and mouse tissues. *Proc. Natl. Acad. Sci. USA* 101 (26), 9740–9744.
- Liu, T., Chen, X., Hong, C.Y., Xu, X.P., Yang, H.H., 2014. Label-free and ultrasensitive electrochemiluminescence detection of microRNA based on long-range self-assembled DNA nanostructures. *Microchim. Acta* 181 (7–8), 731–736.
- Lu, J., Getz, G., Miska, E.A., Alvarez-Saavedra, E., Lamb, J., Peck, D., Sweet-Cordero, A., Ebert, B.L., Mak, R.H., Ferrando, A.A., Downing, J.R., Jacks, T., Horvitz, H.R., Golub, T.R., 2005. MicroRNA expression profiles classify human cancers. *Nature* 435 (7043), 834–838.
- McAlexander, M.A., Phillips, M.J., Witwer, K.W., 2013. Comparison of methods for miRNA extraction from plasma and quantitative recovery of rna from cerebrospinal fluid. *Front. Genet.* 4, 83.
- Peng, Y.F., Gao, Z.Q., 2011. Amplified detection of microRNA based on ruthenium oxide nanoparticle-initiated deposition of an insulating film. *Anal. Chem.* 83 (3), 820–827.
- Piliarik, M., Bockova, M., Homola, J., 2010. Surface plasmon resonance biosensor for parallelized detection of protein biomarkers in diluted blood plasma. *Biosens. Bioelectron.* 26 (4), 1656–1661.
- Ren, Y.Q., Deng, H.M., Shen, W., Gao, Z.Q., 2013. A highly sensitive and selective electrochemical biosensor for direct detection of microRNAs in serum. *Anal. Chem.* 85 (9), 4784–4789.
- Rhysan, G.W., Starczynowski, D.T., 2012. Deregulation of microRNAs in myelodysplastic syndrome. *Leukemia* 26 (1), 13–22.
- Rodriguez-Emmenegger, C., Houska, M., Alles, A.B., Brynda, E., 2012. Surfaces

- resistant to fouling from biological fluids: towards bioactive surfaces for real applications. *Macromol. Biosci.* 12 (10), 1413–1422.
- Ryoo, S.R., Lee, J., Yeo, J., Na, H.K., Kim, Y.K., Jang, H., Lee, J.H., Han, S.W., Lee, Y., Kim, V.N., Min, D.H., 2013. Quantitative and multiplexed microRNA sensing in living cells based on peptide nucleic acid and nano graphene oxide (PANGO). *ACS Nano* 7 (7), 5882–5891.
- Sipova, H., Homola, J., 2013. Surface plasmon resonance sensing of nucleic acids: a review. *Anal. Chim. Acta* 773, 9–23.
- Sipova, H., Zhang, S.L., Dudley, A.M., Galas, D., Wang, K., Homola, J., 2010. Surface plasmon resonance biosensor for rapid label-free detection of microribonucleic acid at subfemtomole level. *Anal. Chem.* 82 (24), 10110–10115.
- Springer, T., Ermini, M.L., Spackova, B., Jablonku, J., Homola, J., 2014. Enhancing sensitivity of SPR biosensors by functionalized gold nanoparticles-size matters. *Anal. Chem.*
- Springer, T., Piliarik, M., Homola, J., 2010. Surface plasmon resonance sensor with dispersionless microfluidics for direct detection of nucleic acids at the low femtomole level. *Sens. Actuators B—Chem.* 145 (1), 588–591.
- Thomson, J.M., Parker, J., Perou, C.M., Hammond, S.M., 2004. A custom microarray platform for analysis of microRNA gene expression. *Nat. Methods* 1 (1), 47–53.
- Turchinovich, A., Weiz, L., Burwinkel, B., 2012. Extracellular miRNAs: the mystery of their origin and function. *Trends Biochem. Sci.* 37 (11), 460–465.
- Vaisocherova, H., Mrkova, K., Piliarik, M., Jinoch, P., Steinbachova, M., Homola, J., 2007. Surface plasmon resonance biosensor for direct detection of antibody against Epstein-Barr virus. *Biosens. Bioelectron.* 22 (6), 1020–1026.
- Vaisocherova, H., Sevcu, V., Adam, P., Spackova, B., Hegnerova, K., Pereira, A.D., Rodriguez-Emmenegger, C., Riedel, T., Houska, M., Brynda, E., Homola, J., 2014. Functionalized ultra-low fouling carboxy- and hydroxy-functional surface platforms: functionalization capacity, biorecognition capability and resistance to fouling from undiluted biological media. *Biosens. Bioelectron.* 51, 150–157.
- Vaisocherova, H., Yang, W., Zhang, Z., Cao, Z., Cheng, G., Piliarik, M., Homola, J., Jiang, S., 2008. Ultralow fouling and functionalizable surface chemistry based on a zwitterionic polymer enabling sensitive and specific protein detection in undiluted blood plasma. *Anal. Chem.* 80 (20), 7894–7901.
- Valoczi, A., Hornyik, C., Varga, N., Burgyan, J., Kauppinen, S., Havelda, Z., 2004. Sensitive and specific detection of microRNAs by northern blot analysis using LNA-modified oligonucleotide probes. *Nucleic Acids Res.* 32 (22).
- Wang, K., Zhang, S.L., Marzolf, B., Troisch, P., Brightman, A., Hu, Z.Y., Hood, L.E., Galas, D.J., 2009. Circulating microRNAs, potential biomarkers for drug-induced liver injury. *Proc. Natl. Acad. Sci. USA* 106 (11), 4402–4407.
- Wark, A.W., Lee, H.J., Corn, R.M., 2008. Multiplexed detection methods for profiling microRNA expression in biological samples. *Angew. Chem.—Int. Ed.* 47 (4), 644–652.
- Wen, Y.L., Liu, G., Pei, H., Li, L.Y., Xu, Q., Liang, W., Li, Y., Xu, L., Ren, S.Z., Fan, C.H., 2013. DNA nanostructure-based ultrasensitive electrochemical microRNA biosensor. *Methods* 64 (3), 276–282.
- Yin, H.S., Wang, M., Zhou, Y.L., Zhang, X.Y., Sun, B., Wang, G.H., Ai, S.Y., 2014. Photoelectrochemical biosensing platform for microRNA detection based on in situ producing electron donor from apoferritin-encapsulated ascorbic acid. *Biosens. Bioelectron.* 53, 175–181.
- Yin, H.S., Zhou, Y.L., Zhang, H.X., Meng, X.M., Ai, S.Y., 2012. Electrochemical determination of microRNA-21 based on graphene, LNA integrated molecular beacon, AuNPs and biotin multifunctional bio bar codes and enzymatic assay system. *Biosens. Bioelectron.* 33 (1), 247–253.
- Zhang, D.C., Yan, Y.R., Cheng, W., Zhang, W., Li, Y.H., Ju, H.X., Ding, S.J., 2013. Streptavidin-enhanced surface plasmon resonance biosensor for highly sensitive and specific detection of microRNA. *Microchim. Acta* 180 (5–6), 397–403.
- Zhu, W.Y., Su, X.P., Gao, X.Y., Dai, Z., Zou, X.Y., 2014. A label-free and PCR-free electrochemical assay for multiplexed microRNA profiles by ligase chain reaction coupling with quantum dots barcodes. *Biosens. Bioelectron.* 53, 414–419.

# Appendix II

Vaisocherová-Lísalová, H., I. Víšová, M. L. Ermini, T. Špringer, X. C. Song, J. Mrázek, J. Lamačová, N. Scott Lynn, P. Šedivák, J. Homola

**Low-fouling surface plasmon resonance biosensor for multi-step detection of foodborne bacterial pathogens in complex food samples.**

*Biosensors and Bioelectronics* **80** (2016): 84-90





ELSEVIER

Contents lists available at ScienceDirect

# Biosensors and Bioelectronics

journal homepage: [www.elsevier.com/locate/bios](http://www.elsevier.com/locate/bios)

## Low-fouling surface plasmon resonance biosensor for multi-step detection of foodborne bacterial pathogens in complex food samples

Hana Vaisocherová-Lísalová<sup>a</sup>, Ivana Víšová<sup>a</sup>, Maria Laura Ermini<sup>a</sup>, Tomáš Špringer<sup>a</sup>, Xue Chadtová Song<sup>a</sup>, Jan Mrázek<sup>a</sup>, Josefína Lamačová<sup>a</sup>, N. Scott Lynn Jr.<sup>a</sup>, Petr Šedivák<sup>b</sup>, Jiří Homola<sup>a,\*</sup>

<sup>a</sup> Institute of Photonics and Electronics, Czech Academy of Sciences, Chaberská 57, Prague, Czech Republic

<sup>b</sup> Police of the Czech Republic, Kapucínská 214/2, Prague, Czech Republic

### ARTICLE INFO

#### Article history:

Received 3 December 2015

Received in revised form

12 January 2016

Accepted 13 January 2016

Available online 14 January 2016

#### Keywords:

Low-fouling biorecognition coatings

Polymer brushes

Surface plasmon resonance biosensor

Gold nanoparticles

Detection of bacterial pathogens

*E. coli* O157:H7

Food safety

### ABSTRACT

Recent outbreaks of foodborne illnesses have shown that foodborne bacterial pathogens present a significant threat to public health, resulting in an increased need for technologies capable of fast and reliable screening of food commodities. The optimal method of pathogen detection in foods should: (i) be rapid, specific, and sensitive; (ii) require minimum sample preparation; and (iii) be robust and cost-effective, thus enabling use in the field. Here we report the use of a SPR biosensor based on ultra-low fouling and functionalizable poly(carboxybetaine acrylamide) (pCBAA) brushes for the rapid and sensitive detection of bacterial pathogens in crude food samples utilizing a three-step detection assay. We studied both the surface resistance to fouling and the functional capabilities of these brushes with respect to each step of the assay, namely: (I) incubation of the sensor with crude food samples, resulting in the capture of bacteria by antibodies immobilized to the pCBAA coating, (II) binding of secondary biotinylated antibody (Ab<sub>2</sub>) to previously captured bacteria, and (III) binding of streptavidin-coated gold nanoparticles to the biotinylated Ab<sub>2</sub> in order to enhance the sensor response. We also investigated the effects of the brush thickness on the biorecognition capabilities of the gold-grafted functionalized pCBAA coatings. We demonstrate that pCBAA-compared to standard low-fouling OEG-based alkanethiolate self-assembled monolayers-exhibits superior surface resistance regarding both fouling from complex food samples as well as the non-specific binding of S-AuNPs. We further demonstrate that a SPR biosensor based on a pCBAA brush with a thickness as low as 20 nm was capable of detecting *E. coli* O157:H7 and *Salmonella* sp. in complex hamburger and cucumber samples with extraordinary sensitivity and specificity. The limits of detection for the two bacteria in cucumber and hamburger extracts were determined to be 57 CFU/mL and 17 CFU/mL for *E. coli* and  $7.4 \times 10^3$  CFU/mL and  $11.7 \times 10^3$  CFU/mL for *Salmonella* sp., respectively. In addition, we demonstrate the simultaneous detection of *E. coli* and *Salmonella* sp. in hamburger sample using a multichannel SPR biosensor having appropriate functional coatings.

© 2016 Elsevier B.V. All rights reserved.

### 1. Introduction

Outbreaks of foodborne illnesses have shown that foodborne bacterial pathogens present a significant threat to public health (CDC, 2014, EFSA, 2014). Recent cases include the discovery of *Staphylococcus aureus* in ice cream (Fetsch et al., 2014), *Escherichia coli* O157:H7 in spinach and ground beef (Heaton and Jones, 2008), *Salmonella* in peanut butter (Gerner-Smidt et al., 2007), and *Listeria monocytogenes* in ready-to-eat meats (Gerner-Smidt et al., 2007). The CDC estimates that every year in the US over 48 million

people are infected, resulting in 128,000 hospitalizations and 3000 deaths (CDC, 2014). Infectious doses for pathogens such as *E. coli* O157:H7 and *Salmonella* are not strictly defined and depend on the host age and health (Food and Drug Administration, 2012, Paton and Paton, 1998). Some of the published data indicates that they may be as low as 1 to 100 organisms (Food and Drug Administration, 2012, Paton and Paton, 1998), while other studies report much higher infective doses (Food and Drug Administration, 2012, Kothary and Babu, 2001). The most commonly infected foods include dairy products, beef, poultry, vegetables, and drinking water. These outbreaks demonstrate an urgent need for an improvement in the screening and diagnosis of food commodities.

Culture and colony counting methods represent the most

\* Corresponding author.

E-mail address: [homola@ufe.cz](mailto:homola@ufe.cz) (J. Homola).

frequent approaches for the detection of foodborne bacterial pathogens in standardized laboratories; however, these methods are excessively time consuming and have been reported to have limited sensitivity to diverse bacterial pathogens (Gracias and McKillip, 2004, Lazcka et al., 2007). In order to improve both sensitivity and selectivity, these approaches can be combined with polymerase chain reaction (PCR)-based techniques (Lampel et al., 2000, Li and Mustapha, 2004, Rodriguez-Lazaro et al., 2005, Simpson and Lim, 2005). Although PCR methods possess relatively high sensitivity (with LODs as low as a few CFU/mL), they require expensive equipment and are likewise time-consuming (Postollec et al., 2011). Currently, the most advanced techniques to detect bacterial pathogens in food and environmental samples are represented by both immunoassay-based methods as well as DNA and fluorescent microarrays (Call et al., 2003, Cudjoe et al., 1995, Disney and Seeberger, 2004, Mansfield and Forsythe, 2001, Yu et al., 2002). These methods are capable of relatively fast detection with respect to culture-based methods, yet they also require trained personnel and expensive equipment.

Biosensors have been shown to provide a simple, cost-effective alternative to conventional methods for the detection of foodborne pathogens and furthermore, are expected to enable the field detection of foodborne pathogens, thus providing significant decreases in the overall analysis time. To date, a variety of biosensors for the detection of bacteria have been demonstrated. These include electrical biosensors based on amperometry (Abdel-Hamid et al., 1999, Li et al., 2012, Lin et al., 2008, Perez et al., 1998) or electrochemical impedance spectroscopy (Barreiros dos Santos et al., 2013, Yang et al., 2004) as well as optical biosensors employing fluorescent labels (Ko and Grant, 2006, Rohde et al., 2015, Sanvicens et al., 2011, Yang and Li, 2006, Zordan et al., 2009) or label-free optical methods (Baccar et al., 2010, Cho et al., 2015, Linman et al., 2010, Rodriguez-Emmenegger et al., 2011a, Tawil et al., 2012, Wang et al., 2011, 2012).

Surface plasmon resonance (SPR) affinity biosensors represent the foremost label-free optical biosensor technology regarding the detection of foodborne pathogens. Typical LODs for bacteria achieved by SPR biosensors are on the order of  $10^4$  CFU/mL or higher for direct detection, where no preconcentration or amplification steps are employed. A lower limit of detection was demonstrated by Yazgan et al. (2014) who reported the detection of *E. coli* in buffer with a LOD of 2.5 CFU/mL through the use of modified carbohydrates as bioreceptors. Another strategy for improving LODs has been demonstrated by Torun et al., who combined an SPR biosensor with immunomagnetic separation and reported the detection of *E. coli* in buffer with a LOD of 3 CFU/mL. They also applied their method to the detection of *E. coli* in moderately complex samples (lake, river, and tap water samples); limits of detection for these matrices were not reported (Torun et al., 2012). Bouguelia et al. (2013) reported the SPR detection of various bacterial pathogens with LODs as low as  $\sim 3$  CFU/mL in matrixes composed of the addition of crude food samples to growth medium. In this sensor a growth chamber was situated directly on the SPR surface, where at a temperature of 37 °C they were able to monitor the growth of each pathogen in real-time; however, the detection of lower pathogen concentrations required analysis times of up to 10 h.

One of the key challenges hindering the application of SPR biosensors for the detection of bacterial pathogens in real-world complex food samples remains interfering effects stemming from the sample matrix, particularly the non-specific adsorption of non-target molecules from the sample to the sensing surface (causing a false positive signal). Correspondingly, a number of research groups have pursued the development of advanced functional coatings in order to suppress this effect. An optimum functional coating for the biosensor-based analysis of food samples is one that combines a high number of functional bioreceptors with an

ability to resist fouling from complex media (Homola, 2008, Vaisocherova et al., 2015a). Among the wide variety of previously reported low-fouling coatings, zwitterionic polymeric coatings have been recently demonstrated as a promising functionalizable low-fouling surface for label-free biosensing in complex media (Brault et al., 2010, Vaisocherova et al., 2015a, 2008). Nevertheless, the biosensor capabilities of such coatings have been primarily demonstrated in complex biological fluids (blood plasma or serum) (Banerjee et al., 2011, Vaisocherova et al., 2008); the use of these coatings has never been explored with food samples. Compared to blood plasma samples, food commodities contain diverse sets of components including lipids, proteins, saccharides, water, vitamins, minerals, and even synthetic low-molecular-weight additives with variable contents. This complexity results in diverse food sample physico-chemical properties (Sikorski, 2002), thus the design of a robust, functional, low-fouling coating for reliable biosensing in crude food samples remains challenging.

In this work, we present the first use of ultra-low fouling, functionalizable poly(carboxybetaine acrylamide) (pCBAA) brushes as a unique sensing surface for the multi-step detection of bacterial pathogens in crude hamburger and cucumber samples. We studied both the functional as well as the surface resistance capabilities of the pCBAA coatings for each step of a detection assay that included: (I.) the capture of *E. coli* O157:H7 and *Salmonella* sp. in hamburger and cucumber samples, (II.) the capture of biotinylated secondary antibody, and (III.) the signal enhancement using streptavidin-coated gold nanoparticles. We compare our results to those using a standard low-fouling carboxy-functional OEG-based AT-SAMs, and show that the pCBAA brushes have similar levels of functionalization while providing over an order of magnitude improvement in fouling resistance. Finally, we demonstrate the effectiveness of these brushes via the use of a pCBAA-based SPR biosensor for the sensitive and specific detection of low levels of *E. coli* O157:H7 and *Salmonella* sp. in complex cucumber and hamburger samples.

## 2. Materials and methods

### 2.1. Reagents and biological materials

*N*-hydroxysuccinimide (NHS) and *N*-ethyl-*N'*-(3-diethylaminopropyl) (EDC) were purchased from PharmaTech, Czech Republic. Ethanol (purity  $\geq 99.9\%$ ) was purchased from Merck, USA. The buffer solutions were prepared using Millipore Q water (18.0 M $\Omega$ .cm). Phosphate buffered saline (PBS, 0.01 M phosphate, 0.138 M sodium chloride, 0.0027 M potassium chloride, pH 7.4 at 25 °C) was prepared from a stock solution purchased from Sigma-Aldrich, Czech Republic. Tween<sup>®</sup> 20 (Tween), ethanolamine (EA), and casein blocking buffer (casein) were purchased from Sigma-Aldrich, Czech Republic. 10 mM 4-(2-hydroxyethyl)-1-piperazine ethanesulfonic acid, pH 8.0 at 25 °C (HEPES) and 10 mM sodium acetate buffer, pH 5.0 at 25 °C (SA) were prepared from stock solutions purchased from Sigma Aldrich, Czech Republic. The bromine-terminated alkanethiol (HS-C<sub>11</sub>-OC(O)-IzoButyrate-Br), HS-C<sub>11</sub>-(EG)<sub>4</sub>-OH, and HS-C<sub>11</sub>-EG<sub>6</sub>-OCH<sub>2</sub>-COOH thiols were purchased from Prochimia, Poland. The carboxybetaine acrylamide monomer (CBAA) was purchased from Zwitter Technology, Seattle, USA. The CuBr, CuBr<sub>2</sub>, 2,2'-dipyridyl (BiPy), were purchased from Sigma-Aldrich, Czech Republic. Tetrahydrofuran (THF, purity  $\geq 99.9\%$ ) was purchased from Penta, Czech Republic.

Heat-killed *Escherichia coli* O157:H7 (*E. coli*), *Salmonella* sp. (*Salmonella*), primary antibodies (Ab<sub>1</sub>), and biotinylated secondary antibodies (Ab<sub>2</sub>) against *E. coli* and *Salmonella* (anti-*E. coli*, b-anti-*E. coli*, anti-*Salmonella*, b-anti-*Salmonella*) were purchased from KPL, Inc., USA.

## 2.2. Preparation of food samples

For detection experiments involving food samples we used cucumbers purchased from a local food store and hamburger from a local fast food restaurant. The cucumber was washed with water and sliced prior to homogenization. Food homogenization was performed for 2 min using a Masticator (IUL Instruments, BioTech, Czech Republic) following a standardized procedure (Andrews et al., 1978). The samples were then centrifuged for 2 min at 1200 rpm to remove any residual large pieces of foods. The supernatant above the sediment was frozen until used. To confirm that these food extracts were free of *Salmonella* and *E. coli*, a series of culture-based reference experiments were performed in the Food control laboratory of the Police of the Czech Republic following standard protocols (ČSN ISO 7251 and ČSN EN ISO 6579).

## 2.3. SPR sensor

In this work we used a four-channel spectroscopic SPR sensor developed at the Institute of Photonics and Electronics (Prague, Czech Republic) (Homola et al., 2002, Vaisocherova et al., 2014) combined with a dispersionless microfluidic system (Springer et al., 2010). The sensor was equipped with a temperature controller with a baseline stability of 0.01 °C.

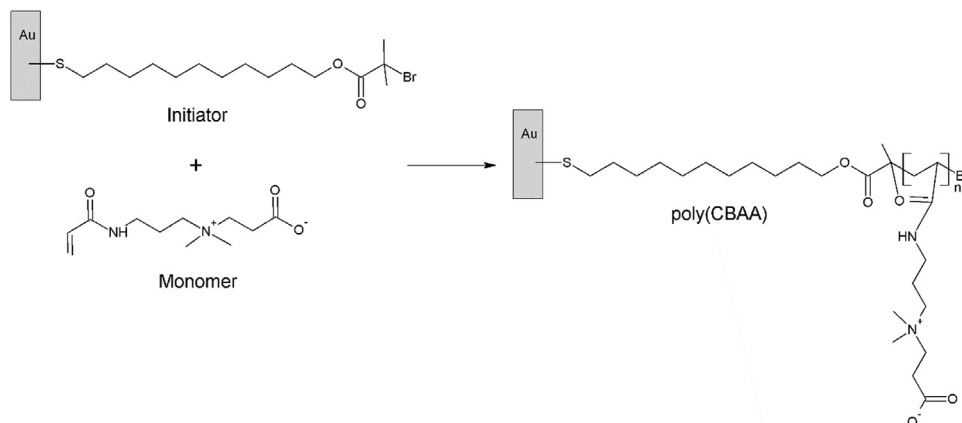
Because SPR is an evanescent field phenomenon, the sensitivity to changes at the polymer/fluid interface will decrease with increasing polymer thickness. To compensate for this effect, the SPR response was calibrated using the transfer-matrix method (Born and Emil, 1999). Briefly, we calculated the reflection spectra of a 4-layer structure consisting of BK-7 glass (RI=1.51 RIU), a 50 nm thick gold layer, a dielectric layer corresponding to polymer brush, and water (RI=1.33 RIU). The RI of gold and the RI and thickness of polymer layers were obtained from ellipsometry measurements, see also (Vaisocherova et al., 2008, 2014). The angle of incidence was derived from experimental values of resonant wavelengths corresponding to unmodified and activated polymer layers in contact with water. The surface sensitivity was calculated as the SPR response upon the addition of a 10 nm thick dielectric layer with RI=1.45 RIU over the polymer brush layer. For the SPR sensor used in this study (resonant wavelength around 750 nm), a 1 nm SPR wavelength shift represents a change in the surface protein concentration of 17 ng/cm<sup>2</sup> (Homola, 2006, Vaisocherova et al., 2007), which assumes the same refractive index for immobilized antibodies, streptavidin, oligonucleotides, and food sample deposits. Typical correction factors for bare polymer brush thickness were 1.2 for a 20 nm thick pCBAA (RI of 1.401 RIU at 750 nm for wet surface).

## 2.4. Preparation and characterization of pCBAA functional coatings

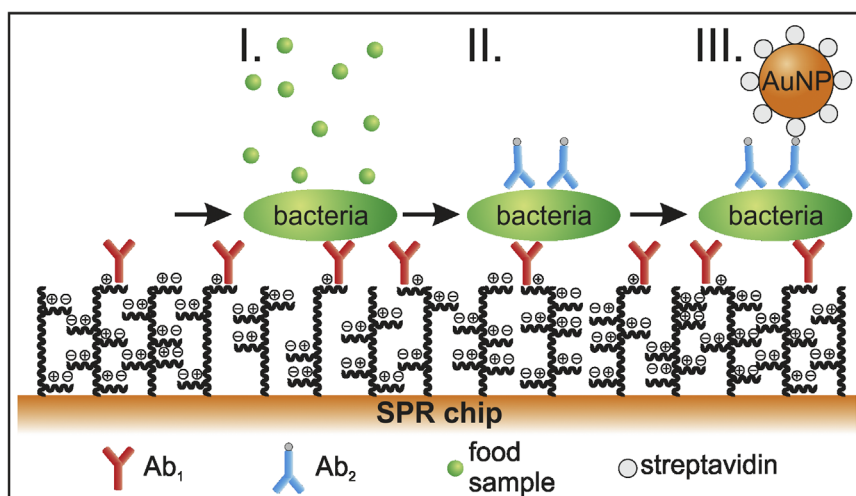
Polymer brushes of poly(3-acryloylamino-propyl)-(2-carboxyethyl)-dimethyl-ammonium) (pCBAA) were prepared on gold substrates via surface-initiated atom transfer radical polymerization (Vaisocherova et al., 2008). Using this procedure, we prepared pCBAA coatings having wet thicknesses of both ~20 and ~80 nm, whereby the pCBAA thickness was varied by changing the water/methanol ratio in the polymerization reaction (Zhang et al., 2006, 2008). The thickness of the wet brushes was measured using a previously described procedure (Vaisocherova et al., 2008, 2014) (Scheme 1).

The SPR chips coated with pCBAA brushes were stored in PBS until use, then washed with MilliQ water, dried with a stream of nitrogen, and mounted into the SPR sensor. The pCBAA surface functionalization included three steps: the activation of carboxyl groups by NHS/EDC chemistry, the covalent attachment of antibodies to activated groups, and the deactivation of residual active groups (Vaisocherova et al., 2014, 2015b). Surface carboxylates were converted to active esters by injection of a freshly prepared solution of *N*-hydroxysuccinimide (NHS, 0.1 M) and *N*-ethyl-*N'*-(3-diethylaminopropyl) (EDC, 0.5 M) in MilliQ water for 15 min at a flow rate of 5 μL/min. Antibodies (25 μg/mL) diluted in HEPES (10 mM, pH 8.0) were filtered using a syringe filter (0.22 μm, TPP Switzerland) and immobilized on the activated surface in a flow-through format at a flow rate of 20 μL/min for 20 min. Any residual active esters were then deactivated using consecutive injections of PBS and SA. The amount of immobilized antibodies on each surface was determined from the difference between the final and initial sensor response.

This surface functionalization protocol was adjusted in order to achieve a maximum loading capacity of immobilized Ab<sub>1</sub> while maintaining a high resistance to fouling. For purposes of comparison we measured the fouling resistance of both the pCBAA brushes as well as surfaces composed of standard low-fouling carboxy-functional mixed oligo(ethylene glycol) alkanethiolate self-assembled monolayers (AT-SAMs); the preparation and functionalization of the AT-SAMs used herein is described in Supplementary Material. Fouling levels were measured by flowing food samples (45 μL/min, 25 °C, 15 min) over both Ab<sub>1</sub>-functionalized pCBAA (~20 nm wet thickness) and AT-SAM surfaces having Ab<sub>1</sub> surface coverages in the range of ~175–275 ng/cm<sup>2</sup>. The fouling characteristics were determined after washing the surface with PBS buffer for 10 min.



**Scheme 1.** Synthesis of pCBAA brushes via surface initiated and surface-initiated atom transfer radical polymerization.



**Scheme 2.** Scheme of the three-step assay for the detection of bacterial pathogens in food samples.

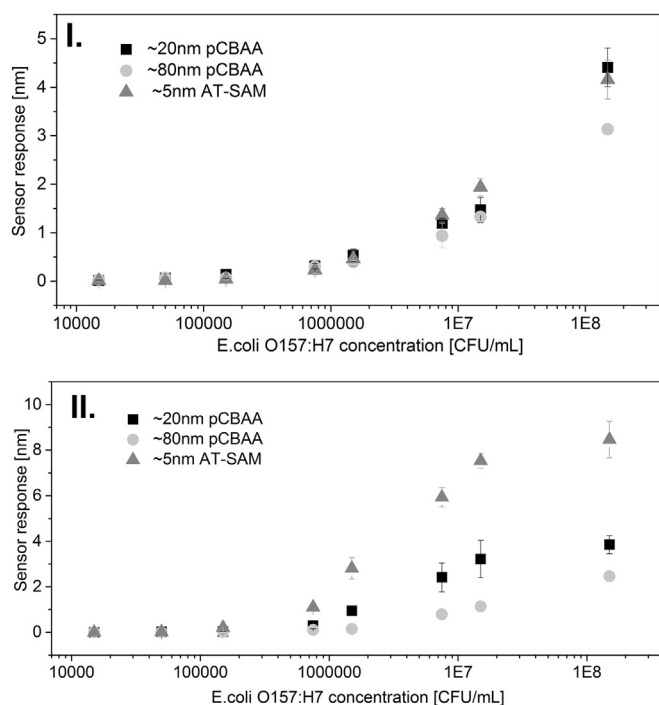


**Fig. 1.** Sensor response to the capture of the *E.coli* O157:H7 (I.) and Ab<sub>2</sub> (II.) regarding 20 and 80 nm thick pCBAA brushes and a 5 nm thick AT-SAM layer. Response of sensors employing alkanethiolate self-assembled monolayers (AT-SAM) are shown for comparison.

### 2.5. SPR biosensor-based detection of bacteria

The detection of bacteria spiked in hamburger and cucumber samples was performed for *E.coli* and *Salmonella* concentrations ranging from  $1.5 \times 10^1$  to  $1.5 \times 10^7$  CFU/mL and  $2.5 \times 10^2$  to  $2.5 \times 10^7$  CFU/mL, respectively. Pathogens spiked in PBS buffer were only used in experiments to characterize the effect of the pCBAA brush thickness on the biosensor biorecognition capabilities. The format of the detection experiments is shown in Scheme 2. All experiments were conducted at 25 °C and proceeded as follows: (I.) food samples spiked with bacteria were flowed along surfaces previously functionalized with respective Ab<sub>1</sub> (45  $\mu$ L/min, 15 min), (II.) followed by an injection of Ab<sub>2</sub> (5  $\mu$ g/mL, 20  $\mu$ L/min, 15 min), and finally (III.) followed by an injection of streptavidin-coated spherical gold nanoparticles (S-AuNPs) having

an OD of 1 (20  $\mu$ L/min, 25 min) in PBS buffer with casein (0.01% w/v) and Tween (0.01% w/v) (Springer and Homola, 2012). Each data point was obtained using data from at least three individual pCBAA coatings and up to eight sensing channels. The procedure for the synthesis and functionalization of S-AuNPs with a diameter of  $\sim 35$  nm was taken from (Springer et al., 2014), and is also described in the Supplementary Material.

Food samples without bacteria (spiked with the same amount of bacteria-free buffer) were injected in a single channel for each coating to detect any potential non-specific binding of S-AuNPs (blank sample). The signal from the reference channel was subtracted from those provided by the detection channels. The limit of detection (LOD) was calculated using a “blank + 3  $\times$  SD” approach.

The simultaneous detection of *E.coli* and *Salmonella* in hamburger samples was performed under the same conditions as used for the detection of individual pathogens. Each sensor chip contained two detection channels and two reference channels, where each pair was functionalized with either anti-*E.coli* or anti-*Salmonella*. Three different mixtures of *E.coli* and *Salmonella* in hamburger samples were analyzed. The concentrations of *E.coli* and *Salmonella* spiked in these samples were  $7.5 \times 10^2$  and  $2.5 \times 10^7$  CFU/mL (MIX-1),  $2.5 \times 10^6$  and  $1.3 \times 10^6$  CFU/mL (MIX-2), and  $7.5 \times 10^9$  and  $1.3 \times 10^4$  CFU/mL (MIX-3), respectively. The results obtained from the measurements on bacteria mixtures were compared with those obtained for individual pathogens.

## 3. Results and discussion

### 3.1. Performance of pCBAA coatings for the multi-step detection of bacterial pathogens in complex food matrices

We measured the effect of the thickness of gold-grafted zwitterionic pCBAA coatings on the biorecognition capabilities of the antibody-functionalized surface. Specifically, we measured the response of the anti-*E.coli*-functionalized pCBAA-coated sensor to both *E.coli* in buffer as well as to the respective secondary antibody (Ab<sub>2</sub>) for two different coating thicknesses (between 20 nm and 80 nm). Due to the rather limited control over the thickness of pCBAA grafted from gold substrates by SI-ATRP (Rodríguez-Emmenegger et al., 2011b, 2011c), we selected these two thicknesses as distinct enough to be reproducibly prepared.

These results are shown in Fig. 1; for purposes of comparison we have included data regarding the use of a thin AT-SAM ( $\sim 5$  nm) (Prime and Whitesides, 1991, Ulman, 1996). It can be seen (upper

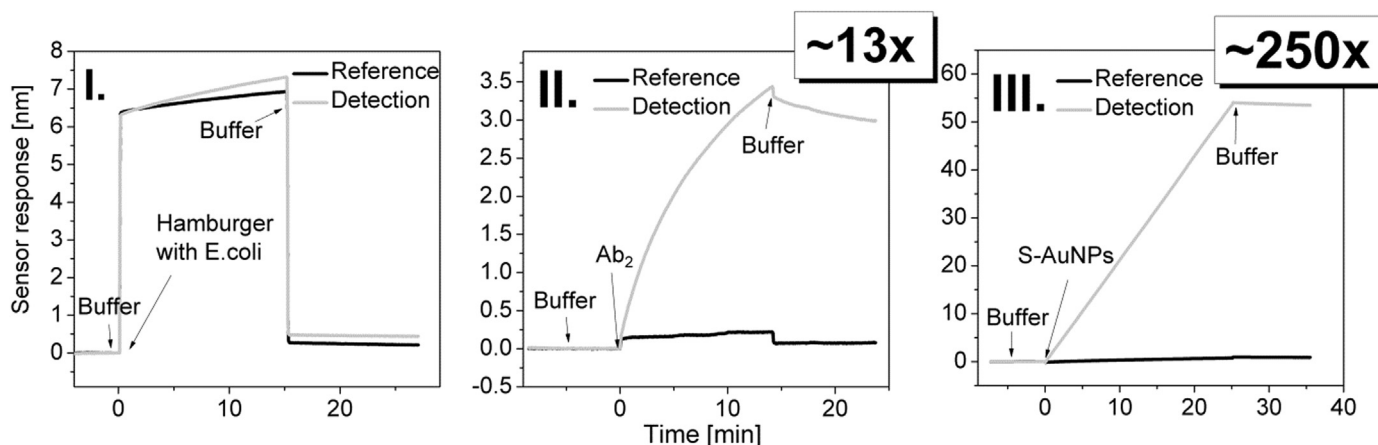


**Fig. 2.** Typical SPR sensorgrams obtained for the detection of *E. coli* O157:H7 ( $7.5 \times 10^5$  CFU/mL) in hamburger sample for each step of the detection assay as depicted in Scheme 2. The sensor response enhancement is given in the boxes.

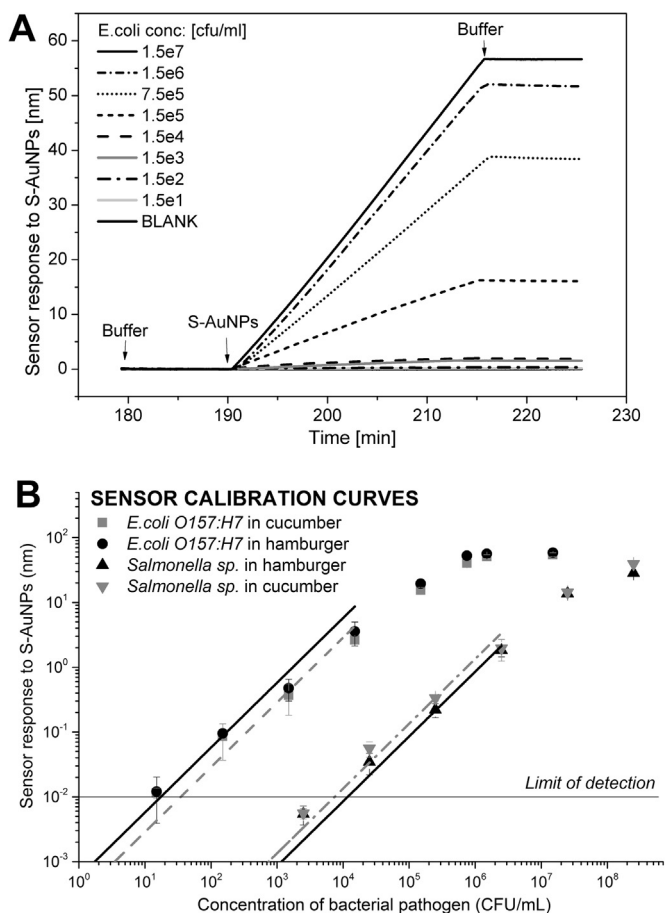


**Fig. 3.** (A) SPR sensor response to the binding of S-AuNPs in step (III) of the assay for the detection of *E. coli* O157:H7 in cucumber sample. (B) Calibration curves for *E. coli* and *Salmonella sp.* in both hamburger and cucumber samples.

graph) that the capture of *E. coli* (Scheme 2/I.) was not significantly influenced by the pCBAA thickness, whereas the effect of the pCBAA thickness was more pronounced in the sensor response to the secondary antibody (Scheme 2/II.). This effect may be attributed to the differences in steric hindrance between the binding of secondary antibody to bacterium bound to brushes of different thicknesses; however, this effect cannot be properly accounted for using the calibration methods used in this study (Homola, 2008). Nevertheless, the discrepancy between the sensor response of all three layers decreases as the concentration of *E. coli* decreases.

In contrast to the pCBAA polymer brushes, the AT-SAMs coatings provided a very limited resistance to fouling from food samples. Specifically, the respective fouling levels from cucumber and hamburger samples for the AT-SAMs were  $22.3 \pm 5.2$  ng/cm<sup>2</sup> and  $69.7 \pm 11.9$  ng/cm<sup>2</sup>, whereas the same levels for  $\sim 20$  nm pCBAA brushes were  $6.2 \pm 1.7$  ng/cm<sup>2</sup> and  $3.4 \pm 1.3$  ng/cm<sup>2</sup>. The superior surface resistance to fouling for pCBAA compared to AT-SAMs is in agreement with previous studies on the fouling from bodily fluids (Vaisocherova et al., 2015a, 2014, 2015b). The average Ab<sub>1</sub> immobilization levels achieved for pCBAA ( $\sim 20$  nm) were  $221 \pm 36$  ng/cm<sup>2</sup> and  $209 \pm 51$  ng/cm<sup>2</sup> for anti-*E. coli* and anti-*Salmonella*, respectively; the same values for AT-SAMs were  $200 \pm 39$  ng/cm<sup>2</sup> and  $169 \pm 13$  ng/cm<sup>2</sup>. Fouling levels from hamburger and cucumber samples on anti-*E. coli*-functionalized pCBAA surface were thus below 2.8% of the anti-*E. coli* immobilization level. This ratio is significantly lower than those observed on AT-SAMs, which had fouling ratios of 11% and 35% for cucumber and hamburger, respectively. Based on these results, a pCBAA coating with a thickness of  $\sim 20$  nm was used for all further bacteria detection experiments. This lower thickness is also beneficial from the perspective of the SPR surface sensitivity (Homola, 2008).

We further compared the nonspecific binding of S-AuNPs to anti-*E. coli*-functionalized pCBAA (having a thickness of  $\sim 20$  nm) with an AT-SAM surface (see Figure S-2 in Supplementary Material). We found that the pCBAA coatings had nearly an order of magnitude better performance. Specifically, based on SPR measurements with *E. coli* O157:H7 spiked in hamburger we found that the levels of nonspecific binding of S-AuNPs to pCBAA and AT-SAM coatings (functionalized with anti-*E. coli* O157:H7 followed with *E. coli* O157:H7 detection in hamburger) were between 0.2 nm and 1.6 nm, respectively. For the blank surfaces (which involve all three detection steps, where bacteria-free food samples were injected instead of bacteria-spiked food sample), the nonspecific binding of S-AuNPs on pCBAA and AT-SAM coatings were 0.9 and 89 nm, respectively. This clearly implies that the nonspecific binding of secondary biotinylated antibody (b-anti-*E. coli* O157:H7) to AT-SAM significantly contributed to a very high level of S-AuNPs in a reference blank surface. Hence, the combination of the high surface resistance to binding of both Ab<sub>2</sub> and S-AuNPs makes the pCBAA coating superior over the AT-SAM.

### 3.2. Detection of individual foodborne pathogens in food samples

We further characterized the high functional and surface-resistance capabilities of pCBAA in a multi-step detection assay through the use of a SPR biosensor based on pCBAA with a thickness

**Table 1**

SPR response to S-AuNPs obtained from the simultaneous detection of *E.coli* and *Salmonella* in hamburger samples. The results were compared to results determined from the respective pathogen's calibration curve ("single pathogen response").

Mix	Bacterial pathogen	Spiked concentration (CFU/mL)	Sensor response (nm)	Single pathogen response (nm)	Recovery (%)
1.	<i>E.coli</i> O157:H7	$7.5 \times 10^2$	$0.026 \pm 0.01$	$0.025 \pm 0.008$	104
	<i>Salmonella</i> sp.	$2.5 \times 10^7$	$10.5 \pm 1.0$	$10.5 \pm 1.1$	100
2.	<i>E.coli</i> O157:H7	$7.5 \times 10^3$	$0.09 \pm 0.03$	$0.10 \pm 0.02$	90
	<i>Salmonella</i> sp.	$1.3 \times 10^6$	$0.7 \pm 0.1$	$0.8 \pm 0.2$	95
3.	<i>E.coli</i> O157:H7	$7.5 \times 10^6$	$95 \pm 20$	$111 \pm 15$	86
	<i>Salmonella</i> sp.	$1.3 \times 10^4$	$0.010 \pm 0.005$	$0.12 \pm 0.005$	83

of 20 nm. Using this three-step assay, two model foodborne pathogens (*E. coli* O157:H7 and *Salmonella* sp.) were detected in crude cucumber and hamburger samples (Scheme 2). Typical sensor data obtained during each step of the assay for both the measuring and reference channel are shown in Fig. 2. Fig. 3A shows the SPR sensor response to the binding of S-AuNPs during step (III) for various concentrations of *E.coli* in cucumber samples. The calibration curves for *E.coli* and *Salmonella* sp. in both hamburger and cucumber samples are shown in Fig. 3B. The limits of detection were determined to be 17 CFU/mL and 57 CFU/mL for *E.coli* in hamburger and cucumber samples, respectively, and  $11.7 \times 10^3$  CFU/mL and  $7.4 \times 10^3$  CFU/mL for *Salmonella* in hamburger and cucumber samples, respectively. The discrepancies between the LODs obtained for *E. coli* and *Salmonella* were most likely due to the differences in the affinity and specificity of the respective antibodies.

Including sample preparation, the detection times for the results herein were ultimately shorter than 80 min, which is remarkably shorter than the time required by standard culture-based techniques (Gracias and McKillip, 2004; Lazcka et al., 2007). The LODs demonstrated herein for *E. coli* were either comparable, or up to one order of magnitude higher, than those of previous reports that are regarded as the most sensitive SPR biosensors for bacterial pathogen detection (Bouguelia et al., 2013; Torun et al., 2012; Yazgan et al., 2014); however, those LOD values regard the detection of pathogens either in buffer or solutions of medium complexity such as tap water. In addition, the LODs for the majority of previous biosensor-based studies reporting the detection of pathogens in complex food samples – including those reporting very low LODs – were not determined through the measurement of sensor calibration curves in said complex media (see also Table S-1 in Supplementary Material). To the best of our knowledge this study represents the first time-efficient (< 80 min) SPR-based biosensor detection of bacterial pathogens in crude food samples with a LOD as low as tens of bacteria per 1 mL of complex food extract without using bacteria enrichment. Furthermore, it is envisioned that these limits of detection can be further improved by adjusting the respective detection assay conditions (e.g. Ab<sub>2</sub> concentrations) or by employing synthetic bioreceptor alternatives to the primary or secondary antibodies (Yazgan et al. 2014).

### 3.3. Simultaneous detection of *E.coli* and *salmonella* in crude food samples

This biosensor was also utilized for the simultaneous detection of *E.coli* and *Salmonella* in hamburger samples. Specifically, crude hamburger samples with three different combinations of *E.coli* and *Salmonella* concentrations were analyzed. A series of control SPR experiments confirmed that there is no significant cross-reactivity between the antibodies (between Ab<sub>1</sub> and Ab<sub>2</sub>) and bacterium used in this study (data not shown). The results of the simultaneous detection experiments are shown in Table 1. We compared the sensor response for each pathogen in mixed samples with the single pathogen responses given by the respective calibration curves. It can be seen that there was a good agreement between the results

obtained in the simultaneous detection experiments and those obtained for the detection of individual pathogens. This indicates that the sensor provides sufficient specificity and indeed allows for the simultaneous detection of the two bacterial pathogens.

## 4. Conclusions

This study demonstrates the use of an ultra-low fouling functionalizable pCBAA coating as a unique biosensor surface platform providing both high functional and surface-resistance capabilities towards the multi-step detection of *E. coli* O157:H7 and *Salmonella* sp. in crude hamburger and cucumber samples. Specifically, the antibody-functionalized pCBAA coatings with a thickness as low as ~20 nm exhibited a high resistance to (i) fouling from hamburger and cucumber samples, to (ii) the nonspecific binding of secondary biotinylated antibodies, and to (iii) the nonspecific binding of streptavidin-functionalized gold nanoparticles. The fouling levels for the pCBAA brushes were up to two orders of magnitude lower when compared to standard low-fouling carboxy-functional oligo (ethylene glycol)-based AT-SAMs. Finally, a SPR biosensor based on a pCBAA coating was capable of the time-efficient (< 80 min) detection of *E. coli* and *Salmonella* with extraordinary sensitivity and specificity: the limits of detection for *E. coli* were 57 CFU/mL and 17 CFU/mL for cucumber and hamburger samples, respectively. In future we plan to further optimize the functional coatings and assay to achieve even higher sensitivity and reproducibility to enable rapid parallelized detection of multiple pathogens in food samples.

## Acknowledgments

This research was supported by the Czech Science Foundation (contract # GP14-35315P) and by Praemium Academiae of the Academy of Sciences of the Czech Republic.

## Appendix A. Supplementary material

Supplementary data associated with this article can be found in the online version at <http://dx.doi.org/10.1016/j.bios.2016.01.040>.

## References

- Abdel-Hamid, I., Ivnitski, D., Atanasov, P., Wilkins, E., 1999. Flow-through immunofiltration assay system for rapid detection of *E. coli* O157:H7. *Biosens. Bioelectron.* 14, 309–316.
- Andrews, W.H., Wilson, C.R., Poelma, P.L., Romero, A., Rude, R.A., Duran, A.P., McClure, F.D., Gentile, D.E., 1978. Usefulness of the stomacher in a microbiological regulatory laboratory. *Appl. Environ. Microbiol.* 35, 89–93.
- Baccar, H., Mejri, M.B., Hafaiedh, I., Ktari, T., Aouni, M., Abdelghani, A., 2010. Surface plasmon resonance immunosensor for bacteria detection. *Talanta* 82, 810–814.
- Banerjee, I., Pangule, R.C., Kane, R.S., 2011. Antifouling coatings: recent developments in the design of surfaces that prevent fouling by proteins, bacteria, and

- marine organisms. *Adv. Mater.* 23, 690–718.
- Barreiros dos Santos, M., Aguilis, J.P., Prieto-Simón, B., Sporer, C., Teixeira, V., Sammiter, J., 2013. Highly sensitive detection of pathogen *Escherichia coli* O157:H7 by electrochemical impedance spectroscopy. *Biosens. Bioelectron.* 45, 174–180.
- Born, Max, Wolf, Emil, 1999. Principles of Optics: Electromagnetic Theory of Propagation, Interference and Diffraction of Light. Cambridge University Press, Cambridge.
- Bouguelia, S., Roupioz, Y., Slimani, S., Mondani, L., Casabona, M.G., Durmort, C., Vernet, T., Calemczuk, R., Livache, T., 2013. On-chip microbial culture for the specific detection of very low levels of bacteria. *Lab Chip* 13, 4024–4032.
- Brault, N.D., Gao, C., Xue, H., Piliarik, M., Homola, J., Jiang, S., Yu, Q., 2010. Ultra-low fouling and functionalizable zwitterionic coatings grafted onto SiO<sub>2</sub> via a biomimetic adhesive group for sensing and detection in complex media. *Biosens. Bioelectron.* 25, 2276–2282.
- Call, D.R., Borucki, M.K., Loge, F.J., 2003. Detection of bacterial pathogens in environmental samples using DNA microarrays. *J. Microbiol. Methods* 53, 235–243.
- CDC. 2014. (23.9.2014); (<http://www.cdc.gov>)).
- Cho, I.H., Bhandari, P., Patel, P., Irudayaraj, J., 2015. Membrane filter-assisted surface enhanced Raman spectroscopy for the rapid detection of *E. coli* O157:H7 in ground beef. *Biosens. Bioelectron.* 64, 171–176.
- Cudjoe, K.S., Hagtvedt, T., Dainty, R., 1995. Immunomagnetic separation of *Salmonella* from foods and their detection using immunomagnetic particle (IMP)-ELISA. *Int. J. Food Microbiol.* 27, 11–25.
- Disney, M.D., Seeberger, P.H., 2004. The use of carbohydrate microarrays to study carbohydrate-cell interactions and to detect pathogens. *Chem. Biol.* 11, 1701–1707.
- EFSA. 2014. (23.09.2014); (<http://www.efsa.europa.eu>)).
- Fetsch, A., Contzen, M., Hartelt, K., Kleiser, A., Maassen, S., Rau, J., Kraushaar, B., Layer, F., Strommenger, B., 2014. Staphylococcus aureus food-poisoning outbreak associated with the consumption of ice-cream. *Int. J. Food Microbiol.* 187, 1–6.
- Food and Drug Administration, 2012. Bad Bug Book, Foodborne Pathogenic Microorganisms and Natural Toxins. Center for Food Safety and Applied Nutrition (CFSAN) of the Food and Drug Administration (FDA), U.S. Department of Health and Human Services.
- Gerner-Smidt, P., Whichard, J.M., Scallan, E., 2007. Foodborne disease trends and reports. *Foodborne Pathog. Dis.* 4, 111–114.
- Gracias, K.S., McKillip, J.L., 2004. A review of conventional detection and enumeration methods for pathogenic bacteria in food. *Can. J. Microbiol.* 50, 883–890.
- Heaton, J.C., Jones, K., 2008. Microbial contamination of fruit and vegetables and the behaviour of enteropathogens in the phyllosphere: a review. *J. Appl. Microbiol.* 104, 613–626.
- Homola, J., 2006. Surface Plasmon Resonance Based Sensors. Springer-Verlag, Germany.
- Homola, J., 2008. Surface plasmon resonance sensors for detection of chemical and biological species. *Chem. Rev.* 108, 462–493.
- Homola, J., Dostalek, J., Chen, S.F., Rasooly, A., Jiang, S.Y., Yee, S.S., 2002. Spectral surface plasmon resonance biosensor for detection of staphylococcal enterotoxin B in milk. *Int. J. Food Microbiol.* 75, 61–69.
- Ko, S., Grant, S.A., 2006. A novel FRET-based optical fiber biosensor for rapid detection of *Salmonella typhimurium*. *Biosens. Bioelectron.* 21, 1283–1290.
- Kothary, M.H., Babu, U.S., 2001. Infective dose of foodborne pathogens in volunteers: a review. *J. Food Saf.* 21, 49–68.
- Lampel, K.A., Orlandi, P.A., Kornegay, L., 2000. Improved template preparation for PCR-based assays for detection of food-borne bacterial pathogens. *Appl. Environ. Microbiol.* 66, 4539–4542.
- Lazcka, O., Campo, F.J.D., Muñoz, F.X., 2007. Pathogen detection: a perspective of traditional methods and biosensors. *Biosens. Bioelectron.* 22, 1205–1217.
- Li, Y., Cheng, P., Gong, J., Fang, L., Deng, J., Liang, W., Zheng, J., 2012. Amperometric immunosensor for the detection of *Escherichia coli* O157:H7 in food specimens. *Anal. Biochem.* 421, 227–233.
- Li, Y., Mustapha, A., 2004. Simultaneous detection of *Escherichia coli* O157:H7, *Salmonella*, and *Shigella* in apple cider and produce by a multiplex PCR. *J. Food Prot.* 67, 27–33.
- Lin, Y.H., Chen, S.H., Chuang, Y.C., Lu, Y.C., Shen, T.Y., Chang, C.A., Lin, C.S., 2008. Disposable amperometric immunosensing strips fabricated by Au nanoparticles-modified screen-printed carbon electrodes for the detection of food-borne pathogen *Escherichia coli* O157:H7. *Biosens. Bioelectron.* 23, 1832–1837.
- Linman, M.J., Sugerman, K., Cheng, Q., 2010. Detection of low levels of *Escherichia coli* in fresh spinach by surface plasmon resonance spectroscopy with a TMB-based enzymatic signal enhancement method. *Sens. Actuators B: Chem.* 145, 613–619.
- Mansfield, L.P., Forsythe, S.J., 2001. The detection of *Salmonella* serovars from animal feed and raw chicken using a combined immunomagnetic separation and ELISA method. *Food Microbiol.* 18, 361–366.
- Paton, J.C., Paton, A.W., 1998. Pathogenesis and diagnosis of Shiga toxin-producing *Escherichia coli* infections. *Clin. Microbiol. Rev.* 11, 450–479.
- Perez, F.G., Mascini, M., Tothill, I.E., Turner, A.P., 1998. Immunomagnetic separation with mediated flow injection analysis amperometric detection of viable *Escherichia coli* O157. *Anal. Chem.* 70, 2380–2386.
- Postollec, F., Falentin, H., Pavan, S., Combrisson, J., Sohier, D., 2011. Recent advances in quantitative PCR (qPCR) applications in food microbiology. *Food Microbiol.* 28, 848–861.
- Prime, K., Whitesides, G., 1991. Self-assembled organic monolayers: model systems for studying adsorption of proteins at surfaces. *Science* 252, 1164–1167.
- Rodríguez-Emmenegger, C., Avramenko, O.A., Brynda, E., Skvor, J., Alles, A.B., 2011a. Poly(HEMA) brushes emerging as a new platform for direct detection of food pathogen in milk samples. *Biosens. Bioelectron.* 26, 4545–4551.
- Rodríguez-Emmenegger, C., Brynda, E., Riedel, T., Houska, M., Subr, V., Alles, A.B., Hasan, E., Gautrot, J.E., Huck, W.T., 2011b. Polymer brushes showing non-fouling in blood plasma challenge the currently accepted design of protein resistant surfaces. *Macromol. Rapid Commun.* 32, 952–957.
- Rodríguez-Emmenegger, C., Kylian, O., Houska, M., Brynda, E., Artemenko, A., Kousal, J., Alles, A.B., Biederman, H., 2011c. Substrate-independent approach for the generation of functional protein resistant surfaces. *Biomacromolecules* 12, 1058–1066.
- Rodríguez-Lazaro, D., D'Agostino, M., Herrewegh, A., Pla, M., Cook, N., Ikononopoulos, J., 2005. Real-time PCR-based methods for detection of *Mycobacterium avium* subsp. *paratuberculosis* in water and milk. *Int. J. Food Microbiol.* 101, 93–104.
- Rohde, A., Hammerl, J.A., Appel, B., Dieckmann, R., Al Dahouk, S., 2015. FISHing for bacteria in food – A promising tool for the reliable detection of pathogenic bacteria? *Food Microbiol.* 46, 395–407.
- Sanvicens, N., Pascual, N., Fernández-Argüelles, M., Adrián, J., Costa-Fernández, J., Sánchez-Baeza, F., Sanz-Medel, A., Marco, M.P., 2011. Quantum dot-based array for sensitive detection of *Escherichia coli*. *Anal. Bioanal. Chem.* 399, 2755–2762.
- Sikorski, Z.E., 2002. Chemical and Functional Properties of Food Components, Second Edition Taylor & Francis, United Kingdom.
- Simpson, J.M., Lim, D.V., 2005. Rapid PCR confirmation of *E. coli* O157:H7 after evanescent wave fiber optic biosensor detection. *Biosens. Bioelectron.* 21, 881–887.
- Springer, T., Ermini, M.L., Spackova, B., Jablonku, J., Homola, J., 2014. Enhancing sensitivity of surface plasmon resonance biosensors by functionalized gold nanoparticles: size matters. *Anal. Chem.* 86, 10350–10356.
- Springer, T., Homola, J., 2012. Biofunctionalized gold nanoparticles for SPR-biosensor-based detection of CEA in blood plasma. *Anal. Bioanal. Chem.* 404, 2869–2875.
- Springer, T., Piliarik, M., Homola, J., 2010. Surface plasmon resonance sensor with dispersionless microfluidics for direct detection of nucleic acids at the low femtomole level. *Sens. Actuators B-Chem.* 145, 588–591.
- Tawil, N., Sacher, E., Mandeville, R., Meunier, M., 2012. Surface plasmon resonance detection of *E. coli* and methicillin-resistant *S. aureus* using bacteriophages. *Biosens. Bioelectron.* 37, 24–29.
- Torun, O., Hakkı Boyacı, I., Temur, E., Tamer, U., 2012. Comparison of sensing strategies in SPR biosensor for rapid and sensitive enumeration of bacteria. *Biosens. Bioelectron.* 37, 53–60.
- Ulman, A., 1996. Formation and structure of self-assembled monolayers. *Chem. Rev.* 96, 1533–1554.
- Vaisocherova, H., Brynda, E., Homola, J., 2015a. Functionalizable low-fouling coatings for label-free biosensing in complex biological media: advances and applications. *Anal. Bioanal. Chem.* 407, 3927–3953.
- Vaisocherova, H., Mrkvova, K., Piliarik, M., Jinoch, P., Steinbachova, M., Homola, J., 2007. Surface plasmon resonance biosensor for direct detection of antibody against Epstein-Barr virus. *Biosens. Bioelectron.* 22, 1020–1026.
- Vaisocherova, H., et al., 2014. Functionalized ultra-low fouling carboxy- and hydroxy-functional surface platforms: functionalization capacity, biorecognition capability and resistance to fouling from undiluted biological media. *Biosens. Bioelectron.* 51, 150–157.
- Vaisocherova, H., et al., 2015b. Rapid and sensitive detection of multiple microRNAs in cell lysate by low-fouling surface plasmon resonance biosensor. *Biosens. Bioelectron.* 70, 226–231.
- Vaisocherova, H., Yang, W., Zhang, Z., Cao, Z., Cheng, G., Piliarik, M., Homola, J., Jiang, S., 2008. Ultra-low fouling and functionalizable surface chemistry based on a zwitterionic polymer enabling sensitive and specific protein detection in undiluted blood plasma. *Anal. Chem.* 80, 7894–7901.
- Wang, Y., Knoll, W., Dostalek, J., 2012. Bacterial pathogen surface plasmon resonance biosensor advanced by long range surface plasmons and magnetic nanoparticle assays. *Anal. Chem.* 84, 8345–8350.
- Wang, Y., Ye, Z., Si, C., Ying, Y., 2011. Subtractive inhibition assay for the detection of *E. coli* O157:H7 using surface plasmon resonance. *Sensors* 11, 2728–2739.
- Yang, L., Li, Y., 2006. Simultaneous detection of *Escherichia coli* O157:H7 and *Salmonella Typhimurium* using quantum dots as fluorescence labels. *Analyst* 131, 394–401.
- Yang, L., Li, Y., Erf, G.F., 2004. Interdigitated array microelectrode-based electrochemical impedance immunosensor for detection of *Escherichia coli* O157:H7. *Anal. Chem.* 76, 1107–1113.
- Yazgan, I., Noah, N.M., Toure, O., Zhang, S., Sadik, O.A., 2014. Biosensor for selective detection of *E. coli* in spinach using the strong affinity of derivatized mannose with fimbrial lectin. *Biosens. Bioelectron.* 61, 266–273.
- Yu, L.S., Reed, S.A., Golden, M.H., 2002. Time-resolved fluorescence immunoassay (TRFIA) for the detection of *Escherichia coli* O157:H7 in apple cider. *J. Microbiol. Methods* 49, 63–68.
- Zhang, Z., Chen, S., Jiang, S., 2006. Dual-functional biomimetic materials: nonfouling poly(carboxybetaine) with active functional groups for protein immobilization. *Biomacromolecules* 7, 3311–3315.
- Zhang, Z., Vaisocherova, H., Cheng, G., Yang, W., Xue, H., Jiang, S., 2008. Nonfouling behavior of polycarboxybetaine-grafted surfaces: structural and environmental effects. *Biomacromolecules* 9, 2686–2692.
- Zordan, M.D., Grafton, M.M., Acharya, G., Reece, L.M., Cooper, C.L., Aronson, A.I., Park, K., Leary, J.F., 2009. Detection of pathogenic *E. coli* O157:H7 by a hybrid microfluidic SPR and molecular imaging cytometry device. *Cytometry A* 75, 155–162.

# Appendix III

Vaisocherová-Lísalová, H., F. Surman, I. Víšová, M. Vala, T. Špringer, M. L. Ermini, H. Šípová, P. Šedivák, M. Houska, T. Riedel, O. Pop-Georgievski, E. Brynda, J. Homola

## **Copolymer Brush-Based Ultralow-Fouling Biorecognition Surface Platform for Food Safety**

*Analytical Chemistry* **88**(21) (2016): 10533-10539.



# Copolymer Brush-Based Ultralow-Fouling Biorecognition Surface Platform for Food Safety

Hana Vaisocherová-Lísalová,<sup>\*,†</sup> František Surman,<sup>‡</sup> Ivana Víšová,<sup>†</sup> Milan Vala,<sup>†</sup> Tomáš Špringer,<sup>†</sup> Maria Laura Ermini,<sup>†</sup> Hana Šípová,<sup>†</sup> Petr Šedivák,<sup>§</sup> Milan Houska,<sup>‡</sup> Tomáš Riedel,<sup>‡</sup> Ognjen Pop-Georgievski,<sup>‡</sup> Eduard Brynda,<sup>‡</sup> and Jiří Homola<sup>\*,†</sup>

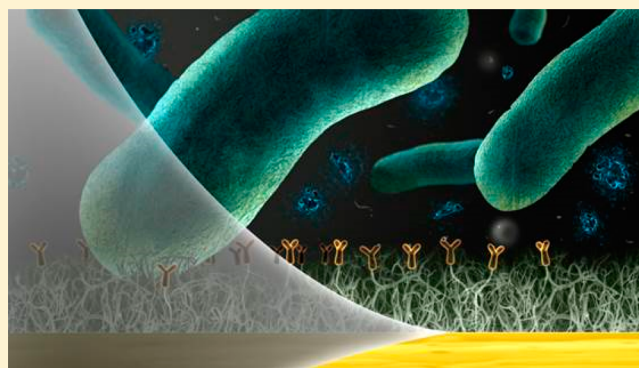
<sup>†</sup>Institute of Photonics and Electronics, Czech Academy of Sciences, Chaberská 57, Prague, Czech Republic

<sup>‡</sup>Institute of Macromolecular Chemistry, Czech Academy of Sciences, Heyrovského nám. 2, Prague, Czech Republic

<sup>§</sup>Police of the Czech Republic, Kapucínská 214/2, Prague, Czech Republic

## S Supporting Information

**ABSTRACT:** Functional polymer coatings that combine the ability to resist nonspecific fouling from complex media with high biorecognition element (BRE) immobilization capacity represent an emerging class of new functional materials for a number of bioanalytical and biosensor technologies for medical diagnostics, security, and food safety. Here, we report on a random copolymer brush surface - poly(CBMAA-*ran*-HPMAA) - providing high BRE immobilization capacity while simultaneously exhibiting ultralow-fouling behavior in complex food media. We demonstrate that both the functionalization and fouling resistance capabilities of such copolymer brushes can be tuned by changing the surface contents of the two monomer units: nonionic *N*-(2-hydroxypropyl) methacrylamide (HPMAA) and carboxy-functional zwitterionic carboxybetaine methacrylamide (CBMAA). It is demonstrated that the resistance to fouling decreases with the surface content of CBMAA; poly(CBMAA-*ran*-HPMAA) brushes with CBMAA molar content up to 15 mol % maintain excellent resistance to fouling from a variety of homogenized foods (hamburger, cucumber, milk, and lettuce) even after covalent attachment of BREs to carboxy groups of CBMAA. The poly(CBMAA 15 mol %-*ran*-HPMAA) brushes functionalized with antibodies are demonstrated to exhibit fouling resistance from food samples by up to 3 orders of magnitude better when compared with the widely used low-fouling carboxy-functional oligo(ethylene glycol) (OEG)-based alkanethiolate self-assembled monolayers (AT SAMs) and, furthermore, by up to 2 orders of magnitude better when compared with the most successful ultralow-fouling biorecognition coatings - poly(carboxybetaine acrylamide), poly(CBAA). When model SPR detections of food-borne bacterial pathogens in homogenized foods are used, it is also demonstrated that the antibody-functionalized poly(CBMAA 15 mol %-*ran*-HPMAA) brush exhibits superior biorecognition properties over the poly(CBAA).



Artificial coatings resistant to the deposition of various biological and chemical species from complex real-world media (i.e., fouling) have been increasingly important in a number of fields, including medical implants, food packaging, and detection technologies.<sup>1–3</sup> In the field of biosensor detection technologies, such coatings are expected to reduce the nonspecific binding of a nontarget species to the biosensor surface. This nonspecific binding poses a major challenge for label-free biosensors, where it can produce a false positive sensor response and imposes limitations on performance, especially at low analyte concentrations.<sup>4,5</sup> In contrast to routinely used label-based bioanalytical methods, such as enzyme-linked immunosorbent assays (ELISA) or fluorescence biosensors, label-free biosensors allow direct real-time observation of interactions among biomolecules and do not require the use of multistep assays or additional reagents (e.g., secondary

antibodies specific to the analyte).<sup>6–8</sup> The development of such bioanalytical techniques tailored for the detection of biomolecules in complex real-world samples nevertheless relies on surface coatings that combine (i) a high surface density of functional groups to attach biorecognition elements (BREs) with (ii) the ability to resist fouling from complex real-world media, even after BRE immobilization (e.g., antibodies or DNA probes). The design of a robust surface coating that maintains its low-fouling properties upon exposure to a variety of complex media remains one of the major challenges for the development of analytical biosensor technologies.<sup>8–11</sup>

Received: July 10, 2016

Accepted: September 30, 2016

Published: September 30, 2016

Various low-fouling functional coatings have been proposed to meet these requirements, including those based on poly(ethylene glycol) (PEG) and its functional derivatives, as well as numerous nonionic or zwitterionic polymer brushes, polymers, or hydrogel materials.<sup>1,5,11–15</sup> Widely used carboxy-functional  $\omega$ -oligo(ethylene glycol) (OEG)-based alkanethiolate self-assembled monolayers (AT SAMs) provide relatively good resistance to fouling from diluted complex media;<sup>16,17</sup> however, their resistance in complex biological samples is rather poor.<sup>11,13,18,19</sup> A higher fouling resistance was demonstrated using thicker layers ( $\sim 25$  nm) of functionalizable polymer brushes with a high density of functional groups along the polymer chains.<sup>5,12</sup> Although the fouling properties of functionalizable polymer brushes have been investigated since the 1990s, systematic studies comparing or enabling direct comparison of various types of coatings remain rather scarce. The resistance to fouling of polymer brushes is often studied for unmodified coatings; only a few reports deal with fouling resistance after functionalization.<sup>5,18,20–22</sup> In addition, the performance of functional coatings has been studied primarily in either model protein solutions or, to a lesser extent, blood plasma and serum.<sup>1,5,11,12,23,24</sup> Compared to blood plasma, foods present a much more diverse group of media, with large differences in contents of lipids, proteins, saccharides, water, vitamins, minerals, and even synthetic additives,<sup>25</sup> further complicating the design of low-fouling biorecognition coatings. To date, only a few publications have reported ultralow-fouling functional coatings for biosensing in complex food samples.<sup>12,19</sup> Rodriguez-Emmenegger et al. reported poly(2-hydroxyethyl methacrylate) (poly(HEMA)) coatings as a surface platform for biosensors for analysis of milk samples;<sup>26</sup> however, it was proven to be difficult to regain the fouling resistance once the hydroxyl groups were activated.<sup>19</sup> We have recently demonstrated that poly(carboxybetaine acrylamide) (poly(CBAA)) brushes represent a promising ultralow-fouling functionalizable surface for the multistep SPR detection of bacterial pathogens in food samples.<sup>27</sup>

In this work, we present a functional coating based on random copolymer brushes that exhibit high fouling resistance and biorecognition capabilities even when used with a variety of food matrices. These functional copolymer brushes combine the high fouling resistance of poly[*N*-(2-hydroxypropyl) methacrylamide] (poly(HPMAA)) with the high functional capacities of carboxy-functional low-fouling poly(carboxybetaine methacrylamide) (poly(CBMAA)). This type of copolymer brush architecture has been recently applied to the detection of antibodies to the hepatitis B virus in moderately complex (10%) serum samples.<sup>24</sup> This work is the first report investigating the potential of this material as a surface biorecognition platform for analysis of real-world complex food samples. Furthermore, in this work, we study the effect of the CBMAA content in random CBMAA/HPMAA copolymer brushes on both the fouling resistance and BRE immobilization capacity by means of PM-IRRAS, SPR, and contact angle methods. The fouling and biorecognition characteristics of copolymer brushes with immobilized BREs are compared to those provided by the carboxy-functional homopolymer poly(CBAA).

## 2. EXPERIMENTAL SECTION

**Reagents.** *N*-hydroxysuccinimide (NHS) and *N*-ethyl-*N'*-(3-diethylaminopropyl)carbodiimide (EDC) were purchased from PharmaTech, Czech Republic. Ethanol (purity  $\geq 99.9\%$ )

was purchased from Merck, Czech Republic. The buffer solutions were prepared using Millipore Q water (18.0 M $\Omega$ -cm, Milli-Q). Phosphate buffered saline (PBS, 0.01 M phosphate, 0.138 M sodium chloride, 0.0027 M potassium chloride, pH 7.4 at 25 °C) was prepared from a stock solution purchased from Sigma-Aldrich, Czech Republic. Tween 20 (Tween), ethanolamine (EA), imidazole, NaCl, streptavidin from *Streptomyces avidinii*, and casein blocking buffer (casein) were purchased from Sigma-Aldrich, Czech Republic. The 10 mM sodium borate, pH 8.5 at 25 °C (SB), and 10 mM sodium acetate buffer, pH 5.0 at 25 °C (SA-10), were prepared from stock solutions purchased from Sigma-Aldrich, Czech Republic. The carboxy-terminated alkanethiols (HS-C<sub>11</sub>-EG<sub>6</sub>-COOH) and HS-C<sub>11</sub>-EG<sub>4</sub>-OH were purchased from Prochimia, Poland. The carboxybetaine acrylamide monomer (CBAA) was purchased from Zwitter Technology, Seattle, Washington. CuBr, CuBr<sub>2</sub>, 2,2'-dipyridyl (BiPy), 1,4,8,11-tetramethyl-1,4,8,11-tetraazacyclotetradecane (Me<sub>4</sub>Cyclam, 98%), CuCl ( $\geq 99.995\%$ ), and CuCl<sub>2</sub> (99.999%) were purchased from Sigma-Aldrich, Czech Republic. Tetrahydrofuran (THF, purity  $\geq 99.9\%$ ) was purchased from Penta, Czech Republic. The amino-modified DNA oligonucleotide probe (ON-probe) was a sequence of NH<sub>2</sub>-(CH<sub>2</sub>)<sub>12</sub>-5'-CGC CAA TAT TTA C-3' that was purchased as HPLC-purified from Integrated DNA Technologies, USA.

For the synthesis of copolymer brushes, we used the following reagents. Initiator  $\omega$ -mercaptoundecylbromoisobutyrate was synthesized by the reaction of  $\alpha$ -bromoisobutyryl bromide (Sigma-Aldrich, 98%) with 11-mercapto-1-undecanol (Sigma-Aldrich, 99%) according to previous literature.<sup>28</sup> *N*-[3-(Dimethylamino)propyl] methacrylamide (DMAPMA, 98%, distilled at reduced pressure prior to use) and  $\beta$ -propiolactone (90%) were purchased from TCI Europe and Serva Electrophoresis GmbH, respectively. Methacryloyl chloride (Sigma-Aldrich, 97%) was distilled prior to use. Water was purified with a Millipore device (Milli-Q). Methylene chloride, diethyl ether, and ethanol (spectroscopy grade) were purchased from LachNer, Czech Republic. The monomers 3-methacryloylamino-propyl-2-carboxyethyl-dimethylammonium betaine (carboxybetaine methacrylamide, CBMAA) and *N*-(2-hydroxypropyl)-methacrylamide (HPMAA) were synthesized using a previously published procedure,<sup>20,29,30</sup> see also [Supporting Information](#). We confirmed by PM-IRRAS measurements that the surface molar contents of CBMAA and HPMAA monomer units in poly(CBMAA-*ran*-HPMAA) were in a good agreement with the monomer contents in polymerization solution (Figure S1 in [Supporting Information](#)). These results suggest similar polymerization rates of CBMAA and HPMAA in the surface-initiated polymerization reaction and, furthermore, indicate a random distribution of CBMAA and HPMAA monomer units in the copolymer brush structure.

Heat-killed *Escherichia coli* O157:H7 (*E. coli* O157:H7), *Escherichia coli* O145:H2 (*E. coli* O145:H2), *Salmonella* serotype *typhimurium* (*Salmonella*), primary antibodies (Ab<sub>1</sub>, anti-*E. coli* O145:H2, anti-*E. coli* O157:H7, anti-*Salmonella*), and biotinylated secondary antibodies (Ab<sub>2</sub>) against *E. coli* O145:H2, *E. coli* O157:H7, and *Salmonella* (b-anti-*E. coli* O145:H2, b-anti-*E. coli* O157:H7, b-anti-*Salmonella*) were purchased from KPL, Inc., USA. The procedure for the preparation of food samples is described in the [Supporting Information](#).

**Preparation of Gold Spherical Nanoparticles.** Gold spherical nanoparticles (AuNPs) with a diameter of 35 nm were

prepared by the reduction of  $\text{HAuCl}_4$  with sodium citrate as described in the literature.<sup>31</sup> Briefly, bare AuNPs were modified with carboxy-terminated OEG-containing AT SAMs, to which streptavidin was covalently bound via amine coupling chemistry. A 200 mL solution of bare AuNPs (absorbance of 0.28) was mixed with a 4 mL solution of 1 mM alkanethiols (in ethanol). This mixture was sonicated in a water bath (50 °C) for 1 h and shaken at a room temperature for 2 h. The unreacted carboxy-thiols were then removed from the solution using four washing cycles: the solution with thiolated AuNPs was centrifuged (9500g, 10 min). The supernatant was discarded, and the pellet was dissolved in Milli-Q water. To activate the carboxyls, 250  $\mu\text{L}$  of thiolated AuNPs with an absorbance of 1.68 were mixed with 120  $\mu\text{L}$  of NHS/EDC solution (1 mM NHS and 5 mM EDC in Milli-Q water) for 2 min. This mixture was then centrifuged at 9500g for 3 min, and the supernatant was removed. The pellet was dissolved in 500  $\mu\text{L}$  of streptavidin solution (12  $\mu\text{g}$  streptavidin in 12  $\mu\text{L}$  SA-10 + 88  $\mu\text{L}$  PBS + 400  $\mu\text{L}$  Milli-Q water), and the solution was shaken for 1 h. Then, 50  $\mu\text{L}$  of 1 M ethanolamine was slowly added during a 5 min period in order to deactivate all of the nonreacted esters. The free streptavidin was removed from the solution in six washing cycles (9500g, 10 min). The cross-linked streptavidin-coated AuNPs (SA-AuNPs) were removed from the solution in 2 “soft” centrifugation cycles: a solution with SA-AuNPs was centrifuged (210g, 5 min). The supernatant was kept, and the pellet was discarded. This solution of SA-AuNPs was stored in a refrigerator until use. Before SPR measurement, the SA-AuNPs solution was centrifuged at 9500g for 10 min, and the pellet was dissolved in a PBS/Tween/Casein solution. To determine the concentration of the SA-AuNPs, the absorption at a wavelength of 528/531 nm was measured using a NanoPhotometer Pearl UV–Vis absorption spectrophotometer (Implen, Germany).

**SPR Measurements.** In this work, we used a four-channel spectroscopic SPR sensor developed at the Institute of Photonics and Electronics (Prague, Czech Republic)<sup>19</sup> combined with a dispersionless microfluidic system.<sup>32</sup> The sensor was equipped with a temperature controller with a baseline stability of 0.01 °C. For this SPR sensor, a 1 nm shift in the SPR resonance wavelength corresponds to a protein coverage of 17  $\text{ng}/\text{cm}^2$  on the bare sensor surface.<sup>17</sup> Because the SPR method exploits the electromagnetic field of a surface plasmon, which exponentially decreases with distance from the surface, the sensitivity of the SPR method to changes occurring at the polymer/fluid interface decreases with increasing polymer thickness. To account for this effect, the SPR sensor response was calibrated as described previously.<sup>5,19</sup> A sensor response calibration factor was determined to be 1.2 for a 20-nm-thick poly(CBMAA 15 mol %-*ran*-HPMAA) (RI of 1.400 RIU at 750 nm for wet surface). The refractive index of polymer layers was obtained by ellipsometry.

SPR chips coated with polymer brushes were removed from water solution, washed with Milli-Q water, dried with a stream of nitrogen, and mounted into the SPR sensor. The surface functionalization procedure was carried out under flow conditions and consisted of three steps: NHS/EDC activation of polymer brushes by converting carboxy groups in CBMAA or CBAA monomer units to NHS esters, covalent attachment of BRE, and deactivation of residual reactive groups.<sup>19</sup> Specifically, surface carboxylates were converted to active esters by injection of a freshly prepared solution of NHS (0.1 M) and EDC (0.5 M) in Milli-Q water (15 min, 5  $\mu\text{L}/\text{min}$ ). Then, the

selected BRE, i.e., antibodies (Ab, 25  $\mu\text{g}/\text{mL}$ ), streptavidin (50  $\mu\text{g}/\text{mL}$ ), or amino-modified oligonucleotide probes (2  $\mu\text{M}$ ), dissolved in sodium borate (SB, 10 mM, pH 8.5) were immobilized on the activated surface (20 min, 20  $\mu\text{L}/\text{min}$ ). The surface was regenerated by consecutive injections of SB (10 mM, pH 8.5, 50 min) containing NaCl (150 mM) and imidazole (10 mM). Finally, Milli-Q water was injected, and the amount of immobilized BRE was determined from the difference between the initial and final sensor response. The carboxy-functional AT SAMs were functionalized with anti-*E. coli* O157:H7 using a previously published procedure.<sup>19</sup>

The fouling from food samples (milk, spinach, cucumber, hamburger, and lettuce) was measured for 10 min (20  $\mu\text{L}/\text{min}$ ); fouling characteristics were determined from the difference between the sensor response to PBS buffer (after food sample injection) after washing the surface for 10 min and the initial sensor response to PBS.

Sensor responses to the binding of bacteria spiked in food samples were measured for *E. coli* O157:H7, *E. coli* O145:H2, and *Salmonella* in food samples at concentrations ranging from  $1.5 \times 10^2$  to  $1.5 \times 10^7$  CFU/mL,  $1.5 \times 10^2$  to  $1.5 \times 10^7$  CFU/mL, and  $2.5 \times 10^2$  to  $2.5 \times 10^7$  CFU/mL, respectively. The measurements were executed in the following steps: (I) food samples flowed along sensor surfaces functionalized with respective Ab<sub>1</sub> (50  $\mu\text{g}/\text{mL}$ , 45  $\mu\text{L}/\text{min}$ , 15 min), (II) injection of Ab<sub>2</sub> (5  $\mu\text{g}/\text{mL}$ , 20  $\mu\text{L}/\text{min}$ , 15 min), and (III) injection of SA-AuNPs (20  $\mu\text{L}/\text{min}$ , 25 min, OD = 1) in PBS buffer with casein (0.01% w/v) and Tween (0.01% w/v).<sup>33</sup> Each sensor response reported in this study was obtained from at least three individual brush coatings. A single channel per each coating was used as a reference channel. The reference surface was treated the same way as measuring channels except for the injection of the food sample (step I), which was only spiked with buffer and did not contain any bacteria (blank sample). To obtain a reference-compensated sensor response, the sensor response in the reference channel was subtracted from the sensor response in the detection channel.

The sensor response to binding of two pathogens in hamburger and cucumber samples was performed for the following combinations of bacteria and concentrations: *E. coli* O157:H7 ( $6 \times 10^2$  CFU/mL) and *E. coli* O145:H2 ( $9 \times 10^4$  CFU/mL) (HAMBURGER-1), *E. coli* O157:H7 ( $6 \times 10^2$  CFU/mL) and *E. coli* O145:H2 ( $9 \times 10^4$  CFU/mL) (CUCUMBER-1), *E. coli* O157:H7 ( $3 \times 10^2$  CFU/mL) and *Salmonella* ( $3 \times 10^4$  CFU/mL) (HAMBURGER-2), and *E. coli* O157:H7 ( $3 \times 10^2$  CFU/mL) and *Salmonella* ( $9 \times 10^3$  CFU/mL) (CUCUMBER-2). Prior to the experiments, control SPR experiments were carried out, and it was confirmed that there is no significant cross-reactivity between nontarget bacteria and antibodies. The assay parameters (e.g., reagent concentration, reaction time) were used as previously optimized and kept constant for all measured polymer brushes;<sup>27</sup> the antibody levels (anti-*E. coli*) for both coatings were also kept constant ( $\sim 200$   $\text{ng}/\text{cm}^2$ ). The analysis of data provided by the SPR sensor was performed using a previously published procedure.<sup>27</sup> The limit of detection (LOD) was calculated using a “blank + 3  $\times$  SD” approach. Recovery values were obtained from a comparison of the measurements on bacteria mixtures with those corresponding to binding of individual pathogens at the same concentrations (see also Supporting Information).

**Ellipsometry and Dynamic Contact Angle Measurements.** The optical characterization of the homopolymer and copolymer layers was performed using a spectral ellipsometer

(SE 850 from Sentech, Germany). In order to facilitate the interpretation of the ellipsometric data and to minimize the influence of the substrate, the thin copolymer layer was prepared on a polished silicon wafer coated with an optically thick (100 nm) gold layer. The refractive index and thickness of the copolymer layer, both dried and in contact with water (wet), was measured on three different substrates per each batch of polymerization and from at least three spots per a substrate. The dried thicknesses of polymer layers were in the range of 19–31 nm. The low-fouling polymer brushes having such thicknesses were previously demonstrated to provide a sufficient resistance to fouling from various biological fluids.<sup>5,8,11</sup>

The dynamic contact angle measurements were performed with a contact angle goniometer OCA 20 (DataPhysics Instruments, Germany) equipped with SCA 21 software (see Supporting Information).

## RESULTS AND DISCUSSION

**Surface Resistance and BRE Immobilization Capacity of Poly(CBMAA-*ran*-HPMAA) Coatings.** We measured the influence of the CBMAA content in poly(CBMAA-*ran*-HPMAA) copolymer brushes on the fouling resistance for nonfunctionalized as well as antibody-functionalized coatings. The coatings were exposed to a multitude of food samples, each selected to contain differing sets of molecular components (e.g., lipids, proteins, saccharides, water, vitamins, and minerals) at different ionic strengths and pH's.<sup>25</sup> The functionalized coatings were prepared by covalent attachment of a model BRE, anti-*Salmonella*; the amount of immobilized antibodies was adjusted to ~200 ng/cm<sup>2</sup> on all the coatings except for poly(HPMAA) and poly(CBMAA 7.5 mol %-*ran*-HPMAA), where respective maximum amounts of 0 ng/cm<sup>2</sup> and 20 ng/cm<sup>2</sup> were obtained under the used experimental conditions.

As follows from Figure 1A, the fouling of poly(HPMAA) and poly(CBMAA 7.5 mol %-*ran*-HPMAA) in all tested food samples was below the SPR sensor sensitivity. The fouling increased with increasing molar content of CBMAA; however, it remained well below 5 ng/cm<sup>2</sup> and therefore could be classified as ultralow fouling.<sup>5,18</sup> This trend was accompanied by a change in surface wettability. The brush wettability, characterized by the dynamic contact angle, increased with increasing CBMAA molar content (Table S-1 in Supporting Information). For example, advancing and receding air/water contact angles of  $\Theta_a = 49.3^\circ \pm 1.4^\circ$  and  $\Theta_r = 19.5^\circ \pm 0.7^\circ$  reflected a medium wettability of poly(HPMAA), whereas a high wettability of poly(CBMAA) was reflected by  $\Theta_a = 11.9^\circ \pm 3.7^\circ$  and unmeasurably low  $\Theta_r$ . The observed higher resistance to fouling for copolymer brushes with a lower wettability is in agreement with recent works showing that poly(HPMAA) coatings may exhibit lower wettability than poly(CBAA), while providing a comparable or even higher resistance to fouling from biological fluids.<sup>27,34</sup>

Fouling levels increased considerably after the brushes were functionalized (i.e., the NHS/EDC activation of carboxy groups in CBMAA, antibody attachment, and surface regeneration; see Figure 1B). Ultralow-fouling capabilities were maintained for the poly(CBMAA-*ran*-HPMAA) brushes with CBMAA molar contents of 7.5 mol % and 15 mol %. The application of NHS/EDC chemistry neither affected the ultralow-fouling of homopolymer poly(HPMAA) brushes (Figure 1B) nor allowed for the covalent attachment of antibody (Figure 2). We hypothesize that the decrease in fouling resistance of the

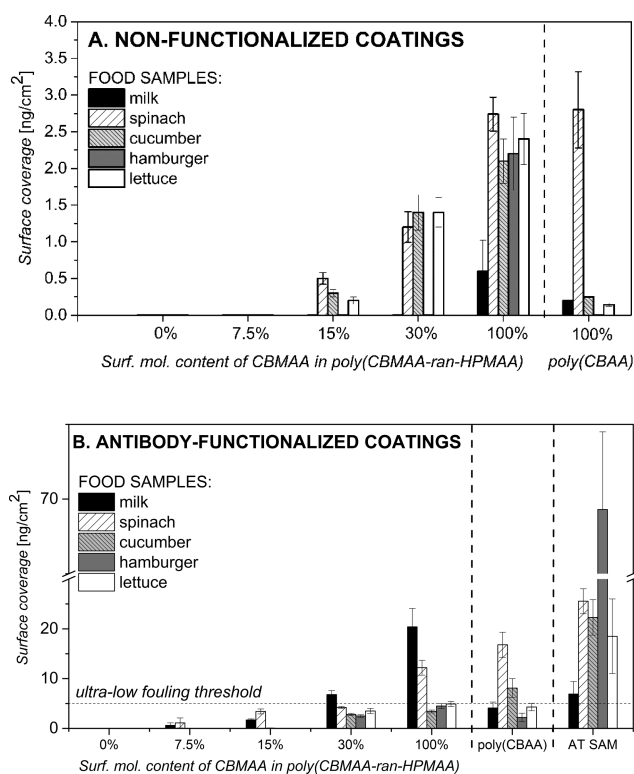


**Figure 1.** Fouling from milk (pH 6.5), spinach (pH 5.8), cucumber (pH 6.9), hamburger (pH 6.8), and lettuce (pH 7.3) on poly(CBMAA-*ran*-HPMAA) brushes containing different surface molar contents of CBMAA. Also included are data from poly(CBAA) brushes and mixed COOH-/OH-OEG-based AT SAMs. (A) Before and (B) after the covalent attachment of anti-*Salmonella*. The molar content of 0% and 100% of CBMAA in poly(CBMAA-*ran*-HPMAA) corresponds to poly(HPMAA) and poly(CBMAA) homopolymers, respectively. The horizontal dashed line corresponding to the surface coverage of 5 ng/cm<sup>2</sup> indicates the ultralow-fouling threshold.<sup>5,18</sup>

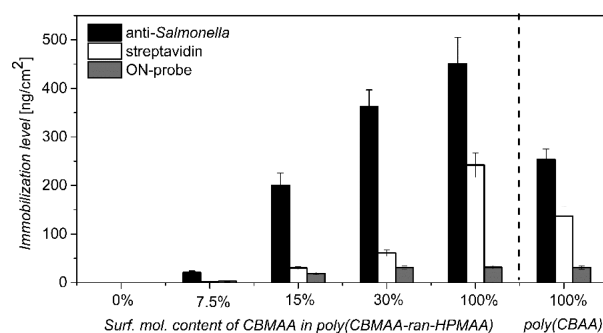


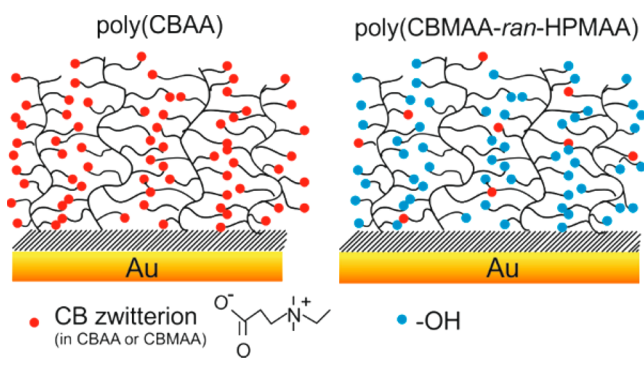
**Figure 2.** Maximum immobilization levels of anti-*Salmonella*, streptavidin, and oligonucleotide probe (ON-probe) covalently bound to poly(CBMAA-*ran*-HPMAA) achievable under the used experimental conditions as a function of the surface molar content of CBMAA in poly(CBMAA-*ran*-HPMAA). Immobilization levels for poly(CBAA) brushes are shown for comparison.

CBMAA-containing brushes after functionalization was due to an incomplete regeneration of carboxy groups which, albeit activated, were not completely employed for the attachment of BRE.

Recent studies have suggested that, to date, homopolymer ultralow-fouling poly(CBAA) brushes exhibit a superior combination of antifouling and biorecognition surface capabilities in undiluted biological fluids over other reported

functional low-/anti-fouling coatings, including OEG-based AT SAMs.<sup>5,11,13,19,27</sup> For purposes of assessment, we compared the performance of these poly(CBAA) brushes (thickness ~25 nm) with the poly(CBMAA-*ran*-HPMAA) brushes developed herein (see Chart 1). It was found out that a copolymer brush with

**Chart 1. Schematic Layout of Homopolymer Poly(CBAA) and Copolymer Poly(CBMAA-*ran*-HPMAA) Brushes Prepared on Gold Surfaces by SI-ATRP**



CBMAA molar content as low as 15% exhibits substantially better fouling resistance compared to poly(CBAA). This effect is even more pronounced for antibody-functionalized coatings, where the poly(CBMAA 15 mol %-*ran*-HPMAA) exhibited fouling resistance better by up to 2 orders of magnitude than poly(CBAA), and even more when compared with AT SAM (Figure 1B). For instance, the fouling level from cucumber samples was 0.05 ng/cm<sup>2</sup> for antibody-functionalized poly(CBMAA 15 mol %-*ran*-HPMAA) compared to 8.1 ng/cm<sup>2</sup> and 18.6 ng/cm<sup>2</sup> for antibody-functionalized poly(CBAA) and OEG-based AT SAMs, respectively. The results indicate a substantial contribution of the inert HPMAA to the net low-fouling properties. Current theories based solely on chemical structure and wettability parameters cannot fully explain the unique ultralow-fouling properties of nonionic poly(HPMAA) and zwitterionic poly(carboxybetaines). It is likely that combined mechanisms of surface hydration via distinct arrangements of water molecules to zwitterionic groups of poly(carboxybetaines) and nonionic poly(HPMAA) moieties contribute to a copolymer surface resistance to fouling from complex media.<sup>11,35–37</sup>

Figure 2 shows the dependence of the BRE maximum immobilization levels achievable under the used experimental conditions on the surface molar CBMAA content in poly(CBMAA-*ran*-HPMAA) for three types of BREs, varying in size and pI. These included the antibody to *Salmonella* (MW of ~150 kDa, pI of ~6.7), streptavidin (MW of ~60 kDa, pI of ~6.4), and amino-modified DNA oligonucleotide probe (MW of 3.4 kDa, pI < 5). For all three BREs, increases in the brush CBMAA content—leading to an increase in the amount of functional groups—led to increased immobilization levels (Figure 2, Figure S6). For the poly(CBMAA-*ran*-HPMAA) with a CBMAA molar content of 15% and higher, the surface concentration of the immobilized antibody was comparable with the values reported for an antibody monolayer, *i.e.*, 200–400 ng/cm<sup>2</sup>.<sup>38</sup>

These results (Figures 1 and 2) indicate that the ratio of BRE immobilization capacity to the fouling resistance can be modified by changing the CBMAA content in the poly(CBMAA-*ran*-HPMAA) brush.

### Biorecognition Capabilities of Antibody-Functionalized Copolymer Brush.

We investigated the biorecognition capabilities of antibody-functionalized poly(CBMAA 15 mol %-*ran*-HPMAA) via the detection of a selected bacterium (*E. coli* O157:H7) in a food sample matrix (cucumber). This study was performed under two analyte concentration regimes given by two different assay formats, the first focusing on the direct detection of high *E. coli* concentrations (from ~10<sup>4</sup> to ~10<sup>7</sup> CFU/mL) and the second focusing on the detection of low *E. coli* concentrations (down to tens of CFU/mL) using a sandwich assay with biotinylated secondary antibodies and functionalized streptavidin-coated gold spherical nanoparticles (SA-AuNPs) for signal enhancement.

The sensor responses obtained for the direct (Figure 3A) as well as SA-AuNP-enhanced detection of *E. coli* (Figure 3B)

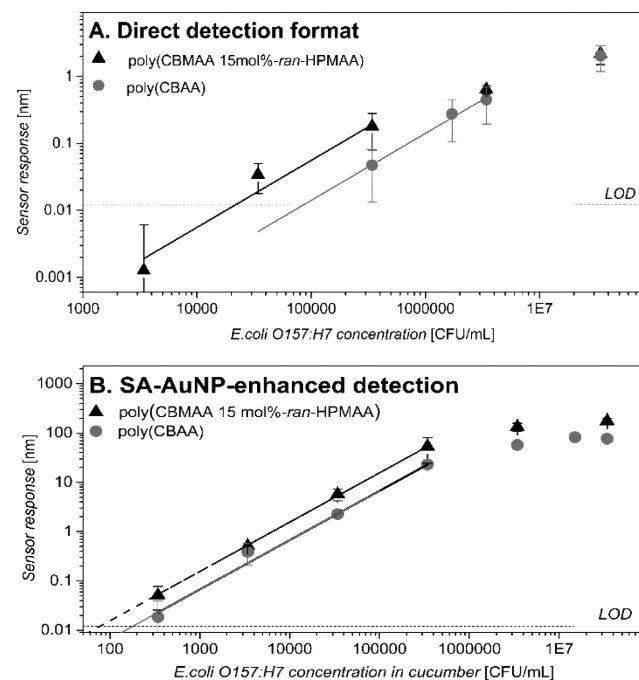


**Figure 3.** SPR reference-compensated response to direct (A) and SA-AuNP-enhanced (B) detection of *E. coli* O157:H7, for functionalized (anti-*E. coli*) poly(CBMAA 15 mol %-*ran*-HPMAA) and poly(CBAA).

demonstrate that anti-*E. coli* maintained its activity after the attachment to poly(CBMAA 15 mol %-*ran*-HPMAA). These results indicate that the presence of inert nonionic HPMAA having a moderate wettability in the copolymer brush improved the net surface fouling resistance and did not significantly interfere with the surface biorecognition capabilities. Furthermore, using the methodology described in ref 27, we determined that the biorecognition capability of anti-*E. coli*-functionalized poly(CBMAA 15 mol %-*ran*-HPMAA) exceeds that of poly(CBAA). The LODs for the direct detection of *E. coli* O157:H7 were  $2.1 \times 10^4$  CFU/mL and  $12.8 \times 10^4$  CFU/mL for poly(CBMAA 15 mol %-*ran*-HPMAA) and poly(CBAA) coatings, respectively; LODs determined for the SA-AuNP-enhanced detection were 81 CFU/mL and 216 CFU/mL for poly(CBMAA 15 mol %-*ran*-HPMAA) and poly(CBAA) coatings, respectively. The differences in surface biorecognition capabilities, particularly in the case of direct detection assay, were most likely due to the higher nonspecific fouling from the cucumber sample observed on anti-*E. coli*

functionalized poly(CBAA) ( $\sim 8.1$  ng/cm<sup>2</sup>) compared to poly(CBMAA 15 mol %-*ran*-HPMAA) ( $\sim 0.1$  ng/cm<sup>2</sup>). We believe that this fouling may have interfered with the capture of *E. coli*, in particular at lower concentrations measured via a direct detection format. This result suggests that although both coatings exhibited low fouling levels after antibody attachment, further suppression of fouling may lead to a considerable improvement in biorecognition characteristics of the coating.

We also characterized the effect of a food matrix on biorecognition capabilities of functionalized poly(CBMAA 15 mol %-*ran*-HPMAA); we used such a surface for the detection of *E. coli* O157:H7 (varying concentration) in four different food matrices. Table 1 shows the sensor responses for both the

**Table 1. Reference-Compensated SPR Sensor Response to Direct (A) and SA-AuNP-enhanced (B) Detection of *E. coli* O157:H7 in Homogenized Cucumber (pH 6.9), Hamburger (pH 6.8), Sprouts (pH 5.9), and Lettuce (pH 7.3) Samples, to Anti-*E. coli*-functionalized Poly(CBMAA 15 mol %-*ran*-HPMAA)**

(A) Sensor Response to <i>E. coli</i> [nm]				
<i>E. coli</i> concentr. [CFU/mL]	cucumber	hamburger	sprouts	lettuce
$3.4 \times 10^4$	$0.03 \pm 0.01$	$0.03 \pm 0.01$	$0.05 \pm 0.05$	$0.02 \pm 0.01$
$3.4 \times 10^5$	$0.18 \pm 0.07$	$0.20 \pm 0.04$	$0.26 \pm 0.05$	$0.17 \pm 0.06$
$3.4 \times 10^6$	$0.64 \pm 0.09$	$0.70 \pm 0.08$	$0.96 \pm 0.23$	$0.64 \pm 0.12$
$3.4 \times 10^7$	$2.2 \pm 0.7$	$1.7 \pm 0.3$	$2.2 \pm 0.5$	$2.0 \pm 0.2$
(B) Sensor Response to SA-AuNPs [nm]				
<i>E. coli</i> concentr. [CFU/mL]	cucumber	hamburger	sprouts	lettuce
$3.4 \times 10^2$	$0.05 \pm 0.03$	$0.08 \pm 0.06$	$0.07 \pm 0.05$	$0.06 \pm 0.02$
$3.4 \times 10^3$	$0.51 \pm 0.11$	$0.86 \pm 0.31$	$0.57 \pm 0.27$	$0.41 \pm 0.21$
$3.4 \times 10^4$	$5.7 \pm 1.5$	$8.2 \pm 2.9$	$4.3 \pm 0.8$	$4.2 \pm 1.4$
$3.4 \times 10^5$	$53.1 \pm 28.6$	$75.0 \pm 23.7$	$46.5 \pm 18.8$	$43.2 \pm 9.2$
$3.4 \times 10^6$	$132 \pm 25$	$140 \pm 15$	$102 \pm 28$	$81 \pm 29$

direct and SA-AuNP-enhanced detection of *E. coli*. The sensor response to the presence of *E. coli* was relatively similar for all four food matrices—across a broad range of concentrations—for both direct as well as SA-AuNP-enhanced detection. These results suggest that the food matrices did not significantly interfere with the binding of bacteria, secondary antibodies, or SA-AuNPs. Furthermore, the results of the measurements in food matrices were in good agreement with both direct and SA-AuNP-enhanced detection of *E. coli* in a buffer (see Supporting Information).

To further demonstrate the biorecognition characteristics of these copolymer brushes, we performed similar detection experiments using two additional antibodies (anti-*Salmonella* and anti-*E. coli* O145:H2), which were immobilized to poly(CBMAA 15 mol %-*ran*-HPMAA) coatings and used toward the detection of their respective counterparts. We found that immobilization levels were comparable:  $\sim 221$  ng/cm<sup>2</sup>,  $\sim 201$  ng/cm<sup>2</sup>, and  $211$  ng/cm<sup>2</sup> for anti-*E. coli* O157:H7, anti-*Salmonella*, and anti-*E. coli* O145:H2, respectively. These functionalized brushes exhibited very high biorecognition capabilities with respect to the binding of *E. coli* O157:H7, *E. coli* O145:H2, and *Salmonella typhimurium*; experiments covered a broad range of bacteria concentrations and food samples. Moreover, we found that copolymer brushes functionalized with anti-*E. coli* O157:H7 and anti-*E. coli* O145:H2 were

capable of the specific recognition of respective *E. coli* serotypes in both hamburger and cucumber samples. These results are shown in the Supporting Information.

## CONCLUSIONS

We report on a ultralow-fouling functionalizable poly(CBMAA-*ran*-HPMAA) copolymer-brush platform, which combines the ability to recognize bimolecular targets with high specificity and high resistance to fouling from real-world complex media, used herein with a variety of food samples. The random character of CBMAA and HPMAA copolymerization allows for an adjustment in the ratio of CBMAA/HPMAA monomer units and can thus be used to tailor the fouling and biorecognition properties of the poly(CBMAA-*ran*-HPMAA) brush. We demonstrate that an antibody-functionalized poly(CBMAA 15 mol %-*ran*-HPMAA) brush exhibits superior biorecognition and fouling properties in food samples compared with the state-of-the-art carboxy-functionalized ultralow-fouling poly(carboxybetaine acrylamide), poly(CBAA). Results of biorecognition and fouling studies in a diverse group of foods (cucumber, hamburger, sprouts, and lettuce) indicate the large potential of the reported coating for biosensors for food safety and security.

## ASSOCIATED CONTENT

### Supporting Information

The Supporting Information is available free of charge on the ACS Publications website at DOI: 10.1021/acs.analchem.6b02617.

SPR and contact angle measurement details as well as procedures of preparation of food samples and polymer brushes (PDF)

## AUTHOR INFORMATION

### Corresponding Authors

\*Tel.: +420 266773547. E-mail: [lisalova@ufe.cz](mailto:lisalova@ufe.cz).

\*Tel.: +420 266773404. E-mail: [homola@ufe.cz](mailto:homola@ufe.cz).

### Author Contributions

The manuscript was written through contributions of all authors. All authors have given approval to the final version of the manuscript.

### Notes

The authors declare no competing financial interest.

## ACKNOWLEDGMENTS

Authors would like to thank Kateřina Mrkvová, Xue Chadtova Song, and Josefína Lamačová from the Institute of Photonics and Electronics of the CAS for their help with PM-IRRAS and SPR experiments reported in this work. This research was supported by the Czech Science Foundation (contracts # GP14-35315P and 15-09368Y), by the Ministry of Education, Youth and Sports of the Czech Republic within the National Sustainability Program II (Project BIOCEV-FAR LQ1604), by the project “BIOCEV” (CZ.1.05/1.1.00/02.0109), and by Praemium Academiae of the Czech Academy of Sciences.

## REFERENCES

- Banerjee, I.; Pangule, R. C.; Kane, R. S. *Adv. Mater.* **2011**, *23*, 690–718.
- Sun, X. H.; Wu, J.; Chen, Z. Q.; Su, X.; Hinds, B. J. *Adv. Funct. Mater.* **2013**, *23*, 1500–1506.

- (3) Yandi, W.; Mieszkin, S.; Martin-Tanchereau, P.; Callow, M. E.; Callow, J. A.; Tyson, L.; Liedberg, B.; Ederth, T. *ACS Appl. Mater. Interfaces* **2014**, *6*, 11448–11458.
- (4) Hucknall, A.; Kim, D. H.; Rangarajan, S.; Hill, R. T.; Reichert, W. M.; Chilkoti, A. *Adv. Mater.* **2009**, *21*, 1968–1971.
- (5) Vaisocherova, H.; Yang, W.; Zhang, Z.; Cao, Z.; Cheng, G.; Piliarik, M.; Homola, J.; Jiang, S. *Anal. Chem.* **2008**, *80*, 7894–7901.
- (6) Fan, X.; White, I. M.; Shopova, S. I.; Zhu, H.; Suter, J. D.; Sun, Y. *Anal. Chim. Acta* **2008**, *620*, 8–26.
- (7) Phelan, M. L.; Nock, S. *Proteomics* **2003**, *3*, 2123–2134.
- (8) Homola, J. *Chem. Rev.* **2008**, *108*, 462–493.
- (9) Calvo, K. R.; Liotta, L. A.; Petricoin, E. F. *Biosci. Rep.* **2005**, *25*, 107–125.
- (10) Huang, R. P. *Front. Biosci., Landmark Ed.* **2003**, *8*, d559–576.
- (11) Vaisocherova, H.; Brynda, E.; Homola, J. *Anal. Bioanal. Chem.* **2015**, *407*, 3927–53.
- (12) Rodriguez-Emmenegger, C.; Brynda, E.; Riedel, T.; Houska, M.; Subr, V.; Alles, A. B.; Hasan, E.; Gautrot, J. E.; Huck, W. T. *Macromol. Rapid Commun.* **2011**, *32*, 952–957.
- (13) Blaszykowski, C.; Sheikh, S.; Thompson, M. *Biomater. Sci.* **2015**, *3*, 1335–1370.
- (14) Prime, K.; Whitesides, G. *Science* **1991**, *252*, 1164–1167.
- (15) Masson, J.-F.; Battaglia, T. M.; Davidson, M. J.; Kim, Y.-C.; Prakash, A. M. C.; Beaudoin, S.; Booksh, K. S. *Talanta* **2005**, *67*, 918–925.
- (16) Lahiri, J.; Isaacs, L.; Tien, J.; Whitesides, G. M. *Anal. Chem.* **1999**, *71*, 777–790.
- (17) Breault-Turcot, J.; Chaurand, P.; Masson, J. F. *Anal. Chem.* **2014**, *86*, 9612–9619.
- (18) Ladd, J.; Zhang, Z.; Chen, S.; Hower, J. C.; Jiang, S. *Biomacromolecules* **2008**, *9*, 1357–1361.
- (19) Vaisocherova, H.; Sevcu, V.; Adam, P.; Spackova, B.; Hegnerova, K.; de los Santos Pereira, A.; Rodriguez-Emmenegger, C.; Riedel, T.; Houska, M.; Brynda, E.; Homola, J. *Biosens. Bioelectron.* **2014**, *51*, 150–157.
- (20) Rodriguez-Emmenegger, C.; Houska, M.; Alles, A. B.; Brynda, E. *Macromol. Biosci.* **2012**, *12*, 1413–1422.
- (21) Bolduc, O. R.; Pelletier, J. N.; Masson, J. F. *Anal. Chem.* **2010**, *82*, 3699–3706.
- (22) Unsworth, L. D.; Sheardown, H.; Brash, J. L. *Biomaterials* **2005**, *26*, 5927–5933.
- (23) Riedel, T.; Riedelova-Reicheltova, Z.; Majek, P.; Rodriguez-Emmenegger, C.; Houska, M.; Dyr, J. E.; Brynda, E. *Langmuir* **2013**, *29*, 3388–3397.
- (24) Riedel, T.; Surman, F.; Hageneder, S.; Pop-Georgievski, O.; Noehammer, C.; Hofner, M.; Brynda, E.; Rodriguez-Emmenegger, C.; Dostalek, J. *Biosens. Bioelectron.* **2016**, *85*, 272–279.
- (25) Sikorski, Z. E. *Chemical and Functional Properties of Food Components*, 2nd ed.; Taylor & Francis, 2002.
- (26) Rodriguez-Emmenegger, C.; Avramenko, O. A.; Brynda, E.; Skvor, J.; Alles, A. B. *Biosens. Bioelectron.* **2011**, *26*, 4545–4551.
- (27) Vaisocherova-Lisalova, H.; Visova, I.; Ermini, M. L.; Springer, T.; Song, X. C.; Mrazek, J.; Lamacova, J.; Scott Lynn, N., Jr.; Sedivak, P.; Homola, J. *Biosens. Bioelectron.* **2016**, *80*, 84–90.
- (28) Jones, D. M.; Brown, A. A.; Huck, W. T. S. *Langmuir* **2002**, *18*, 1265–1269.
- (29) Rodriguez-Emmenegger, C.; Schmidt, B. V.; Sedlakova, Z.; Subr, V.; Alles, A. B.; Brynda, E.; Barner-Kowollik, C. *Macromol. Rapid Commun.* **2011**, *32*, 958–965.
- (30) Ulbrich, K.; Šubr, V.; Strohalm, J.; Plocová, D.; Jelínková, M.; Říhová, B. *J. Controlled Release* **2000**, *64*, 63–79.
- (31) Bastus, N. G.; Comenge, J.; Puentes, V. *Langmuir* **2011**, *27*, 11098–11105.
- (32) Springer, T.; Piliarik, M.; Homola, J. *Sens. Actuators, B* **2010**, *145*, 588–591.
- (33) Springer, T.; Homola, J. *Anal. Bioanal. Chem.* **2012**, *404*, 2869–75.
- (34) Pereira, A. d. I. S.; Rodriguez-Emmenegger, C.; Surman, F.; Riedel, T.; Alles, A. B.; Brynda, E. *RSC Adv.* **2014**, *4*, 2318–2321.
- (35) Kitano, H.; Tada, S.; Mori, T.; Takaha, K.; Gemmei-Ide, M.; Tanaka, M.; Fukuda, M.; Yokoyama, Y. *Langmuir* **2005**, *21*, 11932–11940.
- (36) Laughlin, R. G. *Langmuir* **1991**, *7*, 842–847.
- (37) Leng, C.; Hung, H. C.; Sun, S.; Wang, D.; Li, Y.; Jiang, S.; Chen, Z. *ACS Appl. Mater. Interfaces* **2015**, *7*, 16881–16888.
- (38) Zhou, C.; Friedt, J.-M.; Angelova, A.; Choi, K.-H.; Laureyn, W.; Frederix, F.; Francis, L. A.; Campitelli, A.; Engelborghs, Y.; Borghs, G. *Langmuir* **2004**, *20*, 5870–5878.

# Appendix IV

Lísalová, H., E. Brynda, M. Houska, I. Víšová, K. Mrkvová, X. C. Song, E. Gedeonová, F. Surman, T. Riedel, O. Pop-Georgievski, J. Homola

**Ultralow-Fouling Behavior of Biorecognition Coatings Based on Carboxy-Functional Brushes of Zwitterionic Homo- and Copolymers in Blood Plasma: Functionalization Matters**

*Analytical Chemistry* **89**(6) (2017): 3524-3531.



# Ultralow-Fouling Behavior of Biorecognition Coatings Based on Carboxy-Functional Brushes of Zwitterionic Homo- and Copolymers in Blood Plasma: Functionalization Matters

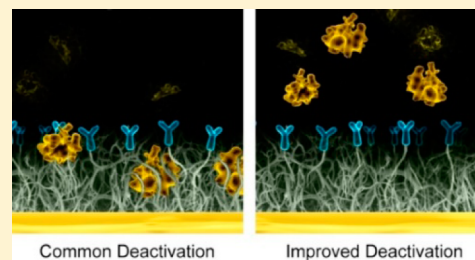
Hana Lísalová,<sup>†</sup> Eduard Brynda,<sup>‡</sup> Milan Houska,<sup>‡</sup> Ivana Víšová,<sup>†</sup> Kateřina Mrkvová,<sup>†</sup> Xue Chadtová Song,<sup>†</sup> Erika Gedeonová,<sup>†</sup> František Surman,<sup>‡</sup> Tomáš Riedel,<sup>‡</sup> Ognen Pop-Georgievski,<sup>‡</sup> and Jiří Homola<sup>\*,†</sup>

<sup>†</sup>Institute of Photonics and Electronics, Czech Academy of Sciences, Chaberská 57, Prague 182 51, Czech Republic

<sup>‡</sup>Institute of Macromolecular Chemistry, Czech Academy of Sciences, Heyrovského nám. 2, Prague 162 00, Czech Republic

## Supporting Information

**ABSTRACT:** Fouling from complex biological fluids such as blood plasma to biorecognition element (BRE)-functionalized coatings hampers the use of affinity biosensor technologies in medical diagnostics. Here, we report the effects the molecular mechanisms involved in functionalization of low-fouling carboxy-functional coatings have on the BRE capacity and resistance to fouling from blood plasma. The specific mechanisms of EDC/NHS activation of carboxy groups, BRE attachment, and deactivation of residual activated groups on recently developed ultra-low-fouling carboxybetaine polymer and copolymer brushes (pCB) as well as conventional carboxy-terminated oligo(ethylene glycol)-based alkanethiolate self-assembled monolayers (OEG-SAMs) are studied using the polarization modulation infrared reflection/absorption spectroscopy, X-ray photoelectron spectroscopy, and surface plasmon resonance methods. It is shown that the fouling resistance of BRE-functionalized pCB coatings is strongly influenced by a deactivation method affecting the ultra-low-fouling molecular structure of the brush and surface charges. It is revealed that, in contrast to free carboxy-group-terminated OEG-SAMs, only a partial deactivation of EDC/NHS-activated zwitterionic carboxy groups by spontaneous hydrolysis is possible in the pCB brushes. The fouling resistance of activated/BRE-functionalized pCB is shown to be recovered only by covalent attachment of amino acid deactivation agents to residual activated carboxy groups of pCB. The developed deactivation procedure is further combined with ultra-low-fouling brushes of random copolymer carboxybetaine methacrylamide (CBMAA) and *N*-(2-hydroxypropyl) methacrylamide (HPMAA) with optimized CBMAA content (15%) providing a BRE-functionalized coating with superior fouling resistance over various carboxy-functional low-fouling coatings including homopolymer pCB brushes and OEG-SAMs. The biorecognition capabilities of pHPMAA-CBMAA(15%) are demonstrated via the sensitive label-free detection of a microRNA cancer biomarker (miR-16) in blood plasma.



Recent advances in optical affinity biosensors have increased their potential for applications in areas such as medical diagnostics, environmental monitoring, food safety, and security.<sup>1,2</sup> Label-free plasmonic biosensors allow for the direct, real-time observation of interactions among biomolecules and, in contrast to commonly used label-based methods such as enzyme-linked immunosorbent assays (ELISA) or fluorescence biosensors, do not require the use of additional reagents (e.g., secondary antibodies). Despite these advantages, label-free biosensors cannot discriminate between the binding of target analytes to biorecognition elements (BREs) immobilized on the sensor surface and deposition of nontarget species (i.e., fouling) from the tested medium.<sup>3</sup> This fouling may be severe from complex biological media, such as blood plasma or serum, and can limit biosensor performance and increase the probability of false positive results.<sup>3,4</sup>

Various approaches have been proposed to suppress the effects of fouling from complex samples on performance of

label-free biosensors. These approaches are based on the use of reference channels or reduction of the fouling by means of surfactants. However, none of these approaches provide perfect compensation for fouling from complex biological fluids.<sup>3,5–8</sup> For instance, in a typical reference-compensated approach, a reference channel is functionalized with a similar (but nontarget) BRE, both the reference and detection channels are exposed to the same sample, and the sensor response in the reference channel is subtracted from that of the detection channel.<sup>3,5</sup> However, it is often difficult to identify BREs yielding a reference channel with fouling properties that are close to those of the sensing channel. Alternatively, both the reference and detection channels are functionalized with the same BREs, and the reference channel is exposed to a reference

**Received:** November 29, 2016

**Accepted:** February 24, 2017

**Published:** February 24, 2017

sample that does not contain a target analyte (e.g., blood plasma obtained from healthy donors or pooled plasma). However, complex biological samples, such as blood plasma samples obtained from different people, exhibit different levels of fouling,<sup>6</sup> which may introduce a bias into the reference-compensated biosensing. In addition to the referencing approaches, various surfactants (e.g., Tween) and protein-based additives (e.g., serum albumin or casein) are commonly used to reduce fouling. However, their use has been shown to negatively affect the biorecognition activity of immobilized BREs.<sup>8</sup>

Therefore, there is an intensive search for functional coatings that effectively resist plasma fouling as well as provide a sufficient amount of functional groups suitable for attachment of BREs. Although there is a variety of antifouling materials, e.g., poly(ethylene glycol) (PEG) and its derivatives, only a few have been demonstrated as functionalized coatings for biosensing in complex media.<sup>4,5,9–14</sup> Currently, carboxy-functional brushes based on zwitterionic carboxybetaine polymers (pCB) provide the best biorecognition platforms for biosensing in complex biological fluids.<sup>4,5,10–15</sup> For example, poly-(carboxybetaine acrylamide) (pCBAA) brushes have been demonstrated to provide superior fouling resistance from blood plasma or serum combined with a relatively high BRE capacity when compared to the widely used carboxy-functional low-fouling  $\omega$ -oligo(ethylene glycol)-based alkanethiolate self-assembled monolayers (OEG-SAMs).<sup>5,11,16</sup> Compared to hydroxy-functional coatings, the activation of the carboxy groups to form the active ester intermediates can be accomplished under mild conditions in a timely manner using protein-compatible water-based solvents.<sup>17,18</sup>

The pCB functionalization consists of the transformation of carboxy groups in zwitterionic carboxybetaine side chains (CB) of the polymers to active esters to which BREs are subsequently covalently coupled via their amine groups. The first step is usually based on *N*-ethyl-*N'*-(3-diethylaminopropyl) carbodiimide (EDC) and *N*-hydroxysuccinimide (NHS) coupling (Figure S1).<sup>19,20</sup> Although the EDC/NHS activation is routinely used in numerous biosensor and bioconjugate techniques,<sup>17,21</sup> the reaction scheme is quite complex and the reaction pathways are influenced by various reaction conditions, including reagent concentrations, incubation times, buffer composition, and functional coating type.<sup>22–25</sup> According to the established reaction scheme, active esters (i.e., NHS ester or *O*-acylurea) spontaneously hydrolyze back to carboxy groups in aqueous solutions.<sup>23,24,26</sup> The same mechanism, i.e., the spontaneous hydrolysis of all activated carboxy groups remaining in pCB after the EDC/NHS activation/attachment of BREs, was supposed to recover the original ultra-low-fouling structure of the pCB brushes. However, a remarkable increase in plasma fouling (beyond the ultra-low-fouling threshold set at 5 ng/cm<sup>2</sup>)<sup>11,16</sup> was observed for pCB brushes after their activation with EDC/NHS, covalent attachment of BREs, and hydrolysis-based deactivation<sup>8,19,27</sup> as well as upon only the EDC/NHS activation and hydrolysis-based deactivation without attachment of any BREs.<sup>8</sup> A similar trend but at a much higher extent was observed for hydroxy-functional brushes upon activation of their functional groups.<sup>8</sup> It is evident that the functionalization processes affect the fouling resistance of functionalized brushes. However, the nature of these effects is not completely understood.

In this work, to the best of our knowledge, it is the first time that the molecular functionalization processes with respect to

both the BRE immobilization capacity and resistance to fouling from blood plasma are investigated. Specifically, the functionalization processes and their relationship with physicochemical properties (surface charge, chemical composition) are studied on the ultra-low-fouling pCB brushes and recently synthesized ultra-low-fouling brushes composed of randomly arranged carboxybetaine methacrylamide (CBMAA) and *N*-(2-hydroxypropyl) methacrylamide (HPMAA) monomer units (pHPMAA-CBMAA)<sup>20,28</sup> using surface plasmon resonance (SPR), polarization modulation infrared reflection/absorption spectroscopy (PM-IRRAS), and X-ray photoelectron spectroscopy (XPS). Results of this study are compared to those obtained on traditional carboxy-functional OEG-SAMs. The studied functionalization processes include EDC/NHS activation, BRE (antibody, amino-modified oligonucleotide probe) attachment, and subsequent deactivation of residual activated carboxy groups. The findings are applied in functionalization of pHPMAA-CBMAA containing an optimized molar content of CBMAA(15%) to characterize its biorecognition capabilities with respect to label-free detection of microRNA (miR-16), a biomarker of various human malignant and cardiovascular diseases,<sup>29–31</sup> in blood plasma.

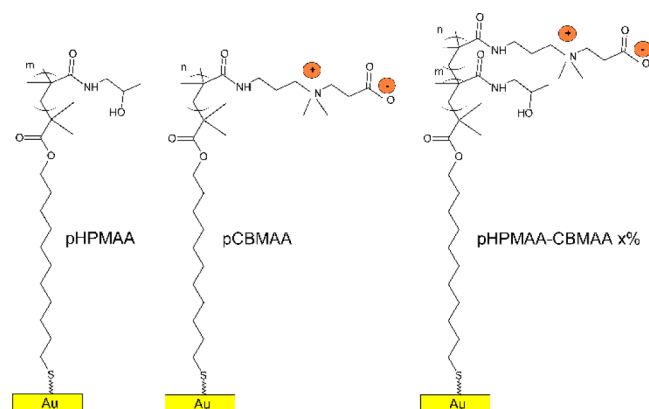
## EXPERIMENTAL SECTION

**Reagents.** *N*-Hydroxysuccinimide (NHS) and *N*-ethyl-*N'*-(3-diethylaminopropyl)carbodiimide (EDC) were purchased from PharmaTech, Czech Republic. Ethanol (purity  $\geq 99.9\%$ ) was purchased from Merck, Czech Republic. Tris-(hydroxymethyl) aminomethane, ethanalamine (EA), imidazole, dextran sulfate (DS; MW  $\approx 8$  kDa), NaCl, glycine, streptavidin, *N*-hydroxysulfosuccinimide sodium salt (sulfo-NHS), ethylenediaminetetraacetic acid (EDTA),  $\gamma$ -aminobutyric acid (99%),  $\beta$ -alanine (99%), sodium dodecyl sulfate (SDS), MgCl<sub>2</sub>, CuBr, CuBr<sub>2</sub>, 2,2'-bipyridyl (BiPy), 1,4,8,11-tetramethyl-1,4,8,11-tetraazacyclotetradecane (Me<sub>4</sub>Cyclam, 98%), CuCl ( $\geq 99.995\%$ ), CuCl<sub>2</sub> (99.999%), and stock solutions for the preparation of phosphate buffered saline (PBS, 0.01 M phosphate, 0.138 M sodium chloride, 0.0027 M potassium chloride, pH 7.4 at 25 °C), 10 mM sodium borate, pH 8 (SB) at 25 °C, and 10 mM sodium acetate buffer, pH 5.0 (SA) at 25 °C were purchased from Sigma-Aldrich, Czech Republic. The buffer solutions were prepared using Milli-Q water (18.0 M $\Omega$ .cm). The (2-aminoethoxy)acetic acid and [2-(2-aminoethoxy)ethoxy]acetic acid were purchased from Iris Biotech, Germany. The alkanethiols HS-(CH<sub>2</sub>)<sub>11</sub>-(EG)<sub>6</sub>-OCH<sub>2</sub>-COOH and HS-(CH<sub>2</sub>)<sub>11</sub>-(EG)<sub>4</sub>-OH were purchased from Prochimia, Poland. Tetrahydrofuran (THF, purity  $\geq 99.9\%$ ) was purchased from Penta, Czech Republic. The amino-modified DNA oligonucleotide probe, 22-mer, NH<sub>2</sub>-(CH<sub>2</sub>)<sub>12</sub>-5'-CGCCAATATTTACGTGCTGCTA-3' (NH<sub>2</sub>-ON-probe), the probe functionalized with attached biotin (biotin-ON-probe), and miR-16 target (5'-r(UAGCAGCAGUAAAUAUUGGCG)-3') were purchased as HPLC-purified from Integrated DNA Technologies, USA. The antibodies (Ab), i.e., anti-*E. coli* O157:H7 (anti-*E. coli*) and anti-*Salmonella* were purchased from KPL Inc., USA. The human blood plasma (pooled, mixed gender) in sodium citrate was donated by the Institute of Hematology and Blood Transfusion, Czech Republic. All of the tested individuals agreed to this study at the time of blood collection. The study was approved by the Institute of Hematology and Blood Transfusion Ethics Committee, and all samples were obtained in accordance with the Ethical Commission's regulations and with a release of

informed consent. The initiator  $\omega$ -mercaptoundecylbromoisobutyrate was synthesized as described previously.<sup>32</sup> The monomers 3-methacryloylaminopropyl-2-carboxyethyl-dimethylammonium betaine (carboxybetaine methacrylamide, CBMAA) and *N*-(2-hydroxypropyl) methacrylamide (HPMAA) were synthesized according to the literature.<sup>33,34</sup>

**Preparation of Functional Coatings.** The brushes of pHPMAA, pCBMAA, pCBAA, and copolymer pHPMAA-CBMAA (Scheme 1) having a thickness of  $\sim 25$  nm (as

**Scheme 1. Chemical Structures of Polymer Brushes Used in This Work<sup>a</sup>**



<sup>a</sup>pHPMAA: poly(*N*-(2-hydroxypropyl) methacrylamide), pCBMAA: poly(carboxybetaine methacrylamide), pHPMAA-CBMAA(*x*%): random copolymer of HPMAA and CBMAA, where *x*% is the molar percentage of CBMAA monomer units in the copolymer.

measured by optical ellipsometry) were grafted from gold-coated substrates (SPR chip or Si wafer) by surface-initiated atom transfer radical polymerization (SI ATRP) as described elsewhere;<sup>20</sup> for details, see the Supporting Information. The molar percentage of CBMAA monomer units  $x = 7.5, 15,$  and  $30$  mol % in pHPMAA-CBMAA(*x*%) brushes corresponded to the molar ratios of CBMAA/(CBMAA + HPMAA) monomers in polymerization solution, indicating that the CBMAA monomer units were randomly distributed in the copolymer chains. The self-assembled monolayers of HS-C<sub>11</sub>-EG<sub>6</sub>-OCH<sub>2</sub>-COOH (COOH-OEG-SAMs) and mixed HS-C<sub>11</sub>-(EG)<sub>6</sub>-OCH<sub>2</sub>-COOH and HS-C<sub>11</sub>-(EG)<sub>4</sub>-OH, 3:7 (mixed OEG-SAMs) were prepared on gold-coated chips according to the procedure described in ref 8, see also the Supporting Information.

**PM-IRRAS Measurements.** The pCBMAA and pHPMAA-CBMAA(15%) coatings formed on SPR chips were analyzed by PM IRRAS (NICOLET 6700 spectrometer with photoelastic

modulation (PEM) module; Thermo Scientific, USA). The laser beam was modulated by ZnSe grid polarizer and ZnSe photoelastic modulator (HINDS Instruments, PEM 90, modulation frequency = 37 kHz) and focused on the sample at an incident angle of 82°. The reflected light was collected by a nitrogen-cooled mercury-cadmium-telluride (MCT) detector. The spectra were obtained from coaddition of 100 scans with a resolution of 4 cm<sup>-1</sup>. A total of four chips for each brush type were washed with Milli-Q water and dried with a stream of nitrogen and immediately mounted to the PEM module of the spectrometer. The coatings were subsequently activated with a solution of 0.1 M NHS/0.5 M EDC + 10 mM NaCl (30 min), washed with Milli-Q water, and dried with nitrogen. The infrared spectrum of a coated SPR chip was recorded immediately after the activation, whereas the other three chips were deactivated by immersion into a solution of (1) 10 mM sodium borate + 10 mM imidazole + 10 mM NaCl, pH 8.0 (D-buffer, 30 min), (2) 1 M glycine, pH 7.0 (30 min), and (3) 1 M EA, pH 8.0 (30 min) as described below.

**XPS Measurements.** The XPS measurements were performed using a K-Alpha + XPS spectrometer (ThermoFisher Scientific, UK) operating at a base pressure of  $1.0 \times 10^{-7}$  Pa. The data acquisition and processing were performed using Thermo Avantage software. All surfaces were analyzed using microfocused, monochromated Al K $\alpha$  X-ray radiation (400  $\mu$ m spot size) with a pass energy of 200 eV for survey and 50 eV for high-energy resolution core level spectra. The X-ray angle of incidence was 30°, and the emission angle was normal to the surface. The K-Alpha charge dual compensation system was employed during analysis using electrons and low-energy argon ions to prevent any localized charge build-up. The high-resolution spectra were fitted/deconvoluted with Voigt profiles. All spectra were referenced to the C 1s peak attributed to C–C, C–H at 285.0 eV binding energy, which was controlled by means of the photoelectron peaks of poly(ethylene terephthalate) and metallic Cu, Ag, and Au.

**Spectral Ellipsometry Measurements.** Polymer brushes were grafted from gold surface of plates cut from a polished silicon wafer coated with an optically thick (100 nm) gold layer. The refractive index and thickness of the dried brush were measured on at least three spots per plate using a spectral ellipsometer (SE 850 Sentech, Germany). For each experiment, the brushes were prepared on three gold-coated silicon plates in one batch together with gold-coated plates for SPR measurements. The dry thicknesses of the brushes were in the range of 22–28 nm.

**SPR Measurements.** A four-channel SPR sensor combined with a near-dispersionless microfluidic system<sup>35</sup> developed at the Institute of Photonics and Electronics (Prague, Czech

**Table 1. Fouling from Undiluted Blood Plasma on the SPR Chip Coated with pCB Brushes<sup>a</sup>**

polymer brush	immobilized antibody [ng/cm <sup>2</sup> ]		fouling from blood plasma [ng/cm <sup>2</sup> ]	
	A	B	C	D
pCBMAA	450.8 $\pm$ 28.5	208.6 $\pm$ 13.2	11.1 $\pm$ 2.8	25.4 $\pm$ 4.1
pHPMAA-CBMAA(30%)	362.2 $\pm$ 21.3	211.3 $\pm$ 10.2	10.0 $\pm$ 3.5	23.4 $\pm$ 3.9
pHPMAA-CBMAA(15%)	201.6 $\pm$ 10.1	201.6 $\pm$ 11.6	2.9 $\pm$ 0.8	11.6 $\pm$ 2.8
pHPMAA-CBMAA(7.5%)	20.1 $\pm$ 5.8	20.1 $\pm$ 3.2	0.0 $\pm$ 0.03	2.6 $\pm$ 1.2

<sup>a</sup>The pHPMAA-CBMAA(*x*%) brushes were functionalized by the covalent attachment of anti-*Salmonella* (Ab) to EDC/NHS-activated pCB. Column A: maximum Ab immobilization capacity; B: adjusted Ab capacity for the measurement of plasma fouling (see column D); C: plasma fouling measured on unmodified polymer brush; D: plasma fouling measured on the Ab-functionalized brush (with the Ab levels shown in column B) and deactivated by hydrolysis.

Republic) was used. More details about SPR measurements are provided in the Supporting Information.

## RESULTS AND DISCUSSION

**Effect of the Surface Content of Carboxy Groups in the pCB Brush on Plasma Fouling and BRE Immobilization.** We investigated the effect of the relative surface content of carboxy groups in the pCB brush on the antibody (Ab) immobilization capacity and fouling from full blood plasma for pHPMAA-CBMAA( $x\%$ ) brushes (where  $x$  denotes mol % of CBMAA). Table 1 shows the antibody (Ab, anti-*Salmonella*) immobilization capacity, i.e., the maximum amount of bound Ab that can be immobilized on the coating under the given experimental conditions (column A) in comparison to homopolymer brushes of pCBMAA. Ab immobilization capacity of pHPMAA-CBMAA( $x\%$ ) brushes pertaining to  $x = 15$  and 30 reached  $\sim 45\%$  and  $\sim 80\%$  of the capacity of pCBMAA, respectively (see also Figure 1). These results show

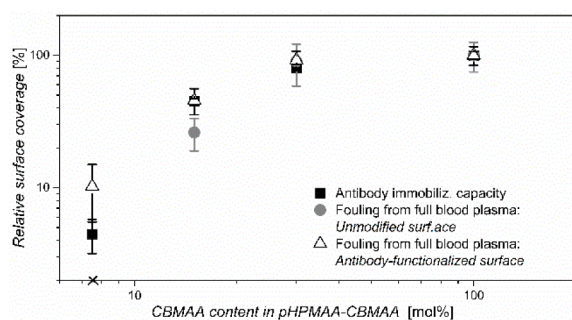


**Figure 1.** Antibody immobilization capacity and fouling from full blood plasma on unmodified and antibody (anti-*Salmonella*)-functionalized pHPMAA-CBMAA random copolymer brushes as a function of the relative surface molar content of CBMAA ( $x$ ) in pHPMAA-CBMAA( $x\%$ ). All the surface coverage values were normalized to maximum values achieved on pCBMAA (Table 1). The symbol “x” refers to the plasma fouling value achieved on unmodified pHPMAA-CBMAA(7.5%) that was below the limit of detection of the SPR sensor used.

that the ratio of the number of CB groups capable of Ab coupling to the total number of CB groups contained in the brush increased with decreasing CBMAA content in the polymer. This trend can be partially attributed to a high density of CB in the surface region of the pCBMAA brush, where CB groups overlapped with an immobilized antibody cannot bind other antibodies. However, this trend can also be associated with the reactivity of ionized carboxy groups to EDC/NHS. Specifically, the PM-IRRAS revealed that whereas only 22% of the ionized carboxy groups present in pCBAA (Figure S4) and 36% in pCBMAA (Figure 2) were converted to active esters, this ratio increased remarkably (to 90%) in pHPMAA-CBMAA(15%) (Figure S3). The results indicate that the incorporation of CBMAA in an inert HPMAA polymer chain increases susceptibility of the CB carboxy groups to EDC/NHS activation.

For the resistance of BRE-functionalized pCB brushes to be compared to fouling from full blood plasma, the amount of immobilized Ab on each brush was adjusted to 215 ng/cm<sup>2</sup>, which corresponded to the maximum achievable immobilization level on pCBAA under the given experimental conditions. Furthermore, prior to this study, we had measured the effect of Ab levels on the fouling resistance for the pHPMAA-

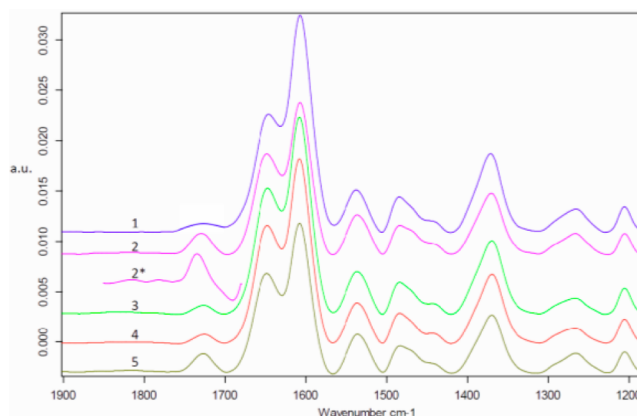


**Figure 2.** PM-IRRAS spectra of pCBMAA on the SPR chip pertaining to the activation with EDC/NHS. (1) pCBMAA before activation ([COO<sup>-</sup>] = 100%), (2) pCBMAA after activation with EDC/NHS ([COO<sup>-</sup>] = 60%), (2\*) difference in the spectra (2 - 1, expanded), (3) pCBMAA after activation and deactivation with glycine ([COO<sup>-</sup>] = 90%), (4) pCBMAA after activation and deactivation with D-buffer ([COO<sup>-</sup>] = 70%), (5) pCBMAA after activation and deactivation with EA ([COO<sup>-</sup>] = 60%).

CBMAA(15%) coatings. We observed that the fouling increases with increasing Ab surface coverage up to the Ab level of  $\sim 180$  ng/cm<sup>2</sup> and then levels off (see Figure S12). For the Ab levels in the range of 180–220 ng/cm<sup>2</sup>, no significant differences in the fouling levels were observed. The Ab level of  $\sim 215$  ng/cm<sup>2</sup> was selected for the evaluation of the fouling resistance of pHPMAA-CBMAA brushes, as variations in the Ab level around this value were expected to have a smaller effect on the results. This level was successfully achieved for all brushes except for pHPMAA-CBMAA(7.5%), for which a maximum Ab level of  $\sim 20$  ng/cm<sup>2</sup> was obtained (column B). The levels of plasma fouling on unmodified copolymers pHPMAA-CBMAA were generally lower than on pCBMAA. A very high Ab level ( $\sim 450$  ng/cm<sup>2</sup>) was achieved on pCBMAA under the given experimental conditions. It should be noted that such a high Ab surface coverage would not be preferable for all biosensing applications due to potentially unfavorable steric effects. Compared to pCBMAA, the plasma fouling on pHPMAA-CBMAA(30%) was lower by 20%, but Ab immobilization capacity was lower by only 8%. Below 30% of CBMAA, both the fouling and immobilization capacity decreased rapidly with decreasing mol % of CBMAA in the copolymer (Table 1, Figure 1). At low CBMAA contents, the decrease in fouling on unmodified copolymer brushes was faster than the decrease in the Ab immobilization capacity (Figure 1).

The attachment of Ab to EDC/NHS-activated pCB followed by spontaneous hydrolysis increased plasma fouling on all of the tested brushes. The fouling exhibited a similar trend as that observed for unmodified copolymer brushes, i.e., fouling decreased with decreasing content of CBMAA (Table 1, Figure 1). The fouling levels on Ab-functionalized pHPMAA-CBMAA(15%) were as low as 11.6 ng/cm<sup>2</sup>, whereby the Ab immobilization capacity was still high ( $\sim 200$  ng/cm<sup>2</sup>). These levels are comparable with those reported for Ab-functionalized pCBAA in refs 8 and 27. On the other hand, even lower fouling values have been achieved for Ab-functionalized pCBAA.<sup>16,27</sup> These variations may in large part be related to differences in composition of plasma samples used in different fouling resistance experiments.<sup>6</sup> Furthermore, the trend of decreasing plasma fouling with decreasing CBMAA molar content in

pHPMAA-CBMAA( $x\%$ ,  $x < 60$ ) was significantly slower for pHPMAA-CBMAA( $x\%$ ,  $x < 60$ ) brushes functionalized with Ab and deactivated by hydrolysis compared to unmodified pHPMAA-CBMAA( $x\%$ ) coatings. It is hypothesized that this phenomenon can be attributed to the presence of immobilized BREs as well as incomplete deactivation of activated carboxy groups in zwitterions of the pCB brush.

**Characterization of Activation/Deactivation Mechanisms in pCB Brushes and OEG-SAMs.** The activation and subsequent deactivation of EDC/NHS-activated carboxy groups were measured by PM-IRRAS and XPS methods for pCB homopolymer and copolymer brushes as well as OEG-SAMs (Figure 2 and Figures S3–S7). Three different deactivation procedures were analyzed: deactivation by hydrolysis in deactivation buffer with optimized composition (D-buffer), glycine, and ethanolamine (EA). Specifically for pCBMAA, the PM-IRRAS spectrum of the pCBMAA brush in the dry state before activation (Figure 2, curve 1) shows that the amide I band at  $1650\text{ cm}^{-1}$  and amide II band at  $1538\text{ cm}^{-1}$  overlapped with the prominent band of ionized carboxy groups at  $1608\text{ cm}^{-1}$  (asym). The ionized carboxy groups also largely contribute to the band at  $1368\text{ cm}^{-1}$  (sym). The band  $1725\text{ cm}^{-1}$  of nonionized carboxy groups is rather weak; however, it suggests that not all carboxy groups are engaged in an internal interaction with quaternary ammonium cation as would be expected in betaines. The spectrum after EDC/NHS activation (curve 2) shows only weak bands of NHS ester at 1818, 1790, and  $1735\text{ cm}^{-1}$  overlapping with the band of nonionized carboxy group at  $1725\text{ cm}^{-1}$ . The intensity of ionized carboxy group at  $1608\text{ cm}^{-1}$  decreased markedly after the activation (down to  $\sim 60\%$ ). This indicates that either some carboxy groups engaged in strong internal hydrogen bonding (the C=O band would shift to the region around  $1660\text{ cm}^{-1}$  and be overlapped by a much stronger amide I band) or some other intermediates might be present. Spectra 3–5 in Figure 2 show the effects of different deactivation approaches, specifically, the deactivation of activated pCBMAA by hydrolysis of NHS ester in D-buffer (spectrum 4) and by reactions with EA (spectrum 5) and glycine (spectrum 3). The hydrolysis in optimized hydrolysis-promoted deactivation buffer (D-buffer) led to the disappearance of NHS ester bands and a decrease in the intensity of nonionized carboxy group; however, the intensity of the band at  $1608\text{ cm}^{-1}$  indicates a regeneration of only  $\sim 70\%$  of the ionized carboxy groups compared to the initial pCBMAA. This observation contrasts with the assumption of spontaneous hydrolysis of NHS esters in aqueous solutions. The reaction with EA (5) does not regenerate carboxy groups (amide group is formed and hydroxy group is attached), and only 60% of ionized carboxy groups are present. Spectrum 3 after the reaction with glycine shows a rather different picture; it indicates an increase in the content of the ionized carboxy groups to 90%, apparently due to the attachment of new carboxy groups. The basic features of the spectra of pCBAA brushes (Figure S4) were rather similar to those of pCBMAA, yet the spectrum of the initial pCBAA does not show any signs of the presence of nonionized carboxy groups. The decrease in the intensity of the band at  $1608\text{ cm}^{-1}$  after activation (to 78%), and nearly no observable bands of NHS ester, suggest that pCBAA is less prone to activation by EDC/NHS than pCBMAA.

Compared to activation with EDC/NHS, a much higher level of activation of carboxy groups was achieved by the reaction of pCBMAA (Figure S5) or pHPMAA-CBMAA(15%) (Figure

S6) brushes with EDC/sulfo-NHS. The spectra of the activated brushes show a decrease in the intensity of the band at  $1608\text{ cm}^{-1}$  (to 45%), the well-developed NHS ester bands at 1815, 1785, and  $1740\text{ cm}^{-1}$  (overlapping with the band  $1725\text{ cm}^{-1}$ ) as well as an intense band at  $1235\text{ cm}^{-1}$  of the sulfo group in sulfo-NHS ester. The sulfo-NHS ester bands disappeared after the deactivation with EA.

The IR data are in a general agreement with the XPS measurements of sulfur present in sulfo-NHS esters bound to the pCBMAA brush (Table S1). The relative content of sulfur (1.95 at. %) in pCBMAA activated by EDC/sulfo-NHS decreased to 0.72 at. % after incubation with D-buffer and to 0 after the reaction with EA. This suggests a complete removal of sulfo-NHS ester. The relative content of sulfur (1.1 at. %) in pHPMAA-CBMAA(15%) activated by EDC/sulfo-NHS decreased to 0 after both incubation with D-buffer and after the reaction with EA.

In summary, the PM-IRRAS results shown in Figure 2 and Figures S3–S6 confirmed that carboxy groups in the pCB brushes were converted to active esters. However, the PM-IRRAS measurements also revealed that carboxy groups were not fully recovered upon hydrolysis of the activated pCB brushes. A relatively low yield of hydrolysis on pCB brushes was further confirmed by XPS analysis. It should be noted that this result is not consistent with the commonly accepted assumption of a fast and complete hydrolysis of active esters in aqueous solutions (see Figure S1). This trend was also assumed to convert all residual active esters in functionalized pCB back to carboxy groups.<sup>16,27</sup> On the other hand, we observed a complete hydrolysis of active esters in activated COOH-OEG-SAMs (Figure S7 and Table S1), where carboxy groups were fully recovered by incubation with D-buffer within 30 min after activation. These results suggest important differences in the reactivity of carboxy groups in CB side chains of polymer brushes and free carboxy groups, such as those on the surface of low-fouling COOH-OEG-SAMs. Compared to the free carboxy groups in COOH-OEG-SAMs, a strong internal electrostatic interaction of carboxy groups with quaternary ammonium cations in zwitterionic CBs seems to make their activation by EDC/NHS and recovery by hydrolysis more difficult.

The effect of different deactivation procedures on plasma fouling in relation to surface charge was further measured for pHPMAA-CBMAA(15%) brushes after the EDC/NHS activation (Table 2). The potential changes in the net surface charge

**Table 2. Effect of Different Deactivation Procedures on Blood Plasma Fouling and Adsorption of Dextran Sulfate (DS) Measured on Activated pHPMAA-CBMAA(15%)**

pHPMAA-CBMAA(15%) functionalization step	plasma fouling [ng/cm <sup>2</sup> ]	DS [ng/cm <sup>2</sup> ]
before activation	4.9 ± 2.0	0.0 ± 0.0
activated	135.5 ± 12.6	76.5 ± 9.4
activ./glycine-deactiv.	5.1 ± 2.6	31.1 ± 5.4
activ./EA-deactiv.	14.8 ± 4.9	69.7 ± 7.3
activ./hydrolysis-deactiv.	12.5 ± 3.1	61.2 ± 5.5

that are associated with EDC/NHS chemical processes were measured by electrostatic adsorption of a strong polyanion, dextran sulfate (DS), to activated/deactivated pHPMAA-CBMAA(15%). Table 2 shows that DS does not adsorb on pHPMAA-CBMAA(15%) before activation, indicating a net surface neutrality even though the PM-IRRAS spectra of

pCBMAA brushes measured in the dry state indicated a small portion of nonionized carboxy groups (see Figure 2 and Supporting Information). After the activation with EDC/NHS, carboxy groups are converted to a neutral NHS ester, resulting in a net positive charge (of quaternary ammonium cation) and an increase of DS adsorption to 77 ng/cm<sup>2</sup>. The strong dependence of DS adsorption on the deactivation procedure is illustrated in Table 2. As expected, deactivation with EA resulting in a replacement of electroneutral NHS ester with neutral amide and hydroxy groups had only a small effect on the surface positive charge; DS adsorption was ~70 ng/cm<sup>2</sup>. A bit smaller but still rather high amount of adsorbed DS, 60 ng/cm<sup>2</sup>, was observed for coatings deactivated by hydrolysis with D-buffer. These results are in agreement with PM-IRRAS spectra and confirm prevailing positive charge, i.e., the deficit of carboxylate anions. The most efficient deactivation procedure with respect to the compensation of the positive charge was reaction with glycine, which led to a DS adsorption of ~30 ng/cm<sup>2</sup>. This is apparently due to the replacement of NHS esters by covalently attached glycine with negatively charged carboxy groups.

As predicted by the surface charge measurements, the lowest plasma fouling was observed on pCB brushes deactivated by the reaction with glycine. Accordingly, the PM-IRRAS and XPS results (see Figure 2 and Supporting Information) demonstrated the highest amount of regenerated carboxy groups after the deactivation with glycine. Furthermore, the same trend was observed on pHPMAA-CBMAA(15%) to which model BRES, i.e., anti-*E. coli* and NH<sub>2</sub>-ON probes were immobilized (Table 3). As a result, the Ab-functionalized and glycine-deactivated

**Table 3. Effect of Different Deactivation Procedures on Blood Plasma Fouling and Adsorption of Dextran Sulfate (DS) Measured on pHPMAA-CBMAA(15%) Brushes Activated with EDC/NHS and Functionalized (via Covalent Attachment) with Either Anti-*E. coli* or NH<sub>2</sub>-ON Probes with Densities 201 ng/cm<sup>2</sup> and 1.4 × 10<sup>13</sup> Probes/cm<sup>2</sup>, Respectively**

deactivation procedure	fouling from undiluted blood plasma [ng/cm <sup>2</sup> ]	
	anti- <i>E. coli</i> functionalized	NH <sub>2</sub> -ON probe functionalized
glycine	6.6 ± 3.6	4.9 ± 2.3
EA	19.6 ± 4.5	12.4 ± 3.8
hydrolysis	10.8 ± 2.7	13.1 ± 2.8

pHPMAA-CBMAA(15%) brush exhibited resistance to fouling from full blood plasma that was comparable to that of the state-of-the-art ultra-low-fouling antibody-functionalized pCBAA coating with a similar Ab level. We hypothesize that a relatively low number of CBMAA monomer units randomly distributed in inert pHPMAA do not influence the formation of a well-packed brush architecture and thus help the copolymer to attain fouling resistance similar to that of the ultra-low-fouling pHPMAA.

Besides glycine, several other amino acids, varying in spacer structure and spacer length between zwitterionic amino and carboxy groups for different binding conditions, were analyzed with respect to DS adsorption and plasma fouling (see Table S2). A trend of decreasing plasma fouling with decreasing spacer length was observed. We believe that this can be attributed to recovery of zwitterionic structure due to a closer proximity of zwitterionic groups. Accordingly, the lowest

plasma fouling was observed for glycine and (2-aminoethoxy)-acetic acid.

**Biorecognition Capabilities of Functionalized pHPMAA-CBMAA(15%) in Blood Plasma.** The biorecognition capabilities of pHPMAA-CBMAA brushes with previously optimized molar content of CBMAA(15%)<sup>28</sup> functionalized with DNA-ON probes and deactivated by glycine were characterized via the direct detection of a microRNA (miR-16) in 50% blood plasma (Figure 3). The surface concentration

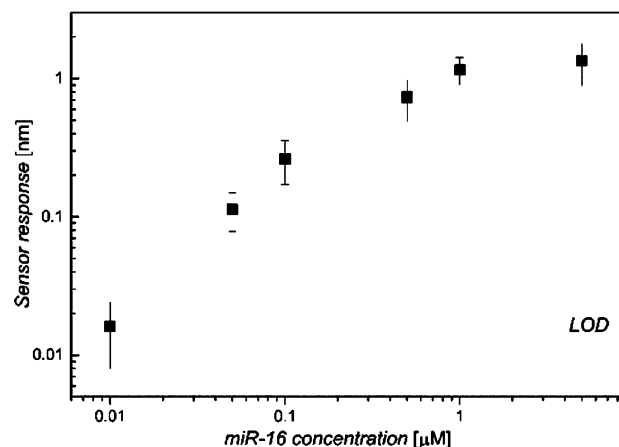


**Figure 3.** Sensor calibration curve for miR-16 spiked into 50% pooled blood plasma measured using pHPMAA-CBMAA(15%) brushes functionalized by covalent attachment of NH<sub>2</sub>-ON probes.

of NH<sub>2</sub>-ON probes (covalently attached to the EDC/NHS activated brush) was ~1.4 × 10<sup>13</sup> probes/cm<sup>2</sup>. The SPR detection experiments revealed a high degree of resistance to fouling; the fouling levels were ~2.9 and ~4.9 ng/cm<sup>2</sup> for 50% and full blood plasma, respectively. To the best of our knowledge, such a high fouling resistance in full blood plasma combined with a very high ON immobilization capacity has not been previously reported for any of the ON-functionalized low-fouling coatings. Furthermore, the pHPMAA-CBMAA(15%) brushes functionalized with NH<sub>2</sub>-ON probes exhibited high biorecognition capabilities in blood plasma: the LOD for the detection of miR-16 was calculated as 6 nmol/L. This LOD is comparable to the values reported for SPR biosensors for the direct label-free detection of miRNAs in buffers.<sup>36,37</sup>

The biorecognition capabilities of pHPMAA-CBMAA(15%) were further compared to mixed OEG-SAMs using the same detection conditions. As it was possible to attach only a negligible amount of NH<sub>2</sub>-ON probes to activated carboxy groups of mixed OEG-SAMs (see Supporting Information), the mixed OEG-SAMs were functionalized with streptavidin to which biotin-ON probes with the same DNA sequence were attached. This approach provided an ON-probe immobilization level of 4.5 × 10<sup>12</sup> probes/cm<sup>2</sup>, and the subsequent fouling from 50% blood plasma was ~151 ng/cm<sup>2</sup>. This level was in very good agreement with previously reported plasma fouling levels for antibody-functionalized unblocked mixed OEG-SAMs.<sup>8</sup> Conversely to the results achieved for ON-functionalized pHPMAA-CBMAA(15%), the ON-functionalized mixed OEG-SAMs did not exhibit any reasonable sensor response to miR-16 detection in 50% blood plasma, even at high analyte concentrations (see Supporting Information). Similar detection experiments for the mixed OEG-SAMs performed in buffer (without any blood plasma) showed a high biorecognition

performance (see Figure S10). It can be concluded that plasma fouling on mixed OEG-SAMs led to a critical impairment of biorecognition capability of the coating.

## CONCLUSIONS

We investigated the fundamental physicochemical processes involved in the functionalization of carboxy-functional low-fouling coatings, including the ultra-low-fouling polymer and copolymer brushes containing zwitterionic carboxybetaine side chains as well as conventional carboxy-terminated OEG-SAMs. The lowering of CBMAA content in pHPMAA-CBMAA was found to increase reactivity of carboxy groups to EDC/NHS activation, increase the ratio of BRE immobilization capacity to the total number of CBs contained in the brush, and decrease the fouling from blood plasma. Furthermore, the results revealed the importance of effective deactivation of residual active esters in pCB after EDC/NHS activation and covalent coupling of BREs with regard to plasma fouling. In contrast to carboxy-terminated OEG-SAMs, the activated pCB brushes were capable of only partial deactivation of EDC/NHS-activated carboxy groups by a spontaneous hydrolysis. The incomplete regeneration of carboxy groups in pCB was accompanied by an excess of surface positive charge promoting the fouling from blood plasma. It was demonstrated that only the covalent coupling of amino acid agents such as glycine to active NHS esters in the brush substantially improved resistance of BRE-functionalized pCB coatings to plasma fouling. We demonstrated that the BRE-functionalized and glycine-deactivated pHPMAA-CBMAA coatings with an optimized CBMAA molar content (15%) provided BRE capacity and resistance to plasma fouling that were comparable with the state-of-the-art ultra-low-fouling carboxy-functional homopolymer coatings. In addition, their resistance to plasma fouling was shown to be better than that of pCBMAA coatings and much better than that of conventional OEG-SAMs.

The pHPMAA-CBMAA(15%) coatings functionalized with DNA-ON probes with high surface concentration ( $\sim 1.4 \times 10^{13}$  probes/cm<sup>2</sup>) and glycine deactivated exhibited fouling resistance to blood plasma that was 2 orders of magnitude better when compared to commonly used DNA ON-functionalized mixed OEG-SAMs. We believe that these findings will benefit future design and functionalization of carboxy-functional ultra-low-fouling biorecognition coatings for effective biosensing in biological fluids.

## ASSOCIATED CONTENT

### Supporting Information

The Supporting Information is available free of charge on the ACS Publications website at DOI: 10.1021/acs.analchem.6b04731.

Synthesis of monomers, procedures of preparation and functionalization of polymer- and SAM-based coatings, and SPR measurement details (PDF)

## AUTHOR INFORMATION

### Corresponding Author

\*Tel.: +420 266773404. E-mail: homola@ufe.cz.

### ORCID

Hana Lísalová: 0000-0002-8755-2398

Ognen Pop-Georgievski: 0000-0001-7938-9271

## Author Contributions

H.L. and E.B. contributed equally to this work.

## Notes

The authors declare no competing financial interest.

## ACKNOWLEDGMENTS

This research was supported by the Czech Science Foundation (contract # P205/12/G118 and 15-09368Y), by the Ministry of Education, Youth and Sports of CR within the National Sustainability Program II (Project BIOCEV-FAR LQ1604), by the project "BIOCEV" (CZ.1.05/1.1.00/02.0109), and by Praemium Academiae of the Academy of Sciences of the Czech Republic.

## REFERENCES

- (1) Murugaiyan, S. B.; Ramasamy, R.; Gopal, N.; Kuzhandaivelu, V. *Adv. Biomed. Res.* **2014**, *3*, 67.
- (2) Vo-Dinh, T.; Fales, A. M.; Griffin, G. D.; Khoury, C. G.; Liu, Y.; Ngo, H.; Norton, S. J.; Register, J. K.; Wang, H. N.; Yuan, H. *Nanoscale* **2013**, *5*, 10127–10140.
- (3) Homola, J. *Chem. Rev.* **2008**, *108*, 462–493.
- (4) Blaszykowski, C.; Sheikh, S.; Thompson, M. *Biomater. Sci.* **2015**, *3*, 1335–1370.
- (5) Vaisocherová, H.; Brynda, E.; Homola, J. *Anal. Bioanal. Chem.* **2015**, *407*, 3927–3953.
- (6) Pereira, A. D.; Rodriguez-Emmenegger, C.; Surman, F.; Riedel, T.; Alles, A. B.; Brynda, E. *RSC Adv.* **2014**, *4*, 2318–2321.
- (7) Špringer, T.; Bocková, M.; Homola, J. *Anal. Chem.* **2013**, *85*, 5637–5640.
- (8) Vaisocherová, H.; Ševců, V.; Adam, P.; Špačková, B.; Hegnerová, K.; Pereira, A. D.; Rodriguez-Emmenegger, C.; Riedel, T.; Houska, M.; Brynda, E.; Homola, J. *Biosens. Bioelectron.* **2014**, *51*, 150–157.
- (9) Rodriguez-Emmenegger, C.; Brynda, E.; Riedel, T.; Houska, M.; Šubr, V.; Alles, A. B.; Hasan, E.; Gautrot, J. E.; Huck, W. T. *Macromol. Rapid Commun.* **2011**, *32*, 952–957.
- (10) Banerjee, I.; Pangule, R. C.; Kane, R. S. *Adv. Mater.* **2011**, *23*, 690–718.
- (11) Ladd, J.; Zhang, Z.; Chen, S.; Hower, J. C.; Jiang, S. *Biomacromolecules* **2008**, *9*, 1357–1361.
- (12) Yang, W.; Chen, S.; Cheng, G.; Vaisocherová, H.; Xue, H.; Li, W.; Zhang, J.; Jiang, S. *Langmuir* **2008**, *24*, 9211–9214.
- (13) Wang, J.; Yuan, S.; Zhang, Y.; Wu, W.; Hu, Y.; Jiang, X. *Biomater. Sci.* **2016**, *4*, 1351–1360.
- (14) Wang, Z.; Ma, G.; Zhang, J.; Yuan, Z.; Wang, L.; Bernards, M.; Chen, S. *Biomaterials* **2015**, *62*, 116–127.
- (15) Sun, F.; Hung, H.-C.; Sinclair, A.; Zhang, P.; Bai, T.; Galvan, D. D.; Jain, P.; Li, B.; Jiang, S.; Yu, Q. *Nat. Commun.* **2016**, *7*, 13437.
- (16) Vaisocherová, H.; Yang, W.; Zhang, Z.; Cao, Z.; Cheng, G.; Piliarik, M.; Homola, J.; Jiang, S. *Anal. Chem.* **2008**, *80*, 7894–7901.
- (17) Löfås, S.; Johnsson, B.; Edström, Å.; Hansson, A.; Lindquist, G.; Hillgren, R. M. M.; Stigh, L. *Biosens. Bioelectron.* **1995**, *10*, 813–822.
- (18) Lahiri, J.; Isaacs, L.; Tien, J.; Whitesides, G. M. *Anal. Chem.* **1999**, *71*, 777–790.
- (19) Brault, N. D.; Gao, C.; Xue, H.; Piliarik, M.; Homola, J.; Jiang, S.; Yu, Q. *Biosens. Bioelectron.* **2010**, *25*, 2276–2282.
- (20) Riedel, T.; Surman, F.; Hageneder, S.; Pop-Georgievski, O.; Noehammer, C.; Hofner, M.; Brynda, E.; Rodriguez-Emmenegger, C.; Dostálek, J. *Biosens. Bioelectron.* **2016**, *85*, 272–279.
- (21) Nakajima, N.; Ikada, Y. *Bioconjugate Chem.* **1995**, *6*, 123–130.
- (22) Sam, S.; Touahir, L.; Salvador Andresa, J.; Allongue, P.; Chazalviel, J.-N.; Gouget-Laemmel, A.; Henry de Villeneuve, C.; Morailon, A.; Ozanam, F.; Gabouze, N.; Djebbar, S. *Langmuir* **2010**, *26*, 809–814.
- (23) Palazon, F.; Montenegro Benavides, C.; Léonard, D.; Souteyrand, E. I.; Chevolut, Y.; Cloarec, J.-P. *Langmuir* **2014**, *30*, 4545–4550.

- (24) Wang, C.; Yan, Q.; Liu, H.-B.; Zhou, X.-H.; Xiao, S.-J. *Langmuir* **2011**, *27*, 12058–12068.
- (25) Booth, M. A.; Kannappan, K.; Hosseini, A.; Partridge, A. *Langmuir* **2015**, *31*, 8033–8041.
- (26) Lim, C. Y.; Owens, N. A.; Wampler, R. D.; Ying, Y.; Granger, J. H.; Porter, M. D.; Takahashi, M.; Shimazu, K. *Langmuir* **2014**, *30*, 12868–12878.
- (27) Brault, N. D.; White, A. D.; Taylor, A. D.; Yu, Q.; Jiang, S. *Anal. Chem.* **2013**, *85*, 1447–1453.
- (28) Vaisocherová-Lisalová, H.; Surman, F.; Višová, I.; Vala, M.; Špringer, T.; Ermini, M. L.; Šípová, H.; Šedivák, P.; Houska, M.; Riedel, T.; Pop-Georgievski, O.; Brynda, E.; Homola, J. *Anal. Chem.* **2016**, *88*, 10533–10539.
- (29) Ikeda, S.; Kong, S. W.; Lu, J.; Bisping, E.; Zhang, H.; Allen, P. D.; Golub, T. R.; Pieske, B.; Pu, W. T. *Physiol. Genomics* **2007**, *31*, 367–373.
- (30) Iorio, M. V.; Ferracin, M.; Liu, C. G.; Veronese, A.; Spizzo, R.; Sabbioni, S.; Magri, E.; Pedriali, M.; Fabbri, M.; Campiglio, M.; Menard, S.; Palazzo, J. P.; Rosenberg, A.; Musiani, P.; Volinia, S.; Nenci, I.; Calin, G. A.; Querzoli, P.; Negrini, M.; Croce, C. M. *Cancer Res.* **2005**, *65*, 7065–7070.
- (31) Wang, K.; Zhang, S. L.; Marzolf, B.; Troisch, P.; Brightman, A.; Hu, Z. Y.; Hood, L. E.; Galas, D. J. *Proc. Natl. Acad. Sci. U. S. A.* **2009**, *106*, 4402–4407.
- (32) Jones, D. M.; Brown, A. A.; Huck, W. T. S. *Langmuir* **2002**, *18*, 1265–1269.
- (33) Rodriguez-Emmenegger, C.; Houska, M.; Alles, A. B.; Brynda, E. *Macromol. Biosci.* **2012**, *12*, 1413–1422.
- (34) Ulbrich, K.; Šubr, V.; Strohalm, J.; Plocová, D.; Jelínková, M.; Říhová, B. *J. Controlled Release* **2000**, *64*, 63–79.
- (35) Špringer, T.; Piliarik, M.; Homola, J. *Sens. Actuators, B* **2010**, *145*, 588–591.
- (36) Šípová, H.; Homola, J. *Anal. Chim. Acta* **2013**, *773*, 9–23.
- (37) Avino, A.; Huertas, C. S.; Lechuga, L. M.; Eritja, R. *Anal. Bioanal. Chem.* **2016**, *408*, 885–893.



# Appendix V

Víšová, I., B. Smolková, M. Uzhytchak, M. Vrabcová, Y. Zhigunova, M. Houska, F. Surman, A. de los Santos Pereira, O. Lunov, A. Dejneka and H. Vaisocherová-Lísalová

**Modulation of Living Cell Behavior with Ultra-Low Fouling Polymer Brush Interfaces.**

*Macromolecular Bioscience* **20**(3) (2020): 1900351



# Modulation of Living Cell Behavior with Ultra-Low Fouling Polymer Brush Interfaces

Ivana Víšová, Barbora Smolková, Mariia Uzhytchak, Markéta Vrabcová, Yulia Zhigunova, Milan Houska, František Surman, Andres de los Santos Pereira, Oleg Lunov, Alexandr Dejneka, and Hana Vaisocherová-Lísalová\*

Ultra-low fouling and functionalizable coatings represent emerging surface platforms for various analytical and biomedical applications such as those involving examination of cellular interactions in their native environments. Ultra-low fouling surface platforms as advanced interfaces enabling modulation of behavior of living cells via tuning surface physicochemical properties are presented and studied. The state-of-art ultra-low fouling surface-grafted polymer brushes of zwitterionic poly(carboxybetaine acrylamide), nonionic poly(*N*-(2-hydroxypropyl)methacrylamide), and random copolymers of carboxybetaine methacrylamide (CBMAA) and HPMAA [p(CBMAA-*co*-HPMAA)] with tunable molar contents of CBMAA and HPMAA are employed. Using a model Huh7 cell line, a systematic study of surface wettability, swelling, and charge effects on the cell growth, shape, and cytoskeleton distribution is performed. This study reveals that ultra-low fouling interfaces with a high content of zwitterionic moieties (>65 mol%) modulate cell behavior in a distinctly different way compared to coatings with a high content of nonionic HPMAA. These differences are attributed mostly to the surface hydration capabilities. The results demonstrate a high potential of carboxybetaine-rich ultra-low fouling surfaces with high hydration capabilities and minimum background signal interferences to create next-generation bioresponsive interfaces for advanced studies of living objects.

biosensors, microarrays, and bio-imaging technologies are aimed to be used in a direct contact with complex biological media such as cell-containing media and clinical samples of bodily fluids. Therefore, an intensive research and development of new ultra-low fouling (or so-called “antifouling”) coatings and materials has been evidenced worldwide.<sup>[2–4]</sup> A specific attention has been paid to antifouling coatings that simultaneously facilitate active target surface functionalities such as biorecognition and the capture of target molecules present in the media.<sup>[2]</sup>

As a result of advances in material sciences and chemical engineering, numerous low-fouling coatings have been reported, such as polyethylene glycol derivatives and zwitterionic and nonionic polymer-based coatings or hydrogels.<sup>[2]</sup> Excellent fouling resistance has been recently reported for ultra-low fouling polymer brushes.<sup>[2]</sup> Examples include nonionic poly(2-hydroxyethyl methacrylate), poly(3-hydroxypropyl methacrylate), poly(*N*-(2-hydroxypropyl)methacrylamide) (pHPMAA), zwitterionic poly(carboxybetaine)-based (pCB) brushes

such as poly(carboxybetaine methacrylamide) (pCBMAA) and poly(carboxybetaine acrylamide) (pCBAA), or recently developed random copolymers combining zwitterionic and nonionic moieties such as p(CBMAA-*co*-HPMAA).<sup>[1,2,5,6]</sup> These platforms are characterized by diverse physicochemical surface properties including structure, architecture, thickness, rigidity, wettability, surface charge, packing density, or swelling properties; all of these parameters have been shown to have an impact on resulting surface resistance to fouling from complex media and biological activity of immobilized biorecognition elements.<sup>[5,7]</sup> Therefore, it is expected that these factors may also significantly influence behavior of living cells in the proximity of such coatings. In fact, when the cells are seeded on such surfaces, the coatings will act as an analogue of extracellular matrix and thus will have a substantial impact on cells, conveying physical and chemical stimuli, and influencing cellular shape, actin cytoskeleton organization, and transcription activity.<sup>[8]</sup>

The cell adhesion and cell behavior in close proximity to surfaces are generally influenced by a number of surface properties including topography, roughness, wettability, electrical

## 1. Introduction

Nonspecific adhesion of biomolecules and cells to synthetic surfaces, that is, “biofouling,” represents a complex and persistent global issue in many fields including biomedical and analytical devices.<sup>[1,2]</sup> A great portion of such rapidly developing technologies such as bioanalytical and medical devices,

I. Víšová, B. Smolková, M. Uzhytchak, M. Vrabcová, Y. Zhigunova, Dr. M. Houska, Dr. O. Lunov, Dr. A. Dejneka, Dr. H. Vaisocherová-Lísalová  
Institute of Physics  
Czech Academy of Sciences  
Na Slovance 2, 182 21 Prague, Czech Republic  
E-mail: lisalova@fzu.cz

Dr. F. Surman, Dr. A. de los Santos Pereira  
Institute of Macromolecular Chemistry  
Czech Academy of Sciences  
Heyrovského nám. 2, 162 00 Prague, Czech Republic

The ORCID identification number(s) for the author(s) of this article can be found under <https://doi.org/10.1002/mabi.201900351>.

DOI: 10.1002/mabi.201900351

charge, biochemical cues, surface stiffness, and presence of functional groups.<sup>[9–11]</sup> The surface wettability has been recognized as one of the most important surface properties affecting the biological response of a biocompatible material.<sup>[11,12]</sup> An optimal cell adhesion has been so far described for moderately wettable polymeric materials with water contact angles in the range of 40°–70°.<sup>[11,13]</sup> Nevertheless, the wettability of polymeric materials required for optimal cell adhesion depends dramatically on the cell type, incubation time, culture conditions, surface chemistry, and topography.<sup>[11,14]</sup> Surface charges have also been found to influence the cell attachment<sup>[9,11,15]</sup> and cell behavior.<sup>[15]</sup> Moreover, many studies reported the improved biocompatibility, cell affinity, and cell differentiation on the implanted surfaces by varying positive and negative charges.<sup>[9,11,16,17]</sup> It is generally accepted that positively charged coating materials such as polylysine improve neuronal attachment in vitro.<sup>[9,11]</sup> The surface charges have also been employed to modify the cell behavior through the chemical functionalities of the polymer materials.<sup>[9,11]</sup> So far, the best cell adhesion, growth, and spreading rate has been shown on polar and positively charged surfaces (amine group-grafted polyethylene) while the negatively charged surfaces usually showed a poor cell growth.<sup>[9,11,16,17]</sup> Moreover, the surfaces grafted with neutral amide and hydroxyl groups showed a similar number of cell attachments. However, the morphology of cells attached at the surfaces was quite distinct. The cells were spread much more on the hydroxyl group-grafted surface than on the amide group-grafted ones.<sup>[9,11,16,17]</sup> Obviously, the molecular mechanisms and approaches of modulation of surface charge-dependent cellular activities still need to be better understood. The study of each individual surface physicochemical parameter and its effect on cellular behavior is a quite complex issue; it is difficult to isolate and assess each surface parameter independently using existing materials and coatings.

Well-defined ultra-low fouling coatings with minimum background nonspecific binding even from complex biological media represent an attractive approach to elucidate the effects of surface physicochemical properties on cellular behavior. Several recent studies dealing with ultra-low fouling surface–cell interactions focused on a specific application without aiming to generalize the observed surface–cell effects.<sup>[4,18–21]</sup> Some complex surface–cell relationships have been recently reported—the ultra-low fouling surface wettability (or hydrophilicity),<sup>[22,23]</sup> hydration and layer thickness,<sup>[24–26]</sup> zwitterionization,<sup>[27]</sup> and charge, and the presence of various functional groups<sup>[28]</sup> have been shown to influence cellular behavior. The differentiation of stem cells was investigated in dependence on surface hydrophilicity and zwitterionization of the coating.<sup>[29]</sup> While in pCBAA hydrogel with zwitterionic hydrophilic cross-linker, stem cells remained in an undifferentiated state, in pCBAA hydrogel with hydrophobic cross-linker, the cells differentiated actively. The direction of differentiation depended on the stiffness of the surface (the amount of hydrophobic spots). In the above reports, coatings with similar chemical composition have been employed with a focus on the effect of a single-surface property. Studies on the complex effects of diverse ultra-low fouling surface physicochemical properties on living cells behavior are still desirable.

In this work, we present a systematic study on the combined effects of varied physicochemical properties of ultra-low fouling

surfaces on behavior of living cells. This work utilizes a set of state-of-art ultra-low fouling polymer brushes with tailored surface properties such as the charge content, wettability, swelling capabilities, and chemical composition. The brushes based on zwitterionic pCB, nonionic pHPMAA, and random p(CBMAA-co-HPMAA) copolymers with the comparable wet thickness were employed. In case of p(CBMAA-co-HPMAA), we take the advantage of easily tunable surface properties achieved by adjusting the molar feed ratio of the monomers with statistically distributed monomer units in the brush structure.<sup>[30]</sup> The tendency of the cell growth, cellular shaping, cytoskeleton distribution, and clustering were analyzed using the high-resolution spinning disk confocal microscopy. The human hepatocellular carcinoma cell line (Huh7) was used as a model cell system for the purpose of this study because of its high sensitivity to external stresses.<sup>[31]</sup> The results highlight the importance of understanding the factors governing the attachment of cells on biofunctional surfaces and may contribute to the development of robust ultra-low fouling platforms for exploration of cellular interactions in complex biological media.

## 2. Results and Discussion

### 2.1. Monitoring Behavior of Living Cells at Ultra-Low Fouling Surfaces

The set of surfaces prepared for the purpose of this study included the state-of-art ultra-low fouling brushes of zwitterionic pCBAA and pCBMAA, nonionic pHPMAA, and p(CBMAA-co-HPMAA) copolymers with randomly distributed monomer units.<sup>[30]</sup> A scheme of the polymer brush structures is shown in **Figure 1**. This surface series was selected to provide a set of diverse surface parameters such as the charge, wettability, and swelling. The brushes were “grafted from” gold substrates by surface-initiated atom transfer radical polymerization as described elsewhere.<sup>[32]</sup> Gold-coated substrates form an excellent platform to create highly dense polymer brushes and these substrates are also easily compatible with advanced surface characterization methods such as surface plasmon resonance (SPR), polarization modulation infrared reflection-absorption spectroscopy (PM-IRRAS), and spectroscopic ellipsometry.<sup>[2,33]</sup> The polymerization conditions such as the time of polymerization or reagent concentrations were optimized for each brush type to achieve the desired wet thickness of ≈75 nm (see Supporting Information for specification of the optimized polymerization conditions). The brush wet thickness of ≈75 nm was selected as an optimum thickness value that provides 1) a sufficient thickness to shield out any potential attractive long-range forces (mostly hydrophobic) from gold (a maximum range of hydrophobic attraction is 50 nm<sup>[34,35]</sup>); 2) a complete resistance to nonspecific protein adsorption even from 100% blood plasma<sup>[2]</sup> (see also results in **Table 1**); and 3) a sensitivity of SPR method is still high enough for the used polymer layers with given optical characteristics to provide reliable measurements.<sup>[36]</sup> Moreover, in order to avoid any potential concerns regarding the thickness variability effects on cell behavior, we performed a control study on cell growth and clustering in dependence on pCBMAA thickness. In particular, the pCBMAA brushes with wet thickness

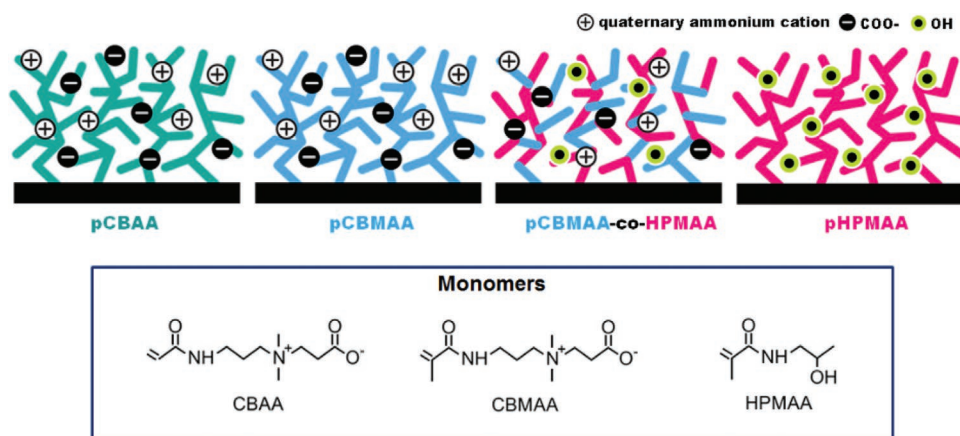


**Figure 1.** Scheme of low-fouling polymer coatings employed in this study.

values of 46, 56, and 128 nm were employed. This thickness range is still reasonable enough to shield out the potential long-range forces (mostly hydrophobic) from gold substrate. The results show no significant differences in cellular behavior for this set of pCBMAA thicknesses, suggesting no influence of brush wet thickness in the range of 46–128 nm on studied cell behavior (see Figure S6, Supporting Information).

The chemical composition of the wet brushes was controlled by means of PM-IRRAS (see Supporting Information).

Hepatocytes are very specific cells: they are polarized, specialized, and species-specific, making them uniquely susceptible to infections.<sup>[37]</sup> Recently, we showed that among widely used hepatic cell lines, Huh7 is the most fragile cell line, which makes it ideal to assess acute toxicity of different substrates.<sup>[31,38]</sup> Therefore, these cell lines were selected for the purpose of this work. The tendency of Huh7 cells to adhere and spread at the ultra-low fouling brushes with the varied charge, swelling, and wettability was studied using high-resolution spinning disk confocal microscopy. First, we confirmed that all the tested brush coatings showed no detectable signs of cytotoxicity. The cells remained viable after 4 days of incubation with each type of the brush (Figure S2 and S3, Supporting Information).

Furthermore, only very few Huh7 cells were settled at all the brushes even after 4 days of cell incubation (Figure 2). It

is important to emphasize that the cells were not fully adhered to any type of the studied brushes, no typical adhesion pattern was found compared to control surface (Figure 2), and the cells could be easily washed out from the brush surfaces using mild solutions such as pure water or PBS buffer (data not shown). The lowest degree of the cell settlement was observed for nonionic pHPMAA ( $10 \pm 2$  cells) and for copolymer with a low content of CBMAA, that is, p(CBMAA 35%-co-HPMAA 65%) ( $9 \pm 1$  cells), and the highest settlement ( $28 \pm 3$  cells) was found for pCBAA. This highest value is substantially lower than  $132 \pm 9$  cells observed on the bare gold, and by order of magnitude lower than that observed using a solution-based positive control ( $235 \pm 11$  cells).

Although no fouling was observed by SPR from 100% human blood plasma and from the cell-free culture medium for any surface studied, a certain but very low fouling from the cells in the culture medium was observed (Table 1) confirming

**Table 1.** Fouling resistance of polymer brushes measured by angular SPR.

Polymer brush	Fouling level [ng cm <sup>-2</sup> ]	
	100% human blood plasma/ cell-free culture medium	Huh7 cells in culture medium
pCBAA	0 <sup>a)</sup> /0 <sup>a)</sup>	3
pCBMAA	0 <sup>a)</sup> /0 <sup>a)</sup>	34
p(CBMAA 65%-co-HPMAA 35%)	0 <sup>a)</sup> /0 <sup>a)</sup>	8.5
p(CBMAA 35%-co-HPMAA 65%)	0 <sup>a)</sup> /0 <sup>a)</sup>	15
pHPMAA	0 <sup>a)</sup> /0 <sup>a)</sup>	0.9

<sup>a)</sup>The value below the detection limit of SPR ( $\approx 0.1$  ng cm<sup>-2</sup>).

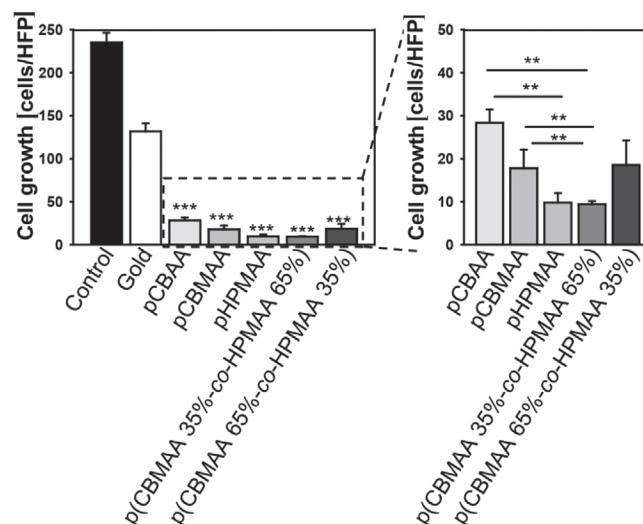


**Figure 2.** Analysis of Huh7 cell settlement on different substrates. Total number of cells per high-power field (HPF)  $700 \mu\text{m} \times 700 \mu\text{m}$  was assessed microscopically. ImageJ software was used for cell counting. One-way analysis of variance with Newman–Keuls multiple comparison test was used. Data are expressed as means  $\pm$  SEM,  $***p < 0.001$ .

a high resistance of studied ultra-low fouling surface to cell adhesion. These results are in general agreement with those observed by confocal microscopy (Figure 2); the differences in quantitative analysis were due to completely different conditions for the cell seeding for confocal microscopy measurements with optimum cell-cultivation conditions and a flow-through regime of SPR measurements (see Experimental Section for more details).

It is generally accepted that the cell adhesion is mediated by a protein preadsorption and correlations between the protein adsorption and cell adhesion were described.<sup>[22,39–41]</sup> Interestingly in our work, even though the fouling resistance from 100% human blood plasma as well as from cell-free culture medium for all the studied coatings was below the detectable limit of SPR measurements ( $\approx 0.1 \text{ ng cm}^{-2}$ ), a certain degree, even very low, of fouling from the cells in culture medium was observed. This observation may suggest that the surface resistance to protein adhesion may not imply the undetectable nonspecific signal from the living cells, as it was

previously reported by Ostuni et al.,<sup>[42]</sup> where the high surface resistance to nonspecific protein adsorption may not be a sufficient prerequisite to prevent cell adhesion or vice versa.<sup>[22]</sup> Our observation of complete resistance to protein adsorption from blood plasma and culture medium and very low nonspecific adsorption from cells seems to be in accordance with these findings. However, one must take into account that the amount of nonspecific protein adsorption was not “zero” but below the limit of SPR detection ( $\approx 0.1 \text{ ng cm}^{-2}$ ) and some extremely low deposits could be present. A very low number of cells on the surfaces and their very loose adhesion correspond well to this situation.

The analysis of cellular shapes showed significant differences depending on the coating types (Figure 3). The cells grown on bare gold show extensive spreading, indicating strong adhesion between the cells and the gold surface. While the cells become round-shaped on the least-adhesive pHPMAA, the cells seeded on pCBAA have irregular shape, although not so prominent as in the positive control. A similar observation of rounded

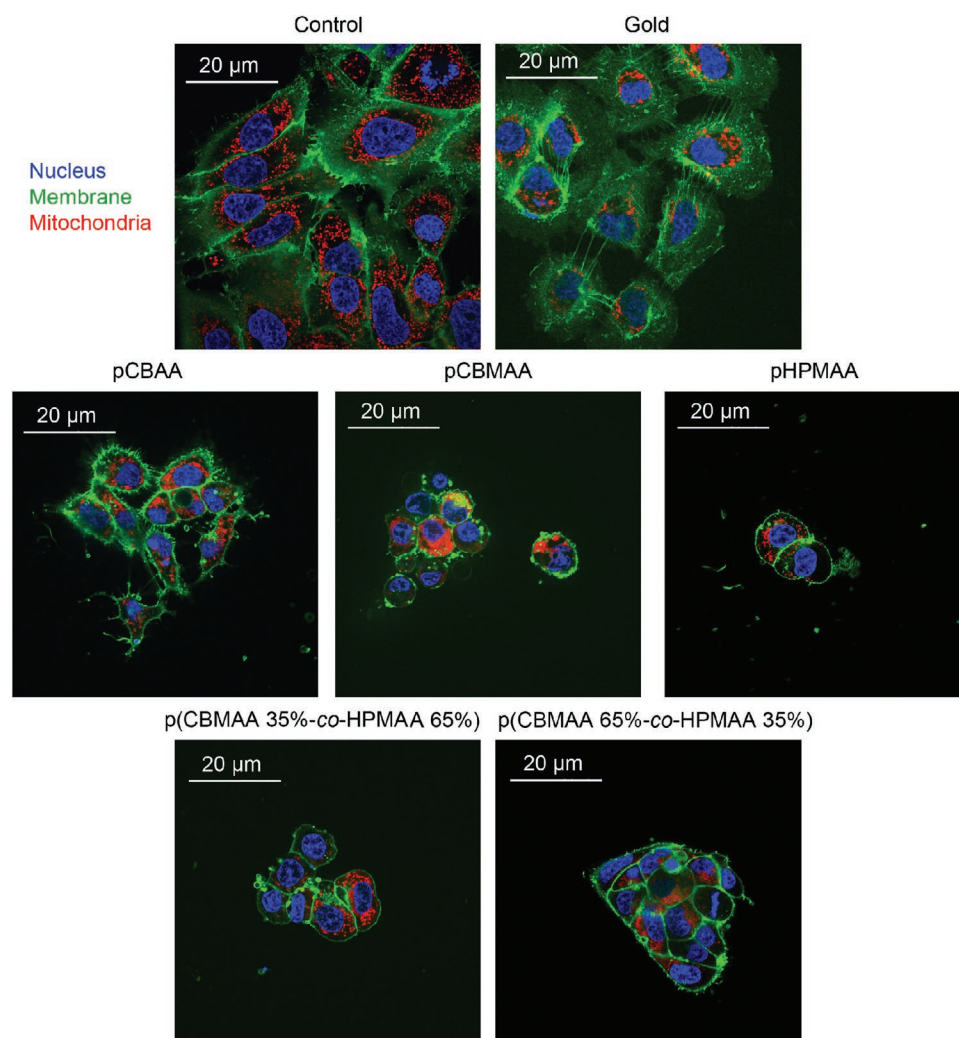


**Figure 3.** Analysis of cellular shape. Cells were seeded on different substrates for 4 days and labeled with MitoTracker Red (red dye) and Hoechst 33342 nuclear stain (blue dye). Cell membranes were labeled with CellMask Green (green dye). Labeled cells were then imaged using high-resolution spinning disk confocal microscopy.

morphology was reported on pHPMAA hydrogel coatings with L929 mouse fibroblast cells after 24 h of incubation.<sup>[43]</sup>

In agreement with a previously published literature dealing with ultra-low fouling coatings, we observed a cluster formation. This is probably due to cell–cell interactions outweighing cell–substrate interactions,<sup>[24,26,43]</sup> which are dramatically weakened on the ultra-low fouling polymer brushes. Consistently with the cell growth analysis and the cell shape assessments, the cell cluster area showed the same tendency. The lowest cell cluster area was measured for nonionic pHPMAA, while the highest area was found for pCBAA (Figure 4). These results correspond to further analysis of cytoskeleton distribution. While for pHPMAA, the cytoskeleton is on periphery of the cells, the cytoskeleton distribution of irregularly shaped cells on pCBAA exhibits a prerequisite of the cell adhesion pattern (Figure 5). Indeed, the cells only on pCBAA exhibited a non-rounded morphology and clear actin fibers, indicating a tendency of a cell to spread. On the contrary, the cells grown on pHPMAA showed decreased cell spreading, a rounded morphology, and the lack of actin fibers (Figure 5). Altogether, this indicates a decreased cell adhesion and spreading tendency on pHPMAA. These results suggest a higher tendency to spreading of cells in the close proximity to the surfaces containing a high content of zwitterionic moieties compared to nonionic ultra-low fouling surfaces.

On standard cell-adhesive substrates, the cells following the initial attachment continue in flattening and spreading on the substrate, resulting in the decrease of the cell height and

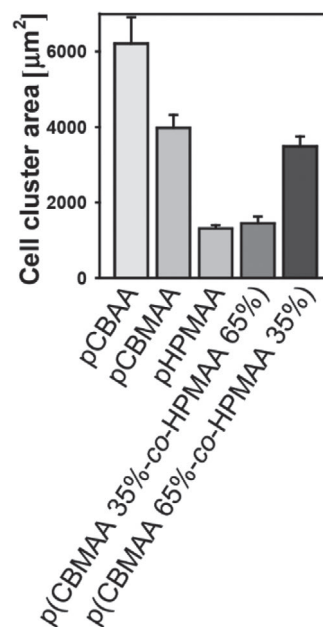


**Figure 4.** Analysis of cell clusters areas. Cells were seeded on different substrates for 4 days and labeled with Hoechst 33342 nuclear stain (blue dye). Cell membranes were labeled with CellMask Green (green dye). Labeled cells were then imaged using high-resolution spinning disk confocal microscopy. Cell cluster area was measured using ImageJ software. Data are expressed as means  $\pm$  SEM.

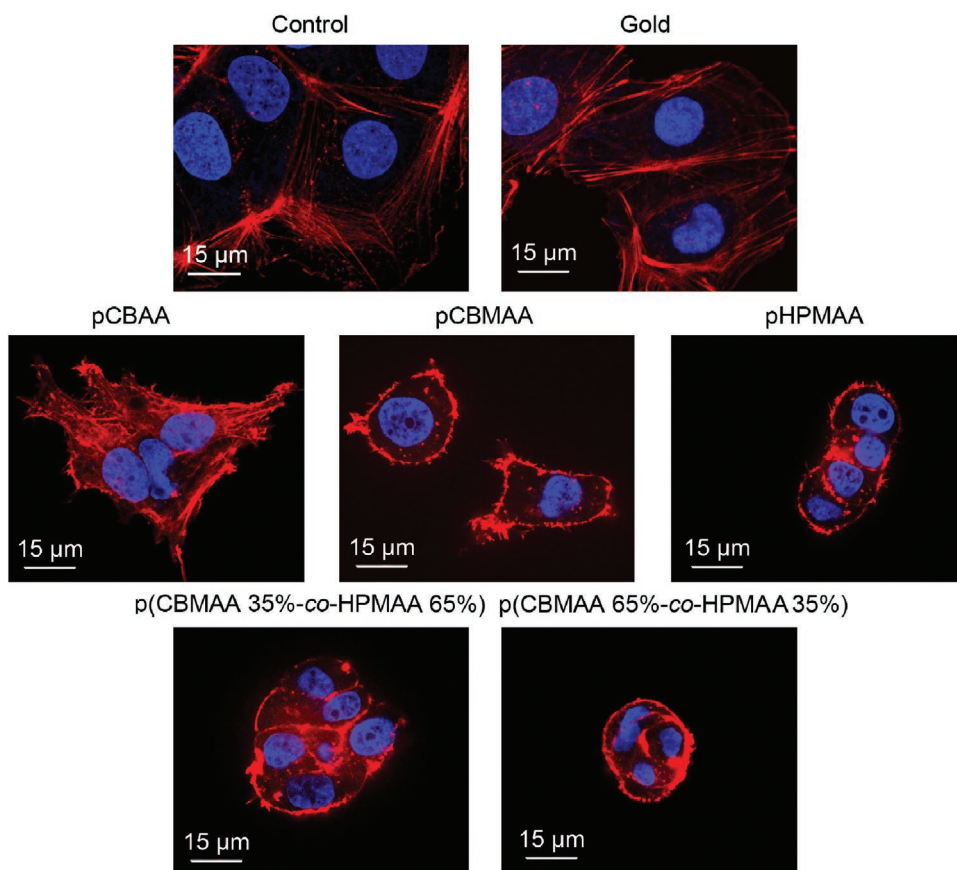


**Figure 5.** Analysis of cytoskeleton remodeling. Cells were seeded on different substrates and labeled with F-actin (red dye) and Hoechst 33342 nuclear stain (blue dye). Labeled cells were then imaged using high-resolution spinning disk confocal microscopy.

**Table 2.** Advancing ( $\Theta_a$ ) and receding ( $\Theta_r$ ) contact angles on the polymer brushes.

Polymer brush	$\Theta_a$ [deg]	$\Theta_r$ [deg]
pCBAA	$10.4 \pm 0.9$	N/A
pCBMAA	$12.2 \pm 1.5$	N/A
p(CBMAA 65%- <i>co</i> -HPMAA 35%)	$16.5 \pm 0.8$	N/A
p(CBMAA 35%- <i>co</i> -HPMAA 65%)	$24.9 \pm 2.0$	$7.9 \pm 0.1$

N/A— $\Theta_r$  could not be determined due to a very high wettability.

increase of the contact area while non-adhered cells remain spherical.<sup>[44,45]</sup> We have observed a similar tendency of the cell behavior on our ultra-low fouling surfaces, namely on CB-rich surfaces (Figure 3 and 5).

## 2.2. Cell Behavior in Relation to Surface Wettability and Swelling

The surface wettability is considered to be one of the major factors governing biological response of biocompatible materials.<sup>[11,12]</sup> Therefore, we focused on analysis of the surface hydration effects in relation to the cell behavior.

**Table 2** shows the results regarding the surface wettability from dynamic water contact angle measurements for each type of the used ultra-low fouling brushes. Apparently, the brush wettability increased with increasing CB molar content. For example, advancing and receding air/water contact angles of  $\Theta_a = 44.7^\circ \pm 0.3^\circ$  and  $\Theta_r = 9.7^\circ \pm 0.6^\circ$  reflected a moderate wettability of pHPMAA, whereas the high wettability of pCBAA and pCBMAA was reflected by  $\Theta_a = 10.4^\circ \pm 0.9^\circ$  and  $\Theta_a = 12.2^\circ \pm 1.5^\circ$ , respectively, and very low  $\Theta_r$ , below  $5^\circ$ . However, while the wettability values of pCBAA and pCBMAA were comparably very high indicating super-hydrophilic surface properties, the cell shaping and clustering exhibited substantial differences. The cells only on pCBAA exhibited growth and shape patterns corresponding to well-spread cells, whereas growth on pCBMAA resulted in decrease in cell spreading in relation with a rounded morphology and peripheral cytoskeleton distribution (Figure 3 and 5). This difference in the cell behavior can be related to differences in swelling characteristics. Therefore, advanced spectroscopic ellipsometry methodology and modeling (see Figure S4, Supporting Information) was employed to determine the swelling parameters for each type of the

coating (**Table 3**). While the thickness of the dry pCBAA brush increased upon hydration in water six times, the thickness of pCBMAA increased four times. Therefore, pCBAA exhibited substantially higher inner layer hydration and this might contribute to the higher cell growth and size of the clusters observed by confocal microscopy (Figure 2 and 4). Surprisingly, there were no significant differences in swelling between the two p(CBMAA-*co*-HPMAA) copolymers; both values were close to that of pHPMAA.

It appears that the presence of HPMAA limits the hydration capabilities even for copolymers with a relatively low content (35 mol%) of HPMAA. Interestingly, the cells grown on p(CBMAA 65%-*co*-HPMAA 35%) showed a similar growth tendency as on pCBMAA (Figure 2). Indeed, the cell cluster area, cellular morphology, and distribution of actin fibers were very similar for the cells seeded on p(CBMAA 65%-*co*-HPMAA 35%) and pCBMAA (Figure 3–5).

The cells seeded on p(CBMAA 35%-*co*-HPMAA 65%) showed a nearly identical degree of cell settlement, cell cluster area, cellular morphology, and distribution of actin fibers as on pHPMAA (Figure 2–5). Thus, it is clearly demonstrated that the inner layer hydration capabilities of ultra-low fouling brushes influence the cell attachment, proliferation, morphology, and cytoskeleton distribution. Indeed, other studies show that cells attach to the super-hydrophilic regions in a highly selective manner.<sup>[46,47]</sup> Therefore, we propose that in the absence of specific protein-integrin-mediated cell interactions on low-fouling surfaces, the cell attachment and following behavior are predominantly mediated by the surface hydration capabilities.

Our data indicate that among the tested low-fouling materials, the pCBAA surfaces exhibiting high hydration capabilities induce a minimum external stress on the living cells. In order to explore these findings for potential application in development of ultra-low fouling microarrays with cells immobilized onto specific microstructure areas, we created a model pCBAA-based microarray containing cell-adhesive squared and circular patterns surrounded by a non-cell-adhesive pCBAA brush background. The Huh7 cells were incubated with these substrates for 72 h and labeled with Hoechst nuclear stain (blue dye). The representative images are shown in **Figure 6**. The microarrays yielded stable either circular or squared printed features on the slides without any cells bound to pCBAA brush background. Indeed, such results are in line with other very recent works demonstrating pCBAA brushes as a suitable low-fouling background in cell microarray applications.<sup>[18,19]</sup> In summary, our

**Table 3.** Thickness and refractive index values (at 670 and 785 nm) of the representative dry and wet polymer brushes.

Polymer brush	Dry		Wet		
	Thickness [nm]	Refractive index (670/785 nm)	Thickness [nm]	Refractive index (670/785 nm)	Swelling [%]
pCBAA	$12.0 \pm 0.9$	1.535/1.531	$71.4 \pm 0.8$	1.360/1.357	616
pCBMAA	$13.1 \pm 0.5$	1.515/1.512	$56.6 \pm 0.3$	1.378/1.375	431
p(CBMAA 65%- <i>co</i> -HPMAA 35%)	$31.3 \pm 1.2$	1.58/1.57	$79.8 \pm 0.3$	1.378/1.377	255
p(CBMAA 35%- <i>co</i> -HPMAA 65%)	$35.5 \pm 0.2$	1.5/1.497	$92.5 \pm 0.4$	1.386/1.384	260
pHPMAA	$29.8 \pm 0.5$	1.448/1.444	$70.6 \pm 0.1$	1.393/1.391	237

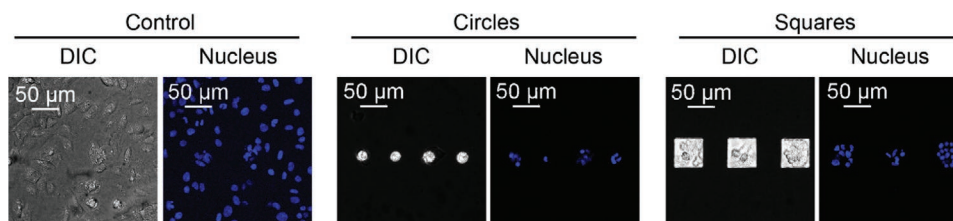


**Figure 6.** Representative confocal microscopy images of Huh7 cells grown on functional spots patterned on pCBAAs brushes.

results show that using the ultra-low fouling pCBAAs brushes, it is possible to create diverse printed features that are stable under cell culture conditions and simultaneously suppress undesirable nonspecific cell adhesion.

### 3. Conclusions

The behavior of living cells upon interaction with ultra-low fouling surfaces with diverse physicochemical properties was explored. Using a model cell line, we demonstrated an ultra-low fouling platform as an advanced interface enabling modulation of living cell behavior via tuning surface physicochemical properties. The systematic study on surface wettability, swelling, and charge effects on the cell growth, shape, and cytoskeleton distribution indicated that ultra-low fouling interfaces with a high content of zwitterionic moieties (>65 mol%) modulate the cell response in a completely different way compared to nonionic pHPMAA and p(CBMAA-co-HPMAA) with a CBMAA molar content as low as 35 mol%. The results suggest the higher tendency of cells to spread in the close proximity to the surfaces with a high content of zwitterionic moieties compared to nonionic ultra-low fouling surfaces. Furthermore, significant differences in the effect of pCBMAA and pCBAAs zwitterionic surfaces on the cell behavior were found. While pCBMAA and pCBAAs exhibited comparable wettability, the swelling characteristics measured using the advanced spectroscopic ellipsometry were substantially different. A higher degree of swelling was observed for pCBAAs, supporting the observation of the higher cell growth and cytoskeleton distribution on pCBAAs compared to pCBMAAs. This also highlights the importance of surface swelling characterization rather than relying only on wettability values. The results indicate that the surface hydration is a critical parameter governing the ultra-low fouling surface–cell interactions. The results demonstrate a high potential of CB-rich ultra-low fouling surfaces with high hydration capabilities to create bioresponsive interfaces for biochip technologies aimed to explore cellular interactions in their native environments. This work highlights the importance of understanding the phenomena governing the processes occurring at material/biological medium interfaces and it can contribute to the development of the next-generation surface-based bioresponsive platforms for advanced studies of living objects.

### 4. Experimental Section

**Reagents:** The buffer solutions were prepared using ultrapure water (Watrex). Phosphate-buffered saline (PBS, 0.01 M phosphate,

0.138 M sodium chloride, 0.0027 M potassium chloride, pH 7.4 at 25 °C) was prepared from a stock solution from Sigma-Aldrich, Czech Republic. The PBS-NaCl buffer (0.01 M phosphate, 0.75 M sodium chloride, 0.0027 M potassium chloride, pH 7.4 at 25 °C) was prepared from PBS stock solution. The initiator  $\omega$ -mercaptoundecyl bromoisobutyrate was from ProChimia, Poland. The carboxybetaine acrylamide, carboxybetaine methacrylamide, and *N*-(2-hydroxypropyl)methacrylamide monomers were from TCI Europe. 1,4,8,11-Tetramethyl-1,4,8,11-tetraazacyclotetradecane (Me<sub>4</sub>Cyclam, 98%), CuCl (≥99.995%), CuCl<sub>2</sub> (99.999%), and methanol (≥99.9%) were from Sigma-Aldrich. Tetrahydrofuran (THF, purity ≥99.9%) and ethanol (purity 96%) was from Penta, Czech Republic. The human blood plasma (pooled, mixed gender) in sodium citrate was from VWR International, Czech Republic.

**Ultra-Low Fouling Polymer Brush-Coated Substrates:** The brushes of pCBMAA, pCBAAs, and random copolymers of CBMAA-HPMAA were synthesized on homogenous gold-coated substrates using surface-initiated atom transfer radical polymerization procedure as described elsewhere giving a resulting wet thickness of ≈75 nm,<sup>[30,48]</sup> see also Supporting Information. The model microarray substrates containing squared (50 μm × 50 μm and a spacing of 50 μm) and circular patterns (with a diameter of 20 μm and a spacing of 50 μm) were prepared via an optical lithography. The gold areas of these substrates were modified with pCBAAs brushes using a procedure employed for synthesis of pCBAAs brushes on homogenous gold-coated substrates.

**Cell Culture:** Human hepatocellular carcinoma cell line (Huh7) from the Japanese Collection of Research Bioresources was cultured in Eagle's minimum essential (EMEM) medium (ATCC) supplemented with 10% fetal bovine serum (Thermo Fisher Scientific) and 0.1% v/v penicillin/streptomycin (Sigma, St. Louis, MO) as recommended by the supplier. The cultures were kept in a humidified 5% CO<sub>2</sub> atmosphere at 37 °C.<sup>[49]</sup>

**Cell Viability Assay:** Cytotoxic activity of the brushes was determined quantitatively by a fluorimetric assay utilizing calcein AM and propidium iodide (PI) (both dyes from Thermo Fisher Scientific), as described earlier.<sup>[50]</sup> This cell viability assay was based on the ability of calcein AM to be retained within live cells, inducing an intense uniform green fluorescence and EthD-1 to bind the nuclei of damaged cells, thus producing a bright red fluorescence in dead cells.<sup>[51]</sup> Prior to the cell seeding, all experimental substrates were sterilized by treatment with 70% ethanol for 20 min, followed by UV exposure for 1 h. For all cell experiments in this study, the cells were seeded on the sterilized substrates at an initial density of 25 000 cells cm<sup>-2</sup> and were maintained under standard cell culture conditions (37 °C, 5% CO<sub>2</sub>). Cells were allowed to grow on substrates for 4 days under standard cell culture conditions.<sup>[38]</sup> When the cells were in the exponential growth phase, the monolayer was washed once in PBS and then stained by the addition of calcein AM (1 μM) and PI (50 μg mL<sup>-1</sup>). The nuclei were counterstained with Hoechst 33342 (Thermo Fisher Scientific). After staining, labeled cells were then imaged using spinning disk confocal microscopy (Spin SR, Olympus). ImageJ (NIH) software was used for image processing and fluorescent micrograph quantification. Cell counting was carried out for 10 fields of view per sample. Two independent samples per each surface were assessed for cell proliferation measurements, and the reported values are the mean ± standard error of the mean (SEM). The cell viability was subsequently calculated using the following equation



Viability (%) = (Calcein AM-positive cells) × 100/Hoechst-positive cells

As the positive control, the cells were treated with 20% ethanol for 30 min.

**Immunofluorescence:** For immunostaining, cells after growth on substrates were fixed with 2% formaldehyde and permeabilized with 0.3% Triton X-100. Subsequently, cells were stained with Alexa Fluor 568 Phalloidin (Thermo Fisher Scientific). Nuclei were counterstained with Hoechst 33342. Samples were covered with mounting medium (VECTASHIELD) and analyzed by spinning disk confocal microscopy (Spin SR).

**Confocal Microscopy:** In order to visualize in great detail morphological changes of Huh7 upon their growth on substrates, we utilized the high-resolution spinning disk confocal microscopy (Spin SR). Huh7 were seeded on different substrates for 3 days and labeled with CellMask Green, Hoechst 33342 nuclear stain and MitoTracker Red (all dyes from Thermo Fisher Scientific). Labeled cells were then imaged using the high-resolution spinning disk confocal microscope. Fluorescence images were taken with the acquisition software cellSens (Olympus, Tokyo, Japan). ImageJ software (NIH) was used for image processing.

**Microstructure Arrays Measurements:** The pCBAA-based microstructure arrays were washed with water and sterilized using the UV light. The Huh7 cells were seeded onto them at a density of 5000 cells cm<sup>-2</sup>. After incubation for 72 h, the loosely attached cells were washed out with PBS and the samples were stained with Hoechst (nucleus) as described above. Labeled cells were then imaged using the high-resolution spinning disk confocal microscope as described above.

**Statistical Analysis:** Data obtained from independent experiments are presented as the mean ± SEM. Statistical analysis was performed using one-way analysis of variance and the Newman–Keuls test. Statistical analysis was performed using MaxStat Pro 3.6. Statistical significance was identified if the tested *p* value was less than 0.05 (\*), 0.01 (\*\*), or 0.001 (\*\*\*). When multiple pairwise comparisons were performed, the Bonferroni correction was used to adjust the significance level.

**Ellipsometric Measurements:** Ellipsometric measurements were performed using J.A. Woollam spectroscopic ellipsometer. Wet-coating measurements were done in ultra-pure water as ambient in custom-made cuvettes with angle of incidence of 70°, spectral range of 300–1200 nm with the step of 2 nm. Polymer-coated substrates were rinsed with water and fixed into the cuvette with ultra-pure water. During the measurement, the depolarization effect of the cuvette windows was considered. Dry-coating measurements were performed at the incidence angle of 70° in the spectral range of 300–1300 nm. Polymer-coated substrates were rinsed with ultra-pure water, dried with a stream of nitrogen, and let 1 h to dry properly. Then they were fixed onto sample holder and ellipsometric data were collected. Experimental data were analyzed using spectral multi-oscillator models (variety of Gaussian, Lorentz or Tauc–Lorentz oscillators) with WVASE32 software. The bare gold surface on BK7 glass with Ti adhesive layer was measured and calculated separately to increase the accuracy of the ellipsometric data analysis.

**SPR Measurements:** A four-channel angular SPR system NAVI 200 (with four-channel flow system, equipped with light-emitting diode sources of 670 and 785 nm, BioNavis Ltd., Finland) was employed herein for all the SPR measurements. For this SPR sensor, a 1 mDeg shift in the SPR resonance angle corresponds to a protein coverage of 0.85 ng cm<sup>-2</sup> on the bare sensor surface at the wavelength of 785 nm. The gold-coated SPR substrates with polymer brushes were removed from PBS, washed with ultra-pure water, dried with a stream of nitrogen, and mounted into the SPR sensor. The fouling resistance was assessed from the difference between the sensor response to PBS–NaCl buffer before and after the 10 min exposition with undiluted blood plasma (10 min exposition is a standard time accepted for comparative purposes<sup>[2,5]</sup>) and 150 min exposure to the cell-free EMEM culture medium. A series of four SPR substrates per each type of coating was employed.

The resistance of surfaces to cell adhesion was monitored in real time with SPR. First, the surface was washed with the EMEM cell culture medium. Then one channel was incubated with cells in the cell

culture medium (50 000 cells mL<sup>-1</sup>) while the other remained in the pure medium as the reference channel. The mass of adhered material from the cell culture solution was determined as difference between the measurement and reference channel after 150 min of incubation within the stopped flow.

**Contact Angle Measurements:** The dynamic water contact angle measurements were performed by the sessile drop method using the contact angle goniometer OCA 20 (DataPhysics Instruments, Germany) equipped with SCA 21 software. A 2 µL drop was placed on the surface and its volume was increased and subsequently decreased by 10 µL at a rate of 0.5 µL s<sup>-1</sup>. The shape of the drop was recorded during the advancing and receding of the contact line and fitted with the tangent leaning algorithm to obtain the contact angles in both stages. The measurements were repeated in the three spots.

**Infrared Spectroscopy:** The chemical structure of the brushes was characterized by the polarization modulation-infrared reflection-absorption spectroscopy using the Thermo Scientific Nicolet iS50 FTIR spectrometer equipped with the PEM module. See also Supporting Information.

## Supporting Information

Supporting Information is available from the Wiley Online Library or from the author.

## Acknowledgements

The authors would like to thank Daniel Špaček for making graphical illustrations. This work was supported by Praemium Lumina quaeeruntur of the Czech Academy of Sciences (LQ100101902) and by Operational Program Research, Development, and Education financed by European Structural and Investment Funds and the Czech Ministry of Education, Youth, and Sports (Project No. SOLID21—CZ.02.1.01/0.0/0.0/16\_019/000760).

## Conflict of Interest

The authors declare no conflict of interest.

## Keywords

antifouling, cell–surface interactions, living cells, surface modification, zwitterionic polymer

Received: September 27, 2019  
Revised: December 12, 2019  
Published online: February 11, 2020

- [1] I. Banerjee, R. C. Pangule, R. S. Kane, *Adv. Mater.* **2011**, *23*, 690.
- [2] H. Vaisocherova, E. Brynda, J. Homola, *Anal. Bioanal. Chem.* **2015**, *407*, 3927.
- [3] S. Y. Jiang, K. Ishihara, Y. Iwasaki, J. Vancso, *Langmuir* **2019**, *35*, 1055.
- [4] X. Lin, P. Jain, K. Wu, D. Hong, H.-C. Hung, M. B. O’Kelly, B. Li, P. Zhang, Z. Yuan, S. Jiang, *Langmuir* **2019**, *35*, 1544.
- [5] C. Blaszykowski, S. Sheikh, M. Thompson, *Biomater. Sci.* **2015**, *3*, 1335.
- [6] F. Sun, H. C. Hung, A. Sinclair, P. Zhang, T. Bai, D. D. Galvan, P. Jain, B. Li, S. Jiang, Q. Yu, *Nat. Commun.* **2016**, *7*, 13437.

- [7] B. S. Liu, X. Liu, S. Shi, R. L. Huang, R. X. Su, W. Qi, Z. M. He, *Acta Biomater.* **2016**, *40*, 100.
- [8] R. G. LeBaron, K. A. Athanasiou, *Tissue Eng.* **2000**, *6*, 85.
- [9] J. S. Hayes, E. M. Czekanska, R. G. Richards, *Advances in Biochemical Engineering Biotechnology*, Vol. 126 (Eds: C. Kasper, F. Witte, R. Pörtner), Springer, Berlin, Heidelberg **2011**.
- [10] M. P. Lutolf, P. M. Gilbert, H. M. Blau, *Nature* **2009**, *462*, 433.
- [11] S. M. Oliveira, N. M. Alves, J. F. Mano, *J. Adhes. Sci. Technol.* **2014**, *28*, 843.
- [12] L. C. Xu, C. A. Siedlecki, *Biomaterials* **2007**, *28*, 3273.
- [13] Y. Arima, H. Iwata, *Biomaterials* **2007**, *28*, 3074.
- [14] A. Ranella, M. Barberoglou, S. Bakogianni, C. Fotakis, E. Stratakis, *Acta Biomater.* **2010**, *6*, 2711.
- [15] J. Ishikawa, H. Tsuji, H. Sato, Y. Gotoh, *Surf. Coat. Technol.* **2007**, *201*, 8083.
- [16] M. R. Bet, G. Goissis, S. Vargas, H. S. Selistre-de-Araujo, *Biomaterials* **2003**, *24*, 131.
- [17] H. Y. Chang, C. C. Huang, K. Y. Lin, W. L. Kao, H. Y. Liao, Y. W. You, J. H. Lin, Y. T. Kuo, D. Y. Kuo, J. J. Shyue, *J. Phys. Chem. C* **2014**, *118*, 14464.
- [18] X. Sun, H. Wang, Y. Wang, T. Gui, K. Wang, C. Gao, *Biosens. Bioelectron.* **2018**, *102*, 63.
- [19] B. L. Leigh, E. Cheng, L. Xu, C. Andresen, M. R. Hansen, C. A. Guymon, *Biomacromolecules* **2017**, *18*, 2389.
- [20] A. E. Rodda, F. Ercole, V. Glattauer, J. Gardiner, D. R. Nisbet, K. E. Healy, J. S. Forsythe, L. Meagher, *Biomacromolecules* **2015**, *16*, 2109.
- [21] B.-Y. Yu, J. Zheng, Y. Chang, M.-C. Sin, C.-H. Chang, A. Higuchi, Y.-M. Sun, *Langmuir* **2014**, *30*, 7502.
- [22] A. C. H. Pape, B. D. Ippel, P. Y. W. Dankers, *Langmuir* **2017**, *33*, 4076.
- [23] O. J. G. M. Goor, J. E. P. Brouns, P. Y. W. Dankers, *Polym. Chem.* **2017**, *8*, 5228.
- [24] H. Chen, M. Zhang, J. Yang, C. Zhao, R. Hu, Q. Chen, Y. Chang, J. Zheng, *Langmuir* **2014**, *30*, 10398.
- [25] F. Yang, Y. Liu, Y. Zhang, B. Ren, J. Xu, J. Zheng, *Langmuir* **2017**, *33*, 13964.
- [26] L. Ye, Y. Zhang, Q. Wang, X. Zhou, B. Yang, F. Ji, D. Dong, L. Gao, Y. Cui, F. Yao, *ACS Appl. Mater. Interfaces* **2016**, *8*, 15710.
- [27] Y.-N. Chou, T.-C. Wen, Y. Chang, *Acta Biomater.* **2016**, *40*, 78.
- [28] W. Li, Q. Liu, L. Liu, *J. Biomater. Sci., Polym. Ed.* **2014**, *25*, 1730.
- [29] T. Bai, F. Sun, L. Zhang, A. Sinclair, S. Liu, J. R. Ella-Menye, Y. Zheng, S. Jiang, *Angew. Chem., Int. Ed.* **2014**, *53*, 12729.
- [30] H. Vaisocherova-Lisalova, F. Surman, I. Visova, M. Vala, T. Springer, M. L. Ermini, H. Sipova, P. Sedivak, M. Houska, T. Riedel, O. Pop-Georgievski, E. Brynda, J. Homola, *Anal. Chem.* **2016**, *88*, 10533.
- [31] B. Smolkova, M. Lunova, A. Lynnyk, M. Uzhytchak, O. Churpita, M. Jirsa, S. Kubinova, O. Lunov, A. Dejneka, *Cell. Physiol. Biochem.* **2019**, *52*, 119.
- [32] H. Lisalova, E. Brynda, M. Houska, I. Visova, K. Mrkvoval, X. C. Song, E. Gedeonova, F. Surman, T. Riedel, O. Pop-Georgievski, J. Homola, *Anal. Chem.* **2017**, *89*, 3524.
- [33] D. Kotlarek, M. Vorobii, W. Ogieglo, W. Knoll, C. Rodriguez-Emmenegger, J. Dostalek, *ACS Sens.* **2019**, *4*, 2109.
- [34] T. Ederth, P. Claesson, B. Liedberg, *Langmuir* **1998**, *14*, 4782.
- [35] J. Israelachvili, R. Pashley, *Nature* **1982**, *300*, 341.
- [36] J. Homola, *Chem. Rev.* **2008**, *108*, 462.
- [37] S. March, V. Ramanan, K. Trehan, S. Ng, A. Galstian, N. Gural, M. A. Scull, A. Shlomai, M. M. Mota, H. E. Fleming, S. R. Khetani, C. M. Rice, S. N. Bhatia, *Nat. Protoc.* **2015**, *10*, 2027.
- [38] M. Jelinek, T. Kocourek, K. Jurek, M. Jelinek, B. Smolkova, M. Uzhytchak, O. Lunov, *Nanomaterials*, **2019**, *9*, 451.
- [39] A. Hucknall, S. Rangarajan, A. Chilkoti, *Adv. Mater.* **2009**, *21*, 2441.
- [40] R. H. Harrison, J. A. Steele, R. Chapman, A. J. Gormley, L. W. Chow, M. M. Mahat, L. Podhorska, R. G. Palgrave, D. J. Payne, S. P. Hettiaratchy, I. E. Dunlop, M. M. Stevens, *Adv. Funct. Mater.* **2015**, *25*, 5748.
- [41] D. Chen, M. Wu, B. Li, K. Ren, Z. Cheng, J. Ji, Y. Li, J. Sun, *Adv. Mater.* **2015**, *27*, 5882.
- [42] E. Ostuni, R. G. Chapman, M. N. Liang, G. Meluleni, G. Pier, D. E. Ingber, G. M. Whitesides, *Langmuir* **2001**, *17*, 6336.
- [43] B. D. Fairbanks, H. Thissen, G. Maurdev, P. Pasic, J. F. White, L. Meagher, *Biomacromolecules* **2014**, *15*, 3259.
- [44] W. Huang, B. Anvari, J. H. Torres, R. G. LeBaron, K. A. Athanasiou, *J. Orthop. Res.* **2003**, *21*, 88.
- [45] S. Hong, E. Ergezen, R. Lec, K. A. Barbee, *Biomaterials* **2006**, *27*, 5813.
- [46] T. Ishizaki, N. Saito, O. Takai, *Langmuir* **2010**, *26*, 8147.
- [47] A. I. Neto, C. A. Custodio, W. L. Song, J. F. Mano, *Soft Matter* **2011**, *7*, 4147.
- [48] S. Zurcher, D. Wackerlin, Y. Bethuel, B. Malisova, M. Textor, S. Tosatti, K. Gademann, *J. Am. Chem. Soc.* **2006**, *128*, 1064.
- [49] M. Lunova, V. Zablotkii, N. M. Dempsey, T. Devillers, M. Jirsa, E. Sykova, S. Kubinova, O. Lunov, A. Dejneka, *Integr. Biol.* **2016**, *8*, 1099.
- [50] A. Lynnyk, M. Lunova, M. Jirsa, D. Egorova, A. Kulikov, S. Kubinova, O. Lunov, A. Dejneka, *Biomed. Opt. Express* **2018**, *9*, 1283.
- [51] N. G. Papadopoulos, G. V. Z. Dedoussis, G. Spanakos, A. D. Gritzapis, C. N. Baxevanis, M. Papamichail, *J. Immunol. Methods* **1994**, *177*, 101.

# Appendix VI

Víšová, I., M. Vrabcová, M. Forinová, Y. Zhigunová, V. Mironov, M. Houska, E. Bittrich, K.-J. Eichhorn, H. Hashim, P. Schovánek, A. Dejneka and H. Vaisocherová-Lísalová

**Surface Preconditioning Influences the Antifouling Capabilities of Zwitterionic and Nonionic Polymer Brushes.**

*Langmuir* **36**(29) (2020): 8485-8493

# Surface Preconditioning Influences the Antifouling Capabilities of Zwitterionic and Nonionic Polymer Brushes

Ivana Víšová, Markéta Vrabcová, Michala Forinová, Yulia Zhigunová, Vasilii Mironov, Milan Houska, Eva Bittrich, Klaus-Jochen Eichhorn, Hisham Hashim, Petr Schovánek, Alexandr Dejneka, and Hana Vaisocherová-Lísalová\*



Cite This: *Langmuir* 2020, 36, 8485–8493



Read Online

ACCESS |



Metrics & More

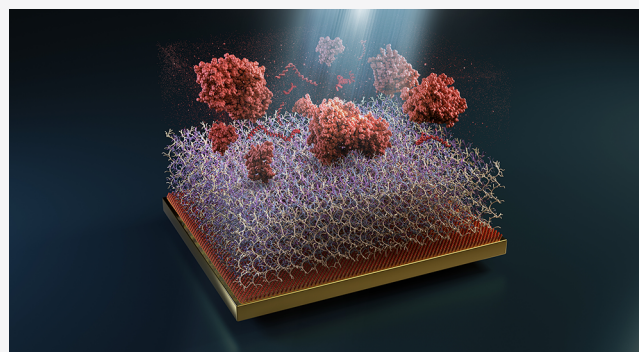


Article Recommendations



Supporting Information

**ABSTRACT:** Polymer brushes not only represent emerging surface platforms for numerous bioanalytical and biological applications but also create advanced surface-tethered systems to mimic real-life biological processes. In particular, zwitterionic and nonionic polymer brushes have been intensively studied because of their extraordinary resistance to nonspecific adsorption of biomolecules (antifouling characteristics) as well as the ability to be functionalized with bioactive molecules. However, the relation between antifouling behavior in real-world biological media and structural changes of polymer brushes induced by surface preconditioning in different environments remains unexplored. In this work, we use multiple methods to study the structural properties of numerous brushes under variable ionic concentrations and determine the impact of these changes on resistance to fouling from undiluted blood plasma. We describe different mechanisms of swelling, depending on both the polymer brush coating properties and the environmental conditions that affect changes in both hydration levels and thickness. Using both fluorescent and surface plasmon resonance methods, we found that the antifouling behavior of these brushes is strongly dependent on the aforementioned structural changes. Moreover, preconditioning of the brush coatings (incubation at a variable salt concentration or drying) prior to biomolecule interaction may significantly improve the antifouling performance. These results suggest a new simple approach to improve the antifouling behavior of polymer brushes. In addition, the results herein enhance the understanding for improved design of antifouling and bioresponsive brushes employed in biosensor and biomimetic applications.



## 1. INTRODUCTION

Surface-grafted polymer brushes, that is, thin polymer films covalently tethered via one end to a substrate, represent a powerful tool for the design of advanced functional surfaces.<sup>1</sup> Aided by advances in surface-initiated polymerization techniques, the molecular structure of a polymer brush can be fine-tuned in composition and density, where brushes with a varying degree of biochemical functionality can be created on many types of surfaces, with areas ranging from  $\sim 10$  cm<sup>2</sup> down to the nanometer scale.<sup>2</sup> In addition to its functionality, these techniques allow for a high degree of control over the physical and chemical characteristics of a material's surface.<sup>3,4</sup>

One tremendously promising use of polymer brushes lies in the development of antifouling coatings, that is, surfaces that inhibit the nonspecific deposition of the biological material.<sup>5–8</sup> Such undesirable fouling, caused by exposure to complex media having the unknown composition (e.g., blood serum and plasma), can inhibit the surface functionality and potentially lead to its failure. Many applications in biology and bioanalytical sciences involve the exposure of a surface to

complex media, and antifouling coatings are now an essential component for many applications, including biosensors and analytical methods,<sup>9</sup> tissue engineering,<sup>10</sup> medical implants,<sup>11</sup> drug delivery,<sup>12</sup> and cell culture.<sup>13</sup>

Among the previously developed antifouling surfaces, zwitterionic polymer brushes are perhaps the most versatile, especially when used in biorecognition platforms for the analysis of biological media.<sup>3,6,14–16</sup> In addition to having antifouling capabilities, zwitterionic polymer brushes are biocompatible, highly hydratable, have long term stability, and provide high biorecognition element loading capacity.<sup>17–20</sup>

Among other factors, there are two key structural parameters that are closely linked to the antifouling capabilities of a

Received: April 7, 2020

Revised: June 2, 2020

Published: June 8, 2020



polymer brush: the brush's hydration capabilities and its thickness.<sup>6,21–23</sup> It has been shown that the fouling resistance of a polymer brush will increase with increase in the brush's hydration level,<sup>24,25</sup> where tightly bound water molecules in the coating present an extra energy barrier for other molecules to be adsorbed. In addition, many studies have shown that fouling resistance increases with increasing brush thickness;<sup>26</sup> however, the bulk of previous data supporting this claim regard measurements of the dried brush thickness.<sup>17,27</sup> Highly hydratable coatings can exhibit a remarkable degree of swelling (the thickness change from a dry to wet state),<sup>28</sup> and as shown in the data herein, small differences in a brush's monomer component can lead to substantial differences in swelling. Therefore, for effective comparison of different brushes, it is necessary to consider the brush thickness in a liquid environment.

It is clear that when exposed to the complex nature of a real-world environment, an antifouling coating can be exposed to a variety of physical and chemical conditions, including changes in pH, ionic concentration and type, environment viscosity, and enzymatic activity. Several studies have shown that such changes in environmental conditions can modify fundamental properties of a polymer brush, but only a few studies focused particularly on zwitterionic polymers.<sup>29</sup> Leng et al. demonstrated that hydration levels of zwitterionic polymer brushes were affected by several environmental parameters, including ionic strength, ionic size, charge, and pH.<sup>30</sup> Zhang et al. studied fouling resistance changes of poly(carboxybetaine acrylamide) (pCBAA) in different salt and pH environments on single protein solution; no complex biological media were employed. Yang et al. synthesized a switchable antifouling polymer [poly(3-(1-(4-vinylbenzyl)-1*H*-imidazol-3-ium-3-yl)-propane-1-sulfonate)] and demonstrated its antifouling properties in different salt environments using undiluted blood plasma.<sup>31</sup> Clearly, it is expected that because of strongly adaptive brush behavior, environmental changes will lead to changes in the polymer brush structures resulting in affecting the antifouling properties. However, it is rather difficult to completely assess such complex relationships based on existing studies dealing with either single-coating types or perform only limited fouling resistance characterization using single-protein solutions instead of complex biological media. Therefore, a thorough understanding of these interrelated mechanisms remains unclear and needs to be explored using a broader set of antifouling brush structures.

In this work, we pursue an extensive research on the effects of structural changes of a set of antifouling zwitterionic and nonionic polymer brushes on surface resistance to fouling from undiluted blood plasma using a combination of ellipsometric, quartz crystal microbalance (QCM), fluorescence, and surface plasmon resonance (SPR) data. The structural changes were induced by surface preconditioning in various environmental conditions including distinct salt concentrations and surface drying/rehydrating. The polymer brushes we used (Figure 1) include the carboxy-functional zwitterionic pCBAA and poly(carboxybetaine methacrylamide) (pCBMAA), sulfo-functional zwitterionic poly(sulfobetaine methacrylamide) (pSBMAA), and the nonionic hydroxyl-functional poly(*N*-(2-hydroxypropyl) methacrylamide) (pHPMAA). This series of antifouling coatings were selected to provide a representative set of antifouling and functionalizable homopolymer brushes with comparable architectures, varying in monomer structures

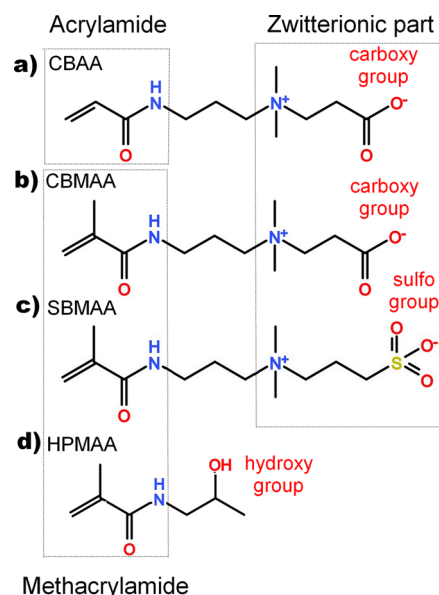


**Figure 1.** Scheme of monomers used for the polymer coatings used in this study, highlighted with important structure characteristics: we used two zwitterionic carboxy-functionalized monomers: (a) CBAA and (b) CBMAA; (c) zwitterionic sulfo-functionalized SBMAA and (d) nonionic HPMAA.

(mostly in functional groups), hence providing a representative set of different surface physicochemical properties.

Specifically, we demonstrate the influence of the ionic strength of the environmental solution on the physical properties of each polymer brush coating, including wet thickness, hydration, and swelling leading to a significant change of antifouling properties. We show that the antifouling properties of zwitterionic and nonionic brushes are strongly influenced by distinct hydration mechanisms. Specifically, based on data taken from both ellipsometry and QCM measurements, we present a hypothesis regarding the mechanism of hydration for each coating. The effect of monovalent and bivalent ions is discussed. In combination with SPR and fluorescence measurements, we relate our results on structural changes to fouling studies using undiluted blood plasma. Finally, discussing an important practical aspect, we compare the effects of drying and rehydrating each coating on their antifouling properties.

## 2. EXPERIMENTAL SECTION

**2.1. Reagents.** We used ultrapure Millipore Q water (18.0 MΩ·cm, Milli-Q) for buffer preparation, measurements in water, and all washing steps. HEPES [4-(2-hydroxyethyl)-1-piperazineethanesulfonic acid; hereafter called buffer], 1,4,8,11-tetramethyl-1,4,8,11-tetraazacyclotetradecane (Me4Cyclam, 98%), phosphate-buffered saline (0.01 M phosphate, 0.138 M sodium chloride, and 0.0027 M potassium chloride), NaCl, MgCl<sub>2</sub>, CuCl (≥99.995%), CuCl<sub>2</sub> (99.999%), and methanol (≥99.9%) were from Sigma-Aldrich, Czech Republic. The initiator ω-mercaptoundecylbromoisobutyrate was from ProChimia, Poland. Carboxybetaine acrylamide (CBAA), carboxybetaine methacrylamide (CBMAA), *N*-(2-hydroxypropyl) methacrylamide (HPMAA), and sulfobetaine methacrylamide (SBMAA) monomers were from Specific Polymers, France. Tetrahydrofuran (purity ≥ 99.9%) and ethanol (purity of 96%) were from Penta, Czech Republic. The Alexa Fluor 568 Protein Labeling Kit was from Thermo Fisher Scientific, USA. QCM crystals with the evaporated gold layer were from Krystaly, Czech Republic.

The human blood plasma (pooled, mixed gender) in sodium citrate was from VWR International, Czech Republic.

**2.2. Polymer Brush Coating Preparation.** Polymer brushes were prepared by surface-initiated atom-transfer radical polymerization using an optimized procedure and a custom-made polymerization system developed in house. More details are presented in the [Supporting Information](#). The monomers used in the polymerization for each brush are shown in [Figure 1](#).

**2.3. Refractometric Measurements of Buffers.** All solutions used in this study were prepared in stock, and their optical constants were characterized by a digital multiwavelength refractometer (DSR- $\lambda$ , Schmidt + Haensch GmbH & Co., Berlin, Germany) measured at room temperature (25 °C). For each solution (water, buffer, and buffer with added salts), we measured the refractive index (RI) at six different wavelengths. Next, these data were extrapolated in the full region of 350–800 nm, taking into account the standard dispersion function of water. Experimental measurements for all solutions, along with fitted (and extrapolated) RI data, are shown in [Figure S2](#) in the [Supporting Information](#).

**2.4. Spectroscopic Ellipsometry and QCM in Liquid Environments.** Ellipsometry is a sensitive surface technique that, when combined with an appropriate modeling procedure, can accurately measure several characteristic parameters of thin polymer brush films, including effective thickness, RI, layer density, surface roughness, and relative structural composition.<sup>32</sup> In this work, ellipsometric measurements were performed using a spectroscopic ellipsometer (VASE, J.A. Woollam, Lincoln, USA) in the spectral range of 3.4–1.5 eV with steps of 0.008 eV and a 70° incidence angle. Measurements were taken at room temperature using a custom-made cell (covered to prevent water evaporation) having an incorporated sample holder to ensure that all data were taken from the same sample spot across all used liquids ([Figure S1](#), more details in [Supporting Information](#)). For a reference, we used a bare Au-coated BK7 glass chip from the same batch as the substrates used for polymer coating. Data analysis was performed with WVASE32 software. Experimental data were fitted with a single- or double-oscillator model (variety of Gaussian and Tauc–Lorentz oscillators), depending on the brush. Model fitting to experimental data with the fits of thickness uniqueness is shown in [Figure S3](#) in the [Supporting Information](#).

QCM measurements were performed at room temperature using a custom-made two-channel apparatus consisting of a portable QCM Analyzer (KEVA, Brno, Czech Republic) and a microfluidic-based crystal holder, previously described in detail.<sup>33</sup> Au-coated QCM crystals with a resistance of max. 30  $\Omega$  and frequency range around 10,000 kHz were used for polymer-brush coated sensor preparation.

More details about QCM and ellipsometric measurements are provided in the [Supporting Information](#).

**2.5. Fouling Resistance Studies by Fluorescent Microscopy.** Coatings from the same batches as those used for ellipsometric studies were immersed in buffer with different concentrations of sodium chloride (0–1000 mM) for 20 min. This incubation time was found to be long enough to complete the surface response to environmental changes as confirmed by spectroscopic ellipsometry (data not shown). Afterward, undiluted human plasma was applied for 10 min and then chips were washed with plain buffer (to avoid the electrostatically induced loss of nonspecifically deposited material). The plasma incubation time of 10 min was selected as it corresponds to a typical detection time used in biosensor applications.<sup>34</sup> All substrates were then labeled with Alexa Fluor 568 using the Alexa Fluor 568 Protein Labeling Kit. Labeled samples were then imaged using a high-resolution spinning disk confocal microscope (Spin SR, Olympus), using the acquisition software cellSens (Olympus, Tokyo, Japan) and processed using ImageJ (NIH). For each polymer type, we measured mean gray values on 30 areas at random positions; this value is proportional to the nonspecifically adsorbed amount of protein (i.e., fouling) on each surface.

**2.6. Fouling Resistance Studies by SPR.** SPR fouling studies were performed on an angular MP-SPR with a four-channel microfluidic system, equipped with light-emitting diode sources of 670 and 785 nm wavelengths (BioNavis Ltd., Finland). To transform

angular units (corresponding to a shift in the SPR resonance angle) to mass units of proteins adsorbed on the surface, we used a value of  $0.001^\circ = 0.85 \text{ ng/cm}^2$  (785 nm). More details on the SPR experiments are provided in the [Supporting Information](#).

### 3. RESULTS AND DISCUSSION

**3.1. Probing Hydrated Polymer Brush Structures by Spectroscopic Ellipsometry and QCM.** The spectroscopic ellipsometry was employed to study four different antifouling hydrophilic polymer brush coatings in different ionic strength liquid environments. The monomers for these polymers are shown in [Figure 1](#): the structures of carboxy-functional pCBAA and pCBMAA differ only in the presence of a methyl group in the backbone; the permanent negative charge of pSBMAA is given by a sulfo-group (more polar than the carboxy-group), and the nonionic pHPMAA-bearing hydroxyl groups is uncharged ([Figure 1](#)). The spectral characteristics of all prepared polymers were measured by infrared spectroscopy ([Figure S5](#)).

To provide reliable ellipsometry characteristics of polymer brushes, accurate model input parameters are an absolute prerequisite for reliable calculation of these parameters, especially regarding highly hydratable polymer brush structures.<sup>28</sup> Therefore, all solutions that were used in a polymer brush environment were prepared in stock and characterized by refractometric measurements prior to ellipsometric data processing. Additionally, the hardware was optimized to ensure accurate measurements, the details of which can be found in the [Supporting Information](#).

Previous work has typically used either the Cauchy or Cauchy–Urbach models for fitting data regarding dielectric molecular layers of polymer structures.<sup>35–38</sup> Conversely, for the more complex zwitterionic brushes used herein, the simple parameters of these models were not found to be sufficient for a best-fit across all measured wavelengths. Moreover, we found that no universal fitting model was sufficient when used alone. Therefore, in order to reflect all the potential differences in brush architectures and thus reliably perform ellipsometric data analysis, we optimized the fitting model for each type of brush structure. Specifically, we used a single-oscillator (Tauc–Lorentz) model for pCBAA and pSBMAA brushes, and a double-oscillator (Gaussians) model for pCBMAA and pHPMAA brushes. Further details on experimental procedures, as well as example spectra ([Figure S3](#)), can be found in the [Supporting Information](#).

All of the brushes in this study had a wet thickness between 60 and 130 nm, for which we used the abovementioned oscillators for data analysis. To characterize the structure in more detail, we prepared a set of thicker pCBAA brushes (206–242 nm). Ellipsometric analysis of these brushes (using a graded layer oscillator model) revealed a gradient RI profile, where the measured RI decreased monotonically away from the surface ([Figure S4](#), [Supporting Information](#)). As RI correlates with the density of the polymer brush, these results suggest that these brushes have a pseudo-ordered structure, where the level of structure periodicity is higher near the gold surface (with polymer chains fixed to the initiator layer) and diminished toward the brush/water blurred interface. More information and all measured spectra can be found in the [Supporting Information](#).

To gain insights into the inner structure of the hydrated polymer brushes, the samples were exposed to HEPES buffer with different concentrations of added monovalent and

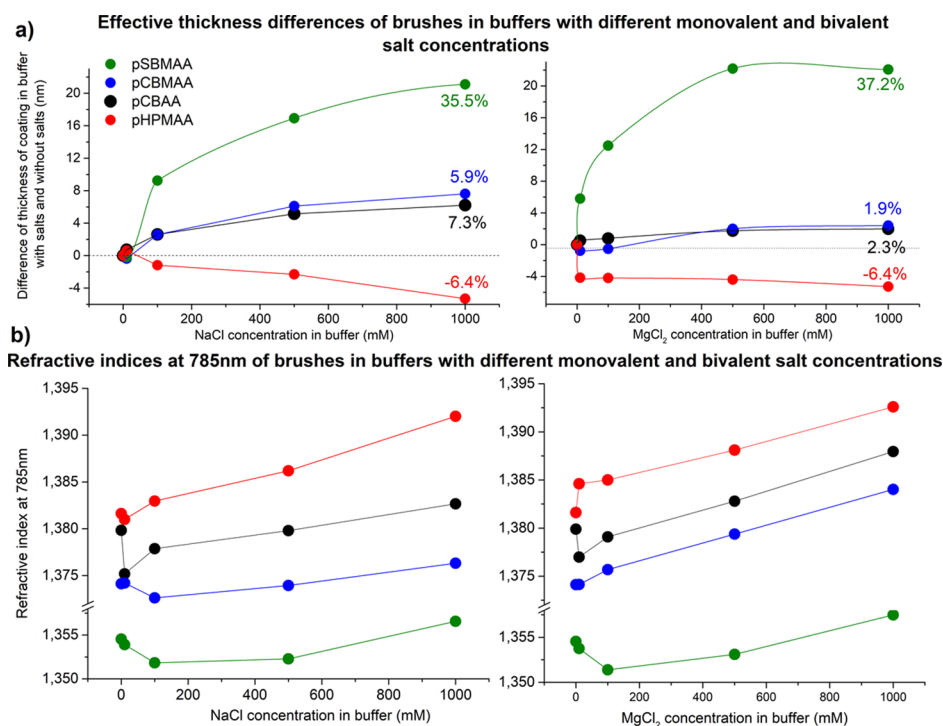


**Figure 2.** Changes in effective thickness and RI (785 nm) of polymer brushes at varying ionic strengths. The effective thickness changes are given as difference between the thicknesses of polymer brushes in buffers with added salts and buffer without added salts. The original thicknesses in buffer without added salts were 86 nm for pCBAA, 129 nm for pCBMAA, 60 nm for pSBMAA, and 82 nm for pHPMAA.

bivalent chloride salts. Other buffer parameters (pH 7.4—physiological pH of normal arterial blood, 25 °C—room temperature) were kept constant.

We monitored changes in the effective thickness and RI using fits to data collected by spectroscopic ellipsometry; this data is shown in Figure 2 for all four polymer brushes. Data for the %-increase is shown for the 1 M data, calculated from the thickness measured in buffer with no added salts. For better clarity, Figure 2 shows RIs only for a wavelength of 785 nm (the wavelength used in SPR experiments); the total set of the RI spectra for wavelengths from 350 to 850 nm can be found in the Figure S6 in the Supporting Information.

With increasing ionic strength, all zwitterionic coatings exhibit an increase in effective thickness, whereas the effective thickness of nonionic pHPMAA systematically decreases. The pCBAA and pCBMAA brushes exhibited an increase in effective thicknesses of 7.3 and 5.9% in 1 M NaCl, with shorter increases of 2.3 and 1.9% in 1 M MgCl<sub>2</sub>, respectively. In comparison, thickness increases for pSBMAA were 5–6 times higher for NaCl and 15 times higher for MgCl<sub>2</sub> (35.5 and 37.2%, respectively).

For carboxy-functional zwitterionic coatings (pCBAA, pCBMAA), increases in effective thickness were about 3 times higher in NaCl than in MgCl<sub>2</sub> solutions, indicating a higher response of both structures to the concentration of monovalent compared to bivalent salt ions. On the other hand, the thicknesses of both pHPMAA and pSBMAA brushes were only weakly affected by the ion type. The response to ionic concentration was the most significant for pSBMAA compared to other polymer brushes.

In higher ionic strength environments, all of the zwitterionic brushes had increased thickness with increasing salt concentration, which was accompanied by increases in the RI (Figures 2b, S6). These results suggest that at higher ionic strength, a

portion of the water molecules in the inner zwitterionic brush structure is substituted or appended with salt-based counterions, ordering themselves around charged groups inside the brush structure and shielding internal electrostatic interactions among chains. This is consistent with prior research, where Leng et al. showed that sum frequency generation vibrational spectroscopy water signals in zwitterionic polymers decreased with increasing NaCl concentration,<sup>30</sup> indicating the disruption of water molecule ordering and increasing amounts of ions binding to the polymers. Hence, zwitterionic brushes will tend to grow thicker and optically denser because of changes in electrostatic interactions between polymer chains and salt ions, redistribution of water bonds, and changes in ambient composition within the polymer structure (Figure S9). On the other hand, nonionic pHPMAA showed systematic decrease in thickness and increase in RI with increasing salt concentration. Such shrinking suggests a different swelling mechanism, incorporating mostly rearrangement of water molecules within the structure and dehydration.

Looking at detailed differences in pCBAA and pCBMAA responses to different ionic strength environments, we can observe a slightly lower tendency for pCBMAA to grow thicker with increasing salt concentration. pCBAA in 1 M NaCl environment exhibits 1.2 times higher thickness increase compared to pCBMAA (similar results for MgCl<sub>2</sub>). We assume that this effect can be caused by the extra methyl group, that is, increased hydrophobicity of the pCBMAA backbone structure, which might bring higher spatial stability and rigidity to the whole brush architecture. In addition, a different affinity of salt ions to methacrylamide compared to acrylamide backbone can be expected. As discussed later, the QCM data in Figure 3 support this hypothesis, showing a slightly lower amount of both salt ion types bound in the pCBMAA structure compared to the pCBAA.

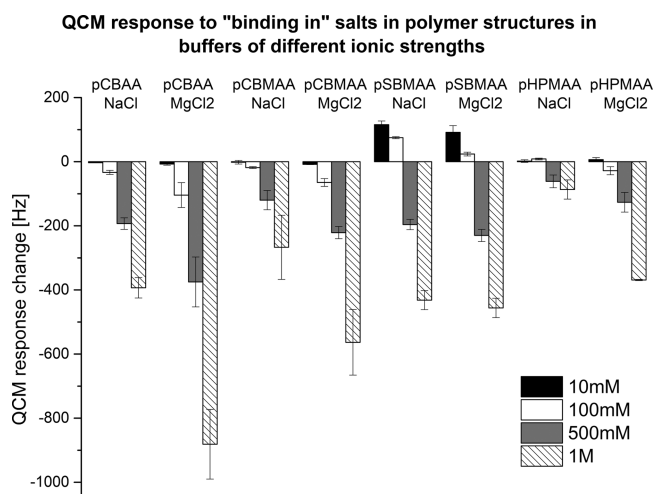


**Figure 3.** QCM response changes of polymer brush-coated quartz crystals in different ionic strength environments with respect to buffer without additional salts.

In pSBMAA, the increment to thickness is up to an order of magnitude higher than the carboxy-group terminated polymers, perhaps caused by the higher polarity of the sulfo-groups in comparison to carboxy-groups. There might also be a remarkable influence on packing density: the pSBMAA shows a significantly lower RI than carboxy-terminated brushes (Figures 2b, S6), suggesting a significantly lower packing density of pSBMAA compared to all studied zwitterionic coatings. Taking into account higher swelling ratio (Table 1) and lower RI (Figure 2b), we hypothesize that instead of being grafted densely, pSBMAA seems to contain longer chains bundled tightly at lower salt ion concentrations and loosening at higher salt ion concentrations when electrostatic interactions between the chains are screened by a higher ionic strength environment.

In all zwitterionic structures, there is a clear dip in the RI in the region of 10–100 mM for both monovalent and divalent salt ion concentrations (Figures 2b and S6) accompanied by systematical increase of the brush thickness. We assume that this dip is related to two competitive processes occurring in the structure during swelling. In particular, it is anticipated that the zwitterionic coatings occupy an equilibrium layout in buffer solution without added salts. Upon increasing ionic strength, electrostatic interactions between the chains become screened by salt counterions and the structure becomes loosened: the RI decreases while the thickness grows. When the concentration of salt ions reaches a threshold value, the binding of counterions into the brush structure starts to compensate for

RI drops caused by loosening of polymer chains, and the RI starts to increase.

We performed additional QCM experiments to further confirm the hypothesis about increasing salt concentration in brush structures at higher ionic strengths. In contrast to ellipsometry or SPR, QCM is insensitive to RI changes. Rather, changes in the QCM response are related to the mass of salt ions bound in the polymer brush structure, the amount of water repelled from the structure, and changes in viscosity of area around the crystal surface (related to the degree of swelling).

A trend of decreasing QCM frequency with increasing ionic strength was observed for all studied types of polymer brushes, suggesting an increasing mass of the salt ions bound to the polymer structures with increasing ionic strength. For all salt concentrations in all samples, the sensor response decrease for  $\text{MgCl}_2$  is greater or equal to NaCl. Taking into account that the molecular weight of the  $\text{MgCl}_2$  molecule is 1.6 times higher than that for NaCl, similar affinities to monovalent and divalent salt ions were observed for carboxybetaines. Conversely, in pSBMAA, the responses are nearly equal, suggesting a higher affinity of the coating to NaCl. The opposite trend was observed in pHPMAA, where the affinity to  $\text{MgCl}_2$  seems to be slightly higher than NaCl (1 M data).

The combination of results shown in Figure 3 with the dry thicknesses of coatings (Table 1) suggests that a significantly lower amount of salt ions was bound in the pHPMAA brush (normalized by dry thickness) in comparison with any zwitterionic brushes. This is in line with the hypothesis of different swelling mechanisms for zwitterionic and nonionic structures. In particular, a decrease of pHPMAA thickness with increasing ionic strength is related mostly to dehydration; only a limited amount of salt ions is attached to the structure. For the zwitterionic brushes, the increase of thickness (with increasing ionic strength) is strongly associated with an increasing amount of salt ions bound in the polymer brush coating.

Interestingly, we observed an increase in the QCM response for pSBMAA for both 10 mM and 100 mM salt ion concentrations (Figure 3). We suggest that this effect is connected with the previously described lower pSBMAA packing density and its dynamics in an ionic environment. Pertaining to the rapid change in brush thickness ( $\leq 100$  mM) in solutions of both salts (Figure 2a): with no added salts, the polymer chains are likely more coil-like near the crystal surface, and at 10 mM, the chains start to uncoil, transferring some mass away from the crystal surface. As the ionic strength of 10 mM salt is relatively low, the effect of binding salt ions in the structure cannot counterweight the effect of chain straightening, and the QCM signal increases. Above 100 mM, the effects

**Table 1.** Comparison of Effective Thickness before Drying and after Rehydration

	pCBAA	pCBMAA	pSBMAA	pHPMAA
effective wet thickness $w_{\text{non-dried}}$ (nm)	119.0 $\pm$ 0.1 <sup>b</sup>	119.2 $\pm$ 0.2 <sup>b</sup>	67.3 $\pm$ 0.8 <sup>b</sup>	82.5 $\pm$ 0.4 <sup>b</sup>
RI $w_{\text{non-dried}}$	1.376	1.373	1.355	1.385
effective dry thickness (nm)	39.3 $\pm$ 0.5 <sup>b</sup>	38.8 $\pm$ 0.4 <sup>b</sup>	16.7 $\pm$ 0.1 <sup>b</sup>	47.7 $\pm$ 0.2 <sup>b</sup>
effective wet thickness $w_{\text{rehydrated}}$ (nm)	125.4 $\pm$ 0.2 <sup>b</sup>	122.1 $\pm$ 0.2 <sup>b</sup>	73.6 $\pm$ 1.1 <sup>b</sup>	85.7 $\pm$ 0.2 <sup>b</sup>
RI $w_{\text{rehydrated}}$	1.373	1.372	1.353	1.378
swelling <sup>a</sup> (%)	319	315	442	180

<sup>a</sup>Swelling was assessed as percentage of rehydrated effective thickness from dry effective thickness. <sup>b</sup>Errors of the effective thicknesses in the table are the errors of parameters given by fit of the ellipsometric data.



are equal and with higher ionic strength, salt-ion binding starts to predominate. This explanation is supported also by Figure 2b, where a decrease of the RI from 0 to 100 mM (“unbounding”) can be seen; with further increases in ionic strength, the RI starts to increase (as salt ions become bound into the structure).

**3.2. Fouling Resistance to Undiluted Blood Plasma Influenced by Preconditioning of Brushes at Different Salt Concentrations.** The fluorescent microscopy was employed to assess the influence of the structural changes of brushes exposed to different salt concentrations (i.e., preconditioning) on the fouling resistance. This method possesses a sensitivity independent of any thickness changes of the brush coating, including those induced by the changes in the surrounding environment. The results of these experiments (Figures 4, S8) show that fouling resistance of the polymer

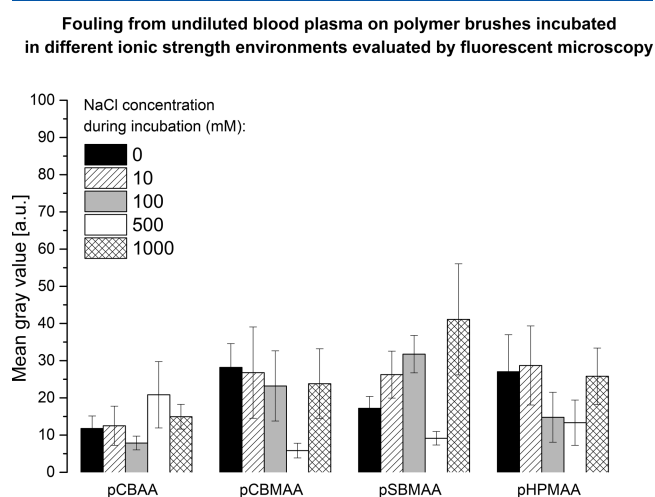


**Figure 4.** Data from fluorescent microscopy measurements for the fouling resistance to undiluted human blood plasma of different polymer brushes incubated (before exposure to plasma) in buffers with different NaCl concentrations.

brushes studied herein is strongly influenced by structural changes caused by preconditioning of the coatings in NaCl solutions with different ionic strengths. Differences between acrylamide- and methacrylamide-based coatings can be observed. The optimum concentration of NaCl in the brush environment before injection of undiluted plasma to achieve a maximum surface fouling resistance was found to be 500 mM NaCl for all methacrylamide-based brushes. On the other hand, the optimum NaCl concentration for the acrylamide-based brush was 100 mM, with fouling that is comparable with the lowest level achieved by the methacrylamide brushes. These data may help to optimize the preconditioning of the coatings to achieve better fouling resistances. It is worth noting, though, that the optimum NaCl concentrations may differ for some types of polymer brushes from physiological levels (ca. 0.15 M).

Zhang et al. observed that protein adsorption to pCBAA tends to decrease in a higher ionic strength environment;<sup>39</sup> however, that study was performed with single protein solutions, and more importantly, the salts were also present in the buffer during the fouling measurement. Hence, electrostatic interactions could have been shielded by higher ionic strengths, leading to a decrease of nonspecific bindings. Moreover, theoretical predictions indicate that polymeric

zwitterions tend to become more hydrated as the NaCl concentration of the environment increases.<sup>22</sup> Nevertheless, it is difficult to straightforwardly apply these findings from these valuable studies for coatings employed in direct contact with real-world biological samples, in which the salt concentrations are fixed. Here, we use the different salt concentration environments prior to plasma injections for brush preconditioning to achieve a specific hydrated structure of the polymer brush.

In summary, compared to previous works, we attempted to provide an extensive study comprising different classes of antifouling monomers on the complex relationships between antifouling properties and environment-induced structural changes of polymer brushes. Based on such a study, more generalized observations highlighting the differences in zwitterionic and nonionic brush-adaptive behavior were determined. For example, we found that relatively small changes in brush thickness (usually lower than 10%) induced by salt concentration changes in a surrounding environment led to significant changes in antifouling properties. For instance, plasma fouling observed for pCBMAA after preincubation in 500 mM NaCl was five times lower than the plasma fouling after preincubation in 0 mM NaCl. Moreover, remarkable difference in environment-induced antifouling behavior between pCBAA and pCBMAA brushes composed of monomers having a very similar structure (differing only in a presence of methyl in a methacrylamide backbone of pCBMAA, Figure 1) was observed. While for pCBAA, the optimum NaCl concentration giving the maximum fouling resistance was 100 mM, which is close to physiological conditions; in the case of pCBMAA (and all other studied methacrylamide-based coatings), the optimum value was much higher, that is, 500 mM NaCl.

It is worth mentioning that in this work, we focus on the initial phase of the brush response to surface preconditioning. We assume that this phase is a critical part of the whole fouling process. Therefore, relatively short blood plasma incubation time (10 min) was employed herein. Moreover, this incubation time is relevant for many biosensor applications, which tend to perform rather a rapid analyte detection. A detailed study on the complex phenomena of fouling dynamics is a subject of our further work.

**3.3. Reversibility of Hydration and Impact of Drying on Fouling Resistance.** We used both spectroscopic ellipsometry and SPR to investigate the ability of polymer brushes to recover their properties after rehydration. Here, we used the SPR method for fouling resistance measurements, as it is considered to be a standard method for fouling evaluation. Moreover, for these experiments, the HEPES buffer with no added salts was used; thus, we expected no changes in swelling in each polymer brush (that might interfere with measured data).

We used ellipsometry to measure the effective thickness and RI of wet brushes that have not been dried ( $wet_{non-dried}$ ), dried brushes, and rehydrated brushes ( $wet_{rehydrated}$ ); these results are shown in Table 1. All coatings exhibited a slight increase in effective thickness after rehydration. The extra methyl group in the pCBMAA structure may bring some differences in recovery after drying, as pCBAA shows two times higher relative increase in rehydrated effective thickness than pCBMAA (5.5 and 2.4%, respectively). The relative thickness increase of pSBMAA (by 9.2%) is the highest of all studied zwitterionic

coatings. Nonionic pHPMAA changes its thickness only by 3.9%.

The swelling, expressed as the ratio of effective thickness of  $wet_{\text{rehydrated}}$  and  $wet_{\text{dried}}$  (Table 1), is the lowest for pHPMAA: from a dry state to a rehydrated, effective thickness increased by a factor of 1.8. In the case of zwitterionic coatings, this ratio was in the range of 3–4.

Besides the effective thickness increase, all studied coatings exhibited a decrease in the RI after being dried and rehydrated; Figure S7 shows the entire RI spectrum for all four brushes. pHPMAA shows the largest decrease in the RI (0.005) with respect to the other brushes ( $\sim 0.002$ ).

We hypothesize that drying after polymerization changes the layout of intermolecular forces in the inner structure of a coating. Rehydrated coatings tend to bind more water in their structure than nondried coatings, leading to the creation of thicker and more hydrated layers having a larger effective thickness and smaller RI. This hypothesis is supported by SPR data, where we compared the fouling resistance of nondried and rehydrated brushes to undiluted blood plasma. These results, shown in Figure 5, clearly show that fouling levels are

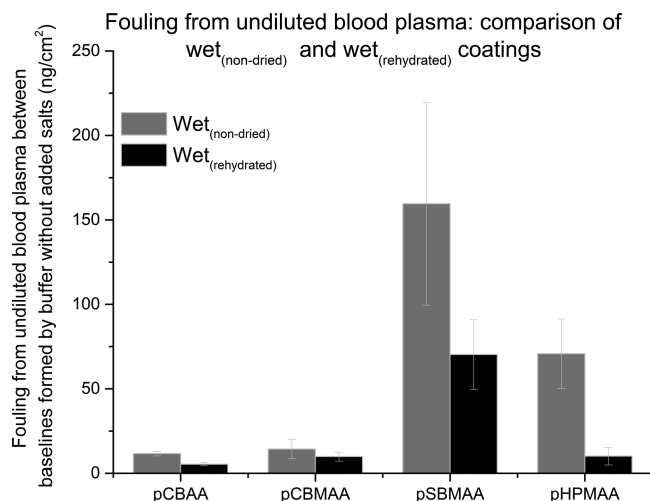


**Figure 5.** Comparison of the fouling level from undiluted blood plasma on  $wet_{\text{(non-dried)}}$  and on  $wet_{\text{(rehydrated)}}$  polymer coatings.

considerably lower on rehydrated brushes with respect to nondried brushes. These findings are consistent with the previous literature, where higher levels of hydration are connected with higher fouling resistance.<sup>24,25,40</sup> The fouling values for rehydrated brushes are in line with those reported in the literature.<sup>17,41,42</sup> The most significant resistance improvement was seen in pHPMAA brushes, which demonstrated the largest RI change (related to the largest relative increase in hydration level after rehydration).

It should be noted that there is a relative difference (compared to other coatings) between the lower fouling of pSBMAA indicated by fluorescent microscopy (in HEPES without salts, Figure 4) when compared to a rather high value determined by SPR (Figure 5). We believe that this difference may be caused by the differences between the applied methods. A comparison of different methods used to assess the fouling of highly hydratable coatings susceptible to a high level of swelling remains the focus of a future study.

## 4. CONCLUSIONS

This extensive study revealed a remarkable dependence of antifouling properties of both zwitterionic (pCBAA, pCBMAA, and pSBMAA) and nonionic (pHPMAA) polymer brushes on the structural changes induced by the adaptive brush response to ionic strength of their surrounding environment. Using spectroscopic ellipsometry, we observed monotonic increases in thickness of carboxy- and sulfo-functional zwitterionic coatings with increasing ionic strength; however, their RI exhibited more complex behavior, which reflected the capture of salt ions, hydration, and the corresponding loosening of the brush chains. On the contrary, nonionic pHPMAA responded to increases in ionic strength by shrinking, which was attributed to dehydration. A series of complementary QCM measurements indicated the same trend of capturing salts for zwitterionic brushes, with much less capture for pHPMAA. The results revealed that brush “preconditioning” at various salt concentrations may improve the antifouling properties by up to 70%; the optimum “preconditioning” parameters providing the highest degree of fouling resistance were determined for each brush type and structure. These results suggest a potential method of how to optimize fouling resistance for practical applications. Another issue important for practice is the ability to store low fouling coatings in a dry state. Rehydration experiments, evaluated by both ellipsometry and SPR, indicated that all brushes exhibited a full recovery, with slightly higher hydration after one drying/rehydration cycle. Correspondingly, all of the brushes exhibited significantly improved fouling resistance from blood plasma after rehydration. The complex responses of antifouling materials to environmental conditions, as shown herein, highlight the importance of an in depth understanding for processes occurring in the brush layers in native environments.

## ■ ASSOCIATED CONTENT

### Supporting Information

The Supporting Information is available free of charge at <https://pubs.acs.org/doi/10.1021/acs.langmuir.0c00996>.

Polymerization procedure, spectroscopic ellipsometry, QCM, and SPR measurements in detail, optimized hardware for ellipsometry in liquid environment, dispersion functions of used liquids, examples of measured and fitted ellipsometric data of polymers, infrared spectra of polymer brushes, and influence of different ionic strengths of environment on swelling of polymer brushes: RI spectra, RI change after rehydration in polymer brush structures (PDF)

## ■ AUTHOR INFORMATION

### Corresponding Author

Hana Vaisocherová-Lisalová – FZU—Institute of Physics of the Czech Academy of Sciences, Prague 182 21, Czech Republic; [orcid.org/0000-0002-8755-2398](https://orcid.org/0000-0002-8755-2398); Phone: +420 266 05 29 93; Email: [lisalova@fzu.cz](mailto:lisalova@fzu.cz)

### Authors

Ivana Višová – FZU—Institute of Physics of the Czech Academy of Sciences, Prague 182 21, Czech Republic  
Markéta Vrabcová – FZU—Institute of Physics of the Czech Academy of Sciences, Prague 182 21, Czech Republic  
Michala Forinová – FZU—Institute of Physics of the Czech Academy of Sciences, Prague 182 21, Czech Republic

**Yulia Zhigunová** – FZU—Institute of Physics of the Czech Academy of Sciences, Prague 182 21, Czech Republic

**Vasilii Mironov** – FZU—Institute of Physics of the Czech Academy of Sciences, Prague 182 21, Czech Republic

**Milan Houska** – FZU—Institute of Physics of the Czech Academy of Sciences, Prague 182 21, Czech Republic

**Eva Bittrich** – Leibniz-Institut für Polymerforschung Dresden e.V., Dresden 01069, Germany; [orcid.org/0000-0003-1484-1786](https://orcid.org/0000-0003-1484-1786)

**Klaus-Jochen Eichhorn** – Leibniz-Institut für Polymerforschung Dresden e.V., Dresden 01069, Germany

**Hisham Hashim** – National University of Science and Technology (MISIS), Moscow 119049, Russia; Faculty of Science, Tanta University, Tanta 31527, Egypt

**Petr Schovánek** – FZU—Institute of Physics of the Czech Academy of Sciences, Prague 182 21, Czech Republic; Palacký University Olomouc, Olomouc 77146, Czech Republic

**Alexandr Dejneka** – FZU—Institute of Physics of the Czech Academy of Sciences, Prague 182 21, Czech Republic; [orcid.org/0000-0002-5116-8781](https://orcid.org/0000-0002-5116-8781)

Complete contact information is available at:

<https://pubs.acs.org/10.1021/acs.langmuir.0c00996>

## Notes

The authors declare no competing financial interest.

## ACKNOWLEDGMENTS

This work was supported by Praemium Lumina quaeruntur of the Czech Academy of Sciences (LQ100101902) and by the project of Operational Programme Research, Development and Education of The Ministry of Education, Youth and Sports (CZ.02.1.01/0.0/0.0/17\_049/0008422). The authors would like to thank Daniel Spaček for his help with the graphic design and N. Scott Lynn Jr. and Djamel Eddine Chafai for their insightful comments.

## REFERENCES

- (1) Krishnamoorthy, M.; Hakobyan, S.; Ramstedt, M.; Gautrot, J. E. Surface-Initiated Polymer Brushes in the Biomedical Field: Applications in Membrane Science, Biosensing, Cell Culture, Regenerative Medicine and Antibacterial Coatings. *Chem. Rev.* **2014**, *114*, 10976–11026.
- (2) Yan, J.; Bockstaller, M. R.; Matyjaszewski, K. Brush-modified materials: Control of molecular architecture, assembly behavior, properties and applications. *Prog. Polym. Sci.* **2020**, *100*, 101180.
- (3) Liu, B.; Liu, X.; Shi, S.; Huang, R.; Su, R.; Qi, W.; He, Z. Design and mechanisms of antifouling materials for surface plasmon resonance sensors. *Acta Biomater.* **2016**, *40*, 100–118.
- (4) Banerjee, I.; Pangule, R. C.; Kane, R. S. Antifouling coatings: recent developments in the design of surfaces that prevent fouling by proteins, bacteria, and marine organisms. *Adv. Mater.* **2011**, *23*, 690–718.
- (5) Jiang, C.; Wang, G.; Hein, R.; Liu, N.; Luo, X.; Davis, J. J. Antifouling Strategies for Selective In Vitro and In Vivo Sensing. *Chem. Rev.* **2020**, *120*, 3852–3889.
- (6) Blaszykowski, C.; Sheikh, S.; Thompson, M. A survey of state-of-the-art surface chemistries to minimize fouling from human and animal biofluids. *Biomater. Sci.* **2015**, *3*, 1335–1370.
- (7) Yu, Q.; Zhang, Y.; Wang, H.; Brash, J.; Chen, H. Anti-fouling bioactive surfaces. *Acta Biomater.* **2011**, *7*, 1550–1557.
- (8) Sun, F.; Hung, H. C.; Sinclair, A.; Zhang, P.; Bai, T.; Galvan, D. D.; Jain, P.; Li, B.; Jiang, S.; Yu, Q. Hierarchical zwitterionic modification of a SERS substrate enables real-time drug monitoring in blood plasma. *Nat. Commun.* **2016**, *7*, 13437.
- (9) Zhang, T.-D.; Zhang, X.; Deng, X. Applications of protein-resistant polymer and hydrogel coatings on biosensors and biomaterials. *Ann. Biotechnol.* **2018**, *1*, 1006–1012.
- (10) Cao, S.; Barcellona, M. N.; Pfeiffer, F.; Bernards, M. T. Tunable multifunctional tissue engineering scaffolds composed of three-component polyampholyte polymers. *J. Appl. Polym. Sci.* **2016**, *133*, 43985–43994.
- (11) Lin, P.; Lin, C.-W.; Mansour, R.; Gu, F. Improving biocompatibility by surface modification techniques on implantable bioelectronics. *Biosens. Bioelectron.* **2013**, *47*, 451–460.
- (12) Chen, W.; Yung, B. C.; Qian, Z.; Chen, X. Improving long-term subcutaneous drug delivery by regulating material-bioenvironment interaction. *Adv. Drug Delivery Rev.* **2018**, *127*, 20–34.
- (13) Višová, I.; Smolková, B.; Uzhytchak, M.; Vrabcová, M.; Zhigunova, Y.; Houska, M.; Surman, F.; de los Santos Pereira, A.; Lunov, O.; Dejneka, A.; Vaisocherová-Lísalová, H. Modulation of Living Cell Behavior with Ultra-Low Fouling Polymer Brush Interfaces. *Macromol. Biosci.* **2020**, *20*, 1900351–1900359.
- (14) Zheng, L.; Sundaram, H. S.; Wei, Z.; Li, C.; Yuan, Z. Applications of zwitterionic polymers. *React. Funct. Polym.* **2017**, *118*, 51–61.
- (15) Lísalová, H.; Brynda, E.; Houska, M.; Višová, I.; Mrkvová, K.; Song, X. C.; Gedeonová, E.; Surman, F.; Riedel, T.; Pop-Georgievski, O.; Homola, J. Ultralow-Fouling Behavior of Biorecognition Coatings Based on Carboxy-Functional Brushes of Zwitterionic Homo- and Copolymers in Blood Plasma: Functionalization Matters. *Anal. Chem.* **2017**, *89*, 3524–3531.
- (16) Lin, X.; Jain, P.; Wu, K.; Hong, D.; Hung, H.-C.; O’Kelly, M. B.; Li, B.; Zhang, P.; Yuan, Z.; Jiang, S. Ultralow Fouling and Functionalizable Surface Chemistry Based on Zwitterionic Carboxybetaine Random Copolymers. *Langmuir* **2019**, *35*, 1544–1551.
- (17) Vaisocherová-Lísalová, H.; Surman, F.; Višová, I.; Vala, M.; Špringer, T.; Ermini, M. L.; Šípová, H.; Šedivák, P.; Houska, M.; Riedel, T.; Pop-Georgievski, O.; Brynda, E.; Homola, J. Copolymer Brush-Based Ultralow-Fouling Biorecognition Surface Platform for Food Safety. *Anal. Chem.* **2016**, *88*, 10533–10539.
- (18) Chou, Y.-N.; Sun, F.; Hung, H.-C.; Jain, P.; Sinclair, A.; Zhang, P.; Bai, T.; Chang, Y.; Wen, T.-C.; Yu, Q.; Jiang, S. Ultra-low fouling and high antibody loading zwitterionic hydrogel coatings for sensing and detection in complex media. *Acta Biomater.* **2016**, *40*, 31–37.
- (19) Vaisocherová-Lísalová, H.; Višová, I.; Ermini, M. L.; Šringere, T.; Song, X. C.; Mrázek, J.; Lamačová, J.; Scott Lynn, N.; Šdivt, L. P.; Homola, J. Low-fouling surface plasmon resonance biosensor for multi-step detection of foodborne bacterial pathogens in complex food samples. *Biosens. Bioelectron.* **2016**, *80*, 84–90.
- (20) Riedel, T.; Hageneder, S.; Surman, F.; Pop-Georgievski, O.; Noehammer, C.; Hofner, M.; Brynda, E.; Rodriguez-Emmenegger, C.; Dostálek, J. Plasmonic Hepatitis B Biosensor for the Analysis of Clinical Saliva. *Anal. Chem.* **2017**, *89*, 2972–2977.
- (21) Leng, C.; Huang, H.; Zhang, K.; Hung, H.-C.; Xu, Y.; Li, Y.; Jiang, S.; Chen, Z. Effect of Surface Hydration on Antifouling Properties of Mixed Charged Polymers. *Langmuir* **2018**, *34*, 6538–6545.
- (22) Schlenoff, J. B. Zwitteration: coating surfaces with zwitterionic functionality to reduce nonspecific adsorption. *Langmuir* **2014**, *30*, 9625–9636.
- (23) Leng, C.; Sun, S.; Zhang, K.; Jiang, S.; Chen, Z. Molecular level studies on interfacial hydration of zwitterionic and other antifouling polymers in situ. *Acta Biomater.* **2016**, *40*, 6–15.
- (24) Chen, S.; Li, L.; Zhao, C.; Zheng, J. Surface hydration: Principles and applications toward low-fouling/nonfouling biomaterials. *Polymer* **2010**, *51*, 5283–5293.
- (25) Herrwerth, S.; Eck, W.; Reinhardt, S.; Grunze, M. Factors that Determine the Protein Resistance of Oligoether Self-Assembled Monolayers – Internal Hydrophilicity, Terminal Hydrophilicity, and Lateral Packing Density. *J. Am. Chem. Soc.* **2003**, *125*, 9359–9366.
- (26) Zhao, C.; Li, L.; Wang, Q.; Yu, Q.; Zheng, J. Effect of Film Thickness on the Antifouling Performance of Poly(hydroxy-functional methacrylates) Grafted Surfaces. *Langmuir* **2011**, *27*, 4906–4913.

- (27) Brault, N. D.; Sundaram, H. S.; Li, Y.; Huang, C.-J.; Yu, Q.; Jiang, S. Dry Film Refractive Index as an Important Parameter for Ultra-Low Fouling Surface Coatings. *Biomacromolecules* **2012**, *13*, 589–593.
- (28) Ogieglo, W.; Wormeester, H.; Eichhorn, K.-J.; Wessling, M.; Benes, N. E. In situ ellipsometry studies on swelling of thin polymer films: A review. *Prog. Polym. Sci.* **2015**, *42*, 42–78.
- (29) Blackman, L. D.; Gunatillake, P. A.; Cass, P.; Locock, K. E. S. An introduction to zwitterionic polymer behavior and applications in solution and at surfaces. *Chem. Soc. Rev.* **2019**, *48*, 757–770.
- (30) Leng, C.; Han, X.; Shao, Q.; Zhu, Y.; Li, Y.; Jiang, S.; Chen, Z. In Situ Probing of the Surface Hydration of Zwitterionic Polymer Brushes: Structural and Environmental Effects. *J. Phys. Chem. C* **2014**, *118*, 15840–15845.
- (31) Yang, J.; Chen, H.; Xiao, S.; Shen, M.; Chen, F.; Fan, P.; Zhong, M.; Zheng, J. Salt-Responsive Zwitterionic Polymer Brushes with Tunable Friction and Antifouling Properties. *Langmuir* **2015**, *31*, 9125–9133.
- (32) Arwin, H. Ellipsometry in Life Sciences. In *Handbook of Ellipsometry*; Tompkins, H. G., Irene, E. A., Eds.; William Andrew Publishing: Norwich, NY, 2005; pp 799–855.
- (33) Farka, Z.; Kovář, D.; Skládal, P. Rapid detection of microorganisms based on active and passive modes of QCM. *Sensors* **2014**, *15*, 79–92.
- (34) Homola, J. *Surface Plasmon Resonance Based Sensors*; Springer-Verlag, 2006; Vol. 4, p 251.
- (35) Bittrich, E.; Burkert, S.; Müller, M.; Eichhorn, K.-J.; Stamm, M.; Uhlmann, P. Temperature-Sensitive Swelling of Poly(N-isopropylacrylamide) Brushes with Low Molecular Weight and Grafting Density. *Langmuir* **2012**, *28*, 3439–3448.
- (36) Kroning, A.; Furchner, A.; Aulich, D.; Bittrich, E.; Rauch, S.; Uhlmann, P.; Eichhorn, K.-J.; Seeber, M.; Luzinov, I.; Kilbey, S. M.; Lokitz, B. S.; Minko, S.; Hinrichs, K. In Situ Infrared Ellipsometry for Protein Adsorption Studies on Ultrathin Smart Polymer Brushes in Aqueous Environment. *ACS Appl. Mater. Interfaces* **2015**, *7*, 12430–12439.
- (37) Tang, Y.; Lu, J. R.; Lewis, A. L.; Vick, T. A.; Stratford, P. W. Swelling of Zwitterionic Polymer Films Characterized by Spectroscopic Ellipsometry. *Macromolecules* **2001**, *34*, 8768–8776.
- (38) Furchner, A.; Bittrich, E.; Uhlmann, P.; Eichhorn, K.-J.; Hinrichs, K. In-situ characterization of the temperature-sensitive swelling behavior of poly(N-isopropylacrylamide) brushes by infrared and visible ellipsometry. *Thin Solid Films* **2013**, *541*, 41–45.
- (39) Zhang, Z.; Vaisocherová, H.; Cheng, G.; Yang, W.; Xue, H.; Jiang, S. Nonfouling Behavior of Polycarboxybetaine-Grafted Surfaces: Structural and Environmental Effects. *Biomacromolecules* **2008**, *9*, 2686–2692.
- (40) Zheng, J.; Li, L.; Tsao, H.-K.; Sheng, Y.-J.; Chen, S.; Jiang, S. Strong repulsive forces between protein and oligo (ethylene glycol) self-assembled monolayers: A molecular simulation study. *Biophys. J.* **2005**, *89*, 158–166.
- (41) Rodriguez Emmenegger, C.; Brynda, E.; Riedel, T.; Sedlakova, Z.; Houska, M.; Alles, A. B. Interaction of blood plasma with antifouling surfaces. *Langmuir* **2009**, *25*, 6328–6333.
- (42) Vaisocherová, H.; Brynda, E.; Homola, J. Functionalizable low-fouling coatings for label-free biosensing in complex biological media: advances and applications. *Anal. Bioanal. Chem.* **2015**, *407*, 3927–3953.

# Appendix VII






Víšová, I., B. Smolková, M. Uzhytchak, M. Vrabcová, D. E. Chafai, M. Houska, M. Pastucha, P. Skládal, Z. Farka, A. Dejneka and H. Vaisocherová-Lísalová

**Functionalizable Antifouling Coatings as Tunable Platforms for the  
Stress-Driven Manipulation of Living Cell Machinery**

*Biomolecules* **10**(8) (2020): 1146.

Article

# Functionalizable Antifouling Coatings as Tunable Platforms for the Stress-Driven Manipulation of Living Cell Machinery

Ivana Víšová <sup>1,†</sup>, Barbora Smolková <sup>1,†</sup>, Mariia Uzhytchak <sup>1,†</sup>, Markéta Vrabcová <sup>1</sup>, Djamel Eddine Chafai <sup>1</sup> , Milan Houska <sup>1</sup>, Matěj Pastucha <sup>2</sup> , Petr Skládal <sup>2</sup>, Zdeněk Farka <sup>2,\*</sup> , Alexandr Dejneka <sup>1</sup>  and Hana Vaisocherová-Lísalová <sup>1,\*</sup> 

<sup>1</sup> Institute of Physics CAS, Na Slovance 1999/2, 182 21 Prague, Czech Republic; visova@fzu.cz (I.V.); smolkova@fzu.cz (B.S.); uzhytchak@fzu.cz (M.U.); vrabcova@fzu.cz (M.V.); chafai@fzu.cz (D.E.C.); houska@fzu.cz (M.H.); dejneka@fzu.cz (A.D.)

<sup>2</sup> Department of Biochemistry, Faculty of Science, Masaryk University, Kamenice 5, 625 00 Brno, Czech Republic; mpastucha@gmail.com (M.P.); skladal@chemi.muni.cz (P.S.)

\* Correspondence: farka@mail.muni.cz (Z.F.); lisalova@fzu.cz (H.V.-L.); Tel.: +420-549497674 (Z.F.); +420-266052993 (H.V.-L.)

† These authors contributed equally to this work.

Received: 20 May 2020; Accepted: 30 July 2020; Published: 5 August 2020



**Abstract:** Cells are continuously sensing their microenvironment and subsequently respond to different physicochemical cues by the activation or inhibition of different signaling pathways. To study a very complex cellular response, it is necessary to diminish background environmental influences and highlight the particular event. However, surface-driven nonspecific interactions of the abundant biomolecules from the environment influence the targeted cell response significantly. Yes-associated protein (YAP) translocation may serve as a marker of human hepatocellular carcinoma (Huh7) cell responses to the extracellular matrix and surface-mediated stresses. Here, we propose a platform of tunable functionable antifouling poly(carboxybetain) (pCB)-based brushes to achieve a molecularly clean background for studying arginine, glycine, and aspartic acid (RGD)-induced YAP-connected mechanotransduction. Using two different sets of RGD-functionalized zwitterionic antifouling coatings with varying compositions of the antifouling layer, a clear correlation of YAP distribution with RGD functionalization concentrations was observed. On the other hand, commonly used surface passivation by the oligo(ethylene glycol)-based self-assembled monolayer (SAM) shows no potential to induce dependency of the YAP distribution on RGD concentrations. The results indicate that the antifouling background is a crucial component of surface-based cellular response studies, and pCB-based zwitterionic antifouling brush architectures may serve as a potential next-generation easily functionable surface platform for the monitoring and quantification of cellular processes.

**Keywords:** zwitterionic material; cell mechanotransduction; cell signaling; functional biointerfaces; antifouling polymer brushes; surface modification

## 1. Introduction

Living cells are continuously sensing their microenvironment and adapt to different physicochemical events during their lifetime [1,2]. Besides soluble chemical signals, mechanical cues influence cells persistently over time, involving the activation or inhibition of different signaling pathways [3]. Mechanotransduction, defined as the conversion of mechanical cues into biochemical signals, leads to cellular responses important for cell function in health (i.e., growth and differentiation) and diseases (i.e., cancer malignant progression) [4]. Among these mechanosensing processes, integrin

mediates cell adhesion, leads to the cell response by recruiting intracellular multiprotein assemblies such as F-actin [5], or influences the Yes-associated protein (YAP) location [6].

YAP is a transcriptional regulator and oncoprotein, tightly controlled by different regulatory systems sensitive for the extracellular matrix and microenvironment [7,8]. In an inactive form, YAP is found mostly in the cytoplasm; when activated, it concentrates in the nucleus to operate the transcription of genes involved in cell division or apoptosis [7]. The regulation of YAP is a complex process, which encompasses several different factors, such as cell density and polarity, mechanical stress, cellular energy status, etc. [9,10]. In detail, the subcellular location of YAP is influenced by the substrate rigidity and topography of the surface [11–13], cell geometry and morphology driven by the surface characteristics and surrounding conditions [14–16], or the density of the population and contact among the cells [17,18].

Surface-based methods are widely used to study cell adhesion and migration. However, surfaces engineered to accurately tailor cell-surface interactions are increasingly needed [19,20]. Recent works focused on the prevention of cell adhesion noticed antifouling coatings as useful platforms to diminish adhesion [21–23] and/or to pattern cell growth [24,25]. Well-defined antifouling coatings with minimum backgrounds of nonspecific bindings, even from complex biological media, represent an attractive approach to elucidate the effects of surface physicochemical properties on cellular behaviors. Surface-based platforms for specific targeting should be rationally designed to (i) integrate functional groups for specific cell receptors targeting, (ii) suppress nonspecific interactions, and (iii) use integrative markers for the assessment of the cell behavior in response to the surface binding. In some portion of the works, the antifouling background was decorated with an arginine, glycine, and aspartic acid (RGD) moiety containing peptides (R: arginine, G: glycine, and D: aspartic acid and further RGD peptides). The RGD peptides are well-known to promote cell adhesion through specific integrin interactions [26]. For example, the study on the effect of the osteogenic differentiation of mesenchymal stem cells proved the possibility to modulate differentiation by using antifouling carboxybetaine-based hydrogel coating functionalized with RGD peptides (RGD-functionalized coatings) [27]. Using a functionalized 3D fiber scaffold covered with antifouling brushes, the authors in [28] showed that cell attachments and spreading are dependent on the RGD moiety surface concentration.

In this work, we demonstrate a smooth approach to control the level of extracellular mechanical stress using the cell adhesion-promoting RGD-functionalized antifouling polymer brushes. To define the level of mechanical stress, we monitored the colocalization of YAP in the cell nucleus. Two distinct types of state-of-art functionable antifouling coatings based on pCB zwitterionic brushes [29–31] were employed and compared. First, a set of RGD-functionalized homopolymers poly(carboxybetaine acrylamide) (pCBAA) was prepared by employing different concentrations of the RGD peptide during the immobilization. Second, a set of RGD-functionalized random copolymers of carboxybetaine methacrylamide (CBMAA) and nonionic poly(*N*-(2-hydroxypropyl) methacrylamide) HPMAA (p(CBMAA-*ran*-HPMAA)) with different molar ratios of functionable CBMAA was prepared. Standard carboxy- or a mix of carboxy-/hydroxy-functional oligo(ethylene glycol) (OEG)-based self-assembled monolayer (SAM) [32,33] commonly used to enhance the resistance of surfaces to fouling were functionalized with the RGD peptide to provide reference systems for comparison of the effects of antifouling properties on mechanotransduction studies.

## 2. Materials and Methods

### 2.1. Reagents

The buffer solutions were prepared using ultrapure water (18.0 M $\Omega$ -cm, Milli-Q<sup>®</sup> system, Merck, Darmstadt, Germany). Phosphate-buffered saline (PBS, 0.01-M sodium phosphate, 0.138-M sodium chloride, 0.0027-M potassium chloride, pH 7.4) and borate buffer (10-mM sodium borate, pH 8.5) were prepared from a stock solution from Sigma-Aldrich, St. Luis, MO, USA. The PBS-NaCl buffer (0.01-M phosphate, 0.75-M sodium chloride, 0.0027-M potassium chloride, pH 7.4) was

prepared from PBS stock solution. The initiator  $\omega$ -mercaptoundecylbromoisobutyrate was from Prochimia, Gdansk, Poland. The carboxybetaine acrylamide, carboxybetaine methacrylamide, and *N*-(2-hydroxypropyl) methacrylamide monomers were from Specific Polymers, Castries, France. 1,4,8,11-tetramethyl-1,4,8,11-tetraazacyclotetradecane (Me<sub>4</sub>Cyclam, 98%), CuCl ( $\geq 99.995\%$ ), CuCl<sub>2</sub> (99.999%), methanol ( $\geq 99.9\%$ ), and ethanol (99.9%) were from Sigma-Aldrich. Tetrahydrofuran (THF,  $\geq 99.9\%$ ) was from Penta, Prague, Czech Republic. The cell adhesion-promoting peptide (RGD peptide) with a sequence of H-RRRGGGGRRGDSP-OH (12 residues), purity  $>98\%$ , was synthesized by Pepscan, Lelystad, The Netherlands. *N*-hydroxysuccinimide (NHS) and *N*-ethyl-*N'*-(3-diethylaminopropyl)carbodiimide (EDC) were purchased from AP Czech, Prague, Czech Republic. 2-(2-aminoethoxy)acetic acid (AEAA) was purchased from VWR International, Radnor, PA, USA. The following fluorescent probes and antibodies were purchased from Thermo Fisher Scientific (Waltham, MA, USA): CellMask™ Green for the cell membrane, propidium iodide for the cell death assessment, Hoechst 33,342 for nuclear staining, Alexa Fluor 568 secondary anti-rabbit antibody, and Alexa Fluor™ 488 Phalloidin (1:500) (A12379). Anti-YAP rabbit antibody (14074S) was purchased from Cell Signaling Technology, Leiden, Netherlands.

## 2.2. Preparation of RGD-Functionalized Coatings

For all experiments, we used rationally designed the RGD moiety with a sequence of H-RRRGGGGRRGDSP-OH (12 residues), containing a primary amine-rich sequence (RRR) at its N-terminus and a cell adhesion-promoting sequence (RGD) near its C-terminus. Thus, the peptide can be easily immobilized on the surface without substantially limiting its cell adhesion-promoting activity. The immobilization of the RGD peptide to the surfaces was performed using amine coupling chemistry via the covalent binding of primary amines with activated carboxy groups of the surface coatings.

### 2.2.1. Preparation of pCB-Based Polymer Brushes

pCB brushes were prepared by surface-initiated atom transfer radical polymerization (SI-ATRP), as described elsewhere [31], and their structures were checked by infrared spectroscopy (data not shown). After polymerization, all coatings were stored in PBS. Before functionalization, coatings were rinsed with ultrapure water and sterilized in 70% ethanol for 30 min. All further steps were carried out under strictly sterile conditions using sterile solutions. After sterilization, coatings were immersed in ultrapure water for 5 min and subsequently activated with a mixture of 0.1-M NHS and 0.5-M EDC for 25 min. Afterwards, the coatings were shortly washed with ultrapure water, and the solution of the RGD peptide in borate buffer (10 mM, pH 8) was added and reacted for 20 min. For functionalization of the pCBAA coating, different concentrations of the RGD peptide were used (0, 1, 10, 50, 100, and 500  $\mu\text{g}/\text{mL}$ ). For immobilization of the RGD peptide on both copolymers, the concentration of 850  $\mu\text{g}/\text{mL}$  was applied. After immobilization, all coatings were rinsed with water and immersed in the deactivation solution of 1-M aminoethoxy acetic acid (AEAA) for 30 min. Finally, all the coatings were rinsed with PBS-NaCl and stored in sterile PBS until use.

### 2.2.2. Preparation of the Carboxy-Functional OEG-Based Self-Assembled Monolayer (OEG-SAM)

Gold-coated glass substrates were rinsed with ultrapure water and isopropyl alcohol and sonicated in isopropyl alcohol for 30 min. Afterwards, the chips were immersed in an ethanol solution of HS-(CH<sub>2</sub>)<sub>11</sub>-(EG)<sub>6</sub>-OCH<sub>2</sub>-COOH and HS-(CH<sub>2</sub>)<sub>11</sub>-(EG)<sub>4</sub>-OH in different molar ratios (0:100, 35:65, 65:35, and 100:0, respectively), with the total concentration of 1 mM of thiol groups, and left for 3 days at room temperature in the dark to form a SAM with different contents of carboxy and hydroxy groups. All further steps were held under strictly sterile conditions using sterile solutions. The coatings were rinsed with ethanol, left in ultrapure water for 10 min, and, subsequently, activated with a mixture of 0.025-M NHS and 0.125-M EDC for 30 min. Afterwards, the coatings were shortly washed with ultrapure water, and a solution of the RGD peptide in 10-mM sodium acetate buffer (pH 5.0) was added and left to react for 12 min. For pure HS-(CH<sub>2</sub>)<sub>11</sub>-(EG)<sub>6</sub>-OCH<sub>2</sub>-COOH coatings, solutions of



different concentrations of RGD peptides were used (0, 0.1, 1, 50, and 100  $\mu\text{g/mL}$ ) for functionalization. For the immobilization of the RGD peptide on the mixed SAM coatings, a concentration of 50  $\mu\text{g/mL}$  was applied. After immobilization, all coatings were subsequently immersed in sodium acetate buffer, PBS-NaCl, sodium acetate, 1-M ethanolamine, and sodium acetate, respectively, each for 5 min. Then, all the coatings were stored in sterile PBS until use.

### 2.3. Surface Characterization by SPR

For the characterization of the functionalization (more details in the Supplementary Materials), a six-channel spectroscopic SPR sensor developed at the Institute of Photonics and Electronics (Prague, Czech Republic) combined with a dispersionless microfluidic system equipped with temperature controller was used. For this sensor at a resonant wavelength around 750 nm, a 1-nm SPR wavelength shift represents a change in the surface protein concentration of 17  $\text{ng/cm}^2$  [2]. Antifouling properties were confirmed using an angular MP-SPR with a 4-channel microfluidic system, equipped with LED sources of 670 nm and 785 nm wavelengths (BioNavis 400 KONTIO, BioNavis, Tampere, Finland). To transform the shift in the SPR resonance angle to mass units of unspecifically adsorbed proteins, a value of 0.001~0.85  $\text{ng/cm}^2$  at 785 nm was used. More details on the SPR experiments can be found in the Supplementary Materials, including the representative SPR sensorgrams for surface functionalization with the RGD-peptide (Figure S1), as well as the obtained immobilization values (Figure S2).

### 2.4. Cell Culture

Human hepatocellular carcinoma cell lines Huh7 obtained from the Japanese Collection of Research Bioresources (JCRB) were cultured in EMEM medium (American-Type Culture Collection, ATCC, Manassas, VA, USA) supplemented with 10% fetal bovine serum (FBS, Thermo Fisher Scientific) as recommended by the supplier. Cells were cultivated at 37 °C in a humidified atmosphere containing 5%  $\text{CO}_2$ , and the medium was changed once a week. The Huh7 cell line was selected as a model system due to its high susceptibility to external physicochemical stresses.

### 2.5. Assessment of Cell Death

Propidium iodide (PI) was used for the cell death assessment. Huh7 cells were seeded on the sterilized substrates at an initial density of 25,000  $\text{cells/cm}^2$  and were grown under standard conditions for 72 h. Cells were afterwards labeled with 1-mL PI (50  $\mu\text{g/mL}$ ) and Hoechst 33,342 as nucleus staining for 5 min in the dark at room temperature. After staining, labeled cells were imaged using spinning disk confocal microscopy (IXplore SpinSR Olympus, Tokyo, Japan). ImageJ software (National Institutes of Health, NIH, Bethesda, MD, USA) was used for image processing and quantification. PI-stained cells were considered to be dead cells. Cells treated with 20% ethanol for 30 min were used as the positive control.

### 2.6. Localization and Quantification of Endogenous YAP

Huh7 cells were seeded on the sterilized substrates at an initial density of 25,000  $\text{cells/cm}^2$  and were grown under standard cell culture conditions. Control cells were seeded onto standard 35-mm Petri dishes (Cellvis, Sunnyvale, CA, USA). After 72 h, the cells were washed with PBS and fixed with 4% paraformaldehyde for 10 min at room temperature. After fixation, the samples were washed with PBS and permeabilized with 0.5% Triton-X 100 in PBS for 20 min at room temperature (RT). Post fixation and permeabilization, cells were incubated with diluted primary anti-YAP antibody (1:500) for 1 h at room temperature. After washing with PBS, the cells were incubated with goat anti-rabbit Alexa Fluor 568 secondary antibody diluted in PBS (1:1000) for 1 to 2 h at room temperature in the dark. Alexa Fluor™ 488 Phalloidin diluted in PBS (1:500) was used sequentially in order to visualize F-actin in cells. Hoechst 33,342 was used as nucleus staining. Post staining, labeled cells were imaged using spinning disk confocal microscopy (Spin SR, Olympus). ImageJ software (NIH) was used for image processing and quantification.

### 2.7. Spinning Disk Confocal Microscopy

High-resolution spinning disk confocal microscopy (Spin SR, Olympus) was used for Huh7 cell visualizations. Huh7 cells were grown on different types of substrates for 72 h and stained with Hoechst 33,342 for nuclear staining in blue, YAP antibody in red, and Alexa Fluor™ 488 Phalloidin was used in order to visualize F-actin in cells in green. Fluorescence images were taken with the acquisition software cellSens (Olympus) and processed using ImageJ.

### 2.8. Statistical Analysis

Data obtained from independent experiments are presented as the mean  $\pm$  standard error of the mean (SEM). Statistical analysis was determined using a one-way analysis of variance and the Newman-Keuls test. Statistical analysis was performed using MaxStat Pro 3.6 (MaxStat Software, Jever, Germany). The differences were considered statistically significant at  $p < 0.05$ .

## 3. Results

### 3.1. Antifouling Properties of RGD-Functionalized Coatings

A set of pCB brush coatings and OEG-based SAM coatings functionalized with variable concentrations of RGD peptides were prepared to investigate the effects of the RGD peptide-decorated antifouling background on mechanotransduction cell signaling. Based on our previous study [31], we used optimized biocompatible and highly hydratable antifouling pCB brush coatings with wet thicknesses around  $\sim 80$  nm (characterized by spectroscopic ellipsometry; data not shown). Two different approaches to the preparation of the coatings functionalized with varying RGD concentrations were employed as follows: first, only carboxy-functional coatings of pCBAA or SAM of HS-(CH<sub>2</sub>)<sub>11</sub>-(EG)<sub>6</sub>-OCH<sub>2</sub>-COOH were RGD-functionalized using immobilization solutions of RGD peptides of different concentrations (Figure 1A1,A2). Second, a gradient of functionalizable elements (Figure 1C1,C2) was prepared by the copolymerization or mixing of different ratios of carboxy-functional and hydroxy-functional components for pCB brushes or OEG SAM coatings, respectively. In the latter case, the concentration of RGD peptides was specified for each type of the coating to be high enough to saturate the activated groups (Figure 1B1,B2).

Depending on the cell line, the first cells can already sense and initiate the adhesion process after 1 h of incubation [1]. Therefore, antifouling properties of RGD-functionalized pCB or OEG SAM coatings were tested (i) after incubation in cell growth medium for 60 min and (ii) after incubation in undiluted human blood plasma for 10 min, as this is a commonly used antifouling characterization method [33]. While in the cell growth medium, the antifouling pCB coatings showed a fouling level under the limit of detection, and OEG SAM showed a fouling level up to 35 ng/cm<sup>2</sup>. RGD peptide concentrations used for the functionalization of both types of carboxy-functional coatings did not have any influence on the fouling level from the cell growth medium (Table 1). To confirm the antifouling properties of all pCB coatings, the coatings were exposed to undiluted human blood plasma. The level of fouling on pCB coatings before the activation of carboxy groups remained below 10 ng/cm<sup>2</sup>. The fouling level after the RGD functionalization was around 27 ng/cm<sup>2</sup>, which is consistent with the previously published data on decreased resistance following the functionalization of antifouling polymer brushes [34]. Fouling from undiluted blood plasma is neither dependent on the volume concentrations of RGD peptides nor the content of carboxy groups in functionalized copolymer coatings (Figure S3). The fouling resistance to the undiluted blood plasma of OEG-based SAM coatings was  $\sim 150$  ng/cm<sup>2</sup>. These values were  $\sim$ five times lower compared to the pCB-based coatings.

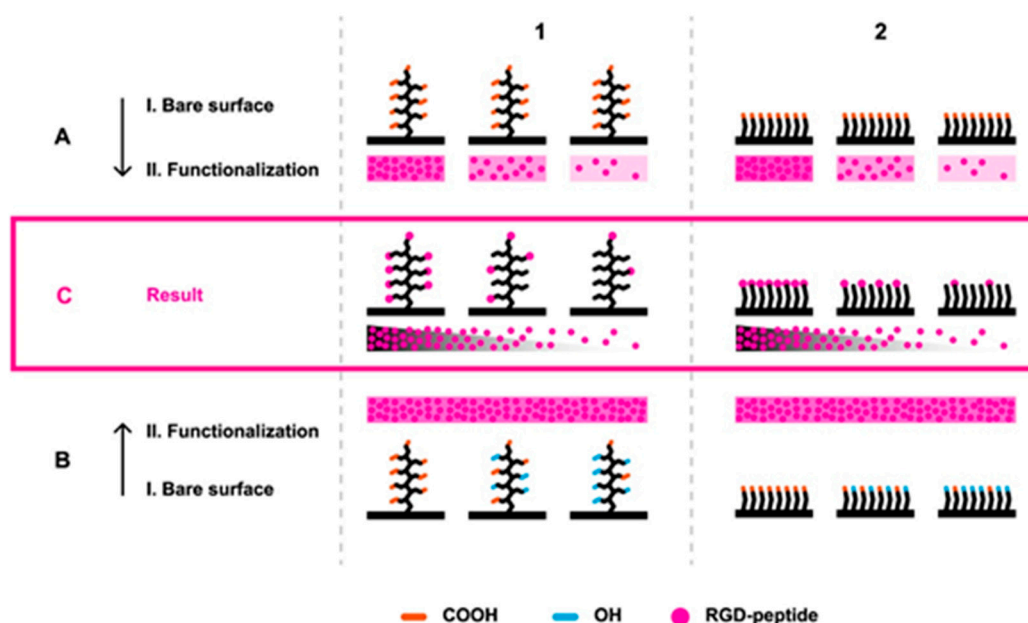


**Figure 1.** Immobilization strategies. Arginine, glycine, and aspartic acid (RGD)-functionalized sets of poly(carboxybetain) (pCB) coatings (C1) and oligo(ethylene glycol) self-assembled monolayer (OEG SAM) coatings (C2) were prepared using two different approaches. First (A), only carboxy-functional coatings were activated and exposed to solutions of RGD peptides with different concentrations. The second (B) set of coatings with different ratios of functionalizable carboxy groups in relation to nonfunctionalizable hydroxy groups was prepared, activated, and exposed to a high concentration of RGD peptides. The functionalization approaches of A and B were performed on pCB homopolymer and copolymer brushes (1) and OEG-based carboxy-functional homogenous and mixed SAM (2) coatings.

**Table 1.** Fouling from the cell growth medium containing 10% fetal bovine serum on arginine, glycine, and aspartic acid (RGD)-functionalized coatings. The incubation time was 60 min; more experimental details are provided in the Supplementary Materials.

RGD Peptide Concentrations Used for Immobilization ( $\mu\text{g/mL}$ )	Fouling on pCBAA ( $\text{ng/cm}^2$ )	RGD Peptide Concentrations Used for Immobilization ( $\mu\text{g/mL}$ )	Fouling on OEG-Based SAM ( $\text{ng/cm}^2$ )
0	Undetectable <sup>1</sup>	0	20.1
1	Undetectable <sup>1</sup>	0.1	32.7
50	Undetectable <sup>1</sup>	1	25.0
500	Undetectable <sup>1</sup>	50	11.5

<sup>1</sup> The value below the detection limit of the gold-coated glass substrates (SPR) ( $\approx 0.1 \text{ ng/cm}^2$ ). pCBAA: poly(carboxybetaine acrylamide) and OEG SAM: oligo(ethylene glycol) self-assembled monolayer.

### 3.2. Modulation of Mechanotransduction Signaling

Hepatocytes are very sensitive cells [35–37], which makes them a good model system for mechanotransduction-signaling studies. Recently we showed that nonfunctionalized antifouling polymer brush coatings pCBAA, pCBMAA, pHPMAA, and their copolymers are not cytotoxic for Huh7 cells [31]. Here, we confirmed no cytotoxicity, even for activated and deactivated or RGD-functionalized pCB antifouling coatings. The cell death ratios of Huh7 cells for all tested coatings remained around 3% after three days of cultivation, which is the same as the cell death ratio of the control (Figure S4). Apparently, the majority of cells cultivated with RGD-functionalized pCB brushes remained alive after three days of incubation.

To assess the influence of the antifouling background on monitoring of the mechanotransduction, we used the prepared variable sets of RGD-functionalized (using method A and method B in Figure 1) pCB- and OEG SAM-based coatings for Huh7 cell cultivations for three days. Figure 2 shows a

significant difference between these coatings. While the functionalized antifouling pCBAA brushes show a clear dependency of cell growth on the RGD peptide-immobilized level, there is no dependency found for the OEG SAM coatings (Figure 2, Figure S5, and Figure S6). Regarding the comparison of the superior antifouling properties of pCB-based brush coatings and rather poor resistance of OEG SAM coatings (given in Table 1 and Figure S3), these results suggest the importance of a proper antifouling background for the studies of cell signaling pathways. Clearly, the pCB-based background diminished most of the nonspecific interactions between the surface and cell cultivation medium or cells themselves, so the number of spots for cell adhesion may be easily controlled.

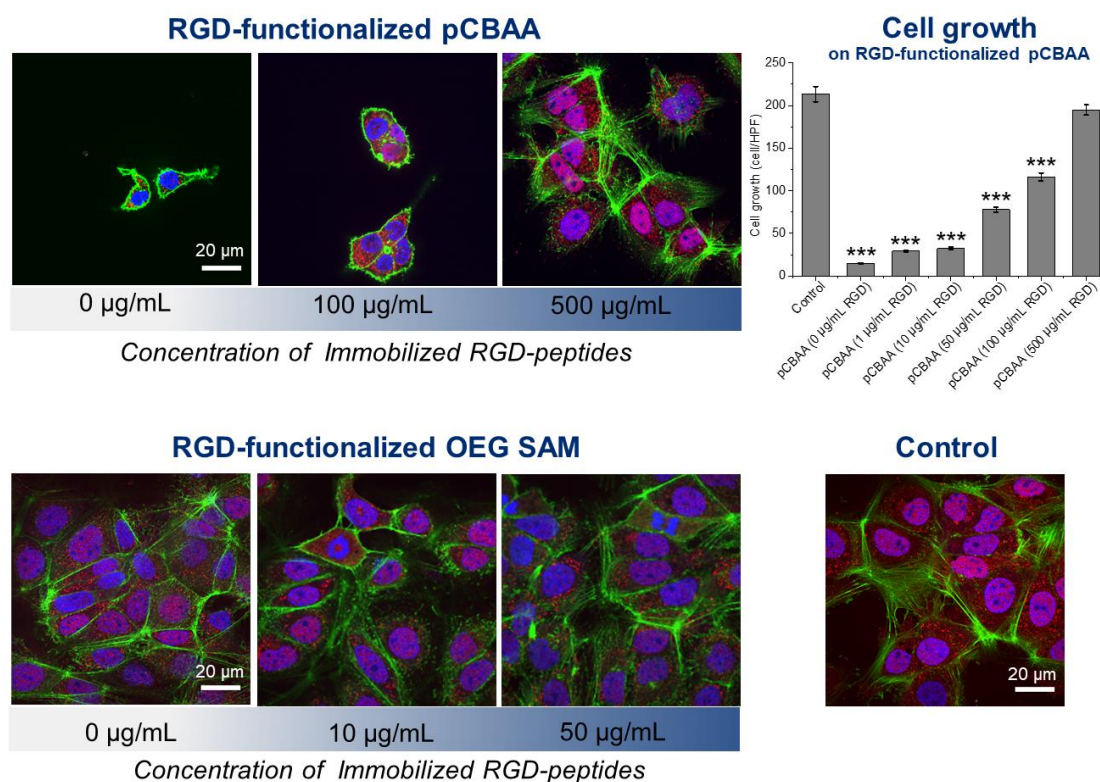


**Figure 2.** Growth of Huh7 cells on RGD-functionalized coatings. Examples of spinning disk confocal microscopy images of coatings functionalized by solutions of different concentrations of RGD peptides. Staining: Yes-associated protein (YAP) (red), F-actin (green), and nucleus (blue). Upper line: RGD-functionalized poly(carboxybetaine acrylamide) (pCBAA) functionalized using the method A-1 in Figure 1 (0, 100, and 500 µg/mL of the RGD peptides in the solution were used for functionalization) and plot of the dependency of the cell growth (number of cells per high-power field) on the RGD peptide concentrations. One-way analysis of variance with the Newman-Keuls test was performed, and data are expressed as means  $\pm$  SEM, \*\*\*  $p < 0.001$ . Bottom line: RGD-functionalized OEG SAMs functionalized using the method A-2 in Figure 1 (0, 10, and 50 µg/mL of the RGD peptides in the solution were used for functionalization; no dependency was found) and the control (cells seeded onto standard 35-mm Petri dishes).

The adhesion number of cells around and the quality of the surface are key parameters directly influencing the mechanical stress-driven cell response. As a measurable parameter of such stress, the colocalization of YAP in the nucleus (“YAP colocalization” further) was determined for all sets of prepared functionalized coatings (Figure 3). The quantified YAP colocalization (shown in Figure 3C, D) shows no significant variation induced by different RGD-functionalized standard OEG SAM (functionalized using both method A-2 and A-3 according to Figure 1)-based coatings compared to the control surface. Apparently, such coatings are ineffective in the modulating of the YAP distribution, as they are ineffective in the modulation of cell growth and adhesion. Additionally, regarding such great

insensitivity, it is not surprising that the functional groups (-COOH, -OH, and -RGD or a combination of them) show no effect on the cell stress response and YAP distribution.

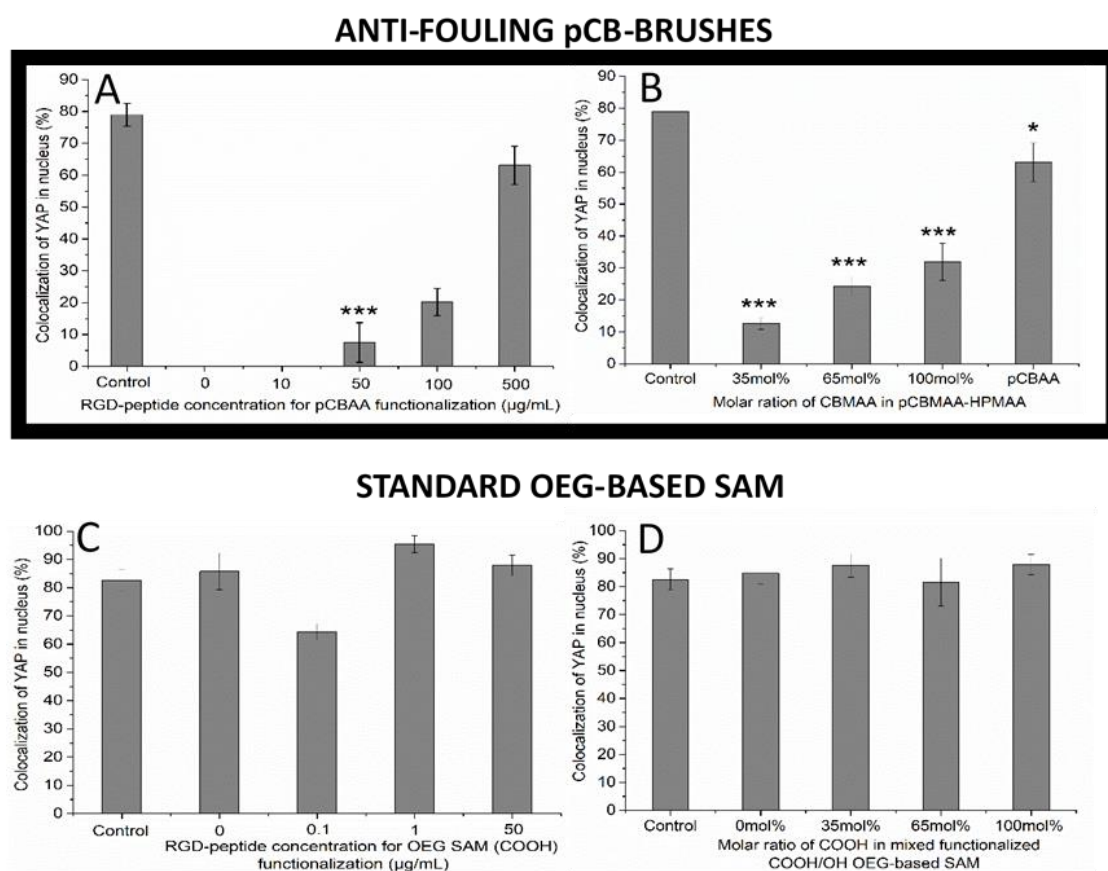


**Figure 3.** Colocalization of the YAP in the nucleus in cells growing on different RGD-functionalized surfaces. (A) Antifouling pCBAA coatings functionalized by solutions with different concentrations of RGD peptides (method A-1 in Figure 1). (B) Set of RGD-functionalized copolymer p(CBMAA-*ran*-HPMAA) antifouling coatings with increasing contents of functionalizable pCBMAA (method B-1 in Figure 1). (C) RGD-functionalized standard carboxy-ended OEG SAM (HS-(CH<sub>2</sub>)<sub>11</sub>-(EG)<sub>6</sub>-OCH<sub>2</sub>-COOH) (method A-2 in Figure 1). (D) RGD-functionalized mix of carboxy- and hydroxy-ended OEG SAM (HS-(CH<sub>2</sub>)<sub>11</sub>-(EG)<sub>6</sub>-OCH<sub>2</sub>-COOH and HS-(CH<sub>2</sub>)<sub>11</sub>-(EG)<sub>4</sub>-OH) (method B-2 in Figure 1). \*\*\*  $p < 0.001$ , \*  $p < 0.05$  mean significant differences with respect to control.

On the other hand, the quantified YAP colocalization presented in Figure 3A shows a significant increase of the YAP level starting from 50 µg/mL of RGD peptide concentrations used to functionalize pCBAA brushes (method A-1 in Figure 1). The YAP colocalization reached almost the same level as on the control surface when the pCBAA brushes were functionalized with the concentration of 500 µg/mL of the RGD peptide. However, it is important to emphasize that there is a threshold of the amount of RGD peptide-functionalized spots on the surface, which is needed to observe the YAP colocalization changes (Figure 3A), despite the fact that the cell growth is tightly related to the RGD peptide concentration, even under such a threshold (Figure 2). Hypothetically, such observation may reveal the limiting “point of break” measure of mechanical stress given by the amount of accessible adhering spots and number of cells around at which cells start or stop the signaling pathway, changing the YAP distribution.

Figure 3B shows YAP colocalization using the set of RGD-functionalized antifouling copolymer coatings (method B-1 in Figure 1). Obviously, the content of CBMAA in the copolymer brushes that correlates with RGD motif abundance modulates the YAP colocalization. However, even the

RGD-functionalized homopolymer of 100% pCBMAA (functionalizable part of the copolymer brushes) did not reach the level of YAP colocalization induced by the control or the RGD-functionalized homopolymer of pCBAA (Figure 3B). In our previous study, the sensitivity of cell growth and spreading on the surface swelling characteristics was noticed, causing the higher growth and cytoskeleton distribution of cells growing on the nonfunctionalized pCBAA compared to pCBMAA [31]. Such a phenomenon can explain the different responses of the cells on functionalized pCBAA (method A-1 in Figure 1) and pCBMAA (method B-1 in Figure 1) and opens new possibilities in the design of coatings for the even finer modulation of cell growth and cell-signaling pathways.

#### 4. Discussion

In the last decades, diverse polymer brushes with a variety of physicochemical properties and different abilities to control cell adhesion have been synthesized [4,38–41]. In the framework of these studies, we have prepared two different sets of RGD-functionalized antifouling coatings based on a zwitterionic pCBAA homopolymer or p(CBMAA-*ran*-HPMAA) copolymers with different contents of CBMAA. Our results demonstrate that, with both types of antifouling coatings, we are not only able to control the cell adhesion via specific integrin receptors but, also, to modulate the cell mechanotransduction signaling pathways. The results of the functionalized pCB-based polymer brushes were also compared with the corresponding RGD-functionalized standard OEG-based SAM coatings (carboxy-terminated or a mixture of carboxy- and hydroxy-terminated SAM). All OEG SAM coatings were ineffective in any modulation of cell adhesion, growth, or mechanotransduction.

The pCB-based polymer brushes exhibit superior antifouling and functionalization properties over numerous types of antifouling functionalizable coatings [34,42]. To achieve comparable RGD peptide immobilized levels on pCB coatings and OEG SAMs, the optimized functionalization procedures described in [42,43] were used and slightly modified to get sets of different surface concentrations of RGD peptides (Figure 1). In-line with previously reported studies [34,43,44], the antifouling character of the pCB brushes was not notably impaired, even after functionalization by RGD peptides. Even though OEG SAM coatings are considered as resistant to fouling from single-protein or diluted biological media, complex solutions challenge their resistance significantly [42,43]. Indeed, comparing foulings from undiluted blood plasma (Figure S3) or cell growth medium (Table 1) on functionalized coatings highlighted the extraordinary resistance of pCB brushes compared to standard OEG SAM coatings. Importantly, the comparison of the data from Figure 3 and Table 1 indicates that only small amounts of adhered materials nonspecifically adsorbed from the cell growth medium to the surface ( $\sim 11.5$  ng/cm<sup>2</sup>) may promote cell-surface interactions significantly. It is worth mentioning that interactions between the cells and OEG SAM substrate itself can contribute to the resulted inefficiency in any modulation of cell behavior. However, it is impossible to separate these two contributions in the used system.

A proper antifouling background appears to be a key parameter to ensure control over the abundance of spots of adhesion and enable the fine-tuning of the mechanically induced stress responses of cells. The control of the YAP distribution in the cell is a complex process influenced by many contradictory factors. Here, we report an increasing concentration of YAP in the nucleus with an increasing RGD motif surface coverage and increasing adhered cell number on functionalized antifouling surfaces. In [17,45], the authors reported decreasing YAP concentrations in the nucleus with an increasing cell population. On the other hand, according to the literature, more round geometry promotes the YAP localization in the cytoplasm. The more cells are spread, the more YAP is activated and localized in the nucleus [14,46]. The pCB-based antifouling coatings without any RGD moiety are not preferable surfaces for adhesion; cells tend to have rather round shapes compared to the standard controls [31,47]. The more spots of adhesion that are presented, the more cells are spreading on the surface, increasing the amount of YAP in the nucleus (Figure 2, Figure S5, and Figure 3). Obviously, in the case of homopolymer pCBAA coatings, there is no remarkable influence of other surface physicochemical properties, such as roughness, thickness, or hydration capabilities, as they do not change across the set of RGD-functionalized samples significantly. Clearly, in the

case of pCBAA coatings with a limited number of spots of adhesion, the biggest contribution to YAP distribution-controlling factors have shape-driven factors. It is highly likely, that for even a higher number of adhered cells, the effect of a contact inhibition of proliferation [45,48] would be more significant, and we would observe the decreasing of YAP in the nucleus subsequently.

In the case of copolymer brush coatings (method B-1 in Figure 1), one can consider even changes of the physicochemical properties of the surface, such as different hydrophilicity or the contents of zwitterionic moieties with changing ratios of the HPMAA content. Nevertheless, we observed the same dependency of YAP localization on the RGD peptide concentration (represented by a pCBMAA ratio in the copolymer), as on the pCBAA coating prepared by method A-1 in Figure 1.

It is worth mentioning that observed results should not be attributed to differences in surface stiffness. In our study, the polymer brushes having a wet thickness of ~80 nm on gold-coated glass substrates were used. It was reported previously that, for example, Petri dish substrates coated with polymers (e.g., PDMS) should be of about 40–200  $\mu\text{m}$  thick to make a reliable change in the substrate stiffness for cell culturing [49–51].

YAP colocalization in the nucleus in cells grown on RGD-functionalized homopolymers pCBAA (method A-1 in Figure 1) and pCBMAA (method B-1 in Figure 1) differ remarkably, even though both coatings exhibit antifouling properties, even after RGD-peptide functionalization. In [31], we showed a higher tendency of F-actin cytoskeleton-spreading on pCBAA in comparison to pCBMAA. In the literature, the connection between F-actin polymerization and YAP nuclear concentration is noted—when F-actin polymerization happens, the nuclear level of YAP increases [45,52]. This is in accordance with our results shown in Figure 3B, and it underlines the influence of physicochemical properties of the surface composition on the cell behavior (even if it is nontoxic and antifouling).

It is worth mentioning that we are aware of the limitations of this study that are related to a lack of quantification of RGD-peptide immobilization levels on pCB-based brushes. Using the available methods (for more details, see also the Supplementary Materials), a direct determination was found to be quite challenging. For example, while the level of immobilized RGD peptides on OEG SAM was quantified by the SPR method, it was not possible to determine the RGD-peptide surface concentration on the pCB-based coatings due to a very high pCB-based zwitterionic surface hydrophilicity [33,39,53] combined with a relatively small molecular weight of the RGD peptide (Figure S2 in the Supplementary Materials). Therefore, we were not able to directly compare the level of functionalization of pCBAA, pCBMAA-based coatings, and OEG-based coatings. However, in [42], we showed that the loading capacity of pCBMAA is quite comparable to pCBAA, so the comparable surface concentration of the RGD peptide can be expected on pCBMAA and pCBAA. Additionally, it should be noted that comparable protein-loading capacities for pCB-based brushes and OEG SAM were reported previously [43,54]. These findings indicate comparable saturation RGD peptide values for the respective functionalized coatings used in this study.

Zwitterionic materials and, namely, pCB-based materials represent emerging and very promising next-generation biomaterials for a wide range of biomedical applications [55]. Due to the excellent nonfouling properties and functionalization capabilities, such materials, in general, can be utilized to create various biomimetic systems, as well as multifunctional nanoparticles for multiple functional tissue scaffolds with cell-adhesive moieties and growth [56–58]. Therefore, the biomedical applications of zwitterionic functional materials continue to be a subject of extensive research and development.

## 5. Conclusions

Here, the RGD-functionalized pCB-based brushes were shown to be suitable and easily tunable platforms for mechanotransduction controlling and cell response manipulation. The results highlight the antifouling background as an essential element of cellular response studies. It was shown that zwitterionic-based antifouling brush architectures should be considered for the advanced design of next-generation surface platforms for the monitoring and quantification of cellular processes.

**Supplementary Materials:** The following are available online at <http://www.mdpi.com/2218-273X/10/8/1146/s1>. Figure S1: Examples of OEG SAM RGD-functionalization (A) and CB-based polymer brush RGD-functionalization (B) measured by SPR. Figure S2: Dependence of the RGD-immobilized level (given by SPR) on the volume concentration of RGD in a functionalization solution (A,B) and on the carboxy group content in the coatings (B,D). (A) 100% OEG-based SAM HS-(CH<sub>2</sub>)<sub>11</sub>-(EG)<sub>6</sub>-OCH<sub>2</sub>-COOH, (B) polymer brush of 100% pCBAA, (C) mixed OEG SAM of HS-(CH<sub>2</sub>)<sub>11</sub>-(EG)<sub>6</sub>-OCH<sub>2</sub>-COOH and HS-(CH<sub>2</sub>)<sub>11</sub>-(EG)<sub>4</sub>-OH, and (D) random copolymer brush of p(CBMAA-ran-HPMAA). Figure S3: Fouling level from undiluted human blood plasma after 10 min of exposure on RGD-functionalized surfaces. Figure S4: Cell death assessment on pCB antifouling RGD-functionalized coatings. Figure S5: Representative pictures from the spinning disk confocal microscope used for the cell growth assessment and images of YAP distributions in cells growing on a CB-containing antifouling background decorated with different RGD peptide concentrations.

**Author Contributions:** Conceptualization, I.V., A.D., and H.V.-L.; data curation, I.V., B.S., and M.U.; formal analysis, I.V., B.S., and M.U.; investigation, I.V., M.V., A.D., and H.V.-L.; methodology, I.V., M.V., and H.V.-L.; project administration, A.D. and H.V.-L.; resources, A.D. and H.V.-L.; supervision, H.V.-L.; visualization, I.V., B.S., and M.U.; writing—original draft, I.V. and D.E.C.; and writing—review and editing, B.S., M.U., M.V., D.E.C., M.H., M.P., P.S., Z.F., A.D., and H.V.-L. All authors have read and agreed to the published version of the manuscript.

**Funding:** This research was funded by Praemium Lumina quaeruntur of the Czech Academy of Sciences (LQ100101902) and by Operational Program Research, Development and Education financed by the European Structural and Investment Funds and the Czech Ministry of Education, Youth and Sports (Project No. SOLID21—CZ.02.1.01/0.0/0.0/16\_019/0000760).

**Acknowledgments:** The authors would like to thank Daniel Špaček for his help with the graphics designs.

**Conflicts of Interest:** The authors declare no conflict of interest.

## References

1. Wolfenson, H.; Yang, B.; Sheetz, M.P. Steps in Mechanotransduction Pathways that Control Cell Morphology. *Annu. Rev. Physiol.* **2019**, *81*, 585–605. [[CrossRef](#)] [[PubMed](#)]
2. Lansky, Z.; Mutsafi, Y.; Houben, L.; Ilani, T.; Armony, G.; Wolf, S.G.; Fass, D. 3D mapping of native extracellular matrix reveals cellular responses to the microenvironment. *JSBX* **2019**, *1*, 100002. [[CrossRef](#)] [[PubMed](#)]
3. Cobbaut, M.; Karagil, S.; Bruno, L.; Diaz de la Loza, M.D.C.; Mackenzie, F.E.; Stolinski, M.; Elbediwy, A. Dysfunctional Mechanotransduction through the YAP/TAZ/Hippo Pathway as a Feature of Chronic Disease. *Cells* **2020**, *9*, 151. [[CrossRef](#)] [[PubMed](#)]
4. Gautrot, J.E.; Malmström, J.; Sundh, M.; Margadant, C.; Sonnenberg, A.; Sutherland, D.S. The Nanoscale Geometrical Maturation of Focal Adhesions Controls Stem Cell Differentiation and Mechanotransduction. *Nano Lett.* **2014**, *14*, 3945–3952. [[CrossRef](#)] [[PubMed](#)]
5. Martino, F.; Perestrello, A.R.; Vinarský, V.; Pagliari, S.; Forte, G. Cellular Mechanotransduction: From Tension to Function. *Front. Physiol.* **2018**, *9*, 824. [[CrossRef](#)] [[PubMed](#)]
6. Elbediwy, A.; Vincent-Mistiaen, Z.I.; Spencer-Dene, B.; Stone, R.K.; Boeing, S.; Wculek, S.K.; Cordero, J.; Tan, E.H.; Ridgway, R.; Brunton, V.G.; et al. Integrin signalling regulates YAP and TAZ to control skin homeostasis. *Development* **2016**, *143*, 1674–1687. [[CrossRef](#)]
7. Mori, M.; Triboulet, R.; Mohseni, M.; Schlegelmilch, K.; Shrestha, K.; Camargo, F.D.; Gregory, R.I. Hippo signaling regulates microprocessor and links cell-density-dependent miRNA biogenesis to cancer. *Cell* **2014**, *156*, 893–906. [[CrossRef](#)]
8. Nardone, G.; Oliver-De La Cruz, J.; Vrbsky, J.; Martini, C.; Pribyl, J.; Skládal, P.; Pešl, M.; Caluori, G.; Pagliari, S.; Martino, F.; et al. YAP regulates cell mechanics by controlling focal adhesion assembly. *Nat. Commun.* **2017**, *8*, 15321. [[CrossRef](#)]
9. Piccolo, S.; Dupont, S.; Cordenonsi, M. The biology of YAP/TAZ: Hippo signaling and beyond. *Physiol. Rev.* **2014**, *94*, 1287–1312. [[CrossRef](#)]
10. Shreberk-Shaked, M.; Oren, M. New insights into YAP/TAZ nucleo-cytoplasmic shuttling: New cancer therapeutic opportunities? *Mol. Oncol.* **2019**, *13*, 1335–1341. [[CrossRef](#)]
11. Halder, G.; Dupont, S.; Piccolo, S. Transduction of mechanical and cytoskeletal cues by YAP and TAZ. *Nat. Rev. Mol. Cell Biol.* **2012**, *13*, 591–600. [[CrossRef](#)] [[PubMed](#)]
12. Schroeder, M.C.; Halder, G. Regulation of the Hippo pathway by cell architecture and mechanical signals. *Semin. Cell Dev. Biol.* **2012**, *23*, 803–811. [[CrossRef](#)] [[PubMed](#)]



13. Thomasy, S.M.; Morgan, J.T.; Wood, J.A.; Murphy, C.J.; Russell, P. Substratum stiffness and latrunculin B modulate the gene expression of the mechanotransducers YAP and TAZ in human trabecular meshwork cells. *Exp. Eye Res.* **2013**, *113*, 66–73. [[CrossRef](#)]
14. Aragona, M.; Panciera, T.; Manfrin, A.; Giullitti, S.; Michielin, F.; Elvassore, N.; Dupont, S.; Piccolo, S. A mechanical checkpoint controls multicellular growth through YAP/TAZ regulation by actin-processing factors. *Cell* **2013**, *154*, 1047–1059. [[CrossRef](#)] [[PubMed](#)]
15. Wada, K.; Itoga, K.; Okano, T.; Yonemura, S.; Sasaki, H. Hippo pathway regulation by cell morphology and stress fibers. *Development* **2011**, *138*, 3907–3914. [[CrossRef](#)] [[PubMed](#)]
16. Gibson, W.T.; Gibson, M.C. Cell topology, geometry, and morphogenesis in proliferating epithelia. *Curr. Top. Dev. Biol.* **2009**, *89*, 87–114. [[CrossRef](#)]
17. Zhao, B.; Wei, X.; Li, W.; Udan, R.S.; Yang, Q.; Kim, J.; Xie, J.; Ikenoue, T.; Yu, J.; Li, L.; et al. Inactivation of YAP oncoprotein by the Hippo pathway is involved in cell contact inhibition and tissue growth control. *Gene. Dev.* **2007**, *21*, 2747–2761. [[CrossRef](#)] [[PubMed](#)]
18. Varelas, X.; Samavarchi-Tehrani, P.; Narimatsu, M.; Weiss, A.; Cockburn, K.; Larsen, B.G.; Rossant, J.; Wrana, J.L. The Crumbs complex couples cell density sensing to Hippo-dependent control of the TGF-beta-SMAD pathway. *Dev. Cell* **2010**, *19*, 831–844. [[CrossRef](#)]
19. Monteiro, A.I.; Kollmetz, T.; Malmstrom, J. Engineered systems to study the synergistic signaling between integrin-mediated mechanotransduction and growth factors (Review). *Biointerphases* **2018**, *13*, 06d302. [[CrossRef](#)]
20. Poreba, R.; de los Santos Pereira, A.; Pola, R.; Jiang, S.; Pop-Georgievski, O.; Sedláková, Z.; Schönherr, H. “Clickable” and Antifouling Block Copolymer Brushes as a Versatile Platform for Peptide-Specific Cell Attachment. *Macromol. Biosci.* **2020**, *20*, 1900354. [[CrossRef](#)]
21. Goor, O.J.G.M.; Brouns, J.E.P.; Dankers, P.Y.W. Introduction of anti-fouling coatings at the surface of supramolecular elastomeric materials via post-modification of reactive supramolecular additives. *Polym. Chem.* **2017**, *8*, 5228–5238. [[CrossRef](#)]
22. Pape, A.C.H.; Ippel, B.D.; Dankers, P.Y.W. Cell and Protein Fouling Properties of Polymeric Mixtures Containing Supramolecular Poly(ethylene glycol) Additives. *Langmuir* **2017**, *33*, 4076–4082. [[CrossRef](#)] [[PubMed](#)]
23. Yang, F.; Liu, Y.; Zhang, Y.; Ren, B.; Xu, J.; Zheng, J. Synthesis and Characterization of Ultralow Fouling Poly(N-acryloyl-glycinamide) Brushes. *Langmuir* **2017**, *33*, 13964–13972. [[CrossRef](#)] [[PubMed](#)]
24. Sun, X.; Wang, H.; Wang, Y.; Gui, T.; Wang, K.; Gao, C. Creation of antifouling microarrays by photopolymerization of zwitterionic compounds for protein assay and cell patterning. *Biosens. Bioelectron.* **2018**, *102*, 63–69. [[CrossRef](#)] [[PubMed](#)]
25. Leigh, B.L.; Cheng, E.; Xu, L.; Andresen, C.; Hansen, M.R.; Guymon, C.A. Photopolymerizable Zwitterionic Polymer Patterns Control Cell Adhesion and Guide Neural Growth. *Biomacromolecules* **2017**, *18*, 2389–2401. [[CrossRef](#)]
26. Hersel, U.; Dahmen, C.; Kessler, H. RGD modified polymers: Biomaterials for stimulated cell adhesion and beyond. *Biomaterials* **2003**, *24*, 4385–4415. [[CrossRef](#)]
27. Chien, H.W.; Fu, S.W.; Shih, A.Y.; Tsai, W.B. Modulation of the stemness and osteogenic differentiation of human mesenchymal stem cells by controlling RGD concentrations of poly(carboxybetaine) hydrogel. *Biotechnol. J.* **2014**, *9*, 1613–1623. [[CrossRef](#)]
28. Rodda, A.E.; Ercole, F.; Glattauer, V.; Gardiner, J.; Nisbet, D.R.; Healy, K.E.; Forsythe, J.S.; Meagher, L. Low Fouling Electrospun Scaffolds with Clicked Bioactive Peptides for Specific Cell Attachment. *Biomacromolecules* **2015**, *16*, 2109–2118. [[CrossRef](#)]
29. Vaisocherová-Lísalová, H.; Víšová, I.; Ermini, M.L.; Špringer, T.; Song, X.C.; Mrázek, J.; Lamačová, J.; Scott Lynn, N.; Šedivák, P.; Homola, J. Low-fouling surface plasmon resonance biosensor for multi-step detection of foodborne bacterial pathogens in complex food samples. *Biosens. Bioelectron.* **2016**, *80*, 84–90. [[CrossRef](#)]
30. Vaisocherova, H.; Sipova, H.; Visova, I.; Bockova, M.; Springer, T.; Laura Ermini, M.; Song, X.; Krejcik, Z.; Chrastinova, L.; Pastva, O.; et al. Rapid and sensitive detection of multiple microRNAs in cell lysate by low-fouling surface plasmon resonance biosensor. *Biosens. Bioelectron.* **2015**, *70*, 226–231. [[CrossRef](#)]
31. Víšová, I.; Smolková, B.; Uzhytchak, M.; Vrabcová, M.; Zhigunova, Y.; Houska, M.; Surman, F.; de los Santos Pereira, A.; Lunov, O.; Dejneka, A.; et al. Modulation of Living Cell Behavior with Ultra-Low Fouling Polymer Brush Interfaces. *Macromol. Biosci.* **2020**, *20*, 1900351. [[CrossRef](#)] [[PubMed](#)]

32. Lokanathan, A.R.; Zhang, S.; Regina, V.R.; Cole, M.A.; Ogaki, R.; Dong, M.; Besenbacher, F.; Meyer, R.L.; Kingshott, P. Mixed poly (ethylene glycol) and oligo (ethylene glycol) layers on gold as nonfouling surfaces created by backfilling. *Biointerphases* **2011**, *6*, 180–188. [[CrossRef](#)] [[PubMed](#)]
33. Vaisocherova, H.; Brynda, E.; Homola, J. Functionalizable low-fouling coatings for label-free biosensing in complex biological media: Advances and applications. *Anal. Bioanal. Chem.* **2015**, *407*, 3927–3953. [[CrossRef](#)] [[PubMed](#)]
34. Lísalová, H.; Brynda, E.; Houska, M.; Víšová, I.; Mrkvová, K.; Song, X.C.; Gedeonová, E.; Surman, F.; Riedel, T.; Pop-Georgievski, O.; et al. Ultralow-Fouling Behavior of Biorecognition Coatings Based on Carboxy-Functional Brushes of Zwitterionic Homo- and Copolymers in Blood Plasma: Functionalization Matters. *Anal. Chem.* **2017**, *89*, 3524–3531. [[CrossRef](#)]
35. Smolkova, B.; Lunova, M.; Lynnyk, A.; Uzhytchak, M.; Churpita, O.; Jirsa, M.; Kubinova, S.; Lunov, O.; Dejneka, A. Non-Thermal Plasma, as a New Physicochemical Source, to Induce Redox Imbalance and Subsequent Cell Death in Liver Cancer Cell Lines. *Cell. Physiol. Biochem.* **2019**, *52*, 119–140. [[CrossRef](#)]
36. March, S.; Ramanan, V.; Trehan, K.; Ng, S.; Galstian, A.; Gural, N.; Scull, M.A.; Shlomai, A.; Mota, M.M.; Fleming, H.E.; et al. Micropatterned coculture of primary human hepatocytes and supportive cells for the study of hepatotropic pathogens. *Nat. Protoc.* **2015**, *10*, 2027–2053. [[CrossRef](#)]
37. Jelinek, M.; Kocourek, T.; Jurek, K.; Jelinek, M.; Smolková, B.; Uzhytchak, M.; Lunov, O. Preliminary Study of Ge-DLC Nanocomposite Biomaterials Prepared by Laser Codeposition. *Nanomaterials* **2019**, *9*, 451. [[CrossRef](#)]
38. Heggestad, J.T.; Fontes, C.M.; Joh, D.Y.; Hucknall, A.M.; Chilkoti, A. In Pursuit of Zero 2.0: Recent Developments in Nonfouling Polymer Brushes for Immunoassays. *Adv. Mater.* **2020**, *32*, 1903285. [[CrossRef](#)]
39. Jiang, C.; Wang, G.; Hein, R.; Liu, N.; Luo, X.; Davis, J.J. Antifouling Strategies for Selective In Vitro and In Vivo Sensing. *Chem. Rev.* **2020**, *120*, 3852–3889. [[CrossRef](#)]
40. Tocce, E.J.; Broderick, A.H.; Murphy, K.C.; Liliensiek, S.J.; Murphy, C.J.; Lynn, D.M.; Nealey, P.F. Functionalization of reactive polymer multilayers with RGD and an antifouling motif: RGD density provides control over human corneal epithelial cell-substrate interactions. *J. Biomed. Mater. Res. Part A* **2012**, *100*, 84–93. [[CrossRef](#)]
41. Yu, S.; Zuo, X.; Shen, T.; Duan, Y.; Mao, Z.; Gao, C. A density gradient of VAPG peptides on a cell-resisting surface achieves selective adhesion and directional migration of smooth muscle cells over fibroblasts. *Acta Biomater.* **2018**, *72*, 70–81. [[CrossRef](#)] [[PubMed](#)]
42. Vaisocherová-Lísalová, H.; Surman, F.; Víšová, I.; Vala, M.; Špringer, T.; Ermini, M.L.; Šípová, H.; Šedivák, P.; Houska, M.; Riedel, T.; et al. Copolymer Brush-Based Ultralow-Fouling Biorecognition Surface Platform for Food Safety. *Anal. Chem.* **2016**, *88*, 10533–10539. [[CrossRef](#)]
43. Vaisocherova, H.; Sevcu, V.; Adam, P.; Spackova, B.; Hegnerova, K.; Pereira, A.D.; Rodriguez-Emmenegger, C.; Riedel, T.; Houska, M.; Brynda, E.; et al. Functionalized ultra-low fouling carboxy- and hydroxy-functional surface platforms: Functionalization capacity, biorecognition capability and resistance to fouling from undiluted biological media. *Biosens. Bioelectron.* **2014**, *51*, 150–157. [[CrossRef](#)] [[PubMed](#)]
44. Brault, N.D.; White, A.D.; Taylor, A.D.; Yu, Q.; Jiang, S. Directly Functionalizable Surface Platform for Protein Arrays in Undiluted Human Blood Plasma. *Anal. Chem.* **2013**, *85*, 1447–1453. [[CrossRef](#)]
45. Low, B.C.; Pan, C.Q.; Shivashankar, G.V.; Bershadsky, A.; Sudol, M.; Sheetz, M. YAP/TAZ as mechanosensors and mechanotransducers in regulating organ size and tumor growth. *FEBS Lett.* **2014**, *588*, 2663–2670. [[CrossRef](#)] [[PubMed](#)]
46. Dupont, S.; Morsut, L.; Aragona, M.; Enzo, E.; Giulitti, S.; Cordenonsi, M.; Zanconato, F.; Le Digabel, J.; Forcato, M.; Bicciato, S.; et al. Role of YAP/TAZ in mechanotransduction. *Nature* **2011**, *474*, 179–183. [[CrossRef](#)]
47. Lin, X.; Jain, P.; Wu, K.; Hong, D.; Hung, H.-C.; O’Kelly, M.B.; Li, B.; Zhang, P.; Yuan, Z.; Jiang, S. Ultralow Fouling and Functionalizable Surface Chemistry Based on Zwitterionic Carboxybetaine Random Copolymers. *Langmuir* **2019**, *35*, 1544–1551. [[CrossRef](#)]
48. Abercrombie, M. Contact inhibition and malignancy. *Nature* **1979**, *281*, 259–262. [[CrossRef](#)]
49. Flammang, P.; Santos, R.; Aldred, N.; Gorb, S. (Eds.) *Biological and Biomimetic Adhesives: Challenges and Opportunities*; Royal Society of Chemistry: London, UK, 2013.
50. Kolahi, K.S.; Donjacour, A.; Liu, X.; Lin, W.; Simbulan, R.K.; Bloise, E.; Maltepe, E.; Rinaudo, E. Effect of Substrate Stiffness on Early Mouse Embryo Development. *PLoS ONE* **2012**, *7*, e41717. [[CrossRef](#)]

51. Durán-Pastén, M.L.; Cortes, D.; Valencia-Amaya, A.E.; King, S.; González-Gómez, G.H.; Hautefeuille, M. Cell Culture Platforms with Controllable Stiffness for Chick Embryonic Cardiomyocytes. *Biomimetics* **2019**, *4*, 33. [[CrossRef](#)]
52. Moroishi, T.; Hansen, C.G.; Guan, K.L. The emerging roles of YAP and TAZ in cancer. *Nat. Rev. Cancer* **2015**, *15*, 73–79. [[CrossRef](#)]
53. Víšová, I.; Vrabcová, M.; Forinová, M.; Zhignuova, Y.; Mironov, V.; Houska, M.; Bittrich, E.; Eichhorn, K.-J.; Hashim, H.; Schovanek, P.; et al. Surface Preconditioning Influences the Antifouling Capabilities of Zwitterionic and Nonionic Polymer Brushes. *Langmuir* **2020**, in press. [[CrossRef](#)]
54. Vaisocherová, H.; Zhang, Z.; Yang, W.; Cao, Z.; Cheng, G.; Taylor, A.D.; Piliarik, M.; Homola, J.; Jiang, S. Functionalizable surface platform with reduced nonspecific protein adsorption from full blood plasma-Material selection and protein immobilization optimization. *Biosens. Bioelectron.* **2008**, *24*, 1924–1930. [[CrossRef](#)] [[PubMed](#)]
55. Jiang, S.; Cao, Z. Ultralow-Fouling, Functionalizable, and Hydrolyzable Zwitterionic Materials and Their Derivatives for Biological Applications. *Adv. Mater.* **2010**, *22*, 920–932. [[CrossRef](#)] [[PubMed](#)]
56. Li, B.; Yuan, Z.; He, Y.; Hung, H.-C.; Jiang, S. Zwitterionic Nanoconjugate Enables Safe and Efficient Lymphatic Drug Delivery. *Nano Lett.* **2020**, *20*, 4693–4699. [[CrossRef](#)] [[PubMed](#)]
57. Li, B.; Yuan, Z.; Jain, P.; Hung, H.-C.; He, Y.; Lin, X.; McMullen, P.; Jiang, S. De Novo Design of Functional Zwitterionic Biomimetic Material for Immunomodulation. *Sci. Adv.* **2020**, *6*, eaba0754. [[CrossRef](#)]
58. Lin, X.; Boit, M.O.; Wu, K.; Jain, P.; Liu, E.J.; Hsieh, Y.-F.; Zhou, O.; Li, B.; Hung, H.-C.; Jiang, S. Zwitterionic carboxybetaine polymers extend the shelf-life of human platelets. *Acta Biomater.* **2020**, *109*, 51–60. [[CrossRef](#)]



© 2020 by the authors. Licensee MDPI, Basel, Switzerland. This article is an open access article distributed under the terms and conditions of the Creative Commons Attribution (CC BY) license (<http://creativecommons.org/licenses/by/4.0/>).

# Appendix VIII

Hashim, H., M. Kozhaev, P. Kapralov, L. Panina, V. Belotelov, I. Víšová, D. Chvostova, A. Dejneka, I. Shpetnyi, V. Latyshev, S. Vorobiov and V. Komanicky

**Controlling the Transverse Magneto-Optical Kerr Effect in Cr/NiFe  
Bilayer Thin Films by Changing the Thicknesses of the Cr Layer**

*Nanomaterials* **10**(2) (2020): 10.



Article

# Controlling the Transverse Magneto-Optical Kerr Effect in Cr/NiFe Bilayer Thin Films by Changing the Thicknesses of the Cr Layer

Hisham Hashim <sup>1,2</sup>, Mikhail Kozhaev <sup>3,4</sup>, Pavel Kapralov <sup>3</sup>, Larissa Panina <sup>1,5,\*</sup>, Vladimir Belotelov <sup>3</sup>, Ivana Víšová <sup>6</sup>, Dagmar Chvostová <sup>6</sup>, Alexandr Dejneka <sup>6</sup>, Ihor Shpetnyi <sup>7</sup>, Vitalii Latyshev <sup>8</sup>, Serhii Vorobiov <sup>7,8</sup> and Vladimír Komanický <sup>8</sup>

<sup>1</sup> Department of Technology of Electronic Materials, National University of Science and Technology (MISIS), Moscow 119049, Russia; hh@science.tanta.edu.eg

<sup>2</sup> Department of Physics, Faculty of Science, Tanta University, Tanta 31527, Egypt

<sup>3</sup> Russian Quantum Center, Skolkovo, Moscow Region 143025, Russia; mikhaikozhaev@gmail.com (M.K.); p.kapralov@rqc.ru (P.K.); v.i.belotelov@ya.ru (V.B.)

<sup>4</sup> Prokhorov General Physics Institute of the Russian Academy of Sciences, Moscow 119991, Russia

<sup>5</sup> Institute of Physics, Mathematics and IT, Immanuel Kant Baltic Federal University, Kaliningrad 236041, Russia

<sup>6</sup> Institute of Physics, Czech Academy of Sciences, Prague 18221, Czech Republic; visova@fzu.cz (I.V.); chvostov@fzu.cz (D.C.); dejneka@fzu.cz (A.D.)

<sup>7</sup> Sumy State University, 2, Rymsky Korsakov Str., 40007 Sumy, Ukraine; i.shpetnyi@aph.sumdu.edu.ua (I.S.); serhii.vorobiov@gmail.com (S.V.)

<sup>8</sup> Institute of Physics, P.J. Šafárik University, 041 80 Košice, Slovak; latyshev.mail@yandex.ua (V.L.); vladimir.komanicky@upjs.sk (V.K.)

\* Correspondence: lpanina@misis.ru; Tel.: +7-9260765513

Received: 30 December 2019; Accepted: 28 January 2020; Published: 1 February 2020



**Abstract:** Here, we demonstrate the impact of ferromagnetic layer coating on controlling the magneto-optical response. We found that the transverse magneto-optical Kerr effect (TMOKE) signal and TMOKE hysteresis loops of Ni<sub>80</sub>Fe<sub>20</sub> thin layers coated with a Cr layer show a strong dependence on the thickness of the Cr layer and the incidence angle of the light. The transmission and reflection spectra were measured over a range of incidence angles and with different wavelengths so as to determine the layers' optical parameters and to explain the TMOKE behavior. The generalized magneto-optical and ellipsometry (GMOE) model based on modified Abeles characteristic matrices was used to examine the agreement between the experimental and theoretical results. A comprehensive theoretical and experimental analysis reveals the possibility to create a TMOKE suppression/enhancement coating at specific controllable incidence angles. This has potential for applications in optical microscopy and sensors.

**Keywords:** transverse magneto-optical Kerr effect (TMOKE); ferromagnetic coupling (FMC); suppression or enhancement of magneto-optical properties; magnetic nanostructure multilayers; reflectivity

## 1. Introduction

Magnetic multilayered structures are of prime interest, as their properties significantly differ from the corresponding bulk materials. Nanostructured thin films are also of great technological importance for applications in nanoelectronics and spintronics [1,2], data storage technologies [3,4], magnetic and biological sensors [5–7] and optical filtering [8,9]. Many practically important physical effects have been discovered in multilayered films, including exchange coupling between ferromagnetic films separated by a non-ferromagnetic layer.

Giant magnetoresistance in Fe/Cr multilayers and antiferromagnetic coupling between ferromagnetic layers assisted by the Cr-spacing generated particular interest in ferromagnetic film systems containing Cr layers. Controlling the properties of the layers and interfaces makes it possible to develop new concepts that would potentially result in novel applications [10–13]. In this paper, we apply ellipsometry and the magneto-optical Kerr effect (MOKE) as effective methods to characterize the ultra-thin bilayer films of NiFe coated with different thicknesses of Cr. It is demonstrated that the functional Cr layer at an optimized thickness and angle of incidence behaves as an enhancement layer.

In general, MOKE is of interest for light modulation, with a magnetic field that typically requires MOKE enhancement by interferometric [14] or resonance [2,15] methods. On the other hand, magneto-optical effects provide a powerful nondestructive technique to investigate magnetization behavior in magnetic nanostructures, such as measuring magnetic hysteresis loops and imaging the magnetic domains [16,17]. The transverse magneto-optical Kerr effect (TMOKE) is a simple, economical and sensitive method to measure thin magnetic films in comparison with superconducting quantum interference device (SQUID) and Vibrating Sample Magnetometer (VSM) [18]. In TMOKE, one examines the changes in the intensity of the reflected light from (or transmitted light through) a magnetized material [19]. This effect arises because the complex refractive indices of the magnetized material are different for left- and right-circularly polarized light.

Spectroscopic ellipsometry methods are well developed to measure the optical parameters and thicknesses of multilayers, with low losses. It is more challenging to characterize absorbing multilayers, as there is a correlation between the complex refractive index and the layer thickness [20]. For magnetic multilayers, it is useful to combine ellipsometry and MOKE methods [21]. In particular, a simple analytical model can be proposed for a generalized magneto-optical and ellipsometry (GMOE) scheme in the transverse magneto-optical configuration. GMOE allows for fitting the unique wavelength-dependent diagonal permittivity of every layer in the multilayer films, and to identify the off-diagonal elements responsible for the magneto-optical signals [22].

In this work, we have investigated the effect of the interface between ferromagnetic and antiferromagnetic materials in bilayer ultra-thin films by employing ellipsometry measurements along with TMOKE. We have compared the experimental results with a theory based on the GMOE model of a ferromagnetic film coated with a non-magnetic layer. It has been revealed that the angular response of TMOKE for a simple structure of NiFe coated with a Cr layer is sensitive to the thickness of the Cr layer, which creates suppression/enhancement points. Such behavior is caused mainly by the interferences between the layers, as the optical properties of thin Cr layers (below 20 nm) are found to be typical of dielectric materials. This could be of interest for the development of optical microscopy [23] and sensing [24,25].

#### *Generalised Magneto-Optical and Ellipsometry (GMOE) Formalism*

In the case of linear, with respect to the layer magnetization, MOKE, the phenomenological description for the multi-layered system is based on the matrix-form permittivity for magnetic layers. Considering the ellipsometry and TMOKE responses, it is convenient to use an extension of the Abeles characteristic matrixes [26].

Assuming that the plane of incidence is the (y, z) plane and the magnetization is in the film plane (along the x-axis for a transverse Kerr effect), as shown in Figure 1, the permittivity of an isotropic magnetic layer has the following form:

$$\hat{\varepsilon} = \varepsilon_m \begin{pmatrix} 1 & 0 & 0 \\ 0 & 1 & -iQ\gamma \\ 0 & iQ\gamma & 1 \end{pmatrix} \quad (1)$$

here,  $\varepsilon_m$  is the diagonal permittivity,  $Q$  is the magneto-optical constant and  $\gamma$  is the x-directional cosine of the magnetization. In this case, the p-polarized ( $H_x$ ,  $E_y$  and  $E_z$ ) and s-polarized ( $E_x$ ,  $H_y$  and  $H_z$ ) waves remain the eigenfunctions of the wave equations.

The amplitudes of the corresponding fields at the zero boundary ( $U_0, V_0$ ) are related to those at the end medium ( $U, V$ ) via a characteristic matrix  $\hat{M}$ , as follows:

$$\begin{pmatrix} U_0 \\ V_0 \end{pmatrix} = \hat{M} \begin{pmatrix} U \\ V \end{pmatrix} \quad (2)$$

The matrix  $\hat{M}$  of the multi-layered film is composed of the characteristic matrices of the individual layers:

$$\hat{M} = \prod_{j=1,2} \hat{M}_j \quad (3)$$

The reflection ( $r$ ) and transmission ( $t$ ) coefficients are found from the following:

$$\begin{pmatrix} 1 + r \\ (-1 + r) \cos \theta_0 / n_0 \end{pmatrix} = \hat{M} \begin{pmatrix} t \\ -t \cos \theta_s / n_s \end{pmatrix} \quad (4)$$

here,  $\theta_0, \theta_s$  are the angles of incidence and refraction, respectively, and  $n_0, n_s$  are the refractive indexes of the medium of incidence and the end medium (substrate), respectively. The form of the characteristic matrices depends on the polarization.

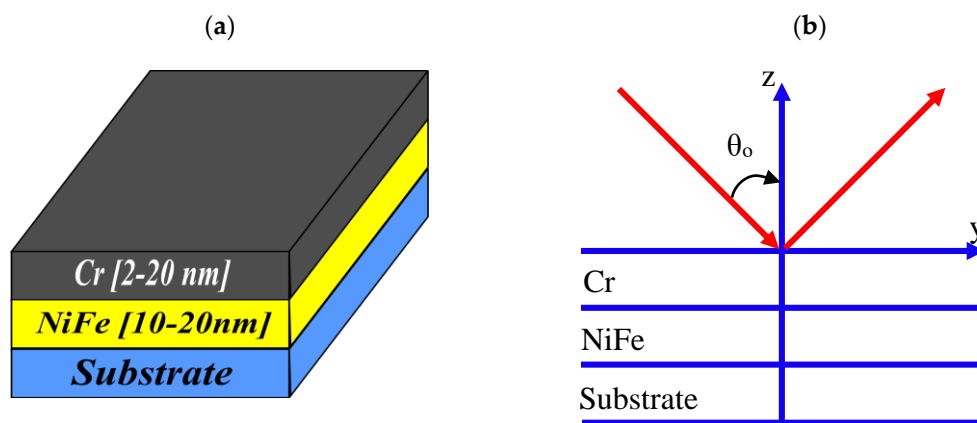


Figure 1. (a) Structure of the fabricated samples and (b) the optical scheme.

This formalism can be extended to the case of linear magneto-optical (MO) effects. A simple analytical expression is obtained for the  $\hat{M}_j$  of the magnetic layer and the TMOKE configuration when the permittivity tensor is given by Equation (1) [27]. In the present work, we demonstrate that the model can be applied to describe the variations in the reflected intensity caused by the layer re-magnetization. The presence of magnetization modifies only the characteristic matrix of the p-polarized waves. The form of the wave equations in the magnetic layer does not change, but there is a modification in the relation between the components of magnetic and electric fields, as follows:

$$\frac{dH_x}{dy} = ik_0 \epsilon_m (iQ\gamma E_y + E_z) \quad (5)$$

$$\frac{dH_x}{dz} = -ik_0 \epsilon_m (E_y - iQ\gamma E_z) \quad (6)$$

In Equations (5) and (6),  $k_0 = 2\pi/\lambda$ ,  $\lambda$  is the wavelength in a vacuum. The characteristic matrix of the magnetic layer is of the following form:

$$\hat{M} = \begin{pmatrix} \cos(\beta h) - \zeta \sin(\beta h) & i \sin(\beta h) / q \\ i q \sin(\beta h) & \cos(\beta h) + \zeta \sin(\beta h) \end{pmatrix} \quad (7)$$

The parameters entering Equation (7) are as follows:

$$\beta = k_0 n_m \cos \theta_m, \quad \zeta = Q\gamma \tan \theta_m, \quad q = \frac{\cos \theta_m}{n_m}, \quad n_m = \sqrt{\varepsilon_m} \quad (8)$$

In Equation (8),  $\theta_m$  is the refraction angle in the magnetic layer and  $h$  is the thickness of the magnetic layer. In a linear approximation with respect to  $\zeta$ , the determinant of the characteristic matrix is equal to 1.

In the case of an s-polarized wave, the characteristic matrix corresponds to that of a non-magnetic layer, that is, the diagonal components of  $\hat{M}$  do not contain the term proportional to  $Q$ , and in the off-diagonal components, the parameter  $q$  is replaced by  $\cos \theta_m n_m$ . Therefore, the formalism of the characteristic matrices makes it possible to calculate both the ellipsometry and TMOKE responses. The ellipsometry parameter  $\rho$  is defined as the ratio of the reflection parameters  $r_p$  and  $r_s$  of the p- and s-polarized waves, as follows:

$$\rho = \tan \psi \exp(i\Delta) = \frac{r_p}{r_s} \quad (9)$$

The TMOKE parameter  $\delta(\gamma)$  is defined as the relative change in the intensity of the p-polarized waves upon magnetization, as follows:

$$\delta(\gamma) = 2 \frac{|r_p(\gamma)|^2 - |r_p(\gamma = -1)|^2}{|r_p(\gamma = 1)|^2 + |r_p(\gamma = -1)|^2} \quad (10)$$

## 2. Materials and Methods

In our experimental measurements, we investigated bilayer thin films of Cr/Ni<sub>80</sub>Fe<sub>20</sub>, which were prepared by magnetron sputtering (ATC Orion 8 Sputtering Systems, AJA International, North Scituate, MA, USA) on glass substrates. The thicknesses of the layers varied from 2 to 20 nm, and from 10 to 20 nm for the Cr and Ni<sub>80</sub>Fe<sub>20</sub> layers, respectively. To obtain the permalloy layer, the Ni<sub>80</sub>Fe<sub>20</sub> target (from AJA International, North Scituate, MA, USA) was used. The sputtering rates were 0.13 nm/s for Ni<sub>80</sub>Fe<sub>20</sub> and 0.28 nm/s for Cr (99.99% purity; AJA International, North Scituate, MA, USA). The sputtering rates were optimized for the material used. The films were prepared in the condition of an ultrahigh vacuum and a high-purity argon atmosphere, therefore, a lower sputtering rate did not affect the layer quality. The thickness was controlled by the quartz resonator method. We also controlled the concentration of components in the NiFe layer after deposition by using energy dispersive X-ray spectroscopy (EDS) (Oxford Instruments, Oxford, UK) analysis. The results show that the deviation from the specified concentration did not exceed 0.5% for all of the samples, which was within the accuracy of the EDS detector used.

The spectroscopic ellipsometry measures  $\psi$  and  $\Delta$  in Equation (9) both represent the elliptical polarization output state after the reflection of linearly polarized light at an oblique incidence off the film sample. They depend on the refractive indexes and thicknesses of the individual layers in the film. Therefore, the method makes it possible to determine the parameters for which a model describing the reflectance spectra of the film system must be built in order to theoretically obtain the values of  $\psi$  and  $\Delta$ . Then, the optical parameters of the individual layers are deduced from fitting the experimental and modelled data [28]. The spectra of  $\psi$  and  $\Delta$  were measured using variable angle spectroscopic ellipsometry (VASE; J.A. Woollam and Co., Nebraska, USA) at two incidence angles of 65° and 70°, working in rotating analyzer mode with an incident wavelength range from 300 to 1050 nm. The WVASE32 software package, containing the refractive index database for a large number of materials, was used as a simulator of a sample to fit and analyze the measured spectra in order to define the optical constants of the individual layers of Cr and NiFe when combined in a bilayer thin film, and to examine if these values depend on a particular layer thickness. In addition, a bare NiFe film with a thickness of 20 nm was inspected to accurately determine the optical constants of the individual



layers of the films. The measured parameters were used in the GMOE model to quantitatively describe the observed magneto-optical response.

A schematic illustration of the TMOKE setup is shown in Figure 2. The experimental measurements were carried out at room temperature. A laser diode with a wavelength of 780 nm and a power of 5 mW was used as the light source. Subsequently, the polarizer light was focused onto the sample, placed in alternating magnetic field with a maximum intensity of 50 mT. The reflected light beam from the surface of the sample was collimated with a lens, and then divided by a Wollaston prism into two beams with vertical and horizontal polarizations. A balanced photodetector was used for the signal measurement. Simultaneously, the signals from the electromagnet and balanced photodetector were recorded and analyzed.

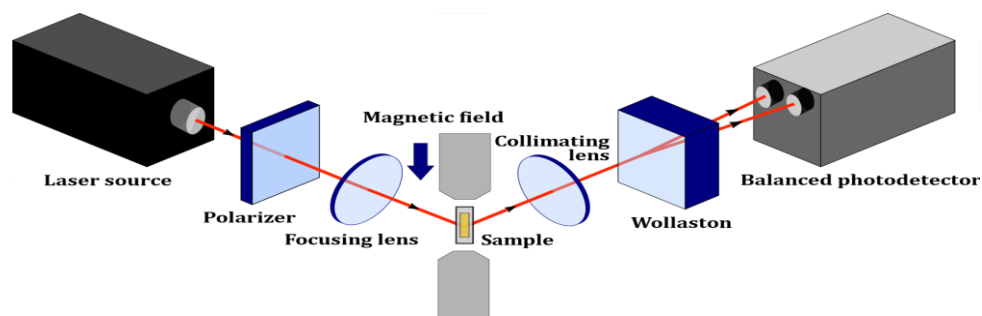


**Figure 2.** Schematic diagram of the transverse magneto-optical Kerr effect (TMOKE) setup.

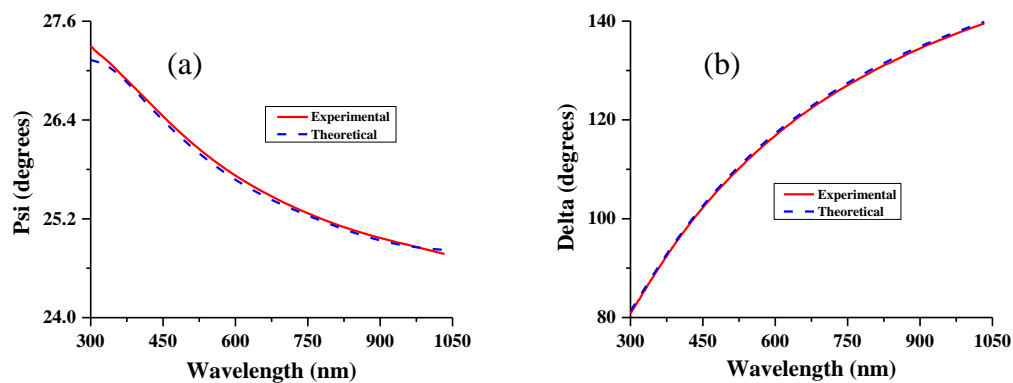
We also measured the reflectance at a zero field and maximum TMOKE signal, which is proportional to the relative change in the reflected light intensity at two opposite directions of the external magnetic field (corresponds to  $\delta(1)$  in Equation (10)) for a range of angles of incidence from 10 to 70°.

### 3. Results and Discussion

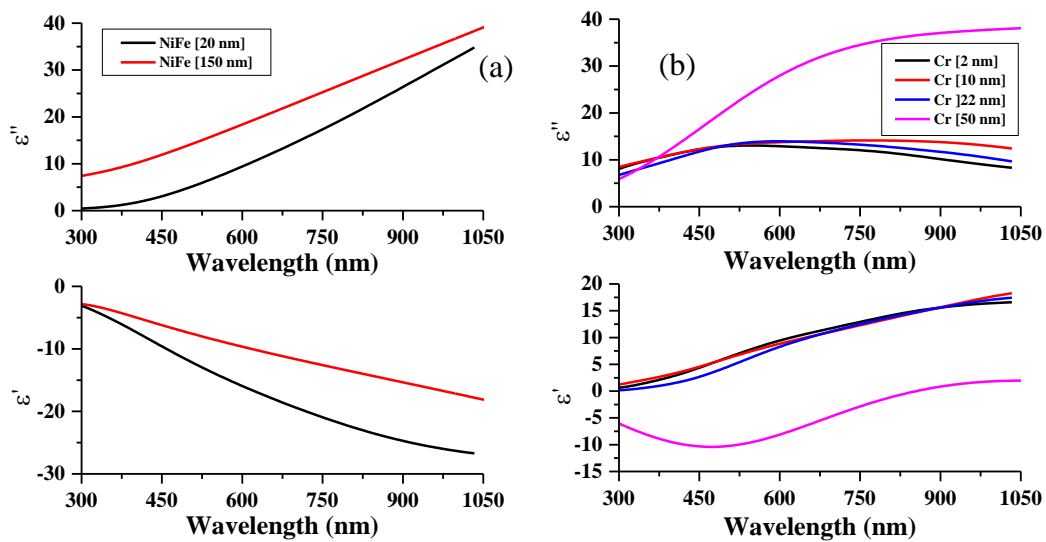
#### Spectroscopic Ellipsometry Characterization

Figure 3 shows an example of the measured ellipsometry parameter spectra for the bilayer Cr/NiFe film, along with the modelled spectra. The calculations are based on a two-layer model. There is an obvious consistency between the measured and the calculated angles of  $\psi$  and  $\Delta$  within the fitting model. The difference is lower than 1%, which ensures the reliability of the data for the optical parameters of thin layers used.

Figure 4 shows the complex-valued permittivity spectra  $\varepsilon = \varepsilon' + i\varepsilon''$  for the individual layers constituting the film system, which were deduced by fitting the experimental ellipsometry angles and theoretical angles calculated within the two-layer model. For comparison, the data for the bulk materials (in the form of thicker films) are given. The permittivity data deduced from fitting for different layer thicknesses are consistent. However, there might be a significant difference between the obtained permittivity values of the thin layers and those known for the bulk materials [29,30]. In the case of the Cr thin film, the permittivity shows a “less” metallic behavior. In particular, the real part of the permittivity for the Cr layer shows positive values. This is consistent with the increase in resistivity with decreasing the Cr layer thickness [10]. We will further demonstrate that the obtained permittivity spectra accurately describe the observed optical and magneto-optical behaviors.



**Figure 3.** Experimental and calculated ellipsometry angles (a) for  $\psi$  and (b) for  $\Delta$ ; were obtained for Cr (2 nm)/NiFe (20 nm) films with a  $70^\circ$  incidence angle at room temperature. The measured and modelled values are represented with solid and dashed lines, respectively.



**Figure 4.** Real ( $\epsilon'$ ) and imaginary ( $\epsilon''$ ) parts of permittivity for (a) NiFe and (b) Cr layers obtained from fitting the ellipsometry measurement of a two-layer film system. For comparison, the data for bulk materials (in the form of thicker films) are given [29,30].

The obtained optical parameters  $\epsilon'$  and  $\epsilon''$  from the ellipsometry measurements of the individual Cr and NiFe thin layers will be used in the GMOE model to obtain the theoretical angular dependence of light reflectance vs. NiFe magnetization and the maximal TMOKE signal of  $\delta_{max}$  within a range of incidence angles.

The angular dependence of reflectance for the p-polarized laser light at a range of incidence angles from  $10^\circ$  to  $70^\circ$  is presented in Figure 5. We simulated the reflectance by using the permittivity values obtained from the ellipsometry data. The experimental and calculated data agree well (with an accuracy of less than 10%), which demonstrates that the obtained permittivity spectra for thin layers quantitatively characterize the optical behavior of the multilayered thin films. The difference may be related to a weak dependence of the layer permittivity on the thickness, as seen in Figure 4. The reflectance shows a reverse dependence on the incidence angle, and it increases alongside the Cr layer thickness.

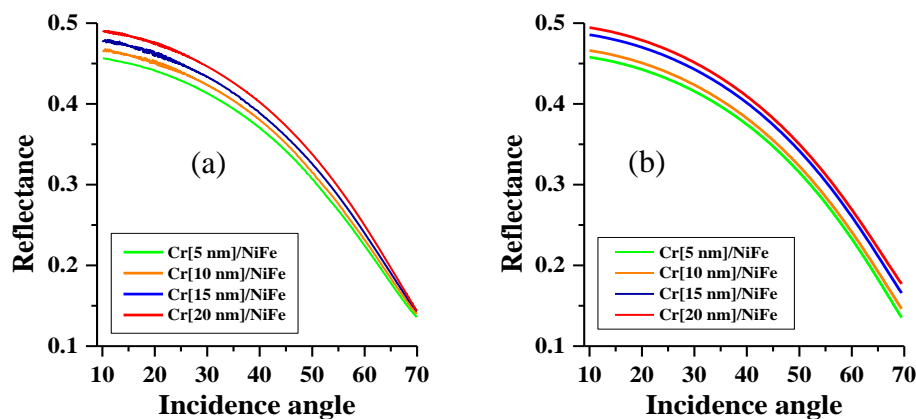


**Figure 5.** Reflectance parameters of p-polarized light vs. incidence angle  $\theta_0$  for Cr/NiFe films with different thicknesses of the Cr layer and with the thickness of NiFe fixed to 10 nm: (a) experimental plots and (b) the theoretical plots calculated with the layer optical parameters deduced from the ellipsometry measurements.

Figure 6 shows the maximal TMOKE signals  $\delta_{max} = \delta(1)$  measured and calculated for the Cr/NiFe thin films as a function of the incidence angle for different thicknesses of the Cr layer. For modelling, the magneto-optical constant for NiFe was taken as  $Q = 0.0177 - i 0.0063$  [31], and the optical constants of the Cr and NiFe layers were taken from our ellipsometry measurements. When increasing the incidence angle  $\theta_0$ , the value of  $\delta_{max}$  changed value, but the angle of the zero signal strongly depended on the thickness of the Cr layer, as follows:  $\theta_0$  changed from 40 to 60° when the thickness increased from 5 to 20 nm. At a fixed  $\theta_0$  within this range of angles, it was possible to observe a changing TMOKE response as the Cr layer thickness increases, as follows: firstly,  $\delta_{max}$  decreased going through zero, and then increased manifold. In particular, a strong increase of four to five times was observed for  $\theta_0 = 45 - 50^\circ$ . The mechanism of TMOKE is related to the dependence of the boundary conditions for fields ( $H_x, E_y$ ) on the x-magnetization of the ferromagnetic layer. The boundary condition also includes the magnitudes of the reflected/transmitted waves. Then, the interference effect of the Cr layer, which is characterized by a relatively large and positive real part of the permittivity, considerably influences the TMOKE signal. The theoretical results describe well the experimental data within the all-optical model. Some discrepancies may be related to the definition of the magneto-optical constant  $Q$  and the possible impact of ferromagnetic/antiferromagnetic coupling causing spin diffusion. Figure 6 also reveals the possibility of analyzing an in-depth profile of the ultra-thin bilayer films by the TMOKE technique, as the signal angular spectra demonstrate different depth sensitivities.

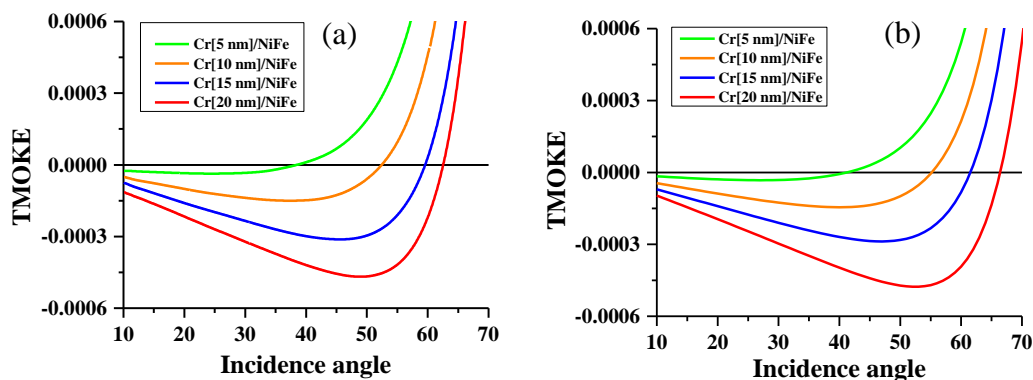


**Figure 6.** Maximal TMOKE signal  $\delta_{max}$  vs. incidence angle  $\theta_0$  for the Cr/NiFe films with different thicknesses of the Cr layer and with the thickness of the NiFe layer fixed to 10 nm: (a) experimental plots and (b) theoretical plots. The theoretical curves are obtained using the deduced results of optical parameters from the ellipsometry experiment.

The investigated thin films were mounted in the TMOKE configuration, as shown in Figure 2. The TMOKE signal is represented by the relative change in intensity  $\delta(\gamma)$  in Equation (10), when the directional cosine  $\gamma$  varies in the presence of the external field. This constitutes the transverse hysteresis loops, which were measured at two different incidence angles of 30 and 50° in the presence of an in-plane magnetic field and are given in Figure 7.

The maximal TMOKE signal  $\delta_{max} = \delta(1)$ , which should correspond to the film magnetization  $M_s$  aligned along the magnetic field, is strongly affected by increasing the thickness of the Cr layer and the angle of incidence. For  $\theta_0 = 30^\circ$ ,  $\delta_{max}$  and the apparent  $M_s$  gradually increase with increasing the Cr layer thickness. Increasing  $\theta_0$  to 50° results in a transformation in the hysteresis loops; the loop shrinks in a vertical direction, increasing the Cr layer thickness as  $M_s$  decreases. With a further increase in the Cr layer thickness, the loops reverse and the value of  $\delta_{max}$  starts to increase. This behavior reflects the change in the TMOKE sign, as the signal increases six times when the Cr layer thickness increases from 5 to 20 nm. Such an unusual behavior could be quantitatively explained within the all-optical model, with the layer optical parameters found from the ellipsometry measurements, as demonstrated in Figure 6b. The coercivity does not change, with the Cr layer thickness confirming that the quality of the interface is not affected by the increase in Cr layer thickness.

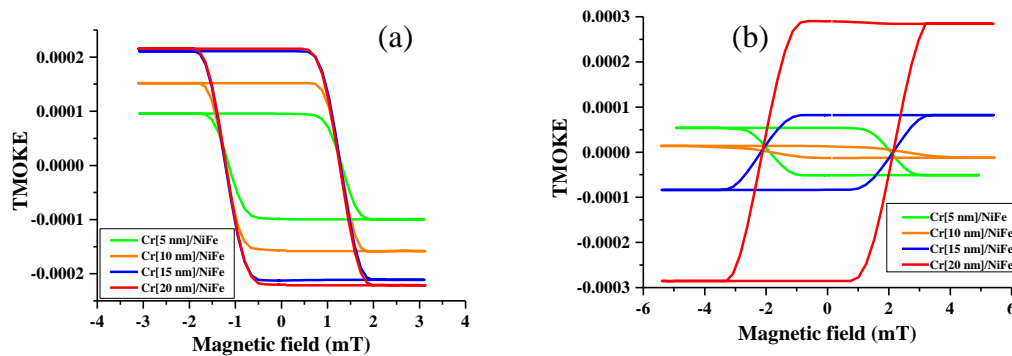


**Figure 7.** TMOKE hysteresis loops with an in-plane applied magnetic field at two different incidence angle Cr/NiFe films, with different thicknesses of the Cr film and the thickness of NiFe fixed to 10 nm: (a) at 30° and (b) at 50°.

#### 4. Conclusions

In summary, this work examined the influence of a top layer of Cr on the optical and magneto-optical properties of the bilayer films based on NiFe, demonstrating that the use of a functional Cr layer may enhance the magneto-optical response. A generalized model for ellipsometry and transverse MOKE analysis based on the extension of the Abeles characteristic matrixes was demonstrated to quantitatively describe the magneto-optical response. To fit the experimental and theoretical data, it was important to determine the optical parameters of the thin layers of Cr and NiFe, which could differ substantially from those of the bulk counterparts. The optical parameters of the individual layers were extracted from the ellipsometry measurements. Some additional contributions to the enhancement of the transverse MOKE response could also be due to the coupling between NiFe and antiferromagnetic Cr.

**Author Contributions:** L.P. did the conceptualization, supervision, validation, wrote the original draft, reviewing and editing; H.H. did the experiments, data curation, formal analysis, investigation, visualization and wrote the original draft of this paper; M.K. did the formal analysis, methodology, visualization, review and editing; P.K. did the investigation, methodology and visualization; V.B. and A.D. did the supervision, project administration and methodology; V.K., V.L., I.S., S.V. did the methodology and resources; D.C. and I.V. did the formal analysis and methodology. All authors have read and agree to the published version of the manuscript.

**Funding:** The authors gratefully acknowledge the financial support of the Ministry of Science and Higher Education of the Russian Federation in the framework of the Increases Competitiveness Program of MISiS (a support project for young research engineers). L.V. Panina acknowledges the support for this work under the Russian Federation State Contract for organizing a scientific work (grant no. 3.8022.2017). M.A. Kozhaev, P.O. Kapralov and V.I. Belotelov acknowledge the support by the Russian Foundation for Basic Research (grant no. 18-52-80038). This work was partially supported by Operational Program Research, Development and Education financed by the European Structural and Investment Funds and the Czech Ministry of Education, Youth and Sports (project no. SOLID21-CZ.02.1.01/0.0/0.0/16\_019/0000760). Work at Safarik University was supported by grant VEGA No. 1/0204/18, and the grant of the Slovak Research and Development Agency under the contract No. APVV-17-0059.

**Conflicts of Interest:** The authors declare no conflict of interest.

## References

1. Hashim, H.; Singkh, S.P.; Panina, L.V.; Pudonin, F.A.; Sherstnev, I.A.; Podgornaya, S.V.; Shpetny, I.A.; Beklemisheva, A.V. Spectral ellipsometry as a method for characterization of nanosized films with ferromagnetic layers. *Phys. Solid State* **2017**, *59*, 2211. [[CrossRef](#)]
2. Dyakov, S.A.; Klompaker, L.; Spitzer, F.; Yalcin, E.; Akimov, I.; Yavsin, D.A.; Pavlov, S.I.; Pevtsov, A.B.; Verbin, S.Y.; Tikhodeev, S.G.; et al. Wide band enhancement of transverse magneto-optic Kerr effect in magnetite-based plasmonic crystals. *Phys. Rev. B* **2019**, *100*, 214411. [[CrossRef](#)]
3. Betzig, E.; Trautman, J.K.; Wolfe, R.; Gyorgy, E.M.; Finn, P.L.; Kryder, M.H.; Chang, C.H. Near-field magneto-optics and high density data storage. *Appl. Phys. Lett.* **1992**, *61*, 142. [[CrossRef](#)]
4. Mok, K.; Kovács, G.J.; McCord, J.; Li, L.; Helm, M.; Schmidt, H. Magneto-optical coupling in ferromagnetic thin films investigated by vector-magneto-optical generalized ellipsometry. *Phys. Rev. B* **2011**, *84*, 094413. [[CrossRef](#)]
5. Didosyan, Y.S.; Hauser, H.; Wolfmayr, H.; Nicolics, J.; Fulmek, P. Magneto-optical rotational speed sensor. *Sensor. Actuat. A Phys.* **2003**, *106*, 168. [[CrossRef](#)]
6. Sepúlveda, B.; Calle, A.; Lechuga, L.M.; Armelles, G. Highly sensitive detection of biomolecules with the magneto-optic surface-plasmon-resonance sensor. *Opt. Lett.* **2006**, *31*, 1085. [[CrossRef](#)] [[PubMed](#)]
7. Regatos, D.; Sepúlveda, B.; Fariña, D.; Carrascosa, L.G.; Lechuga, L.M. Suitable combination of noble/ferromagnetic metal multilayers for enhanced magneto-plasmonic biosensing. *Opt. Express* **2011**, *19*, 8336. [[CrossRef](#)]
8. Rotondaro, M.D.; Zhdanov, B.V.; Knize, R.J. Generalized treatment of magneto-optical transmission filters. *Opt. Soc. Am. B* **2015**, *32*, 2507. [[CrossRef](#)]
9. Keaveney, J.; Wrathmall, S.A.; Adams, C.S.; Hughes, I.G. Optimized ultra-narrow atomic bandpass filters via magneto-optic rotation in an unconstrained geometry. *Opt. Lett.* **2018**, *43*, 4272. [[CrossRef](#)]
10. Qu, D.; Huang, S.Y.; Chien, C.L. Inverse spin Hall effect in Cr: Independence of antiferromagnetic ordering. *Phys. Rev. B* **2015**, *92*, 020418. [[CrossRef](#)]
11. Turgut, E.; Laovorakiat, C.; Shaw, J.M.; Grychtol, P.; Nembach, H.T.; Rudolf, D.; Adam, R.; Aeschlimann, M.; Schneider, C.M.; Silva, T.J.; et al. Controlling the Competition between Optically Induced Ultrafast Spin-Flip Scattering and Spin Transport in Magnetic Multilayers. *Phys. Rev. Lett.* **2013**, *110*, 197201. [[CrossRef](#)] [[PubMed](#)]
12. Petrița, I.; Ungureanu, F.; Manta, V. Effects of laser beam modulation on all-optical switching phase diagrams in magneto-optical ultrafast storage device. *J. Comput. Electron.* **2015**, *14*, 627–633. [[CrossRef](#)]
13. Petrița, I.; Manta, V. Metropolis Monte Carlo analysis of all-optical switching. *Comput. Phys. Commun.* **2014**, *185*, 2874–2878. [[CrossRef](#)]
14. Ghanaatshoar, M.; Moradi, M. Magneto-optical Kerr-effect enhancement in glass/Cu/SnO<sub>2</sub>/Co/SnO<sub>2</sub> thin films. *Opt. Eng.* **2011**, *50*, 093801.
15. Belotelov, V.I.; Akimov, I.A.; Pohl, M.; Kotov, V.A.; Kasture, S.; Vengurlekar, A.S.; Gopal, A.V.; Yakovlev, D.R.; Zvezdin, A.K.; Bayer, M. Enhanced magneto-optical effects in magnetoplasmonic crystals. *Nat. Nanotechnol.* **2011**, *6*, 370–376. [[CrossRef](#)]
16. Barman, A.; Sinha, J. *Spin Dynamics and Damping in Ferromagnetic Thin Films and Nanostructures*; Springer International Publishing: Kolkata, India, 2017; Volume 3, pp. 48–50.

17. Borovkova, O.V.; Hashim, H.; Kozhaev, M.A.; Dagesyan, S.A.; Chakravarty, A.; Levy, M.; Belotelov, V.I. TMOKE as efficient tool for the magneto-optic analysis of ultra-thin magnetic films. *Appl. Phys. Lett.* **2018**, *112*, 063101. [[CrossRef](#)]
18. Pathak, S.; Sharma, M. Polar magneto-optical Kerr effect instrument for 1-dimensional magnetic nanostructures. *Appl. Phys.* **2014**, *115*, 043906. [[CrossRef](#)]
19. Singh, V.; Annadi, A.; Bhoi, B.; Madugundo, R.; Muthu, M.; Bohra, M. Synthesis, Properties, and Applications of Multifunctional Magnetic Nanostructures. *J. Nanomater.* **2019**, 2638715. [[CrossRef](#)]
20. Hilfiker, J.N.; Singh, N.; Tiwald, T.; Convey, D.; Baker, J.H.; Tompkins, H.G. Survey of methods to characterize thin absorbing films with Spectroscopic Ellipsometry. *Thin Solid Films* **2008**, *516*, 7979. [[CrossRef](#)]
21. Postava, K.; Maziewski, A.; Stupakiewicz, A.; Wawro, A.; Baczewski, L.T.; Visnovsky, S.; Yamaguchi, T. Transverse magneto-optical Kerr effect measured using phase modulation. *JEOS:RP* **2006**, *1*, 06017. [[CrossRef](#)]
22. Allen, G.A.; Dionne, G.F. Accurate analysis of the magneto-optical permittivity tensor of  $Y_3Fe_5O_{12}$ . *Appl. Phys.* **2003**, *93*, 6951. [[CrossRef](#)]
23. Liu, J.; Singh, A.; Llandro, J.; Duffy, L.B.; Stanton, M.R.; Holmes, S.N.; Applegate, M.J.; Phillips, R.T.; Hesjedal, T.; Barnes, C.H.W. A low-temperature Kerr effect microscope for the simultaneous magneto-optic and magneto-transport study of magnetic topological insulators. *Meas. Sci. Technol.* **2019**, *30*, 125201. [[CrossRef](#)]
24. Armelles, G.; Cebollada, A.; García-Martín, A.; González, M.U. Magnetoplasmonics: Combining Magnetic and Plasmonic Functionalities. *Adv. Opt. Mater.* **2013**, *1*, 10–35. [[CrossRef](#)]
25. Piskin, H.; Akdogan, N. Interface-induced enhancement of sensitivity in NiFe/Pt/IrMn-based planar hall sensors with nanoTesla resolution. *Sensor. Actuat.* **2019**, *292*, 24–29. [[CrossRef](#)]
26. Born, M.; Wolf, E. *Principles of Optics*, 7th ed.; Cambridge University Press: New York, NY, USA, 2002; pp. 1–70.
27. Hashim, H.; Singkh, S.P.; Panina, L.V.; Pudonin, F.A.; Sherstnev, I.; Podgornaya, S.V.; Shpetny, I.A. Optical and magnetic properties of Al/NiFe and Al/Ge/NiFe nanosized films. *EPJ Web Confer.* **2018**, *185*, 04014. [[CrossRef](#)]
28. Rebib, F.; Tomasella, E.; Gaston, J.P.; Eypert, C.; Cellier, J.; Jacquet, M. Determination of optical properties of a-SiOxNy thin films by ellipsometric and UV-visible spectroscopies. *J. Phys.* **2008**, *100*, 082033. [[CrossRef](#)]
29. McPeak, K.M.; Jayanti, S.V.; Kress, S.; Meyer, S.; Iotti, S.; Rossinelli, A.; Norris, D.J. Plasmonic films can easily be better: Rules and recipes. *ACS Photonics* **2015**, *2*, 326. [[CrossRef](#)]
30. Rakić, A.D.; Djurišić, A.B.; Elazar, J.M.; Majewski, M.L. Optical properties of metallic films for vertical-cavity optoelectronic devices. *Appl. Opt.* **1998**, *37*, 5271. [[CrossRef](#)]
31. Neuber, G.; Rauer, R.; Kunze, J.; Backstrom, J.; Rübhausen, M. Generalized magneto-optical ellipsometry in ferromagnetic metals. *Thin Solid Films* **2004**, *455*, 39–42. [[CrossRef](#)]



# Appendix IX

Víšová, I., M. Forinová, A. Pilipenco, K. Mezuláníková, M. Tomandlová, M. Vrabcová, M. Houska, A. Dejneka, J. Dostálek, H. Vaisocherová-Lísalová

**Recovery of Antifouling Properties of Zwitterionic Brushes after Postmodification with Bioactive Molecules Significantly Improves Label-Free Biosensing in Complex Media.**

Submitted in *ACS Applied Materials & Interfaces* (2021)

This document is confidential and is proprietary to the American Chemical Society and its authors. Do not copy or disclose without written permission. If you have received this item in error, notify the sender and delete all copies.

**Recovery of Antifouling Properties of Zwitterionic Brushes after Postmodification with Bioactive Molecules Significantly Improves Label-Free Biosensing in Complex Media**

Journal:	<i>ACS Applied Materials &amp; Interfaces</i>
Manuscript ID	am-2021-03472z
Manuscript Type:	Article
Date Submitted by the Author:	22-Feb-2021
Complete List of Authors:	V&iacute;acute;&scaron;ov&aacute;acute;, Ivana; Institute of Physics Czech Academy of Sciences, Optics Forinová, Michala; Institute of Physics Czech Academy of Sciences, Department of Optical and Biophysical Systems Pilipenco, Alina; Institute of Physics Czech Academy of Sciences, Department of Optical and Biophysical Systems Mezuláníková, Kateřina; Imperial College London, Department of Life Sciences; Institute of Physics Czech Academy of Sciences, Optics Tomandlová, Markéta; Institute of Physics Czech Academy of Sciences, Department of Optical and Biophysical Systems Vrabcová, Markéta; Institute of Physics Czech Academy of Sciences, Department of Optical and Biophysical Systems Houska, Milan; Institute of Physics Czech Academy of Sciences, Department of Optical and Biophysical Systems Dejneka, Alexandr; Institute of Physics Czech Academy of Sciences, Dostalek, Jakub; Austrian Institute of Technology, BioSensor Technologies; Institute of Physics Czech Academy of Sciences, Department of Optical and Biophysical Systems Vaisocherová - Lísalová, Hana; Institute of Physics Czech Academy of Sciences, Department of Optical and Biophysical Systems

SCHOLARONE™  
Manuscripts



# Recovery of Antifouling Properties of Zwitterionic Brushes after Postmodification with Bioactive Molecules Significantly Improves Label-Free Biosensing in Complex Media

Ivana Víšová<sup>1</sup>, Michala Forinová<sup>1</sup>, Alina Pilipenco<sup>1</sup>, Kateřina Mezuláníková<sup>2</sup>, Markéta Tomandlová<sup>1</sup>, Markéta Vrabcová<sup>1</sup>, Milan Houska<sup>1</sup>, Alexandr Dejneka<sup>1</sup>, Jakub Dostálek<sup>1,3</sup>, Hana Vaisocherová-Lísalová<sup>1\*</sup>

<sup>1</sup> Institute of Physics of the CAS, Na Slovance 2, Prague, Czech Republic

<sup>2</sup> Department of Life Sciences, Imperial College London, London SW7 2AZ

<sup>3</sup> Austrian Institute of Technology GmbH, Konrad-Lorenz-Strasse 24, Tulln, Austria

Corresponding Author: Hana Vaisocherová-Lísalová, Ph.D., Institute of Physics, Academy of Sciences of the Czech Republic, Na Slovance 2, 18221 Prague, Czech Republic; Tel.: +420 266 05 29 93, E-mail: lisalova@fzu.cz.

---

## ABSTRACT:

---

Robust antifouling coatings with specific biofunctional moieties are of the utmost importance in a range of biomedical and bioanalytical technologies. In particular, they are highly attractive in conjunction with devices that operate in contact with bodily fluids, tissues, or food samples, in which the nonspecific deposition of biomaterial (fouling) could severely impair their performance. To anchor functional biomolecules, the majority of antifouling coatings are designed to bear carboxy groups enabling their convenient postmodification via the amine coupling. Here we show that the process of

1  
2  
3 deactivation of unreacted carboxy groups after the postmodification is crucial for  
4 preserving the coating antifouling properties. We investigate the postmodification of  
5 carboxybetaine-based functionalized polymer and copolymer brushes representing  
6 biosensor-attractive antifouling functionalizable materials and report on the tailoring of  
7 the deactivation of residual active esters remaining in the coating after its conjugating  
8 with functional biomolecules. The deactivation by a mixture of small molecules with  
9 primary amines and carboxy-, sulfate- or sulfo- groups allows restoring the optimum  
10 charge balance and fouling resistance of the coating as characterized by FT-IRRAS,  
11 and SPR methods. We show that the surface mass density of nonspecifically adsorbed  
12 species onto functionalized zwitterionic coatings can be suppressed by one order of  
13 magnitude when challenged with undiluted blood plasma or crude minced meat  
14 samples. The ability to improve the functionality of biorecognition element-modified  
15 antifouling coating is further demonstrated by the label-free SPR detection of *E.coli*  
16 O157:H7 in crude minced meat. The optimized deactivation procedure enables  
17 improving the limit of detection (LOD) in a direct detection format by two orders of  
18 magnitude compared to previously published procedures, resulting in LOD in a food  
19 sample  $< 10^2$  CFU/mL. The reported approach is generic and may be readily applied  
20 in other zwitterionic systems, which suffer from impaired antifouling properties after the  
21 surface postmodifications.  
22  
23  
24  
25  
26  
27  
28  
29  
30  
31  
32  
33  
34  
35  
36  
37  
38  
39  
40  
41  
42  
43  
44  
45

---

46  
47 **Keywords:** resistance to fouling; antifouling polymer brush; zwitterion;  
48 functionalization; EDC/NHS; biosensor  
49  
50  
51

---

## 52 53 54 55 **1. Introduction**

56  
57 The rapid progress in important fields of bioanalytics, biomedicine, or food safety and  
58 security trigger demands for efficient functional coatings that are resistant to fouling  
59  
60

1  
2  
3 from complex real-world samples <sup>1-4</sup>. Through the last several decades, this problem  
4  
5 has been addressed by intensive research, and various strategies were pursued to  
6  
7 protect artificial surfaces against nonspecific adsorption <sup>5-7</sup>. Depending on the  
8  
9 application, such protection aims solely at the resistance to fouling (antifouling  
10  
11 coatings) or has to provide antifouling properties that are combined with functionality  
12  
13 provided by anchoring additional bioactive moieties (functionalized antifouling  
14  
15 coatings) <sup>8-14</sup>. Applications that rely on such functionalized antifouling coatings span  
16  
17 from various bioanalytical platforms for rapid detection of chemical and biological  
18  
19 species, coatings of nanoparticles used in drug delivery, membranes for separation  
20  
21 and cleaning technologies, scaffolds for tissue engineering, to the protection of ship  
22  
23 hulls. Among all these fields that can benefit from efficient and versatile functionalized  
24  
25 antifouling coatings, this paper is primarily focused on polymer architectures that are  
26  
27 typically, but not exclusively, used for biosensing.

28  
29  
30  
31  
32  
33 Zwitterionic poly(carboxybetaine)-based (pCB) polymer brushes or hydrogels that are  
34  
35 'grafted from' or 'grafted to' the surface stand out from a variety of investigated  
36  
37 antifouling functionalizable coatings <sup>15-16</sup>. For example, such coatings were developed  
38  
39 based on poly(carboxybetaine acrylamide) (pCBAA) polymer <sup>16</sup>, poly(carboxybetaine  
40  
41 methacrylamide) (pCBMAA) polymer <sup>17</sup>, or recently investigated random p(CBMAA-co-  
42  
43 HPMAA) copolymer <sup>10, 18</sup> of CBMAA and non-ionic poly[*N*-(2-hydroxypropyl)  
44  
45 methacrylamide] (HPMAA). Their hydrophilicity and zwitterionic structure endow with  
46  
47 superior fouling resistance <sup>19-21</sup>, offer high loading capacity for the attachment of  
48  
49 biorecognition elements (BREs), and also can provide attractive biocompatible  
50  
51 characteristics <sup>18, 22-25</sup>.

52  
53  
54  
55  
56  
57 Arguably, the most common method for the postmodification of polymer antifouling  
58  
59 coatings with BREs is based on the amine coupling chemistry <sup>1, 26-28</sup>. In the most  
60

1  
2  
3 frequently used approach, the carboxy groups present at the surface are activated by  
4  
5 sequential reaction with 1-ethyl-3-(3-dimethylaminopropyl)carbodiimide hydrochloride  
6  
7 (EDC) and *N*-hydroxysuccinimide (NHS) or sulfo-NHS to form active NHS esters <sup>29</sup>.  
8  
9  
10 Afterward, the surface with the active NHS esters is brought in contact with BREs and  
11  
12 allowed to react with their primary amine groups to form stable covalent bonds.  
13  
14 However, typically only a small portion of available active esters can react with BREs  
15  
16 due to the steric restrictions. Following the generally accepted scheme, the unreacted  
17  
18 active esters spontaneously hydrolyze in aqueous solutions, restoring the initial  
19  
20 carboxy groups <sup>30</sup>. Even though NHS esters in solution were reported to hydrolyze fast  
21  
22 and easily <sup>31</sup>, for instance, Schönherr et al. showed a significant decrease in the rate  
23  
24 constants of active esters hydrolysis at surfaces caused by in-plane confinement  
25  
26 effects <sup>32</sup>. When the NHS ester hydrolysis was applied in postmodification of the  
27  
28 antifouling zwitterionic brushes, the unreacted active NHS esters and molecular  
29  
30 changes in postmodified brush structure significantly impaired the resistance to fouling  
31  
32 <sup>17, 25</sup>. A modified deactivation route based on a reaction of active NHS esters with a  
33  
34 glycine, a small molecule carrying primary amine and carboxy-groups, was suggested  
35  
36 to address this problem <sup>17, 33</sup>.  
37  
38  
39  
40  
41

42  
43 Importantly, the deactivation step has to remove all active esters and restore the  
44  
45 neutral net charge of the functionalized polymer brush structure, which is a key  
46  
47 prerequisite for its antifouling characteristics. In general, the zwitterionic balance  
48  
49 between negative and positive charges is disrupted either through the use of carboxy  
50  
51 groups for the conjugation with BRE, the net charge of the BRE itself, or by the limited  
52  
53 performance of the subsequent deactivation step.  
54  
55

56  
57 Here, we explore the compensating of these effects by deactivation of active NHS  
58  
59 esters using an optimized mixture of selected low molecular weight molecules bearing  
60

1  
2  
3 primary amines and additional negatively charged moieties. These include two  
4  
5 carboxy-terminated compounds: a synthetic derivative modified with an inserted  
6  
7 ethoxy group, 2-(2-aminoethoxy)acetic acid (AEAA), and natural amino acid glycine as  
8  
9 a reference <sup>17, 33</sup>. The AEAA ethoxy group is more hydrophilic than hydrophobic  
10  
11 aliphatic chain <sup>34</sup> and thus is hypothesized to restore the antifouling properties more  
12  
13 effectively. In addition, two deactivating agents bearing permanent negative charges  
14  
15 2-aminoethyl hydrogen sulfate (D1) and aminomethanesulfonic acid (D2), and their  
16  
17 mixtures with glycine or AEAA were tested.  
18  
19  
20  
21

22 To investigate versatility of such approach, two established zwitterionic  
23  
24 carboxybetaine-based polymer brushes, poly(carboxybetaine acrylamide) (pCBAA)  
25  
26 and random copolymer [p(CBMAA-co-HPMAA)] of carboxybetaine methacrylamide  
27  
28 (CBMAA) and poly[*N*-(2-hydroxypropyl) methacrylamide] (HPMAA) were employed.  
29  
30 The introduction of a specific surface density of permanent negative charge in  
31  
32 deactivated structure is assumed to neutralize the surplus positive charge of the  
33  
34 quaternary ammonium group associated with the functionalization of the betaine  
35  
36 moiety.  
37  
38  
39  
40

41 Fourier transform infrared reflection-absorption spectroscopy (FT-IRRAS) was used to  
42  
43 analyze respective molecular changes after the EDC/NHS-based activation and  
44  
45 deactivation steps. A surface plasmon resonance (SPR) sensor was employed to  
46  
47 assess the impact of the deactivation protocols on the resistance to fouling from  
48  
49 undiluted human blood plasma (i.e., commonly accepted reference complex sample <sup>1</sup>)  
50  
51 and crude minced meat sample (employed in the food control analysis for the presence  
52  
53 of pathogens). The optimized deactivation procedures of anti-bacteria antibody-  
54  
55 functionalized pCBAA were utilized in the label-free SPR detection of a foodborne  
56  
57 bacterial pathogen *E.coli* O157:H7 from a food sample. A crude minced meat sample,  
58  
59  
60

1  
2  
3 which is a relevant complex sample for pathogen analysis in food control <sup>35</sup> was used.  
4  
5 The results show a strong improvement (up to two orders of magnitude compared to  
6  
7 previously published procedures) of the determined LOD and LOQ values highlighting  
8  
9 the importance of the surface deactivation method for the development of highly  
10  
11 sensitive biosensors.  
12  
13  
14  
15  
16  
17

## 18 **2. Materials and methods**

### 19 **2.1. Reagents**

20  
21 All aqueous solutions were prepared using ultrapure water (18.0 MΩ.cm, Milli-Q®  
22  
23 system, Merck). Stock chemicals for the preparation of phosphate-buffered saline  
24  
25 (PBS, 0.01 M phosphate, 0.138 M sodium chloride, 0.0027 M potassium chloride, pH  
26  
27 7.4 at 25 °C), borate buffer (10 mM sodium borate, pH 8 at 25°C), glycine (1 M glycine,  
28  
29 pH 7.0 at 25 °C), 2-aminoethyl hydrogen sulfate (D1, 0.8 M, pH 7.0 at 25 °C),  
30  
31 aminomethanesulfonic acid (D2, 0.8 M, pH 7.0 at 25 °C) were from Sigma-Aldrich,  
32  
33 Czech Republic. 2-(2-aminoethoxy)acetic acid (AEAA) was from VWR International,  
34  
35 Czech Republic. The PBS-NaCl buffer (0.01 M phosphate, 0.75 M sodium chloride,  
36  
37 0.0027 M potassium chloride, pH 7.4) was prepared from PBS stock solution. The  
38  
39 carboxybetaine acrylamide, carboxybetaine methacrylamide, and N-(2-hydroxypropyl)  
40  
41 methacrylamide monomers were from Specific Polymers, France. 1,4,8,11-  
42  
43 tetramethyl-1,4,8,11-tetraazacyclotetradecane (Me4Cyclam, 98%), CuCl (≥ 99.995%),  
44  
45 CuCl<sub>2</sub> (99.999%), methanol (≥ 99.9%) and ethanol (99,9%) were from Sigma-Aldrich.  
46  
47 Tetrahydrofuran (THF, ≥99.9%) was from Penta, Czech Republic. N-  
48  
49 hydroxysuccinimide (NHS) and N-ethyl-N'-(3-diethylaminopropyl)carbodiimide (EDC)  
50  
51 were from AP Czech, Czech Republic. Anti- *E.coli* O157:H7 antibody (anti- *E.coli*) and  
52  
53  
54  
55  
56  
57  
58  
59  
60

1  
2  
3 heat-killed *Escherichia coli* O157:H7 (*E.coli*) were from KPL Inc., USA. The procedure  
4 for the preparation of the minced meat sample is described in the Supporting  
5 Information. Human blood plasma (pooled, mixed gender) in sodium citrate was from  
6 VWR International, Czech Republic.  
7  
8  
9  
10  
11  
12  
13  
14

## 15 **2.2. Preparation of polymer brush coatings**

16  
17  
18 pCBAA and p(CBMAA-co-HPMAA) polymer brush coatings were prepared on the SPR  
19 chip (substrates made from BK7 glass coated with 5 nm thick Ti and 50 nm thick gold  
20 layers) by surface-initiated atom transfer radical polymerization (SI-ATRP) according  
21 to the procedure described elsewhere <sup>22</sup>. A random copolymer p(CBMAA-co-HPMAA)  
22 was composed of CBMAA (15% monomer concentration) and HPMAA (85% monomer  
23 concentration). Successful polymerization was checked by FT-IRRAS and  
24 spectroscopic ellipsometry measurements (data not shown). A detailed description of  
25 the procedure can be found in Supporting Information.  
26  
27  
28  
29  
30  
31  
32  
33  
34  
35  
36  
37  
38  
39

## 40 **2.3. Preparation of deactivation solutions**

41  
42  
43 AEAA was dissolved in ultra-pure water (1 M, pH set to 7), aliquoted, and stored at -  
44 20 °C till used. Glycine dissolved in ultra-pure water (1M, pH set to 7) was prepared  
45 fresh every week and stored at 6 °C till used. 2-aminoethyl hydrogen sulfate (D1) or  
46 aminomethanesulfonic acid (D2) were dissolved in ultra-pure water (both 0.8 M, pH set  
47 to 7) and stored at 6 °C till used. To prevent oversaturation and subsequent  
48 precipitation, the procedure described in Supporting Information was applied.  
49  
50  
51  
52  
53  
54  
55

56  
57 It should be noted that 2-aminoethyl hydrogen sulfate tends to crystalize when placed  
58 in the fridge. This can be overcome by heating the solution to 45 °C in a lidded  
59  
60

1  
2  
3 container. Once cooled to room temperature, the solution remains fully homogeneous.  
4  
5 Although aminomethanesulfonic acid does not precipitate at low temperatures, it is  
6  
7 more prone to oversaturation during the process of dissolution.  
8  
9

#### 10 **2.4. SPR measurements**

11  
12  
13 SPR experiments were performed using the angular multiparametric SPR with a 4-  
14  
15 channel microfluidic system (BioNavis Ltd, Finland) and a LED source emitting at a  
16  
17 wavelength of 670 nm. The SPR sensor response change measured in angular units  
18  
19 were converted into surface mass density units using  $0.001^\circ = 0.85 \text{ ng/cm}^2$ .  
20  
21

22  
23 SPR experiments to probe the fouling resistance of functionalized pCB-coatings (i) and  
24  
25 biorecognition calibration-curves experiments (ii) were performed as follows: pCB  
26  
27 coatings were washed with ultra-pure water, dried with airflow, and mounted into the  
28  
29 SPR system. After a few minutes of washing the surface with water to establish a  
30  
31 baseline in the SPR response, the aqueous solution of 0.5 M EDC and 0.1 M NHS was  
32  
33 injected for 20 minutes (12  $\mu\text{L}/\text{min}$ ), followed by injections of ultrapure water for 2  
34  
35 minutes, 50  $\mu\text{g}/\text{mL}$  of anti-*E.coli* antibody in borate buffer (10 mM borate buffer, pH 8,  
36  
37 15  $\mu\text{L}/\text{min}$ ) for 20 minutes, and water for 2 minutes to reach baseline again. The  
38  
39 deactivation reaction was held for 30 minutes at a flow rate of 12  $\mu\text{L}/\text{min}$  by using  
40  
41 deactivation solutions described in Supporting Information (Table S1). Subsequently,  
42  
43 ultrapure water (2 min, 30  $\mu\text{L}/\text{min}$ ) and PBS (10 min, 30  $\mu\text{L}/\text{min}$ ) were flowed over the  
44  
45 sensor surface to create a baseline.  
46  
47  
48  
49

50  
51 Then, in (i) experiments, the undiluted human blood plasma (annealed to 50°C and  
52  
53 cooled down to room temperature, pH 7.9) was injected for 10 minutes (30  $\mu\text{L}/\text{min}$ ),  
54  
55 followed by injections of PBS for 10 minutes, PBS-NaCl for 5 minutes, and PBS for  
56  
57 further 10 minutes. The fouling level was assessed either as the difference between  
58  
59 baseline established upon the flow of PBS before and 10 minutes after the plasma  
60



1  
2  
3 injection or as the difference between the SPR response upon the flow of PBS before  
4 the plasma injection and after 5 minutes incubation with PBS-NaCl. The typical SPR  
5 sensorgram is shown in Supporting Information (Figure S14).  
6  
7  
8  
9

10 In (ii), a set of concentrations ( $10^4$  -  $10^7$  CFU/mL) of heat-killed *E.coli* in a minced meat  
11 sample (pH 6.8) were prepared and subsequently flowed over the functionalized and  
12 deactivated surface for 10 minutes (30  $\mu$ L/min). The level of detection was assessed  
13 as the difference between SPR sensor response baseline upon the flowing PBS before  
14 and 10 minutes after the sample injection.  
15  
16  
17  
18  
19  
20  
21  
22  
23  
24

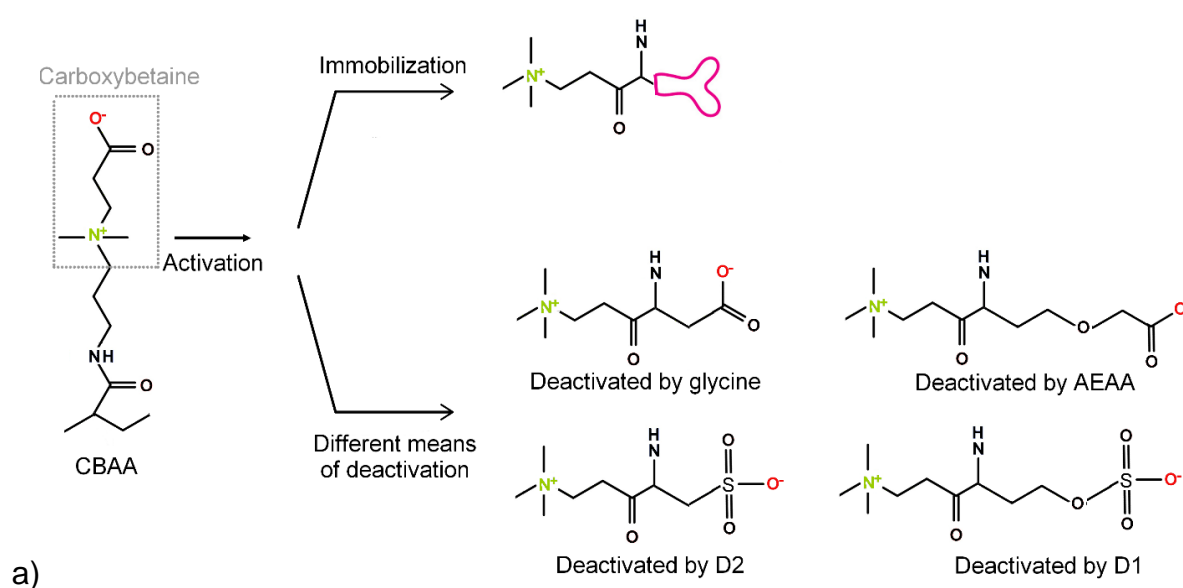
## 25 **2.5. FT-IRRAS measurements**

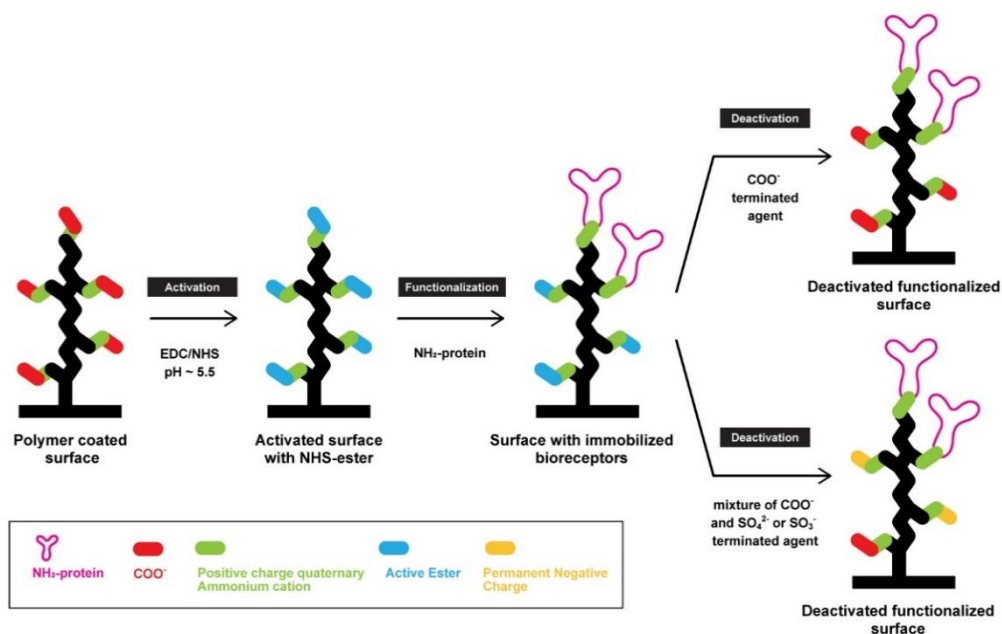
26  
27  
28 FT-IRRAS spectra of dry polymer brushes on gold were scanned using Thermo  
29 Scientific™ Nicolet™ iS50 FTIR Spectrometer equipped with Thermo Scientific™  
30 Smart SAGA™ Accessory. The spectra were collected with 200 scans at 4  $\text{cm}^{-1}$   
31 resolution and an 80° reflection angle.  
32  
33  
34  
35  
36  
37

38 The polymer brushes on the gold-coated SPR sensor chips were rinsed with ultrapure  
39 water, dried and reference spectra of bare unmodified coatings were recorded for every  
40 single chip. Afterward, the chips were immersed in an aqueous solution of 0.1 M NHS  
41 and 0.5 M EDC and let react for 20 minutes, while horizontally shaken at 250 rpm. The  
42 activated coatings were then rinsed with ultrapure water and deactivated for 30 minutes  
43 by different deactivating solutions, while horizontally shaken at 250 rpm. Finally, the  
44 chips were rinsed with ultrapure water, dried and the spectra were immediately  
45 measured.  
46  
47  
48  
49  
50  
51  
52  
53  
54  
55  
56  
57  
58  
59  
60

## **3. Results and discussion**

1  
2  
3 The deactivation approach for recovering the antifouling properties of functionalized  
4 pCB-based brushes was evaluated by using a set of SPR and FTIR experiments. To  
5  
6 pCB-based polymer brushes were synthesized by the 'grafting from' method on gold-  
7  
8 coated SPR sensor chips. They were composed of pCBAAs homopolymer and  
9  
10 p(CBMAA-co-HPMAA) copolymer exhibiting a wet thickness of ~75 nm and ~90 nm,  
11  
12 and swelling ratio of ~616 % and ~260 %, respectively, as determined in previous  
13  
14 studies <sup>22</sup>. In SPR experiments, the pCB-brushes were functionalized with  
15  
16 immunoglobulin G antibody (anti-*E.coli* O157:H7 antibody). The surface mass density  
17  
18 of the anchored IgG in the pCBAAs brush ( $350 \pm 50 \text{ ng/cm}^2$ ) was about 4.3-fold higher  
19  
20 than on the p(CBMAA-co-HPMAA) copolymer brush ( $81 \pm 35 \text{ ng/cm}^2$ ) due to the higher  
21  
22 amount of carboxy groups in the homopolymer pCBAAs brush. As Figure 1 summarizes,  
23  
24 after functionalization the unreacted NHS esters were deactivated by covalent  
25  
26 attachment of glycine, AEAA, D1, or D2 and by using their mixtures (see also Table  
27  
28 S1).  
29  
30  
31  
32  
33  
34  
35  
36  
37  
38  
39  
40  
41  
42  
43  
44  
45  
46  
47  
48  
49  
50  
51  
52  
53  
54  
55  
56  
57  
58  
59  
60





b)

Figure 1: a) CBAA monomer unit before activation (left), the detail of the structure after BRE immobilization (right-top), and products of active ester deactivation by four different small molecules (glycine, AEAA, D1, and D2, right bottom). Positively charged atoms are depicted green, negatively charged atoms are depicted red. b) Schematics of the brush architecture changes after the functionalization and deactivation by restoring carboxy groups, the positive charge of the coating is in abundance (upper case). The mixture of the optimized ratio of permanent negative charges along with carboxy groups (bottom case) allows the surface to optimize its charge balance and to restore better its resistance to fouling.

### 3.1. Effect of deactivation agents on fouling resistance of pCB brushes

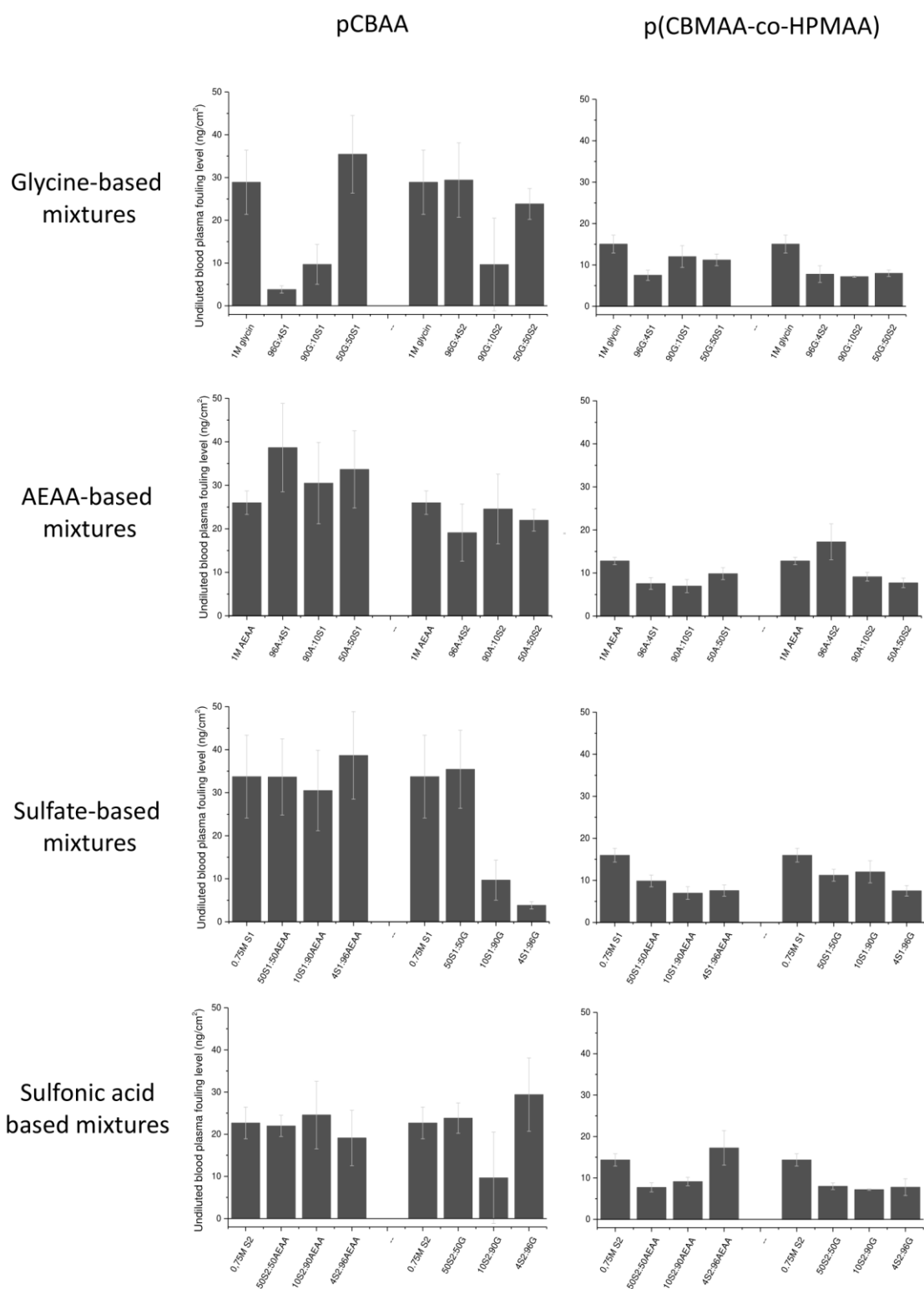
The fouling level from undiluted blood plasma discussed further was determined from SPR sensorgrams (see example in Figure S14) as the difference between SPR response baseline before and after the 10 min of undiluted plasma injection over the surface. In total 16 combinations of the deactivation compounds (glycine, AEAA, D1,

1  
2  
3 and D2) used individually and in mixtures were investigated for both pCBAA and  
4  
5 p(CBMAA-co-HPMAA) brushes.  
6  
7

8 The complete summary of the results can be found in Figure 2. For pCBAA, the  
9  
10 deactivation with single-component solution (1 M AEAA and 0,75 M D2) perform  
11  
12 slightly better compared to that with already published 1M glycine <sup>17</sup>. A significant  
13  
14 improvement in the fouling resistance (7.5 times reduction of fouling level,  
15  
16 corresponding to ~3.8 ng/cm<sup>2</sup>) was observed after the addition of a very small amount  
17  
18 of negative permanent charge of D1 (4%) to the glycine solution (960 mM glycine + 40  
19  
20 mM D1, 96G:4D1). The higher content of D1 deteriorates the resistance again. The  
21  
22 optimal concentration of D2 in the deactivation solution was found to be around 10%  
23  
24 of D2 (900 mM glycine + 100 mM D2, 90G:10D2; corresponding fouling level ~9.7  
25  
26 ng/cm<sup>2</sup>), which is roughly 2 times higher than the concentration of D1. For the  
27  
28 copolymer brush p(CBMAA-co-HPMAA), similar trends can be observed but the  
29  
30 magnitude of the change is smaller due to the smaller concentration of carboxy groups  
31  
32 in the copolymer. The fouling levels after deactivation with glycine, 90G:10D2 or  
33  
34 96G:4D1 were ~9.7 ng/cm<sup>2</sup>, 7.2 ng/cm<sup>2</sup>, and 7.5 ng/cm<sup>2</sup>, respectively. Interestingly,  
35  
36 AEAA-based mixtures didn't bring any improvement to the resistance recovery of  
37  
38 pCBAA and only a negligible improvement was observed for p(CBMAA-co-HPMAA)  
39  
40 resistance after using 4-10% of D1 and around 50% of D2 in mixtures with AEAA  
41  
42 compared to pure AEAA solution (corresponding to ~7.6 ng/cm<sup>2</sup>, ~7.0 ng/cm<sup>2</sup>,  
43  
44 ~7.7 ng/cm<sup>2</sup> and ~12.8 ng/cm<sup>2</sup> respectively.  
45  
46  
47  
48  
49  
50

51  
52 It is worth mentioning, that only the levels of fouling without using any extra washing  
53  
54 step (only PBS baseline after plasma exposure) are considered in this work. Increasing  
55  
56 the ionic strength of the running buffer during the additional washing step after  
57  
58 detection/complex sample exposure is a commonly used method to release the deposit  
59  
60

1  
2  
3 kept by nonspecific electrostatic interactions. So, the levels of fouling here could be  
4  
5 rather higher compared to previously published results. However, in <sup>19</sup> we show  
6  
7 remarkable sensitivity of zwitterionic structures to salt ions exposure. Here, in  
8  
9 Supporting Information (Figure S15 with the following discussion) we show how  
10  
11 significantly the ionic strength-based swelling can interfere with the SPR fouling  
12  
13 measurements, bringing up the question, what the most feasible method of resistance  
14  
15 assessment of highly swollen structures is.  
16  
17  
18  
19  
20  
21  
22  
23  
24  
25  
26  
27  
28  
29  
30  
31  
32  
33  
34  
35  
36  
37  
38  
39  
40  
41  
42  
43  
44  
45  
46  
47  
48  
49  
50  
51  
52  
53  
54  
55  
56  
57  
58  
59  
60



1  
2  
3 Figure 2: Fouling levels quantified by SPR on functionalized and deactivated pCBAA  
4 (left column) and p(CBMAA-co-HPMAA) (right column) polymer brushes after  
5 exposure to undiluted human plasma.  
6  
7  
8  
9

### 10 11 12 13 **3.2. FT-IRRAS spectra of deactivated pCB brushes** 14

15  
16 The deactivation of pCB-based brushes with a set of the best performing conditions  
17 was followed by using infrared spectroscopy (Figure S1-S13).  
18

19  
20  
21 The FT-IRRAS spectra acquired for both pCBAA and p(CBMAA-HPMAA) show an  
22 absorption peak at about  $1730\text{ cm}^{-1}$ , which corresponds to the unionized carboxy  
23 group. This peak indicates that not all carboxy groups are permanently involved in  
24 creating a zwitterionic (betaine) structure and appear not to be involved in the  
25 activation/deactivation reactions as it is not significantly affected by the treatment (see  
26 Figures S2-S14). The deactivation of activated pCBAA by spontaneous hydrolysis in  
27 water or water-based buffer (30 min) does not recover zwitterionic form, as witnessed  
28 by a decreased intensity of the bands of the ionized carboxyl at  $1608\text{ cm}^{-1}$  and  
29  $1370\text{ cm}^{-1}$  compared to non-activated brush spectra (Figure S1 and following  
30 discussion in Supporting Information material, <sup>17</sup>).  
31  
32  
33  
34  
35  
36  
37  
38  
39  
40  
41  
42  
43

44  
45 The reactions with deactivating agents bearing carboxy group never result in the  
46 complete recovery of the bands of the ionized carboxyl at  $1608\text{ cm}^{-1}$  and  $1370\text{ cm}^{-1}$   
47 neither. The attachment of glycine or AEAA cannot be demonstrated directly via some  
48 specific band and only the changes of absorptions of carboxy groups can be assessed.  
49  
50  
51  
52  
53  
54 Nevertheless, Figure S2 and Figure S3 indicate that AEAA restores the ionic form of  
55 the carboxy group more effectively than glycine.  
56  
57  
58  
59  
60

1  
2  
3 In contrast to the interaction of active esters with glycine and AEAA, reactions with D1  
4 and D2 may be easily observed due to strong absorption bands of sulfate and sulfo  
5 groups, respectively. The spectra after the deactivation with D1 (Figure S4) and D2  
6 (Figure S5) (in absence of glycine or AEAA) show a decreased absorption of ionized  
7 carboxyl and the additional strong bands of sulfate group at 1253, 1229, and 1010  $\text{cm}^{-1}$   
8 (Figure S4) and the bands of sulfo group at 1230 and 1010  $\text{cm}^{-1}$  (Figure S5) appears  
9 confirming the attachment of D1 and D2. The deactivation with mixed agents  
10 containing D1 or D2 and glycine or AEAA shows a similar picture. It appears that D2,  
11 in contrast to D1, binds more effectively and preferentially from the mixed solutions of  
12 D2 with glycine or AEAA, as the intensity of D2 bands remains high irrespective of its  
13 concentration in the mixtures.  
14  
15  
16  
17  
18  
19  
20  
21  
22  
23  
24  
25  
26  
27  
28

29 The spectra of p(CBMAA-co-HPMAA) show an analogical behavior as pCBAA,  
30 however, because of the lower content of the reactive component the changes after  
31 the treatment of copolymer are less pronounced (see the differential spectrum in Figure  
32 S12 and Figures S8-S13).  
33  
34  
35  
36  
37  
38

39 It is to be noted that the infrared spectra of polymer brushes measured in the dry state  
40 may somewhat differ from the spectra of hydrated polymer brushes where the state is  
41 further affected by factors like pH, type of ions, and ionic strength. However, the  
42 measurements in water environment would bring additional issues related to inference  
43 with water environment spectra. As the purpose of the presented work is to pursue a  
44 comparative study on deactivation methods, it is anticipated that the spectra of the  
45 dried coatings supplement adequate information on the reactions of interest.  
46  
47  
48  
49  
50  
51  
52  
53  
54  
55  
56  
57  
58

### 59 **3.3. Enhancing biorecognition capabilities of optimally deactivated pCB brush**

60



1  
2  
3 The lowest postmodification fouling level was achieved for pCBAA, where the impact  
4 of the deactivation protocol was more pronounced compared to the copolymer  
5 structure. Therefore, the potential of selected deactivation protocols in affinity  
6 biosensor applications was investigated using optimally deactivated functionalized  
7 pCBAA coatings for label-free detection of *E.coli* O157:H7 in a minced meat sample.  
8 This foodborne bacterial pathogen and corresponding medium were chosen as a  
9 model system for biorecognition studies due to its attractiveness in the field of  
10 biosensor development for modern food safety applications and the possibility to  
11 compare the data with results published earlier <sup>18, 35</sup>. The pCBAA brush was  
12 functionalized by covalent attachment of anti-*E.coli* antibody with a surface mass  
13 density of  $350 \pm 50$  ng/cm<sup>2</sup> and subsequently deactivated by the three deactivation  
14 mixtures (96G:4D1, AEAA, or 90G:10D2 ) and glycine as the reference to already  
15 published results <sup>17, 33</sup>. The average fouling levels from minced meat sample on  
16 functionalized coatings were for all deactivation procedures below 3% of antibody  
17 functionalized level – specifically, 3.0%, 2.4%, 0.6%, and 0.3% for coatings deactivated  
18 by glycine, 96G:4D1, 90G:10D2, and AEAA, respectively. These ratios are comparable  
19 to or significantly lower than 2.8%, the ratio previously reported for pCB-based anti-  
20 *E.coli* functionalized coatings in a hamburger sample <sup>36</sup>.

21  
22  
23  
24  
25  
26  
27  
28  
29  
30  
31  
32  
33  
34  
35  
36  
37  
38  
39  
40  
41  
42  
43  
44  
45 Figure 3 shows the calibration curves for label-free *E.coli* detection in a crude minced  
46 meat sample for 4 different deactivation strategies. Table 1 summarizes the LODs and  
47 LOQs determined according to standard “3 $\sigma$ ” and “10 $\sigma$ ” approaches <sup>37-38</sup>. The  
48 qualitative confirmation of the results was achieved also by another data analysis  
49 approach, taking into account the chip-to-chip blank deviations, which are more  
50 relevant for real-world applications (see Supporting Information for more details).  
51  
52  
53  
54  
55  
56  
57  
58  
59  
60

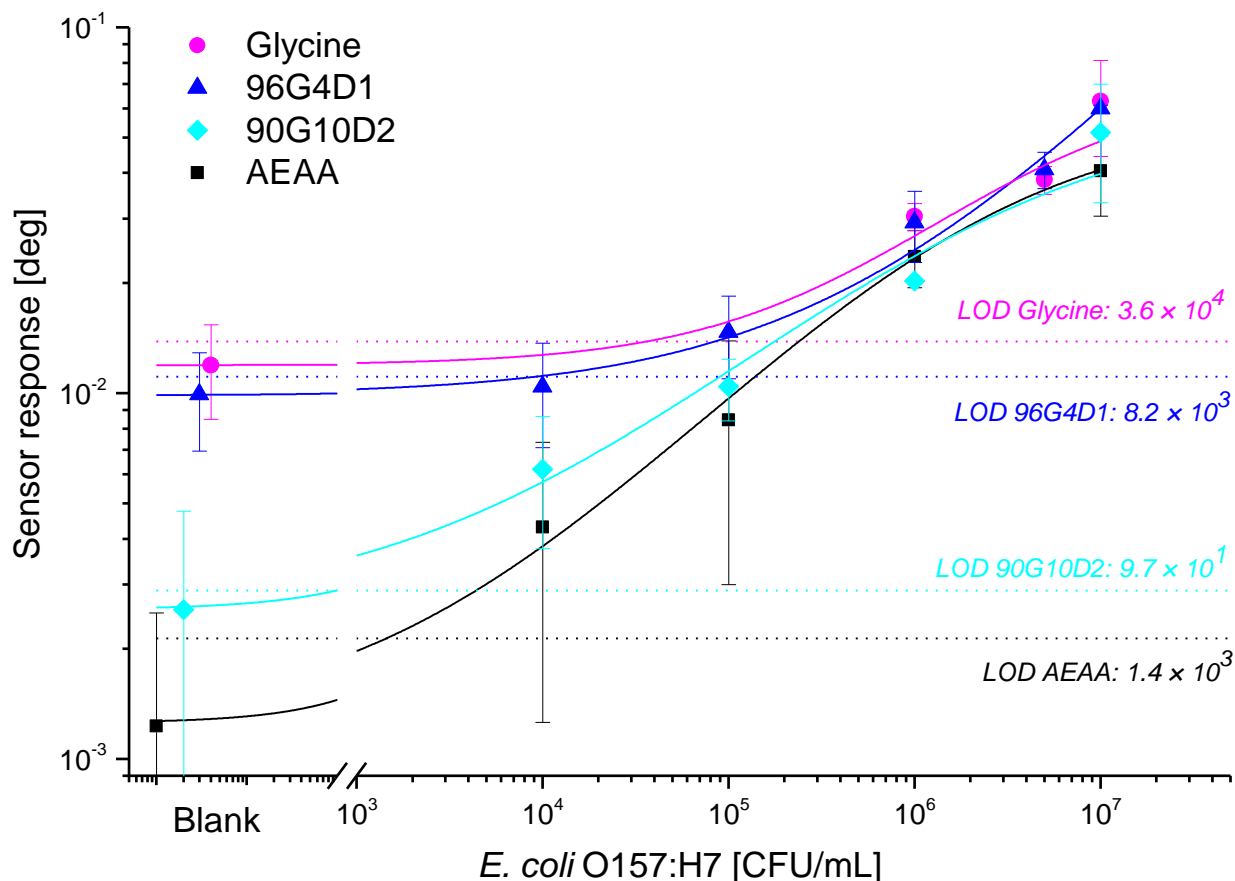


Figure 3: Calibration curves in a logarithmic scale of the primary detection of *E.coli* O157:H7 in minced meat samples using functionalized antifouling pCBAA brush deactivated by 4 different optimized deactivation solutions. LODs are indicated as a cross-section of fitted calibration curves (solid lines) with the response to blank sample with added three-times standard deviation of the SPR sensor baseline (dashed lines).

Table 1: The summary of LODs and LOQs for the label-free detection of *E.coli* O157:H7 in the minced meat sample, estimated for four different deactivation mixtures applied after functionalization.

Deactivation agent	Blank (ng/cm <sup>2</sup> )	LOD	LOQ
Glycine	10.1	$3.6 \times 10^4$	$2.3 \times 10^5$

<b>96G:4D1</b>	8.4	$8.2 \times 10^3$	$7.4 \times 10^4$
<b>AEAA</b>	1.0	$1.4 \times 10^3$	$1.3 \times 10^4$
<b>90G:10D2</b>	2.1	$9.7 \times 10^1$	$1.1 \times 10^3$

The limit of detection (LOD) and limit of quantification (LOQ) decreased by up to two orders of magnitude compared to glycine deactivation in the label-free assay when deactivation mixture 90G:10D2 or AEAA was used (Table 1, Figure 3). Using infrared spectroscopy, both solutions AEAA and 90G:10D2 were proved to restore negative charge in the zwitterionic structure effectively (by restoring ionic form COO<sup>-</sup> or by adding extra permanent negative charge into the structure, respectively).

Interestingly, Table 1 shows a higher LOD and LOQ for 96G:4D1 deactivation mixture compared to AEAA or 90G:10D2, even though the resistance to undiluted blood plasma was superior using 96G:4D1. The fouling resistance generally depends on the type and composition of the complex sample<sup>25</sup>. A high resistance to non-specific adsorption from blood does not necessarily mean the high resistance to adsorption from food samples (Figure S16), the composition of which varies greatly<sup>39</sup>. As the infrared data indicate, D2 in the mixtures with glycine reacts with active esters of the surface preferentially, while using the mixture of D1 and glycine, the D1 attachment is concentration-dependent. Therefore, due to the permanent charge of D2, the charge balance after deactivation with G:D2 mixtures should be rather stable in a wider range of pH. Specifically, the lower pH of the minced meat sample (6.8) compared to the pH of human blood plasma (7.9) may promote a higher amount of carboxy groups in the undissociated form of COOH. A higher amount of pH-insensitive negatively charged moieties can be then used to restore and keep the neutrality and zwitterionicity of functionalized coating with an advantage.

1  
2  
3 Typically, detectable concentrations and LODs for *E.coli* detection achieved by label-  
4 free direct optical or non-optical biosensors are in the order of  $10^2$ - $10^5$  CFU/mL in a  
5 buffer solution <sup>40-48</sup>. As shown in Table 1, functionalized pCBAA coating deactivated  
6 by an optimized deactivation mixture achieves the lower limit of such range for LOD  
7 and even LOQ in complex crude food samples, without any extra sample  
8 preconditioning or extra after-detection washing steps needed, in a reasonably short  
9 time (~20 minutes). Moreover, such assay allows further amplification steps <sup>36</sup>,  
10 possibly further improving LOD by 2-3 orders of magnitude.  
11  
12  
13  
14  
15  
16  
17  
18  
19  
20  
21  
22  
23  
24

## 25 **Conclusions**

26  
27  
28 A new effective approach is reported for recovering antifouling properties of zwitterionic  
29 poly(carboxybetaine)-based brushes after their postmodification with functional  
30 biomolecules using an amine coupling. It addresses the misbalanced charge density  
31 and disrupted structure of the zwitterionic moieties, which occur after the surface  
32 postmodification with biorecognition elements. These changes severely impair fouling  
33 resistance of the coating and we report on its recovery through the tailored deactivation  
34 of residual active esters by covalent attachment of small molecules carrying amine  
35 group and additional carboxy, sulfate, and sulfo groups in an optimized mixture. Such  
36 treatment allows restoring the charge layout leading to suppressing the fouling from  
37 complex biological fluids.  
38  
39  
40  
41  
42  
43  
44  
45  
46  
47  
48  
49

50  
51 The use of a deactivation mixture of glycine and 2-aminoethyl hydrogen sulfate in a  
52 ratio of 96:4 allowed reducing the fouling from undiluted human blood plasma on  
53 pCBAA and p(CBMAA-co-HPMAA) brushes that were postmodified with IgG antibody  
54 (specific to an analyte not presented in the plasma) by a factor of 7.5 and 1.3,  
55  
56  
57  
58  
59  
60

1  
2  
3 respectively, when compared to previously published deactivation procedure (glycine  
4 based deactivation). The surface mass density of the deposits from the undiluted blood  
5 plasma was 3.8 ng/cm<sup>2</sup> and 7.5 ng/cm<sup>2</sup>, respectively, which are comparable to levels  
6 reported for the pristine pCBAA and p(CBMAA-co-HPMAA) brushes (17, 25).  
7  
8  
9

10  
11  
12 To demonstrate the versatility of the proposed approach and the biorecognition  
13 abilities, the functionalization of pCBAA brush coating with IgG antibody against  
14 bacterial pathogen and subsequently optimized deactivation was employed in label-  
15 free SPR biosensor for the detection of *E.coli* H157:O7 in the crude minced meat  
16 sample. The mixtures of glycine with aminomethanesulfonic acid, or 2-(2-  
17 aminoethoxy)acetic acid suppressed the fouling to 2.1 ng/cm<sup>2</sup> and 1.0 ng/cm<sup>2</sup>,  
18 respectively, improving the limit of detection to  $9.7 \times 10^1$  and  $1.4 \times 10^3$  CFU/mL  
19 respectively, which is two orders of magnitude better than that we observed for the  
20 reference deactivation by glycine ( $3.6 \times 10^4$  CFU/mL).  
21  
22  
23  
24  
25  
26  
27  
28  
29  
30  
31  
32

33  
34 The proposed strategy relying on using tailored deactivation compositions offers an  
35 attractive means to individually tune characteristics of the functionalized  
36 poly(carboxybetaine)-based polymer brushes and in particular to restore their  
37 antifouling properties that are compromised by the postmodification step. Moreover,  
38 this approach holds the potential to provide generic means to post-functional  
39 modification of the antifouling surface (without impairing its resistance), which we  
40 believe makes it attractive for high-performance label-free biosensors applications, as  
41 well as for other fields including studies on cell interactions with surface and cell-on-  
42 chip technologies.  
43  
44  
45  
46  
47  
48  
49  
50  
51  
52  
53

## 54 55 56 57 58 **Acknowledgments** 59 60

This work was supported by Praemium Lumina quaeruntur of the Czech Academy of Sciences (LQ100101902) and by the Czech Science Foundation (contract # P205/21-19779S). The authors would like to thank Daniel Špaček for his help with the graphic design. In addition, J.D. acknowledges support from the ESIF and MEYS (Project 'FZU researchers, technical and administrative staff mobility' – CZ.02.2.69/ 0.0/ 0.0/18\_053/0016627).

## References

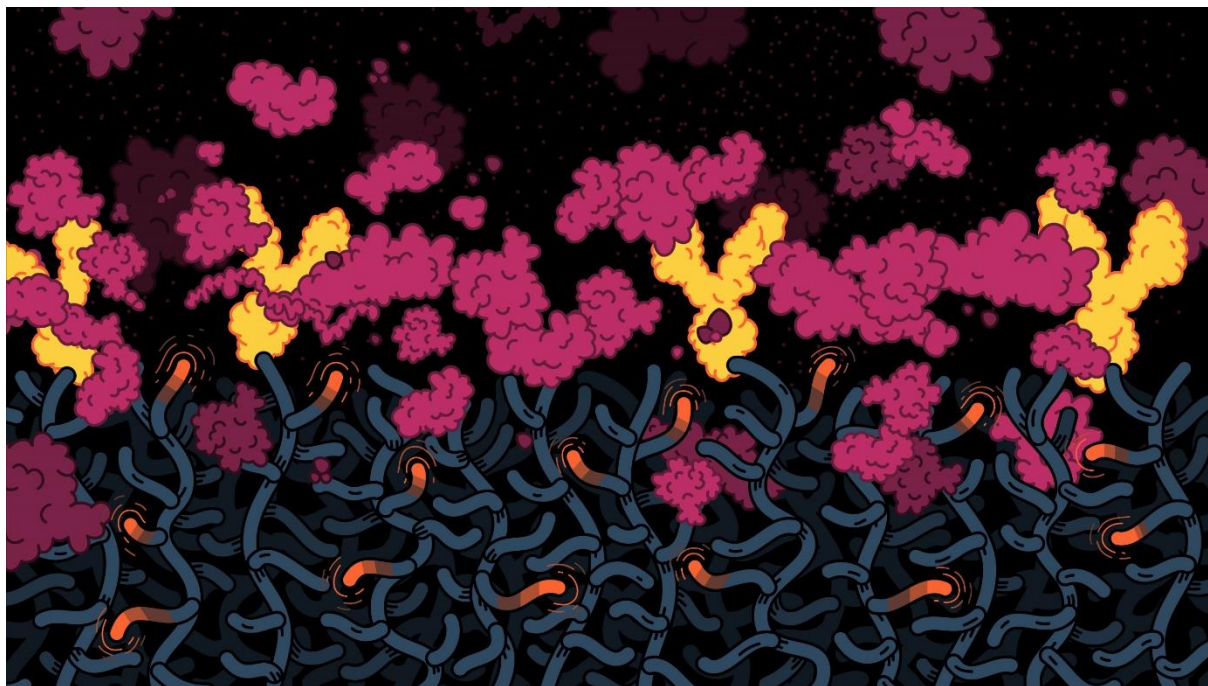
- (1) Vaisocherova, H.; Brynda, E.; Homola, J. Functionalizable low-fouling coatings for label-free biosensing in complex biological media: advances and applications. *Anal. Bioanal. Chem.* **2015**, *407* (14), 3927-3953, DOI: 10.1007/s00216-015-8606-5.
- (2) Liu, J.; Qu, S.; Suo, Z.; Yang, W. Functional hydrogel coatings. *National Science Review* **2020**, DOI: 10.1093/nsr/nwaa254.
- (3) Srey, S.; Jahid, I. K.; Ha, S.-D. Biofilm formation in food industries: A food safety concern. *Food Control* **2013**, *31* (2), 572-585, DOI: <https://doi.org/10.1016/j.foodcont.2012.12.001>.
- (4) Bixler, G. D.; Bhushan, B. Biofouling: lessons from nature. *Philosophical Transactions of the Royal Society A: Mathematical, Physical and Engineering Sciences* **2012**, *370* (1967), 2381-2417, DOI: doi:10.1098/rsta.2011.0502.
- (5) Lin, P.-H.; Li, B.-R. Antifouling strategies in advanced electrochemical sensors and biosensors. *Analyst* **2020**, *145* (4), 1110-1120, DOI: 10.1039/C9AN02017A.
- (6) Jiang, C.; Wang, G.; Hein, R.; Liu, N.; Luo, X.; Davis, J. J. Antifouling Strategies for Selective In Vitro and In Vivo Sensing. *Chemical Reviews* **2020**, *120* (8), 3852-3889, DOI: 10.1021/acs.chemrev.9b00739.
- (7) Blaszykowski, C.; Sheikh, S.; Thompson, M. A survey of state-of-the-art surface chemistries to minimize fouling from human and animal biofluids. *Biomater. Sci.* **2015**, *3* (10), 1335-1370, DOI: 10.1039/c5bm00085h.
- (8) Wang, F.; Zhang, H.; Yu, B.; Wang, S.; Shen, Y.; Cong, H. Review of the research on anti-protein fouling coatings materials. *Prog. Org. Coat.* **2020**, *147*, 105860, DOI: <https://doi.org/10.1016/j.porgcoat.2020.105860>.
- (9) Zhao, C.; Li, L.-Y.; Guo, M.-M.; Zheng, J. Functional polymer thin films designed for antifouling materials and biosensors. *Chemical Papers* **2012**, *66* (5), 323, DOI: <https://doi.org/10.2478/s11696-012-0147-1>.
- (10) Víšová, I.; Smolková, B.; Uzhytchak, M.; Vrabcová, M.; Chafai, D. E.; Houska, M.; Pastucha, M.; Skládal, P.; Farka, Z.; Dejneka, A.; Vaisocherová-Lísalová, H. Functionalizable Antifouling Coatings as Tunable Platforms for the Stress-Driven Manipulation of Living Cell Machinery. *Biomolecules* **2020**, *10* (8), 1146.
- (11) Chen, S. F.; Cao, Z. Q.; Jiang, S. Y. Ultra-low fouling peptide surfaces derived from natural amino acids. *Biomaterials* **2009**, *30* (29), 5892-5896.
- (12) Nie, W.; Wang, Q.; Zou, L.; Zheng, Y.; Liu, X.; Yang, X.; Wang, K. Low-Fouling Surface Plasmon Resonance Sensor for Highly Sensitive Detection of MicroRNA in a Complex Matrix Based on the DNA Tetrahedron. *Analytical Chemistry* **2018**, DOI: 10.1021/acs.analchem.8b02686.
- (13) Ratel, M.; Provencher-Girard, A.; Zhao, S. S.; Breault-Turcot, J.; Labrecque-Carbonneau, J.; Branca, M.; Pelletier, J. N.; Schmitzer, A. R.; Masson, J.-F. Imidazolium-Based Ionic Liquid Surfaces for Biosensing. *Analytical Chemistry* **2013**, *85* (12), 5770-5777, DOI: 10.1021/ac400386z.
- (14) Mi, L.; Jiang, S. Integrated Antimicrobial and Nonfouling Zwitterionic Polymers. *Angewandte Chemie International Edition* **2014**, *53* (7), 1746-1754, DOI: 10.1002/anie.201304060.

- 1  
2  
3 (15) Zheng, L.; Sundaram, H. S.; Wei, Z.; Li, C.; Yuan, Z. Applications of zwitterionic polymers. *Reactive and Functional Polymers* **2017**, *118*, 51-61, DOI: <https://doi.org/10.1016/j.reactfunctpolym.2017.07.006>.
- 4 (16) Jiang, S.; Cao, Z. Ultralow-Fouling, Functionalizable, and Hydrolyzable Zwitterionic Materials and Their  
5 Derivatives for Biological Applications. *Adv. Mater.* **2010**, *22* (9), 920-932.
- 6 (17) Lísalová, H.; Brynda, E.; Houska, M.; Víšová, I.; Mrkvová, K.; Song, X. C.; Gedeonová, E.; Surman, F.; Riedel,  
7 T.; Pop-Georgievski, O.; Homola, J. Ultralow-Fouling Behavior of Biorecognition Coatings Based on Carboxy-  
8 Functional Brushes of Zwitterionic Homo- and Copolymers in Blood Plasma: Functionalization Matters.  
9 *Analytical Chemistry* **2017**, *89* (6), 3524-3531, DOI: 10.1021/acs.analchem.6b04731.
- 10 (18) Vaisocherová-Lísalová, H.; Surman, F.; Víšová, I.; Vala, M.; Špringer, T.; Ermini, M. L.; Šípová, H.; Šedivák, P.;  
11 Houska, M.; Riedel, T.; Pop-Georgievski, O.; Brynda, E.; Homola, J. Copolymer Brush-Based Ultralow-Fouling  
12 Biorecognition Surface Platform for Food Safety. *Analytical Chemistry* **2016**, *88* (21), 10533-10539, DOI:  
13 10.1021/acs.analchem.6b02617.
- 14 (19) Víšová, I.; Vrabcová, M.; Forinová, M.; Zhigunová, Y.; Mironov, V.; Houska, M.; Bittrich, E.; Eichhorn, K.-J.;  
15 Hashim, H.; Schovánek, P.; Dejneka, A.; Vaisocherová-Lísalová, H. Surface Preconditioning Influences the  
16 Antifouling Capabilities of Zwitterionic and Nonionic Polymer Brushes. *Langmuir* **2020**, *36* (29), 8485-8493, DOI:  
17 10.1021/acs.langmuir.0c00996.
- 18 (20) Riedel, T.; Hageneder, S.; Surman, F.; Pop-Georgievski, O.; Noehammer, C.; Hofner, M.; Brynda, E.;  
19 Rodriguez-Emmenegger, C.; Dostálek, J. Plasmonic Hepatitis B Biosensor for the Analysis of Clinical Saliva.  
20 *Analytical Chemistry* **2017**, *89* (5), 2972-2977, DOI: 10.1021/acs.analchem.6b04432.
- 21 (21) Chou, Y. N.; Sun, F.; Hung, H. C.; Jain, P.; Sinclair, A.; Zhang, P.; Bai, T.; Chang, Y.; Wen, T. C.; Yu, Q. M.;  
22 Jiang, S. Y. Ultra-low fouling and high antibody loading zwitterionic hydrogel coatings for sensing and detection  
23 in complex media. *Acta Biomaterialia* **2016**, *40*, 31-37, DOI: 10.1016/j.actbio.2016.04.023.
- 24 (22) Víšová, I.; Smolková, B.; Uzhychak, M.; Vrabcová, M.; Zhigunova, Y.; Houska, M.; Surman, F.; de los Santos  
25 Pereira, A.; Lunov, O.; Dejneka, A.; Vaisocherová-Lísalová, H. Modulation of Living Cell Behavior with Ultra-Low  
26 Fouling Polymer Brush Interfaces. *Macromolecular Bioscience* **2020**, *20* (3), 1900351, DOI:  
27 10.1002/mabi.201900351.
- 28 (23) Huang, C.-J.; Li, Y.; Jiang, S. Zwitterionic Polymer-Based Platform with Two-Layer Architecture for Ultra Low  
29 Fouling and High Protein Loading. *Analytical Chemistry* **2012**, *84* (7), 3440-3445, DOI: 10.1021/ac3003769.
- 30 (24) Brault, N. D.; Gao, C.; Xue, H.; Piliarik, M.; Homola, J.; Jiang, S.; Yu, Q. Ultra-low fouling and functionalizable  
31 zwitterionic coatings grafted onto SiO<sub>2</sub> via a biomimetic adhesive group for sensing and detection in complex  
32 media. *Biosensors and Bioelectronics* **2010**, *25* (10), 2276-2282, DOI: 10.1016/j.bios.2010.03.012.
- 33 (25) Vaisocherova, H.; Sevcu, V.; Adam, P.; Spackova, B.; Hegnerova, K.; Pereira, A. D.; Rodriguez-Emmenegger,  
34 C.; Riedel, T.; Houska, M.; Brynda, E.; Homola, J. Functionalized ultra-low fouling carboxy- and hydroxy-  
35 functional surface platforms: functionalization capacity, biorecognition capability and resistance to fouling from  
36 undiluted biological media. *Biosensors & bioelectronics* **2014**, *51*, 150-157, DOI: DOI  
37 10.1016/j.bios.2013.07.015.
- 38 (26) El-Faham, A.; Albericio, F. Peptide Coupling Reagents, More than a Letter Soup. *Chemical Reviews* **2011**,  
39 *111* (11), 6557-6602, DOI: 10.1021/cr100048w.
- 40 (27) Yüce, M.; Kurt, H. How to make nanobiosensors: surface modification and characterisation of  
41 nanomaterials for biosensing applications. *RSC Adv.* **2017**, *7* (78), 49386-49403, DOI: 10.1039/C7RA10479K.
- 42 (28) Hermanson, G. T. *Bioconjugate techniques* Second Edition ed.; Elsevier: Illinois, USA, 2008.
- 43 (29) Palazon, F.; Montenegro Benavides, C.; Léonard, D.; Souteyrand, É.; Chevolut, Y.; Cloarec, J.-P.  
44 Carbodiimide/NHS Derivatization of COOH-Terminated SAMs: Activation or Byproduct Formation? *Langmuir*  
45 **2014**, *30* (16), 4545-4550, DOI: 10.1021/la5004269.
- 46 (30) Lim, C. Y.; Owens, N. A.; Wampler, R. D.; Ying, Y.; Granger, J. H.; Porter, M. D.; Takahashi, M.; Shimazu, K.  
47 Succinimidyl Ester Surface Chemistry: Implications of the Competition between Aminolysis and Hydrolysis on  
48 Covalent Protein Immobilization. *Langmuir* **2014**, *30* (43), 12868-12878, DOI: 10.1021/la503439g.
- 49 (31) Cline, G. W.; Hanna, S. B. Kinetics and mechanisms of the aminolysis of N-hydroxysuccinimide esters in  
50 aqueous buffers. *The Journal of Organic Chemistry* **1988**, *53* (15), 3583-3586, DOI: 10.1021/jo00250a031.
- 51 (32) Schönherr, H.; Feng, C.; Shovsky, A. Interfacial Reactions in Confinement: Kinetics and Temperature  
52 Dependence of Reactions in Self-Assembled Monolayers Compared to Ultrathin Polymer Films. *Langmuir* **2003**,  
53 *19* (26), 10843-10851, DOI: 10.1021/la034887z.
- 54 (33) Lísalová, H.; Brynda, E.; Víšová, I.; Houska, M.; Surman, F.; Mrkvová, K.; Chadtová, S. X.; Homola, J.  
55 Způsob přípravy povrchu substrátu obsahujícího karboxybetainové funkční skupiny. 2016.
- 56 (34) Lai, H.; Wu, P. Hydration capabilities and structures of carbonyl and ether groups in poly(3-(2-  
57 methoxyethyl)-N-vinyl-2-pyrrolidone) film. *Polymer Chemistry* **2013**, *4* (11), 3323-3332, DOI:  
58 10.1039/C3PY00239J.
- 59  
60

- 1  
2  
3 (35) Tuttle, J.; Gomez, T.; Doyle, M. P.; Wells, J. G.; Zhao, T.; Tauxe, R. V.; Griffin, P. M. Lessons from a large  
4 outbreak of Escherichia coli O157[ra]tio JH7 infections: insights into the infectious dose and method of  
5 widespread contamination of hamburger patties. *Epidemiology and Infection* **1999**, *122* (2), 185-192, DOI:  
6 10.1017/S0950268898001976.
- 7 (36) Vaisocherová-Lísalová, H.; Víšová, I.; Ermini, M. L.; Špringer, T.; Song, X. C.; Mrázek, J.; Lamačová, J.; Scott  
8 Lynn, N.; Šedivák, P.; Homola, J. Low-fouling surface plasmon resonance biosensor for multi-step detection of  
9 foodborne bacterial pathogens in complex food samples. *Biosensors and Bioelectronics* **2016**, *80*, 84-90, DOI:  
10 https://doi.org/10.1016/j.bios.2016.01.040.
- 11 (37) Uhrovčík, J. Strategy for determination of LOD and LOQ values – Some basic aspects. *Talanta* **2014**, *119*,  
12 178-180, DOI: https://doi.org/10.1016/j.talanta.2013.10.061.
- 13 (38) Thompson, M.; Ellison, L. R. S.; Wood, R. Harmonized guidelines for single-laboratory validation of  
14 methods of analysis (IUPAC Technical Report). *Pure and Applied Chemistry* **2002**, *74*, 835-855.
- 15 (39) Sikorski, Z. E. *Chemical and functional properties of food components*, CRC press: 2006.
- 16 (40) Shin, H. J.; Lim, W. K. Rapid label-free detection of E. coli using a novel SPR biosensor containing a  
17 fragment of tail protein from phage lambda. *Preparative Biochemistry & Biotechnology* **2018**, *48* (6), 498-505,  
18 DOI: 10.1080/10826068.2018.1466154.
- 19 (41) Tawil, N.; Sacher, E.; Mandeville, R.; Meunier, M. Surface plasmon resonance detection of E. coli and  
20 methicillin-resistant S. aureus using bacteriophages. *Biosensors & bioelectronics* **2012**, *37* (1), 24-9, DOI:  
21 10.1016/j.bios.2012.04.048.
- 22 (42) Dudak, F. C.; Boyacı, İ. H. Rapid and label-free bacteria detection by surface plasmon resonance (SPR)  
23 biosensors. *Biotechnology journal* **2009**, *4* (7), 1003-1011, DOI: 10.1002/biot.200800316.
- 24 (43) Elgiddawy, N.; Ren, S. W.; Yassar, A.; Louis-Joseph, A.; Sauriat-Dorizon, H.; El Rouby, W. M. A.; El-Gendy, A.  
25 O.; Farghali, A. A.; Korri-Youssoufi, H. Dispersible Conjugated Polymer Nanoparticles as Biointerface Materials  
26 for Label-Free Bacteria Detection. *ACS applied materials & interfaces* **2020**, *12* (36), 39979-39990, DOI:  
27 10.1021/acsami.0c08305.
- 28 (44) Lamanna, L.; Rizzi, F.; Bhethanabotla, V. R.; De Vittorio, M. Conformable surface acoustic wave biosensor  
29 for E-coli fabricated on PEN plastic film. *Biosensors & bioelectronics* **2020**, *163*, 10, DOI:  
30 10.1016/j.bios.2020.112164.
- 31 (45) Huang, Y. Y.; Wu, Z. Y.; Zhao, G. Y.; Dou, W. C. A Label-Free Electrochemical Immunosensor Modified with  
32 AuNPs for Quantitative Detection of Escherichia coli O157:H7. *J. Electron. Mater.* **2019**, *48* (12), 7960-7969,  
33 DOI: 10.1007/s11664-019-07527-6.
- 34 (46) van Grinsven, B.; Eersels, K.; Akkermans, O.; Ellermann, S.; Kordek, A.; Peeters, M.; Deschaume, O.; Bartic,  
35 C.; Diliën, H.; Steen Redeker, E.; Wagner, P.; Cleij, T. J. Label-Free Detection of Escherichia coli Based on  
36 Thermal Transport through Surface Imprinted Polymers. *ACS sensors* **2016**, *1* (9), 1140-1147, DOI:  
37 10.1021/acssensors.6b00435.
- 38 (47) Steen Redeker, E.; Eersels, K.; Akkermans, O.; Royakkers, J.; Dyson, S.; Nurekeyeva, K.; Ferrando, B.;  
39 Cornelis, P.; Peeters, M.; Wagner, P.; Diliën, H.; van Grinsven, B.; Cleij, T. J. Biomimetic Bacterial Identification  
40 Platform Based on Thermal Wave Transport Analysis (TWTA) through Surface-Imprinted Polymers. *ACS*  
41 *Infectious Diseases* **2017**, *3* (5), 388-397, DOI: 10.1021/acsinfecdis.7b00037.
- 42 (48) Taylor, A. D.; Ladd, J.; Yu, Q.; Chen, S.; Homola, J.; Jiang, S. Quantitative and simultaneous detection of four  
43 foodborne bacterial pathogens with a multi-channel SPR sensor. *Biosensors & bioelectronics* **2006**, *22* (5), 752-  
44 8.  
45  
46  
47  
48  
49

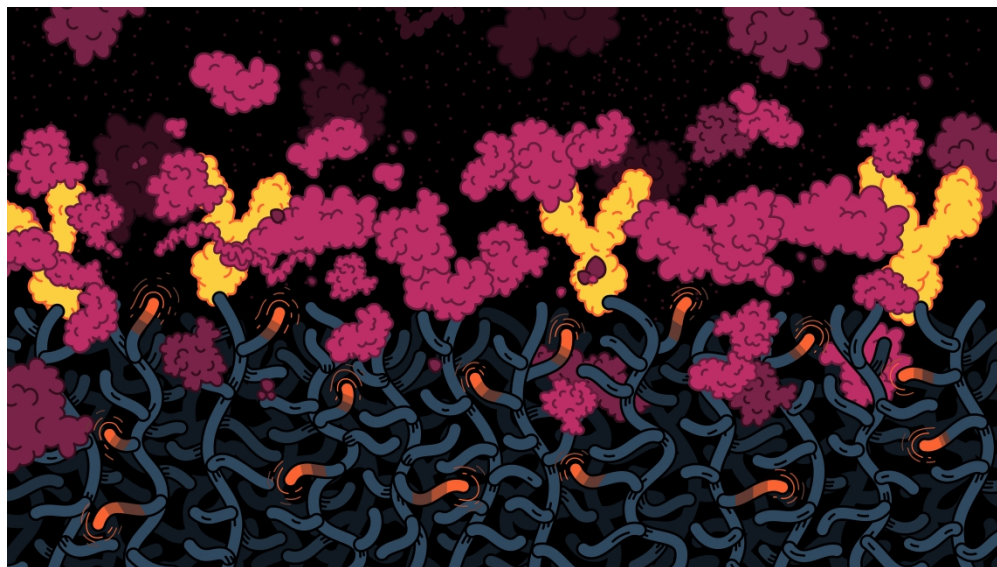
50 For Table of Contents Only:  
51  
52  
53  
54  
55  
56  
57  
58  
59  
60





1  
2  
3  
4  
5  
6  
7  
8  
9  
10  
11  
12  
13  
14  
15  
16  
17  
18  
19  
20  
21  
22  
23  
24  
25  
26  
27  
28  
29  
30  
31  
32  
33  
34  
35  
36  
37  
38  
39  
40  
41  
42  
43  
44  
45  
46  
47  
48  
49  
50  
51  
52  
53  
54  
55  
56  
57  
58  
59  
60

Molecular coupling-based recovery of antifouling properties of carboxybetaine polymer brushes after amino coupling-based functionalization significantly improves biorecognition performance.



Molecular coupling-based recovery of antifouling properties of carboxybetaine polymer brushes after amino coupling-based functionalization significantly improves biorecognition performance.

# Appendix X

Víšová, I., M. Houska, H. Vaisocherová-Lísalová

**Coatings Exhibiting Anti-Fouling Behavior and Biorecognition  
Activity in Complex Biological Media: A Review of Functionalization  
Aspects**

In preparation. To be submitted in *Analyst*.

# Coatings Exhibiting Anti-Fouling Behavior and Biorecognition Activity in Complex Biological Media: A Review of Functionalization Aspects

Ivana Víšová, Milan Houska, Hana Lísalová\*

Institute of Physics CAS, Na Slovance 1999/2, 182 21 Prague 8, Czech Republic

## ABSTRACT

The review focuses on various aspects of functionalization of the most frequently used platforms resistant to non-specific deposition from complex biological media like blood plasma and raw food extracts. It shows examples and emphasizes the importance of careful consideration of the choice of functionalization methods and their conditions for maintaining good antifouling characteristics of the platforms.

## 1 Introduction

The development of functional coatings in the last two decades has significantly contributed to many breakthrough scientific achievements and triggered new practical applications in various biomedical fields. Novel functional coatings have been intensively developed for use in a number of advanced biotechnologies such as bioanalytical devices, biosensors and microarrays, drug delivery carriers, medical implants, marine coatings, water treatment, or food packaging. The ultimate goal of such development is to create robust application platforms with advanced functional coatings operating in a direct contact with complex biological media such as clinical body fluids or crude food extracts [1-3].

A common element of such functional coatings is a synthetic surface coating that is exposed to the analysed biological medium. However, when almost all common materials come into contact with biological media, undesirable formation of biological deposits, so-called "fouling", occurs on their surface [2-5]. The fouling process is considered to be initiated by a formation of a hydrated layer followed by the adsorption of biological molecules, especially proteins, by means of dynamic molecular exchange processes [6-9]. Depending on the type of the medium, microorganisms or cells can adhere to protein deposits, followed by other biological processes such as blood clotting, inflammatory and immune reactions, or the formation of bacterial biofilms [2-5]. The resulting biological deposits can significantly impair the function of materials and equipment operating in biological media, such as body fluids, media containing cells, food and media from biological production and the biological environment in general.

The problem is particularly critical for materials and “dual-functional” coatings that are supposed to effectively resist fouling from complex media and simultaneously facilitate binding of bioactive elements enabling specific interactions of the surface with target components in biological media. Such combination of coating functionalities is very important for a wide range of biotechnological and medical applications, including biosensors, membranes and particles for separation and accumulation of biological agents and cells, drug carriers, or diagnostic particles applied to blood stream, blood-contacting materials and cell carriers or scaffolds for tissue engineering.

Ultra-low/low fouling functionalizable coatings are exploited especially for applications in the field of biosensors. They pose a modification of the transducer surface to prevent non-specific adsorption from a complex matrix, while supporting biomolecular recognition elements to capture the analyte, which is critical for any biosensing or detection. Finding such a combination of resistance and functionalizability is challenging, and this fragile balance can be easily disrupted after the attachment of bioreceptors.

## **2 Methods for studying fouling**

Recently, a huge effort has been made to research antifouling coatings and a wide range of different characterisation techniques has been used. In such diverse studies it is not easy to find a way to compare results and draw conclusions. First of all, authors usually do not convert results to some easily comparable quantitative units (i.e. mass per area), rather leave them in sensor response units. Therefore, it is difficult to compare the fouling resistance of different coatings. Second, a great range of different conditions for estimating the resistance can be found in the literature – different complex solutions and deposition times or different flow rates of a complex solution – all these parameters affect the resulting level of fouling. Third, there is difference in data evaluation. Some authors read the fouling-related sensor response as the difference between the sensor response before introduction and a certain time after the introduction of the complex sample. Others use so called “real-time nonspecific fouling” approach [10], where the fouling level is determined as the difference between the change in sensor response at time zero after a bulk refractive index change of complex sample and response after some time in the sample, before introducing washing buffer. Obviously, both approaches are observing different fouling levels, as they both look at slightly different phenomena. The first takes into account the creation of a complete irreversible, in the buffer spontaneously non-removable fouling, and the second monitors rather dynamics of the fouling progress after the introduction of a complex sample. As there is no comprehensive approach to the topic, it is difficult to draw reasonable conclusions.

For fouling studies, the method based on surface plasmon resonance (SPR), such as surface plasmon resonance spectroscopy or surface plasmon resonance imaging, is the most commonly used. The method has a very good limit of detection of  $\sim\text{ng}/\text{cm}^2$ . The relationship between the sensor response and mass of the deposit per surface area is known and so most authors report fouling in units of mass per surface area. A certain limitation of this method consists in the need to use a plasmonic material (such as gold,

silver, platinum, etc.) for the sensor substrate, which determines the methods of coating design and its preparation.

Less frequently other methods can be encountered like fluorescent microscopy, quartz crystal microbalances (QCM) and microring resonators or electrochemistry methods (i.e. DPV, EIS). Fluorescent spectroscopy usually indicates the resistance to nonspecific deposition of fluorescent labels, which is not a real measure of fouling and so it is not discussed further in this review. A general disadvantage of the rest of other mentioned methods is that the authors usually display the results in sensor response units, so that such results are not directly comparable with the others.

A comparison of the frequency of use of these methods according to the reviewed literature is shown in Table 1.

**Table 1 – Methods for fouling studies and frequency of their use**

<b>Method</b>	<b>Frequency of use [%]</b>	<b>Units reported</b>
SPR based	78	ng/cm <sup>2</sup>
Electrochemistry methods (EIS, DPV)	15	% change of some initial or reference signal
Microring resonators	5	relative wavelength shift
QCM	2	ng/cm <sup>2</sup>

As shown in Table 2, the great majority of studies claiming ultra-low fouling used for testing undiluted complex media or media diluted to a maximum 10%. Undiluted blood plasma and blood serum and food samples, were most frequently tested, which reflects the fact, that most of functionalizable ultra-low fouling coatings are needed in medical research and food industry. It is worth emphasizing here that the composition of different body fluids and food samples varies greatly, so that one coating may have excellent fouling resistance for one type of sample and not for another.

**Table 2 – The complex media most frequently tested in studies of fouling**

<b>Medium (% dilution)</b>	<b>Frequency of use [%]</b>
Blood plasma (100%)	48
Blood serum (100%)	45
Food samples (100%)	13
Cell lysate (> 50%)	13
Food samples (10%)	13
Blood plasma (10%)	10
Blood serum (10%)	10
Saliva (100%)	6
Saliva (10%)	3
Whole blood (100%)	3

### **3 Functionalization**

Any functionalization, i.e., the attachment of an additional entity to a surface may have some influence on its fouling properties. Both, the attachment technique and the attached biorecognition element (BRE) itself have more or less pronounced effect. It is obvious that the technique used, either physical or covalent, should minimally disrupt the structure of antifouling platform and retain as much as possible activity and specificity of the attached BRE. The choice of suitable functionalization techniques depends on the type of antifouling platform and BRE to be attached, and in case of covalent attachment on functional groups available for the binding reaction.

In most articles dealing with ultra-low or low-fouling coatings, it is possible to find data on fouling before functionalization. However, for analytical applications the fouling after functionalization is important, as it correlates with non-specific interactions that interfere with the detection. Such changes of fouling may be caused not only by non-specific interactions with the structure of the platform disrupted by functionalization reactions, but also by some non-specific interactions inherent to BRE.

#### **3.1 Antifouling functionalizable platforms**

During the years of search for the efficient antifouling and functionalizable platforms several types have been selected from an enormous number of designs. The initially used simple strategy of passivating surfaces by adsorption of a non-interfering protein has later evolved into sophisticated platforms like specific polypeptide matrices [11-15] or complex

matrices based on DNA tetrahedron probes on gold surface [16]. For some time, the most widespread nonfouling strategies used to be the coating with functionalizable hydrophilic polymers like oligosaccharides, various hydrogels and deposition of self-assembled monolayers, often containing oligo(ethylene glycol) moiety [17-19]. Carboxymethyl dextran platform enables efficient binding of high amounts of BREs via its carboxyl groups, but its architecture makes it prone to nonspecific adsorption from undiluted complex media and it is not a well suited platform for such demanding uses [20]. Poly(ethylene glycol) (PEG) and its derivatives can be functionalized via its terminal hydroxyl or carboxyl group. However, its fouling characteristics has been surpassed by newer platforms and, moreover, PEG appeared susceptible to oxidation damage in biological environments, which limits its use for longer-term applications [21], [22], [23] [24].

Nowadays the most frequently used nonfouling platforms are based on dense polymer brushes prepared by controlled surface-initiated polymerization of zwitterionic monomers [25], [26] bearing phosphorylcholine [27], sulfobetaine [28] or carboxybetaine group [29]. Poly(carboxybetaines) allow easy functionalization with various BREs via their carboxyl group [30, 31] which makes them a rather universal platform existing in various variations. We have described ATRP copolymerization of carboxybetaine methacrylamide with another antifouling component, hydroxypropyl methacrylamide, yielding outstandingly antifouling brushes in which the ratio of the both units can be tailored to optimize their BRE immobilization capacity [32]. Interestingly, it was reported that copolymers of carboxybetaine acrylamide or carboxybetaine methacrylate with a substantial portion of hydrophobic n-butyl methacrylate also retain a rather good antifouling characteristics. These copolymers can be deposited by a simple dip-coating on surfaces of hydrophobic supports like polypropylene and polystyrene, which makes them promising for blood contacting medical devices [33]. An another reported approach is the spin coating of a thin layer of crosslinked poly(carboxybetaine acrylamide) hydrogel. Such films 15nm to 150 nm thick on gold and silicon dioxide exhibited fouling from undiluted human blood serum below 5 ng/cm<sup>2</sup> [34]. There are various variations of the above types of antifouling platforms which are listed in other reviews, e.g., in [35].

### **3.2 Functionalization techniques**

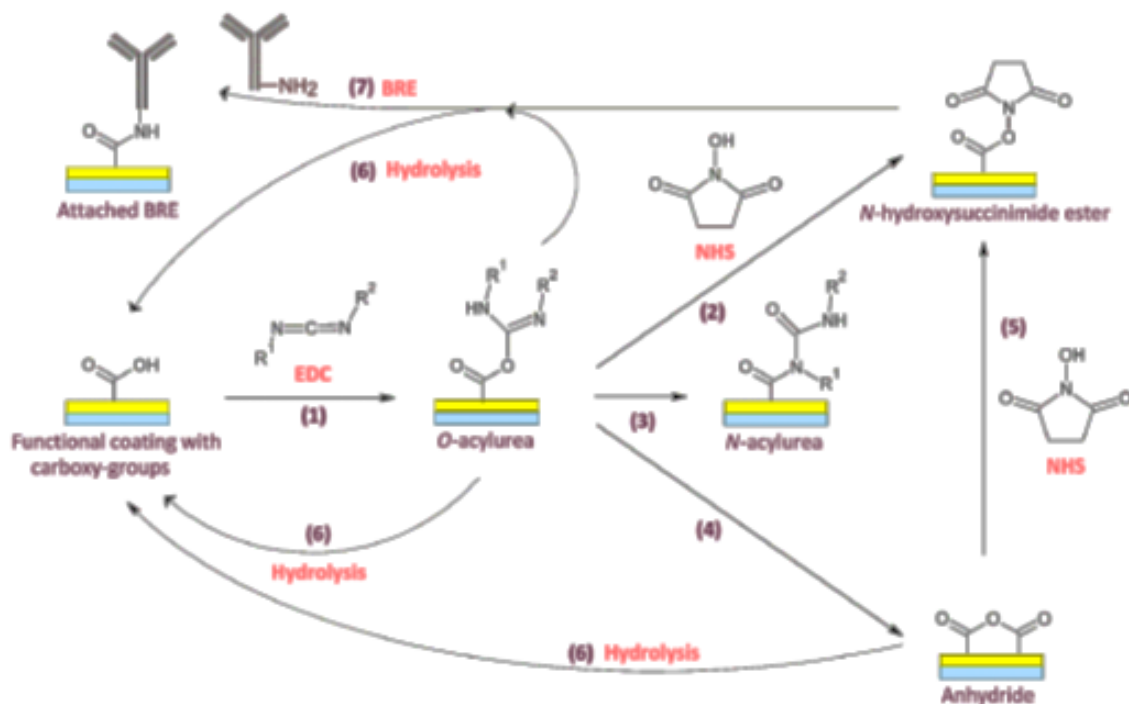
A large number of procedures for coupling BREs have been described in detail in many papers and reviews [31, 36-39] but we shall briefly list only the most important techniques utilized in the papers overviewed in this review and focus on their potential to affect antifouling properties of functionalized matrices.

#### **EDC/NHS**

By far the most frequently used method for the covalent attachment of BREs to biosensing platforms is the activation of surface carboxyl groups with EDC [1-ethyl-3-(3-dimethylaminopropyl)carbodiimide hydrochloride] and NHS (N-hydroxysuccinimide) or sulfo-NHS followed by the reaction of NHS active esters with BREs' amino groups and resulting in stable amide linkages [31], [35], [40], [41], see also [42-51].



A general course of the reactions is indicated in the scheme below.



Carboxyl groups react with EDC [ $R^1 = -CH_2CH_3$ ;  $R^2 = -(CH_2)_3NH(CH_3)_2Cl$ ] to form *O*-acylisourea esters (1) which can react directly with amino groups of BRE to form amide bond (7) while EDC is transformed to the corresponding nonreactive isourea byproduct (not shown in the scheme). However, *O*-acylisourea esters are prone to fast hydrolysis (6) and for this reason the reaction is performed in tandem with NHS (or sulfo-NHS). NHS converts *O*-acylisourea esters rapidly to NHS esters (2) which also readily react with amines (7) but are much more resistant to hydrolysis. The other effect of NHS is the reduction of undesirable and irreversible rearrangement ( $O \rightarrow N$  displacement) of *O*-acylisourea esters to *N*-acylisourea (3) which is unreactive towards primary amines and remains attached to the surface. It has been suggested that in certain cases NHS active ester may not be the prevailing product of activation [52]. Although the reaction of NHS esters proceeds preferentially with primary amine groups, such as those found on the N-terminus and on lysine residues in proteins, other nucleophiles like sulfhydryl and hydroxyl groups may react with NHS esters, even though less efficiently, and the products are less stable compared to amide bond. The reaction is not site specific so that multiple coupling and BRE orientations may occur at the substrate surface influencing BRE activity.

The efficacy of immobilization procedure via NHS esters is very sensitive to pH due to electrostatic interactions between the activated substrate and BRE. For instance, polycarboxybetaines activated with NHS have a positive charge, while activation with sulfo-NHS brings a strong negative charge. Hence, BRE can be attracted to or repulsed from the activated surface depending on its  $pI$  and pH and the conditions must be carefully

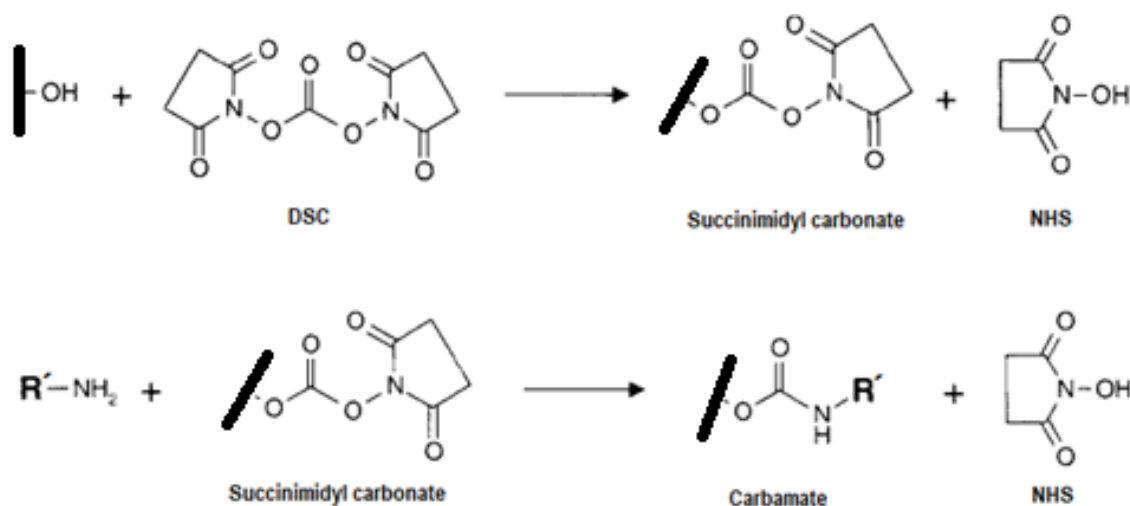
optimized not only to attract BRE to the surface (preconcentration) but also facilitate the reaction with amine group. The optimum pH is a compromise between the rate of hydrolysis of NHS esters, which is enhanced in alkaline region, and the rate of reaction with amino group which should not be protonated. The attachment via sulfo-NHS esters is generally more effective due to its better solubility in water and the chance to better tune electrostatic attraction between the sulfo-substituted substrate and the attached molecule [30, 36]. However, the search of literature shows that for the attachment of BREs to antifouling surfaces sulfo-NHS has been utilized much less frequently than NHS. The reason may be the rate of hydrolysis of sulfo-NHS esters that is substantially lower than that of their NHS analogs [30] and due to strong charge interactions the residuals may be difficult to efficiently remove.

The great advantage of EDC/NHS technique is that BRE is attached via peptide bond. However, like other techniques, it has several drawbacks discussed in more detail in clause 3.3.

### DSC-DMAP

Some platforms like poly[N-(2-hydroxypropyl) methacrylamide], poly(2-hydroxyethyl methacrylate) or poly(oligohydroxyethylene methacrylate) can be functionalized via hydroxyl group. This group is not very reactive but may be activated for coupling with amino groups using various reagents [30].

The most frequently used reagent DSC (N,N'-disuccinimidyl carbonate) consists essentially of two NHS esters. It is not soluble in water but in water readily hydrolyzes to two molecules of NHS and carbon dioxide. In non-aqueous media it reacts with hydroxyl group to carbonate derivative which can conjugate with amine group to form highly stable carbamate bond. Hence, the activation must be carried out in non-aqueous media, which may cause undesirable stress to hydrophilic matrix, but subsequent coupling with an amine-containing BRE may be done in an aqueous solution. .



The reaction is sometimes performed in presence of 4-(dimethylamino)pyridine (DMAP) which acts as a catalytic base deprotonating the hydroxyl group and thus making it more

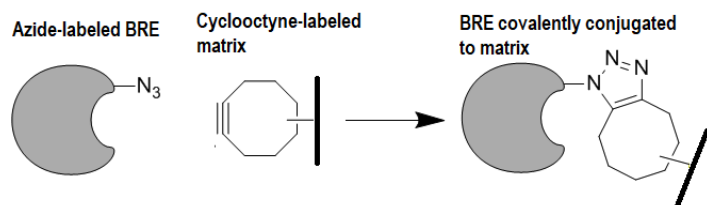
reactive towards DSC. This technique gives higher coupling yields, and what is important, with less side reactions than methods utilizing another reagents, as for instance carbonyldiimidazole [30]. It was used for the attachment of antibody to SPR sensing layer of poly(2-hydroxyethyl methacrylate) [48] and poly[N-(2-hydroxypropyl) methacrylamide] [53] without an apparent increase of fouling in milk and blood plasma, respectively.

### **Biotin-Streptavidin**

This frequently used method of bioconjugation is based on strong noncovalent interaction between small molecule biotin (5-[(3aS,4S,6aR)-2-oxohexahydro-1H-thieno[3,4-d]imidazol-4-yl]pentanoic acid) and glycoprotein streptavidin which has four binding sites for biotin. There are many designs of this technique all of which require covalent preconjugation of biotin to BRE and/or substrate surface. This biotinylation proceeds through the end carboxylic group of biotin which may be coupled either directly to amino group via NHS ester or various biotinylation reagents may be prepared having a spacer with an end binding group for the reaction at the specific site of the protein. These biotinylated conjugates retain good activity of BRE. The binding of biotinylated BRE to the surface requires the presence of streptavidin in between the surface and BRE. This may be achieved by biotinylation of the surface followed by adsorption of streptavidin onto the surface and the adsorption of biotinylated BRE to streptavidin. This technique, is widely used for the conjugation in ELISA assays, and for direct label-free biosensing systems. It has been successfully used for coupling of biotinylated antibody to SPR platform made of diblock of poly[oligo(ethylene glycol) methylether methacrylate] and click chemistry biotinylated poly(glycidylmethacrylate) [55-57]. The method is also frequently used for the attachment of aptamers [58].

### **Site-specific, bioorthogonal coupling**

If immobilization of BRE relies on its endogenous functional groups which are not present at a unique and a site-specific location on BRE surface, a specific orientation of BRE can hardly be controlled. The issue may be solved by the site-specific introduction of bioorthogonal functional group, i.e, the group which is not appearing in, or cross-reacting with BRE endogenous groups, which does not alter its bioactivity, and which can react with the complementary functional group of the surface [59]. This may be achieved using a click chemistry reactions [60] consisting in a catalyst-free, strain-promoted alkyne-azide cycloaddition (SPAAC) which enables the specific immobilization of target BREs in a spatially confined fashion under mild conditions. The azide group is particularly bioorthogonal because it is small, metabolically stable and has no competing biological side reactions. It has been successfully used for coupling of biotinylated antibody to SPR platform made of diblock of poly[oligo(ethylene glycol) methylether methacrylate] and click chemistry biotinylated poly(glycidyl methacrylate). The resulting platform was useful for detection in blood plasma [55]. The SPAAC has been used for the attachment of BRE to zwitterion poly(sulfobetaine) preserving its antifouling properties [61].



## Functionalization with aptamers

Whereas in the past, the detection capability of the great majority of BREs was based on antigen-antibody interactions, nowadays an important part is played by aptamers. As there is a huge amount of literature on aptamer based biosensors [62-70], we shall mention them only briefly. Aptamers are synthetically produced oligonucleotides of ribonucleic acid and single-stranded deoxyribonucleic acid or peptide molecules. They can bind with a high affinity and specificity due to their specific 3D structure even to non-immunogenic target molecules. The range of target molecules is very wide ranging from ions and small molecules to toxins drugs, proteins, cells, etc. [65]. Aptamers can be prepared much easier than antibodies by the SELEX method [62] and they are much more stable allowing repeated use of the sensor.

The choice of immobilization method depends on a number of factors, as it may essentially affect the affinity of aptasensor. Immobilized aptamers are also susceptible to changes of conformation due to interactions with the surface as negative charges of the aptamer phosphate moiety may interact with charged surfaces and originally unfolded random coil may change to folded conformation. The nature of surface chemistry and immobilization methods affect orientation and accessibility of the bound aptamer as well as nonspecific binding.

The immobilization techniques used include physical adsorption, covalent binding, self-assembly, (strept)avidin-biotin interactions, and hybridization, however, not all techniques are suitable for demanding applications such as biosensing. The physical adsorption is not universal enough and due to obvious reasons it cannot meet requirements of demanding applications.

The self/assembly method has been used mainly for electrochemical sensors [67]. Aptamers can be thiolated either directly or via suitable linkers and the modified aptamers are densely attached to gold (metallic) surface by chemisorption. This immobilization is much stronger than physisorption, and even though the coverage with aptamer selfassembled layers suffer of surface defects, such acceptable low fouling impedance-based aptasensor were designed [58].

The main advantage of covalent binding of aptamers lies, in addition to high bond stability, in the possibility of immobilization to chemically diverse surfaces including non-fouling platforms. Both, the 5'-end or the 3'-end of the aptamer can be used for covalent attachment to functionalized surfaces and the choice depends on the type of functionality of the surface. To an amino functionalized surface aptamer can be attached via 5'-end of

ssDNA using EDC and NHS, which results to stable covalent phosphoramidate bond. The same linkage is formed using reactive anhydride or activated ester methods. The spectrum of immobilization methods becomes wider when aptamers are modified with linkers terminated with functional groups. Aptamers having functionalized termini can be immobilized by the same chemical methods used for similar applications of other biomolecules.

Another widely used technique for aptamer immobilization is biotin-(strept)avidin affinity coupling. However, some authors describe instability of the immobilized aptamers and lower sensitivity and specificity [66].

A specific method for attachment of aptamers is hybridization of aptamers to partially complementary sequences immobilized on a surface like planar gold, nanoparticles etc [55]. The hybridization may be tuned in such a way that the interaction with analyte will either lead to its binding, or to the complexation of analyte with aptamer and dissociation of the aptamer complex from the complementary sequence. This binding method is limited by large electrostatic repulsion and steric hindrance that require stringent control of experimental conditions.

### **3.3 Impact of functionalization on fouling**

#### **Polycarboxybetaine-based platforms**

As mentioned above, polybetaine brushes are currently considered to be the best nonfouling platforms for highly demanding applications such as biosensors, while polycarboxybetaines are highly suitable for universal functionalization with various BREs. For this reason, the issue of the effect of functionalization on antifouling characteristics of polycarboxybetaines is given the utmost attention.

As shown in 3.2, the most frequently used method for BRE immobilization to platforms bearing carboxyl group is the EDC/NHS technique. Antifouling characteristics of polycarboxybetaine platforms can be close or below the ultra-low fouling limit defined for undiluted blood plasma as  $<5\text{ng/cm}^2$ , and in some less demanding media it can be even below the SPR limit of detection ( $0.5\text{ ng/cm}^2$ ). There are examples where immobilization did not appear to lead to a marked deterioration in fouling [78-80] but with ever-increasing demands on the sensitivity of assays this becomes an issue.

The immobilization of BREs can lead to significant deterioration of fouling which is due not only to changes introduced by BRE itself, but also to changes of polymer chain arrangements, the presence of residual byproducts and activated groups that may impair antifouling properties of the platform.

We have studied this issue in detail [32] and shown that only a part of NHS esters close to the surface is accessible for the reaction with bulky BREs. If some NHS esters remaining in the platform after the attachment of BRE were not completely deactivated, they can react with smaller non-target nucleophiles present in the analyzed medium and cause false results. It used to be assumed that unreacted NHS esters (and *O*-acylisourea)

may be efficiently hydrolyzed and all corresponding carboxyl groups recovered. We have shown that this may be true if NHS esters are located on top of the platform, like in carboxy terminated oligo(ethylene glycol) SAMs. However, it may not be true if the surface is grafted with polymer that bears functionalizable groups along the whole chain, like in polycarboxybetaines. The common approach to resolve this problem is deactivation of residual NHS esters by hydrolysis in slightly alkaline buffers, which should recover carboxy groups. As this way may not be efficient enough, reactions with small amino compounds, usually ethanolamine or glycine are used instead. While ethanolamine introduces hydroxyl group, the use of amino acid glycine for deactivation of polycarboxybetaines brings an obvious benefit. Each carboxyl group converted to amide group means a loss of one negative charge and disturbs the charge balance essential for outstanding antifouling of polycarboxybetaines. The reaction with glycine formally compensates for this loss and helps to keep antifouling properties.

We have recently shown [32] that the effect of recovered carboxyl groups on antifouling depends on the structure of deactivator and for instance deactivation with (2-aminoethoxy)acetic acid appears to be more effective than deactivation with glycine.

However, we have also observed [using FTIR IRRAS, not published yet] that none of the deactivating compounds, neither glycine nor (2-aminoethoxy)acetic acid (AEAA), lead to a full recovery of zwitterion structure, i.e. the full number of ionized carboxy groups. Even though AEAA itself behaves slightly better than glycine, additionally introduced carboxyl groups apparently are not in a proper position for interaction with quaternary ammonium cation.

It further follows from the above that it is reasonable to optimize the number of functionalizable groups and thus to restrict the extent of chemical modification of antifouling coating to a minimum level indispensable for binding a sufficient amount of BRE for achievement of optimum recognition capacity. There are two practically feasible approaches to this optimization. The first one is to coat the surface with hierarchically structured double layer in which the bottom part is antifouling but non-functionalizable by the immobilization technique used so that only the top part is reactive and bears just the necessary number of functional groups. This is achieved for instance by controlled stepwise surface-initiated polymerization forming two-layer brushes [50, 54]. The optimum antifouling/BRE attachment capacity is tuned by the density and length of the functionalizable block.

We described [32] the second strategy consisting in surface-initiated copolymerization leading to a brush of copolymer in which both monomer units are antifouling but only one is functionalizable. The optimum antifouling/BRE attachment capacity is controlled by varying the ratio of the both monomer units in the copolymer chain and their distribution. We have pursued this approach further [not published yet] by introducing a third nonfouling monomer unit with an ionizable group so that the charge of the whole terpolymer system can be tuned and optimized for a specific BRE and immobilization procedure.

To illustrate further the above discussion, we tested the EDC/NHS activation procedure without binding any BRE and followed by deactivation with various primary amines containing carboxy, sulfate or sulfo groups [71]. This approach excludes interfering effect of added BREs. We observed significant differences in fouling resistance of poly(carboxybetaine acrylamide) (pCBAA) to undiluted human blood plasma using different ways of deactivation. The best result  $\sim 3.8 \text{ ng/cm}^2$  (by SPR) was achieved with a mixture of glycine and 2-aminoethyl hydrogen sulfate, which corresponds to 7.5time reduction of fouling level compared to glycine.

An optimal deactivation also enhances biorecognition capability. The pCBAA brush was functionalized with anti-*E.coli* antibody in a final surface concentration of  $350 \pm 50 \text{ ng/cm}^2$  and subsequently deactivated by various deactivators [71]. This foodborne bacterial pathogen and corresponding medium – minced meat – were chosen as a model system due to its attractiveness in the field of biosensor development for modern food safety applications and possibility to compare the data with results published earlier. The best average fouling level ratio achieved with AEAA was 0,3% of antibody functionalized level, which is significantly better than the ratio 2.8% reported previously [72]. Typically, concentrations of *E.coli* detectable in a buffer solution by direct label-free optical or non-optical biosensors are in the order of  $10^3$  to  $10^5$  CFU/mL [73-77]. This functionalized pCBAA coating deactivated by an optimized deactivation mixtures reached the bottom limit of this range with the LOD  $2.8 \times 10^3$  CFU/mL and LOQ  $1,8 \times 10^4$  CFU/mL, moreover in complex crude food samples, without any extra sample preconditioning or extra after-detection washing steps needed and in a reasonably short time ( $\sim 20$  minutes) [71].

We observed an interesting feature when compared poly(carboxybetaine acrylamide) (pCBAA) and poly(carboxybetaine methacrylamide) (pCBMAA). Though pCBMAA brush shows worse resistance to fouling from undiluted human blood plasma than pCBAA, it keeps resistance after functionalization better if the same EDC/NHS procedure is used [78], [32].

### **pHEMA and AT-SAM platforms**

While blood and other bodily fluids represent the most important media for medical analyses, food industry requires testing of a variety of samples for food safety reasons. The design of nonfouling platforms for analysis of food matrices is challenging because the composition of these samples is very complex and varies enormously. The main attention is focused to detection of food pathogens in meat and milk products, which represent a highly demanding medium from the point of fouling. For milk, the platform made of poly(2-hydroxyethyl methacrylate) (pHEMA) brush seems to be promising. The DSC-DMAP is used for hydroxy group activation and antibody immobilization. This platform was reported [53] to show nearly no fouling (by SPR) from undiluted fresh-whole milk, 10% whole-fat milk from powder or 10% infant formula from powder before or after anti-Cronobacter ex-situ immobilization with LOD  $10^4$  cells/mL. In another work [48] an extremely low fouling of  $0.1 \text{ ng/cm}^2$  from milk on pHEMA and just a few ngs after

immobilization of BSA-aflatoxin M1 conjugates was reported. The DSC-DMAP was used for hydroxy group activation and immobilization.

In [43] the fouling was tested from native orange, tomato and cucumber juices, milk and blood plasma onto pHEMA, OEG-based carboxy-functional alkanethiolate self-assembled monolayer (AT-SAM) and pCBAA. The fouling from all the media was measured on unmodified platforms, after activation (with DMS-DMAP or EDC/NHS) and deactivation (with ethanolamine or glycine) without attaching antibody, and after functionalization with anti-*E. coli* or anti-*Salm* (fouling values were determined for equal amounts of anti-*E. coli* and anti-*Salm*). The fouling after activation/deactivation slightly increased on pCBAA, in contrast to pHEMA that lost a substantial part of its resistance to fouling towards all media. The fouling from milk ca. 40 ng/cm<sup>2</sup> improved slightly to 30 ng/cm<sup>2</sup> after the attachment of antibodies. This example clearly demonstrates that activation/deactivation cycle must be carefully controlled and that the platform may not return to its initial state. AT-SAM performed reasonably well for orange, tomato and cucumber, however, its fouling from blood plasma was in all cases very high (>100 ng/cm<sup>2</sup>). LODs of *Escherichia coli* O157:H7 in undiluted milk were determined to be  $6 \times 10^4$ ,  $8 \times 10^5$ , and  $6 \times 10^5$  cells/ml for pCBAA, pHEMA, and AT-SAM, respectively.

There are many platforms and immobilization methods not discussed here. Unfortunately, they scarcely compare the platform fouling performances before and after the activation/functionalization/deactivation and so the efficacy of these systems can only be judged from the sensitivity of the detection of individual specific targets.

## CONCLUSIONS

The requirements for rapid determination of various pathogens, markers and toxic substances are constantly increasing. The basic problem of label-free methods is the non-specific interaction of the sensor with non-target analytes, and for these reasons more attention needs to be paid to methods for bioreceptor immobilization. As the examples presented here show, the methods and their detailed conditions can have a significant effect on the preservation or deterioration of the antifouling characteristics and thus the performance of the whole system.



## REFERENCES

- [1] Ratner, B. D. and S. J. Bryant (2004). "Biomaterials: where we have been and where we are going." Annu Rev Biomed Eng **6**: 41-75
- [2] Chen, S., L. Li, C. Zhao and J. Zheng (2010). "Surface hydration: Principles and applications toward low-fouling/nonfouling biomaterials." Polymer **51**(23): 5283-5293
- [3] Jiang, S. and Z. Cao (2010). "Ultralow-Fouling, Functionalizable, and Hydrolyzable Zwitterionic Materials and Their Derivatives for Biological Applications." Advanced Materials **22**(9): 920-932
- [4] Blaszykowski, C., S. Sheikh and M. Thompson (2015). "A survey of state-of-the-art surface chemistries to minimize fouling from human and animal biofluids." Biomater Sci **3**(10): 1335-137
- [5] Vaisocherova, H., E. Brynda and J. Homola (2015). "Functionalizable low-fouling coatings for label-free biosensing in complex biological media: advances and applications." Anal Bioanal Chem
- [6] Andrade, J. D., V. L. Hlady and R. A. Vanwageningen (1984). "Effects of Plasma-Protein Adsorption on Protein Conformation and Activity." Pure and Applied Chemistry **56**(10): 1345-1350
- [7] Schmaier, A. H., L. Silver, A. L. Adams, G. C. Fischer, P. C. Munoz, L. Vroman and R. W. Colman (1984). "The effect of high molecular weight kininogen on surface-adsorbed fibrinogen." Thrombosis Research **33**(1): 51-67
- [8] Andrade, J. D., Ed. (1985). Surface and Interfacial Aspects of Biomedical Polymers. New York, Plenum Press
- [9] Vroman, L. (2008). "Finding seconds count after contact with blood (and that is all I did)." Colloids and Surfaces B: Biointerfaces **62**(1): 1-4
- [10] Aubé, A., S. Campbell, A. R. Schmitzer, A. Claing and J.-F. Masson (2017). "Ultra-low fouling methylimidazolium modified surfaces for the detection of HER2 in breast cancer cell lysates." Analyst **142**(13): 2343-2353
- [11] New peptidomimetic polymers for antifouling surfaces. Statz AR, Meagher RJ, Barron AE, Messersmith PB, J. Am. Chem. Soc. 2005 127 7972-7973
- [12] Antifouling glycoalkalix-mimetic peptoids. H.O. Ham, S.H. Park, J.W. Kurutz, I.G. Szleifer, P.B. Messersmith, J. Am. Chem. Soc. 2013 135 13015-13022
- [13] Antifouling poly(beta-peptoid)s. S. Lin, B. Zhang, M.J. Skoumal, B. Ramunno, X. Li, C. Wesdemiotis, L. Liu, L. Jia, Biomacromolecules 2011 12 2573-2582
- [14] An integrated, peptide-based approach to site-specific protein immobilization for detection of biomolecular interactions. Kruis IC, Löwik DW, Boelens WC, van Hest JC, Pruijn GJ, Analyst 2016, 141, 5321

- [15] Low Fouling Protein Detection in Complex Biological Media Supported by a Designed Multifunctional Peptide. Nianzu Liu, Ni Hui, Davis JJ, Xiliang Luo, ACS Sens. 2018 36 1210-1216
- [16] Low-Fouling Surface Plasmon Resonance Sensor for Highly Sensitive Detection of MicroRNA in a Complex Matrix Based on the DNA Tetrahedron. Wenyan Nie, Qing Wang, Liyuan Zou, Yan Zheng, Xiaofeng Liu, Xiaohai Yang, Kemin Wang, Anal. Chem. 2018 90 21 2584-12591
- [17] A novel hydrogel matrix on gold surfaces in surface plasmon resonance sensors for fast and efficient covalent immobilization of ligands. Lofas S., Johnsson B., J. Chem. Soc., Chem. Commun. 1990 1526-1528
- [18] High Salt Stability and Protein Resistance of Poly(L-lysine)-g-poly(ethylene glycol) Copolymers Covalently Immobilized via Aldehyde Plasma Polymer Interlayers on Inorganic and Polymeric Substrates. Blattler T M, Pasche S, Textor M, Griesser HJ, Langmuir 2006 22 5760-769
- [19] Effects of ionic strength and surface charge on protein adsorption on PEGylated surfaces. Pasche S, Vörös J, Griesser HJ, Spencer N D, Textor M, J. Phys. Chemistry B 2005 1745-17552
- [20] Preparation of analyte-sensitive polymeric supports for biochemical sensors, Masson J F, Battaglia T M, Davidson MJ, Kim YC, Prakash AMC, Beaudoin S, Booksh KS, Talanta 2004 64 716-725
- [21] A Survey of Structure–Property Relationships of Surfaces that Resist the Adsorption of Protein. Ostuni E, Chapman RG, Holmlin RE, Takayama S, Whitesides GM Langmuir 2001, 17, 5060-5620
- [22] Protein interactions with oligo(ethylene glycol) (OEG) self-assembled monolayers: OEG stability, surface packing density and protein adsorption. Li L, Chen S, Jiang S, J. Biomater. Sci., Polym. Ed. 2007 18 1415-1427
- [23] Antifouling polymer interfaces: poly(ethylene glycol) and other promising candidates. Lowe S, O'Brien-Simpson N, Connal LA, Polym. Chem. 2015 6 198-212
- [24] On the biodegradability of polyethylene glycol, polypeptoids and poly(2-oxazoline)s. Ulbricht J, Jordan R, Luxenhofer R, Biomaterials 2014 35 (17) 4848-4861
- [25] Zwitterionic polymers exhibiting high resistance to nonspecific protein adsorption from human serum and plasma. Ladd J, Zhang Z, Chen S, Hower JC, Jiang S, Biomacromolecules 2008 9 (5) 1357-1361
- [26] Zwitteration: coating surfaces with zwitterionic functionality to reduce nonspecific adsorption. Schlenoff J B, Langmuir 2014 30 9625-9636

- [27] Non-biofouling materials prepared by atom transfer radical polymerization grafting of 2-methacryloyloxyethyl phosphorylcholine: separate effects of graft density and chain length on protein repulsion. Feng W, Brash JL, Zhu S, *Biomaterials* 2006 27 847-855
- [28] A highly stable nonbiofouling surface with well-packed grafted zwitterionic polysulfobetaine for plasma protein repulsion. Chang Y, Liao SC, Higuchi A, Ruaan RC, Chu CW, Chen WY, *Langmuir* 2008 24 5453–5458
- [29] Pursuing "zero" protein adsorption of poly(carboxybetaine) from undiluted blood serum and plasma. Yang W, Xue H, Li W, Zhang J, Jiang S, *Langmuir* 2009 25 11911-11916
- [30] *Bioconjugate Techniques*, 3rd Edition, Greg T. Hermanson, Academic Press, 2013
- [31] Poly(carboxybetaine methacrylamide)-modified nanoparticles: A model system for studying the effect of chain chemistry on film properties, adsorbed protein conformation, and clot formation kinetics. Abraham S, So A, Unsworth LD, *Biomacromolecules* 2011 12 3567-3580
- [32] Ultralow-Fouling Behavior of Biorecognition Coatings Based on Carboxy-Functional Brushes of Zwitterionic Homo- and Copolymers in Blood Plasma: Functionalization Matters. Lísalová H, Brynda E, Houska M, Víšová I, Mrkvová K, Song XC, Gedeonová E, Surman F, Riedel T, Pop-Georgievski O, Homola J, *Anal. Chem.* 2017 89 6 3524-3531
- [33] Ultra-low Fouling and Functionalizable Surface Chemistry Based on Zwitterionic Carboxybetaine Random Copolymers. Xiaojie Lin, Priyesh Jain, Kan Wu, Daewha Hong, Hsiang-Chieh Hung, Mary Beth O'Kelly, Bowen Li, Peng Zhang, Zhefan Yuan, and Shaoyi Jiang. *Langmuir* 2019 35 (5) 1544–155
- [34] Ultra-low fouling and high antibody loading zwitterionic hydrogel coatings for sensing and detection in complex media. Ying-Nien Chou, Fang Sun, Hsiang-Chieh Hung, Priyesh Jain, Andrew Sinclair, Peng Zhang, Tao Bai, Yung Chang, Ten-Chin Wenb, Qiuming Yu, Shaoyi Jiang. *Acta Biomaterialia*, 2016 40 31-37
- [35] Design and mechanisms of antifouling materials for surface plasmon resonance sensors. Boshi Liu, Xia Liu, Se Shi, Renliang Huang, Rongxin Su, Wei Q, Zhimin He. *Acta Biomaterialia* 2016 40 100–118
- [36] Protein Engineering for direct immobilization. Reddeker ES, Duy Tien Ta, Cortens, Bllen B, Guedens W, Adriansens P. *Bioconjugate Chem.* 2013 24 1761-1777
- [37] Bioconjugation and stabilisation of biomolecules in biosensors. Li'ébana S, Drago GA, *Essays in Biochemistry* 2016 60 (1) 59-68
- [38] *Advances in Bioconjugation*. Kalia J, Raines RT. *Current Organic Chemistry*, 2010 14 138-147

- [39] Bioconjugation Protocols Strategies and Methods. Mark SS (Editor). Methods in Molecular Biology, Vol. 751, Humana Press 2011
- [40] Amine coupling through EDC/NHS: A practical approach. Fischer MJ, Methods. Mol. Biol. 2010 627 55-73
- [41] Optimizing immobilization on two-dimensional carboxyl surface: pH dependence of antibody orientation and antigen binding capacity. Zchiao Pei, Anderson H, Myrskog A, Dunér G, Ingemarsson B, Aastrup T. Analytical Biochemistry 2010 398 161-168
- [42] Low-fouling surface plasmon resonance biosensor for multi-step detection of foodborne bacterial pathogens in complex food samples. Vaisocherová-Lísalová H, Víšová I, Ermini ML, Špringer T, Chadtová-Song X, Mrázek J, Lamačová J, .Scott Lynn N Jr., Šedivák P, Homola J, Biosensors and Bioelectronics 2016 80 84-90
- [43] Functionalized ultra-low fouling carboxy- and hydroxy-functional surface platforms: functionalization capacity, biorecognition capability and resistance to fouling from undiluted biological media. Vaisocherová H, Ševců V, Adam P, Špačková B, Hegnerová K, de los Santos Pereira A, Rodriguez-Emmenegger C, Riedel T, Houska M, Brynda E, Homola J. Biosensors and Bioelectronics 2014 51 150-157
- [44] Plasmonic Hepatitis B Biosensor for the Analysis of Clinical Saliva. Riedel T, Hageneder S, Surman F, Pop-Georgievski O, Noehammer C, Hofner M, Brynda E, Rodriguez-Emmenegger C, Dostálek J. Anal. Chem. 2017 89 2972-2977
- [45] Copolymer Brush-Based Ultralow-Fouling Biorecognition Surface Platform for Food Safety. Vaisocherova-Lísalová H, Surman F, Víšova I, Vala M, Špringer T, Ermini ML, Šípová H, Šedivák P, Houska M, Riedel T, Pop-Georgievski O, Brynda E, Homola J. Anal. Chem. 2016 88 10533-10539
- [46] Hepatitis B plasmonic biosensor for the analysis of clinical serum samples. Riedel T, Surman F, SimoneHageneder b, Pop-Georgievski O, Christa Noehammer c, ManuelaHofner c, Brynda E, Rodriguez-Emmenegger C, Dostálek J. Biosensors and Bioelectronics 2016 85 72-279
- [47] Directly Functionalizable Surface Platform for Protein Arrays in Undiluted Human Blood Plasma. Brault ND, White AD, Taylor AD, Qiuming Yu, Jiang S. Anal. Chem. 2013 85 1447-1453
- [48] Sensitive and rapid detection of aflatoxin M1 in milk utilizing enhanced SPR and p(HEMA) brushes. Karczmarczyk A, Dubiak-Szepietowska M, Vorobii M, Rodriguez-Emmenegger C, Dostálek J, Feller KH. Biosensors and Bioelectronics 2016 81 159-165
- [49] Ultra-low fouling and functionalizable zwitterionic coatings grafted onto SiO<sub>2</sub> via a biomimetic adhesive group for sensing and detection in complex media. Brault ND,

- Changlu Gao, Hong Xue, Piliarik M, Homola J, Shaoyi Jiang, Qiuming Yu.  
Biosensors and Bioelectronics 2010 25 2276-2282
- [50] Zwitterionic Polymer-Based Platform with Two-Layer Architecture for Ultra Low Fouling and High Protein Loading. Chun-Jen Huang, Yuting Li, Shaoyi Jiang. Anal. Chem. 2012 85 3440-3445
- [51] SPR Biosensing in Crude Serum Using Ultralow Fouling Binary Patterned Peptide SAM. Bolduc OR, Pelletier JN, Masson J-F. Anal. Chem. 2010 82 3699-3706
- [52] Different EDC/NHS Activation Mechanisms between PAA and PMAA Brushes and the Following Amidation Reactions. Cuie Wang, Qin Yan, Hong-Bo Liu, Xiao-Hui Zhou, Shou-Jun Xiao. Langmuir 2011 27 (19) 12058-12068
- [53] Polymer Brushes Showing Non-Fouling in Blood Plasma Challenge the Currently Accepted Design of Protein Resistant Surfaces. Rodriguez-Emmenegger C, Brynda E, Riedel T, Houska M, Šubr V, Aldo Bologna Alles, Hasan E, Gautrot JE, Huck WTS. Macromol. Rapid Commun. 2011 32 952-957
- [54] Two-Layer Architecture Using Atom Transfer Radical Polymerization for Enhanced Sensing and Detection in Complex Media. Brault ND, Harihara S Sundaram, Chun-Jen Huang, Yuting Li, Qiuming Yu, and Shaoyi Jiang. Biomacromolecules 2012 13 4049-4056
- [55] Catalyst-free “click” functionalization of polymer brushes preserves antifouling properties enabling detection in blood plasma. Parrillo V, de Los Santos Pereira A, Riedel T, Rodriguez-Emmenegger C. Analytica Chimica Acta 971 (2017) 78-87
- [56] Regenerative biosensor for use with biotinylated bait molecules. Knoglinger C, Zich A, Traxler L, Poslední K, Friedl G, Ruttmann B, Schorpp A, Müller K, Zimmermann M, Gruber HJ. Biosensors and Bioelectronics 2018 99 684-690
- [57] Fc-specific biotinylation of antibody using an engineered photoactivatable Z–Biotin and its biosensing application. Yang HM, Bao RM, Yu CM, Lv YN, Zhang WF, Tang JB. Analytica chimica acta 2017 949 76-82
- [58] Optimisation and Characterisation of Anti-Fouling Ternary SAM Layers for Impedance-Based Aptasensors, Anna Miodek, Edward M. Regan, Nikhil Bhalla, Neal A.E. Hopkins, Sarah A. Goodchild and Pedro Estrela. Sensors (Basel) 2015 15(10) 25015–25032
- [59] The future of Bioorthogonal Chemistry. Devaraj NK. ACS Cent. Sci. 2018 4 8 952-959
- [60] Click Chemistry Immobilization of Antibodies on Polymer Coated Gold Nanoparticles. Finetti C, Sola L, Pezzullo M, Prospero D, Colombo M, Riva B, Avvakumova S, Morasso C, Picciolini S, Chiari M. Langmuir 2016 32 29 7435-7441

- [61] Generic top-functionalization of patterned antifouling zwitterionic polymers on indium tin oxide. Li Y, Giesbers M, Gerth M, Zuilhof H. *Langmuir* 2012 28(34) 12509-17
- [62] Detection and beyond: challenges and advances in aptamer-based biosensors, Hyebin Yoo, Hyesung Jo and Seung Soo Oh. *Mater. Adv.*, 2020 1 2663-2687
- [63] Aptamer based tools for environmental and therapeutic monitoring: A review of developments, applications, future perspectives, Błażej Kudłak, Monika Wiczerzak. *Critical Reviews in Environmental Science and Technology* Volume 50, 2020 - Issue 8
- [64] Aptamer-based biosensors for biomedical diagnostics, Wenhui Zhou, Po-Jung Jimmy Huang, Jinsong Ding and Juewen Liu. *Analyst*, 2014 139 2627-2640
- [65] Aptasensors for Detection of Avian Influenza Virus H5N1. Li Y, Wang R. *Methods in Molecular Biology* (Clifton, N.J.), 2017 1572 379-402
- [66] Aptamers for Analytical Applications: Affinity Acquisition and Method Design, Chapter: Immobilization of Aptamers on Substrates, Maria C. DeRosa, Marina Cortese, Michelangelo Pascale, et al. John Wiley and Sons, Oct 26, 2018
- [67] Immobilization Techniques for Aptamers on Gold Electrodes for the Electrochemical Detection of Proteins: A Review. Franziska V. Oberhaus \*, Dieter Frense and Dieter Beckmann. *Biosensors* 2020 10 45
- [68] Aptasensors in Health, Environment and Food Safety Monitoring, Arghya Sett, Suradip Das, Pragma Sharma, Utpal Bora. *Open Journal of Applied Biosensor*, 2012 1 9-19
- [69] Surface immobilization of DNA aptamers for biosensing and protein interaction analysis. Zhang X, Yadavalli VK. *Biosens Bioelectron.* 2011 26(7) 3142-7
- [70] Surface immobilization methods for aptamer diagnostic applications, Subramanian Balamurugan, Anne Obubuafo, Steven A Soper, David A Spivak. *Anal Bioanal Chem.* 2008 390(4) 1009-21
- [71] Recovery of Antifouling Properties of Zwitterionic Brushes After Carboxy Groups Activation and Functionalization, Ivana Víšová, Michala Forinová, Alina Pilipenco, Kateřina Mezulániková, Markéta Tomandlová, Markéta Vrabcová, Milan Houska, Alexandr Dejnek, Jakub Dostálek, Hana Vaisocherová-Lísalová. Submitted to
- [72] Low-fouling surface plasmon resonance biosensor for multi-step detection of foodborne bacterial pathogens in complex food samples, Vaisocherová-Lísalová, H., Víšová, I., Ermini, M.L., Špringer, T., Song, X.C., Mrázek, J., Lamačová, J., Scott Lynn, N., Šedivák, P., Homola. J., *Biosensors and Bioelectronics* 2016 80 84-90

- [73] Rapid and label-free bacteria detection by surface plasmon resonance (SPR) biosensors, Dudak, F.C., Boyacı, İ.H. *Biotechnology journal* 2009 4(7) 1003-1011
- [74] Conformable surface acoustic wave biosensor for E-coli fabricated on PEN plastic film, Lamanna, L., Rizzi, F., Bhethanabotla, V.R., De Vittorio, M. *Biosensors & bioelectronics* 2020 163 10
- [75] Rapid label-free detection of E. coli using a novel SPR biosensor containing a fragment of tail protein from phage lambda, Shin, H.J., Lim, W.K. *Preparative Biochemistry & Biotechnology* 2018 48(6) 498-505
- [76] Biomimetic Bacterial Identification Platform Based on Thermal Wave Transport Analysis (TWT) through Surface-Imprinted Polymers, Steen Redeker, E., Eersels, K., Akkermans, O., Royackers, J., Dyson, S., Nurekeyeva, K., Ferrando, B., Cornelis, P., Peeters, M., Wagner, P., Diliën, H., van Grinsven, B., Cleij, T.J. *ACS Infectious Diseases* 2017 3(5) 388-397
- [77] Label-Free Detection of Escherichia coli Based on Thermal Transport through Surface Imprinted Polymers, van Grinsven, B., Eersels, K., Akkermans, O., Ellermann, S., Kordek, A., Peeters, M., Deschaume, O., Bartic, C., Diliën, H., Steen Redeker, E., Wagner, P., Cleij, T.J.. *ACS sensors* 2016 1(9) 1140-1147
- [78] Ultralow fouling and functionalizable surface chemistry based on a zwitterionic polymer enabling sensitive and specific protein detection in undiluted blood plasma, Vaisocherova, H., W. Yang, Z. Zhang, Z. Cao, G. Cheng, M. Piliarik, J. Homola and S. Jiang. *Analytical Chemistry* 2008 80(20) 7894-7901.
- [79] Polymer brushes showing non-fouling in blood plasma challenge the currently accepted design of protein resistant surfaces, Rodriguez-Emmenegger, C., E. Brynda, T. Riedel, M. Houska, V. Subr, A. B. Alles, E. Hasan, J. E. Gautrot and W. T. Huck. *Macromol Rapid Commun* 2011 32(13): 952-957
- [80] Zwitterionic Polymer-Based Platform with Two-Layer Architecture for Ultra Low Fouling and High Protein Loading, Huang, C.-J., Y. Li and S. Jiang. *Analytical Chemistry* 2012 84(7) 3440-3445

# Appendix XI

Obořilová, R., H. Šimečková, M. Pastucha, Š. Klimovič, I. Víšová, J. Příbyl, H.  
Vaisocherová-Lísalová, R. Pantůček, P. Skládal, I. Mašlaňová, Z. Farka

**Atomic Force Microscopy for Real-time Single-cell Study of the  
Bacteriophage-mediated Lysis.**

In preparation. To be submitted in *Nanoscale*.



# Atomic Force Microscopy for Real-time Single-cell Study of the Bacteriophage-mediated Lysis of Bacteria

Radka Obořilová<sup>1,†</sup>, Hana Šimečková<sup>2,†</sup>, Matěj Pastucha<sup>1,3</sup>, Šimon Klimovič<sup>1,3</sup>, Ivana Víšová<sup>4</sup>, Jan Příbyl<sup>3</sup>, Hana Vaisocherová-Lísalová<sup>4</sup>, Roman Pantůček<sup>2</sup>, Petr Skládal<sup>1,3</sup>, Ivana Mašlaňová<sup>2,\*</sup>, Zdeněk Farka<sup>1,3,\*</sup>

<sup>1</sup> Department of Biochemistry, Faculty of Science, Masaryk University, Kamenice 5, 625 00 Brno, Czech Republic

<sup>2</sup> Department of Experimental Biology, Faculty of Science, Masaryk University, Kamenice 5, 625 00, Brno, Czech Republic

<sup>3</sup> CEITEC MU, Masaryk University, Kamenice 5, 625 00 Brno, Czech Republic

<sup>4</sup> Institute of Physics of the CAS, Na Slovance 1999/2, 182 21 Prague, Czech Republic

† R.O. and H.Š. contributed equally to the work

\* Corresponding authors: [maslanova@mail.muni.cz](mailto:maslanova@mail.muni.cz) (I.M.), [farka@mail.muni.cz](mailto:farka@mail.muni.cz) (Z.F.)

## Abstract

The growing incidence of multidrug-resistant bacterial strains is one of the key challenges in the current medicine. Antibiotic resistance is often exhibited by *Staphylococcus aureus*, which causes severe infections in human and animal hosts and leads to significant economic losses. Enzybiotics and phage therapy represent promising and effective alternatives to classic antibiotics. New tools are necessary to study the phage-bacteria interactions and bacterial lysis process with high resolution and in real-time. Electron microscopy can provide a high resolution; however, it is limited to static observation of the dynamic biological processes. Here, we introduce a methodology to study the lysis of *S. aureus* on a single-cell level in real-time using the atomic force microscopy (AFM). We demonstrated the potential of the method to follow the effect of enzybiotic lysostaphin on *S. aureus* and the lytic action of the *Podoviridae* phage P68. AFM allowed monitoring of topographic and biomechanical properties of the bacteria in the course of lysis at high resolution and in near-physiological conditions. The force-distance curves were evaluated to determine Young's modulus characterizing the changes in stiffness of *S. aureus* during the lysis. This allowed us to reveal progressive disintegration of the cell envelope was

accompanied by the decrease of cell stiffness. The AFM experiments were complemented by surface plasmon resonance (SPR), which provided details on the kinetics of the phage-bacterium binding and subsequent lysis processes. The approach forms a foundation of an innovative framework for studying the lysis of individual bacteria, with the potential to obtain results that will support the development of phage therapy.

## 1 Introduction

Antibiotic resistance is one of the major threats of the current medicine, which is highlighted by the steep increase in the number of multidrug-resistant (MDR) bacterial strains [[10.1146/annurev.biochem.78.082907.145923](#)]. The antibiotic resistance can lead to prolonged treatment, increased healthcare costs, and even the inability to cure the patients. Therefore, development of alternative therapies to fight bacterial infections, independent of antibiotics, is required. *Staphylococcus aureus* is a clinically relevant opportunistic pathogen that exhibits multidrug resistance and a wide range of virulence factors [10.3389/fmicb.2019.00539]. In particular, the increasing emergence and prevalence of virulent clones of methicillin-resistant *S. aureus* (MRSA) represents a significant medical problem [10.1016/j.jgar.2016.04.004].

Phage therapy promises an alternative treatment approach based on the highly specific host-phage interaction enabling selective antimicrobial action [[10.4161/viru.25991](#)]. The experimental utilization of virulent phages with a broad host range has proven to be effective in the treatment of incurable bacterial infections [10.1128/CMR.00066-18] [[10.1038/s41564-019-0666-4](#)]; [[10.1038/s41564-019-0634-z](#)]. Besides the high specificity, the application of phages provides other advantages compared to the antibiotic treatment, in particular, natural dosing by phage multiplication in the presence of the pathogen, minimal effect on normal microflora, and smaller potential for inducing resistance [[10.4161/bact.1.2.14590](#)]. Therefore, the applications of phages in human and veterinary medicine, as well as in the food industry and biotechnology, are intensively studied [[10.1146/annurev-food-032818-121747](#)], [[10.1111/jam.13207](#)], [[10.1016/j.tibtech.2006.03.003](#)]. Lytic phages from the families *Myoviridae* and *Podoviridae* are highly promising candidates for phage therapy of *S. aureus* infections. This work focuses on phage P68, member of the short-tailed *Podoviridae* family [10.1038/s41467-020-16669-9].

The enzybiotics represent another promising class of antimicrobial agents, most of which belong to phage lysins or bacterial cell wall hydrolases. Lysostaphin is an endopeptidase isolated from *Staphylococcus simulans*, which targets the pentaglycine bridge of peptidoglycan of most staphylococcal species [[10.3390/ph3041139](#)]. Due to the highly specific interaction and the precise mechanism of action [10.1038 / s41589-019-0393-4], lysostaphin can provide rapid lysis of bacterial cells and biofilms where antibiotics fail [10.1128 / AAC.47.11.3407–3414.2003].

For the successful introduction of phage therapy, it is necessary to study the phage-host interactions at various levels (from genome to phenotype) [10.1080/14712598.2019.1651287], including cell-level monitoring of the process in real-time. Conventional approaches for studying phage-mediated lysis include plaque assays on agar plates resulting in visual evaluation of bacterial sensitivity. The kinetics of the infection process can be further investigated by monitoring the decrease in the optical density of the bacterial culture exposed to the phage. This method allows efficient evaluation of the lytic activity of phages based on the mathematical description of bacterial growth curves. This approach has been already optimized and applied for rapid phage detection and quantification [10.1371/journal.pone.0216292]. Phage activity can be quantitatively characterized by a Virulence Index [10.1089/phage.2019.0001] or a Phage Score [10.1016/j.bej.2020.107652]. The high-resolution images of the interaction of phages with bacteria at the nanoscale level can be provided by electron microscopy (EM), in particular by Cryo-EM [10.1007/978-1-4939-7395-8\_5]. It provides the best results in terms of the resolution and structural view of the sample; however, the information about the dynamics of the living system is given only in combination with molecular modeling simulations. Further disadvantages of EM include complicated sample preparation, only static exploration of the sample, and the inability to evaluate the biomechanical changes happening during the process.

Due to its capability to visualize phage-mediated bacterial lysis in real-time, atomic force microscopy (AFM) can provide useful data complementary to the conventional techniques. AFM examines the topology of a sample by moving or tapping a probe on a surface. The method is recently gaining popularity for nanoscale bioimaging due to gentle sample handling and the possibility of measuring in native conditions. Another significant advantage of AFM compared to EM is the possibility to investigate the biomechanical properties of the sample. For this purpose, Young's modulus (YM) is most typically examined, which is defined as the ratio of stress to proportional deformation and expresses the stiffness or elasticity of the studied object. YM values of bacteria vary based on the composition and condition of the bacterial envelope [10.1021/acs.biochem.7b00346]. AFM enables scanning in liquid and simultaneous monitoring of multiple properties of the studied object. Thus, it can be used to study the dynamic process of bacterial lysis in the natural environment of the growth medium (**Figure 1**).

AFM was previously used for the study of the phage-mediated bacterial lysis [10.1016/j.mimet.2011.10.006, 10.1021/la8022612, 10.1371/journal.pone.0047348]; however, these measurements were done only in the air and, therefore, provided only a static assessment without the possibility to examine living cells under the native conditions. On the other hand, near-physiological conditions can be achieved for visualization in liquid. The only deviation from the natural system is the necessity to attach the bacteria to the surface. The bacterial adhesion to solid surfaces is commonly observed during biofilm formation as a part of its infection strategy [10.1038/nrmicro3161]. The most straightforward method of gentle attachment of bacteria to the surface without the need for fixation is adsorption. It can be done either directly on the surface or mediated by electrostatic interactions after activation of the surface with poly-L-lysine (PLL),

gelatin [10.1016/S0304-3991(03)00045-7], polyethyleneimine, or silanization [10.1016/j.ultramic.2010.06.010]. Another possibility for a non-invasive attachment is physical capture in microwells, such as in the pores of a polycarbonate membrane [10.1111/j.1365-2818.2009.03333.x]. Finally, adhesive proteins or peptides can be used for a more specific capture [10.1016/j.ultramic.2010.06.010]. Several authors studied bacteria in liquid by AFM; however, most capture the static image without monitoring the changes over time.

Surface plasmon resonance (SPR) is a technique that is routinely used to study the interactions of biomacromolecules. It can be used as a complementary method to AFM, allowing the study of the real-time kinetics of the bacterial lysis. Bacteria need to be immobilized on the sensing surface, similarly to AFM. As the lysis agent binds to the bacteria and causes their degradation, the optical properties close to the surface change substantially. This is detected by the SPR instrument as the shift of the resonance angle. In this way, SPR can be used also for sensitive detection of the lysis agent, when the bacteria serve as a “biorecognition element” [10.1128/AEM.02806-07], [10.1016/j.bios.2004.11.019], [10.1016/j.snb.2020.127945], [10.1021/ac950844e].

Here, we introduce a methodology to employ the AFM and SPR to follow the dynamic processes of bacterial lysis in a growth medium in real-time. Our results reveal not only topographic changes during the lysis but also significant differences in biomechanical properties. As far as we know, this is the first report on the monitoring of phage-mediated bacterial lysis at the single-cell level under native conditions using AFM. Furthermore, SPR was used to study the kinetics of the interaction of the antibacterial agent with *S. aureus*.

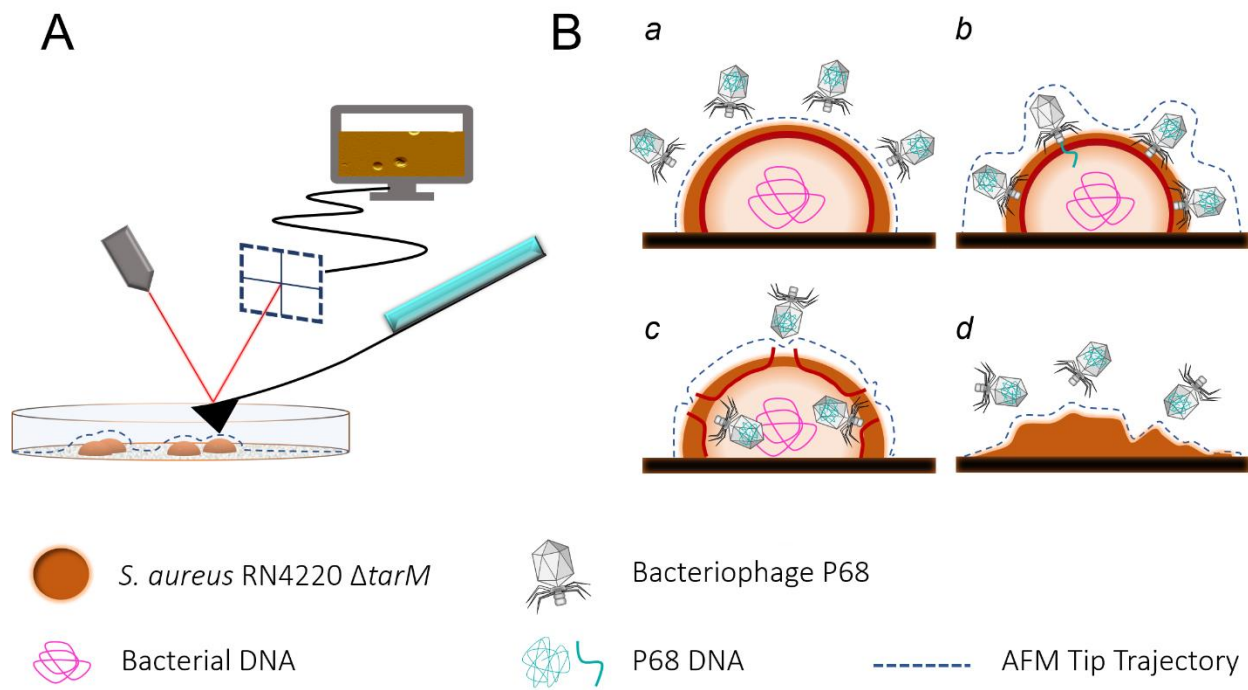


**Figure 1:** (A) Scheme of AFM imaging of bacterial lysis. The scanning provides information on the topography and mechanical properties of the immobilized bacterial cells. (B) A lytic cycle consisting of (a) phage binding to the bacterium, (b) injection of phage DNA, (c) release of assembled virions, and (d) completed lysis of the bacterium.

## 2 Materials and Methods

### 2.1 Chemicals, Buffers, and Cultivation Media

Poly-L-lysine (PLL) and bovine serum albumin (BSA) were purchased from Sigma-Aldrich (USA). Lysostaphin (specific activity  $\geq 3990$  U/mg) was obtained from AMBI Products (USA). Growth media were obtained from Oxoid (UK). All other common chemicals were obtained from Sigma-Aldrich (USA), Carl Roth (Germany), and Penta (Czech Republic). Polystyrene Petri dishes were obtained from TPP (Switzerland).

The used buffers and cultivation media included phosphate-buffered saline (PBS; 50 mM  $\text{NaH}_2\text{PO}_4/\text{Na}_2\text{HPO}_4$ , 150 mM NaCl, pH 7.4), Tris-buffer saline (Tris; 50 mM Tris, 150 mM NaCl, pH 7.5), Tris-buffer saline with additional  $\text{CaCl}_2$  (Tris+; 50 mM Tris, 150 mM NaCl, 2 mM  $\text{CaCl}_2$ , pH 7.5), phage buffer (50 mM Tris, 10 mM NaCl, 10 mM  $\text{CaCl}_2$ , pH 8.0), tryptone soya broth with 2 mM  $\text{CaCl}_2$  (TSB), tryptone soya broth without the addition of  $\text{Ca}^{2+}$  (TSB without  $\text{CaCl}_2$ ), tryptone soya agar (1.5% TSA), and soft agar (0.7% TSA). The full composition of the cultivation media is provided in the Supporting Information (SI).

### 2.2 Cultivation of *S. aureus*

*S. aureus* strains RN4220 and RN4220  $\Delta tarM$  [10.1038/srep17219] were kindly provided by prof. Andreas Peschel (University of Tübingen, Germany). The *tarM* deletion mutant of strain RN4220 was used as a suitable host [10.1038/srep17219], and RN4220 without gene deletion was chosen as a phage-resistant control. To enable an effective infection, Staphylococcal podoviruses, including P68, require a specific stereochemistry of O-linked  $\beta$ -N-acetylglucosamine to the 4 position of the ribitol phosphate wall teichoic acid monomer attached by glycosyltransferase TarS [10.1371/journal.ppat.1006067]. It is assumed that in the case of *S. aureus* RN4220, the additional attachment of  $\alpha$ -O-GlcNAc mediated by TarM glycosyltransferase prevents effective infection by phage P68.

The bacteria were grown overnight in TSB at 37 °C to an optical density at 600 nm ( $OD_{600}$ ) of  $\sim 1.8$ . The cells were harvested by centrifugation at 4,600 g for 10 min and resuspended in a buffer, depending on the following experiments. The concentration of viable bacteria was determined by cultivation and quantification as colony-forming units (CFU) per mL.

### 2.3 Preparation of Phage P68

Phage vB\_SauP\_P68 (P68) was purchased from Félix d'Hérelle Reference Center for Bacterial Viruses (Université Laval, Quebec, Canada). The propagating strain *S. aureus* RN4220  $\Delta tarM$  was freshly grown to  $OD_{600}$  of 0.4 in TSB. Afterward, the lysate of phage P68 was added to achieve the multiplicity of infection (MOI) of ~10 and allowed to propagate at 37 °C with mild shaking until the bacterial lysis occurred. The resulting bacterial lysate was filtered through a 0.45- $\mu$ m polyethersulfone syringe filter (TPP, Switzerland). The sterile lysate was stored at 4 °C for further processing.

The phages were purified by centrifugation at 64,000 g for 2.5 h at 4 °C (Avanti J-30I with JA-30.50 Ti rotor, Beckman Coulter, USA). The pellet was resuspended in 300  $\mu$ L of phage buffer overnight at 4 °C. The residual dissolved proteins were removed by extraction with chloroform (1:1 of total sample volume). The viral particles were purified by ultracentrifugation in CsCl gradient as described previously [10.1038/s41467-020-16669-9]. The viable viral particles were quantified by double agar layer plaque assay as plaque-forming units (PFU) per mL.

The protocols for the determination of the adsorption kinetics of the phage and for the use of qPCR to evaluate the expression of the major capsid protein (mcp) gene of phage P68 are provided in the Supporting Information.

### 2.4 Lysis Evaluated as Changes of Optical Density

The lysis experiments in solution were performed in non-binding 96-well polystyrene microtiter plates (Greiner, Austria) and the lysis was evaluated using Synergy 2 reader (BioTek, USA) as a decrease of  $OD_{600}$ . First, the bacterial culture of *S. aureus* was transferred to the TSB, TSB with  $Ca^{2+}$ , and Tris buffer. Varying concentrations of lysis agents – either lysostaphin or phage P68 in corresponding buffers were added in a ratio of 1:4 (v/v). The lysis was monitored for 6 h at 25 °C and 37 °C. The lysostaphin-mediated lysis was tested for concentrations of 0.1, 0.3, 1, 3, 10, 30, and 100  $\mu$ g/mL with the *S. aureus* concentration of  $1.1 \times 10^9$  CFU/mL. In the case of phages, the number of phages was expressed as a multiplicity of infection (MOI), defined as the ratio of the phage P68 to *S. aureus*. The MOI values of 0.0001, 0.001, 0.01, 0.1, 1, and 10 were tested.

### 2.5 Optical Microscopy

Bright-field optical microscopy without staining the sample was performed using an Olympus BX41 microscope equipped with a 100 $\times$  immersion objective and an Olympus E-510 camera (Olympus, Japan). For the immobilization of the bacteria, the surface of the polystyrene Petri dish was coated with 10  $\mu$ g/mL of PLL for 1 h, washed with distilled water, and *S. aureus* bacterial culture in PBS ( $1.4 \times 10^9$  CFU/mL) was applied for 1 h, followed by rinsing with distilled water and drying with compressed air. The bacteria were rehydrated by either the Tris buffer or the TSB immediately after that. The initial state of immobilized bacteria was imaged, followed by the

addition of the enzyme or phage and incubation at room temperature or at 37 °C. After 1.5 h and then every 30 min, the lysis progress was evaluated under the microscope. Samples with different lysostaphin concentrations (0.1, 1, 10, and 100 µg/mL) and a control sample (without the enzyme) were examined. The control sample (either in the absence of the lysing agent or using the phage-resistant culture of *S. aureus* RN4220) was treated by the same procedure. The phage concentration was  $8 \times 10^9$  PFU/mL; however, some non-specific adsorption of phages on the Petri dish surface must be considered. Therefore, the exact MOI value cannot be reliably determined.

## 2.6 SPR Characterization of Bacterial Lysis

SPR system MP-SPR Navi 210A (Bionavis, Finland) was employed to follow the lysis in real-time. The system allows to measure simultaneously in two independent flow channels and utilizes two lasers, 670 and 785 nm. The measurement was carried out in the angular scan mode, where the selected spectral range (58–78°) was monitored. The response was evaluated as the shift in the surface plasmon resonance angle determined by a centroid fitting function.

Before the measurement, the bacteria were captured on the chip. A bare gold SPR chip was first cleaned with acetone and isopropanol (each for 10 min in an ultrasonic bath), washed with water, dried with compressed air, and covered with PLL (10 µg/mL in water). After 1 h, the chip was washed with water, dried, and 500 µL of the bacterial suspension ( $OD_{600}$  of 1.5) in PBS was applied for 1 h at room temperature. The bacterial suspension was applied off-line outside of the flow cell to prevent non-specific adsorption to the fluidic system. The chip was washed with PBS, water and dried with compressed air. For lysostaphin-mediated lysis experiments, it was incubated with a blocking solution (1 mg/mL BSA in PBS) for 1 h. For phage-mediated lysis experiments, the blocking step was omitted since the surface was blocked in the system by the running solution of TSB. After washing with PBS, water, and drying with compressed air, the chip was immediately inserted into the SPR system, and the flow channels were filled with the running solution (Tris buffer for lysostaphin and TSB medium for phage experiments, respectively).

The running buffer was flown continuously over the surface at the flow rate of 10 µL/min until the response was stabilized. Then, the solution of the lytic agent (0.3 to 100 µg/mL of lysostaphin and  $4 \times 10^9$  to  $4 \times 10^{10}$  PFU/mL of phage P68) in the running buffer was injected for 20 min at the same flow rate, followed again by the flow of running buffer.

## 2.7 Real-time AFM Monitoring of Bacterial Lysis in Liquid

For the activation of Petri dish surfaces, 10 µg/mL solution of PLL in distilled water was applied for 1 h, followed by the incubation with a bacterial suspension of *S. aureus* ( $1.6 \times 10^9$  CFU/mL) in

PBS for 1.5 h. The immobilized bacteria were rinsed by distilled water, dried with compressed air, and immediately rehydrated in TSB for scanning in liquid.

The real-time AFM scanning of lysostaphin-mediated bacteria lysis was performed at 25 °C in Tris buffer. First, the initial state of the bacteria on the surface was recorded, followed by the addition of 10 µg/mL of lysostaphin in Tris buffer and subsequent monitoring of the topography and mechanical properties of the bacteria. The phage-mediated lysis took place in the TSB, which contains sufficient growth factors for the metabolic activity of the bacteria and the complete realization of the lytic cycle; the experiments were carried out at temperatures of 25 °C and 37 °C. The concentration of phage P68 was  $1.2 \times 10^9$  PFU/mL. The control experiments were performed for 3 h without the addition of the lysing agent to verify the stability of the bacteria under the experimental conditions and to exclude any adverse effect of the repeated scanning on the integrity of the bacterial envelope.

The AFM system NanoWizard 3 (JPK, Germany) was operated in the QI tapping mode to dynamically capture the lysis progress. The expected height of the bacterium was around 1 µm [10.22203/ecm.v004a04]; therefore, it was necessary to choose a probe with a longer tip. Silicon nitride probe NITRA-TALL-B with a spring constant  $k$  of 0.02 N/m, tip length of 14–16 µm was used. Calibration of sensitivity and spring constant was performed before each measurement. The  $10 \times 10$  µm images were recorded at  $256 \times 256$  pixels, with pixel time of 10 ms, amplitude of 500 nm, and the setpoint of 0.4 nN.

The AFM images were processed in Gwydion software [10.2478/s11534-011-0096-2]. The calculation of mechanical properties was performed using the JPK data processing software. YM values were evaluated using the Hertz-Sheldon model based on the quadratic pyramid tip shape.

## 3 Results and Discussion

### 3.1 Turbidimetric Study of the Lysis of Free Bacteria

Appropriate conditions for lysostaphin and phage-mediated lysis were optimized in solution, followed by optical density measurements. First, the bacterial lysis mediated by lysostaphin was tested with free bacteria in Tris buffer at 25 °C and monitored as changes in the optical density. A wide range of enzyme concentrations from 0.1 to 100 µg/mL was tested (**Figure 2A**). The highest concentrations (30 and 100 µg/mL) lysed most bacteria within 1 h. As the enzyme concentration decreased, the lysis rate declined. At concentrations below 1 µg/mL, the bacteria did not disintegrate at all. The obtained results agree with the literature [10.1016/j.fm.2019.103245].

Effective phage propagation is a complex process, and lysis of infected bacteria requires adsorption of virions to the host cells, injection of phage DNA into the cell, expression of phage genes, and assembly of functional virions. To find optimal conditions for phage-mediated lysis in



solution, the ability of phages to adsorb to the cells (**Figure S3**) was first tested. More than 90% of P68 virions were adsorbed on both *S. aureus* strains RN4220 and RN4220  $\Delta tarM$  within 3–5 min in both TSB and Tris buffer (**Figure S3**). Then, the turbidimetric study of the efficiency of phage infection in various solutions and at different temperatures (**Figure 2B**) was observed. As the MOI decreased, the onset of lysis was delayed and rate was slower. The highest MOI of \_\_\_ lysed the bacteria completely while with the MOI below 0.1, the OD began to rise slightly after the end of the lysis.

No bacterial lysis was observed in Tris buffer for all tested phage concentrations (**Figure S2D**). This agrees with the expression analysis of the P68 *mcp* gene revealed that phage structural proteins are not expressed in Tris buffer, whereas in TSB, the phage infection was effective both at 37 °C and 25 °C (**Figure S4**). Afterward, the lysis experiments were performed in TSB. In most of the staphylococcal phages,  $Ca^{2+}$  ions support the adsorption and penetration of phage genomes into the host cells [[10.1002/jobm.201300051](https://doi.org/10.1002/jobm.201300051)]. However, in our experiments, the addition of 2 mM  $CaCl_2$  to the TSB had no significant effect on the bacterial lysis. In contrast, the temperature and lysing agent concentration significantly affected the lysis kinetics (**Figure S2**). The phage-mediated lysis was examined at two different temperatures. At 25 °C, the phage replication was slower; in the case of the highest tested MOI of 10, the lysis began after 2 h, and complete degradation of bacteria was observed after another 1 h (**Figure S1A**). At 37 °C, the onset of lysis happened already after 45 min, and the complete degradation of bacteria was observed after another 30 min (**Figure S2B**). Again, this agrees with the PCR expression analysis of the P68 *mcp* gene (**Figure S4**).

In the case of the resistant *S. aureus* RN4220, high amounts of P68 (MOI 0.1–10) showed disintegration at 25 °C, but a delayed onset of the lysis and a smaller decrease of *OD* were observed compared to sensitive *S. aureus* RN4220  $\Delta tarM$  (**Figure S2C**). Partial lysis of the resistant strain at the highest concentration of P68 (MOI 10) was also observed at 37 °C, demonstrating only a limited level of resistance [[10.1038/srep17219](https://doi.org/10.1038/srep17219)]. The results for all the tested lysis conditions are summarized in **Figure S2**.

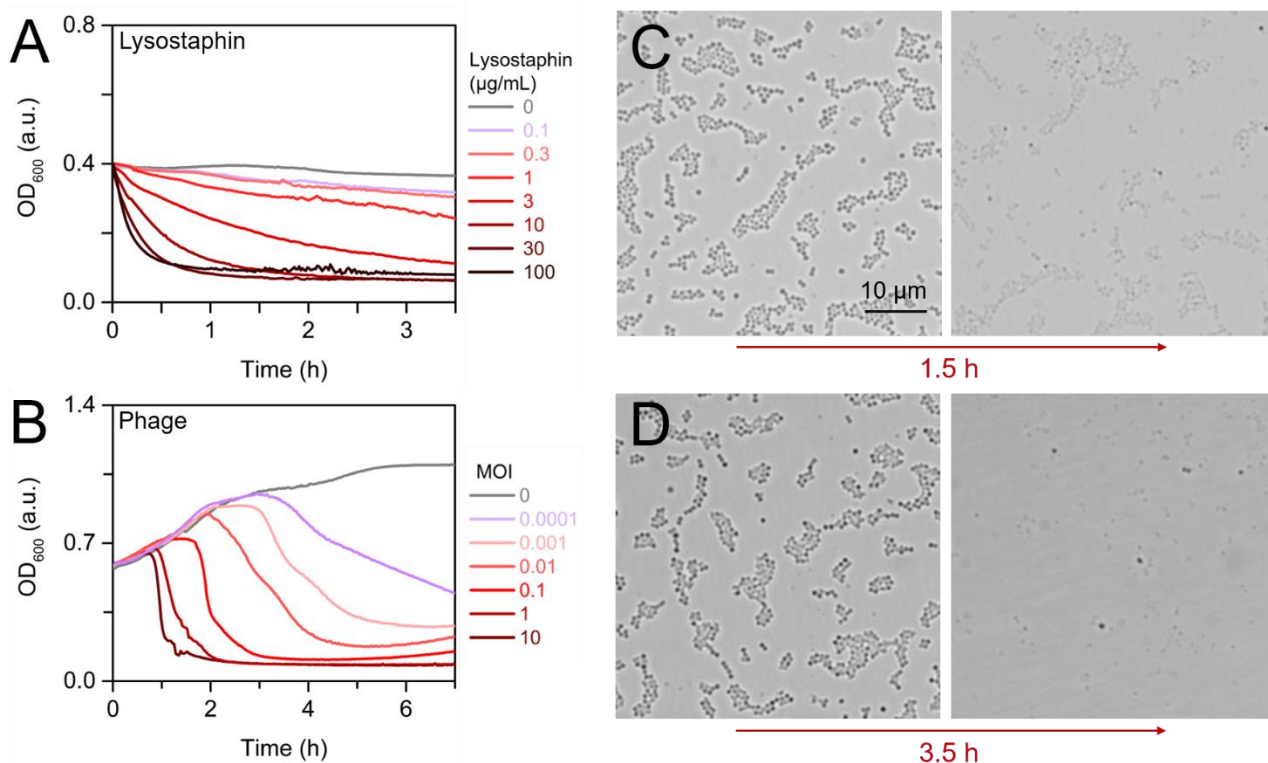


**Figure 2:** Turbidimetric study of *S. aureus* RN4220  $\Delta tarM$  lysis in solution by (A) lysostaphin in Tris buffer, and (B) by phage P68 in the TSB. MOI is the ratio of the phages to bacteria. Optical microscopy visualization of lysis of captured bacteria by (C) lysostaphin (10  $\mu\text{g}/\text{mL}$ ) in Tris buffer, and (D) by phage P68 ( $8 \times 10^9$  PFU/mL) in TSB medium.

### 3.2 Optical Microscopy Study of the Lysis of Surface-Bound Bacteria

To monitor changes in lysis conditions after immobilization, the lysis on the surface was initially tested and visualized using optical microscopy (Figures S5 and 2C, D). To perform gentle immobilization using physical adsorption, the bacterial culture was resuspended either in the TSB medium or PBS buffer and introduced to the Petri dish surface. Unlike TSB, the PBS allowed immobilizing more bacteria on the surface and was preferred thereafter. The lower immobilization efficiency in TSB can be explained TSB components blocking the Petri dish surface.

Lysis of surface-bound bacteria requires a different evaluation strategy compared to the lysis in volume. The approximate number of bacteria on the surface was determined by counting under the microscope. Compared to the experiments in solution, surface-bound experiments are based on a reduced total number of bacteria involved in the reaction, and only a smaller part of the bacterial envelope is exposed to the lytic agent due to the steric hindrance of the surface. It is important to mention that the enzyme also binds non-specifically to the Petri dish surface, decreasing the effective concentration of the lytic agent in the solution.

**Figure S5** shows the lysis with lysostaphin in the Tris buffer at 25 °C for the concentrations between 0.1 and 100 µg/mL. For the lysis of surface-bound bacteria, the optimal lysostaphin concentration appears to be 10 µg/mL (**Figure 2C**). Interestingly, no difference was optically visible for the other investigated enzyme concentrations of 0, 0.1, 1, and the high concentration of 100 µg/mL. This is in contrast to the lysis in solution, where the lysis was faster with the increasing enzyme concentration, and the most efficient disintegration took place at the highest tested concentration of 100 µg/mL.

For the phage-mediated lysis, various media and buffers (TSB, TSB with Ca<sup>2+</sup>, and Tris buffer) were again compared. All negative controls with the resistant bacterium, as well as controls with the absence of phage, did not show any lysis within the 3.5 h interval of monitoring. Furthermore, no lysis was observed in the Tris buffer even with the sensitive bacterial strain (**Figure S6**). However, in the case of TSB, some bacteria detached from the surface and became visible floating in the medium. When the lysis was performed in TSB and TSB with Ca<sup>2+</sup>, most bacteria disintegrated and detached after 3.5 h (**Figure S6**). When monitoring the time course of the lysis with the optical microscopy, there were no noticeable changes during the first 2 hours of the lysis; therefore, it is difficult to evaluate the onset and duration of the lytic cycle (**Figure S7**).

It is worth mentioning that the lysis by lysostaphin was optically observed as “fading”, and the outline of the bacteria remained visible on the surface. In contrast, the phage-mediated lysis led to complete disintegration and detachment of the bacteria from the surface (compare **Figure 2C** and **2D**). This can be explained by the different lysis mechanism. The lytic action of the phage is destructive as the release of virions from the cell is accompanied by both membrane damage by P68 holin and cell wall degradation by endolysin [[10.2217/fmb.12.97](#)]. On the other hand, lysostaphin acts from the outside and gradually disrupts the cell wall by cleaving the peptidoglycan [[10.3390/ph3041139](#)].

### 3.3 SPR Characterization of Lysostaphin-mediated Lysis

SPR was used to monitor the interactions during the lysis of *S. aureus* RN4220  $\Delta tarM$  in real-time at two different wavelengths (**Figure 4**). The resulting sensorgrams are given by a combination of two effects: (i) the binding of the lysostaphin on the bacterial envelope (specific) or on the chip surface (non-specific adsorption; **Figure S8**), observed as the increase of the resonance angle, and (ii) the bacterial lysis caused by cleavage of the pentaglycine crosslinks in the peptidoglycan layer, observed as the decrease of the response. At the very low lysostaphin concentrations ( $\leq 1$  µg/mL), the lysis was observed only at a longer timescale of 90 min. Probably, a small number of breaks in the peptidoglycan does not cause immediate disruption of the cells. At higher concentrations ( $\geq 3$  µg/mL), lysis was observed immediately after applying the enzyme, resulting in a significant signal decrease corresponding to material loss. Starting from 10 µg/mL, the binding of the enzymes was also observed. The highest concentrations ( $\geq 30$  µg/mL) resulted in the highest binding

signals, but the apparent lysis speed was slower. The optimal concentration of lysostaphin to cause the lysis but limit the interferences of the lysostaphin binding was 10  $\mu\text{g}/\text{mL}$ .

There was a notable signal difference between the two SPR wavelengths, especially for higher lysostaphin concentrations of 30 and 100  $\mu\text{g}/\text{mL}$ . At 670 nm (**Figure 4A**), an increase of the signal with a small decline around 10 min after the injection was noticeable, and the lysis was subsequently visible for 30  $\mu\text{g}/\text{mL}$  of lysostaphin. However, at 785 nm (**Figure 4B**), a short increase followed by a signal decrease was observed in the association phase, followed by a second increase. Immediately after the end of the enzyme injection, the signal decreases, similarly to 670 nm. This can be explained by the different penetration depths of the plasmons created at wavelengths of 670 and 785 nm. The plasmon at 670 nm decays faster with distance, so nonspecific binding of the enzyme happening directly at the sensor surface is more pronounced. Whereas the penetration depth of plasmons excited by 785 nm is higher, and the plasmon resonance changes are more sensitive to refractive index changes further above the sensor surface [[10.1063/1.4879830](#)].

After the measurement, the surface of the SPR chip was imaged by AFM in the air to provide detailed information on the situation after the lysis (**Figure 5A**). The average height of the bacteria on the SPR chip not treated by lysostaphin was  $480\pm 50$  nm. This is significantly different from the size of the native bacteria, which is around 0.5–1  $\mu\text{m}$  in TSB [[10.22203/ecm.v004a04](#)]. This difference is caused by the adhesion of the bacteria to the substrate and drying of the cells [[10.1021/la026440g](#)]. In contrast to the SPR, the AFM showed noticeable changes in the bacteria shape already at the low lysostaphin concentrations of 0.3 and 1  $\mu\text{g}/\text{mL}$ ; the average heights of the lysed bacteria were  $320\pm 70$  nm and  $200\pm 20$  nm, respectively. The most significant deformation of cells and the decrease of their height to  $60\pm 15$  nm was observed at a lysostaphin concentration of 10  $\mu\text{g}/\text{mL}$ . This corresponds to the concentration with the most significant decrease of the SPR response. The lysis was also noticeable at the highest concentration of 100  $\mu\text{g}/\text{mL}$ . The bacteria did not degrade completely; the cells preserved their shape, but the height of the lysed bacteria was as low as  $93\pm 10$  nm. At the high concentrations, the lysis progresses in the background of lysostaphin binding to the chip surface and is not easily detectable (**Figure S8**). This demonstrates that the AFM is useful for imaging of the situation on the chip surface after the lysis, and it is an important part of the SPR bacterial lysis examination. It provides detailed insight into the bacterial structure changes that cannot be obtained directly by the SPR. As an alternative evaluation method, the integrated area under the height profile (area under the curve, AUC) was calculated (**Figure 5B**). The lowest area under the curve, corresponding to the most disintegrated bacteria, was again achieved with the lysostaphin concentration of 10  $\mu\text{g}/\text{mL}$ .

### 3.4 SPR Detection of Phage-mediated Lysis

After successfully monitoring lysostaphin-mediated lysis, the SPR was also used to study the lysis mediated by the phage. The most notable difference between both lytic approaches is in the time of the lysis onset. While the lysostaphin-mediated lysis begins immediately after the injection, a delay of 60 min for higher phage P68 concentrations ( $4 \times 10^{10}$  PFU/mL) and 80 min for lower concentration ( $4 \times 10^9$  PFU/mL) was observed (**Figure S9**). This agrees with the SPR assay results describing a difference in the lytic action of different concentrations of a coliphage  $\phi$ X174 [[10.1128/AEM.02806-07](#)]. In contrast to our results, this report describes an increase of the SPR response after the lysis, which can be attributed to the different surface chemistry (biotinylated bacteria bound to avidin adsorbed on the surface), resulting in rebinding of the lysed material to the surface.

The resonance angle decreases of 0.45 deg upon the lysis was comparable for both P68 concentrations, indicating similar final effectivity of the bacteria disintegration. It is also higher compared to the lysostaphin-mediated lysis (0.2 deg), proposing more successful blocking of the surface by the TSB culture medium than by BSA, and thus limited rebinding of the lysed material (**Figure S10**). The injection of P68 in the concentration of  $4 \times 10^{10}$  PFU/mL led to the signal increase corresponding to the phage binding to the bacteria and chip surface; this difference (inset of **Figure S9**) was retained even after the end of the injection. These results agree with the study of lysis in solution by turbidimetry (**Figure S2**), where a similar time of lysis onset and its duration were observed with respect to the MOI approximation. Compared to the lysis with lysostaphin, the difference between the SPR sensorgrams of the phage-based lysis at the wavelengths of 670 nm and 785 nm was not significant (**Figure S9**).

After the lysis by phage, the surface of the SPR chip was again imaged by AFM (**Figure S11**). Lysis by both phage concentrations led to similar results, which agrees with the SPR data. At the concentration of  $4 \times 10^9$  PFU/mL (**Figure S11B**), the indistinct spots (lysed clusters of bacteria) almost did not occur, and the chip rather remained covered with compact bacteria, at  $4 \times 10^{10}$  PFU/mL (**Figure S11C**), the areas of lysed clusters predominated. Thus, a higher concentration leads to more massive lysis, and the bacteria in the indistinct spots are completely lysed, while the lower concentration leaves a compact but damaged bacterium. The negative control without phage injection provided an average bacteria height of  $440 \pm 90.0$  nm (**Figure S11A**). On the other hand, even though the bacteria were not completely destroyed after the phage application, the bacteria were deformed and smaller after the lysis, resulting in an average size of only  $130 \pm 80$  nm (**Figure S11B**).

### 3.5 Real-time AFM Visualization of Lysis by Lysostaphin

The first experiments with AFM studying the real-time lysis in liquid were performed using the enzyme lysostaphin in Tris buffer at room temperature. The AFM allowed observing the gradual

progress of lysis in time (**Figure 6**). The beginning of the lysis was observed after 15 min of exposure to lysostaphin. After 40 min, the bacteria were significantly lysed, and after 50 min, only the remnants of the envelopes remained visible on the surface. The lysis continued until the remaining envelopes were removed; the bacteria were completely disintegrated after 1.5 h, leaving only cell debris on the surface. The quantitative evaluation of the changes of the bacteria size is shown in **Figure 6B** as the changes of the integrated cross-sections of height profiles, where gradual decreases of the area under the curve can be observed.

Furthermore, the stiffness changes (evaluated as YM) were monitored as an additional indicator of cell disintegration (**Figure 6C**). As the cell wall peptidoglycan was hydrolyzed by lysostaphin, the YM decreased from  $8\pm 2$  MPa to  $0.08\pm 0.07$  MPa. The completion of the lysis relates to a dramatic increase of YM to  $50\pm 30$  MPa, caused by the disappearance of the biological mass and revealing of the Petri dish surface decorated with bacterial fragments and proteins. This YM value approximately corresponds to the stiffness of the poly-L-lysine layer on the Petri dish determined before the lysis ( $98\pm 30$  MPa); the small difference is probably caused by the presence of bacterial fragments and proteins.

Monitoring of changes in the peptidoglycan cell wall of *S. aureus* RN4220  $\Delta tarM$  by AFM during the lysostaphin cleavage was investigated previously [[10.1128/JB.01116-08](#)]. In the study, the bacteria were mechanically trapped in a porous polycarbonate membrane. After applying lysostaphin, the increased surface roughness and decreased YM were observed, which is in accordance with our results. On the other hand, the bacterium height changes after the exposure to lysostaphin were completely different from our observation. The bacterium did not disintegrate within 260 min of the measurement as in our case, but instead, it swelled by 100 nm, which was explained as the formation of osmotically fragile cells after the peptidoglycan hydrolysis. However, another work [[10.1128/jb.103.1.116-119.1970](#)] revealed that fragile cells occur only within 2 min of exposure to the lysostaphin. After extended treatment with lysostaphin, the bacteria can lose their osmotic pressure due to the disintegration of peptidoglycan and rupture of the cell membrane [[10.3390/ph3041139](#)], which agrees more with our observations.

As a control, *S. aureus* RN4220  $\Delta tarM$  was scanned in Tris buffer for 3 h without the addition of lysostaphin (**Figure S12**). The height of the bacteria was stable during this period ( $780\pm 20$  nm), and YM slightly increased from  $1.4\pm 0.3$  MPa to  $3.9\pm 1.1$  MPa. This can be caused by changes in the bacterial envelope composition and structure as a reaction to new conditions (Tris buffer and attachment to the surface). In the Tris buffer without nutrients, the bacteria do not replicate and have reduced movement.

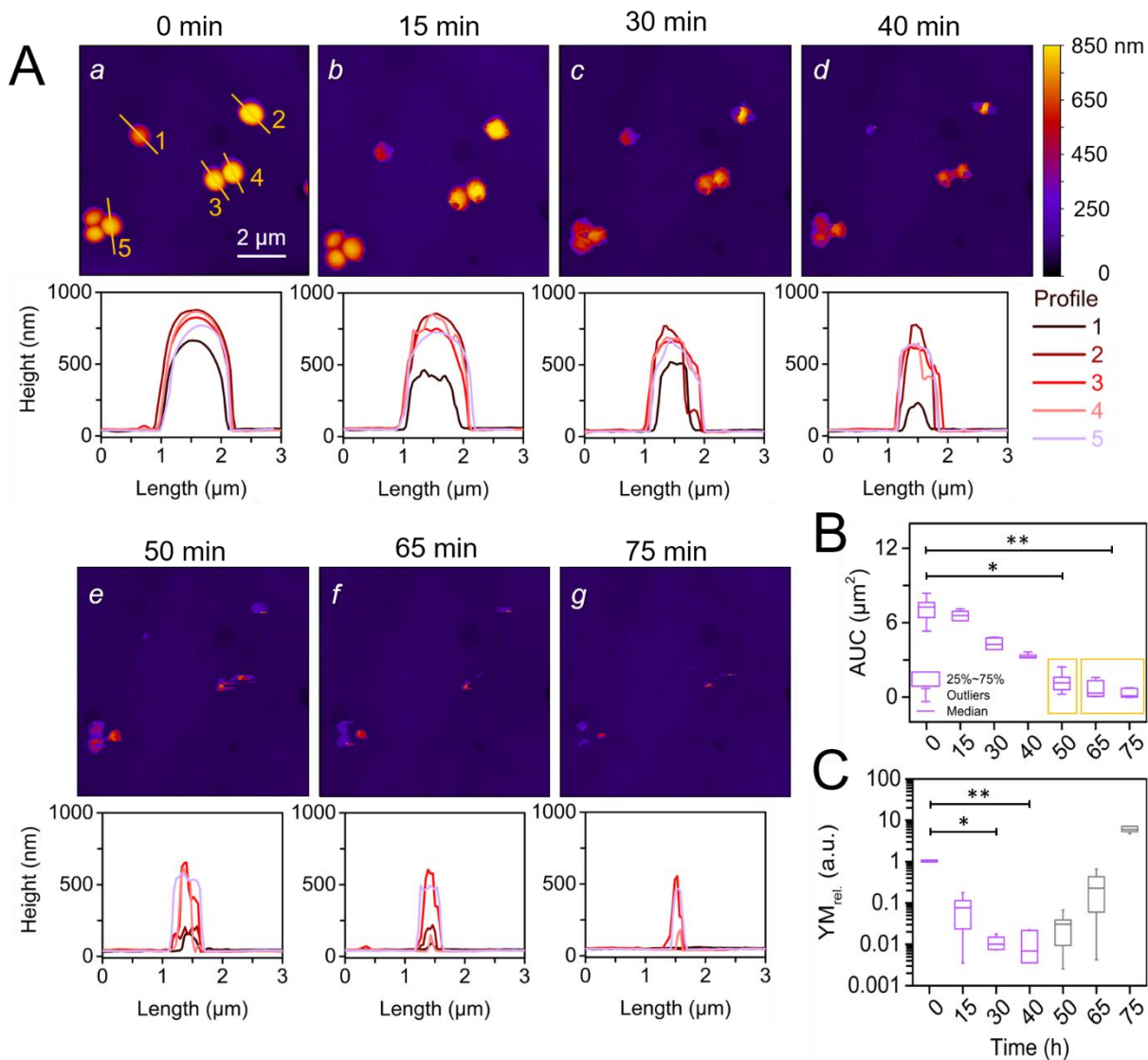


**Figure 6:** Lysostaphin-mediated lysis of *S. aureus* RN4220  $\Delta tarM$  in Tris buffer. (A) AFM images and height profiles of bacteria (a) before the addition of lysostaphin (10  $\mu\text{g}/\text{mL}$ ), and after (b) 15 min, (c) 30 min, (d) 40 min, (e) 50 min, (f) 65 min, and (g) 75 min. (B) The time dependency of the area under curves corresponding to the integrated bacterial cross-sections; and (C) changes of YM during the lysis.

### 3.6 Real-time AFM Visualization of Lysis by Phage P68 in Liquid

After successfully imaging the lysostaphin-mediated lysis by AFM in liquid, the same approach was used to study the lysis by phage P68. Based on the previous results, the TSB medium was used to preserve the bacterial viability and the reproduction ability of the phages; the experiments were performed at 25 °C and 37 °C. The better viability of the bacteria at 37 °C resulted in its increased movement; therefore, measurement at 25 °C was carried out to provide more stable scanning at the cost of the prolonged lysis (~ 2 h).

Real-time phage-mediated lysis of *S. aureus* RN4220  $\Delta tarM$  at 25 °C is shown in **Figure S13A**. The average height of the bacteria before the lysis ( $860\pm 20$  nm) corresponds to the native state [[10.22203/ecm.v004a04](#)]. After 1 h, the phage bound to the bacteria could be discerned (**Figure 7**). The phage was visible as small humps on the bacteria surface, clearly visible on the cross-section. The lysis began 2.5 h after the phage injection. The scanning proceeds from the bottom to the top; **Figure S13A d** is taken immediately after the previous one, and the disappearance of the top bacterial cluster is visible. The complete removal of the bacteria from the surface is visible 3.25 h after the addition of phage. **Figure S13B** indicates the changes in the AUC of the bacteria cross-section in time; the trend differs from the lysis by lysostaphin and resembles to the results of the turbidimetric measurements of the phage-mediated lysis in solution (**Figure 2B**). In the case of lysostaphin, the lysis begins immediately and proceeds linearly with time. In contrast, the phage-mediated lysis takes place as a fast transition after a longer time delay, depending on the temperature and MOI. The evaluation of the stiffness changes during the lysis (**Figure S13C**) revealed that the value of YM first rose slightly from  $3.9\pm 1.2$  MPa to  $4.8\pm 1.3$  MPa, followed by a drop to  $0.8\pm 1.6$  MPa. The end of the lysis was again connected with the steep increase of the YM value ( $139\pm 16$  MPa) to the level corresponding to the background of PLL on the polystyrene surface ( $180\pm 40$  MPa).

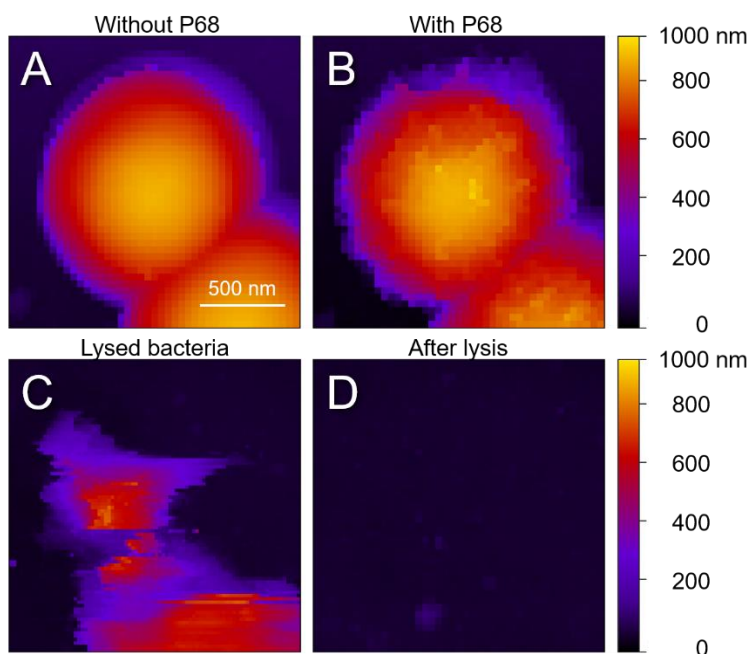


**Figure 7:** AFM visualization of lysis of *S. aureus* by phage P68 at 25 °C. (A) Before and (B) after the binding of P68 on *S. aureus* RN4220  $\Delta tarM$ , (C) partially lysed bacterium, and (D) surface after the complete lysis.



When the phage-mediated lysis was visualized by AFM at 37 °C (**Figure 8A**), the bacteria were more mobile compared to 25 °C. This led to lower imaging quality, but lysis was significantly faster. There were no significant changes in the bacteria shape immediately after the addition of the phage. The increased bacterial movement, together with the interferences from the Petri dish heater, caused slightly blurred images at higher temperatures (37 °C), which prevented us from the visualization of phages as bumps in the cross-sections. Thus, the binding of phage to bacteria cannot be directly observed, as in the case of scanning at 25 °C. However, the lysis began sooner, and after 1.5 h, the bacteria were completely disintegrated. **Figure 8B** shows the dependence of the integrated bacteria cross-sections on time. The areas under the curve began to decrease after 1 h of incubation with the P68. The time of lysis onset and duration were comparable to the turbidimetric measurements (**Figure S2B**). The YM value decreased during the lysis from  $2.0 \pm 0.5$  MPa to  $0.2 \pm 0.2$  MPa, followed by the rise to  $79 \pm 20$  MPa when the bacteria were disintegrated (**Figure 8C**). The value of the YM background of PLL on the polystyrene surface before the lysis was  $51 \pm 30$  MPa. The large variability of the YM values of the individual cells can be related to the state of the bacterium before the infection, the phase of the lysis cycle, and the influence of the surface in reducing the height of the bacterium during the disintegration.

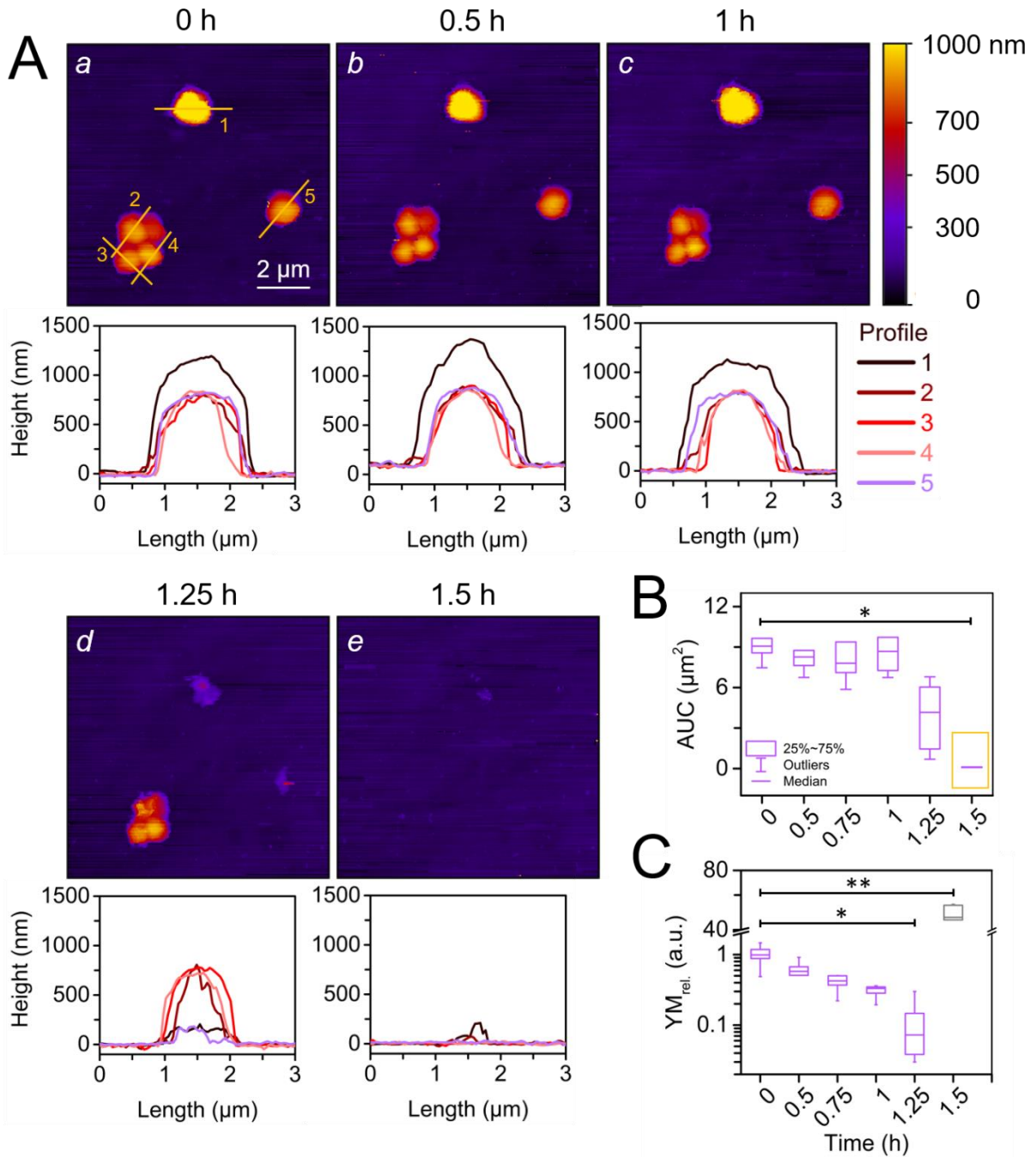


**Figure 8:** (A) AFM visualization of *S. aureus* RN4220  $\Delta tarM$  lysis by  $1.2 \times 10^9$  CFU/mL of phage P68 at 37°C with height profiles of the individual bacteria. (a) Bacteria before the lysis and (b) 0.5 h, (c) 1 h, (d) 1.25 h, and (e) 1.5 h after the addition of the phage. The time dependences of (B) cross-section areas under the curve and (C) change of YM of the bacteria.

## 4 Conclusions

For the first time, this work reports on the real-time monitoring of bacterial lysis at the single-cell level by AFM in the native conditions of the growth medium. We studied lysis of *S. aureus* RN4220  $\Delta tarM$  mediated by the enzyme lysostaphin and phage P68. The kinetics of lysis by the phage P68 strongly depended on the phage concentration and working temperature. Gradual degradation of the cell wall, followed by the complete lysis of the bacterial cell, was monitored. The mechanical data acquitted by AFM were used for the detailed evaluation of the associated changes of bacterial stiffness (Young's modulus). Furthermore, SPR provided deeper insight into the interaction kinetics, but without the possibility to monitor individual cells. The methodology introduced in this work is important not only for the basic research but it also has a considerable application potential in biotechnology and medicine. The acquired knowledge will provide better insight into bacterial lysis, which can be utilized in the fight against antibiotic-resistant bacterial strains.

## Acknowledgments

This work was financially supported by the Ministry of Education, Youth and Sports of the Czech Republic (MEYS CR) under the projects CEITEC 2020 (LQ1601) and INTER-ACTION (LTAB19011). Support from the Czech Science Foundation (project GA18-13064S) is gratefully acknowledged. CIISB, Instruct-CZ Centre of Instruct-ERIC EU consortium, funded by MEYS CR infrastructure project LM2018127, is gratefully acknowledged for the financial support of the measurements at the CF Nanobiotechnology.

# Appendix XII

Forinová, M., A. Pilipenco, I. Víšová, N. S. Lynn, J. Dostálek, V. Honig, M. Palus, J. Stěrba, M. Houska, M. Vrabcová, P. Horák, C-P. Tung, C-M. Yu, C-Y. Chen, Y-C. Huang, P-H. Tsai, S-Y. Lin, H-J. Hsu, A-S. Yang, A. Dejneka, H. Vaisocherová-Lísalová

**Rapid one-step quantitative detection of SARS-CoV-2 virus in crude clinical samples using antifouling quartz crystal microbalance biosensor**

In preparation. To be submitted in *Science Advances*.

## Rapid one-step quantitative detection of SARS-CoV-2 virus in crude clinical samples using quartz crystal microbalance biosensor and antifouling biointerface architecture

### Authors

*Michala Forinová<sup>1</sup>, Alina Pilipenco<sup>1</sup>, Ivana Víšová<sup>1</sup>, N. Scott Lynn<sup>1</sup>, Jakub Dostálek<sup>1,2</sup>, Václav Honig<sup>3,4</sup>, Martin Palus<sup>3,4</sup>, Jan Stěrba<sup>5</sup>, Milan Houska<sup>1</sup>, Markéta Vrabcová<sup>1</sup>, Petr Horák<sup>1</sup>, Chao-Ping Tung<sup>6</sup>, Chung-Ming Yu<sup>6</sup>, Chi-Yung Chen<sup>6</sup>, Yu-Chuan Huang<sup>6</sup>, Pei-Hsun Tsai<sup>6</sup>, Szu-Yu Lin<sup>6</sup>, Hung-Ju Hsu<sup>6</sup>, An-Suei Yang<sup>6</sup>, Alexandr Dejneka<sup>1</sup>, Hana Vaisocherová-Lísalová<sup>1\*</sup>*

### Affiliations

<sup>1</sup> Institute of Physics of the CAS, Na Slovance 2, Prague, Czech Republic

<sup>2</sup> Austrian Institute of Technology GmbH, Konrad-Lorenz-Strasse 24, Tulln, Austria

<sup>3</sup> Institute of Parasitology, Biology Centre CAS, Branisovska 31, Ceske Budejovice, Czech Republic

<sup>4</sup> Veterinary Research Institute, Hudcova 70, Brno, Czech Republic

<sup>5</sup> Faculty of Science, University of South Bohemia, Branisovska 31a, Ceske Budejovice, Czech Republic

<sup>6</sup> Genomics Research Center, Academia Sinica, 128 Academia Rd., Sec.2, Nankang Dist., Taipei 115, Taiwan

Corresponding Author: Hana Vaisocherová-Lísalová, Ph.D., Institute of Physics, Academy of Sciences of the Czech Republic, v.v.i., Na Slovance 2, 18221 Prague, Czech Republic; Tel.: +420 266 05 29 93, E-mail: lisalova@fzu.cz

### Abstract

The outbreak of worldwide COVID-19 pandemic revealed a critical lack of reliable methods for cost-efficient, rapid, and sensitive detection of infectious agents in real-world biological samples. Here, we report on a biosensor that

addresses these needs based on quartz crystal microbalance (A-QCM) biosensor with direct immunoassay readout that is enabled by an antifouling biointerface architecture. It combines extraordinary sensitivity with short detection time, and furthermore, it allows for quantification of SARS-CoV-2 in clinical samples without any extra sample pre-treatment steps. Such performance is made possible by the use of terpolymer brush carrying a unique composition of zwitterionic and non-ionic moieties that is postmodified with human cell-expressed specific antibodies against SARS-CoV-2 nucleocapsid protein. The fouling resistance of the functionalized polymer brush on the sensor surface is documented via exposure to a variety of crude biological samples (such as stool, oropharyngeal or nasopharyngeal swabs). The LOD was determined to be  $6.7 \times 10^3$  PFU/mL, which is in the clinically relevant range. The results from A-QCM biosensor were validated by RT-qPCR for a set of clinical nasopharyngeal samples and they document the potential of A-QCM biosensor to serve as a tool for rapid COVID-19 diagnostic and disease prognosis, as well as for the SARS-CoV-2 contamination monitoring.

## Keywords

SARS-CoV-2, rapid detection, QCM, clinical samples, COVID-19, biosensors, antifouling, polymer brush

## Introduction

Coronavirus disease 2019 (COVID-19) is caused by severe acute respiratory syndrome coronavirus 2 (SARS-CoV-2) and manifests itself by various symptoms including pneumonia, fever, cough, myalgia, fatigue and gastrointestinal symptoms (1–3). This virus is highly contagious and after there were recorded the first cases of COVID-19 in December 2019 in Wuhan, China, it has rapidly spread worldwide with more than 62 million people infected and 1.4 million deaths reported until November 2020 (4). In March 2020, the COVID-19 was classified as a pandemic by World Health Organization (WHO). SARS-CoV-2 belongs to the virus family *Coronaviridae*, which carries in their body enveloped positive-sense single stranded RNA. They can infect vertebrates (3) and seven species of coronaviruses that can infect humans are known. Among these, SARS-CoV, MERS-CoV and SARS-CoV-2 (belonging to genera *Betacoronavirus*) are of particular danger for human health as they can cause severe acute respiratory symptoms (5). The body of CoVs is mainly assembled from four structural proteins: spike protein (S), envelope protein (E), membrane protein (M), and nucleocapsid protein (N). S and N proteins are dominantly used as antigen biomarkers for the specific detection of SARS-CoV-2 and diagnosis of COVID-19 (7, 8). However, several additional proteins interfering with the innate immune response of the host have been identified and others with unknown or poorly understood function are under investigation (6).

69 Even though the rapid development of several vaccines gives prospects to  
70 overcome the COVID-19 pandemics, the potential for SARS-CoV-2 mutations and  
71 expected long-term vaccination process make it still extremely dangerous and poorly  
72 controlled global problem. Therefore, it is of utmost importance to deploy tools for  
73 rapid monitoring SARS-Cov-2 presence in order to early identify SARS-CoV-2  
74 infections and thus enable to impose efficient measures to prevent its fast outbreaks.  
75 The molecular diagnosis tools for SARS-CoV-2 are mainly based on the detection  
76 of SARS-CoV-2 constituents (i.e., vRNA, antigens or proteins) present in bodily  
77 fluids or the analysis of person's immune response to the infection (antibodies or  
78 other biomarkers) (9). An immune response can be typically recognized in four days  
79 after the onset of COVID-19 symptoms, when it produces detectable amounts of  
80 immunoglobulin M and G antibodies (10, 11)(12, 13). Therefore, this time lag, after  
81 which the antibodies are present, does not allow for using this approach for  
82 identification of ongoing infections.

83 Currently, the detection of unique SARS-CoV-2 vRNA sequences by real-time  
84 reverse-transcription polymerase chain reaction (RT-qPCR) represents a standard  
85 method for the diagnosis of COVID-19 and for the infection confirmation (15). It  
86 provides the limit of detection (LOD) in range of  $10^2 - 10^4$  copies/ml (15–17), but  
87 is relatively time consuming (takes approx. 1-4 hours, including sample  
88 preparation). Thus, there were developed other faster PCR-based assays including  
89 reverse transcription loop-mediated isothermal amplification (RT-LAMP) (18, 19)  
90 and clustered regularly interspaced short palindromic repeat (CRISPR)-Cas12 (21,  
91 22). By these less equipment-demanding methods, the readout time of the SARS-  
92 CoV-2 vRNA assay can be then shorten to about 30 min with the LOD as low as 10  
93 copies/mL. Nevertheless, to achieve similar sensitivity, compare to RT-qPCR, RNA  
94 has to be isolated from the primary samples, which take another 30-60 minutes and  
95 represents another laborious and cross-contamination prone step. Moreover, all these  
96 assays rely on the infrastructure that has to be deployed in specialized laboratories  
97 and operated with highly trained personnel and cross-contamination complicates the  
98 PCR-based analysis and often leads to necessity of repeating the assay for large  
99 number of samples.

100 Lateral flow immunoassay tests (LFIA), often referred to as antigenic test,  
101 become increasingly used method that complement the PCR-based screening of  
102 COVID-19. LFIA enables fulfilling the requirements for fast, simple and cost-  
103 efficient detection of SARS-Cov-2 (23–29) and it typically utilizes sandwich  
104 immunoassay format with a qualitative readout providing limited LOD  $> 10^4$   
105 PFU/ml. Moreover, LFIA still needs pre-preparation of sample (30) and thus the  
106 sensitivity of the test provided by the manufacturer may be significantly reduced for  
107 the on-site use that is prone for sampling errors (31, 32). Hence, this platform is  
108 useful mostly for frontline less accurate testing or as a tool in situations when RT-  
109 qPCT is not available.

110 The still unmet challenge of rapid and sensitive point-of-care COVID-19 testing  
111 can be addressed by novel biosensor technologies that are pursued for alternative  
112 SARS-CoV-2 detection methods in a format that significantly simplifies analysis  
113 and reduces overall detection time (33–35). Biosensors can be developed for  
114 detection of SARS-CoV-2 based on its both vRNA and protein constituents and we  
115 witness a great variety of physicochemical transducers applied. Electrochemical-  
116 based detection of SARS-CoV-2 RNA with the LOD of 200 copies/ml was reported  
117 by using vRNA sandwich assay on calixarene functionalized graphene oxide (36)  
118 with the total detection time is about 3 hours (without additional vRNA extraction).  
119 Amperometric detection of nCovid-19 spike antigen by using sandwich  
120 immunoassays on screen-printed carbon electrode was utilized for the analysis of  
121 saliva samples with LOD of 90 fM (37). Potentiometric measurement on an  
122 biointerface carrying membrane-engineered cells with human chimeric antibody  
123 against S1 protein allowed to reach LOD of 1 fg/ml results in 3 minutes (38). Direct  
124 detection based on field-effect transistor with antibody against S protein was  
125 investigated on graphene transducer surface (40). The LOD for SARS CoV-2 spike  
126 protein S of 1 fg/ml was reached in model buffer samples and the implementation of  
127 the assay for the analysis of SARS CoV-2 in culture medium at 16 PFU/ml and 242  
128 copies/mL in heat-deactivated diluted clinical samples was documented. Another  
129 class of biosensors were researched based on optical probing of the affinity captured  
130 vRNA or protein markers on the metallic surface by the use of surface plasmon  
131 resonance (SPR). Pig serum-derived antibodies against SARS Cov-2 N protein were  
132 used to affinity bind of target analyte in culture fluid and the LOD of 1 pM was  
133 reported (41). A biosensor combining the plasmonic photothermal effect and  
134 localized surface plasmon resonance (LSPR) sensing transduction was employed for  
135 detection of vRNA with the LOD of 0.22 pM in nuclease-free water (42). Another  
136 LSPR biosensor based on gold nanoparticles capped with thiol-modified DNA  
137 specific for nucleocapsid phosphoprotein gene of SARS-CoV-2 was used for  
138 detecting vRNA. Simple colorimetric readout allowed for the detection within 10  
139 minutes from the isolated RNA samples with LOD of 0.18 ng/ $\mu$ L (43).

140 In general, the electrochemical or optical biosensors typically enables reaching  
141 only partially the goal of rapid, sensitive, and automatized analysis of SARS-CoV-  
142 2 samples. The reported implementations reveal the potential for sufficient  
143 sensitivity and short analysis time, however, only in proof-of-concept experiments  
144 performed in model environment. When applied for the analysis of clinical samples,  
145 they still did overcome the necessity of extensive sample pre-treatment steps. Their  
146 performance in complex clinical samples is not convincingly documented and thus  
147 their deployment to serve as a rapid tool in real setting remains elusive. This  
148 important aspect is related to the design of the biosensor interface, and in particularly  
149 its resistance to nonspecific binding of abundant biomolecules present in complex  
150 media. Unspecific interactions at affinity-based biosensors eventually blocks the  
151 sensor surface and can mask the response to specific capture of target analyte.  
152 Remarkable research efforts have been devoted to the development of appropriate



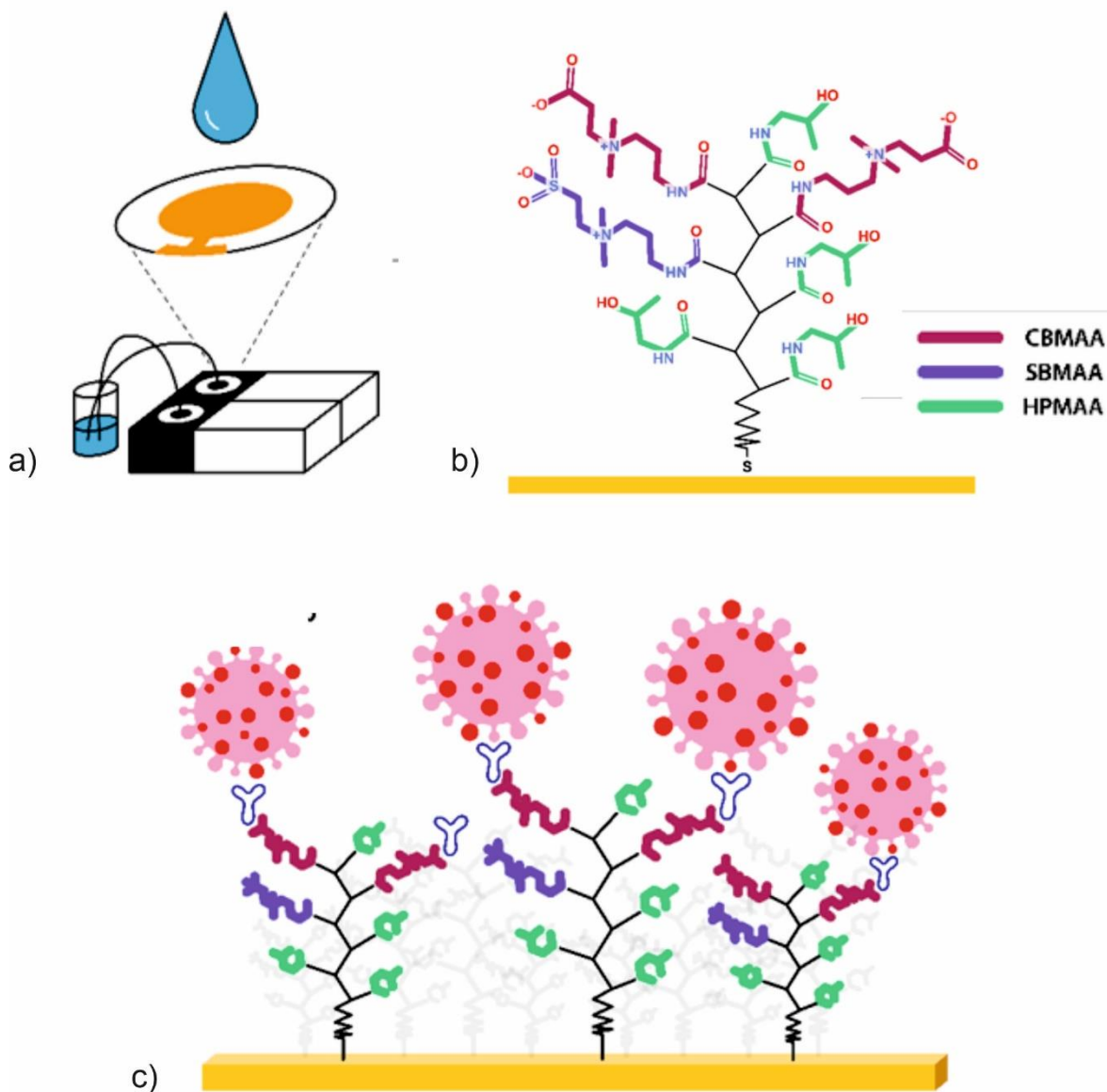
153 biofunctional interface architectures, mainly addressing the need of anchoring of  
154 sufficient density biorecognition elements without impairing the resistance to  
155 nonspecific sorption (fouling) [ref]. Polymer brushes composed from grafted chains  
156 with zwitterionic and non-ionic pendant groups represent one of the most efficient  
157 architectures for affinity biosensors with direct detection format (44, 45)(46, 47).

158 This paper reports on a new antifouling quartz crystal microbalance (A-QCM)  
159 biosensor for rapid, sensitive, and quantitative detection of SARS-CoV-2 in crude  
160 clinical samples that takes advantage of tailored antifouling polymer brush  
161 biointerface. This platform is based on the monitoring of surface mass density  
162 changes, and it was implemented in previous works to biosensors for rapid detection  
163 of a range of bacterial (48)(49, 50)(51, 52) as well viral (53, 54)(55) pathogens. The  
164 present work reveals the utmost importance design of the QCM sensor interface that  
165 is detrimental in the application for diagnosis COVID-19 in clinical samples. This  
166 problem is solved by a combination of sensitive QCM detection, tailored  
167 biointerface resistant to nonspecific binding of the non-target constituents in the  
168 clinical liquid samples, and direct immunoassay detection format for rapid one-step  
169 detection of SARS-CoV-2. The key biosensor performance characteristics are  
170 determined and validated by comparing to standard RT-qPCR experiments  
171 performed in parallel on a series of clinical nasal swab samples.

172

## 173 **Results**

174 Antifouling quartz crystal microbalance (A-QCM) biosensor was pursued for  
175 direct detection of SARS Cov-2 present minimally processed liquid samples. As  
176 schematically shown in Figure 1, the biosensor relies on a gold-coated quartz crystal  
177 that carries a tailored antifouling polymer brush architecture with anchored custom-  
178 produced high-affinity antibodies against N protein of SARS Cov-2 virus (AbN).  
179 The analysed liquid samples were delivered to the sensor surface via a microfluidic  
180 device and the specific capture of target analyte was monitored in realtime from  
181 detuning of the resonance oscillation frequency  $f$  of the quartz sensor chip due to the  
182 increase in the surface mass density. As described further, the sensor biointerface  
183 architecture was established for detecting of SARS-CoV-2 virus in a set of standards  
184 prepared in culture medium with the analyte expressed in Vero E6 cells. Then, the  
185 custom-made antibodies AnB were characterized in terms of specificity and  
186 recognition of the target part of SARS Cov-2 virus. Afterwards, there was  
187 investigated the performance of sensor biointerface architecture in terms of  
188 elimination of unspecific sorption of abundant molecules from a set of real matrices  
189 originating from nasopharyngeal, oropharyngeal, stool and surface swabs. Finally,  
190 the fully characterized biosensor system is validated for the analysis of clinical  
191 samples of patients that were identified with a standard RT-qPCR as positive or  
192 negative.



193  
 194 *Figure 1 a) Schematics of the A-QCM sensor chip that is contacted with the analysed liquid sample, b) chemical*  
 195 *structure of the used antifouling polymer brush architecture prepared from random terpolymer of CBMAA, HPMAA,*  
 196 *and SBMAA and c) its post-modification with custom-produced antibodies for affinity capture of SARS Cov-2.*

197

## 198 **Monoclonal antibody to SARS-CoV-2 nucleocapsid protein**

199 Human cell culture-produced monoclonal antibody (AbN) to SARS-CoV-2  
 200 nucleocapsid protein was developed. This antibody was selected from a panel of 46  
 201 immunoglobulin G (IgG) antibodies based on their performance assessed by  
 202 immunoblotting and enzyme-linked immunosorbent assay (ELISA). The specificity  
 203 of the selected AbN was further confirmed by immunoblot. High specificity of the  
 204 antibody was confirmed – binding to N protein of SARS-CoV-1 and 2, whereas no  
 205 binding was observed for any other human coronavirus N protein nor other common  
 206 respiratory viruses, see Table 1.

Protein	Strain	Source	Concentration	Results
SARS-coronavirus-2 N protein	BL21(DE3)	Escherichia coli	1ug/well	POS
SARS-coronavirus N protein	BL21(DE3)	Escherichia coli	1ug/well	POS
MERS- coronavirus N protein	BL21(DE3)	Escherichia coli	1ug/well	NEG
229E- coronavirus N protein	BL21(DE3)	Escherichia coli	1ug/well	NEG
NL63- coronavirus N protein	BL21(DE3)	Escherichia coli	1ug/well	NEG
OC43- coronavirus N protein	BL21(DE3)	Escherichia coli	1ug/well	NEG
HKU1- coronavirus N protein	BL21(DE3)	Escherichia coli	1ug/well	NEG

208

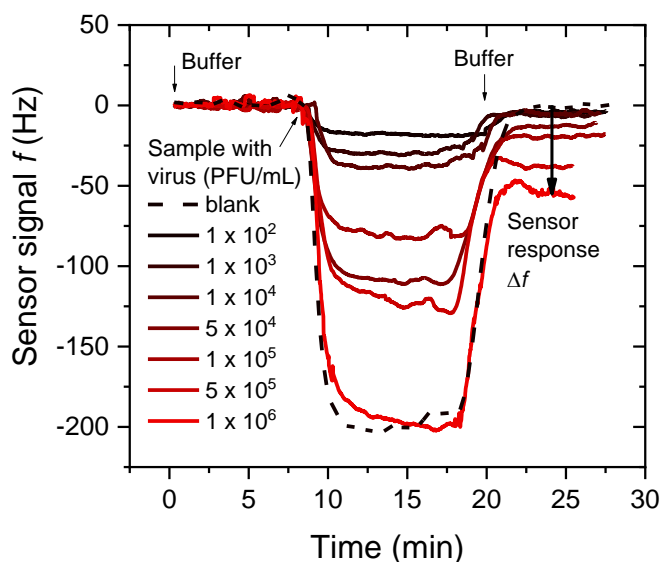
### 209 **Detection of SARS-CoV-2 virus by A-QCM**

210 In order to directly detect the presence of SARS Cov-2 virus in complex  
 211 biological fluids, a gold coated QCM sensor chip was chemically modified by  
 212 antifouling layer composed of polymer chains that take a brush architecture with a  
 213 thickness of  $70 \pm 10$  nm when contacted with aqueous environment (data not shown).  
 214 The polymer chains were synthesized as a terpolymer with random distribution of  
 215 *N*-(2-hydroxypropyl) methacrylamide (HPMAA), carboxybetaine methacrylamide  
 216 (CBMAA), and sulfobetaine methacrylamide (SBMAA) and optimized ratios of  
 217 each monomer unit in polymerization feed (77 mol%, 20 mol%, and 3 mol% for  
 218 HPMAA, CBMAA, and SBMAA, respectively). In this poly(HPMAA-*co*-CBMAA-  
 219 *co*-SBMAA brush coating, (Figure 1b), each monomer unit has a certain role. The  
 220 HPMAA forms a robust non-ionic background (46, 47) and the chosen portion of  
 221 CBMAA units provide a sufficient amount of carboxy-groups for the  
 222 postmodification with functional biomolecules. The incorporation of the monomer  
 223 SBMAA introduces a permanent charge, which during the postmodification reaction  
 224 helps preserving the net charge electroneutrality. The thickness of terpolymer brush  
 225 was of  $40 \pm 8$  nm and it served as a binding matrix, to which the antibody against  
 226 the SARS-CoV-2 N protein – AbN – was immobilized by using amine coupling.

227 In the first stage of the A-QCM biosensor experiments, the sensor chip was  
 228 clamped to a flow-cell and series of samples with SARS-CoV-2 virus concentrations  
 229 ranging between  $1 \times 10^2$  to  $1 \times 10^6$  PFU/mL were flowed over its surface. These  
 230 samples originated from Vero E6 cell culture and the virus concentration in the  
 231 whole cell culture medium was determined by a plaque assay. Typical A-QCM  
 232 sensor signal kinetics upon the flow of the analysed sample can be seen in in Figure  
 233 2a. It shows that after the contacting of the sample the sensor chip surface, a rapid  
 234 decrease in the QCM signal  $f$  occurs with respect to the baseline established in a  
 235 buffer. After 10 min flow, the sensor signal reaches a plateau and after a subsequent

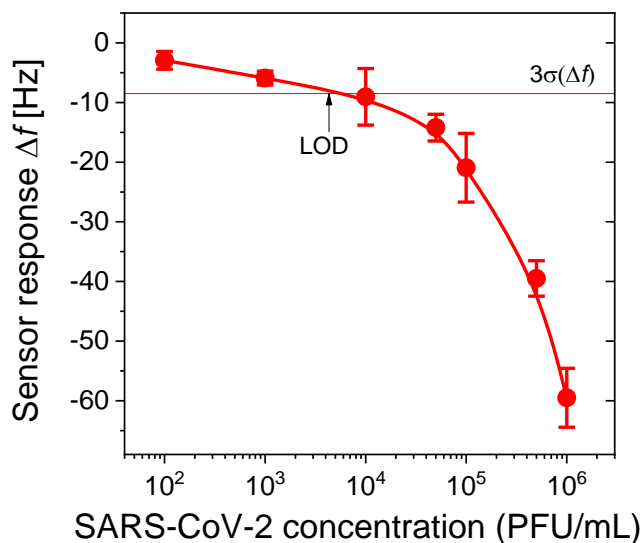
236 rinsing with a buffer it rapidly increases. After the rinsing, the QCM signal  $f$  levels  
237 below the original baseline value. When increasing the concentration of target  
238 analyte SARS-CoV-2, the QCM signal decrease is more pronounced. The sensor  
239 response  $\Delta f$  was defined as difference between the sensor signal baseline before  
240 injecting the analyse sample and after 5-minute washing with the same buffer. The  
241 resulting A-QCM calibration curve for direct detection of SARS-CoV-2 in  
242 minimally processed cell culture medium is presented in Figure 2b. The LOD was  
243 determined to be  $6.7 \times 10^3$  PFU/mL based on the noise of sensor signal baseline.  
244 This value is in the range that was currently determined to be clinically relevant (58)  
245 and it is worth mentioning that these samples exhibited a very high degree of  
246 biological complexity as they contained cells debris, virions, and cell culture  
247 medium without any dilutions. These results clearly demonstrate a high sensitivity  
248 of developed A-QCM method and highlights a potential of quantitative analysis in  
249 virus-containing complex biological samples.

250



251

a)



252

b)

253

254

255

Figure 2 a) Kinetics of the -QCM biosensor response to series of cultured SARS-CoV-2 virus samples. b) Established calibration curve of A-QCM biosensor for SARS-CoV-2 detection in cell culture medium. The cell culture medium was spiked with SARS-CoV at concentrations from  $1 \times 10^2$  PFU/mL to  $1 \times 10^6$  PFU/mL.

256

257

258

259

260

261

262

263

264

265

266

267

268

269

270

271

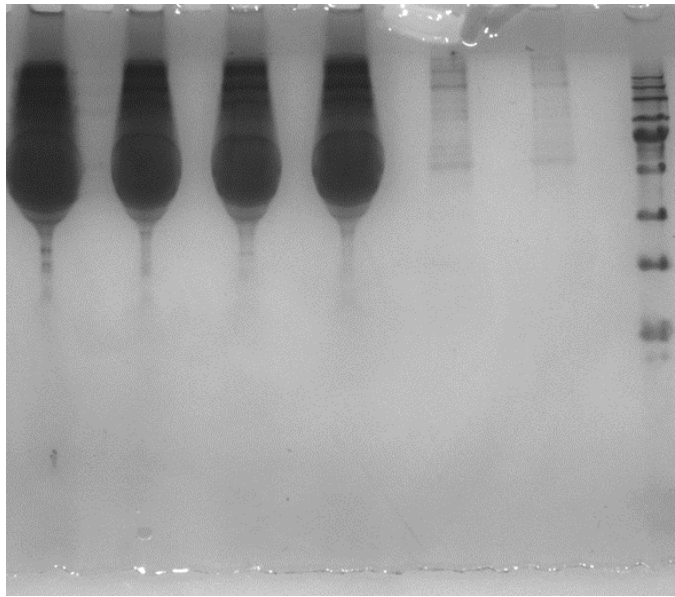
272

273

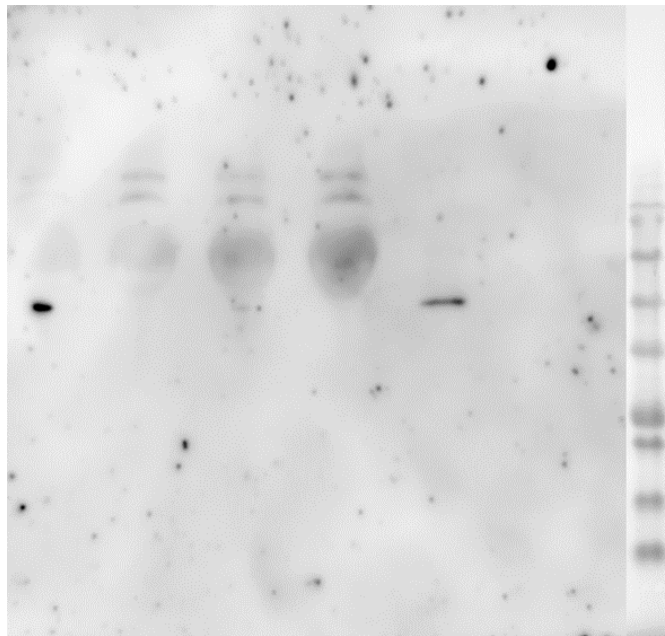
274

275

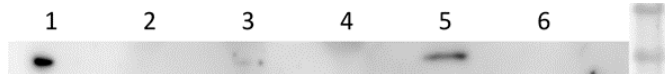
As sample pre-treatment steps were completely avoided, let us point out that no protein lysis or sample dilution was used. Indeed, then one can assume that the used antibody AbN (tethered at the sensor surface) would be able to recognize the SARS Cov-2 protein N. The N- (nucleocapsid) protein is a viral structural protein forming the viral capsid, in which it is hidden from the outside environment. However, it is apparent that the analysed samples contain N protein that is not part of the virion structure and that probably leaches from infected cells expressing the virus. Thus, we verified the presence of free N protein in medium using the same specific antibodies AbN, which were used also for biochip coating. N protein was detected in the medium after polyethylene glycol (PEG) precipitation, which was used to remove the SARS-CoV-2 virions from the cell culture medium. The gel electrophoresis data presented in Figure 3 confirm the presence of free N-protein in the medium. However, interestingly it also shows that the majority of the N protein is detected in the fraction with precipitated (and subsequently lysed) virions. Therefore, it can be anticipated that strongly improved A-QCM sensitivity can be achieved if a specific sample pre-treatment such as virus sample lysis was used. However, in this work we aimed to develop a robust simple one-step method to maximize the simplicity of virus detection.



276



277



278

279

280 *Figure 3 Immunodetection of N protein in the samples. Majority of SARS-CoV-2 N protein was detected in the*  
 281 *virions and not as a free protein in the medium. (A) SDS-PAGE separated proteins stained by Coomassie Brilliant*  
 282 *Blue. (B) Immunodetection of N protein after electroblotting. 1 – medium containing SARS-CoV-2, 2 – control*  
 283 *medium, 3 – SARS-CoV-2 medium supernatant after PEG precipitation, 4 – control medium supernatant after PEG*  
 284 *precipitation, 5 – SARS-CoV-2 medium pellet after PEG precipitation, 6 – control medium pellet after PEG*  
 285 *precipitation.*

286

287 **Antifouling properties of AbN-functionalized terpolymer brush on A-**  
 288 **QCM**

289 In order to provide a versatile tool for the direct rapid analysis of SARS-CoV-2,  
 290 the sensor design has to eliminate the false response due to the constituent of  
 291 analysed sample matrix that interfere with the specific recognition of target analyte.  
 292 Therefore, the herein reported terpolymer brush with immobilized antibody to  
 293 SARS-CoV-2 N-protein – AbN – was challenged with a set of complex biological  
 294 samples, which possess a clinical relevance towards SARS-CoV-2 detection. These  
 295 solutions included SARS-CoV-2 virus-free oropharyngeal, nasopharyngeal and  
 296 stool swabs and swabs from an indoor surface. These swabs were collected by  
 297 standard protocol and no additional pre-treatment step was employed prior to their  
 298 injecting to the sensor.

299 Following the detection protocol used for the calibration of the A-QCM  
 300 biosensor (see Figure 2a), the QCM signal was monitored upon the 10-minute flow  
 301 of the analysed swab matrices over the surface of antifouling polymer brush  
 302 architecture with immobilized AbN. Consequently, the sensor response  $\Delta f$  was  
 303 determined as a difference in the QCM signal  $f$  before after the sample incubation.  
 304 The obtained results are summarized in Table 3 below and they show that for all  
 305 samples the magnitude of the response  $\Delta f$  was below 6 Hz. This value is below the  
 306 uncertainty  $3\sigma$  (determined based on the baseline noise) and therefore undetectable.  
 307 These results clearly confirm a very high degree of antifouling properties of AbN-  
 308 functionalized terpolymer brush and negligible interaction of various SARS-CoV-  
 309 2-free biological matrices with AbN biorecognition layer.

310 In addition, the specificity of the AbN immobilized in the antifouling polymer  
 311 brush architecture was tested by QCM-based monitoring of its interaction with  
 312 control hepatitis A virus protein (10  $\mu\text{g}/\text{mL}$ ) and *Escherichia coli* O157:H7 (10<sup>6</sup>  
 313 CFU/mL) that were spiked in a buffer. Similar to the swab samples, there measured  
 314 sensor response for these control analytes was below measurable values as can be  
 315 seen in Table 3. These data were measured in at least two replicates and in addition,  
 316 the detection specificity was further confirmed by incubation of non-target antibody  
 317 (anti-*E. coli*)-functionalized terpolymer brush with a medium spiked with SARS-  
 318 CoV-2 virus with a high concentration (5  $\times 10^4$  PFU/mL). No detectable sensor  
 319 response was observed. The same result was also obtained when only activated and  
 320 deactivated coating (without any biorecognition elements immobilized) was  
 321 incubated with virus-spiked medium (data not shown). Apparently, no potential  
 322 interactions of the coating material with target virus were found.

323  
 324 Table 2 A-QCM sensor response to the unspecific sorption from selected set of clinically relevant SARS Cov-2  
 325 – free swab samples and control analytes.

Sample type	Frequency shift $\Delta f$ [Hz $\pm$ SD]
Nasopharyngeal swab	5.5 $\pm$ 0.9
Oropharyngeal swab	1.0 $\pm$ 1.4

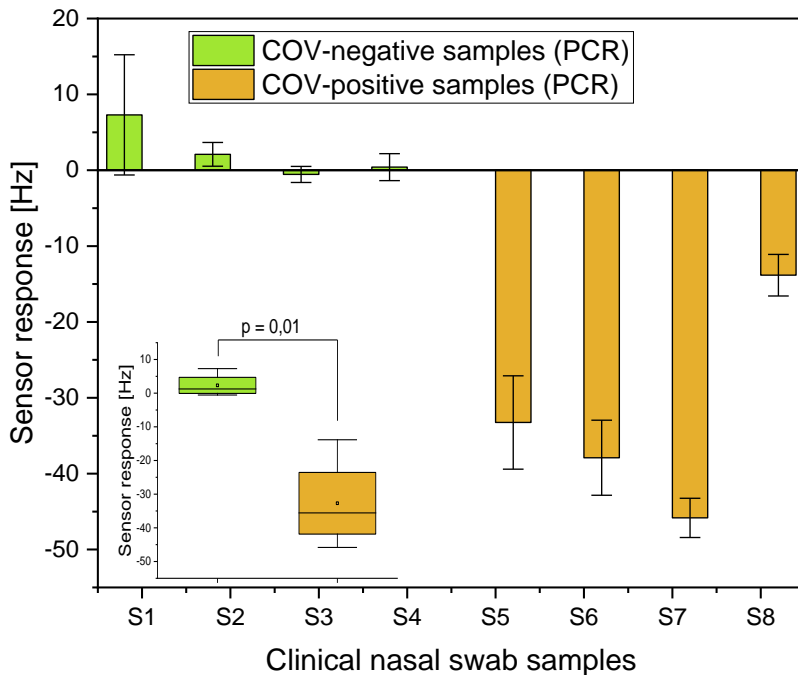
326	Stool swab	1.8 ± 2.6
327	Surface swab	0.9 ± 1.0
328	Hepatitis A Virus protein	2.0 ± 0.8
329	Escherichia coli	1.7 ± 2.0
330		

331  
332  
333

### 334 **Validation of A-QCM SARS Cov-2 biosensor for crude clinical samples**

335 There was investigated the employment of the developed biosensor assay for  
336 routine use in COVID-19 diagnosis by using a comparative A-QCM and RT-qPCR  
337 study on a set of clinical samples. In a blinded study, we tested a series of  
338 nasopharyngeal swabs (Figure S2) acquired by using standard certified protocol  
339 from COVID-19 negative and positive patients. These samples were analyzed in  
340 parallel at the clinical diagnostic unit using RT-qPCR and by A-QCM platform. In  
341 total, eight clinical samples were used and RT-qPCR showed four samples negative  
342 and four were positive having the vRNA concentration in the range  $4.1 \times 10^5$  to  
343  $7.4 \times 10^6$  copies/ml. The qualitative results achieved by A-QCM were in 100%  
344 agreement with the standardized RT-qPCR as all positive and negative samples were  
345 recognized identically when using the cut-off value of  $\Delta f = 3\sigma = -9$  Hz, see Figure 4.  
346 In addition, the magnitude of the measured A-QCM sensor response was  
347 investigated for possible quantitative detection of SARS Cov-2 employing the  
348 previously established calibration curve (see Figure 2b). Indeed, these results have  
349 shown only partial agreement with RT-qPCR, which was be ascribed to the fact that  
350 RT-qPCR quantifies the number of viral vRNA copies, whereas the A-QCM based  
351 serves for the detection of a protein antigen, the viral N protein in our case (Table  
352 S1). Partial discrepancy between the quantitative result of A-QCM and RT-qPCR  
353 can be thus attributed to the differences in vRNA and protein production that is either  
354 present in the virion capsule or also can be found in a free form (61).





355  
356  
357

Figure 4 Statistically significant difference between RT-qPCR positive and negative clinical samples (i.e. nasopharyngeal swab).

358

## Discussion

359

360 Current detection methods of SARS CoV-2 rely mostly on detection of viral  
 361 genetic information (vRNA) by reverse transcription quantitative polymerase chain  
 362 reaction (RT-qPCR) or isothermal amplification methods (62). This approach is  
 363 considered a gold standard method with high analytical sensitivity and specificity  
 364 (65–67). However, when applied for the routine diagnostics the sensitivity RT-qPCR  
 365 of might be significantly lower (68, 69) due to its complex multistep protocol. In  
 366 addition, the presence of vRNA in does not necessarily mean the presence of  
 367 replicating and thus infectious virus. There are multiple reports of individuals with  
 368 long-term RT-qPCR SARS-CoV-2 positivity in nasopharyngeal swabs (70, 71).  
 369 However, the prolonged RNA shedding was not associated with production of  
 370 infectious viral particles as described in several studies (61, 72, 73). On the other  
 371 hand, rare cases of (immunodeficient) patients with long-term production of  
 372 infectious virus were also recorded (74). An alternative to approach to viral RNA is  
 373 based on detection of viral proteins and it has been utilized in numerous antigen-  
 374 based tests. These tests usually provide with lower sensitivity (and specificity)  
 375 compared to RT-qPCR (24, 75–77), but they offer the advantage of less demanding  
 376 operation and possible on place rapid analysis in the order of minutes.

377 The reported approach combines the advantages of antigen-based approach,  
 378 which is more closely related to the presence of replicating virus in the sample, and

379 sensitivity and specificity comparable with RT-qPCR. Importantly, unlike in the  
380 case of RT-qPCR, extensive sample preparation (that would require transport into a  
381 specialized laboratory) is avoided, and the whole process from sample collection by  
382 standard protocol to the test readout takes only approximately 30-45 minutes. The  
383 detection by a A-QCM based biochip showed sensitivity in the range of the most of  
384 commonly used RT-qPCR tests without the using specialized laboratory equipment,  
385 necessity of operating the device with trained personnel, and lengthy and laborious  
386 sample processing (RNA isolation).

387 Unlike the already used lateral flow antigen tests, the A-QCM can be used for  
388 quantitative analysis of SARS-Cov-2, but it should be noted that the response due to  
389 the presence of target SARS-Cov-2 protein N is not proportional to the amount of  
390 infectious viral particles (78, 79). This does not allow for direct comparison between  
391 the methods based on vRNA and viral protein detection. Nevertheless, we have  
392 shown that the number of viral particles (as inferred from a calibration curve)  
393 roughly corresponds with the number of vRNA copies present in the original sample.  
394 Partial discrepancy between the quantitative result of A-QCM and RT-qPCR can be  
395 attributed to the differences in vRNA and protein production (61).

396 The A-QCM immunoassay was established by using antibody specific to SARS-  
397 CoV nucleocapsid (N) protein. This structural protein plays a crucial role in  
398 coronavirus replication cycle ([10.1016/j.antiviral.2013.12.009](https://doi.org/10.1016/j.antiviral.2013.12.009)). Transcriptomic and  
399 proteomic studies in multiple cell culture systems and human clinical samples show  
400 that it belongs to the most abundant viral protein, whereas the surface exposed S  
401 protein is usually relatively less represented (78–81). However, the majority of  
402 antigenic tests relies on targeting the S protein as it is exposed on the surface of viral  
403 particles. Importantly, the currently developed vaccines also dominantly target the  
404 S protein of SARS-CoV-2 ([10.1038/s41577-020-00480-0](https://doi.org/10.1038/s41577-020-00480-0)). It can be assumed that  
405 the vaccine-based selection pressure will potentially lead to the occurrence of  
406 antibody escape mutants ([10.7554/eLife.61312](https://doi.org/10.7554/eLife.61312); [10.1101/2020.12.21.20248640](https://doi.org/10.1101/2020.12.21.20248640);  
407 [10.1101/2021.01.22.427567](https://doi.org/10.1101/2021.01.22.427567)) that will complicate the use of antigenic tests specific  
408 to the S protein. The alternative whole virus vaccines elicit the antibody response  
409 to multiple virus epitopes, and makes the generation of escape mutants far less  
410 probable ([10.1126/science.abd0831](https://doi.org/10.1126/science.abd0831), [10.1126/science.abd0827](https://doi.org/10.1126/science.abd0827)). The stability of N  
411 protein sequence is, among others, illustrated by the high degree sequence homology  
412 between SARS-CoV-1 and 2 (90% similarity of the amino acid sequence)  
413 ([10.1016/j.chom.2020.03.002](https://doi.org/10.1016/j.chom.2020.03.002)). Considering the mutation rate, the SARS-CoV-2 N  
414 protein was shown to have lower variability than S protein  
415 ([10.1016/j.chom.2020.03.002](https://doi.org/10.1016/j.chom.2020.03.002)), it suggests that the performance of the presented  
416 detection method is less likely to be affected by mutations and new virus variants.  
417 Moreover, the specificity to both SARS-CoV-1 and 2 (and no other human  
418 coronaviruses or other respiratory viruses) can be seen as advantage as these viruses  
419 are highly pathogenic, the clinical features of the diseases they cause are very similar  
420 and they never reported to co-occur.

421 In summary, a combination of the interdisciplinary research in the area of surface  
422 chemistry, physics, bioengineering, and biology paved the way to rapid, direct,  
423 sensitive, and potentially low-cost method for SARS-CoV-2 detection that does not  
424 rely on sample pre-treatment. It is enabled by using a unique biointerface  
425 architecture that allows to eliminate unspecific sorption from complex biological  
426 samples used in the COVID-19 diagnosis. The chosen QCM biosensor platform is  
427 ideally suited for developed type of polymer brush-based antifouling coating, as the  
428 optimum thickness assuring the antifouling performance has to be of several tens of  
429 nanometer. Therefore, other biosensor platforms proposed for the analysis of SARS-  
430 CoV-2 including field effect transistor (FET) and surface plasmon resonance (SPR)  
431 cannot fully benefit from this approach. The reason is the short probing depth  
432 dictated by the Debye length and confined evanescent field of surface plasmons that  
433 are comparable or much lower than the needed antifouling brush thickness.  
434 Moreover, QCM monitoring of SARS-CoV-2 virus affinity capture can be  
435 implemented by established readers. The key advantage is the possibility of rapid  
436 direct analysis of untreated clinical samples with a sensitivity comparable to RT-  
437 qPCR with additional opportunity of quantitative characterization of the  
438 concentration of viral antigens. These features may have critical impacts into clinics  
439 for precise COVID-19 diagnosis, as well as in disease prognosis or individual  
440 infectivity characterization. In addition, the potential of A-QCM can be also seen in  
441 detecting virus in other scenarios, such as various swabs from public-accessible  
442 surface in public transportation or the supermarket's shelves (82–84).

## 443 **Materials and Methods**

### 444 **Reagents**

445 The buffer solutions were prepared using ultrapure water (18.0 M $\Omega$ .cm, Milli-Q®  
446 system, Merck). Phosphate-buffered saline (PBS, 0.01-M sodium phosphate, 0.138-  
447 M sodium chloride, 0.0027-M potassium chloride, pH 7.4) was prepared from tablets  
448 from Sigma-Aldrich, Czech Republic. The PBS-NaCl buffer (0.01-M phosphate,  
449 0.75-M sodium chloride, 0.0027-M potassium chloride, pH 7.4) was prepared from  
450 PBS stock solution. The PBS-T buffer and Laemmli sample buffer. NaCl. 5mM 4-  
451 (2-hydroxyethyl)-1-piperazine ethanesulfonic acid (HEPES), pH 7.0 and pH 6.00 at  
452 25°C were prepared from stock solutions purchased from Sigma Aldrich, Czech  
453 Republic. N-hydroxysuccinimide (NHS) and N-ethyl-N'-(3-  
454 diethylaminopropyl)carbodiimide (EDC) were purchased from AP Czech, Czech  
455 Republic. 2-(2-aminoethoxy)acetic acid (AEAA) was purchased from VWR  
456 International, Czech Republic. Gold-coated quartz crystals of resonant frequency 10  
457 MHz were purchased from Krystaly, Hradec Králové, Czech Republic. The  
458 sulfobetaine methacrylamide (SBMAA), carboxybetaine methacrylamide  
459 (CBMAA), and N-(2-hydroxypropyl) methacrylamide (HPMAA) monomers were  
460 from Specific Polymers, France. 1,4,8,11-tetramethyl-1,4,8,11-  
461 tetraazacyclotetradecane (Me4Cyclam, 98%), CuCl ( $\geq 99.995\%$ ), CuCl<sub>2</sub> (99.999%),

462 methanol ( $\geq 99.9\%$ ), and ethanol (99,9%) were from Sigma-Aldrich.  
463 Tetrahydrofuran (THF,  $\geq 99.9\%$ ) was from Penta, Czech Republic. The chloroform.  
464 The PEG6000 SDS-PAGE. The cell cultivation medium Dulbecco's Modified Eagle  
465 Medium (DMEM) low glucose and fetal bovine serum were from Biosera, France.  
466 L-glutamine, penicillin, streptomycin, amphotericin B were purchased from  
467 Biowest, France. Nucleic Acid Extraction Kit B-200 was purchased from Zybico,  
468 China. Seegene AllPlex™ 2019-nCoV Assay kit was from Seegene, South Korea.  
469 Hepatitis A Virus protein inactivated with formaldehyde was purchased from  
470 Abbexa, UK. Heat-killed *E. coli* O157:H7 was from SeraCare, USA.

#### 471 **Preparation of Terpolymer Brushes**

472 Terpolymer brush coatings were prepared using modified procedure as described  
473 previously, and their composition was verified by infrared spectroscopy (85).  
474 Briefly, crystals were cleaned in UV-ozone cleaner for 10 min and then were rinsed  
475 with ultra-pure water and ethanol. Immediately after the cleaning, the slides were  
476 immersed in an initiator solution of a 1 mM  $\omega$ -mercaptoundecyl bromoisobutyrate  
477 in ethanol to form a self-assembled monolayer (SAM) and were left in the solution  
478 for 3 days at room temperature in darkness. Methanol and water were degassed via  
479 6 freeze-pump-thaw cycles. For the amount of 80 coatings, the catalyst solution was  
480 prepared as follows: under the nitrogen atmosphere CuCl (151.9 mg), CuCl<sub>2</sub> (29.4  
481 mg), and Me<sub>4</sub>Cyclam (338.8 mg) in a Schlenk tube were mixed with 7.1 mL of  
482 degassed methanol. The mixture was sonicated for 5 min to dissolve all solids. In a  
483 second Schlenk tube, monomers SBMAA (0.483 g, 3 mol %), CBMAA (2.667 g, 20  
484 mol %) or HPMMA (6.069 g, 77 mol %) were dissolved in 13.3 mL degassed water  
485 and 46.1 mL degassed methanol and stirred. After the dissolution was completed,  
486 the catalyst solution was added to the monomer solution using a gastight syringe.  
487 The polymerization mixture was added into the reactor containing the substrates  
488 coated with the initiator SAM. The polymerization was carried out for 2 h at room  
489 temperature. Finally, the samples were washed with ultra-pure water and stored in  
490 PBS at 6 °C until used.

491 The verification of the presence of all three monomers was performed using  
492 infrared spectroscopy (Figure S1). The thickness of terpolymer brush was measured  
493 using spectroscopic ellipsometry according to previously described procedure (86).

#### 494 **Production of the 7 human coronavirus nucleocapsid proteins**

495 The 7 human coronavirus nucleocapsid protein genes were derived from NCBI  
496 protein databank. These proteins were codon optimized and synthesized for  
497 expression in *E. coli* and mammalian cells with pET15b (Novagen) and pcDNA3.1  
498 (Thermo Fisher Scientific) vectors, respectively. These coronavirus N protein  
499 constructs with pET15b vector were overexpressed in *E. coli* BL21 (DE3) cells with  
500 0.5 mM IPTG induction at 16°C. The recombinant coronavirus N proteins were  
501 purified using Ni<sup>2+</sup> charged Chelating Sepharose FF (for His<sub>6</sub>-tag binding) with A  
502 (binding) buffer containing 50 mM Tris-HCl, pH 8.0 and 600 mM NaCl, and B

503 (elution) buffer containing 50 mM Tris-HCl, pH 8.0, 600 mM NaCl, and 500 mM  
504 Imidazole by using an Akta prime plus chromatography system (GE Healthcare Life  
505 Sciences). The fractions containing coronavirus N proteins were pooled for size  
506 exclusion separation with Superose12 10/300GL columns (GE Healthcare) and  
507 elution buffer containing 50 mM Tris, pH 8.0, 600 mM NaCl. These recombinant  
508 coronavirus N proteins would be contained RNA from *E. coli*, and then the  
509 A260/A280 ratio would be larger than 0.8. The concentration of recombinant  
510 coronavirus N proteins with BCA protein assay (Thermo Fisher Scientific) would  
511 be lower than optical detection with NanoDrop™ 2000 Spectrophotometer (Thermo  
512 Fisher Scientific) and the extinction coefficient of each coronavirus N protein.  
513 Purified coronavirus N proteins were confirmed by SDS-PAGE.  
514

#### 515 **Characterization of the IgG1s derived from the selection and screening procedure with** 516 **phage-displayed synthetic single chain variable fragment libraries**

517 The construction and characterization of the phage-displayed synthetic single  
518 chain variable fragment (scFv) libraries followed the same procedure, without  
519 modification, as described in the previous work (Ref 1 & 2). The experimental  
520 procedures for panning the phage display libraries, selecting and screening of phage-  
521 displayed scFv binders, characterizing the scFvs binding to the cognate antigens and  
522 Protein A/L with ELISA, reformatting scFvs into IgG1s, expressing in and purifying  
523 IgG1s, and determining EC50 for the antibody-antigen interaction with ELISA have  
524 been described in previous works (Ref 1-4).  
525

#### 526 **Construction and expression of IgG**

527 VH and VL DNA fragments were PCR amplified separately. The VH and VL  
528 DNA fragments were assembled into the plasmid for IgG1 expression with the pIgG  
529 expression system (U.S. patent no. 5736137) with Gibson assembly cloning kit  
530 (NEB Cat no. E5510S). IgGs were expressed by Expi293 cells following the  
531 manufacture's instruction manual and purified through protein A column, eluted  
532 with 0.2 M glycine/HCl buffer, pH 2.5, and neutralized with 1 M Tris buffer, pH  
533 9.0.  
534

#### 535 **Detection of recombinant N proteins with immunoblotting**

536 The recombinant N proteins (1 µg) were resolved on an SDS containing 4%-  
537 20% gradient gel polyacrylamide gel, transferred to polyvinylidene difluoride nylon  
538 (PVDF) membrane, and probed with 46 hIgG antibodies (1 µg/mL). The specific  
539 bands were detected by horseradish peroxidase-conjugated antibody and revealed by  
540 SuperSignal® West Pico Chemiluminescent Substrate (Thermo Scientific) and  
541 chemiluminescent imaging system.  
542

#### 543 **Detection of recombinant N proteins with sandwich ELISA**

544 Horseradish peroxidase (HRP) was conjugated to detection antibody with HRP  
545 Conjugation Kit (Abcam, ab102890). 50 µg of purified IgG was added to HRP mix  
546 with molar ratio IgG:HRP = 1:2 and the conjugation reaction was quenched  
547 according to manufacturer's instruction. Sandwich ELISAs were carried out with  
548 96-well Nunc plate, which was coated with 1 µg of purified capture IgG for each  
549 well at 4°C overnight. The Recombinant N proteins were added to each well coated  
550 with capture antibody for one hour. After washing, 0.625 µg/ml HRP conjugated  
551 detection IgG (100 µL per well) was added to each well. The color was developed  
552 by adding TMB (ScyTek Laboratories, Inc.) (100 µL per well) to each well for 5  
553 min before adding 1 N HCl (100 µL per well) to stop the chromogenic reaction  
554 before the absorbance at 450 nm was measured. EC50 of sandwich ELISA with  
555 pairing IgGs was also measured. 1µg of purified capture IgG was coated for each  
556 well at 4°C overnight. The recombinant N proteins were diluted by 2-fold serial  
557 dilution. 0.313 µg/mL of HRP conjugated detection IgG (100 µL per well) was  
558 added to each well. EC50 was calculated as previously published (Ref. 1-4).  
559

#### 560 *IgG binding to N protein from transfected 293T cells*

561 pcDNA3.1-SARS-CoV-2-N-His was transfected into HEK 293T cells by transient  
562 transfection using ExpiFectamine (Gibco) and the cell were seeded into 96-well  
563 plates (Thermo Fisher) at a density of  $6 \times 10^6$  cells/100 µl/well and cultured for 48 h.  
564 After the removal of medium, cells were fixed with 200 µl/well of fixation reagent  
565 (Methanol:Acetone (1:1)) 10 min at room temperature (RT). After the removal of  
566 fixation reagent and air dry incubation for 10 min at RT, the cells were rinsed with  
567 200 µl of PBS. After the removal of PBS, 100 µl of 0.5% Triton X-100 in PBS was  
568 added to each well then incubated for 5 min at RT. After the removal of 0.5% Triton  
569 X-100, the cells were rinsed with 200 µl of PBS. Cells were then washed twice with  
570 PBS and blocked with 5% skim milk in PBST for 1h at RT. Immunostaining was  
571 performed with each of the anti-SARS-COV-2-N mAb (1 µg/100µl in PBST) as the  
572 primary antibody for at least 2 h at RT, washed twice with PBST and diluted  
573 (1:5000) HRP-conjugated anti-human IgG Fc (A80-304P, Bethyl Laboratories) was  
574 applied as the secondary antibody for 1 h at RT and subsequently washed twice with  
575 PBST. Colorimetric measurements were carried out after the color development by  
576 adding TMB (ScyTek) substrate (100 µL per well) to each well for 5 min before  
577 adding 1 N HCl (100 µL per well) to stop the chromogenic reaction. The absorbance  
578 at 450 nm was measured, each anti-SARS-CoV-2-N mAb was assayed with  
579 triplicate.  
580

#### 581 **Virus and cell culture**

582 Virus infection experiments were performed in a biosafety level 3 laboratory.  
583 SARS-CoV-2 (SARS-CoV-2/human/Czech Republic/951/2020, EPI\_ISL\_414477,  
584 isolated from a clinical sample at The National Institute of Public Health Centre for  
585 Epidemiology and Microbiology, Prague, Czech Republic), kindly provided by Dr.  
586 Jan Weber, Institute of Organic Chemistry and Biochemistry, Prague, Czech

587 Republic, was passaged in Vero E6 cells (African green monkey kidney cells,  
588 ATCC® CRL-1586™) up to six times before its use in this study. Vero E6 cells  
589 were cultured at 37°C and 5% CO<sub>2</sub> in DMEM low glucose supplemented with 10%  
590 fetal bovine serum, 1% L-glutamine, 100 U/ml penicillin, 100 µg/ml streptomycin,  
591 0.25 µg/ml amphotericin B. To produce high titer viral stocks we used 100 kDa  
592 Amicon Ultra-15 Centrifugal Filter Unit (Merck Millipore, Germany) followed by  
593 filtration through 0.22µm filter (VWR, USA). The titer of the virus was measured  
594 by plaque assay. Virus was diluted in cultivation media as required for further  
595 experiments.

#### 596 **Plaque assay**

597 Plaque assays were performed as previously described (87) with slight  
598 modifications. Suspension culture of Vero E6 cells were seeded ( $1.3 \times 10^5$  cells per  
599 well) to 24-well tissue culture plate with 10-fold dilutions of virus. After 4 hours of  
600 incubation at 37 °C with 5% CO<sub>2</sub>, each well was overlaid by complete medium with  
601 carboxymethylcellulose (1.5%). After a 5-day incubation at 37 °C and 5% CO<sub>2</sub>, the  
602 cell monolayers were visualized using naphthalene black. Viral titers were expressed  
603 as plaque-forming units (PFU) per millilitre.

#### 604 **Clinical Samples**

605 Oropharyngeal, nasopharyngeal, stool and throat swabs were collected in native  
606 conditions and placed to a transport solution according to a standard sampling WHO-  
607 approved protocol. Surface samples were taken from indoor table; the surface (with  
608 an area 225 cm<sup>2</sup>) was wiped for 30 seconds. After addition of 1 ml of PBS the  
609 samples were vortexed and incubated for 5 min at room temperature. After brief  
610 centrifugation the whole volume was transferred into a microtube. Then 200 µl from  
611 were taken for RNA isolation. All swabs were collected with certified swab kits.

#### 612 **RNA extraction and RT-qPCR for SARS-CoV-2**

613 RNA was extracted from 200 µl of samples with the Nucleic Acid Extraction Kit  
614 B-200 (88) using Nucleic acid isolation system (Zybio EXM3000). RT-qPCR was  
615 performed using the Seegene AllPlex™ 2019-nCoV (89) Assay kit in the CFX96  
616 Touch Real-time PCR Detection cyler System (Bio-Rad, USA). The evaluation  
617 was performed on the basis of the manufacturer's manual using the CFX Maestro  
618 software (Bio-Rad, USA).

#### 619 **Functionalization of the polymeric brush**

620 For the functionalization and real time detection, the A-QCM device developed  
621 at the Institute of Physics (Prague, Czech Republic) combined with openQCM Q-1  
622 (Novaetech, Italy) and microfluidic system, was used. Before functionalization,  
623 coatings were rinsed with ultrapure water. After it, coatings were washed with PBS  
624 buffer for 5 min with a flow rate of 45 ul/min and after were submerged in ultrapure  
625 water for 5 min with the same flow rate. Subsequently brushes were activated with

626 a freshly prepared solution of 0.1-M NHS and 0.5-M EDC for 20 min (7 ul/min).  
627 Afterwards, the coatings were washed for 3 min (60 ul/min) with HEPES buffer (5  
628 mM, pH 6). The solution with antibody diluted in HEPES buffer (5 mM, pH 7) was  
629 added with flow rate 60 ul/min, after a minute, the speed was reduced by 45 ul/min,  
630 then by 30 ul/min, and then it was left reacted for 12 min with flow rate 15 ul/min.  
631 After immobilization, all coatings were rinsed again with HEPES buffer (5 mM, pH  
632 6) (10 min, 30 ul/min) and immersed in the deactivation solution of 1M AEAA for  
633 25 min at a flow rate of 7 ul/min. Deactivated coatings with immobilized antibodies  
634 were used for detection of SARS-CoV-2 virus in the next step.

#### 635 **Detection of SARS-CoV-2 Virus by A-QCM**

636 The SARS-CoV-2 virus was detected in real time using the software using the  
637 crystals with immobilized antibodies from the previous step. A stable flow rate of  
638 30  $\mu$ L / min was used in this part. All the coatings were rinsed with PBS buffer for  
639 10 min. Afterwards, the sample was added and reacted for 12 min. Finally, all the  
640 coatings were rinsed with PBS buffer for 10 min. The amount of detected SARS-  
641 CoV-2 virus was calculated from sensor response in PBS buffer before and after  
642 detected solution.

#### 643 **Precipitation of SARS-CoV-2 using PEG6000**

644 Virus particles were precipitated from 1 mL of growth medium from Vero E6  
645 cells infected with SARS-CoV-2 using PEG6000 (90). Shortly, medium was  
646 centrifuged at 5000 x g for 10 minutes, and 20g/l NaCl was added to the supernatant  
647 together with 50 % PEG6000 in 0.5 M NaCl (final concentration of PEG 8 %). The  
648 mixture was incubated overnight at 4°C and was centrifuged the next day at 7000 x  
649 g, 4°C for 15 min. Virions in the pellet were resuspended in 1 mL of PBS and  
650 together with the virion-free supernatant were methanol/chloroform precipitated  
651 (91). The resulting protein pellets were resuspended in 1 mL of PBS; thus, volume  
652 of the resulting virion-containing and virion-free samples was the same, as the  
653 volume of the original medium. A similar procedure was performed with medium  
654 from uninfected Vero E6 cells (negative controls).

#### 655 **Immunodetection of SARS-CoV-2 N protein by Western blot**

656 A reducing Laemmli sample buffer was added to the protein samples, the  
657 resulting mixtures were boiled for 5 min and loaded onto a 12% SDS-PAGE gel  
658 together with prestained protein marker VI (10-245 kDa, Applichem, Germany).  
659 Electrophoresis was performed in a Mini-Protean Tetra Cell (Bio-Rad, USA). The  
660 separated proteins were transferred to a PVDF membrane (company, country) for 1  
661 h at 20 V by semi-dry transfer in TRANS-BLOT SD (Bio-Rad, USA). Membrane  
662 was blocked (5% skimmed milk in PBS-T) and incubated with SARS-CoV-2 N  
663 protein-specific antibody and subsequently secondary antibody conjugated with  
664 HRP (VectorLabs, USA); between each incubation step, membranes were washed  
665 three times in PBS-T. Chemiluminescent signal was developed using WesternBright



666 Quantum kit for horseradish peroxidase (Advansta, USA). The images of gels and  
667 membranes were captured and digitalized using G:BOX Chemi XX6 system  
668 (Syngene, UK).

#### 669 Statistical Analysis

670 Data obtained from independent experiments are presented as the mean  $\pm$   
671 standard error of the mean (SEM). The limit of detection (LOD) was calculated using  
672 a “blank + 3 $\times$ SD” approach.

#### 673 References and Notes

- 674 1. C. Huang, Y. Wang, X. Li, L. Ren, J. Zhao, Y. Hu, L. Zhang, G. Fan, J. Xu,  
675 X. Gu, Z. Cheng, T. Yu, J. Xia, Y. Wei, W. Wu, X. Xie, W. Yin, H. Li, M.  
676 Liu, Y. Xiao, H. Gao, L. Guo, J. Xie, G. Wang, R. Jiang, Z. Gao, Q. Jin, J.  
677 Wang, B. Cao, Clinical features of patients infected with 2019 novel  
678 coronavirus in Wuhan, China. *Lancet*. **395**, 497–506 (2020).
- 679 2. J. Zhang, X. Dong, Y. Cao, Y. Yuan, Y. Yang, Y. Yan, C. A. Akdis, Y. Gao,  
680 Clinical characteristics of 140 patients infected with SARS-CoV-2 in Wuhan,  
681 China. *Allergy*. **75**, 1730–1741 (2020).
- 682 3. C. S. G. of the I. C. on T. of Viruses, The species Severe acute respiratory  
683 syndrome-related coronavirus: classifying 2019-nCoV and naming it SARS-  
684 CoV-2. *Nat. Microbiol.* **5**, 536–544 (2020).
- 685 4. World Health Organization, in press (available at  
686 [https://www.who.int/docs/default-source/coronaviruse/situation-](https://www.who.int/docs/default-source/coronaviruse/situation-reports/20201012-weekly-epi-update-9.pdf)  
687 [reports/20201012-weekly-epi-update-9.pdf](https://www.who.int/docs/default-source/coronaviruse/situation-reports/20201012-weekly-epi-update-9.pdf)).
- 688 5. J. Cui, F. Li, Z.-L. Shi, Origin and evolution of pathogenic coronaviruses.  
689 *Nat. Rev. Microbiol.* **17**, 181–192 (2019).
- 690 6. E. De Wit, N. Van Doremalen, D. Falzarano, V. J. Munster, SARS and  
691 MERS: Recent insights into emerging coronaviruses. *Nat. Rev. Microbiol.*  
692 **14**, 523–534 (2016).
- 693 7. X. Y. Che, L. W. Qiu, Y. X. Pan, K. Wen, W. Hao, L. Y. Zhang, Y. Di  
694 Wang, Z. Y. Liao, X. Hua, V. C. C. Cheng, K. Y. Yuen, Sensitive and  
695 specific monoclonal antibody-based capture enzyme immunoassay for  
696 detection of nucleocapsid antigen in sera from patients with severe acute  
697 respiratory syndrome. *J. Clin. Microbiol.* **42**, 2629–2635 (2004).
- 698 8. P. C. Y. Woo, S. K. P. Lau, B. H. L. Wong, H. W. Tsoi, A. M. Y. Fung, R.  
699 Y. T. Kao, K. H. Chan, J. S. M. Peiris, K. Y. Yuen, Differential sensitivities  
700 of severe acute respiratory syndrome (SARS) coronavirus spike polypeptide  
701 enzyme-linked immunosorbent assay (ELISA) and SARS coronavirus  
702 nucleocapsid protein ELISA for serodiagnosis of SARS coronavirus  
703 pneumonia. *J. Clin. Microbiol.* **43**, 3054–3058 (2005).
- 704 9. World Health Organization, “Laboratory testing for coronavirus disease 2019

- 705 (COVID-19) in suspected human cases” (2020).
- 706 10. L. Hueston, J. Kok, A. Guibone, D. McDonald, G. Hone, J. Goodwin, I.  
707 Carter, K. Basile, I. Sandaradura, S. Maddocks, V. Sintchenko, N. Gilroy, S.  
708 Chen, D. E. Dwyer, M. V. N. O’Sullivan, The Antibody Response to SARS-  
709 CoV-2 Infection. *Open Forum Infect. Dis.* **7**, 1–8 (2020).
- 710 11. B. Demey, N. Daher, C. François, J.-P. Lanoix, G. Duverlie, S. Castelain, E.  
711 Brochot, Dynamic profile for the detection of anti-SARS-CoV-2 antibodies  
712 using four immunochromatographic assays. *J. Infect.* **81**, e6–e10 (2020).
- 713 12. Z. Li, Y. Yi, X. Luo, N. Xiong, Y. Liu, S. Li, R. Sun, Y. Wang, B. Hu, W.  
714 Chen, Y. Zhang, J. Wang, B. Huang, Y. Lin, J. Yang, W. Cai, X. Wang, J.  
715 Cheng, Z. Chen, K. Sun, W. Pan, Z. Zhan, L. Chen, F. Ye, Development and  
716 clinical application of a rapid IgM-IgG combined antibody test for SARS-  
717 CoV-2 infection diagnosis. *J. Med. Virol.* **92**, 1518–1524 (2020).
- 718 13. Y. Li, Z. Wang, X.-X. Xu, S. Song, L. Liu, M. Xin, C. Xu, Rapid,  
719 Ultrasensitive and Highly Specific Biosensor for the Diagnosis of SARS-  
720 CoV-2 in Clinical Blood Samples. *Mater. Chem. Front.* **4**, 2000–2005  
721 (2020).
- 722 14. J. Xiang, M. Yan, H. Li, T. Liu, C. Lin, S. Huang, C. Shen, *medRxiv*, in  
723 press, doi:10.1101/2020.02.27.20028787.
- 724 15. V. M. Corman, O. Landt, M. Kaiser, R. Molenkamp, A. Meijer, D. K. Chu,  
725 T. Bleicker, S. Brünink, J. Schneider, M. Luisa Schmidt, D. GJC Mulders, B.  
726 L. Haagmans, B. van der Veer, S. van den Brink, L. Wijsman, G. Goderski,  
727 J.-L. Romette, J. Ellis, M. Zambon, M. Peiris, H. Goossens, C. Reusken, M.  
728 P. Koopmans, C. Drosten, C. M. Victor, L. Olfert, K. Marco, M. Richard, M.  
729 Adam, C. K. Daniel, B. Tobias, B. Sebastian, S. Julia, S. Marie Luisa, M.  
730 Daphne GJC, H. L. Bart, V. der Veer Bas, V. den Brink Sharon, W. Lisa, G.  
731 Gabriel, R. Jean-Louis, E. Joanna, Z. Maria, P. Malik, G. Herman, R.  
732 Chantal, Detection of 2019 -nCoV by RT-PCR. *Euro Surveill.* **25**, 1–8  
733 (2020).
- 734 16. X. Wang, H. Yao, X. Xu, P. Zhang, M. Zhang, J. Shao, Y. Xiao, H. Wang,  
735 Limits of Detection of 6 Approved RT-PCR Kits for the Novel SARS-  
736 Coronavirus-2 (SARS-CoV-2). *Clin. Chem.* **66**, 977–979 (2020).
- 737 17. D. K. W. Chu, Y. Pan, S. M. S. Cheng, K. P. Y. Hui, P. Krishnan, Y. Liu, D.  
738 Y. M. Ng, C. K. C. Wan, P. Yang, Q. Wang, M. Peiris, L. L. M. Poon,  
739 Molecular Diagnosis of a Novel Coronavirus (2019-nCoV) Causing an  
740 Outbreak of Pneumonia. *Clin. Chem.* **66**, 549–555 (2020).
- 741 18. W. E. Huang, B. Lim, C.-C. Hsu, D. Xiong, W. Wu, Y. Yu, H. Jia, Y. Wang,  
742 Y. Zeng, M. Ji, H. Chang, X. Zhang, H. Wang, Z. Cui, RT-LAMP for rapid  
743 diagnosis of coronavirus SARS-CoV-2. *Microb. Biotechnol.* **13**, 950–961  
744 (2020).

- 745 19. Y. H. Baek, J. Um, K. J. C. Antigua, J.-H. Park, Y. Kim, S. Oh, Y. Kim, W.-  
746 S. Choi, S. G. Kim, J. H. Jeong, B. S. Chin, H. D. G. Nicolas, J.-Y. Ahn, K.  
747 S. Shin, Y. K. Choi, J.-S. Park, M.-S. Song, Development of a reverse  
748 transcription-loop-mediated isothermal amplification as a rapid early-  
749 detection method for novel SARS-CoV-2. *Emerg. Microbes Infect.* **9**, 998–  
750 1007 (2020).
- 751 20. J. S. Chen, E. Ma, L. B. Harrington, M. Da Costa, X. Tian, J. M. Palefsky, J.  
752 A. Doudna, CRISPR-Cas12a target binding unleashes indiscriminate single-  
753 stranded DNase activity. *Science* (80-. ). **360**, 436–439 (2018).
- 754 21. J. P. Broughton, X. Deng, G. Yu, C. L. Fasching, V. Servellita, J. Singh, X.  
755 Miao, J. A. Streithorst, A. Granados, A. Sotomayor-Gonzalez, K. Zorn, A.  
756 Gopez, E. Hsu, W. Gu, S. Miller, C. Y. Pan, H. Guevara, D. A. Wadford, J.  
757 S. Chen, C. Y. Chiu, CRISPR–Cas12-based detection of SARS-CoV-2. *Nat.*  
758 *Biotechnol.* **38**, 870–874 (2020).
- 759 22. T. Hou, W. Zeng, M. Yang, W. Chen, L. Ren, J. Ai, J. Wu, Y. Liao, X. Gou,  
760 Y. Li, X. Wang, H. Su, B. Gu, J. Wang, T. Xu, Development and evaluation  
761 of a rapid CRISPR-based diagnostic for COVID-19. *PLoS Pathog.* **16**, 1–12  
762 (2020).
- 763 23. H. Gremmels, B. M. F. Winkel, R. Schuurman, A. Rosingh, N. A. M. Rigter,  
764 O. Rodriguez, J. Ubijaan, A. M. J. Wensing, M. J. M. Bonten, L. M. Hofstra,  
765 Real-life validation of the Panbio™ COVID-19 antigen rapid test (Abbott) in  
766 community-dwelling subjects with symptoms of potential SARS-CoV-2  
767 infection. *EClinicalMedicine*, 100677 (2020).
- 768 24. A. Scohy, A. Anantharajah, M. Bodéus, B. Kabamba-Mukadi, A. Verroken,  
769 H. Rodriguez-Villalobos, Low performance of rapid antigen detection test as  
770 frontline testing for COVID-19 diagnosis. *J. Clin. Virol.* **129**, 104455 (2020).
- 771 25. Y. Hirotsu, M. Maejima, M. Shibusawa, Y. Nagakubo, K. Hosaka, K.  
772 Amemiya, H. Sueki, M. Hayakawa, H. Mochizuki, T. Tsutsui, Y. Kakizaki,  
773 Y. Miyashita, S. Yagi, S. Kojima, M. Omata, Comparison of automated  
774 SARS-CoV-2 antigen test for COVID-19 infection with quantitative RT-PCR  
775 using 313 nasopharyngeal swabs, including from seven serially followed  
776 patients. *Int. J. Infect. Dis.* **99**, 397–402 (2020).
- 777 26. F. Cerutti, E. Burdino, M. G. Milia, T. Alice, G. Gregori, B. Bruzzone, V.  
778 Ghisetti, Urgent need of rapid tests for SARS CoV-2 antigen detection:  
779 Evaluation of the SD-Biosensor antigen test for SARS-CoV-2. *J. Clin. Virol.*  
780 **132**, 104654 (2020).
- 781 27. F. M. Liotti, G. Menchinelli, E. Lalle, I. Palucci, S. Marchetti, F. Colavita,  
782 M. La Sorda, G. Sberna, L. Bordi, M. Sanguinetti, P. Cattani, M. R.  
783 Capobianchi, B. Posteraro, Performance of a novel diagnostic assay for rapid  
784 SARS-CoV-2 antigen detection in nasopharynx samples. *Clin. Microbiol.*

- 785 *Infect.*, S1198-743X(20)30583–8 (2020).
- 786 28. A. Krüttgen, C. G. Cornelissen, M. Dreher, M. W. Hornef, M. Imöhl, M.  
787 Kleines, Comparison of the SARS-CoV-2 Rapid antigen test to the real star  
788 Sars-CoV-2 RT PCR kit. *J. Virol. Methods*. **288**, 114024 (2021).
- 789 29. A. Berger, M. T. Ngo Nsoga, F. J. Perez-Rodriguez, Y. A. Aad, P. Sattoune-  
790 Roche, A. Gayet-Ageron, C. Jaksic, G. Torriani, E. Boehm, I. Kronig, J. A.  
791 Sacks, M. de Vos, F. J. Bausch, F. Chappuis, L. Kaiser, M. Schibler, I.  
792 Eckerle, *medRxiv*, in press, doi:10.1101/2020.11.20.20235341.
- 793 30. H.-Y. Kim, J.-H. Lee, M. J. Kim, S. C. Park, M. Choi, W. Lee, K. B. Ku, B.  
794 T. Kim, E. Changkyun Park, H. G. Kim, S. Il Kim, Development of a SARS-  
795 CoV-2-specific biosensor for antigen detection using scFv-Fc fusion  
796 proteins. *Biosens. Bioelectron.*, 112868 (2020).
- 797 31. B. D. Grant, C. E. Anderson, J. R. Williford, L. F. Alonzo, V. A. Glukhova,  
798 D. S. Boyle, B. H. Weigl, K. P. Nichols, SARS-CoV-2 Coronavirus  
799 Nucleocapsid Antigen-Detecting Half-Strip Lateral Flow Assay Toward the  
800 Development of Point of Care Tests Using Commercially Available  
801 Reagents. *Anal. Chem.* **92**, 11305–11309 (2020).
- 802 32. G. Guglielmi, Fast coronavirus tests: what they can and can't do. *Nature*.  
803 **585**, 496–498 (2020).
- 804 33. N. Bhalla, Y. Pan, Z. Yang, A. F. Payam, Opportunities and Challenges for  
805 Biosensors and Nanoscale Analytical Tools for Pandemics: COVID-19. *ACS*  
806 *Nano*. **14**, 7783–7807 (2020).
- 807 34. R. Samson, G. R. Navale, M. S. Dharne, Biosensors: frontiers in rapid  
808 detection of COVID-19. *3 Biotech*. **10**, 385 (2020).
- 809 35. M. Asif, M. Ajmal, G. Ashraf, N. Muhammad, A. Aziz, T. Iftikhar, J. Wang,  
810 H. Liu, The role of biosensors in coronavirus disease-2019 outbreak. *Curr.*  
811 *Opin. Electrochem.* **23**, 174–184 (2020).
- 812 36. H. Zhao, F. Liu, W. Xie, T.-C. Zhou, J. OuYang, L. Jin, H. Li, C.-Y. Zhao,  
813 L. Zhang, J. Wei, Y.-P. Zhang, C.-P. Li, Ultrasensitive supersandwich-type  
814 electrochemical sensor for SARS-CoV-2 from the infected COVID-19  
815 patients using a smartphone. *Sensors Actuators B Chem.* **327**, 128899 (2021).
- 816 37. S. Mahari, A. Roberts, D. Shahdeo, S. Gandhi, *bioRxiv*, in press,  
817 doi:10.1101/2020.04.24.059204.
- 818 38. S. Mavrikou, G. Moschopoulou, V. Tsekouras, S. Kintzios, Development of  
819 a Portable, Ultra-Rapid and Ultra-Sensitive Cell-Based Biosensor for the  
820 Direct Detection of the SARS-CoV-2 S1 Spike Protein Antigen. *Sensors*. **20**,  
821 3121 (2020).
- 822 39. S. Kintzios, E. Pistola, P. Panagiotopoulos, M. Bomsel, N. Alexandropoulos,  
823 F. Bem, G. Ekonomou, J. Biselis, R. Levin, Bioelectric recognition assay

- 824 (BERA). *Biosens. Bioelectron.* **16**, 325–336 (2001).
- 825 40. G. Seo, G. Lee, M. J. Kim, S. H. Baek, M. Choi, K. B. Ku, C. S. Lee, S. Jun,  
826 D. Park, H. G. Kim, S. J. Kim, J. O. Lee, B. T. Kim, E. C. Park, S. Il Kim,  
827 Rapid Detection of COVID-19 Causative Virus (SARS-CoV-2) in Human  
828 Nasopharyngeal Swab Specimens Using Field-Effect Transistor-Based  
829 Biosensor. *ACS Nano.* **14**, 5135–5142 (2020).
- 830 41. J.-H. Bong, T.-H. Kim, J. Jung, S. J. Lee, J. S. Sung, C. K. Lee, M.-J. Kang,  
831 H. O. Kim, J.-C. Pyun, Pig Sera-derived Anti-SARS-CoV-2 Antibodies in  
832 Surface Plasmon Resonance Biosensors. *BioChip J.* **14**, 358–368 (2020).
- 833 42. G. Qiu, Z. Gai, Y. Tao, J. Schmitt, G. A. Kullak-Ublick, J. Wang, Dual-  
834 Functional Plasmonic Photothermal Biosensors for Highly Accurate Severe  
835 Acute Respiratory Syndrome Coronavirus 2 Detection. *ACS Nano.* **14**, 5268–  
836 5277 (2020).
- 837 43. P. Moitra, M. Alafeef, K. Dighe, M. B. Frieman, D. Pan, Selective Naked-  
838 Eye Detection of SARS-CoV-2 Mediated by N Gene Targeted Antisense  
839 Oligonucleotide Capped Plasmonic Nanoparticles. *ACS Nano.* **14**, 7617–  
840 7627 (2020).
- 841 44. J. Ladd, Z. Zhang, S. Chen, J. C. Hower, S. Jiang, Zwitterionic Polymers  
842 Exhibiting High Resistance to Nonspecific Protein Adsorption from Human  
843 Serum and Plasma. *Biomacromolecules.* **9**, 1357–1361 (2008).
- 844 45. H. Vaisocherová, W. Yang, Z. Zhang, Z. Cao, G. Cheng, M. Piliarik, J.  
845 Homola, S. Jiang, Ultralow Fouling and Functionalizable Surface Chemistry  
846 Based on a Zwitterionic Polymer Enabling Sensitive and Specific Protein  
847 Detection in Undiluted Blood Plasma. *Anal. Chem.* **80**, 7894–7901 (2008).
- 848 46. H. Vaisocherová-Lísalová, F. Surman, I. Víšová, M. Vala, T. Špringer, M. L.  
849 Ermini, H. Šípová, P. Šedivák, M. Houska, T. Riedel, O. Pop-Georgievski, E.  
850 Brynda, J. Homola, Copolymer Brush-Based Ultralow-Fouling  
851 Biorecognition Surface Platform for Food Safety. *Anal. Chem.* **88**, 10533–  
852 10539 (2016).
- 853 47. I. Víšová, B. Smolková, M. Uzhytchak, M. Vrabcová, D. E. Chafai, M.  
854 Houska, M. Pastucha, P. Skládal, Z. Farka, A. Dejneka, H. Vaisocherová-  
855 Lísalová, Functionalizable Antifouling Coatings as Tunable Platforms for the  
856 Stress-Driven Manipulation of Living Cell Machinery. *Biomolecules.* **10**  
857 (2020), , doi:10.3390/biom10081146.
- 858 48. L. M. Pandey, Design of engineered surfaces for prospective detection of  
859 SARS-CoV-2 using quartz crystal microbalance-based techniques. *Expert*  
860 *Rev. Proteomics.* **17**, 425–432 (2020).
- 861 49. F. Salam, Y. Uludag, I. E. Tohill, Real-time and sensitive detection of  
862 *Salmonella Typhimurium* using an automated quartz crystal microbalance

- 863 (QCM) instrument with nanoparticles amplification. *Talanta*. **115**, 761–767  
864 (2013).
- 865 50. X.-L. Su, Y. Li, A QCM immunosensor for Salmonella detection with  
866 simultaneous measurements of resonant frequency and motional resistance.  
867 *Biosens. Bioelectron.* **21**, 840–848 (2005).
- 868 51. F. Liu, Y. Li, X.-L. Su, M. F. Slavik, Y. Ying, J. Wang, QCM immunosensor  
869 with nanoparticle amplification for detection of Escherichia coli O157:H7.  
870 *Sens. Instrum. Food Qual. Saf.* **1**, 161–168 (2007).
- 871 52. X. Guo, C.-S. Lin, S.-H. Chen, R. Ye, V. C. H. Wu, A piezoelectric  
872 immunosensor for specific capture and enrichment of viable pathogens by  
873 quartz crystal microbalance sensor, followed by detection with antibody-  
874 functionalized gold nanoparticles. *Biosens. Bioelectron.* **38**, 177–183 (2012).
- 875 53. R. Wang, Y. Li, Hydrogel based QCM aptasensor for detection of avian  
876 influenza virus. *Biosens. Bioelectron.* **42**, 148–155 (2013).
- 877 54. T. M. Peduru Hewa, G. A. Tannock, D. E. Mainwaring, S. Harrison, J. V  
878 Fecondo, The detection of influenza A and B viruses in clinical specimens  
879 using a quartz crystal microbalance. *J. Virol. Methods.* **162**, 14–21 (2009).
- 880 55. B. Zuo, S. Li, Z. Guo, J. Zhang, C. Chen, Piezoelectric Immunosensor for  
881 SARS-Associated Coronavirus in Sputum. *Anal. Chem.* **76**, 3536–3540  
882 (2004).
- 883 56. A. Karczmarczyk, K. Haupt, K.-H. Feller, Development of a QCM-D  
884 biosensor for Ochratoxin A detection in red wine. *Talanta*. **166**, 193–197  
885 (2017).
- 886 57. Ş. Ş. Pirinçci, Ö. Ertekin, D. E. Laguna, F. Ş. Özen, Z. Z. Öztürk, S. Öztürk,  
887 Label-free QCM immunosensor for the detection of ochratoxin A. *Sensors*.  
888 **18**, 1161 (2018).
- 889 58. R. Wölfel, V. M. Corman, W. Guggemos, M. Seilmaier, S. Zange, M. A.  
890 Müller, D. Niemeyer, T. C. Jones, P. Vollmar, C. Rothe, M. Hoelscher, T.  
891 Bleicker, S. Brünink, J. Schneider, R. Ehmann, K. Zwirgmaier, C. Drosten,  
892 C. Wendtner, Virological assessment of hospitalized patients with COVID-  
893 2019. *Nature*. **581**, 465–469 (2020).
- 894 59. L. D. Blackman, P. A. Gunatillake, P. Cass, K. E. S. Locock, An introduction  
895 to zwitterionic polymer behavior and applications in solution and at surfaces.  
896 *Chem. Soc. Rev.* **48**, 757–770 (2019).
- 897 60. I. Víšová, M. Vrabcová, M. Forinová, Y. Zhigunová, V. Mironov, M.  
898 Houska, E. Bittrich, K.-J. Eichhorn, H. Hashim, P. Schovánek, A. Dejneka,  
899 H. Vaisocherová-Lísalová, Surface Preconditioning Influences the  
900 Antifouling Capabilities of Zwitterionic and Nonionic Polymer Brushes.  
901 *Langmuir*. **36** (2020), doi:10.1021/acs.langmuir.0c00996.

- 902 61. J. Bullard, K. Dust, D. Funk, J. E. Strong, D. Alexander, L. Garnett, C.  
903 Boodman, A. Bello, A. Hedley, Z. Schiffman, K. Doan, N. Bastien, Y. Li, P.  
904 G. Van Caesele, G. Poliquin, Predicting Infectious Severe Acute  
905 Respiratory Syndrome Coronavirus 2 From Diagnostic Samples. *Clin. Infect.*  
906 *Dis.*, 1–4 (2020).
- 907 62. O. Vandenberg, D. Martiny, O. Rochas, A. van Belkum, Z. Kozlakidis,  
908 Considerations for diagnostic COVID-19 tests. *Nat. Rev. Microbiol.*, 1–13  
909 (2020).
- 910 63. T. Ai, Z. Yang, H. Hou, C. Zhan, C. Chen, W. Lv, Q. Tao, Z. Sun, L. Xia,  
911 Correlation of Chest CT and RT-PCR Testing for Coronavirus Disease 2019  
912 (COVID-19) in China: A Report of 1014 Cases. *Radiology*. **296**, E32–E40  
913 (2020).
- 914 64. T. C. Kwee, R. M. Kwee, Chest CT in COVID-19: What the Radiologist  
915 Needs to Know. *RadioGraphics*. **40**, 1848–1865 (2020).
- 916 65. X. Lu, L. Wang, S. K. Sakthivel, B. Whitaker, J. Murray, S. Kamili, B.  
917 Lynch, L. Malapati, S. A. Burke, J. Harcourt, A. Tamin, N. J. Thornburg, J.  
918 M. Villanueva, S. Lindstrom, US CDC real-time reverse transcription PCR  
919 panel for detection of severe acute respiratory syndrome Coronavirus 2.  
920 *Emerg. Infect. Dis.* **26**, 1654–1665 (2020).
- 921 66. A. K. Nalla, A. M. Casto, A. M. Casto, M. L. W. Huang, G. A. Perchetti, R.  
922 Sampoleo, L. Shrestha, Y. Wei, H. Zhu, K. R. Jerome, K. R. Jerome, A. L.  
923 Greninger, Comparative performance of SARS-CoV-2 detection assays using  
924 seven different primer-probe sets and one assay kit. *J. Clin. Microbiol.* **58**, 1–  
925 6 (2020).
- 926 67. C. B. F. Vogels, A. F. Brito, A. L. Wyllie, J. R. Fauver, I. M. Ott, C. C.  
927 Kalinich, M. E. Petrone, A. Casanovas-Massana, M. Catherine Muenker, A.  
928 J. Moore, J. Klein, P. Lu, A. Lu-Culligan, X. Jiang, D. J. Kim, E. Kudo, T.  
929 Mao, M. Moriyama, J. E. Oh, A. Park, J. Silva, E. Song, T. Takahashi, M.  
930 Taura, M. Tokuyama, A. Venkataraman, O. El Weizman, P. Wong, Y. Yang,  
931 N. R. Cheemarla, E. B. White, S. Lapidus, R. Earnest, B. Geng, P.  
932 Vijayakumar, C. Odio, J. Fournier, S. Bermejo, S. Farhadian, C. S. Dela  
933 Cruz, A. Iwasaki, A. I. Ko, M. L. Landry, E. F. Foxman, N. D. Grubaugh,  
934 Analytical sensitivity and efficiency comparisons of SARS-CoV-2 RT-qPCR  
935 primer-probe sets. *Nat. Microbiol.* **5**, 1299–1305 (2020).
- 936 68. R. Weissleder, H. Lee, J. Ko, M. J. Pittet, COVID-19 diagnostics in context.  
937 *Sci. Transl. Med.* **12**, 1–7 (2020).
- 938 69. S. Woloshin, N. Patel, A. S. Kesselheim, *N. Engl. J. Med.*, in press,  
939 doi:10.1056/nejmp2015897.
- 940 70. C. Chirathaworn, M. Sripramote, P. Chalongsiriyaalert, S. Jirajariyavej, P.  
941 Kiatpanabhikul, J. Saiyarin, C. Soudon, O. Thienfaidee, T. P. N. Ayuthaya,

- 942 C. Brukesawan, D. Chaiwanichsiri, D. Intharasongkroh, N. Wanlapakorn, J.  
943 Chansaenroj, J. Puenpa, R. Yorsaeng, A. Thitithanyanont, R. Kitphati, A.  
944 Mungaomklang, P. Nagavajara, Y. Poovorawan, SARS-CoV-2 RNA  
945 shedding in recovered COVID-19 cases and the presence of antibodies  
946 against SARS-CoV-2 in recovered COVID-19 cases and close contacts,  
947 Thailand, April-June 2020. *PLoS One*. **15**, 1–11 (2020).
- 948 71. Q. Li, X.-S. Zheng, X.-R. Shen, H.-R. Si, X. Wang, Q. Wang, B. Li, W.  
949 Zhang, Y. Zhu, R.-D. Jiang, K. Zhao, H. Wang, Z.-L. Shi, H.-L. Zhang, R.-  
950 H. Du, P. Zhou, Prolonged shedding of severe acute respiratory syndrome  
951 coronavirus 2 in patients with COVID-19. *Emerg. Microbes Infect.*, 1–28  
952 (2020).
- 953 72. P. Vetter, C. S. Eberhardt, B. Meyer, P. A. Martinez Murillo, G. Torriani, F.  
954 Pigny, S. Lemeille, S. Cordey, F. Laubscher, D.-L. Vu, A. Calame, M.  
955 Schibler, F. Jacqueroiz, G. Blanchard-Rohner, C.-A. Siegrist, L. Kaiser, A.  
956 M. Didierlaurent, I. Eckerle, Daily Viral Kinetics and Innate and Adaptive  
957 Immune Response Assessment in COVID-19: a Case Series. *Msphere*. **5**, 1–  
958 35 (2020).
- 959 73. R. Wölfel, V. M. Corman, W. Guggemos, M. Seilmaier, S. Zange, M. A.  
960 Müller, D. Niemeyer, T. C. Jones, P. Vollmar, C. Rothe, M. Hoelscher, T.  
961 Bleicker, S. Brünink, J. Schneider, R. Ehmann, K. Zwirgmaier, C. Drosten,  
962 C. Wendtner, Virological assessment of hospitalized patients with COVID-  
963 2019. *Nature*. **581**, 465–469 (2020).
- 964 74. V. A. Avanzato, M. J. Matson, S. N. Seifert, R. Pryce, B. N. Williamson, S.  
965 L. Anzick, K. Barbian, S. D. Judson, E. R. Fischer, C. Martens, T. A.  
966 Bowden, E. de Wit, F. X. Riedo, V. J. Munster, Case Study: Prolonged  
967 Infectious SARS-CoV-2 Shedding from an Asymptomatic  
968 Immunocompromised Individual with Cancer. *Cell*, 1–12 (2020).
- 969 75. G. C. Mak, P. K. Cheng, S. S. Lau, K. K. Wong, C. S. Lau, E. T. Lam, R. C.  
970 Chan, D. N. Tsang, Evaluation of rapid antigen test for detection of SARS-  
971 CoV-2 virus. *J. Clin. Virol.* **129**, 104500 (2020).
- 972 76. L. Porte, P. Legarraga, V. Vollrath, X. Aguilera, Since January 2020 Elsevier  
973 has created a COVID-19 resource centre with free information in English and  
974 Mandarin on the novel coronavirus COVID- 19 . The COVID-19 resource  
975 centre is hosted on Elsevier Connect , the company ’ s public news and  
976 information. *Int. J. Infect. Dis.* **99**, 328–333 (2020).
- 977 77. T. Weitzel, P. Legarraga, M. Iruretagoyena, G. Pizarro, V. Vollrath, L. Porte,  
978 R. Araos, J. M. Munita, Comparative evaluation of four rapid SARS-CoV-2  
979 antigen detection tests using universal transport medium. *Travel Med. Infect.*  
980 *Dis.* **Dec 2**, 328–333 (2020).
- 981 78. A. D. Davidson, M. K. Williamson, S. Lewis, D. Shoemark, M. W. Carroll,

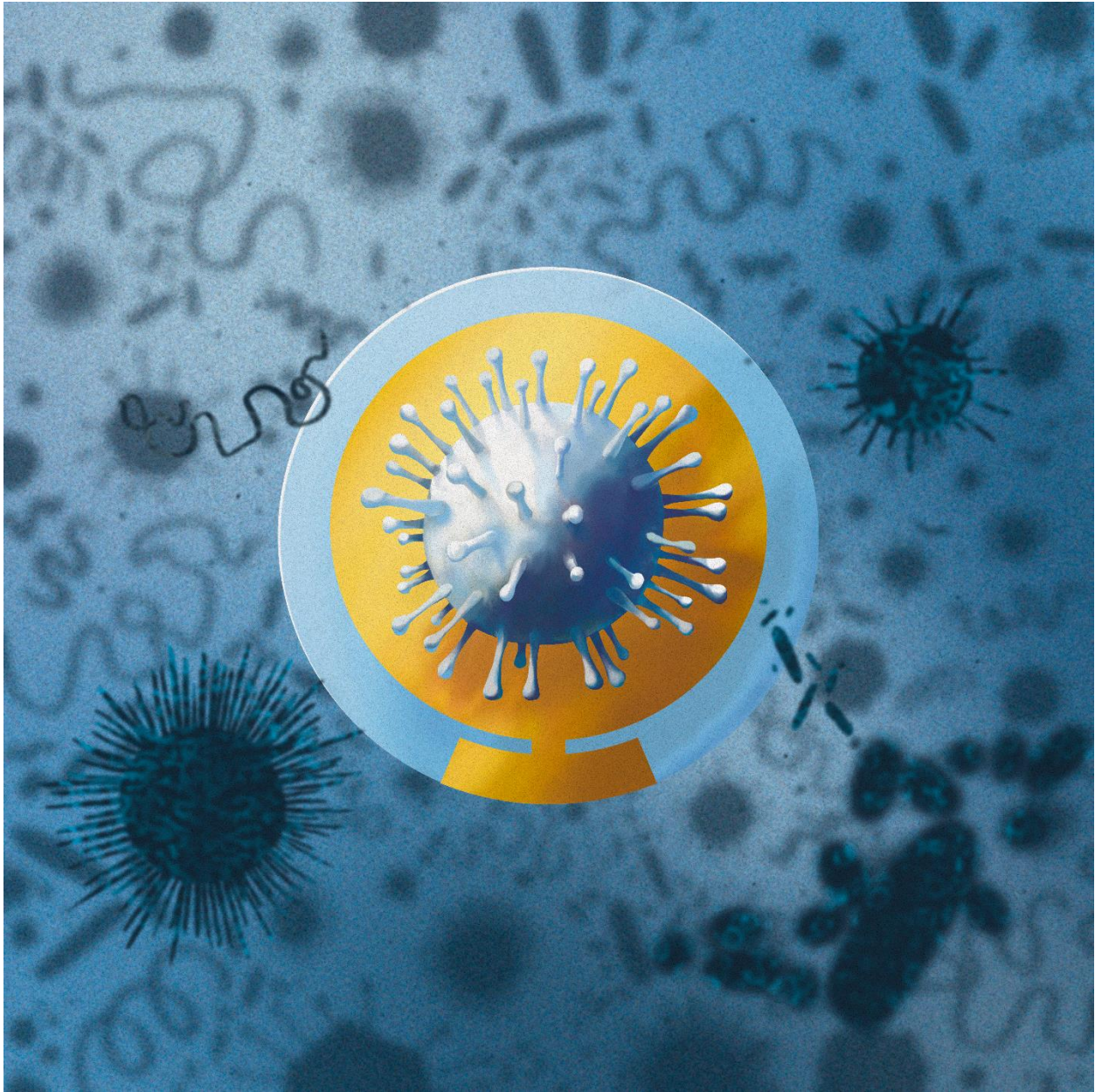


- 982 K. J. Heesom, M. Zambon, J. Ellis, P. A. Lewis, J. A. Hiscox, D. A.  
983 Matthews, Characterisation of the transcriptome and proteome of SARS-  
984 CoV-2 reveals a cell passage induced in-frame deletion of the furin-like  
985 cleavage site from the spike glycoprotein. *Genome Med.* **12**, 1–15 (2020).
- 986 79. D. Kim, J. Y. Lee, J. S. Yang, J. W. Kim, V. N. Kim, H. Chang, The  
987 Architecture of SARS-CoV-2 Transcriptome. *Cell.* **181**, 914-921.e10 (2020).
- 988 80. D. Bojkova, K. Klann, B. Koch, M. Widera, D. Krause, S. Ciesek, J. Cinatl,  
989 C. Münch, Proteomics of SARS-CoV-2-infected host cells reveals therapy  
990 targets. *Nature.* **583**, 469–472 (2020).
- 991 81. L. Grenga, F. Gallais, O. Pible, J. C. Gaillard, D. Gouveia, H. Batina, N.  
992 Bazaline, S. Ruat, K. Culotta, G. Miotello, S. Debroas, M. A. Roncato, G.  
993 Steinmetz, C. Foissard, A. Desplan, B. Alpha-Bazin, C. Almunia, F. Gas, L.  
994 Bellanger, J. Armengaud, Shotgun proteomics analysis of SARS-CoV-2-  
995 infected cells and how it can optimize whole viral particle antigen production  
996 for vaccines. *Emerg. Microbes Infect.* **9**, 1712–1721 (2020).
- 997 82. W. Zeng, G. Liu, H. Ma, D. Zhao, Y. Yang, M. Liu, A. Mohammed, C.  
998 Zhao, Y. Yang, J. Xie, C. Ding, X. Ma, J. Weng, Y. Gao, H. He, T. Jin,  
999 Biochemical characterization of SARS-CoV-2 nucleocapsid protein.  
1000 *Biochem. Biophys. Res. Commun.* **527**, 618–623 (2020).
- 1001 83. K. Razzini, M. Castrica, L. Menchetti, L. Maggi, L. Negroni, N. V Orfeo, A.  
1002 Pizzoccheri, M. Stocco, S. Muttini, C. M. Balzaretto, SARS-CoV-2 RNA  
1003 detection in the air and on surfaces in the COVID-19 ward of a hospital in  
1004 Milan, Italy. *Sci. Total Environ.* **742**, 140540 (2020).
- 1005 84. S. Westhaus, F.-A. Weber, S. Schiwiy, V. Linnemann, M. Brinkmann, M.  
1006 Widera, C. Greve, A. Janke, H. Hollert, T. Wintgens, S. Ciesek, Detection of  
1007 SARS-CoV-2 in raw and treated wastewater in Germany – Suitability for  
1008 COVID-19 surveillance and potential transmission risks. *Sci. Total Environ.*  
1009 **751**, 141750 (2021).
- 1010 85. N. van Doremalen, T. Bushmaker, D. H. Morris, M. G. Holbrook, A.  
1011 Gamble, B. N. Williamson, A. Tamin, J. L. Harcourt, N. J. Thornburg, S. I.  
1012 Gerber, J. O. Lloyd-Smith, E. de Wit, V. J. Munster, Aerosol and Surface  
1013 Stability of SARS-CoV-2 as Compared with SARS-CoV-1. *N. Engl. J. Med.*  
1014 **382**, 1564–1567 (2020).
- 1015 86. I. Víšová, B. Smolková, M. Uzhytchak, M. Vrabcová, Y. Zhigunova, M.  
1016 Houska, F. Surman, A. de los Santos Pereira, O. Lunov, A. Dejneka, H.  
1017 Vaisocherová-Lísalová, Modulation of Living Cell Behavior with Ultra-Low  
1018 Fouling Polymer Brush Interfaces. *Macromol. Biosci.* **20**, 1–9 (2020).
- 1019 87. H. Vaisocherová, V. Ševců, P. Adam, B. Špačková, K. Hegnerová, A. de los  
1020 Santos Pereira, C. Rodriguez-Emmenegger, T. Riedel, M. Houska, E.  
1021 Brynda, J. Homola, Functionalized ultra-low fouling carboxy- and hydroxy-

- 1022 functional surface platforms: functionalization capacity, biorecognition  
1023 capability and resistance to fouling from undiluted biological media. *Biosens.*  
1024 *Bioelectron.* **51**, 150–157 (2014).
- 1025 88. J.-W. Jian, H.-S. Chen, Y.-K. Chiu, H.-P. Peng, C.-P. Tung, I.-C. Chen, C.-  
1026 M. Yu, Y.-L. Tsou, W.-Y. Kuo, H.-J. Hsu, A.-S. Yang, Effective binding to  
1027 protein antigens by antibodies from antibody libraries designed with  
1028 enhanced protein recognition propensities. *MAbs.* **11**, 373–387 (2019).
- 1029 89. H.-S. Chen, S.-C. Hou, J.-W. Jian, K.-S. Goh, S.-T. Shen, Y.-C. Lee, J.-J.  
1030 You, H.-P. Peng, W.-C. Kuo, S.-T. Chen, M.-C. Peng, A. H.-J. Wang, C.-M.  
1031 Yu, I.-C. Chen, C.-P. Tung, T.-H. Chen, K. Ping Chiu, C. Ma, C. Yuan Wu,  
1032 S.-W. Lin, A.-S. Yang, Predominant structural configuration of natural  
1033 antibody repertoires enables potent antibody responses against protein  
1034 antigens. *Sci. Rep.* **5**, 12411 (2015).
- 1035 90. S.-C. Hou, H.-S. Chen, H.-W. Lin, W.-T. Chao, Y.-S. Chen, C.-Y. Fu, C.-M.  
1036 Yu, K.-F. Huang, A. H.-J. Wang, A.-S. Yang, High throughput cytotoxicity  
1037 screening of anti-HER2 immunotoxins conjugated with antibody fragments  
1038 from phage-displayed synthetic antibody libraries. *Sci. Rep.* **6**, 31878 (2016).
- 1039 91. C.-P. Tung, I.-C. Chen, C.-M. Yu, H.-P. Peng, J.-W. Jian, S.-H. Ma, Y.-C.  
1040 Lee, J.-T. Jan, A.-S. Yang, Discovering neutralizing antibodies targeting the  
1041 stem epitope of H1N1 influenza hemagglutinin with synthetic phage-  
1042 displayed antibody libraries. *Sci. Rep.* **5**, 15053 (2015).
- 1043 92. A. T. De Madrid, J. S. Porterfield, A simple micro-culture method for the  
1044 study of group B arboviruses. *Bull. World Health Organ.* **40**, 113–121  
1045 (1969).
- 1046 93. Zybionics Inc., “Nucleic Acid Extraction Kit Handbook” (2020), (available at  
1047 <http://www.poctservices.com/uploads/biker/130f140fa034e9c9b3b61f2f610f40e5.pdf>).  
1048
- 1049 94. Seegene Inc., “Allplex™ 2019-nCoV Assay” (2020), (available at  
1050 [http://www.seegene.com/upload/product/IFU\\_FDA\\_COVID19\\_Seegene.pdf](http://www.seegene.com/upload/product/IFU_FDA_COVID19_Seegene.pdf))  
1051 .
- 1052 95. M. R. Alexander, C. L. Rootes, P. J. van Vuren, C. R. Stewart, Concentration  
1053 of infectious SARS-CoV-2 by polyethylene glycol precipitation. *J. Virol.*  
1054 *Methods.* **286**, 113977 (2020).
- 1055 96. D. Wessel, U. I. Flügge, A method for the quantitative recovery of protein in  
1056 dilute solution in the presence of detergents and lipids. *Anal. Biochem.* **138**,  
1057 141–143 (1984).

1058

1059 **TOC**



1060  
1061

# Appendix XIII

H. Lísalová, E. Brynda, I. Víšová, X. Song Chadtová, K. Mrkvová, F. Surman, M.

Riedel, M. Houska, E. Brynda, J. Homola

**Způsob přípravy povrchu substrátu obsahujícího karboxybetainové  
funkční skupiny**

Patent application (CZ) PV 2016-361 filed in 6/2016, approved 10/2017

# PŘIHLÁŠKA VYNÁLEZU

Zveřejněná podle §31 zákona č. 527/1990 Sb.

(21) Číslo dokumentu:

## 2016-361

(13) Druh dokumentu: **A3**

(51) Int. Cl.:

*C08F 292/00* (2006.01)  
*C08F 20/58* (2006.01)  
*C08F 20/60* (2006.01)  
*C08F 8/30* (2006.01)  
*C07C 231/02* (2006.01)  
*G01N 33/483* (2006.01)  
*G01N 33/543* (2006.01)

(19)  
ČESKÁ  
REPUBLIKA



ÚŘAD  
PRŮMYSLOVÉHO  
VLASTNICTVÍ

(22) Přihlášeno: **17.06.2016**

(40) Datum zveřejnění přihlášky vynálezu: **22.11.2017**  
(Věstník č. 47/2017)

(71) Přihlašovatel:  
Ústav fotoniky a elektroniky AV ČR, v. v. i., Praha  
8, Kobylisy, CZ  
Ústav makromolekulární chemie AV ČR, v. v. i.,  
Praha 6, Břevnov, CZ

(72) Původce:  
RNDr. Hana Lísalová, Ph.D., Praha 8, CZ  
RNDr. Eduard Brynda, CSc., Praha 2, CZ  
Mgr. Ivana Víšová, Česká Třebová, CZ  
Ing. Milan Houska, CSc., Praha 5, CZ  
Ing. František Surman, Velké Pavlovice, CZ  
Mgr. Kateřina Mrkvová, Praha 5, CZ  
dipl. Ing. Xue Chadtová Song, Praha 9, CZ  
prof. Ing. Jiří Homola, CSc., DSc., Praha 10, CZ

(74) Zástupce:  
INVENTIA s.r.o., RNDr. Kateřina Hartvichová, Na  
Bělidle 3, 150 00 Praha 5

(54) Název přihlášky vynálezu:

**Způsob přípravy povrchu substrátu  
obsahujícího karboxybetainové funkční  
skupiny**

(57) Anotace:

Předkládané řešení se týká způsobu přípravy povrchu substrátu obsahujícího karboxybetainové funkční skupiny s navázanými bioaktivními látkami a majícího rezistenci proti nežádoucí depozici složek biologických médií na povrchu substrátu, obsahujícího kroky chemické aktivace karboxybetainových funkčních skupin na povrchu substrátu převedením karboxylátové složky karboxybetainu na aktivní ester, kovalentního navázání bioaktivní látky na část aktivních esterů a podrobení produktu z předchozího kroku reakci s kyselinou (2-aminoethoxy)octovou, přičemž s kyselinou (2-aminoethoxy)octovou reagují aktivní estery, na nichž nedošlo ke kovalentnímu navázání bioaktivní látky.

CZ 2016 - 361 A3

~~10.10.16~~

PV 2016-361

PV 361-2016

## Způsob přípravy povrchu substrátu obsahujícího karboxybetainové funkční skupiny

### Oblast techniky

Vynález se týká způsobu přípravy povrchu substrátu obsahujícího karboxybetainové funkční skupiny s navázanými bioaktivními látkami, která zvyšuje rezistenci povrchu proti nežádoucí biologické depozici při kontaktu s biologickými médii.

### Dosavadní stav techniky

Při styku prakticky všech běžných materiálů s biologickým médiem dochází na jejich povrchu k biologické depozici, tzv. „fouling“, začínající adsorpcí biologických molekul, hlavně proteinů, na které podle složení daného média mohou adherovat buňky a mikroorganismy následované dalšími biologickými procesy, jako je koagulace krve, zánětlivé a imunitní reakce nebo tvorba bakteriálních biofilmů. Výsledné biologické depozity mohou zhoršovat funkci materiálů a zařízení, která pracují v biologických médiích, jako jsou tělní tekutiny, média obsahující buňky, potraviny a média z biologických výrob a z biologického prostředí obecně. Problém je zvláště kritický pro materiály používané v kontaktu s krevním sérem, plasmou nebo krví. Proto jsou povrchy, které v biologických médiích brání nespecifické tvorbě biologických depozitů a současně umožňují navázání bioaktivních prvků zprostředkujících specifickou interakci povrchu s cílovými složkami biologického prostředí, velmi důležité pro mnoho biotechnologických a lékařských aplikací, např. jako biosenzory, membrány a částice pro separaci a akumulaci biologických látek a buněk, nosiče léčiv a diagnostické částice aplikované do krevního oběhu, materiály přicházející do kontaktu s krví a nosiče buněk, tzv. scaffolds, pro tkáňové inženýrství.

Za nejvíce odolné proti biologické depozici (tzv. „antifouling“) jsou v současné době považovány povrchy připravené roubováním hydrofilních elektroneutrálních polymerů, jako jsou neionogenní poly(oligo(hydroxyethylen glykol) methakrylát) (polyHOEGMA), poly(2-hydroxyethyl methakrylát) (polyHEMA), poly(3-hydroxypropyl methakrylát) (polyHPMA), poly(N-(2-hydroxypropyl) methakrylamid) (polyHPMAA) a zwitteriontové poly(karboxybetain methakrylát) (polyCBMA) a poly(karboxybetain akrylamid) (polyCBAA), z povrchu substrátů (tzv. „grafting from“) pomocí povrchem iniciované radikálové polymerizace s přenosem atomu (SI ATRP). Výsledný kartáč polymerních řetězců, tzv. „polymer brush“, je vrstva hustě uspořádaných polymerních řetězců navázaných jedním koncem k povrchu. Kartáče z

polyCBAA, polyCBMA a polyHPMAA jako jediné účinně potlačují i depozici z neředěné krevní plasmy a séra.

Alternativní metodou je připojení polymerních řetězců připravených polymerací v roztoku k povrchu (tzv. „grafting to“). Menší hustota polymerních řetězců dosahovaná v kartáčích připravených touto metodou oproti kartáčům připraveným metodou „grafting from“ poskytuje povrchu slabší odolnost proti biologické depozici.

Ještě slabší odolnost zejména proti depozici z krevní plasmy a séra poskytují často používané vrstvy karboxymetyldextranu nebo povlaky ze samoorganizovaných monovrstev (SAMs) ze směsi molekul  $(\text{CH}_2)_{11}(\text{EO})_4$  a  $(\text{CH}_2)_{11}(\text{EO})_6\text{OOH}$ , kde EO je ethylenoxid, jejichž povrch je tvořen hustě uspořádanými oligoethylenoxidy obsahujícími v některých pozicích karboxylové skupiny používané pro navázání bioaktivních látek.

Pro navázání bioaktivních látek na neionogenní polymerní řetězce je používána aktivace hydroxylových skupin v jejich postranních řetězcích. Zbytkové produkty této aktivace, které zůstávají na polymerech po navázání bioaktivních látek, do velké míry zhoršují odolnost kartáčů proti biologické depozici. Povrchy s požadovanou biologickou aktivitou a lepší odolností proti depozici byly připraveny navázáním bioaktivních látek na kartáče z polyCBMA nebo polyCBAA, mající karboxybetainové zwitterionty jako postranní skupiny polymerních řetězců. Kartáče z polyCBMA a polyCBAA s bioaktivními látkami navázanými na karboxybetainové postranní skupiny polymerů jsou zahrnuty mimo jiné v dokumentech US20140370567 a US20130244249. Patentová přihláška PV 2015-313 popisuje kartáče z poly(HPMAA-co-CBMAA) roubované kopolymerizací monomerů HPMAA a karboxybetainakrylamidu (CBMAA) z povrchu různých substrátů včetně polymerních nanočástic a navázání bioaktivních látek na jejich aktivované karboxybetainové skupiny. PCT/CZ2016/050011, která navazuje na PV 2015-313, zahrnuje i přípravu kartáčů z poly(HPMAA-co-CBMAA) připravených polymerací v roztoku a kovalentně roubovaných na povrch substrátu. Ke stavu techniky patří i hydrogely z kopolymerů poly(HEMA-co-CBMAA) odolné proti biologické depozici (Kostina, et al., Biomacromolecules 2012, 13, 4164–4170) nebo sorbenty, jejichž povrch je modifikován připojením karboxybetainových zwitteriontů (WO2014165421 A1).

Bioaktivní látky obsahující jednu nebo více aminoskupin se na karboxybetainové skupiny navazují prakticky výhradně reakcí s karboxylem karboxybetainového zwitteriontu, který se

napřed aktivuje na meziprodukt snadno reagující s nukleofilní aminoskupinou navazované bioaktivní látky. Tato aktivace se provádí převážně reakcí s různými N-substituovanými karbodiimidy (DCI) za vzniku aktivního esteru O-acylisolurey<sup>močoviny</sup>. Tento meziprodukt však má ve vodném prostředí extrémně nízkou životnost a rychle se hydrolyzuje, takže vazebná reakce s aminoskupinou má nedostatečný výtěžek. Z tohoto důvodu se reakce provádí v přítomnosti N-hydroxysukcinimidu (NHS) nebo jeho derivátů, který rychle reaguje s O-acylisolureou<sup>močovinou</sup> za vzniku aktivního NHS-esteru. NHS-ester má vyšší reaktivitu vůči aminoskupině než O-acylisolurea<sup>močovina</sup> a je stabilnější vůči hydrolyze, takže se lépe dosahuje požadovaného výtěžku. Reakce NHS-aktivního esteru i O-acylisolurey<sup>močoviny</sup> s aminoskupinou vede v obou případech ke stejné vazbě bioaktivní látky na karboxybetainovou skupinu amidickou vazbou.

Nezreagované NHS-aktivní estery vytvořené aktivací 1-ethyl-3-(3-dimethylaminopropyl)karbodiimid/N-hydroxysukcinimidem (EDC/NHS) pouze karboxylových skupin (nikoli karboxybetainů), např. na povrchu výše zmíněných SAMs, se ve vodném prostředí samovolně hydrolyzují zpět na karboxylové skupiny. Deaktivace NHS-aktivních esterů zlepšuje odolnost povrchu vůči depozici biologických látek, proto je často pro lepší zajištění deaktivace aktivních esterů, zbylých po navázání bioaktivních substancí na karboxylové skupiny v SAMs nebo karboxymethyldextranu, používána inkubace s roztokem ethanolaminu (US 5561069 A). Popsána byla také deaktivace aldehydových skupin na modifikovaném polyethylenglykolu, PEG-CH=O, reakcí s ethanolaminem a glycinem (Wildling et al. Bioconjugate Chem. 2011, 22, 1239–1248), nicméně deaktivace glycinem vedla v porovnání s ethanolaminem ke zvýšení nespecifické depozice, zřejmě v důsledku zavedení nadbytečného náboje karboxylu.

Přestože se obecně předpokládalo, že meziprodukty O-acylisolurey<sup>močovina</sup> i NHS-aktivní estery, které nezreagovaly s aminoskupinou, se po vazebné reakci mohou kvantitativně hydrolyzovat zpět na karboxylové skupiny, k regeneraci karboxylových skupin karboxybetainových zwitteriontů po aktivaci metodou DCI/NHS samovolnou hydrolyzou nedochází. Naše studie založené na reflexní IČ spektroskopii ukázaly, že v případě po aktivaci karboxybetainů reakcí s 1-ethyl-3-(3-dimethylaminopropyl)karbodiimidem (EDC), který je nejčastěji používaným DCI, a NHS nedochází ke kvantitativní regeneraci karboxylových skupin, a to ani dlouhodobým působením vodných roztoků s různým složením elektrolytů, iontovou silou a pH.

Vzhledem k míře a šíři použití karboxybetainových skupin pro navázání biologicky aktivních látek na různé povrchy se regenerace nezreagovaných aktivních esterů na molekulu zakončenou



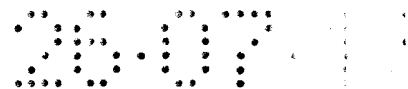
karboxylovou skupinou jeví jako klíčová pro snížení biologické depozice (fouling) na těchto površích.

US 7 943 370 B2 popisuje přípravu povrchu substrátu obsahujícího karboxybetainové skupiny převedením karboxybetainu na aktivní ester, kovalentním navázáním bioaktivní látky a deaktivaci nezreagovaných aktivních esterů pomocí glycinu nebo  $\beta$ -alaninu. Dokumenty Chou Y.-N. a kol., *Acta Biomaterialia* 2016, 40, 31 – 37 a Vaisocherová H. a kol., *Biosensors and Bioelectronics* 2014, 51, 150 – 157 popisují přípravu povrchu substrátu obsahujícího karboxybetainové skupiny převedením karboxybetainu na aktivní ester, kovalentním navázáním bioaktivní látky a deaktivaci nezreagovaných aktivních esterů pomocí glycinu. WO 2009/130 233 A1 popisuje přípravu halogenovaných povrchů s potenciálním obsahem karboxybetainových skupin převedením karboxylové skupiny na aktivní ester, kovalentní navázání bioaktivní látky a deaktivaci nezreagovaných aktivních esterů pomocí glycinu. Vaisocherová H. a kol., *Biosensors and Bioelectronics* 2014, 51, 150 – 157 popisují přípravu povrchu substrátu obsahujícího karboxybetainové skupiny převedením karboxybetainu na aktivní ester, kovalentní navázání bioaktivní látky a deaktivaci nezreagovaných aktivních esterů pomocí glycinu.

### Podstata vynálezu

Předkládaný vynález se týká regenerace aktivních esterů karboxybetainových skupin způsobem přípravy povrchu substrátu, obsahujícího karboxybetainové funkční skupiny, který vede k nahrazení nezreagovaných aktivních esterů, zbylých po navázání bioaktivní látky na některé z aktivovaných karboxybetainových zwitteriontů, kyselinou (2-aminoethoxy)octovou. Části výrobku nebo zařízení, jejichž povrch má vykonávat nějakou aktivní funkci v biologickém médiu, která by mohla být ovlivněna biologickou depozicí, a jejichž povrch obsahuje karboxybetainové skupiny, mohou být z organických i anorganických materiálů, mohou mít libovolnou morfologii, např. částice, membrány, trubky, hadičky, destičky, porézní materiál, sítě vláken, a různé použití v kontaktu s biologickým médiem, např. jako biosenzory, afinitní částice a membrány pro separaci a akumulaci biologických látek, cílené nosiče pro dopravu léčiv, biomateriály pro tkáňové inženýrství, antitrombogenní materiály pro kontakt s krví.

Předkládaný vynález spočívá v tom, že ihned po aktivaci karboxybetainových skupin a navázání biologicky aktivních látek se povrch substrátu inkubuje s roztokem kyseliny (2-aminoethoxy)octové. Během této inkubace koncová aminoskupina této molekuly reaguje s aktivními estery, které nebyly spotřebovány při předchozím navázání biologicky aktivních



látek. Volná karboxylová skupina v části molekuly, která nahradila aktivní ester, vytvoří nový zwitteriont s kationtem kvarterního dusíku zbylým po aktivaci původní karboxylové skupiny. Uvedeným postupem je neutralizována reaktivita zbytkových aktivních esterů a současně kompenzován kladný náboj kationtů kvarterního dusíku a tím opět zvýšena odolnost povrchu proti biologické depozici. Technický efekt způsobu přípravy povrchu substrátu obsahujícího karboxybetainové funkční skupiny se projeví zejména (ale nikoliv pouze) u polymerních kartáčů s vysokou hustotou polymerních řetězců obsahujících karboxybetainové postranní skupiny. Malé molekuly aktivačních reagentů mohou pronikat mezi polymerní řetězce a reagovat s karboxybetainy v celém objemu kartáče, zatímco pro navázání velkých bioaktivních látek, např. proteinů, jsou dostupné pouze karboxybetainy blízko povrchu vrstvy.

Předmětem předkládaného vynálezu je způsob přípravy povrchu substrátu obsahujícího karboxybetainové skupiny, se zvýšenou odolností proti nežádoucí depozici složek biologických médií na povrch substrátu, obsahující kroky:

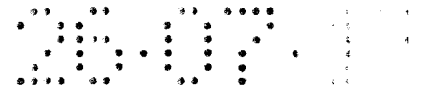
- a) chemická aktivace karboxybetainových skupin na povrchu substrátu převedením karboxylové skupiny karboxybetainu na aktivní ester;
- b) kovalentní navázání bioaktivní látky reakcí její aminoskupiny s aktivním esterem připraveným v kroku a);

příčemž po kroku b) se provede krok c), ve kterém produkt z kroku b) reaguje s kyselinou (2-aminoethoxy)octovou,

kdy s kyselinou (2-aminoethoxy)octovou reagují aktivní estery, na nichž nedošlo v kroku b) ke kovalentnímu navázání bioaktivní látky. S výhodou se krok c) provede při zásaditém pH, výhodněji při pH v rozmezí od 7,5 do 9, nejvýhodněji při pH 8.

Karboxybetainové skupiny mohou být buď přímo součástí materiálu substrátu, nebo mohou být připojeny k povrchu substrátu, např. jako součást molekul naroubovaných na povrch substrátu nebo substrát může být pokryt vrstvou obsahující tyto skupiny, např. polymerním kartáčem připraveným povrchem iniciovanou polymerací z povrchu substrátu (grafting from) nebo připraveným připojením polymerních řetězců připravených polymerací v roztoku k povrchu (grafting to).

Karboxybetainové skupiny jsou odborníkovi v oboru dobře známé a jsou obecně definované jako neutrální chemické skupiny obsahující kvarterní amoniový kationt, který nenesé žádný vodíkový atom, a negativně nabitou karboxylovou skupinu, která nesousedí přímo s kvarterním amoniovým kationtem (IUPAC, Compendium of Chemical Terminology).



Substrátem se pro účely předkládaného vynálezu rozumí objekt, který je odolný proti depozici složek biologických médií, nebo který je třeba pokrýt polymerní vrstvou propůjčující mu odolnost proti depozici složek biologických médií (lze na něj naroubovat polymerní kartáč, nebo na něj lze nanést polymerní povlak).

Substrátem tak může být:

(1) objekt, jehož povrch je pokryt vrstvou polymerního kartáče roubovanou z povrchu (grafting from) živou radikálovou polymerizací, viz PV 2015-313 a <sup>WO 2016/177354</sup> PCT/CZ2016/050011,

(2) objekt, jehož povrch je pokryt vrstvou polymerů připravených v roztoku a následně připojených k povrchu kovalentní vazbou nebo fyzikální adsorpcí (grafting to), viz <sup>WO 2016/177354</sup> PCT/CZ2016/050011,

(3) objekt, jehož povrch je pokryt polymerací iniciovanou radikály vytvořenými chemickou nebo fyzikální aktivací povrchu objektu,

(4) objekt, jehož povrch je povlečen adhezující vrstvou polymerů nanesenou z roztoku (polymerní povlak),

(5) objekt, jehož povrch lze modifikovat navázáním molekuly obsahující karboxybetainové zwitterionty,

(6) objekt, který obsahuje karboxybetainové zwitterionty ve své struktuře, např. polymerní gel, kde některé monomerní jednotky obsahují karboxybetainové zwitterionty.

Polymerní vrstvy vytvořené na objektech (1), (2), (3) a (4) vždy obsahují alespoň jeden homopolymer nebo kopolymer obsahující karboxybetainové zwitterionty v bočních řetězcích. Ve vrstvách na objektech (2) a (4) mohou být polymery obsahující karboxybetainové zwitterionty ve směsi s hydrofilními polymery, s výhodou vybranými z polyHPMAA, polyHOEGMA, polyHEMA, a polyHPMA.

S výhodou jsou vrstvy na objektech (1), (2), (3) a (4) vytvořené z homopolymeru vybraného ze skupiny zahrnující polyCBMAA, polyCBMA a polyCBAA nebo z kopolymeru poly(A-co-B), kde A je monomerní jednotka vybraná ze skupiny obsahující HPMAA, HOEGMA, HEMA, HPMA a B je monomerní jednotka v koncentraci 1 až 99 mol%, vybraná ze skupiny obsahující CBMAA, CBMA, CBAA.

Tvar, rozměry, morfologie a chemická povaha substrátu není rozhodující, může se jednat o planární či různě tvarované objekty, trubice, vlákna, částice, membrány, mikročástice, nanočástice, porézní materiály, kovy, křemík, materiály na bázi křemičitanů či hlinitokřemičitanů (např. sklo), polymery, anorganické materiály, apod.

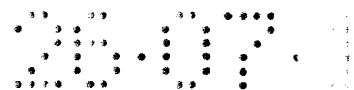
Biologické médium je pro účely předkládaného vynálezu tekutina obsahující biologické látky, tj. biomolekuly a jejich asociáty (proteiny, sacharidy, polysacharidy lipidy, nukleové kyseliny, lipoproteiny, glykoproteiny, organely atd.), viry, buňky, mikroorganismy a jejich fragmenty. Biologickým médiem je tedy např. krev a ostatní tělní tekutiny, krevní plasma a sérum, tkáňové extrakty, buněčné lyzáty a suspense, potravinové extrakty.

Bioaktivní (biologicky aktivní) látkou v předkládaném vynálezu je látka, obsahující alespoň jednu  $\text{NH}_2$  skupinu, selektivně interagující s cílovou složkou biologického média. Bioaktivní látka může mít afinitu k cílové složce, typicky je bioaktivní látkou přírodní protilátka, antigen, lektin a buněčný receptor a jejich umělé analogy a části připravené rekombinantní technikou a syntetické oligopeptidové sekvence, nukleové kyseliny a jejich části a syntetické oligonukleotidové sekvence a aptamery. Bioaktivní látka může katalyzovat chemickou přeměnu cílové látky, např. enzym, koenzym a jejich syntetické analogy. Nebo může bioaktivní látka vyvolávat biologickou odezvu, jako např. antikoagulant, např. heparin, proteiny a oligopeptidové sekvence reagující s buněčnými integriny, růstové faktory, hormony, a deriváty léčiv a vitamínů. Bioaktivními látkami mohou být také například nanočástice funkcionalizované  $\text{NH}_2$  skupinou, zejména kovové, polymerní, silikonové nanočástice, nanočástice na bázi oxidů kovů či polymerní nanočástice s magnetickým jádrem.

Aktivní ester karboxybetainu je produkt reakce karboxylové skupiny karboxybetainu s N-substituovanými karbodiimidy, tj. O-acyl<sup>mocovina</sup>urea, a/nebo produkt reakce karboxylové skupiny karboxybetainu s N-substituovanými karbodiimidy a N-hydroxysukcinimidem (NHS) nebo jeho deriváty, s výhodou je aktivním esterem NHS-ester nebo sulfo NHS-ester.

Ve výhodném provedení se krok c) se provede tak, že se nejprve produkt z kroku b) opláchně pufr, který byl použit jako rozpouštědlo v kroku b), následně se opláchně pufr, který bude použit v následujícím kroku k inkubaci, s výhodou je takovým pufr pufr o pH 8, následně se produkt inkubuje s roztokem kyseliny (2-aminoethoxy)octové v pufru, následně se opláchně pufr předtím použitým k inkubaci, a následně se opláchně roztokem, do kterého je pak vložen pro skladování, nebo vodou a vysuší se.

V jednom provedení jsou karboxybetainové skupiny obsaženy v polymerní vrstvě na povrchu substrátu jako polymerní kartáč, připravený polymerací z povrchu nebo roubováním polymerů



na povrch substrátu, nebo polymerní povlak, s výhodou má tato vrstva tloušťku v rozmezí od 5 nm do 5  $\mu$ m.

Ve výhodném provedení je polymerní vrstvou obsahující karboxybetainové skupiny polymerní kartáč z polyCBMAA, polyCBMA, polyCBAA nebo poly(HPMAA-co-CBMAA/x mol%), kde x (molární koncentrace CBMAA) je v rozmezí od 1 mol% do 99 mol%. S výhodou má tato vrstva tloušťku v rozmezí od 5 nm do 5  $\mu$ m.

V jednom provedení je substrát vybraný ze skupiny zahrnující částice, porézní membrány, nosiče buněk („scaffolds“) a biosenzory.

Částice jsou s výhodou z materiálu vybraného ze skupiny obsahující zlato, stříbro, magnetické materiály, křemík, SiO<sub>2</sub>, polymery, spadají do definice substrátu (1) až (6) a mají s výhodou průměr od 5 nm do 1 mm. Částice s bioaktivními látkami navázanými na aktivované karboxybetainové skupiny na povrchu částic včetně vnitřního povrchu porézních částic jsou aplikovatelné jako nosiče pro cílenou terapii a diagnostiku *in vivo*, separaci a akumulaci biologických látek a enzymatickou katalýzu v bioreaktorech.

Porézní membrány jsou membrány určené pro afinitní separaci biologických látek z biologických médií.

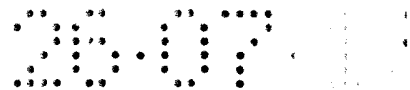
Nosiče buněk („scaffolds“) jsou odborníkovi v oboru dobře známé, jejich využití je např. pro tkáňové inženýrství (viz např.

[http://www.wikiskripta.eu/index.php/Tk%C3%A1%C5%88ov%C3%A9\\_in%C5%BEen%C3%BDrstv%C3%AD](http://www.wikiskripta.eu/index.php/Tk%C3%A1%C5%88ov%C3%A9_in%C5%BEen%C3%BDrstv%C3%AD)).

V jednom provedení je substrátem detekční povrch biosenzoru pro přímou detekci nebo více-stepňovou detekci analytů v komplexních biologických médiích, např. pomocí optických nebo hmotnostních biosenzorů. S výhodou je detekční povrch pokryt polymerním kartáčem z polyCBMAA, polyCBMA, polyCBAA nebo poly(HPMAA-co-CBMAA) s navázanými bioreceptory. Bioreceptory v této aplikaci jsou bioaktivní láky mající selektivní afinitu k cílovým složkám analyzovaného média.

V jednom provedení je substrát určený pro kontakt s krví *in vitro*, *ex vivo* a *in vivo*.

Způsob přípravy povrchu substrátu obsahujícího karboxybetainové skupiny podle předkládaného vynálezu, který má zvýšenou odolnost proti nežádoucí depozici složek biologických médií na



povrch substrátu, poskytuje velmi rychlé, levné a efektivní zmírnění problémů s depozicí nežádoucích složek biologických médií oproti řešením nabízeným v dosavadním stavu techniky.

*uskutečnění*  
Příklady ~~provedení~~ vynálezu

Příklad 1: *Obecný způsob úpravy povrchu substrátu obsahujícího karboxybetainové funkční skupiny*

V kroku (a) dochází k chemické aktivaci přítomných karboxybetainových skupin tím, že se karboxylové skupiny karboxybetainu převedou na aktivní NHS-ester nebo sulfo-NHS-ester reakcí s 1-ethyl-3-(3-dimethylaminopropyl)karbodiimidem (EDC) a N-hydroxysukcinimidem (NHS) nebo sulfo-NHS. V kroku (b) dojde k inkubaci vzorku s roztokem obsahujícím bioaktivní látky (BAL), během které jsou tyto látky kovalentně navázány na některé z aktivních esterů vytvořených v kroku (a). V kroku (c) probíhá reakce těch aktivních NHS-esterů nebo sulfo-NHS-esterů, které nezreagovaly s bioaktivní látkou, s molekulami kyseliny (2-aminoethoxy)octové. V průběhu inkubace vzorku s vodným roztokem kyseliny (2-aminoethoxy)octové jsou tyto molekuly kovalentně navázány na povrch stálou amidickou vazbou.

Příklad 2: *Odolnost karboxybetainových polymerních kartáčů proti biologické depozici z neředěné krevní plazmy a potravinových vzorků po EDC/NHS aktivaci, a po reakci s deaktivními činidly.*

Zlatý povrch čipu pro měření rezonance povrchových plasmonů (SPR), skleněná destička s napařenou vrstvou zlata o tloušťce 50 nm, byl metodou SI ATRP pokryt kartáčem z polyCBMAA nebo kartáčem z kopolymeru obsahujícího 15 mol% CBMAA (poly(HPMAA-co-CBMAA/15 mol%) s tloušťkou v rozsahu 19 až 31 nm dle protokolu popsáno v PV 2015-313. Následně byl čip opláchnut vodou a upevněn do komory SPR senzoru s 6 průtokovými mikrofluidními kanály. Karboxybetainové skupiny kartáče byly v 2. a 6. kanálu aktivovány reakcí s vodným roztokem N-hydroxysukcinimidu (NHS; 0,1 M) a 1-ethyl-3-(3-dimethylaminopropyl)karbodiimidu (EDC; 0,5 M) 20 min při 20°C (krok (a) v Příkladu 1). Po oplachování vodou po dobu 5 min a PBS a vodou pH 8 (10 mM Na<sub>2</sub>HPO<sub>4</sub>, 1,8mM KH<sub>2</sub>PO<sub>4</sub>, 137mM NaCl, 2,7mM KCl, pH 7,4) 10 min byl aktivovaný kartáč vystaven působení roztoku glycinu (1 M, voda pH 8) 30 min v 3. kanálu, roztoku kyseliny (2-aminoethoxy)octové (0,1 M, voda pH 8) 30 min v 4. kanálu, roztoku ethanolaminu (1 M, voda pH 8) 30 min v 5. kanálu a deaktivnímu pufru (10mM borát sodný + 10mM imidazol + 10mM NaCl, pH 8) 40 min v 6. kanálu při 20°C (krok (c) v Příkladu 1). Tímto způsobem by připraven SPR senzor, ve kterém 1.



kanál obsahoval neaktivovaný kartáč, 2. kanál kartáč po aktivaci, 3. kanál kartáč po deaktivaci glycinem, 4. kanál kartáč po deaktivaci kyselinou (2-aminoethoxy)octovou, 5. kanál kartáč po deaktivaci ethanolaminem a 6. kanál kartáč po deaktivaci deaktivčním pufrém. Vždy po modifikaci kartáče provedené v příslušném kanále byl kartáč opláchnut vodou 5 min a PBS 10 min, změřena SPR rezonanční vlnová délka ( $\lambda_1$ ), povrch byl inkubován s neředěnou krevní plazmou po dobu 10 min, opláchnut PBS a opět změřena  $\lambda_2$ . Velikost biologického depositu v  $\text{ng/cm}^2$  byla vypočtena z rozdílu  $\lambda_2 - \lambda_1$ .

Stejným způsobem byly na dalších čípech změřeny biologické deposity z komplexních vzorků potravin připravených <sup>uč</sup>homogenizací dle protokolu popsaneho v ČSN ISO 7251 a ČSN EN ISO 6579. Výsledky jsou uvedeny v <sup>t</sup>Tabulce 1 a 2.

Tabulka 1: Depozice z komplexních biologických roztoků na kartáč z poly(HPMAA-co-CBMAA/15 mol%<sup>1</sup>) aktivovaný EDC/NHS a deaktivovaný deaktivčními činidly.

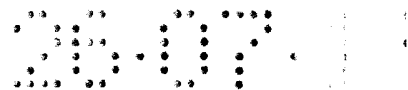
Deaktivční činidlo	Depozit [ $\text{ng/cm}^2$ ]			
	Krevní plazma	Mléko	Hamburger	Okurka
Před aktivací	4,9 ± 2,0	3,1	0,0	0,0
Po aktivaci	135,5	74,3	55,3	21,4
Glycin <sup>*1</sup>	5,1	1,9	1,4	0,2
Kyselina (2-aminoethoxy)octová <sup>*2</sup>	5,9	1,9	0,7	1,4
Ethanolamin <sup>*3</sup>	14,8	11,4	6,6	1,4
Deaktivční pufr <sup>*4</sup>	12,5 ± 3,1	5,8	2,4	3,4

\*<sup>1</sup> 1M glycin, pH 8, 30 min

\*<sup>2</sup> 100mM kyselina (2-aminoethoxy)octová, pH 5, 30 min

\*<sup>3</sup> 1M ethanolamin, pH 8, 30 min

\*<sup>4</sup> 10mM borát sodný + 10mM imidazol + 10mM NaCl, pH 8, 40 min



Tabulka 2 Depozice z komplexních biologických roztoků na kartáč z polyCBMAA aktivovaný EDC/NHS a deaktivovaný deaktivujícími činidly

Deaktivující činidlo	Depozit [ng/cm <sup>2</sup> ]			
	Krevní plazma	Mléko	Hamburger	Okurka
Před aktivací	9,6 ± 1,3	10,7	4,1	10,9
Ihned po aktivaci	222,7	897,6	73,1	135,5
Glycin <sup>*1</sup>	75,7	317,9	11,2	13,6
Kyselina (2-aminoethoxy)octová <sup>*2</sup>	71,9	316,1	14,6	11,1
Ethanolamin <sup>*3</sup>	90,4	364,6	16,3	15,1
Deaktivující pufr <sup>*4</sup>	92,9	380,8	63,9	43,4

\*<sup>1</sup> 1M glycin, pH 8, 30 min

\*<sup>2</sup> 100mM kyselina (2-aminoethoxy)octová, pH 5, 30 min

\*<sup>3</sup> 1M ethanolamin, pH 8, 30 min

\*<sup>4</sup> 10mM borát sodný + 10mM imidazol + 10mM NaCl, pH 8, 40 min

Tabulky 1 a 2 ukazují signifikantně sníženou depozici ze všech testovaných biologických vzorků na oba typy karboxybetainových polymerních kartáčů po deaktivaci kovalentním navázáním aminokyselinových činidel (glycin nebo NH<sub>2</sub>-CH<sub>2</sub>-CH<sub>2</sub>-O-CH<sub>2</sub>-COOH) oproti zavedené deaktivaci hydrolýzou v deaktiválním pufru nebo navázáním ethanolaminu.



## PATENTOVÉ NÁROKY

1. Způsob přípravy povrchu substrátu obsahujícího karboxybetainové skupiny, se zvýšenou odolností proti nežádoucí depozici složek biologických médií na povrch substrátu, obsahující kroky:

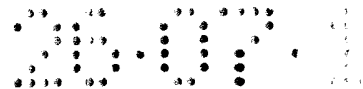
- a) chemická aktivace karboxybetainových skupin na povrchu substrátu převedením karboxylové skupiny karboxybetainu na aktivní ester;
- b) kovalentní navázání bioaktivní látky reakcí její aminoskupiny s aktivním esterem připraveným v kroku a)\*

**vyznačený tím, že** po kroku b) se provede krok c), ve kterém produkt z kroku b) reaguje s kyselinou (2-aminoethoxy)octovou,

kdy s kyselinou (2-aminoethoxy)octovou reagují aktivní estery, na nichž nedošlo v kroku b) ke kovalentnímu navázání bioaktivní látky.

2. Způsob podle nároku 1, **vyznačený tím, že** krok c) se provede tak, že se nejprve produkt z kroku b) opláchne puforem, který byl použit jako rozpouštědlo v kroku b), následně se opláchne puforem, který bude použit v následujícím kroku k inkubaci, následně se produkt inkubuje s roztokem kyseliny (2-aminoethoxy)octové v pufru, následně se opláchne puforem použitým k inkubaci, a následně se opláchne roztokem, do kterého je pak vložen pro skladování, nebo vodou a vysuší se.

3. Způsob podle kteréhokoliv z předcházejících nároků, **vyznačený tím, že** bioaktivní látka je látka obsahující alespoň jednu  $\text{NH}_2$  skupinu a selektivně interagující s cílovou složkou biologického média, s výhodou je bioaktivní látkou látka s afinitou k cílové složce, vybraná ze skupiny zahrnující protilátku, antigen, lektin, buněčný receptor a jejich analogy, části připravené rekombinantní technikou, syntetické oligopeptidové sekvence, nukleové kyseliny a jejich části, syntetické oligonukleotidové sekvence, aptamery; látka katalyzující chemickou přeměnu cílové látky, vybraná ze skupiny zahrnující enzymy, koenzymy a jejich syntetické analogy; látka vyvolávající biologickou odezvu, vybraná ze skupiny zahrnující antikoagulanty, proteiny a oligopeptidové sekvence reagující s buněčnými integriny, růstové faktory, hormony a léčiva.



4. Způsob podle kteréhokoliv z předcházejících nároků, **vyznačený tím, že** biologické médium je tekutina obsahující biomolekuly a jejich asociáty, vybrané ze skupiny zahrnující proteiny, sacharidy, polysacharidy, lipidy, nukleové kyseliny, lipoproteiny, glykoproteiny, organely; buňky, viry a mikroorganismy a/nebo jejich fragmenty.
5. Způsob podle kteréhokoliv z předcházejících nároků, **vyznačený tím, že** karboxybetainové skupiny jsou obsaženy v polymerní vrstvě na povrchu substrátu, vybrané ze skupiny obsahující polymerní kartáč, připravený polymerací z povrchu nebo roubováním polymerů na povrch substrátu, a polymerní povlak, přičemž s výhodou má tato vrstva tloušťku v rozmezí od 5 nm do 5  $\mu\text{m}$ .
6. Způsob podle nároku 5, **vyznačený tím, že** polymerní vrstva obsahuje alespoň jeden polymer obsahující karboxybetainové skupiny.
7. Způsob podle nároku 5, **vyznačený tím, že** polymerní vrstvou obsahující karboxybetainové skupiny je polymerní kartáč z poly(karboxybetain methakrylamid)u, poly(karboxybetain methakrylát)u, poly(karboxybetain akrylamid)u nebo kopolymeru poly(A-co-B), kde A je monomerní jednotka ze skupiny N-(2-hydroxypropyl) methakrylamid, 2-hydroxyethyl methakrylát, 3-hydroxypropyl methakrylát a oligo(hydroxyethylen glykol) methakrylát a B je monomerní jednotka ze skupiny karboxybetain methakrylamid, karboxybetain methakrylát a karboxybetain akrylamid v koncentraci od 1 do 99/mol %.
8. Způsob podle kteréhokoliv z předcházejících nároků, **vyznačený tím, že** substrát je vybrán ze skupiny zahrnující částice s výhodou o velikosti v rozmezí od 5 nm do 1 mm, porézní membrány, nosiče buněk a biosenzory.
9. Způsob podle nároku 8, **vyznačený tím, že** substrátem je detekční povrch biosenzoru pro přímou detekci nebo víceúrovňovou detekci analytů v komplexních biologických médiích.

# Appendix XIV

H. Lísalová, E. Brynda, I. Víšová, X. Song Chadtová, K. Mrkvová, F. Surman, M. Riedel, M. Houska, E. Brynda, J. Homola

**Method of preparation of a substrate containing carboxybetaine groups and bound bioactive substances which is resistant against undesirable deposition from biological media.**

Patent application (international) PCT/CZ2017/050025 filed in 6/2017,



(51) International Patent Classification:

G01N 33/543 (2006.01) C08F 122/22 (2006.01)

(21) International Application Number:

PCT/CZ20 17/050025

(22) International Filing Date:

16 June 2017 (16.06.2017)

(25) Filing Language:

Czech

(26) Publication Language:

English

(30) Priority Data:

PV 2016-361 17 June 2016 (17.06.2016) CZ

(71) Applicants: USTAV MAKROMOLEKULARNI CHEMIE AV CR, V.V.I. [CZ/CZ]; Heyrovskeho nam. 2/1888, 16206 Praha 6 (CZ). USTAV FOTONIKY A ELEKTRONIKY AV CR, V.V.I. [CZ/CZ]; Chaberska 57, 1825 1 Praha 8 (CZ).

(72) Inventors: LISALOVA, Hana; K Brezince 380/2, 18200 Praha 8 (CZ). BRYNDA, Eduard; Belehradska 450/39, 12000 Praha 2 (CZ). VISOVA, Ivana; Husova 163,

56002 Ceska Trebova (CZ). HOUSKA, Milan; Na Rymani 8 11/42, 15300 Praha 5 (CZ). SURMAN, Frantisek; Zelnice 5, 691 06 Velke Pavlovice (CZ). MRKVOVA, Kateřina; Krivatcova 277/6, 15521 Praha 5 (CZ). CHADTOVA SONG, Xue; Cakovicka 328/43, 19000 Praha 9 (CZ). HO-MOLA, Jiri; Secska 17/1878, 10000 Praha 10 (CZ).

(74) Agent: HARTVICOVA, Katerina; INVENTIA s.r.o., Na Belidle 3, 15000 Praha 5 (CZ).

(81) Designated States (unless otherwise indicated, for every kind of national protection available): AE, AG, AL, AM, AO, AT, AU, AZ, BA, BB, BG, BH, BN, BR, BW, BY, BZ, CA, CH, CL, CN, CO, CR, CU, CZ, DE, DJ, DK, DM, DO, DZ, EC, EE, EG, ES, FI, GB, GD, GE, GH, GM, GT, HN, HR, HU, ID, IL, IN, IR, IS, JO, JP, KE, KG, KH, KN, KP, KR, KW, KZ, LA, LC, LK, LR, LS, LU, LY, MA, MD, ME, MG, MK, MN, MW, MX, MY, MZ, NA, NG, NI, NO, NZ, OM, PA, PE, PG, PH, PL, PT, QA, RO, RS, RU, RW, SA, SC, SD, SE, SG, SK, SL, SM, ST, SV, SY, TH, TJ, TM, TN, TR, TT, TZ, UA, UG, US, UZ, VC, VN, ZA, ZM, ZW.

(54) Title: METHOD OF PREPARATION OF A SUBSTRATE CONTAINING CARBOXYBETAINE GROUPS AND BOUND BIOACTIVE SUBSTANCES WHICH IS RESISTANT AGAINST UNDESIRABLE DEPOSITION FROM BIOLOGICAL MEDIA

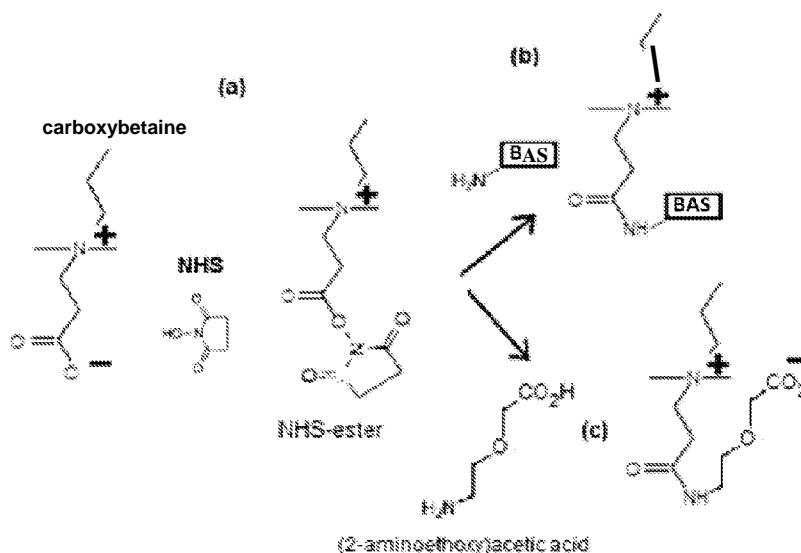


Fig. 1

(57) Abstract: The present invention relates to a method of preparation of a substrate surface containing carboxybetaine groups with bound bioactive substances, having resistance to undesirable deposition of biological media components on the substrate surface, comprising the steps of chemical activation of carboxybetaine groups on the surface of the substrate by converting the carboxybetaine carboxyl group into an active ester, covalent binding of a bioactive substance to some of the active esters, and reaction of the product from the previous step with an acid of general formula (I) NH<sub>2</sub>-(CH<sub>2</sub>-CH<sub>2</sub>-O)<sub>n</sub>-CH<sub>2</sub>-COOH, where n = 1 to 4, wherein the acid of general formula (I) reacts with those active esters, which have not undergone covalent bonding of the bioactive substance.



**(84) Designated States** (*unless otherwise indicated, for every kind of regional protection available*): ARIPO (BW, GH, GM, KE, LR, LS, MW, MZ, NA, RW, SD, SL, ST, SZ, TZ, UG, ZM, ZW), Eurasian (AM, AZ, BY, KG, KZ, RU, TJ, TM), European (AL, AT, BE, BG, CH, CY, CZ, DE, DK, EE, ES, FI, FR, GB, GR, HR, HU, IE, IS, IT, LT, LU, LV, MC, MK, MT, NL, NO, PL, PT, RO, RS, SE, SI, SK, SM, TR), OAPI (BF, BJ, CF, CG, CI, CM, GA, GN, GQ, GW, KM, ML, MR, NE, SN, TD, TG).

**Published:**

— *with international search report (Art. 21(3))*

Method of preparation of a substrate containing carboxybetaine groups and bound bioactive substances which is resistant against undesirable deposition from biological media

#### Field of Art

5

The present invention relates to a method of preparation of a substrate surface containing carboxybetaine functional groups with bound bioactive substances, which significantly increases surface resistance against undesirable biological deposition upon contact with biological media.

#### 10 Background Art

At contact of virtually all common materials with biological media, biological deposition (so-called "fouling") on their surface takes place, which begins with the adsorption of biological molecules, especially proteins. Depending on composition of the medium, cells and microorganisms can  
15 adhere on them, followed by other biological processes such as blood coagulation, inflammatory and immune reactions, or formation of bacterial biofilms. Resulting biological deposits may impair the function of materials and equipment that work in biological media such as body fluids, cell-containing media, food and media from biological production, and from biological environment in general. The problem is particularly critical for materials used in contact with blood serum, plasma,  
20 or blood. Therefore, surfaces that prevent non-specific formation of biological deposits in biological media and simultaneously facilitate binding of bioactive elements enabling the specific interaction of the surface with target components of the biological environment are very important for many biotechnological and medical applications. Such applications include biosensors, membranes and particles for separation and accumulation of biological agents and cells, drug  
25 carriers and diagnostic particles applied to blood stream, blood-contacting materials and cell carriers or scaffolds for tissue engineering.

Currently, the most resistant "antifouling" surfaces are considered those prepared by grafting hydrophilic electroneutral polymers such as non-ionogenic (poly(oligo(hydroxy ethylene glycol) methacrylate) (polyHOEGMA), poly(2-hydroxyethyl methacrylate) polyHEMA, poly(3-  
30 hydroxypropyl methacrylate) (polyHPMA), poly(N-(2-hydroxypropyl methacrylamide) (polyHPMAA), and zwitterionic poly(carboxybetaine methacrylate) (polyCBMA), and poly(carboxybetaine acrylamide) (polyCBAA) from the substrate surface (the "grafting from" method) using the surface-initiated atom transfer radical polymerization (SI-ATRP). The resulting  
35 so-called polymer brush is a layer of densely arranged polymer chains bonded with one end to the

surface. Brushes made of polyCBAA, polyCBMA, and polyHPMAA are the only ones effectively suppressing even deposition from undiluted blood plasma and serum.

5 An alternative method is to graft polymer chains prepared by polymerization in solution to a surface, or the so-called "grafting to" method. Smaller density of polymer chains achieved in the brushes prepared by this method versus brushes prepared by the "grafting from" method gives the surface a weaker resistance to biological deposition.

10 Even weaker resistance, particularly against plasma and serum deposition, provide frequently used coatings of carboxymethyl dextran or self-assembled monolayers (SAMs) from a mixture of  $(\text{CH}_2)_n(\text{EO})_4\text{OH}$  and  $(\text{CH}_2)_n(\text{EO})_6\text{COOH}$  molecules where EO is an ethylene oxide unit. Their surface is formed by densely arranged oligoethylene oxides containing in certain positions carboxyl groups used for binding of bioactive substances.

15 Functionalization of non-ionogenic polymer chains by binding of bioactive substances uses activation of hydroxyl groups in their side chains. The residual products of this activation, which remain on the polymers after functionalization, greatly aggravate the resistance of brushes against biological deposition. Surfaces with desired biological activity and better resistance to deposition were prepared by binding bioactive substances to polyCBMA or polyCBAA brushes that have  
20 zwitterionic carboxybetaine as side groups of polymer chains. Brushes of polyCBMA and polyCBAA with bioactive substances bound to side carboxybetaine groups of polymers are included, among others, in US20140370567 and US20130244249. Patent application PV 2015-313 describes poly(HPMAA-co-CBMAA) brushes grafted via copolymerization of HPMAA monomers and carboxybetaine acrylamide (CBMAA) from surfaces of various substrates including polymer  
25 nanoparticles and binding of bioactive substances to their activated carboxybetaine groups. PCT/CZ20 16/0500 11, which relates to PV 2015-313, also includes the preparation of brushes from poly(HPMAA-co-CBMAA) prepared by polymerization in a solution and covalently grafted onto the surface of substrate. The state of the art also include hydrogels of poly(HEMA-co-CBMAA) copolymers resistant to biological deposition (Kostina et al., *Biomacromolecules* 2012,13,4164-  
30 4170) or sorbents whose surface is modified by grafting of carboxybetaine zwitterions (WO2014165421 A1).

Bioactive substances containing one or more amino groups are bound to the carboxybetaine groups virtually exclusively by reaction with the carboxybetaine zwitterion carboxylate which is first  
35 activated into an intermediate product easily reacting with the nucleophilic amino group of the bound bioactive substance. This activation is mainly accomplished by reacting with 1-ethyl-3-(3-

dimethylaminopropyl)carbodiimide (EDC) in the presence of N-hydroxysuccinimide (NHS) or its derivatives, resulting in the formation of an active NHS ester (EDC/NHS activation). The bioactive substance is subsequently bonded by reaction of its amino group with an active NHS ester formed by activating the carboxyl in the carboxybetaine group.

5

After binding of bioactive substances, it is necessary to deactivate the residual active NHS esters in order to avoid, when the surface is in contact with complex solutions, the non-specific deposition, or binding of biological substances, especially proteins, by covalent bonds of their amino groups. NHS esters formed from free carboxyl groups, e.g. on the surface of the above-mentioned SAMs, are deactivated back to carboxyl groups using spontaneous hydrolysis in aqueous media. . Another traditional method is the deactivation of residual active NHS esters by ethanolamine binding, for example deactivation of functionalized carboxymethyl dextran by incubation with a solution of ethanolamine (US 5561069 A).

10

15

Several documents describe the use of glycine as a deactivating agent for deactivating of active NHS esters in activated carboxybetaine groups. US 7 943 370 B2 describes the preparation of a substrate surface containing carboxybetaine groups by converting carboxybetaine into active ester, covalent binding of a bioactive substance and deactivating unreacted active esters with glycine or  $\beta$ -alanine. WO 2009/130 233 A1 describes the preparation of halogenated surfaces with a potential content of carboxybetaine groups by converting the carboxyl group to an active ester, covalent binding of a bioactive substance and deactivating the unreacted active esters with glycine. Non-patent documents by Chou Y.-N. et al., *Acta Biomaterialia* 2016, 40, 31-37 and Vaisocherova H. et al., *Biosensors and Bioelectronics* 2014, 51, 150-157 describe the preparation of a substrate surface containing carboxybetaine groups by converting carboxybetaine into active ester, covalent binding of bioactive substance and deactivating unreacted active esters using glycine.

20

25

The current state of the art of technology provides a method of deactivating the aforementioned active esters using amino acids, especially glycine. However, the present invention describes a significantly more efficient method of deactivating active esters on the substrate surface. Compared to the current state of the art, the use of this more efficient method of deactivation leads, in most cases, to complete or almost complete restoration of the original (prior to activation and binding of bioactive substances) ability of the surface to withstand non-specific deposition from biological media.

30

35



Disclosure of the Invention

The present invention relates to a method for preparing surfaces which by reacting with an acid of general formula (I) regenerate carboxyl groups from active NHS esters remaining after binding of bioactive substances.

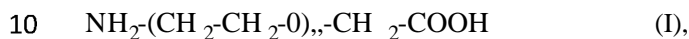
Parts of a product or device, the surface of which in a biological medium has an active function to perform that could be affected by biological deposition, and whose surface contains carboxybetaine groups, may be from organic and inorganic materials. They may have any morphology such as particles, membranes, pipes, hoses, wafers, porous material, and fibre webs and may have various uses in contact with biological media, such as biosensors, affinity particles and membranes for separation and accumulation of biological agents, targeted drug delivery carriers, biomaterials for tissue engineering, and antithrombogenic materials for contact with blood.

The present invention relates on the fact that immediately after the activation of carboxybetaine groups and binding of bioactive substances, the substrate surface is incubated with a solution of an acid of general formula (I). During this incubation, the terminal amino group of this molecule reacts with active esters that were not consumed in the prior binding of bioactive substances. The terminal carboxyl group in the part of the molecule that replaced the active ester forms a new zwitterion with the quaternary nitrogen cation left over after activation of the original carboxyl group. The above procedure on one hand neutralizes the reactivity of the residual active esters while at the same time compensates the positive charge of quaternary nitrogen cations, thereby increasing the resistance of the surface against biological deposition. The technical effect of this method for preparing substrate surface containing carboxybetaine functional groups takes shape particularly, but not only, in high density polymer brushes containing carboxybetaine side groups. Small molecules of activating reagents can penetrate between the polymer chains and react with carboxybetaines throughout the whole volume of the brush, while for binding of large bioactive substances, such as proteins, only activated carboxybetaines near the surface of the layer are available. It has been found that the deactivation of active esters by the acid of the present invention is significantly more effective than the deactivation conventionally carried out by glycine or by other methods. Even with 10 times lower concentrations of the acid according to the present invention, the deactivation efficiency was comparable or slightly higher than deactivation by glycine. Using the same concentrations of glycine and acid according to the present invention, the deactivation efficiency of the present invention was significantly higher. This more efficient method of deactivation leads, in most cases, to a complete or almost complete restoration of the original ability of the surface to resist nonspecific deposition from biological media.

The subject of the present invention is a method of preparation of a substrate surface containing carboxybetaine groups, with increased resistance to undesirable deposition of biological media components on the substrate surface, comprising the following steps:

- a) chemical activation of carboxybetaine groups on the surface of the substrate by converting the carboxybetaine carboxyl group into active ester;
- b) covalent binding of a bioactive substance by reacting of its amino group with the active ester prepared in step a);

wherein following step b), step c) is carried out in which the product of step b) reacts with an acid of general formula (I)



where  $n = 1$  to  $4$ ,

wherein the acid of general formula (I) reacts with those active esters, which have not undergone covalent bonding of the bioactive substance in step b).

15 Carboxybetaine groups can either be directly a part of the substrate material or may be attached to the substrate surface, e.g., as a part of molecules grafted onto the substrate surface, or the substrate can be coated with a layer containing these groups, e.g. a polymer brush prepared by grafting from the substrate surface using surface initiated polymerization ("grafting from") or prepared by grafting of the polymer chains prepared by polymerization in solution to surface ("grafting to").

20

Carboxybetaine groups are well known to a person skilled in the art, and are generally defined as neutral chemical groups containing a quaternary ammonium cation that carries no hydrogen atom and a negatively charged carboxyl group not directly adjacent to quaternary ammonium cation (IUPAC, Compendium of Chemical Terminology).

25

In one preferred embodiment, the acid of general formula (I) is (2-aminoethoxy)acetic acid (AEAA).

30 In one preferred embodiment, concentration of the acid of general formula (I) in step c) of the method according to the present invention is in the range of from 0.5 M to 2 M, more preferably in the concentration range of from 0.7 M to 1.5 M, most preferably at the concentration of 1 M. The pH of step c) is preferably neutral or basic in the range of from pH 7 to 9, more preferably from pH 7 to 8.5, most preferably at pH 8.

35 For the purposes of the present invention, the substrate is an object which is resistant to the deposition of biological media components or which is to be coated with a polymeric layer giving it

resistance to the deposition of biological media components. A polymer brush can be grafted to it or it can be coated with a polymer. A substrate thus can be:

- (1) An object whose surface is covered by a polymer brush layer ("grafted from") by live radical polymerization, see PV 2015-313 and PCT/CZ20 16/0500 11,
- 5 (2) An object whose surface is covered by a layer of polymers prepared in solution and subsequently attached to the surface by covalent bonding or by physical adsorption ("grafted to"), see PCT/CZ20 16/0500 11,
- (3) An object whose surface is covered by polymerization initiated by radicals formed by chemical or physical activation of the surface of the object,
- 10 (4) An object whose surface is coated with an adhesive polymeric layer deposited from a solution (polymeric coating),
- (5) An object whose surface can be modified by binding to a molecule containing carboxybetaine zwitterions,
- (6) An object containing carboxybetaine zwitterions in its structure, such as a polymer gel, where  
15 some monomer units contain carboxybetaine zwitterions.

The polymeric layers formed on objects (1), (2), (3), and (4) always contain at least one homopolymer or copolymer containing carboxybetaine zwitterions in side chains. The layers on objects (2) and (4) may contain polymers containing carboxybetaine zwitterions in a mixture with  
20 hydrophilic polymers, preferably selected from polyHPMAA, polyHOEGMA, polyHEMA, and polyHPMA.

Preferably, the layers on objects (1), (2), (3), and (4) are formed from a homopolymer selected from the group comprising polyCBMAA, polyCBMA, and polyCBAA or from a copolymer poly(A-co-B), where A is a monomeric unit selected from the group comprising HPMAA, HOEGMA,  
25 HEMA, HPMA, and B is a monomeric unit at a concentration from 1 to 99 mol%, selected from the group comprising CBMAA, CBMA, CBAA.

The shape, dimensions, morphology, and chemical nature of the substrate are not critical. They may be planar or differently shaped objects, tubes, fibres, particles, membranes, microparticles,  
30 nanoparticles, porous materials, metals, silicon, silicate- or aluminosilicate-based materials (such as glass), polymers, inorganic materials, and the like.

The active carboxybetaine ester is a product of a reaction of carboxyl group of carboxybetaine with N-substituted carbodiimides, i.e. O-acylurea, and/or a product of a reaction of carboxyl group of  
35 carboxybetaine with N-substituted carbodiimides and N-hydroxysuccinimide (NHS) or derivatives thereof. Preferably, active esters are NHS ester or sulfo-NHS ester.

In a preferred embodiment, step c) is carried out by first rinsing the product of step b) with a solution or buffer, which was used as the solvent in step b), preferably water, an aqueous NaCl or PBS, followed by rinsing with a buffer, which will be used in the next step for incubation, preferably PBS buffer. Then the product is incubated with a solution of aminoethoxyacetic acid of general formula (I) in a buffer (preferably PBS buffer). Then it is rinsed with the buffer previously used for incubation, and then rinsed with a solution into which it is then deposited for storage or with water and dried.

10 In a preferred embodiment, the bioactive substance of the present invention is a substance containing at least one  $\text{NH}_2$  group selectively interacting with the target component of the biological medium. The bioactive substance may have affinity for the target component. Typically, the bioactive substance is a natural antibody, antigen, lectin and the cellular receptor and their synthetic analogues and parts prepared by recombinant techniques as well as synthetic oligopeptide sequences, nucleic acids and portions thereof, and synthetic oligonucleotide sequences and aptamers. The bioactive substance can catalyse chemical conversion of the target substance, such as enzyme, coenzyme, and their synthetic analogues. Alternatively, the bioactive substance can induce a biological response, such as an anticoagulant including heparin, proteins and oligopeptide sequences responding to cellular integrins, growth factors, hormones, and derivatives of drugs and vitamins. Bioactive substances may also include nanoparticles functionalized by the  $\text{NH}_2$  group, in particular metallic, polymeric, and silicon nanoparticles, as well as nanoparticles based on metal oxides, or polymeric nanoparticles with magnetic core. Preferably, the bioactive substance is a substance with affinity for the target component, selected from the group consisting of antibody, antigen, lectin, cellular receptor and analogues thereof, as well as parts prepared by recombinant techniques, synthetic oligopeptide sequences, nucleic acids and parts thereof, synthetic oligonucleotide sequences, and aptamers; a substance catalysing chemical transformation of the target substance, selected from the group comprising enzymes, coenzymes, and synthetic analogues thereof; a substance that induces biological response, selected from the group comprising anticoagulants, proteins and oligopeptide sequences reacting with cellular integrins, growth factors, hormones, and drugs.

The biological medium for the purposes of the present invention is a fluid containing biological agents, that is biomolecules and their associates (proteins, saccharides, polysaccharides, lipids, nucleic acids, lipoproteins, glycoproteins, organelles etc.), viruses, cells, microorganisms, and fragments thereof. The biological medium is, for example, blood and other body fluids, blood plasma and serum, tissue extracts, cell lysates and suspensions, as well as food extracts.

In one embodiment, the carboxybetaine groups are contained in a polymeric layer on the substrate surface as a polymer brush, prepared by surface polymerization or grafting of polymers to the substrate surface, or a polymer coating, preferably having a thickness ranging between 5 nm and 5  
5  $\mu\text{m}$ .

In one preferred embodiment, the polymeric layer containing carboxybetaine groups is a polymer brush of poly(carboxybetaine methacrylamide) (polyCBMAA), poly(carboxybetaine methacrylate) (polyCBMA), poly(carboxybetaine acrylamide) (polyCBAA) or copolymer poly (A-co-B), where  
10 A is a monomeric unit from the group of N-(2-hydroxypropyl) methacrylamide (HPMAA), 2-hydroxyethyl methacrylate, 3-hydroxypropyl methacrylate and oligo(hydroxy ethylene glycol) methacrylate, and B is a monomeric unit from the group of carboxybetaine methacrylamide, carboxybetaine methacrylate and carboxybetaine acrylamide at a concentration of from 1 to 99 mol%, especially poly(HPMAA-co-CBMAA/xmol%), where x (molar concentration of CBMAA)  
15 ranges between 1 and 99 mol%. Preferably, this layer has a thickness in the range of from 5 nm to 5  $\mu\text{m}$ .

In one embodiment, the substrate is selected from the group comprising particles, porous membranes, cell carriers ("scaffolds"), and biosensors.  
20

Particles are preferably from material selected from the group containing gold, silver, magnetic materials, silicon, SiO<sub>2</sub>, and polymers falling within the definitions of substrate (1) to (6) and preferably have their diameter of from 5 nm to 1 mm. Particles with bioactive substances bound on activated carboxybetaine groups on the surface of particles including the inner surfaces of porous  
25 particles are applicable as carriers for targeted therapy and *in vivo* diagnostics, separation and accumulation of biological agents, and for enzymatic catalysis in bioreactors.

Porous membranes are membranes designed for affinity separation of biological substances from biological media.

Cells carriers or scaffolds, well known to a person skilled in the art, are used for example for tissue  
30 engineering such as:

[http://www.wikiskripta.eu/index.php/Tk%C3%A11%C5%88ov%C3%A9\\_in%C5%BEen%C3%BDrstv%C3%AD](http://www.wikiskripta.eu/index.php/Tk%C3%A11%C5%88ov%C3%A9_in%C5%BEen%C3%BDrstv%C3%AD)).

In one embodiment, the substrate is a biosensor detection surface for direct detection or multistage  
35 detection of analytes in complex biological media, such as by optical or mass biosensors. Preferably, the detection surface is coated with a polyCBMAA, polyCBMA, polyCBAA or poly

(HPMAA-co-CBMAA) polymer brush with bound bioreceptors. Bioreceptors in this application are bioactive agents that have selective affinity for the target components of the analysed medium.

In one embodiment, the substrate is intended for contact with blood *in vitro*, *ex vivo*, and *in vivo*.

5

The method of preparation of a substrate surface containing carboxybetaine groups according to the present invention, which has an increased resistance to undesirable deposition of biological media components on the surface of the substrate, provides a very rapid, cheap, and effective mitigation of problems with deposition of undesirable components of biological media. In contrast to the current solutions of the background art (use of glycine), the claimed use of (2-aminoethoxy)acetic acid is more effective, as illustrated in the following comparative examples.

10

#### Brief description of figures

15 Fig. 1: Diagram of activation of carboxybetaine groups (a), binding of bioactive substance (b), and incubation with an aqueous solution of (2-aminoethoxy)acetic acid (AEAA) (c).

Fig. 2: Example of detection of carcinoembryonic antigen (CEA, 10 ug/mL) in undiluted blood plasma using an SPC biosensor coated with a polyCBAA brush functionalized by anti-CEA binding and subsequently deactivated by AEAA. The figure shows the compensated reference data that was obtained by subtracting the SPR response from the reference channel with anti-CEA incubated in undiluted plasma from the measuring channel with anti-CEA incubated in undiluted blood plasma with added CEA (10  $\mu\text{g}/\text{mL}$ ).

20

Fig. 3: Example of detection of *Salmonella typhimorium* ( $1 \times 10^7$  CFU/mL) in a homogenized cucumber solution using a SPR biosensor coated with a polyCBAA brush functionalized by anti-Salm binding and subsequently deactivated by AEAA. The figure shows reference compensatory data obtained by subtracting the SPR response from the reference channel with anti-Salm incubated in a homogenized cucumber solution from the anti-Salm measuring channel incubated in *Salmonella-added* homogenized cucumber solution ( $1 \times 10^7$  CFU/mL).

25

#### Examples

30

*Example 1: Method of treating a surface of the substrate containing activated carboxybetaine functional groups by reaction with (2-aminoethoxy)acetic acid*

Fig. 1 shows the method of treating a surface of the substrate containing carboxybetaine functional groups. In step (a), the carboxybetaine groups are chemically activated by converting the carboxyl groups of carboxybetaine into an active NHS ester or sulfo-NHS ester by reaction with 1-ethyl-3-

35

(3-dimethylaminopropyl)carbodiimide (EDC) and N-hydroxysuccinimide (NHS) or sulfo NHS. In step (b), incubation with a solution containing the bioactive substances (BAS) takes place during which these substances are covalently bound to some of the active esters formed in step (a). In step (c), a reaction of those active NHS esters or sulfo-NHS esters with (2-aminoethoxy)acetic acid (AEAA) takes place, which did not react with bioactive substance in step b). During the sample incubation with AEAA aqueous solution, the AEAA molecules are covalently bound to the surface by a permanent amide bond.

**Comparative Example 1:** *Regeneration of resistance of EDC/NHS activated polyCBAA brushes against biological deposition by a reaction with deactivating agents*

The golden surface of a chip for measuring of the surface plasmon resonance (SPR), a 50 nm gold-plated glass plate, was incubated with a 1 mM solution of co-mercaptopundecyl bromoisobutyrate initiator in ethanol and left overnight in the dark. From the initiator layer immobilized on the golden surface, a polyCBAA brush from the CBAA monomer solution of the catalyst mixture containing CuCl, CuCl<sub>2</sub> and Me<sub>4</sub>Cyclam was grafted using the SI ATRP method.

The chip covered with the polyCBAA brush was rinsed with water and mounted into the SPR sensor chamber with four flow microfluidic channels. Carboxybetaine groups of brush in the 2<sup>nd</sup>, 3<sup>rd</sup>, and 4<sup>th</sup> channels were activated by reaction with an aqueous solution of N-hydroxysuccinimide (NHS, 0.1 M) and 1-ethyl-3-(3-dimethylaminopropyl)carbodiimide (EDC; 0.5 M) for 20 minutes with 10 mM NaCl at 20 °C (step (a) in Example 1). After rinsing with water for 5 minutes, the activated brush was exposed to deactivation buffer (10 mM sodium borate + 10 mM imidazole + 10 mM NaCl, pH 8) for 30 minutes or 40 minutes in the 2<sup>nd</sup> channel, to the solution of (2-aminoethoxy)acetic acid (1 M, water pH 7, 30 minutes) in the 3<sup>rd</sup> channel, and to the glycine solution (1 M, water pH 7, 30 minutes) in the 4<sup>th</sup> channel at 20 °C (step (c) in Example 1).

Specifically, a SPR sensor was prepared in this way, in which the 1<sup>st</sup> channel contained an inactivated brush; the 3<sup>rd</sup> channel contained the brush after deactivation by (2-aminoethoxy)acetic acid; and the 4<sup>th</sup> channel contained the brush after deactivation by glycine. After brush modification in each channel, the brush was always rinsed for 5 minutes with water and 10 minutes with PBS. The SPR resonance wavelength ( $\lambda_1$ ) was measured, the surface was incubated with undiluted blood plasma for 10 minutes, rinsed with PBS, measured  $\lambda_2$ , incubated with high ionic strength solution (PBS\*<sup>1</sup>, PBS containing 0.75 M NaCl, pH 7.4) for 5 minutes, rinsed with PBS, and measured  $\lambda_3$ . The size of biological deposits in ng/cm<sup>2</sup> was calculated from the differences  $\lambda_2 - \lambda_1$  and  $\lambda_3 - \lambda_1$ .

In the same way, biological deposits from undiluted cerebrospinal fluid were measured on other chips. The results are shown in Table 1.

Table 1: Deposition from undiluted human blood plasma and cerebrospinal fluid on polyCBAA brushes activated by EDC/NHS and deactivated by deactivating agents.

	Deposit [ng/cm <sup>2</sup> ]			
	Blood plasma		Cerebrospinal fluid	
Rinsing deposits with	PBS	PBS <sup>*1</sup>	PBS	PBS <sup>*1</sup>
Before activation	7.1 ± 5.2	1.3 ± 0.5	0.5	< LOD
Activation/deactivation by AEAA <sup>*2</sup>	34.1 ± 6.4	1.9 ± 0.4	7.0	0.2
Activation/deactivation by glycine <sup>*3</sup>	44 ± 3.2	13.3 ± 2.6	18.8	7.7

<sup>\*1</sup> PBS, 0.75 M NaCl, pH 7.4

5 <sup>\*2</sup> (2-aminoethoxy)acetic acid (AEAA), 1M, pH 7, 30 minutes

<sup>\*3</sup> glycine, 1M, pH 7, 30 minutes

< LOD below the detection limit of the SPR method

The effect of the reaction of EDC/NHS activated polyCBAA brush with AEAA solution was compared with that of a known reaction of activated carboxyl groups with glycine solution of the same concentration. Deposition from undiluted blood plasma on activated polyCBAA brushes after deactivation by AEAA was 7 times lower, and deposition from undiluted cerebrospinal fluid was 39 times lower than after deactivation by glycine. The effect of AEAA is therefore significantly higher than that of glycine. Moreover, the resulting values of deposits from both tested complex biological media after deactivation by AEAA (1M, pH 7, 30 minutes) are comparable to the original size of deposits from the same media prior to activation. These results demonstrate a unique complete regeneration of the surface resistance to non-specific deposition from biological media after activation and deactivation using AEAA.

20 **Comparative Example 2:** *Reaction of functionalized polyCBAA brushes with (2-aminoethoxy)acetic acid increases their resistance to biological deposition*

Activation of the polyCBAA brush, binding of bioactive substances, and incubation with deactivating agents (step (b) in Example 1) was carried out in four microfluidic channels. The brush was activated by EDC/NHS as described in Comparative example 1. After rinsing with water, the brush was incubated with an antibody against carcinoembryonic antigen solution (anti-CEA, 50 µg/ml, 10 mM borate buffer, pH 8) for 15 minutes, the achieved level of bound antibody was 200 ng/cm<sup>2</sup> according to SPR, or with solution of NH<sub>2</sub>-DNA oligonucleotide probes (NH<sub>2</sub>-DNA-ON, 22-mer, 2 µM, 10 mM borate buffer, pH 8), the level of bound probes was 75 ng/cm<sup>2</sup> according to SPR, or with *anti-Salmonella typhimorium* (Anti-Salm, 50 µg / ml, 10 mM borate



buffer, pH 8), the achieved levels of bound antibody were 180, 102, or 98 ng/cm<sup>2</sup> according to the SPR. After rinsing with borate buffer, the brush was deactivated by (2-aminoethoxy)acetic acid or glycine or deactivation buffer (10 mM sodium borate + 10 mM imidazole + 10 mM NaCl, pH 8, 40 minutes) and then incubated with undiluted blood plasma as described in Comparative example 1.

- 5 Plasma deposits which remained on the surface after rinsing with PBS, and deposits after further rinsing with a high ionic strength solution (PBS\*<sup>1</sup>, PBS containing 0.75 M NaCl, pH 7.4) were determined by SPR measurement as in Comparative example 1.

10 Table 2: Deposition from undiluted human blood plasma and undiluted human cerebrospinal fluid on the polyCBAA brush functionalized by antibody against carcinoembryonic antigen (anti-CEA) or NH<sub>2</sub>-DNA oligonucleotide probes for detection of microRNA (NH<sub>2</sub>-DNA-ON) and subsequently deactivated by deactivation reagents

Functionalization	anti-CEA 200 ± 22 ng/cm <sup>2</sup>		NH <sub>2</sub> -DNA-ON 75 ng/cm <sup>2</sup>			
	Blood plasma [ng/cm <sup>2</sup> ]		Blood plasma [ng/cm <sup>2</sup> ]		Cerebrospinal fluid [ng/cm <sup>2</sup> ]	
Rinsing deposits with	PBS	PBS* <sup>1</sup>	PBS	PBS* <sup>1</sup>	PBS	PBS* <sup>1</sup>
Before activation	< LOD	< LOD	16.7	11.6	7	7
Functionalization/deactivation by AEAA* <sup>2</sup>	21.8 ± 0.6	< LOD	36.7	10.8	13.1	< LOD
Functionalization/deactivation by glycine* <sup>3</sup>	30.5 ± 0.1 37.1* <sup>6</sup>	7.5±2.1 7.0* <sup>6</sup>	40.6	13.6	15.8	1.6
Functionalization/deactivation by ethanolamine* <sup>4</sup>	41.5* <sup>6</sup>	13.6* <sup>6</sup>				
Functionalization/deactivation by hydrolysis* <sup>5</sup>	54.6 40.9* <sup>6</sup>	10.8 10.3* <sup>6</sup>				

\*<sup>1</sup> PBS, 0.75 M NaCl, pH 7.4, 5 minutes

\*<sup>2</sup> (2-aminoethoxy)acetic acid, AEAA, 1M, pH 7, 30 minutes

- 15 \*<sup>3</sup> glycine, 1M, pH 7, 30 minutes

\*<sup>4</sup> ethanolamine 1M, pH 8, 30 minutes

\*<sup>5</sup> deactivation buffer (10 mM sodium borate + 10 mM imidazole + 10 mM NaCl, pH 8) 40 minutes

\*<sup>6</sup> anti-CEA, 125 ng/cm<sup>2</sup>

< LOD deposit was below the SPR detection limit of 0.03 ng/cm<sup>2</sup>

The effect of the reaction of functionalized polyCBAA brush with AEAA solution was compared with the effect of traditional reaction of activated carboxyl groups with glycine solution of the same concentration and with regeneration of carboxyl groups by spontaneous hydrolysis of active esters in a deactivation buffer.

- 5 Blood plasma deposit on polyCBAA with bound anti-CEA and deactivated by AEAA was under the SPR detection limit. On the same brush deactivated by glycine,  $7.5 \text{ ng/cm}^2$  of blood plasma was deposited. Only slightly more, namely  $10.8 \text{ ng/cm}^2$ , was deposited on the brush deactivated by spontaneous hydrolysis of active esters in the deactivation buffer.

- 10 The effect of the reaction of polyCBAA brush functionalized with  $125 \text{ ng/cm}^2$  of anti-CEA with traditional deactivating agents was evaluated in a separate experiment. Deactivation by glycine did not lead to significantly higher blood plasma deposition than deactivation by ethanolamine or deactivation buffer.

- 15 After binding of small molecules of  $\text{NH}_2\text{-DNA-ON}$ , which, unlike large antibodies, can penetrate to active esters of side groups of polymers inside the brush, the deactivation of a small number of residual active esters by deactivating agents has only a little effect on the regeneration of the brush structure.

- 20 This example demonstrates that the extraordinarily high efficiency of deactivation by AEAA (1M, pH 7, 30 minutes) approaches the complete recovery of the original ability of the polyCBAA surface to withstand non-specific deposition from biological media even after binding of different types of bioactive substances, such as antibodies or  $\text{NH}_2$ -oligonucleotide probes, at high surface concentrations by SPR biosensor coated with polyCBAA brush with bound anti-CEA ( $198 \text{ ng/cm}^2$ ) and deactivated by AEAA was detected with CEA ( $10 \text{ }\mu\text{g/mL}$ ) added to the undiluted blood plasma in the detection channel. The signal of the detection channel was compensated by a signal from the  
25 reference channel containing plasma without CEA (see Fig. 2).

Table 3: Deposition from homogenized hamburger, undiluted blood plasma, and cerebrospinal fluid on the polyCBAA brush functionalized by *anti-Salmonella* (anti-Salm) binding followed by deactivation by deactivating agents

Functionalization	anti-Salm $180 \pm 0.9 \text{ ng/cm}^2$		anti-Salm $102 \pm 5.5 \text{ ng/cm}^2$		anti-Salm $98 \text{ ng/cm}^2$	
	Deposits [ $\text{ng/cm}^2$ ]					
	Hamburger		Blood plasma		Cerebrospinal fluid	
Rinsing deposits with	PBS	PBS <sup>*1</sup>	PBS	PBS <sup>*1</sup>	PBS	PBS <sup>*1</sup>

Before activation	0.5	0.3	$5.2 \pm 0.5$	$1.3 \pm 1.1$	0.5	< LOD
Functionalization/deactivation by AEAA <sup>*2</sup>	10.9	< LOD	$24.9 \pm 2.9$	$4.1 \pm 0.9$	1.8	< LOD
Activation/deactivation by glycine <sup>*3</sup>	18.7	10.4	$32.3 \pm 1.3$	$11.1 \pm 0.8$	6.5	0.3

<sup>\*1</sup> PBS, 0.75 M NaCl, pH 7.4, 5 minutes

<sup>\*2</sup> (2-aminoethoxy)acetic acid, AEAA, 1M, pH 7, 30 minutes

<sup>\*3</sup> glycine, 1M, pH 7, 30 minutes

< LOD deposit was below the SPR detection limit of 0.03 ng/cm<sup>2</sup>

5

The effect of the reaction of the functionalized polyCBAA brush with AEAA solution was compared with that of a known reaction of activated carboxyl groups with a glycine solution of the same concentration.

On polyCBAA with bound anti-Salm, the deactivation by AEAA led, compared to deactivation by glycine, to hamburger and cerebrospinal fluid deposition under the SPR detection limit and 2.7 times lower plasma deposition. Anti-Salm has been tested here as a typical receptor for the detection of pathogenic bacteria in food and as a model antibody to obtain information on purely non-specific blood plasma and cerebrospinal fluid deposition not affected by specific antigen bond. Salmonella is present neither in plasma nor cerebrospinal fluid.

15 Using an SPR biosensor coated with polyCBAA brush with bound anti-Salm (175 ng/cm<sup>2</sup>) and deactivated by reaction with AEAA, *Salmonella* (10<sup>7</sup> CFU/mL) was detected, which was added to the cucumber extract in the detection channel. The detection channel signal was compensated by the signal from the reference channel containing *Salmonella-free* extract. Fig. 3 shows reference-compensated data obtained by subtracting the SPR response from the reference channel with anti-Salm incubated in a homogenized cucumber solution from the measuring channel with anti-Salm incubated in *Salmonella-added* homogenized cucumber solution (1 × 10<sup>7</sup> CFU/mL).

**Comparative Example 3:** *Reaction of functionalized poly(HPMAA-co-CBMAA/ 15 mol%) brushes with (2-aminoethoxy)acetic acid increases their resistance to biological deposition*

25 The golden surface of the SPR chip was covered with a copolymer brush containing 15 mol% CBMAA (poly(HPMAA-co-CBMAA/15 mol%)) with a thickness ranging from 19 nm to 31 nm according to the protocol described in PCTCZ20 160500 11, PV 2015-3 13. The brush was activated, functionalized by covalent bonding of an antibody to Staphylococcal enterotoxin B (anti-SEB) or NH<sub>2</sub>-DNA oligonucleotide probes, deactivated by AEAA or glycine by the procedure described in  
30 Comparative example 2.

Table 4: Deposition from non-diluted blood plasma on poly(HPMAA-co-CBMAA/15 mol%) brushes functionalized by binding of an antibody to Staphylococcal enterotoxin B (anti-SEB) or NH<sub>2</sub>-DNA-oligonucleotide probes (NH<sub>2</sub>-DNA-ON) for detection of microRNA and subsequently deactivated by deactivating agents.

Functionalization	Non-functionalized brush		Anti-SEB 133 ± 6.1 ng/cm <sup>2</sup>		NH <sub>2</sub> -DNA-ON 43.5 ± 0.6 ng/cm <sup>2</sup>	
	Deposits from blood plasma [ng/cm <sup>2</sup> ]					
Rinsing deposits with	PBS	PBS <sup>*1</sup>	PBS	PBS <sup>*1</sup>	PBS	PBS <sup>*1</sup>
Before activation	7.5 ± 1.3	4.8 ± 1.3	6.1 ± 1.1	3.8 ± 1.5	8.9 ± 3.7	6.2 ± 4.2
Functionalization/ deactivation by AEAA <sup>*2</sup>	4.6 ± 1.0	3.2 ± 0.9	12.6 ± 0.6	5.2 ± 0.6	7.1 ± 1.6	4.5 ± 1.2
Activation/ deactivation by glycine <sup>*3</sup>	9.2 ± 1.0	7.1 ± 0.6	16.5 ± 1.9	10.0 ± 1.3	9.6 ± 1.9	7.9 ± 1.8

5

<sup>\*1</sup> PBS, 0.75 M NaCl, pH 7.4, 5 minutes

<sup>\*2</sup> (2-aminoethoxy)acetic acid, AEAA 1M, pH 7, 30 minutes

<sup>\*3</sup> glycine, 1M, pH 7, 30 minutes

10 Also in this example, the effect of AEAA deactivation on blood plasma deposits was more significant than with glycine deactivation. In addition, the example shows that as in the case of polyCBAA, in poly(HPMAA-co-CBMAA/15 mol%), after activation, binding of bioactive substances and deactivation by AEAA (1 M, pH 7, 30 minutes), even total regeneration of original surface resistance to biological deposition may take place.

15

**Comparative Example 4:** *Resistance of carboxybetaine polymer brushes to biological deposition from undiluted blood plasma and food samples after EDC/NHS activation and after reaction with deactivating agents at different concentrations*

20 The golden surface of the chip for measuring surface plasmon resonance (SPR), a glass plate coated with 50 nm thick, gold film, was coated using SI ATRP method with a polyCBMAA brush or a copolymer brush containing 15 mol% CBMAA (poly(HPMAA-co-CBMAA/15 mol%)) with a thickness ranging from 19 nm to 31 nm, according to the protocol described in PV 2015-313. Subsequently, the chip was rinsed with water and mounted in the SPR sensor chamber with six flow microfluidic channels. Carboxybetaine groups of the brush were activated in the 2<sup>nd</sup> to 6<sup>th</sup>

channel by reaction with an aqueous solution of N-hydroxysuccinimide (NHS, 0.1 M) and 1-ethyl-3-(3-dimethylaminopropyl)carbodiimide (EDC, 0.5 M) for 20 minutes at 20 °C (step (a) in Example 1). After rinsing with water for 5 minutes and with PBS and water pH 8 (10 mM Na<sub>2</sub>HPO<sub>4</sub>, 1.8 mM KH<sub>2</sub>PO<sub>4</sub>, 137 mM NaCl, 2.7 mM KCl, pH 7.4) for 10 minutes, the activated brush was exposed to glycine solution (1 M, water pH 8) for 30 minutes in the 3<sup>rd</sup> channel, (2-aminoethoxyacetic) acid solution (0.1 M, water pH 8) for 30 minutes in the 4<sup>th</sup> channel, ethanolamine solution (1M, water, pH 8) for 30 minutes in the 5<sup>th</sup> channel, and deactivation buffer (10 mM sodium borate + 10 mM imidazole + 10 mM NaCl, pH 8) for 40 minutes in the 6<sup>th</sup> channel at 20 °C (step (c) in Example 1). In this way, the SPR sensor was prepared in which the 1<sup>st</sup> channel contained an inactivated brush, the 2<sup>nd</sup> channel brush after activation, the 3<sup>rd</sup> channel brush after deactivation by glycine, the 4<sup>th</sup> channel brush after deactivation by (2-aminoethoxy)acetic acid, the 5<sup>th</sup> channel brush after deactivation by ethanolamine, and the 6<sup>th</sup> channel brush after deactivation by deactivation buffer. Always after the brush modification carried out in the respective channel, the brush was rinsed with water for 5 minutes and with PBS for 10 minutes. Then the SPR resonance wavelength ( $\lambda_1$ ) was measured, the surface was incubated with undiluted blood plasma for 10 minutes, rinsed with PBS and again  $\lambda_2$  was measured. The size of the biological deposit in ng/cm<sup>2</sup> was calculated from the difference  $\lambda_2 - \lambda_1$ .

In the same way, the biological deposits were measured on other chips from the complex food samples prepared by homogenization according to the protocol described in ČSN ISO 7251 and ČSN EN ISO 6579. The results are shown in Tables 5 and 6.

Table 5: Deposition from complex biological solutions on the poly(HPMAA-co-CBMAA/15 mol%) brush activated by EDC/NHS and deactivated by deactivating agents

Deactivating agent	Deposit [ng/cm <sup>2</sup> ]			
	Blood plasma	Milk	Hamburger	Cucumber
Before activation	4.9 ± 2.0	3.1	0.0	0.0
After activation	135.5	74.3	55.3	21.4
Glycine <sup>*1</sup>	5.1	1.9	1.4	0.2
(2-aminoethoxy)acetic acid <sup>*2</sup>	5.9	1.9	0.7	1.4
[2-(2-Aminoethoxy) ethoxy]acetic acid <sup>*3</sup>	11.3			
Ethanolamine <sup>*4</sup>	14.8	11.4	6.6	1.4
Deactivation buffer <sup>*5</sup>	12.5 ± 3.1	5.8	2.4	3.4

<sup>\*1</sup> 1 M glycine, pH 8, 30 minutes

<sup>\*2</sup> 100 mM, (2-aminoethoxy)acetic acid, pH 5, 30 minutes

<sup>\*3</sup> 70 mM, [2-(2-aminoethoxy) ethoxy]acetic acid, pH 9, 30 minutes

\*4 1 M ethanolamine, pH 8, 30 minutes

\*5 10 mM sodium borate + 10 mM imidazole + 10 mM NaCl, pH 8, 40 minutes

Table 6: *Deposition from complex biological solutions on the polyCBMAA brush activated by EDC/NHS and deactivated by deactivating agents*

Deactivating agent	Deposit [ng/cm <sup>2</sup> ]			
	Blood plasma	Milk	Hamburger	Cucumber
Before activation	9.6 ± 1.3	10.7	4.1	10.9
Immediately after activation	222.7	897.6	73.1	135.5
Glycine <sup>*1</sup>	75.7	317.9	11.2	13.6
(2-aminoethoxy)acetic acid <sup>*2</sup>	71.9	316.1	14.6	11.1
Ethanolamine <sup>*3</sup>	90.4	364.6	16.3	15.1
Deactivation buffer <sup>*4</sup>	92.9	380.8	63.9	43.4

\*1 1 M glycine, pH 8, 30 minutes

\*2 100 mM (2-aminoethoxy)acetic acid, pH 5, 30 minutes

\*3 1 M ethanolamine, pH 8, 30 minutes

\*4 10 mM sodium borate + 10 mM imidazole + 10 mM NaCl, pH 8, 40 minutes

10

Tables 5 and 6 present deposition from all tested biological samples for both types of carboxybetaine polymer brushes after deactivation by incubation with a solution of (2-aminoethoxy)acetic acid. This is comparable or slightly lower than deposition after deactivation by incubation with 10 times more concentrated glycine solution and significantly lower compared with traditional deactivation by hydrolysis in deactivation buffer or by ethanolamine binding. This example demonstrates that even at much lower concentrations of (2-aminoethoxy)acetic acid compared to glycine, deactivation by AEAA is comparable or even more effective than deactivation by glycine.

15

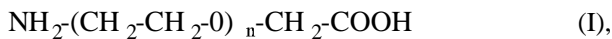
## CLAIMS

1. A method of preparation of a substrate surface containing carboxybetaine groups, with increased resistance to undesirable deposition of biological media components on the substrate surface, comprising the following steps:

a) chemical activation of carboxybetaine groups on the surface of the substrate by converting the carboxybetaine carboxyl group into an active ester;

b) covalent binding of a bioactive substance by reacting of its amino group with the active ester prepared in step a);

10 **characterized in that** following the step b), step c) is carried out in which the product of step b) reacts with an acid of general formula (I)



where  $n = 1$  to  $4$ ,

15 wherein the acid of general formula (I) reacts with those active esters, which have not undergone covalent bonding of the bioactive substance in step b).

2. The method according to claim 1, **characterized in that** the acid of general formula (I) is (2-aminoethoxy)acetic acid.

20

3. The method according to claims 1 or 2, **characterized in that** the concentration of the acid of general formula (I) in step c) is in the range of from 0.5 M to 2 M.

4. The method according to claims 1, 2 or 3, **characterized in that** step c) is carried out by first rinsing the product of step b) with a buffer, which was used as a solvent in step b), followed by rinsing with a buffer, which will be used in the next step for incubation, then the product is incubated with a solution of aminoethoxyacetic acid of general formula (I) in a buffer, and then it is rinsed with the buffer previously used for incubation, and then rinsed with a solution into which it is then deposited for storage or with water and dried.

30

5. The method according to any one of the preceding claims, **characterized in that** the carboxybetaine groups are contained in a polymeric layer on the substrate surface, selected from a group comprising a polymer brush, prepared by surface polymerization or grafting of polymers to the substrate surface, or a polymer coating, whereas preferably the polymeric layer has a thickness ranging from 5 nm to 5  $\mu\text{m}$ .

35

6. The method according to claim 5, **characterized in that** the polymeric layer contains at least one polymer comprising carboxybetaine groups.

7. The method according to claim 5, **characterized in that** the polymeric layer comprising  
5 carboxybetaine groups is a polymer brush of poly(carboxybetaine methacrylamide),  
poly(carboxybetaine methacrylate), poly(carboxybetaine acrylamide) or copolymer poly (A-co-B),  
wherein A is a monomeric unit from the group of N-(2-hydroxypropyl) methacrylamide, 2-  
hydroxyethyl methacrylate, 3-hydroxypropyl methacrylate and oligo(hydroxy ethylene glycol)  
methacrylate, and B is a monomeric unit from the group of carboxybetaine methacrylamide,  
10 carboxybetaine methacrylate and carboxybetaine acrylamide at a concentration of from 1 to 99  
mol%.

8. The method according to any one of the preceding claims, **characterized in that** the substrate  
is selected from the group comprising particles with preferable size of from 5 nm to 1 mm, porous  
15 membranes, cell carriers, and biosensors.

9. The method according to claim 8, **characterized in that** the substrate is a biosensor detection  
surface for direct detection or multistage detection of analytes in complex biological media.



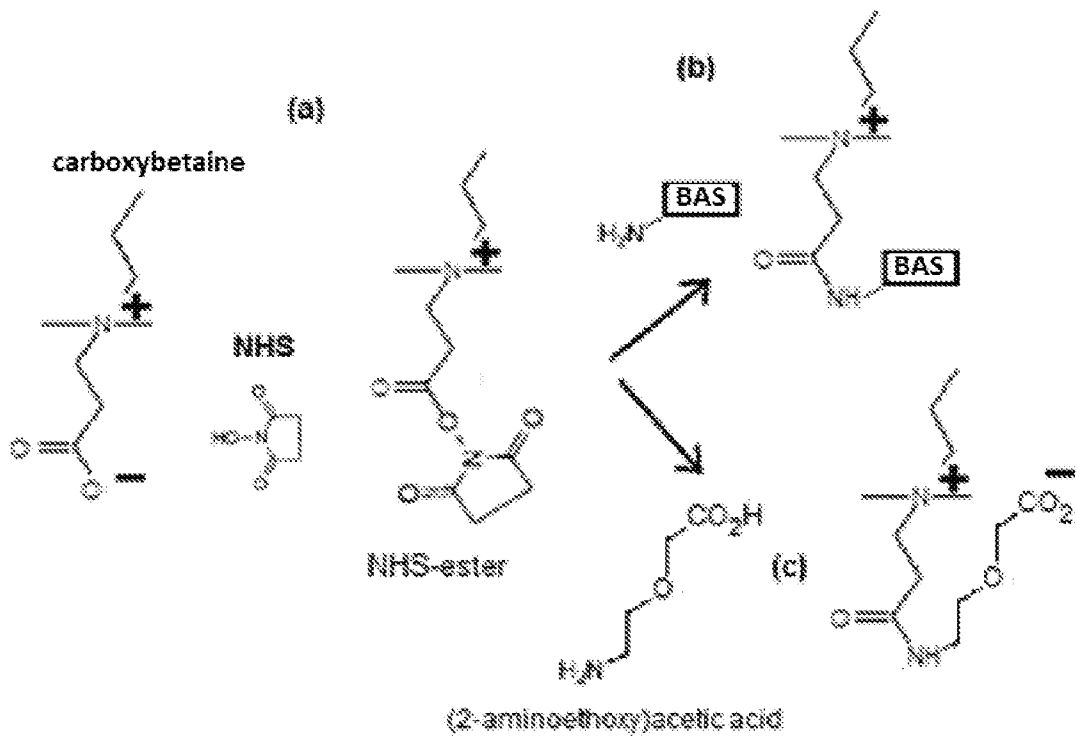


Fig. 1

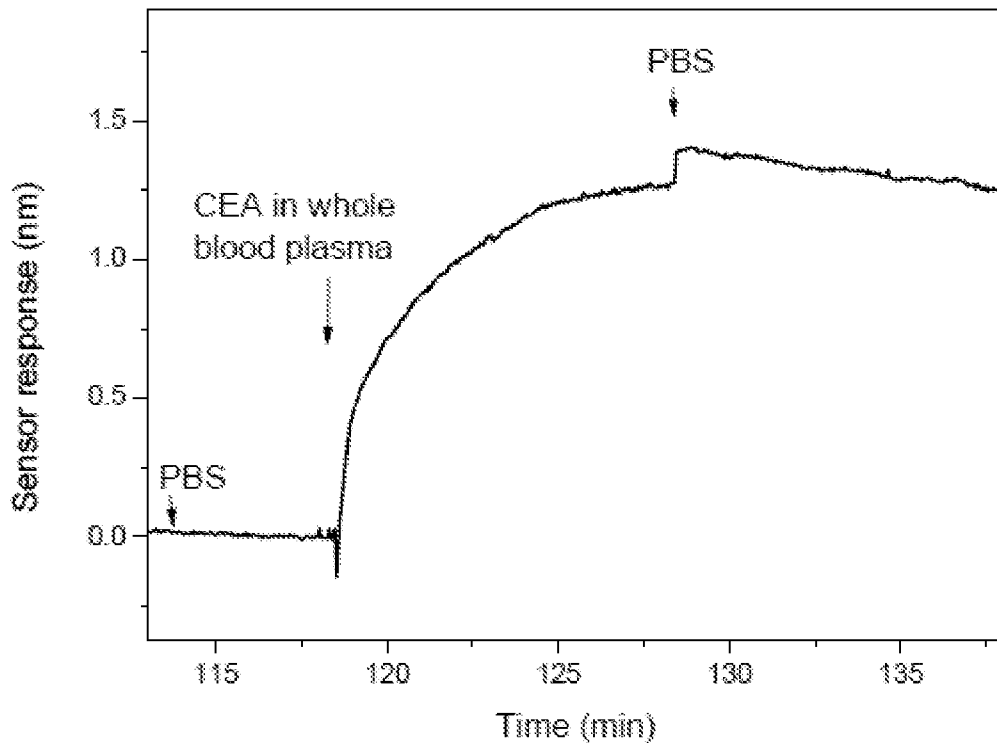


Fig. 2

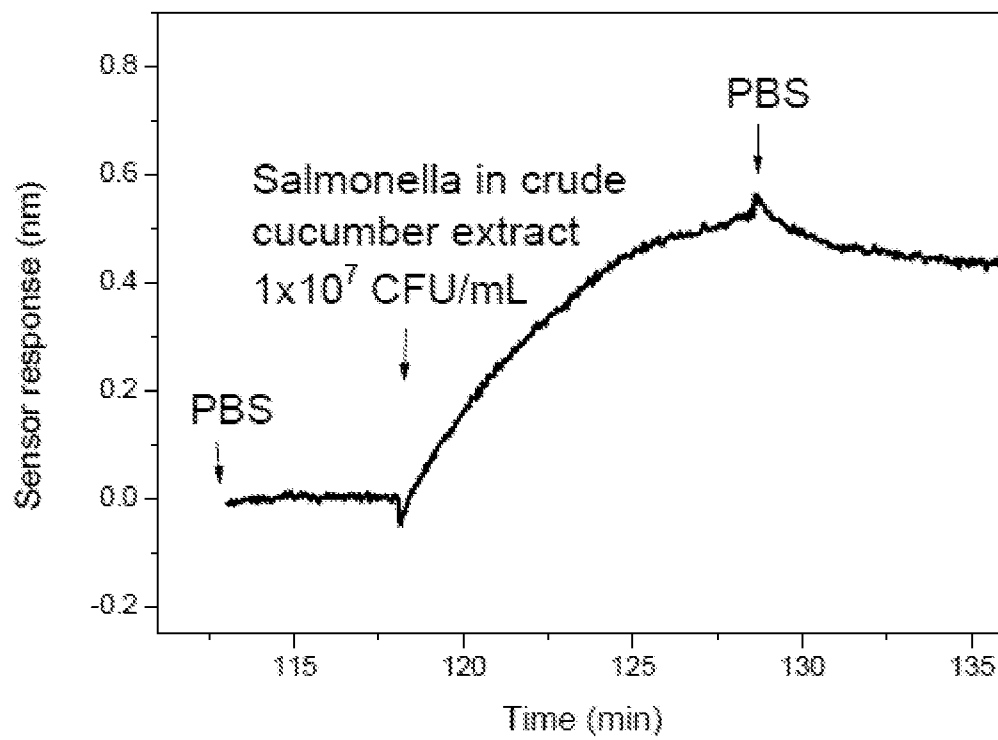


Fig. 3

# Appendix XV

H. Lísalová, M. Vrabcová, I. Víšová, M. Houska, A. Dejneka

**Terpolymer pro použití proti nespecifické adsorpci látek z  
biologických médií.**

Patent application (CZ) PV 2020-270 filed in 5/2020,

## **Terpolymer pro použití proti nescifické adsorpci látek z biologických médií, polymerní kartáče jej obsahující**

### Oblast techniky

Vynález se týká nového statistického antifoulingového terpolymeru, polymerních kartáčů jej obsahujících, a jejich použití proti nescifické adsorpci látek z biologických médií.

### Dosavadní stav techniky

Nescifická adsorpce je nežádoucí depozice látek z komplexních biologických vzorků, která představuje kritický problém pro vývoj řady moderních bioanalytických a biomedicínských metod, zařízení a materiálů. Jedná se např. o biosenzory, separační metody, funkční nanočástice a nanostrukturované povrchy, nosiče léčiv, membrány, diagnostické částice pro analýzu v tělních tekutinách, obecně o libovolné bioanalytické metody a funkční materiály, které přicházejí do přímého styku s biologickým médiem. Proto je velké úsilí věnováno vývoji tzv. ultrarezistentních materiálů a povrchů, které účinně kombinují schopnost navázání funkčních, např. biorekogničních prvků, a které jsou současně odolné proti nescifické adsorpci látek i z velmi komplexních biologických médií, jako jsou např. neředěné tělní tekutiny, potravinové extrakty, média obsahující buňky, vzorky z tkání a částí organismů obecně, či tekutiny z prostředí obecného charakteru.

V současné době jsou považovány za nejvíce odolné (tzv. „antifouling“, či „ultra-low fouling“) a přitom funkcionalizovatelné povrchy, které se připravují polymerizací z povrchu („grafting from“) hydrofilních elektroneutrálních polymerů, jako jsou neionogenní poly(oligo(hydroxyethylenglykol methakrylát) (polyHOEGMA), poly(2-hydroxyethyl methakrylát) (polyHEMA), poly(3-hydroxypropyl methakrylát) (polyHPMA) poly[N-(2-hydroxypropyl methakrylamid) (polyHPMAA) a ionogenní zwitteriontové poly(karboxybetain methakrylát) (polyCBMA), poly(karboxybetain akrylamid) (polyCBAA) a statistický kopolymer N-(2-hydroxypropyl) methakrylamidu (HPMAA) s karboxybetain methakrylamidem (CBMAA) (poly(HPMAA-co-CBMAA), z povrchu substrátů pomocí povrchem iniciované radikálové polymerizace s přenosem atomu (ATRP). Postup se skládá z

kovalentního navázání iniciátoru ATRP na povrch substrátu (S). Po přidání polymerizačního roztoku obsahujícího monomery rostou polymerní řetězce od upoutaného zbytku iniciátoru (R) postupným navazováním monomerních jednotek, přičemž iniciační atom halogenu se vždy přenáší na konec rostoucího řetězce polymeru. Výsledkem postupu je tzv. kartáč polymerních řetězců („polymer brush“), což je vrstva hustě uspořádaných polymerních řetězců navázaných jedním koncem k povrchu substrátu dle schématu S-R-polymerní řetězec. Při současném stavu techniky nelze u polymerních kartáčů roubovaných z povrchu spolehlivě stanovit délku jednotlivých řetězců ani hustotu kartáče. Proto bývá kartáč charakterizován pouze tloušťkou měřenou elipsometrickou metodou s využitím metody rezonance povrchových plasmonů (SPR) nebo pomocí mikroskopie atomárních sil (AFM).

Příprava a aktivace kartáčů z homopolymerů polyCBMA a polyCBAA jsou zahrnuty v dokumentu US20140370567. Tento dokument mimo jiné popisuje antifouling povrchy připravené roubováním polyCBMA a polyCBAA homopolymerů z povrchu substrátu polymerizací ATRP nebo RAFT, a blokové kopolymery, které obsahují blok z hydrofobního polymeru a blok z homopolymeru polyCBMA nebo polyCBAA, roubované polymerizací z povrchu nebo vazbou na povrch substrátu. Dokument US20130244249 popisuje postup používající dvoustupňovou ATRP, při níž se napřed na povrch naroubuje vrstva polymeru s vysokou hustotou řetězců a dobrými antifouling vlastnostmi. Na tuto vrstvu je naroubována druhá vrstva z polyCBMA nebo polyCBAA o nízké hustotě polymerních řetězců s reaktivními skupinami podél řetězce, které slouží k imobilizaci bioaktivních prvků. Výslovně uvedeným cílem tohoto postupu je zvýšení dostupnosti reaktivních skupin pro vazbu velkých molekul v druhé vrstvě, přičemž otázkou vedlejších reakcí a nežádoucích reakčních reziduí se nezabývá. Dokument PV 2015-313 se zabývá přípravou a využitím statistického kopolymeru poly(HPMAA-co-CBMAA) a srovnává jeho antifoulingové vlastnosti po ukotvení funkčních prvků s polyCBAA.

I když všechny výše zmíněné polymerní kartáče potlačují nesespecifickou adsorpci z modelových proteinových roztoků a snižují depozici z neředěné krevní plasmy pod  $50 \text{ ng/cm}^2$ , jsou kartáče na bázi HPMAA, CBMA a CBAA v současnosti jedinými „ultra-low fouling“ povrchy snižujícími nesespecifické vazby látek z krevní plasmy pod  $5 \text{ ng/cm}^2$ . Obecně se uznává, že vysoká odolnost proti nesespecifické adsorpci je dána kombinací vysoké hydrofility, která omezuje hydrofobní interakce, a celkové elektroneutality, omezující elektrostatické interakce.

Vazba funkčních entit, což mohou být látky a velké molekuly s různými doménami a velkým počtem nábojů, může tuto charakteristiku povrchu podstatně změnit a původně vynikající odolnost zhoršit.

Např. pro vazbu na neionogenní polymerní řetězce je využívána aktivace jejich bočních hydroxylových skupin, která však vede k tvorbě produktů, které do velké míry zhoršují odolnost kartáčů, příp. tyto schopnosti zcela ztratí.

Elektroneutrální zwitteriontové boční skupiny polyCBMA a polyCBAA řetězců obsahují karboxylový aniont a kvarterní amoniový kationt. Karboxylová skupina zwitteriontu se, obvykle pomocí EDC-NHS chemie, ale lze použít i jiná odborníkovi známá aktivační činidla pro aktivaci karboxylu (Bioconjugate Techniques, G.T.Hermanson, Elsevier, 2008), přemění na aktivní ester, který potom reaguje s aminoskupinou funkčního prvku za vzniku amidové vazby. V polymeru ovšem vždy zůstane část nezreagovaných aktivních esterů, které musí být kvantitativně odstraněny, jednak aby při následném styku s biologickým médiem nemohly nespecificky reagovat s jeho složkami, a dále aby se pokud možno zachovala původní elektroneutralita polymeru, tj. kompenzovala převaha permanentního kladného náboje kvarterní amoniové skupiny. K tomu nepostačuje prostá hydrolyza aktivního esteru, a proto se s výhodou zbylé aktivní estery eliminují reakcí s malou molekulou obsahující aminoskupinu a karboxylovou skupinu, např. s glycinem (PV 2016-361). Nicméně žádný z těchto postupů se doposud neukázal jako plně vyhovující, a právě ztráta celkové elektroneutrálnosti povrchu je považována za jeden z klíčových faktorů, který vede ke snížené odolnosti kartáče po vazbě funkčních prvků.

Předkládaný vynález si klade za cíl odstranit výše uvedené nevýhody.

#### Podstata vynálezu

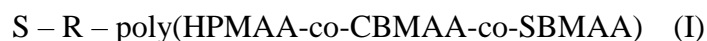
Předmětem vynálezu je statistický terpolymer N-(2-hydroxypropyl) methakrylamidu (HPMAA), karboxybetain methakrylamidu (CBMAA) a sulfobetain methakrylamidu (SBMAA). Tento terpolymer lze zapisovat jako poly(HPMAA-co-CBMAA-co-SBMAA).

S výhodou tento statistický terpolymer obsahuje od 0,1 mol % do 40 mol % SBMAA, s výhodou od 0,5 mol % do 30 mol % SBMAA.

S výhodou statistický terpolymer podle vynálezu obsahuje od 0,1 mol % do 50 mol % CBMAA, výhodněji od 5 mol % do 30 mol % CBMAA, ještě výhodněji od 10 mol % do 20 mol % CBMAA.

HPMAA tvoří v terpolymeru zbytek do 100 mol %.

Předmětem vynálezu je dále tzv. polymerní kartáč (angl. „polymer brush“) statistického terpolymeru N-(2-hydroxypropyl) methakrylamidu (HPMAA), karboxybetain methakrylamidu (CBMAA) a sulfobetain methakrylamidu (SBMAA), jehož řetězce jsou jedním koncem navázány na substrát (angl. „end-tethered“), přičemž polymerní kartáč má strukturu I,



kde

S je substrát, na jehož povrch lze kovalentně navázat iniciátory polymerizace;

R je zbytek iniciátoru, vybraného ze skupiny zahrnující iniciátory radikálové polymerizace s přenosem atomu ATRP, iniciátory živé radikálové polymerizace s přenosem jednotlivého elektronu SET-LRP a činidla pro polymerizaci s reverzibilním adičně-fragmentačním přenosem RAFT;

– je kovalentní vazba.

Polymerní kartáč je struktura, která se skládá z polymerních řetězců jedním koncem navázaných na substrát, přičemž polymerní řetězce jsou uspořádány hustě vedle sebe, takže směřují od substrátu. Výsledná struktura polymerních řetězců připomíná vlákna kartáče, odtud název.

S výhodou je tloušťka vrstvy statistického terpolymeru v polymerním kartáči 10 nm až 500 nm, výhodněji 20 nm až 200 nm, měřeno elipsometrickou metodou ve vodě.

Předmětem vynálezu je rovněž funkcionalizovaný polymerní kartáč statistického terpolymeru N-(2-hydroxypropyl) methakrylamidu (HPMAA), karboxybetain methakrylamidu (CBMAA) a sulfobetain methakrylamidu (SBMAA), mající strukturu II



kde

S je substrát, na jehož povrch lze kovalentně navázat iniciátory polymerizace;

R je zbytek iniciátoru, vybraného ze skupiny zahrnující iniciátory radikálové polymerizace s přenosem atomu ATRP, iniciátory živé radikálové polymerizace s přenosem jednotlivého elektronu SET-LRP a činidla pro polymerizaci s reverzibilním adičně-fragmentačním přenosem RAFT;

– je kovalentní vazba;

F je alespoň jedna funkční entita kovalentně navázaná na polymer amidovou vazbou.

Předkládaný vynález řeší výše popsaný problém ztráty celkové elektroneutrálnosti povrchu při problematických hydrolyzách reziduálních aktivních esterů, který vede ke snížené odolnosti kartáče po vazbě funkčních molekul. V dosud známých postupech se hydrolyzou reziduálních aktivních esterů, i s použitím látek obsahujících karboxylovou slupinu, sice mohou karboxylové skupiny regenerovat, nikoli však úplně, protože se nenahradí úbytek způsobený vazbou funkčního prvku. Takto nahrazený zwitterion také není strukturně identický s původním zwitterionem. Je také obecně známo, že elektroneutralita karboxybetainů je závislá na pH v důsledku změn ionizace karboxylové skupiny při zachování permanentního kladného náboje kvarterního amoniového kationtu. Vazba funkční entity, což může být například velká molekula s různými doménami a velkým počtem vlastních nábojů, vytváří na povrchu podstatně změněné mikrookolí, tedy i lokální pH, a tím ovlivňuje nábojovou rovnováhu. Předložený vynález řeší tento nedostatek novým způsobem, a to doladěním rovnováhy přidáním monomerní jednotky SBMAA, což je betain s trvale ionizovanou sulfoskupinou. Sulfoskupina se neúčastní vazebné reakce při aktivaci karboxylových skupin pomocí aktivačních činidel (např. EDC-NHS nebo jiných odborníkovi známých aktivačních činidel pro aktivaci karboxylu), takže samotný homopolymer polySBMAA by nemohl být takto funkcionalizován, a jako homopolymer ostatně také nemá příliš dobrou odolnost proti nespecifické adsorpci. V poly(HPMAA-co-CBMAA-co-SBMAA) zajišťuje funkcionalizovatelnost přítomnost CBMAA. Použití SBMAA v kombinaci s HPMAA a CBMAA pro polymerní kartáč dosud nebylo známo, přičemž, jak je doloženo dále, použití SBMAA je pro popsany účel velmi výhodné a účinné.

Obsah SBMAA ve statistickém terpolymeru se v rámci výše uvedeného rozmezí od 0,1 mol % do 30 mol % optimalizuje podle navazované funkční entity tak, aby se po jejím navázání



dosáhlo nejvyšší odolnosti proti nespecifické adsorpci. Tuto optimalizaci lze provést přípravou několika vzorků s různými obsahy SBMAA v rámci uvedeného rozmezí, a volbou vhodného obsahu SBMAA podle změřených požadovaných parametrů.

Terpolymer podle předkládaného vynálezu má vysokou odolnost proti nespecifické adsorpci látek z biologických médií, a stejně tak i polymerní kartáče, které jej obsahují, mají tuto vysokou odolnost, a to i po aktivaci (tj. reakci tvorby aktivních esterů), navázání funkční entity a deaktivaci.

Biologickými médii jsou zde míněny zejména tělní tekutiny, jako je například krev, mozkomíšní mok, moč, sliny, ascitická tekutina, ale i další média biologického původu, jako je například krevní plasma a sérum, buněčné lyzáty, tkáňové extrakty, buněčné suspenze, média z biologických výrob, pitná či odpadní voda a potraviny.

Substrátem S je materiál, který se pokrývá funkcionalizovatelnou vrstvou terpolymeru odolnou proti nespecifické adsorpci. Substrátem je jakýkoliv materiál, na jehož povrch lze kovalentně navázat iniciátory polymerizace. Vhodnými substráty jsou tedy zejména materiály obsahující reaktivní skupiny na povrchu nebo inertní materiály povlečené vrstvou dobře adheující k jejich povrchu a obsahující reaktivní skupiny pro navázání iniciátoru, typicky polydopaminem připraveným autopolymerizací na povrchu materiálu. Tvar, rozměry, morfologie a chemická povaha substrátu nejsou rozhodující, může se jednat o planární či různě tvarované objekty, trubice, vlákna, částice, membrány, mikročástice, nanočástice, porézní materiály, kovy, křemík, materiály na bázi křemičitanů či hlinitokřemičitanů (např. sklo), polymery, anorganické materiály – zejména oxidy kovů či nekovů, apod. Ve výhodném provedení se zejména jedná o kovy, křemík, oxidy kovů či nekovů, včetně křemičitanů či hlinitokřemičitanů. Substrátem může být například povrch senzoru, povrch biosenzoru, nebo sorbent, nebo povrch zařízení či materiálu používaného ve zdravotnictví.

Skupina R je zbytek iniciátoru. Pro ukotvení řetězce kopolymeru je potřeba nejprve na substrát navázat iniciátor polymerizace. Vhodné iniciátory a vhodné typy polymerizace pro roubování z povrchu jsou odborníkovi v oboru známy, jedná se o iniciátory polymerizace ATRP (atom transfer radical polymerization), iniciátory polymerizace SET-LRP (single-electron transfer living radical polymerization) nebo RAFT (reversible addition fragmentation transfer

polymerization) činidla. Způsob vazby, kterou se iniciátor váže k substrátu, závisí na tom, o jaký substrát a jaký iniciátor se jedná, ale její určení, stejně jako určení vhodného iniciátoru pro každý substrát, je plně v rozsahu znalostí a schopností odborníka v oboru, bez potřeby vynaložení dalšího inventivního úsilí (odborník v oboru má k dispozici řadu monografií, učebnic a přehledových článků, jako příklad lze uvést *Advanced Materials by Atom Transfer Radical Polymerization*, Krysztof Matyjaszewski, Wiley Online Library, 2018).

F je funkční entita kovalentně navázaná amidovou vazbou k polymernímu kartáči, přesněji ke zbytku karboxylové skupiny monomerní jednotky CBMAA. F je entita obsahující aminoskupinu, např. proteiny, peptidy, protilátky, oligonukleotidy, nukleové kyseliny, DNA sondy. F může být biorekogniční entita, která specificky interaguje s cílovým analytem, kterým může být například protein, peptid, nukleová kyselina, oligonukleotid a jiné organické nebo anorganické analyty.

Terpolymer poly(HPMAA-co-CBMAA-co-SBMAA) se připravuje známými technikami, např. metodou tzv. živé radikálové polymerizace. Polymerní kartáč obsahující tento terpolymer se připravuje živou radikálovou polymerizací z povrchu substrátu za vzniku řetězců polymerních kartáčů jedním koncem vázaných na povrchu substrátu. Lze použít i metody „grafting to“, kdy se již uskupená polymerní entita naváže na substrát.

Vhodné způsoby polymerizace pro přípravu statistického terpolymeru podle vynálezu či polymerního kartáče obsahujícího tento terpolymer, např. ATRP polymerizace, SET-LRP polymerizace, RAFT polymerizace, jejich použití pro jednotlivé typy substrátů, odpovídající iniciátory a odpovídající vazebné skupiny pro kombinace iniciátoru a substrátu jsou známy z literatury. Jako příklady kombinací iniciátorů vhodných pro substráty lze uvést 11-(trichlorsilyl)undecyl-2-bromo-2-methyl propanoát na sklo a křemík pokrytý oxidem, nebo  $\omega$ -merkaptoundecyl bromisobutyrylát na zlato, nebo iniciátor navázaný na povrchu substrátu obsahujícím karboxylové skupiny, který se připraví inkubací s roztokem kyseliny  $\alpha$ -bromisomáselné, NHS a EDC, nebo 2-brom-2-methylpropanoyl bromid jako iniciátor pro substrát obsahující na povrchu amino nebo hydroxylové skupiny, což je i případ vrstvy polydopaminu. Všechny monomery jsou methakrylamidy z hlediska polymerizace podobného typu, mají podobnou rychlostní konstantu polymerizace, a statistický charakter polymerizace dokládá

molární poměr koncentrací monomerních jednotek SBMAA, HPMAA a CBMAA v terpolymerech, shodný se složením polymerizační násady.

Příprava funkcionalizovaných polymerních kartáčů se provádí tak, že se karboxylové skupiny polykarboxybetainů (CBMAA jednotek) v polymerním kartáči podrobí reakci s aktivačními činidly, jako jsou například EDC (1-ethyl-3-(3-dimethylaminopropyl)-karbodiimid) a NHS (N-hydroxysukcinimid), za vzniku aktivních esterových skupin. Vzniklé aktivní esterové skupiny se dále podrobí reakci s aminovou skupinou funkční entity za vzniku amidové kovalentní vazby. Zbylé nezreagované aktivní esterové skupiny se pak podrobí reakci s deaktivčním činidlem, například ethanolamin-O-sulfátem a/nebo amino-PEG2-octovou kyselinou a/nebo glycinem. Výhodnost použití ethanolamin-O-sulfátu spočívá v možnosti optimalizovat celkový náboj povrchu.

Vynález umožňuje univerzální modifikaci různých substrátů obsahujících reaktivní skupiny pro navázání iniciátorů polymerizace. Na povrch inertních substrátů, na které nelze iniciátory polymerizací navázat přímo, je možné napřed deponovat kotvicí mezivrstvu, na příklad polydopaminu, která obsahuje reaktivní skupiny pro navázání iniciátorů.

Předmětem předkládaného vynálezu je pak také použití statistického terpolymeru poly(HPMAA-co-CBMAA-co-SBMAA) pro zvýšení odolnosti povrchů proti nespecifické adsorpci látek z biologických médií. Povrch lze při takovém použití pokrýt terpolymerem poly(HPMAA-co-CBMAA-co-SBMAA), například ve formě povlaku či ve formě polymerního kartáče.

Konkrétněji je předmětem vynálezu použití statistického terpolymeru poly(HPMAA-co-CBMAA-co-SBMAA) nebo polymerního kartáče jej obsahujícího nebo funkcionalizovaného polymerního kartáče jej obsahujícího pro dosažení odolnosti povrchu (substrátu) proti nežádoucí nespecifické interakci se složkami biologických médií, zejména molekul proteinů a buněk, a proti adsorpci/depozici složek biologických médií na povrchy chráněné tímto polymerem.

Použití funkcionalizovaného polymerního kartáče obsahujícího statistický terpolymer poly(HPMAA-co-CBMAA-co-SBMAA) pro specifickou a selektivní interakci s cílovými analyty, zahrnujícími zejména proteiny, peptidy, nukleové kyseliny, oligonukleotidy.

Předkládaný vynález dále zahrnuje senzory, zejména biosenzory pro přímou detekci analytů nebo víceúrovňovou detekci s použitím přidaných reagentů, jako jsou senzory rezonance povrchových plasmonů (SPR senzory), křemenné krystalové mikrováhy (quartz crystal microbalance) nebo fluorescenční senzory, které obsahují polymerní kartáč či funkcionalizovaný polymerní kartáč podle vynálezu.

Předkládaný vynález dále zahrnuje membrány obsahující polymerní kartáč či funkcionalizovaný polymerní kartáč podle vynálezu. Substrátem je pak typicky membrána, vrstva polymerních řetězců je naroubována na povrch membrány. Je-li membrána porézní, je vrstva polymerních řetězců naroubována na povrchu pórů.

#### Objasnění výkresů

Obr. 1 ukazuje typické IRRAS spektrum kartáče poly[HPMAA(70 mol %)-co-CBMAA(15 mol %)-co-SBMAA(15 mol %)] na zlatě. Vyznačeny jsou charakteristické absorpční pásy skupin jednotlivých složek: Am I a Am II amidové pásy řetězce, -OH pás hydroxylové skupiny HPMAA,  $\text{-COO}^-$  pás ionizované karboxylové skupiny CBMAA,  $\text{-SO}_3^-$  pás ionizované sulfoskupiny SBMAA.

Obr. 2 je záznam odezvy SPR senzoru s čipem se zlatým povrchem opatřeným polymerním kartáčem, dle Příkladů 3 a 4.

Obr. 3 je záznam odezvy SPR senzoru při detekci *E.coli* na funkcionalizovaném terpolymerním kartáči, dle příkladu 5.

#### Příklady provedení vynálezu

Příklad 1: Příprava polymerního kartáče na zlatě

Skleněná destička s napařenou vrstvou zlata byla čištěna 10 min v UV ozonovém generátoru, ihned poté byla opláchnuta vodou a ethanolem. Potom byla destička ponořena do 0,1mM

roztoku iniciátoru  $\omega$ -merkaptoundecyl bromoisobutyrate v ethanolu na 48 hodin v pokojové teplotě bez přístupu světla. Katalytická směs byla připravena ve Schlenkové baňce rozpuštěním CuCl (28 mg), CuCl<sub>2</sub> (8,4 mg) a Me<sub>4</sub>cyclam (96,8 mg) v odplyněném methanolu (2 ml) pod dusíkovou atmosférou a sonikována 5 min do úplného rozpuštění. Ve druhé Schlenkové baňce byly rozpuštěny monomery SBMAA (138 mg, 3 mol %), CBMAA (572 mg, 15 mol %) a HPMAA (1847 mg, 82 mol %) v odplyněné vodě (16,9 ml) a methanolu (0,1 ml). Příklady dalších navážek pro přípravu povrchů s jiným procentuálním zastoupením složek jsou uvedeny v Tabulce 1. Po rozpuštění byla katalytická směs pod dusíkem přidána ke směsi monomerů. Homogenní polymerační směs byla pod dusíkem přidána do reaktoru s destičkou pokrytou iniciátorem. Polymerace probíhala v uzavřeném reaktoru 2 hod při pokojové teplotě. Poté byla destička opláchnuta vodou a před dalším použitím byla skladována ve fosfátovém pufru (pH 7,4) při teplotě 4 °C.

Metodou infračervené reflexní absorpční spektroskopie (PM-IRRAS) byla ověřena chemická struktura terpolymerního kartáče. Na obrázku 1 je ukázáno typické IRRAS spektrum pro jedno provedení terpolymerního kartáče.

Tabulka 1: Vybrané příklady navážek pro přípravu terpolymeru s různým obsahem jednotlivých monomerů.

Složení polymerizační násady [mol %]			Složení polymerizační násady [mg]		
HPMAA	CBMAA	SBMAA	HPMAA	CBMAA	SBMAA
84,5	15,0	0,5	1903	572	23
82,0	15,0	3,0	1847	572	138
80,0	15,0	5,0	1802	572	230
75,0	15,0	10,0	1689	572	460
70,0	15,0	15,0	1576	572	690
55,0	15,0	30,0	1239	572	1379

#### Příklad 2: Příprava polymerního kartáče na skle

Skleněná destička byla opláchnuta acetonem, čištěna 20 min ultrazvukem v 50% methanolu při teplotě 20 °C a poté sonikována dalších 20 min v chloroformu. Potom byla destička opláchnuta vodou, osušena vzduchem a čištěna 4 min v UV ozonovém generátoru. Po čištění byla destička dehydratována 1 hod při teplotě  $\geq 90$  °C v přítomnosti silikagelu a ihned poté byla

na 2 hod ponořena do 3mM roztoku iniciátoru  $(\text{MeO})_3\text{-Si-(CH}_2\text{)}_{11}\text{-Br}$  v bezvodém n-heptanu při pokojové teplotě. Potom byla destička opláchnuta ethanolem a vodou a vložena do reaktoru k polymeraci. Další postup přípravy polymerního kartáče je analogický s výše uvedeným příkladem 1. Katalytická směs byla připravena ve Schlenkově baňce rozpuštěním  $\text{CuCl}$  (28 mg),  $\text{CuCl}_2$  (8,4 mg) a  $\text{Me}_4\text{cyclam}$  (96,8 mg) v odplyněném methanolu (2 ml) pod dusíkovou atmosférou a sonikována ultrazvukem 5 min do úplného rozpuštění. Ve druhé Schlenkově baňce byly rozpuštěny monomery SBMAA (138 mg, 3 mol %), CBMAA (572 mg, 15 mol %) a HPMMA (1847 mg, 82 mol %) v odplyněné vodě (16,9 ml) a methanolu (0,1 ml). (Další příklady navážek jsou stejné jako příklady navážek uvedených v Tabulce 1). Po rozpuštění byla katalytická směs pod dusíkem přidána ke směsi monomerů. Homogenní polymerační směs byla pod dusíkem přidána do reaktoru s destičkou s navázaným iniciátorem. Polymerace probíhala v uzavřeném reaktoru 2 hod při pokojové teplotě. Poté byla destička opláchnuta vodou a před dalším použitím byla skladována ve fosfátovém pufru (pH 7,4) při teplotě 4 °C.

#### Příklad 3: Vazba bakteriální protilátky

Dle příkladu 1 byl na zlaté vrstvě čipu připraven terpolymerní kartáč poly[(HPMAA(80 mol %)-co-CBMAA(15 mol %)-co-SBMAA(5 mol %))]. Čip byl opláchnut vodou, vložen do SPR senzoru a karboxylové skupiny CBMAA byly aktivovány 20 min za průtoku 10  $\mu\text{l/min}$  roztokem 0,1M NHS a 0,5M EDC v deionizované vodě na aktivní ester. Po aktivaci byla zaznamenána hladina odezvy senzoru pro povrch ve vodě. 50  $\mu\text{g/ml}$  bakteriální protilátky anti-Salmonella bylo rozpuštěno v borátovém pufru (10 mM, pH 8,5), napuštěno rychlostí 30  $\mu\text{l/min}$  do mikrofluidického systému SPR senzoru a reakcí s aktivovaným kartáčem kovalentně navázáno (20 minut). Po imobilizaci protilátky byla opět zaznamenána hladina odezvy senzoru ve vodě. Množství navázané protilátky bylo určeno z rozdílu odezvy senzoru ve vodě před nástřikem protilátky a odezvy ve vodě po ukončení imobilizace (Obrázek 2, červeně označená „hladina imobilizace“ odpovídá hodnotě 206  $\text{ng/cm}^2$ ).

#### Příklad 4: Funkcionalizační kapacita a odolnost proti nespecifické adsorpci po navázání funkčních entit

Dle příkladu 1 byly připraveny terpolymerní kartáče poly(HPMAA-co-CBMAA-co-SBMAA) obsahující (a) 84,5 mol % HPMAA, 15 mol % CBMAA, 0,5 mol % SBMAA, (b) 82 mol % HPMAA, 15 mol % CBMAA, 3 mol % SBMAA a (c) 55 mol % HPMAA, 15 mol % CBMAA, 30 mol % SBMAA na zlaté vrstvě. Dále byly připraveny dva již známé referenční antifoulingové povrchy, vykazující vysokou míru rezistence k nescifickým vazbám a zároveň dostatečnou funkcionalizační kapacitu - kopolymer obsahující 85 mol % HPMAA a 15 mol % CBMAA (WO2016177354A3) a homopolymer polyCBAA. Dále je uveden postup přípravy těchto polymerů:

#### poly[HPMAA(85 mol %)-co-CBMAA(15 mol %)]

Skleněná destička s napařenou vrstvou zlata byla čištěna 10 min v UV ozonovém generátoru, ihned poté byla opláchnuta vodou a ethanolem. Potom byla destička ponořena do 0,1mM roztoku iniciátoru  $\omega$ -merkaptoundecyl bromoisobutyrate v ethanolu na 48 hodin v pokojové teplotě bez přístupu světla. Katalytická směs byla připravena ve Schlenkově baňce rozpuštěním CuCl (28 mg), CuCl<sub>2</sub> (8,4 mg) a Me<sub>4</sub>cyclam (96,8 mg) v odplyněném methanolu (2 ml) pod dusíkovou atmosférou a sonikována 5 min do úplného rozpuštění. Ve druhé Schlenkově baňce byly rozpuštěny monomery CBMAA (572 mg, 15 mol %) a HPMAA (1914 mg, 85 mol %) v odplyněné vodě (16,9 ml) a methanolu (0,1 ml). Po rozpuštění byla katalytická směs pod dusíkem přidána ke směsi monomerů. Homogenní polymerační směs byla pod dusíkem přidána do reaktoru s destičkou pokrytou iniciátorem. Polymerace probíhala v uzavřeném reaktoru 2 hod při pokojové teplotě. Poté byla destička opláchnuta vodou a před dalším použitím byla skladována ve fosfátovém pufru při teplotě 4 °C.

#### polyCBAA

Skleněná destička s napařenou vrstvou zlata byla čištěna 10 min v UV ozonovém generátoru, ihned poté byla opláchnuta vodou a ethanolem. Potom byla destička ponořena do 0,1mM roztoku iniciátoru  $\omega$ -merkaptoundecyl bromoisobutyrate v ethanolu na 48 hodin v pokojové teplotě bez přístupu světla. Katalytická směs byla připravena ve Schlenkově baňce rozpuštěním CuCl (28 mg), CuCl<sub>2</sub> (8,4 mg) a Me<sub>4</sub>cyclam (96,8 mg) v odplyněném methanolu (2 ml) pod dusíkovou atmosférou a sonikována 5 min do úplného rozpuštění. Ve druhé Schlenkově baňce byly rozpuštěny monomer CBAA (3590 mg) v odplyněné vodě (16,9 ml) a methanolu (0,1 ml). Po rozpuštění byla katalytická směs pod dusíkem přidána ke směsi monomerů. Homogenní polymerační směs byla pod dusíkem přidána do reaktoru s destičkou pokrytou iniciátorem.

Polymerace probíhala v uzavřeném reaktoru 2 hod při pokojové teplotě. Poté byla destička opláchnuta vodou a před dalším použitím byla skladována ve fosfátovém pufru (pH 7,4) při teplotě 4 °C.

Výše uvedené polymerní kartáče byly zkoušeny na odolnost proti nespecifické adsorpci: (a) aktivovaný a deaktivovaný povrch, (b) aktivovaný a funkcionalizovaný povrch po deaktivaci. Pro všechny kartáče byl dále uvedený analogický postup. Čip s kartáčem byl opláchnut vodou, vložen do SPR senzoru a za průtoku 10 µl/min aktivován 20 min roztokem 0,1 M NHS a 0,5 M EDC v deionizované vodě. V případě ad (a) byl povrch dále 25 min omýván borátovým pufrem (10 mM, pH 8,5, průtok 30 µl/min), v případě ad (b) byl povrch 25 min omýván borátovým (10 mM, pH 8,5, průtok 30 µl/min) obsahujícím konkrétní rozpuštěnou funkční entitu obsahující primární aminy. Na následující povrchy byly imobilizovány dále uvedené entity:

poly[HPMAA(84,5 mol %)-co-CBMAA(15 mol %)-co-SBMAA(0,5 mol %)]:

DNA oligonukleotid s koncovou amino skupinou (roztok o koncentraci 4 µM);

poly[HPMAA(82 mol %)-co-CBMAA(15 mol %)-co-SBMAA(3 mol %)]:

anti-bakteriální protilátka anti-Salmonella (roztok o koncentraci 50 µg/ml);

poly[HPMAA(55 mol %)-co-CBMAA(15 mol %)-co-SBMAA(30 mol %)]:

poly L-lysin (roztok o koncentraci 50 µg/ml);

poly[HPMAA(85 mol %)-co-CBMAA(15 mol %)]:

anti-bakteriální protilátka anti-Salmonella (roztok o koncentraci 50 µg/ml), nebo DNA oligonukleotid s koncovou amino skupinou (roztok o koncentraci 4 µM), nebo poly L-lysin (roztok o koncentraci 50 µg/ml);

polyCBAA: anti-bakteriální protilátka anti-Salmonella (roztok o koncentraci 50 µg/ml), nebo DNA oligonukleotid s koncovou amino skupinou (roztok o koncentraci 4 µM), nebo poly L-lysin (roztok o koncentraci 50 µg/ml).

Dále byl v obou případech ad (a) a (b) u všech povrchů použit stejný postup. Kartáč byl deaktivován reakcí s 1M kyselinou (2-aminoethoxy)octovou (30 min, průtok 10 µl/min) a potom inkubován v PBS (10 mM fosfátový pufr + 150 mM NaCl + 2,7 mM KCl, pH 7,4) pro dosažení rovnováhy a konstantní odezvy senzoru. Poté byla injektována 100% lidská krevní plasma rychlostí 30 µl/min při 25 °C po dobu 10 min, následovaná opláchnutím PBS. Po 10 min oplachování PBS byl na 5 minut injektován PBS s vyšší iontovou silou (10 mM fosfátový pufr



+ 750 mM NaCl + 2,7 mM KCl, pH 7,4) pro odmytí elektrostaticky adsorbovaného nespecifického depozitu a nakonec byl celý povrch relaxován opět v normálním PBS. Hladina nespecifické adsorpce byla určena z rozdílu odezvy senzoru v PBS před injektací krevní plasmy a 10 min po ukončení injektace. Hladina nespecifické adsorpce po odmytí v PBS s vyšší iontovou silou byla určena z rozdílu odezvy senzoru v PBS před nástřikem krevní plasmy a 10 min po ukončení odmytí v PBS s vyšší iontovou silou. Výsledky jsou ukázány v Obrázku 2, Tabulce 2 a Tabulce 3.

Obrázek 2 dokládá, že i při koncentraci 15 mol % CBMAA v terpolymeru se na povrch naváže dostatečné množství funkčního prvku ( $206 \text{ ng/cm}^2$  anti-Salmonella), a přitom se dosáhne vysoké odolnosti proti nespecifické adsorpci – nespecifická adsorpce z neředěné lidské plasmy byla  $0 \text{ ng/cm}^2$ .

Tabulka 2 – Nespecifická adsorpce z neředěné krevní plasmy po aktivaci a deaktivaci a aktivaci/kovalentním navázáním protilátky anti-Salmonella a deaktivaci.

Nespecifická adsorpce z neředěné krevní plasmy [ $\text{ng/cm}^2$ ]			
	poly[HPMAA(82 mol %)- co-CBMAA(15 mol %)- co-SBMAA(3 mol %)]	polyCBAA	poly[HPMAA(85 mol %)- co-CBMAA(15 mol %)]
Po aktivaci/deaktivaci	8,1	66,1	20,8
Po aktivaci/deaktivaci a odmytí PBS s vyšší iontovou silou	0	2,5	16,9
Po aktivaci/ukotvení anti-Salmonella/deaktivaci	10,9	51,9	39,5
Po aktivaci/ukotvení anti-Salmonella/deaktivaci a odmytí PBS s vyšší iontovou silou	4,5	8,5	40,9

Tabulka 2 dokládá zlepšené antifoulingové vlastnosti terpolymerního kartáče poly(HPMAA-co-CBMAA-co-SBMAA) po aktivaci a imobilizaci funkčních prvků v porovnání se známými antifoulingovými karboxy-funkčními povrchy. Zároveň ukazuje významně nižší hladinu nespecifické adsorpce i bez nutnosti odmytí elektrostaticky adsorbovaného nespecifického depozitu.

Tabulka 3 – Nespecifická adsorpce z neředěné krevní plasmy po aktivaci a kovalentním navázáním kladně (poly L-lysin) a záporně (DNA oligonukleotid zakončený amino skupinou) nabitého ligandu za daných funkcionalizačních podmínek na terpolymerních kartáčích s různým molárním zastoupením jednotlivých monomerních jednotek.

Nespecifická adsorpce z neředěné krevní plasmy [ng/cm <sup>2</sup> ]		
	<b>poly[HPMAA(84,5 mol %)- co-CBMAA(15 mol %)- co-SBMAA(0,5 mol %)]</b>	<b>poly[HPMAA(85 mol %)- co-CBMAA(15 mol %)]</b>
Po aktivaci/ukotvení DNA oligonukleotidů s koncovou amino skupinou /deaktivaci	1,7	4,1
Po aktivaci/ ukotvení DNA oligonukleotidů s koncovou amino skupinou /deaktivaci a odmytí PBS s vyšší iontovou silou	0	3,0
	<b>poly[HPMAA(55 mol %)- co-CBMAA(15 mol %)- co-SBMAA(30 mol %)]</b>	<b>poly[HPMAA(85 mol %)- co-CBMAA(15 mol %)]</b>
Po aktivaci/ukotvení poly L-lysinu/deaktivaci a odmytí PBS s vyšší iontovou silou	6,0	11,7

Tabulka 3 ukazuje výhodu laditelnosti složení terpolymerního kartáče v širokém rozmezí obsahu sulfobetainové složky. Pro různé ligandy lze na základě rozložení nábojů vyhodnotit vhodné složení kartáče tak, aby po imobilizaci zůstal povrch co nejvíce neutrální a tedy odolný proti nespecifické adsorpci. Lze tak docílit ještě nižší hladiny nespecifické adsorpce, než u známých funkcionalizovatelných antifoulingových povrchů bez sulfobetainové složky.

Příklad 5: Biorekogniční schopnost terpolymerního kartáče po navázání funkčních entit

Dle příkladu 1 byl na zlatém povrchu čipu připraven poly[HPMAA(75 mol %)-co-CBMAA(15 mol %)-co-SBMAA(10 mol %)]. Čip byl vložen do SPR senzoru a postupem dle příkladu 3 byl funkcionalizován protilátkou proti bakterii *Escherichia coli* (*E.coli*), anti-*E.coli*, a protilátkou proti karcinoembryonálnímu antigenu (CEA), anti-CEA. Druhá zmíněná protilátka byla použita jako reference pro ukázání specifičnosti detekce bakterie *E.coli*. Po funkcionalizaci byly zbylé aktivní estery deaktivovány 30 min reakcí s roztokem 1M kyseliny (2-aminoethoxy)octové (30 min, průtok 10 μl/min) a potom se čip nechal ustálit v PBS (10 mM

fosfátový pufr + 150 mM NaCl + 2,7 mM KCl, pH 7,4). Po ustálení odezvy senzoru byl na čip injektován roztok inaktivované bakterie *E.coli* o koncentraci  $1 \times 10^7$  KTJ/mL (kolonie tvořících jednotek na ml) v PBS (15 min, průtok 45  $\mu$ l/min). Potom byl čip opět oplachován PBS do ustálení odezvy senzoru.

Obrázek 3 ukazuje záznam odezvy SPR senzoru. Odezva z referenčního kanálu (černá barva), ve kterém byla imobilizovaná protilátka anti-CEA, byla zanedbatelná proti specifické odezvě SPR senzoru (červená barva), kde byla imobilizovaná protilátka anti-*E.coli*.

Polymerní kartáče v příkladech 3, 4 a 5 byly připraveny v rozmezí tlouštěk vrstvy statistického polymeru 80 nm až 100 nm (tloušťka byla ověřena elipsometrií a metodou SPR ve vodě).

#### Příklad 6

Dle příkladu 1 byl na zlatém povrchu čipu připraven terpolymerní kartáč o složení 81 mol % HPMAA, 15 mol % CBMAA, 4 mol % SBMAA. Čip byl opláchnut vodou, vložen do SPR senzoru a karboxylové skupiny CBMAA byly 20 min za průtoku 10  $\mu$ l/min aktivovány roztokem 0,5M EDC a 0,1M NHS v deionizované vodě za vzniku aktivního esteru. Po aktivaci byla zaznamenána hladina odezvy senzoru pro povrch ve vodě. 50  $\mu$ g/ml bakteriální protilátky anti-*E.coli* v borátovém pufru (10 mM, pH 8,5) bylo za průtoku 30  $\mu$ l/min napuštěno do mikrofluidického systému SPR senzoru a imobilizováno  $104 \pm 25$  ng/cm<sup>2</sup> protilátky. Následně byly reziduální aktivní estery deaktivovány 36 min jedním ze tří roztoků deaktivčních činidel: (1) roztok glycinu (1M v deionizované vodě, pH 7), nebo (2) roztok kyseliny (2-aminoethoxy)octové (1M v deionizované vodě, pH 7), a nebo (3) roztok ethanolamin-O-sulfátu (0,9 M v deionizované vodě, pH 8).

Takto připravené povrchy byly dále 10 min promývány PBS (10 mM fosfátový pufr + 150 mM NaCl + 2,7 mM KCl, pH 7,4). Potom byla injektována 100% lidská krevní plazma rychlostí 30  $\mu$ l/min při 25 °C po dobu 10 min, následovaná opět promýváním PBS. Po 10 min promývání PBS byl na 5 minut injektován PBS s vyšší iontovou silou (10 mM fosfátový pufr + 750 mM NaCl + 2,7 mM KCl, pH 7,4) a nakonec byl celý povrch relaxován opět v PBS. Nespecifická adsorpce byla určena z rozdílu odezvy senzoru v PBS před injektováním krevní plasmy a 10 min po ukončení injektace. Nespecifická adsorpce po odmytí PBS s vyšší iontovou silou byla určena z rozdílu odezvy senzoru v PBS před injektací krevní plasmy a 10 min po ukončení injektace PBS s vyšší iontovou silou.

Tabulka 4: Porovnání deaktivace reziduálních aktivních esterů - nespecifická adsorpce z neředěné krevní plasmy po deaktivaci dvěma referenčními, v literatuře používanými, činidly a novým činidlem ethanolamin-O-sulfátem.

<b>Deaktivační činidlo</b>	<b>Nespecifická adsorpce ze 100% krevní plasmy (ng/cm<sup>2</sup>)</b>	<b>Nespecifická adsorpce ze 100% krevní plasmy/odmytí PBS s vyšší iontovou silou (ng/cm<sup>2</sup>)</b>
glycin	20,3	13,7
kyselina (2-aminoethoxy)octová	21,2	18,1
ethanolamin-O-sulfát	16,6	6,0

Tabulka 4 dokládá nižší nespecifickou adsorpci z komplexního roztoku po deaktivaci funkcionalizovaného terpolymerního povrchu ethanolamin-O-sulfátem v porovnání s referenčními již publikovanými metodami a dokládá tak zlepšení regenerace antifoulingových vlastností po deaktivaci ethanolamin-O-sulfátem.

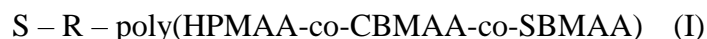
## PATENTOVÉ NÁROKY

1. Statistický terpolymer N-(2-hydroxypropyl) methakrylamidu, karboxybetain methakrylamidu a sulfobetain methakrylamidu.

2. Statistický terpolymer podle nároku 1, vyznačený tím, že obsahuje

- od 0,1 mol % do 40 mol % sulfobetain methakrylamidu;
- od 0,1 mol % do 50 mol % karboxybetain methakrylamidu; a
- N-(2-hydroxypropyl) methakrylamid tvoří v terpolymeru zbytek do 100 mol %.

3. Polymerní kartáč mající strukturu I



kde

S je substrát, na jehož povrch lze kovalentně navázat iniciátory polymerizace;

R je zbytek iniciátoru, vybraného ze skupiny zahrnující iniciátory radikálové polymerizace s přenosem atomu ATRP, iniciátory živé radikálové polymerizace s přenosem jednotlivého elektronu SET-LRP a činidla pro polymerizaci s reverzibilním adičně-fragmentačním přenosem RAFT;

poly(HPMAA-co-CBMAA-co-SBMAA) je statistický terpolymer podle nároku 1 nebo 2;

– je kovalentní vazba.

4. Funkcionalizovaný polymerní kartáč mající strukturu II



kde

S je substrát, na jehož povrch lze kovalentně navázat iniciátory polymerizace;

R je zbytek iniciátoru, vybraného ze skupiny zahrnující iniciátory radikálové polymerizace s přenosem atomu ATRP, iniciátory živé radikálové polymerizace s přenosem jednotlivého elektronu SET-LRP a činidla pro polymerizaci s reverzibilním adičně-fragmentačním přenosem RAFT;

poly(HPMAA-co-CBMAA-co-SBMAA) je statistický terpolymer podle nároku 1 nebo 2;

– je kovalentní vazba;

F je alespoň jedna funkční entita kovalentně navázaná na statistický terpolymer amidovou vazbou prostřednictvím aminoskupiny funkční entity, přičemž s výhodou je funkční entita vybrána ze skupiny zahrnující proteiny, protilátky, peptidy, nukleové kyseliny, oligonukleotidy.

5. Polymerní kartáč podle nároku 3 nebo funkcionalizovaný polymerní kartáč podle nároku 4, vyznačený tím, že je tloušťka vrstvy statistického terpolymeru v polymerním kartáči 10 nm až 500 nm, s výhodou 20 nm až 300 nm, měřeno elipsometrickou metodou ve vodě.

6. Způsob přípravy funkcionalizovaných polymerních kartáčů podle nároku 4, vyznačený tím, že se karboxylové skupiny polykarboxybetainů v polymerním kartáči podrobí reakci s aktivačními činidly pro aktivaci karboxylu za vzniku aktivních esterových skupin; vzniklé aktivní esterové skupiny se dále podrobí reakci s aminovou skupinou funkční molekuly za vzniku amidové kovalentní vazby; a zbylé nezreagované aktivní esterové skupiny se pak podrobí reakci s ethanolamin-O-sulfátem a/nebo amino-PEG2-octovou kyselinou a/nebo glycinem.

7. Použití statistického terpolymeru podle nároku 1 nebo 2 pro zvýšení odolnosti povrchů proti nespecifické adsorpci látek z biologických médií a/nebo proti nespecifické interakci se složkami biologických médií.

8. Použití polymerního kartáče podle nároku 3 nebo funkcionalizovaného polymerního kartáče podle nároku 4 pro zvýšení odolnosti povrchu substrátu proti nespecifické adsorpci látek z biologických médií a/nebo proti nespecifické interakci se složkami biologických médií.

9. Použití funkcionalizovaného polymerního kartáče podle nároku 4 pro specifickou a selektivní interakci s cílovými analyty, zahrnujícími zejména proteiny, peptidy, nukleové kyseliny, oligonukleotidy.

10. Senzor, zejména vybraný ze skupiny zahrnující senzory rezonance povrchových plasmonů, křemenné krystalové mikrováhy nebo fluorescenční senzory, vyznačený tím, že obsahuje polymerní kartáč podle nároku 3 či funkcionalizovaný polymerní kartáč podle nároku 4.

11. Membrána, vyznačená tím, že obsahuje polymerní kartáč podle nároku 3 či funkcionalizovaný polymerní kartáč podle nároku 4.

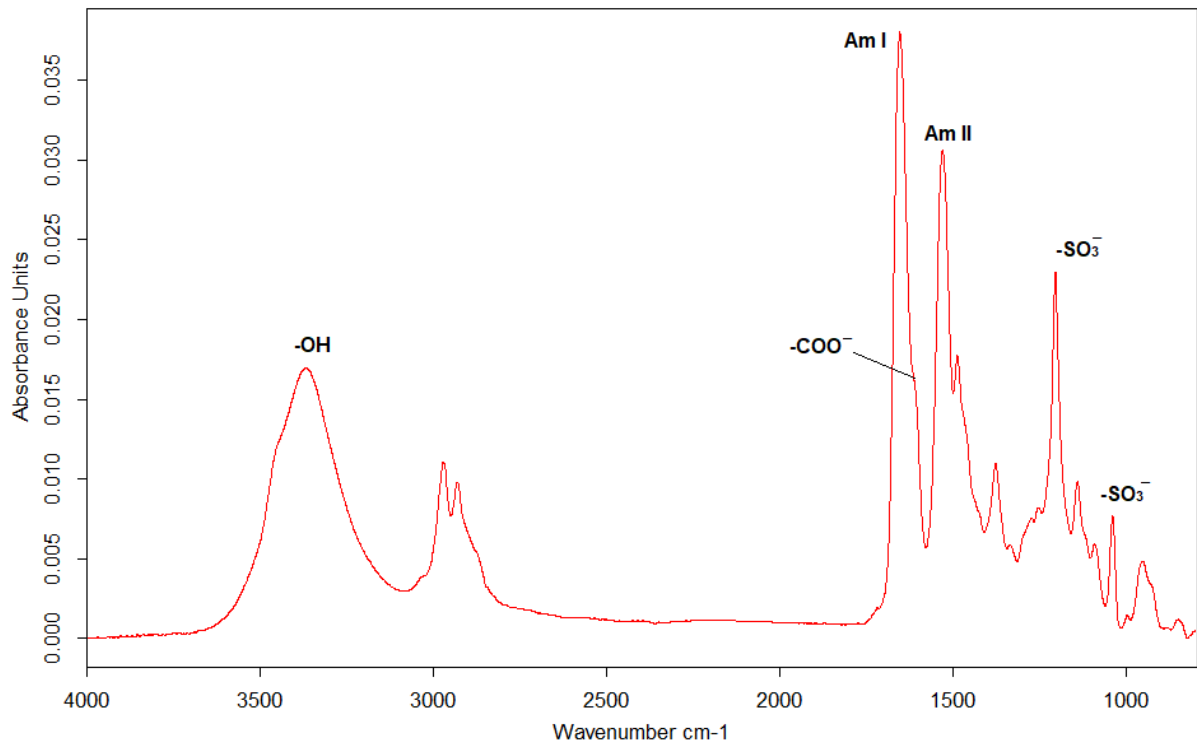
## Anotace

Název vynálezu: Terpolymer pro použití proti nespecifické adsorpci látek z biologických médií, polymerní kartáče jej obsahující

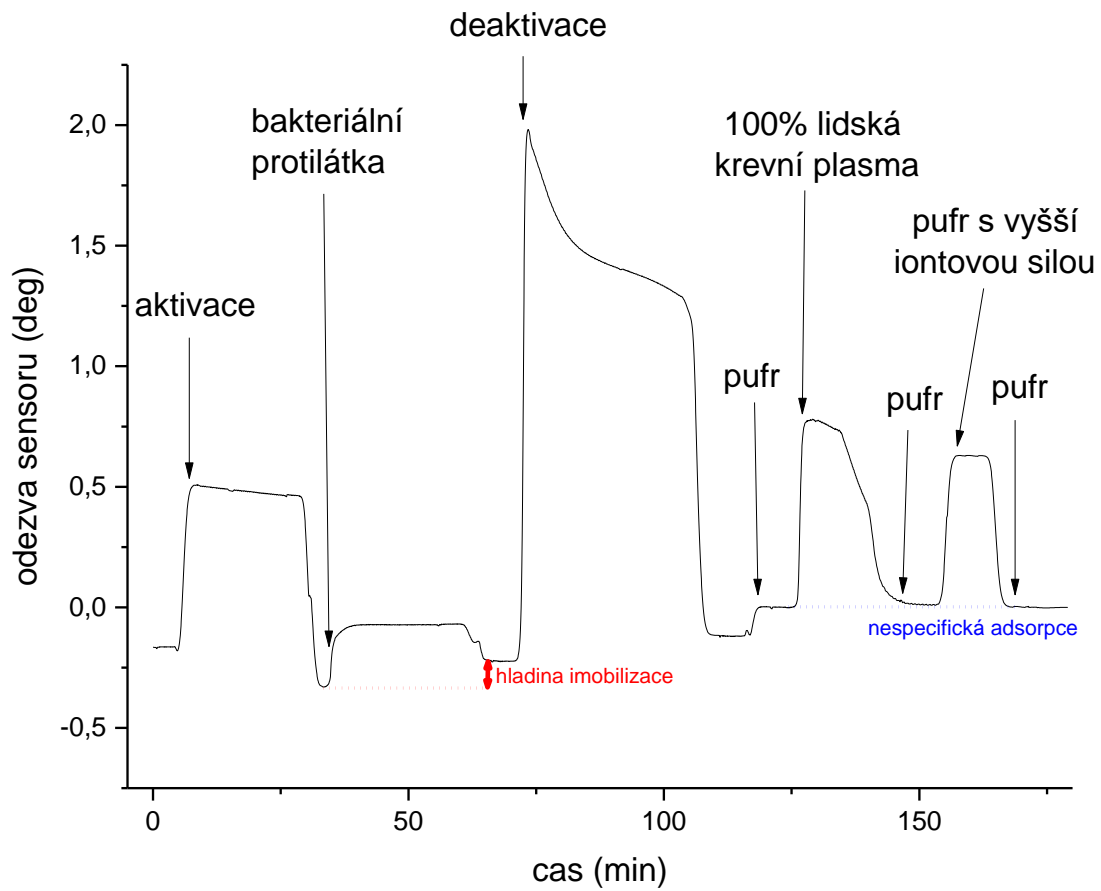
Předmětem předkládaného řešení je statistický terpolymer N-(2-hydroxypropyl) methakrylamidu, karboxybetain methakrylamidu a sulfobetain methakrylamidu, polymerní kartáč a funkcionalizovaný polymerní kartáč obsahující tento terpolymer.

Uvedený statistický terpolymer zvyšuje odolnost povrchu substrátu proti nespecifické adsorpci látek z biologických médií a/nebo proti nespecifické interakci se složkami biologických médií, a je vhodný pro použití ve formě polymerního kartáče např. v senzorech nebo na membránách.

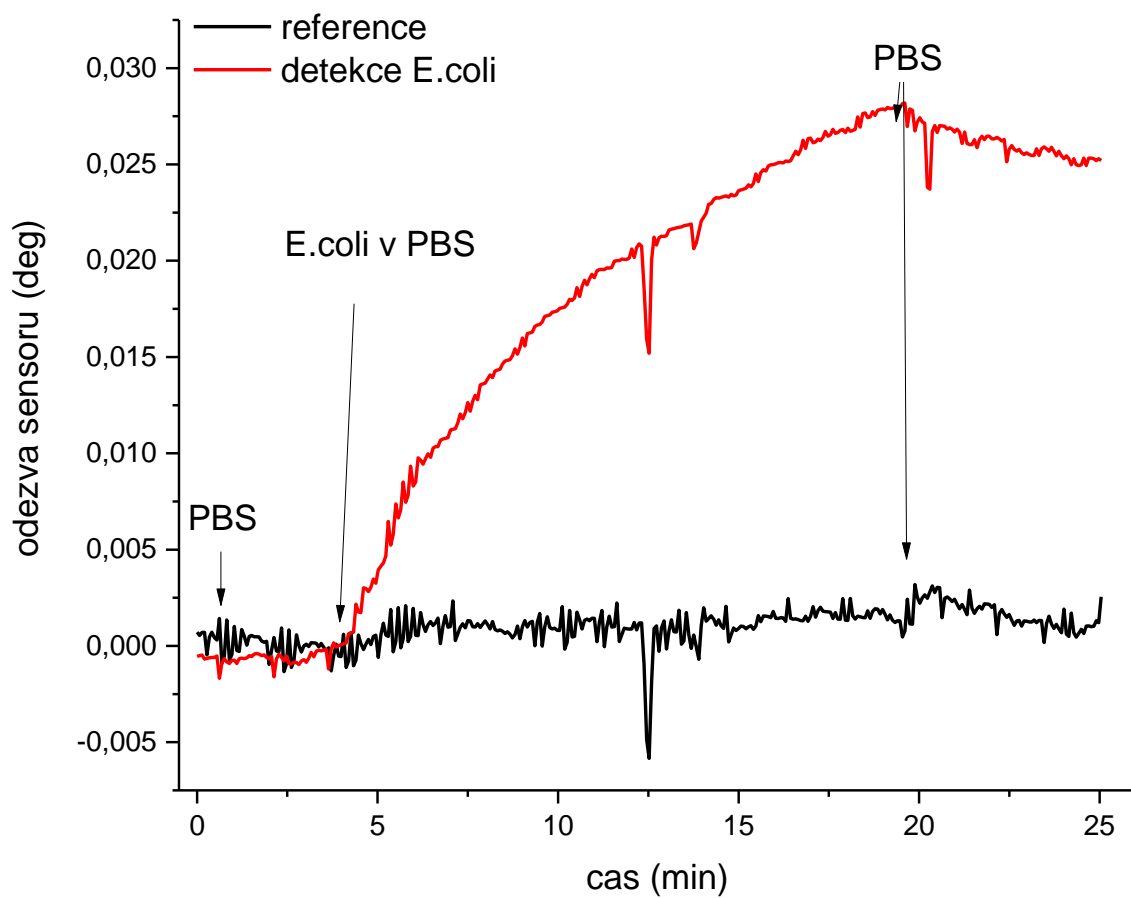




Obr. 1



Obr. 2



Obr. 3

# Appendix XVI

Víšová I., H. Lísalová, M. Vrabcová, M. Houska, M. Forinová, A. Pilipenco

**Vylepšení resistantnosti substrátu obsahujícího karboxybetainové  
funkční skupiny po aktivaci či aktivaci a funkcionalizaci**

Patent application (CZ) to be filed in 3/2021

## **Postup pro zvýšení odolnosti funkcionalizovaného substrátu obsahujícího karboxybetainové funkční skupiny proti nežádoucí depozici z biologických médií**

### Oblast techniky

Vynález se týká způsobu přípravy substrátu obsahujícího karboxybetainové skupiny, na který se navazují bioaktivní látky či jiné funkční molekuly aktivací karboxylové skupiny substrátu na aktivní ester a následnou reakcí s amino skupinou bioaktivní látky. Vynález zásadním způsobem zvyšuje odolnost povrchu proti nežádoucí depozici z biologických médií při zachování funkčnosti navázaných bioaktivních látek tím, že umožňuje individuálně optimalizovat nábojové poměry substrátu s navázanou bioaktivní látkou.

### Dosavadní stav techniky

Při styku prakticky všech běžných materiálů s biologickými médii dochází ke spontánní depozici složek média, tzv. „foulingu“ na povrch materiálu. Největší podíl tvoří nespecificky adsorbované proteiny, na které podle složení daného média mohou dále adherovat buňky a mikroorganismy, následované dalšími biologickými procesy, jako je koagulace krve, zánětlivé a imunitní reakce nebo tvorba bakteriálních biofilmů. Výsledné biologické depozity zhoršují funkci a životnost materiálů a zařízení, a způsobují tak značné komplikace v biotechnologických a lékařských aplikacích (biosenzory, membrány a částice pro separaci a akumulaci biologických látek a buněk, nosiče léčiv a diagnostické částice aplikované do krevního oběhu, materiály přicházející do kontaktu s tělními tekutinami – implantáty, kompenzační pomůcky, lékařské nástroje či nosiče buněk, tzv. scaffolds, pro tkáňové inženýrství, atd.), a také v potravinářství a dalších průmyslových odvětvích (balení a hygiena potravin, životnost podvodních staveb a lodí) a v dalších oblastech, kde se pracuje s komplexními a biologickými médii, jako jsou tělní tekutiny, média obsahující buňky, potraviny a média z biologických výrob a z biologického prostředí obecně. Proto jsou povrchy, které jsou odolné proti nespecifické tvorbě depozitů, a zároveň umožňující navázání bioaktivních látek zprostředkujících specifickou interakci povrchu s cílovými složkami biologického prostředí, velmi důležité a pro následující rozvoj výše zmíněných metod a odvětví nezbytné.

V současné době jsou proti biologické depozici nejvíce odolné substráty („antifouling povrchy“), tzv. polymerní kartáče připravené roubováním elektroneutrálních polymerů, zejména hydrofilních, na povrchy substrátů povrchem iniciovanou radikálovou polymerizací s přenosem atomu (SI-ATRP, „grafting from“). Polymery takových antifouling povrchů jsou s

výhodou buď neionogenní - například poly[N-(2-hydroxypropyl) methakrylamid] (polyHPMAA) a/nebo zwitterionické, například poly(karboxybetain akrylamid) (polyCBAA) nebo poly(karboxybetain methakrylamid) (polyCBMAA). Tyto polymery mohou účinně potlačit i depozici z neředěné krevní plazmy a séra.

Polymerní kartáče s bioaktivními látkami navázanými na karboxybetainové postranní skupiny polyCBAA a polyCBMAA jsou zahrnuté v řadě dokumentů, např. v US20140370567 a US20130244249. Patentová přihláška PV 2015-313, navazující na PCT/CZ2016/050011, popisuje kartáče poly(HPMAA-co-CBMAA) připravené kopolymerizací monomerů HPMAA a CBMAA na povrchu různých substrátů a navázání bioaktivních látek na jejich aktivované karboxybetainové skupiny. Ke stavu techniky patří i hydrogely z kopolymerů poly(HEMA-co-CBMAA) (HEMA = 2-hydroxyethyl methakrylát) odolné proti biologické depozici (Kostina, et al., *Biomacromolecules* 2012, 13, 4164–4170) nebo sorbenty jejichž povrch je modifikován připojením karboxybetainových zwitteriontů (WO2014165421 A1).

Funkcionalizace substrátů obsahujících karboxylovou skupinu se provádí prakticky výhradně tak, že se karboxylová skupina nejprve aktivuje za použití různých N-substituovaných karbodiimidů (CDI) za vzniku aktivního esteru O-acylisourey. Tento meziprodukt velmi ochotně reaguje s nukleofilní aminoskupinou navazované látky za vzniku kovalentní amidické vazby. Výhodněji se reakce provádí za přítomnosti N-hydroxysukcinimidu (NHS) nebo jeho derivátů, který s O-acylisoureu reaguje za vzniku ve vodě stabilnějšího a s aminoskupinou reaktivnějšího aktivního NHS-esteru. Navazovaná látka, zvláště pokud je objemnější, jako například proteiny, nemůže ze sterických důvodů reagovat se všemi aktivními estery uvnitř povrchové vrstvy. Přítomnost reziduálních aktivních esterů po navázání látky je nežádoucí neboť mohou jednak reagovat s jinými (méně objemnými) složkami biologického média a tím způsobovat falešné výsledky, např. při využití pro biosenzory, a dále jejich přítomnost narušuje původní zwitteriontovou nábojovou rovnováhu důležitou pro antifoulingové vlastnosti. Je tedy snahou reziduální aktivní estery deaktivovat, tj. kvantitativně hydrolyzovat zpět na karboxyl ideálně za vzniku původní betainové struktury.

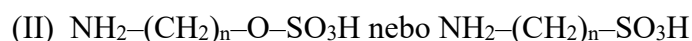
Ovšem kvantitativně regenerovat karboxybetainovou strukturu po aktivaci metodou EDC/NHS pouhou hydrolyzou prakticky nelze. Hydrolyza byla proto poměrně nedávno vystřídaná reakcí reziduálních aktivních esterů s malou molekulou látky obsahující amino- a karboxylovou skupinu, která pomáhá alespoň částečně obnovit počet karboxylových skupin (PV 2016-361). Ukázalo se však, že i přes částečnou obnovu množství karboxylových skupin ve struktuře reakcí například s glycinem se nevytvoří původní betainová struktura

s ionizovaným karboxylem v rovnováze kationtem kvarterního amoniového dusíku. Navíc, při navázání látky na aktivní ester vznikají amidické vazby a zanikají karboxylové skupiny, které již nemohou být obnoveny. Dalším důležitým faktorem je, že sama navázaná látka může svými náboji podstatně změnit nábojový stav povrchu. Všechny tyto faktory mohou vést ke zhoršení antifoulingových vlastností v porovnání s původním substrátem. Pro zachování antifoulingových vlastností celé platformy po funkcionalizaci je tedy třeba nejen pokud možno co nejlépe obnovit původní zwitteriontovou strukturu polymerního substrátu, ale optimálně kompenzovat nábojové změny v důsledku funkcionalizace, tj. navázání bioaktivní látky. To žádný z dosud známých způsobů neumožňuje.

### Podstata vynálezu

Předmětem vynálezu je způsob chemické úpravy substrátu obsahujícího karboxybetainové skupiny po navázání bioaktivní látky metodou EDC/NHS, který vede ke zvýšení odolnosti funkcionalizovaného substrátu proti nežádoucí depozici z biologických médií při zachování funkčnosti navázané bioaktivní látky.

Podstata vynálezu spočívá v deaktivaci reziduálních aktivních esterů a optimalizaci nábojového stavu reakcí s vícesložkovým deaktivčním činidlem. Složky deaktivčního činidla popsané obecnými vzorci (I) a (II) jsou malé molekuly obsahující vždy aminoskupinu pro reakci s aktivním esterem a karboxylovou skupinu (I), nebo sulfátovou nebo sulfo skupinu (II). Složka (II) nese skupinu s permanentním záporným nábojem a jak je ukázáno na příkladech, vhodnou kombinací poměru obou složek se slabou a silnou kyselinou se u funkcionalizovaných povrchů dosáhne zásadního zvýšení odolnosti proti nežádoucí depozici na takové povrchy.



Vynález je vhodný pro úpravy libovolných organických i anorganických povrchů obsahujících karboxybetainové struktury, které se funkcionalizují aktivací karboxylové skupiny (nejběžnější způsob funkcionalizace). Takto připravené biologicky aktivní povrchy vykonávající funkci v biologickém médiu (odolnost proti nespecifické adsorpci, biorekogniční funkce, biomodulační funkce, atd.), mohou mít libovolnou morfologii - např. částice, membrány, trubky, hadičky, destičky, porézní materiál, sítě vláken, a různé použití - např. jako biosenzory, afinitní částice a membrány pro separaci a akumulaci biologických látek, cílené nosiče pro

dopravu léčiv, biomateriály pro tkáňové inženýrství, antitrombogenní materiály určené pro styk s krví.

Podrobněji, předkládaný vynález spočívá v tom, že ihned po aktivaci karboxybetainových skupin a volitelném navázání biologicky aktivní látky se povrch substrátu inkubuje s deaktivčním činidlem obsahujícím minimálně po jedné složce ze dvou skupin látek popsaných obecnými vzorci (I) a (II). Během této inkubace koncové aminoskupiny deaktivčních činidel reagují s reziduálními aktivními estery, které zůstaly v substrátu po navázání bioaktivních látek. Kvarterní amoniová skupina karboxybetainu se reakce neúčastní a její permanentní kladný náboj zůstává zachován, přičemž ani deaktivací slabou karboxy kyselinou [složka (I)] nemusí dojít k jeho účinné neutralizaci. Vhodnou volbou složení deaktivčního činidla obsahujícího složku s permanentním záporným nábojem [složka (II)] se může vyrovnat tento deficit i optimalizovat změny v důsledku funkcionalizace.

Díky použití malých molekul je postup vhodný zejména (nikoli pouze) pro deaktivaci struktur s vysokou hustotou polymerních řetězců obsahujících karboxybetainy, jako jsou polymerní kartáče připravené metodou „grafting from“ nebo zesíťované hydrogely. Malé molekuly EDC/NHS mohou pronikat mezi polymerní řetězce a reagovat s karboxybetainy v celém objemu kartáče, zatímco pro navázání velkých bioaktivních látek, např. proteinů, jsou dostupné pouze karboxybetainy u povrchu kartáče.

Postup, který je předmětem vynálezu, je popsán třemi kroky:

- a) chemická aktivace karboxybetainových skupin na povrchu substrátu převedením karboxylových skupin karboxybetainu na aktivní ester;
- b) kovalentní navázání bioaktivní látky reakcí její aminoskupiny s aktivním esterem připraveným v kroku a); a
- c) reakce produktu z kroku b) s deaktivčním činidlem obsahujícím nejméně po jedné složce z každé ze dvou skupin látek, popsaných obecnými vzorci (I) a (II). Ve výhodném provedení se krok c) se provede tak, že se nejprve produkt z kroku b) opláchnou vodou či pufrům, který byl použit jako rozpouštědlo v kroku b), následně se produkt inkubuje s deaktivčním činidlem, s výhodou při pH 8, následně se opláchnou vodou či pufrům použitým k inkubaci, a následně se opláchnou roztokem, do kterého je pak vložen pro skladování, nebo se opláchnou vodou, vysuší a skladuje suchý.

Substrátem se pro účely předkládaného vynálezu rozumí:

(1) objekt, jehož povrch je pokryt vrstvou polymerního kartáče roubovanou z povrchu (grafting from) živou radikálovou polymerizací, viz PV 2015-313 a PCT/CZ2016/050011,

(2) objekt, jehož povrch je pokryt vrstvou polymerů připravených v roztoku a následně připojených k povrchu kovalentní vazbou nebo fyzikální adsorpcí (grafting to), viz. PCT/CZ2016/050011,

(3) objekt, jehož povrch je pokryt polymerací iniciovanou radikály vytvořenými chemickou nebo fyzikální aktivací povrchu objektu,

(4) objekt, jehož povrch je povlečen adhezující vrstvou polymerů nanesenou z roztoku (polymerní povlak),

(5) objekt, jehož povrch lze modifikovat navázáním molekuly obsahující karboxybetainové skupiny,

(6) objekt, který obsahuje karboxybetainové skupiny ve své struktuře, např. polymerní gel, kde některé monomerní jednotky obsahují karboxybetainové skupiny.

Polymerní vrstvy vytvořené na objektech (1), (2), (3) a (4) vždy obsahují alespoň jeden homopolymer nebo kopolymer obsahující karboxybetainové skupiny v bočních řetězcích. Ve vrstvách na objektech (2) a (4) mohou být polymery obsahující karboxybetainové skupiny ve směsi s hydrofilními polymery, s výhodou vybranými z polyHPMAA, polyHOEGMA [poly(oligo-ethylenglykol methakrylát)], polyHEMA [poly(2-hydroxyethyl methakrylát)] a polyHPMA [poly(2-hydroxypropyl methakrylát)].

S výhodou jsou vrstvy na objektech (1), (2), (3) a (4) vytvořené z homopolymeru vybraného ze skupiny zahrnující polyCBMAA, polyCBMA [poly(karboxybetain methakrylát)] a polyCBAA nebo z kopolymeru poly(A-co-B), kde A je monomerní jednotka vybraná ze skupiny obsahující HPMAA, HOEGMA, HEMA, HPMA a B je monomerní jednotka v koncentraci 1 až 99 mol%, vybraná ze skupiny obsahující CBMAA, CBMA, CBAA.

V jednom provedení je substrát vybraný ze skupiny zahrnující částice, porézní membrány, nosiče buněk („scaffolds“) a biosenzory. Částice jsou s výhodou z materiálu vybraného ze skupiny obsahující zlato, stříbro, magnetické materiály, křemík, SiO<sub>2</sub>, polymery, spadají do definice substrátu (1) až (6) a mají s výhodou průměr od 5 nm do 1 mm. Částice s bioaktivními látkami navázanými na aktivované karboxybetainové skupiny na povrchu částic včetně vnitřního povrchu porézních částic jsou aplikovatelné jako nosiče pro cílenou terapii a



diagnostiku *in vivo*, separaci a akumulaci biologických látek a enzymatickou katalýzu v bioreaktorech.

V jednom provedení je substrátem detekční povrch biosenzoru pro přímou detekci nebo více-  
stupňovou detekci analytů v komplexních biologických médiích, např. pomocí optických nebo  
hmotnostních biosenzorů. S výhodou je detekční povrch pokryt polymerním kartáčem z  
polyCBMAA, polyCBMA, polyCBAA nebo poly(HPMAA-co-CBMAA) s navázanými  
bioreceptory. Bioreceptory v této aplikaci jsou bioaktivní láky mající selektivní afinitu k  
cílovým složkám analyzovaného média.

Biologické (komplexní) medium je pro účely předkládaného vynálezu tekutina obsahující  
biologické látky, tj. biomolekuly a jejich asociáty (proteiny, sacharidy, polysacharidy lipidy,  
nukleové kyseliny, lipoproteiny, glykoproteiny, organely atd.), viry, buňky, mikroorganismy a  
jejich fragmenty. Biologickým médiem je tedy např. krev a ostatní tělní tekutiny, krevní plasma  
a sérum, tkáňové extrakty, buněčné lyzáty a suspence, potravinové extrakty.

Bioaktivní (biologicky aktivní) látkou je pro účely předkládaného vynálezu látka, obsahující  
alespoň jednu primární aminoskupinu, selektivně interagující s cílovou složkou biologického  
média. Bioaktivní látka může mít afinitu k cílové složce, může katalyzovat chemickou přeměnu  
cílové látky, nebo může vyvolávat biologickou odezvu. Bioaktivními látkami mohou být také  
například nanočástice funkcionalizované primární aminoskupinou skupinou, zejména kovové,  
polymerní, silikonové nanočástice, nanočástice na bázi oxidů kovů či polymerní nanočástice  
s magnetickým jádrem.

Aktivní ester karboxybetainu je produkt reakce karboxylové skupiny karboxybetainu s N-  
substituovanými karbodiimidy, tj. O-acyisourea, a/nebo produkt reakce karboxylové skupiny  
karboxybetainu s N-substituovanými karbodiimidy a N-hydroxysukcinimidem (NHS) nebo  
jeho deriváty, s výhodou je aktivním esterem NHS-ester nebo sulfo NHS-ester.

Způsob přípravy povrchu substrátu obsahujícího karboxybetainové skupiny podle  
předkládaného vynálezu poskytuje oproti dosavadnímu stavu techniky účinné, rychlé a  
provedení nenáročné řešení nedostatků plynoucích z depozice nežádoucích složek  
biologických médií na povrchy funkcionalizované bioaktivní látkou a tím i zlepšení funkce  
celého systému.

Deaktivací se pro účely vynálezu rozumí odstranění reziduálních aktivních esterů a jejich  
nahrazení reakcí se deaktivčním činidlem.

## Stručný<sup>[M1]</sup> popis obrázků

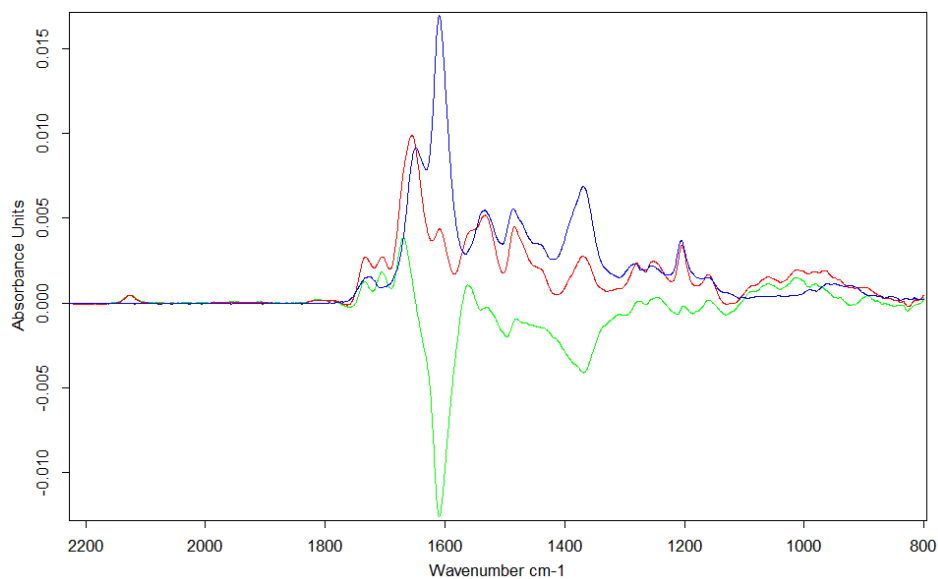
### OBRÁZKY

#### Příklady provedení vynálezu

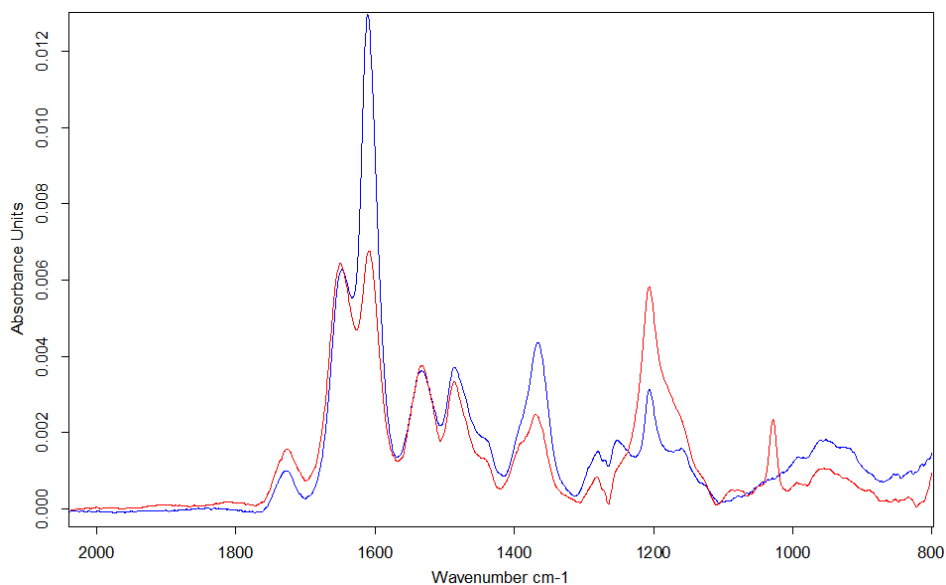
*Příklad 1: PolyCBMAA kartáč aktivovaný EDC/NHS a deaktivovaný činidlem podle vynálezu.*

Polymerní kartáč polyCBMAA byl připraven metodou SI-ATRP následujícím postupem. Zlatý čip (BK7/Ti/Au, 50nm) byl opláchnut ethanolem a vodou a dočištěn 10 min v UV ozonolyzátoru. Čip byl poté ponořena do 0,1 M roztoku iniciátoru  $\omega$ -merkaptoundecyl bromoisobutyrátu v ethanolu na 24 hodin bez přístupu světla. Do Schlenkovy ampule obsahující CuCl (20,0 mg), CuCl<sub>2</sub> (6,0 mg) a Me<sub>4</sub>Cyclam (69,1 mg) bylo přidáno 1,5 ml odplyněného methanolu a katalytická směs byla míchána do úplného rozpuštění. Ve druhé Schlenkově ampuli bylo za chlazení ledem rozpuštěno 2,722 g monomer CBMAA v 12,1 ml odplyněné vody. Po rozpuštění byl do ampule přidán pod dusíkem katalytický roztok. Homogenní polymerační směs byla nadávkována pod dusíkem do druhé Schlenkovy ampule s vloženou destičkou pokrytou iniciátorem a směs byla polymerována 120 min při laboratorní teplotě. Čip byl poté opláchnut vodou a před dalším použitím byl uchována v PBS pufru při 6 °C.

Čip byl opláchnut ultračistou vodou, osušen proudem dusíku a změřeno FT-IRRAS spektrum. Tento čip byl poté 20 min aktivován ve vodném roztoku EDC (0,5 M) a NHS (0,1 M). Po aktivaci a osušení bylo ihned změřeno FT-IRRAS spektrum. Spektrum v obrázku 1 dokládá aktivaci povrchu velkým poklesem intenzity pásů karboxylové skupiny při 1610 cm<sup>-1</sup> a 1370 cm<sup>-1</sup> a zároveň novými pásy NHS esteru v oblasti 1850 cm<sup>-1</sup> až 1700 cm<sup>-1</sup>. Čip připravený stejným způsobem jako čip předchozí byl dále po aktivaci 30 min inkubován v dvousložkovém deaktivčním činidle o složení 0,5M kyselina 2-(2-aminoethoxy)octová (I) + 0,5 M kyselina aminomethansulfonová (II), pH 7. Po inkubaci byl čip krátce opláchnut ultračistou vodou a změřeno FT-IRRAS spektrum. Spektrum v obrázku 2 ukazuje, že vymizely pásy NHS esteru, zvýšila se intenzita pásů karboxylové skupiny a zároveň se objevily intenzivní pásy 1205 cm<sup>-1</sup> a 1030 cm<sup>-1</sup> sulfo skupiny dokládající navázání kyseliny aminomethansulfonové.



**Obrázek 1: Aktivace polyCBMAA. Modrá: nemodifikovaný povrch před aktivací; Červená: povrch ihned po aktivaci EDC/NHS; Zelená: rozdílové spektrum.**



**Obrázek 2: Deaktivace polyCBMAA. Modrá: nemodifikovaný povrch před aktivací; Červená: povrch po deaktivaci 0,5M 2-(2-aminoethoxy)octovou kyselinou + 0,5M amino-methansulfonovou kyselinou při pH 7.**

Příklad 2: *Odolnost kartáčů polyCBAA a poly(HPMAA-co-CBMAA/15 mol%) proti biologické depozici z neředěné krevní plazmy po EDC/NHS aktivaci, funkcionalizaci anti-E.coli a deaktivaci aktivních esterů činidly podle vynálezu.*

Polymerní kartáč polyCBAA byl připraven stejným postupem jako v Příkladu 1.

Polymerní kartáč poly(HPMAA/85 mol%-*co*-CBMAA/15 mol%) byl připraven metodou SI-ATRP následujícím postupem. Zlatý čip (BK7/Ti/Au, 50nm) byl opláchnut ethanolem a vodou a dočištěn 10 min v UV ozonolyzátoru. Čip byl poté ponořena do 0,1 M roztoku iniciátoru  $\omega$ -merkaptoundecyl bromoisobutyrátu v ethanolu na 24 hodin bez přístupu světla. Do Schlenkovy ampule obsahující CuCl (40,0 mg), CuCl<sub>2</sub> (12,0 mg) a Me<sub>4</sub>Cyclam (138,3 mg) bylo přidáno 2,9 ml odplyněného methanolu a katalytická směs byla míchána do úplného rozpuštění. Ve druhé Schlenkově ampuli bylo za chlazení ledem rozpuštěno 0,817 g monomeru CBMAA a 2,734 g HPMAA ve 24,1 ml odplyněné vody. Po rozpuštění byl do ampule přidán pod dusíkem katalytický roztok. Homogenní polymerační směs byla nadávkována pod dusíkem do druhé Schlenkovy ampule s vloženou destičkou pokrytou iniciátorem a směs byla polymerována 120 min při laboratorní teplotě. Čip byl poté opláchnut vodou a před dalším použitím byl uchována v PBS pufru při 6 °C.

Oba čipy s polyCBAA a poly(HPMAA/85 mol%-*co*-CBMAA/15 mol%) byly postupně opláchnuty vodou, osušeny dusíkem, vloženy do SPR senzoru se 4 mikrofluidickými kanály a 5 min omývány ultračistou vodou. Poté byly karboxybetainové skupiny ve všech kanálech 20 min aktivovány vodným roztokem 0,5 M EDC a 0,1 M NHS. Následoval oplach čistou vodou po dobu 1 min. 50  $\mu$ g/ml bakteriální protilátky anti-E.coli bylo rozpuštěno v 10 mM borátovém pufru, pH 8,5 a roztok byl rychlostí 30  $\mu$ l/min injikován do mikrofluidického systému SPR senzoru. Reakcí s aktivovaným povrchem bylo na polyCBAA navázáno  $350 \pm 180$  ng/cm<sup>2</sup> a na poly(HPMAA/85 mol%-*co*-CBMAA/15 mol%)  $80 \pm 35$  ng/cm<sup>2</sup>. Následně byly oba čipy deaktivovány 30 min reakcí s různými deaktivujícími činidly podle vynálezu. Pro oba povrchy byly jako referenční metody deaktivace použité již publikované postupy deaktivace povrchů přeměnou aktivních esterů zpět na karboxylové skupiny reakcí s 1 M roztokem samotné kyseliny 2-(2-aminoethoxy)octové anebo 1 M roztokem glycinu při pH 7. Zkušební čipy byly deaktivovány 30 min dvousložkovými činidly MIX 1 až MIX 5 podle vynálezu, jejichž složení je uvedeno v tabulce 1.

Tabulka 1: Deaktivací dvousložková činidla použitá pro demonstraci vynálezu na dvou polymerních kartáčích.

polyCBAA		poly(HPMAA/85 mol%- <i>co</i> -CBMAA/15 mol%)	
MIX 1	960 mM glycin + 40 mM 2-aminoethyl hydrogen sulfát, pH 7	MIX 4	900 mM 2-(2-aminoethoxy) octová kyselina + 100mM aminomethansulfonová kyselina, pH 7
MIX 2	900 mM glycin + 100 mM aminomethansulfonová kyselina, pH 7	MIX 5	500 mM glycin + 500 mM aminomethansulfonová kyselina, pH 7
MIX 3	900 mM glycin + 100 mM 2-aminoethyl hydrogen sulfát, pH 7		

Následně byl každý čip opláchnut vodou a inkubován v pufru PBS (10 mM fosfátový pufr + 150 mM NaCl + 2,7 mM KCl, pH 7,4) pro dosažení rovnováhy a konstantní odezvy senzoru. Poté byla injektována 100% lidská krevní plasma rychlostí 30 $\mu$ l/min při 25 °C po dobu 10 min, následovaná opět pufrům PBS. Hmotnost nespecifického depozitu byla určena z rozdílu odezvy senzoru v pufru před injektováním krevní plasmy a 10 min po ukončení injektace. Tabulka 2 udává výsledný nespecifický fouling z neředěné krevní plasmy na površích připravených různým způsobem. Pro přepočítání odezvy senzoru na povrchovou hustotu hmotnosti byl použit vztah  $0,001^\circ = 0,85 \text{ ng/cm}^2$ .

Tabulka 2: Hmotnost nespecifického depozitu z neředěné krevní plasmy na dvou rozdílných funkcionalizovaných kartáčích deaktivovaných pěti různými činidly podle vynálezu a porovnání s dvěma referenčními již publikovanými způsoby.

polyCBAA	AEAA (reference)	GLYCIN (reference)	MIX 1	MIX 2	MIX 3
	19 ng/cm <sup>2</sup>	19 ng/cm <sup>2</sup>	5 ng/cm <sup>2</sup>	7 ng/cm <sup>2</sup>	9 ng/cm <sup>2</sup>
poly(HPMAA/85 mol%- <i>co</i> -CBMAA/15mol%)	AEAA (reference)	GLYCIN (reference)	MIX 4	MIX 2	MIX 5
	9 ng/cm <sup>2</sup>	11 ng/cm <sup>2</sup>	5 ng/cm <sup>2</sup>	5 ng/cm <sup>2</sup>	5 ng/cm <sup>2</sup>

Příklad 3: *Odolnost karboxybetainových polymerních kartáčů proti biologické depozici ze vzorků potravin po EDC/NHS aktivaci, funkcionalizaci anti-E.coli a deaktivaci aktivních esterů činidly podle vynálezu.*

Polymerní kartáč polyCBAA byl připraven postupem uvedeným v Příkladu 1 a funkcionalizován  $350 \pm 180 \text{ ng/cm}^2$  anti-*E.coli*, postupem uvedeným v Příkladu 2. Následně byl čip deaktivován 30 min reakcí s různými deaktivujícími činidly. Jako referenční metoda deaktivace byla použita již publikovaná metoda přeměny aktivních esterů zpět na karboxylové skupiny reakcí s 1 M roztokem glycinu při pH 7. Zkušební čipy byly deaktivovány 30 min dvousložkovými činidly MIX 1 a MIX 2 podle vynálezu, jejich složení je uvedeno v tabulce 1 u příkladu 1.

Následně byl čip opláchnut vodou a inkubován v pufru PBS (10 mM fosfátový pufr + 150 mM NaCl + 2,7 mM KCl, pH 7,4) pro dosažení rovnováhy a konstantní odezvy senzoru. Poté byl injektován vzorek hovězího mletého masa (připravený homogenizací dle protokolu popsáno v ČSN ISO 7251 a ČSN EN ISO 6579) rychlostí 30  $\mu\text{l/min}$  při 25 °C po dobu 10 min, a potom opět pufr PBS. Hmotnost nescifického depozitu uvedená v tabulce 3 byla určena z rozdílu odezvy senzoru v pufru před injektováním vzorku potravin a 10 min po ukončení injektace. Pro přepočítání odezvy senzoru na povrchovou hustotu hmotnosti byl použit vztah  $0,001^\circ = 0,85 \text{ ng/cm}^2$ .

Tabulka 3: Hmotnost nescifického depozitu ze vzorku potravin - hovězího mletého masa - na funkcionalizovaném polyCBAA deaktivovaném dvěma různými činidly podle vynálezu a porovnání s referenčním již publikovaným způsobem.

polyCBAA	Glycin	MIX 1	MIX 2
	10 $\text{ng/cm}^2$	8 $\text{ng/cm}^2$	2 $\text{ng/cm}^2$

*Příklad 4: Příklad aplikace vynálezu při detekci bakterie E.coli ve vzorcích potravin.*

Polymerní kartáč polyCBAA byl připraven postupem uvedeným v Příkladu 1 a funkcionalizován  $350 \pm 180 \text{ ng/cm}^2$  anti-*E.coli* postupem uvedeným v Příkladu 2. Následně byl čip deaktivován 30 min reakcí s různými deaktivujícími činidly. Jako referenční metoda deaktivace byla použita již publikovaná metoda přeměny aktivních esterů zpět na karboxylové skupiny reakcí s 1 M roztokem glycinu při pH 7. Zkušební čip byl deaktivován 30 min dvousložkovým činidlem MIX 2 podle vynálezu, jehož složení je uvedeno v tabulce 1 u příkladu 1. Následně byl čip opláchnut vodou a inkubován v pufru PBS (10 mM fosfátový pufr + 150 mM NaCl + 2,7 mM KCl, pH 7,4) pro dosažení rovnováhy a konstantní odezvy senzoru. Poté byl injektován vzorek hovězího mletého masa (připravený homogenizací dle protokolu popsáno v ČSN ISO 7251 a ČSN EN ISO 6579) infikovaný různými

koncentracemi bakterie Ecoli ( $0 - 1 \times 10^7$  CFU/ml) rychlostí 30  $\mu$ l/min při 25 °C po dobu 10 min. Následovalo opět propláchnutí PBS. Hladina detekce byla určena z rozdílu odezvy senzoru v pufru před injektováním vzorku potravin a 10 min po ukončení injektace. Data byla poté kompenzována odezvou referenčního kanálu s nulovou koncentrací bakterie *E.coli*. Tabulka 4 udává výsledné meze detekce (LOD, hodnota blanku + 3 $\times$  směrodatná odchylka šumu) a meze stanovitelnosti (LOQ, hodnota blanku + 10 $\times$  směrodatná odchylka šumu) dopočítané ze získaných kalibračních křivek. Pro přepočítání odezvy senzoru na hmotnost na jednotku povrchu byl použit vztah  $0,001^\circ = 0,85$  ng/cm<sup>2</sup>.

Tabulka 4: LOD a LOQ kalibračních křivek detekce *E.coli* ve vzorcích potravin (hovězí mleté maso) za použití referenční (již publikované) přípravy vzorku a podle vynálezu.

polyCBAA	LOD (Glycin)	LOD (MIX 2)	LOQ (Glycin)	LOQ (MIX 2)
	[ng/cm <sup>2</sup> ]			
	$7 \times 10^5$	$6 \times 10^3$	$1 \times 10^6$	$9 \times 10^4$

## PATENTOVÉ NÁROKY

1. Postup pro zvýšení odolnosti funkcionalizovaného substrátu obsahujícího karboxybetainové funkční skupiny proti nežádoucí depozici z biologických médií vyznačený tím, že po funkcionalizaci substrátu EDC/NHS metodou se odstraní reziduální aktivní estery reakcí s vícesložkovým deaktivčním činidlem, které se na substrát naváže amidickou vazbou.

2. Postup podle nároku 1. vyznačený tím, že vícesložkové deaktivční činidlo obsahuje dvě složky (I) a (II) obsahující látky obecného vzorce:

(I)  $\text{NH}_2-(\text{CH}_2)_n-\text{COOH}$  nebo  $\text{NH}_2-(\text{CH}_2-\text{CH}_2-\text{O})_n-\text{CH}_2-\text{COOH}$ ;

(II)  $\text{NH}_2-(\text{CH}_2)_n-\text{O}-\text{SO}_3\text{H}$  nebo  $\text{NH}_2-(\text{CH}_2)_n-\text{SO}_3\text{H}$ ,

příčemž složky deaktivčního činidla popsané obecnými vzorci (I) a (II) jsou malé molekuly obsahující vždy aminoskupinu pro reakci s aktivním esterem a karboxylovou skupinu (I) nebo sulfátovou nebo sulfo skupinu (II), tj. skupinu s permanentním záporným nábojem.

3. Postup podle nároku 1. a 2. vyznačený tím, že vhodným výběrem a poměrem obou složek se slabou a silnou kyselinou se upraví nábojové poměry a dosáhne zvýšení odolnosti funkcionalizovaných povrchů proti nežádoucí depozici na takové povrchy.

4.



# Appendix XVII

H. Lísalová, M. Vrabcová, I. Víšová, M. Houska, A. Dejneka

**Terpolymer and polymer brushes for use against non-specific  
adsorption of substances from biological media**

Patent application (International) to be filed in 3/2021

## **Terpolymer and polymer brushes for use against non-specific adsorption of substances from biological media**

### Field of Art

The invention relates to a new random anti-fouling terpolymer, to polymer brushes containing the terpolymer, and to their use against non-specific adsorption of substances from biological media.

### Background Art

Non-specific adsorption is an undesirable deposition of substances from complex biological samples, which represents a critical problem for the development of many modern bioanalytical and biomedical methods, equipment and materials. These include biosensors, separation methods, functional nanoparticles and nanostructured surfaces, drug carriers, membranes, diagnostic particles for analysis in body fluids, generally any bioanalytical methods and functional materials that come into direct contact with the biological medium. Therefore, great efforts are devoted to the development of so-called ultra-resistant materials and surfaces which effectively combine the ability to bind functional, e.g. biorecognition elements, and which are also resistant to non-specific adsorption of substances even from very complex biological media such as undiluted body fluids, food extracts, media containing cells, tissue samples and parts of organisms in general, or fluids from environments of a general nature.

Currently, the most resistant (so-called 'anti-fouling' or 'ultra-low fouling') and at the same time functionalizable surfaces are those prepared by polymerization from the surface ('grafting from') of hydrophilic electroneutral polymers, such as non-ionogenic poly(oligo (hydroxyethyleneglycol methacrylate) (polyHOEGMA), poly(2-hydroxyethyl methacrylate) (polyHEMA), poly(3-hydroxypropyl methacrylate) (polyHPMA), poly[N-(2-hydroxypropyl methacrylamide)] (polyHPMAA) and ionogenic zwitterionic poly(carboxybetain methacrylate) (polyCBMA), poly(carboxybetaine acrylamide) (polyCBAA) and a random copolymer of N-(2-hydroxypropyl) methacrylamide (HPMAA) with carboxybetaine methacrylamide (CBMAA) (poly(HPMAA-co-CBMAA)), from the surface of substrates by surface-initiated atom-transfer radical polymerization (ATRP). The procedure involves covalently attaching an ATRP initiator to the surface of the substrate (S). After the addition of the polymerization solution containing the monomers, the polymer chains grow from the bound initiator residue (R) by successive attachment of the monomer units, the halogen initiating atom always being transferred to the end of the growing polymer chain. The result of the procedure is a so-called polymer brush, which is a layer of densely arranged polymer chains linked by one end to the surface of the

substrate according to the formula: S-R-polymer chain. In the current state of the art, it is not possible to reliably determine the length of the individual chains nor the density of the brush for polymer brushes grafted from the surface. Therefore, the brush is usually characterized only by the thickness measured by the ellipsometric method with surface plasmon resonance (SPR) or by atomic force microscopy (AFM).

Preparation and activation of brushes from polyCBMA and polyCBAA homopolymers are disclosed in the document US20140370567. This document describes, inter alia, anti-fouling surfaces prepared by grafting polyCBMA and polyCBAA homopolymers from a substrate surface by ATRP or RAFT polymerization, and block copolymers comprising a hydrophobic polymer block and a polyCBMA or polyCBAA homopolymer block grafted by polymerization from the surface or bonded to the substrate surface. Document US20130244249 describes a procedure using a two-stage ATRP in which a polymer layer with a high chain density and good anti-fouling properties is first grafted onto the surface. Onto this layer, a second layer of polyCBMA or polyCBAA of low density polymer chains with reactive groups along the chain is grafted, which serves to immobilize the bioactive elements. The explicitly claimed aim of this procedure is to increase the availability of reactive groups for the binding of large molecules in the second layer, but the document does not address the issue of side reactions and undesired reaction residues. Document PV 2015-313 discloses the preparation and use of random copolymer poly(HPMAA-co-CBMAA) and compares its anti-fouling properties after anchoring functional elements with polyCBAA.

Although all of the above polymer brushes suppress non-specific adsorption from model protein solutions and reduce deposition from undiluted blood plasma below 50 ng/cm<sup>2</sup>, HPMAA, CBMA and CBAA brushes are currently the only 'ultra-low fouling' surfaces that reduce non-specific binding of substances from blood plasma below 5 ng/cm<sup>2</sup>. It is generally accepted that high resistance to non-specific adsorption is due to a combination of high hydrophilicity, which limits hydrophobic interactions, and net electroneutrality, which limits electrostatic interactions. The binding of functional entities, which can be substances and large molecules with different domains and a large number of charges, can significantly change this surface characteristic and worsen the initially excellent resistance.

E.g. for binding of functional entities to the non-ionogenic polymer chains, the activation of their side hydroxyl groups is used, which, however, leads to the formation of products which significantly impair or completely destroy the resistance of the brushes to non-specific adsorption.

The electroneutral zwitterionic side groups of the polyCBMA and polyCBAA chains contain a carboxylate anion and a quaternary ammonium cation. The carboxyl group of the zwitterion is usually

converted to an active ester by EDC-NHS chemistry, but other carboxyl activating agents known to those skilled in the art (Bioconjugate Techniques, G.T.Hermanson, Elsevier, 2013) can be used, which then reacts with the amino group of the functional element to form an amide bond. However, part of the unreacted active esters always remain in the polymer and then must be removed quantitatively, so that upon subsequent contact with the biological medium they cannot react non-specifically with its components, as well as to preserve as much as possible the original electroneutrality of the polymer, i.e. to compensate for the predominance of the permanent positive charge of the quaternary ammonium group. Simple hydrolysis of the active ester is not sufficient for this, and therefore the remaining active esters are preferably eliminated by reaction with a small molecule containing an amino group and a carboxyl group, e.g. with glycine (PV 2016-361). However, none of these methods has so far proved to be entirely satisfactory, and it is the loss of the overall electroneutrality of the surface that is considered to be one of the key factors leading to reduced brush anti-fouling ability after binding of functional elements.

The present invention aims to overcome the above disadvantages.

#### Disclosure of the Invention

The present invention relates to a random terpolymer of N-(2-hydroxypropyl) methacrylamide (HPMAA), carboxybetaine methacrylamide (CBMAA) and sulfobetaine methacrylamide (SBMAA). This terpolymer is designated as poly(HPMAA-co-CBMAA-co-SBMAA).

Preferably, the random terpolymer contains from 0.1 to 40 mol% SBMAA, more preferably from 0.5 to 30 mol% SBMAA.

Preferably, the random terpolymer of the invention contains from 0.1 to 50 mol% CBMAA, more preferably from 5 to 30 mol% CBMAA, even more preferably from 10 to 20 mol% CBMAA.

HPMAA forms the balance to 100 mol% in the terpolymer.

The invention further relates to a polymer brush containing the random terpolymer of N-(2-hydroxypropyl) methacrylamide (HPMAA), carboxybetaine methacrylamide (CBMAA) and sulfobetaine methacrylamide (SBMAA), the chains of which are linked by one end (end-tethered) to a substrate, the polymer brush having the structure I,



wherein

S is a substrate having a surface suitable for binding of polymerization initiators;

R is a residue of a polymerization initiator selected from the group consisting of ATRP initiators, SET-LRP initiators and RAFT agents;

– is a covalent bond.

A polymer brush is a structure that consists of polymer chains end-tethered (linked by one end) to a substrate, the polymer chains being arranged densely next to each other so as to extend away from the substrate. The resulting structure of the polymer chains resembles the fibres of a brush, hence the name.

Preferably, the thickness of the random terpolymer layer in the polymer brush is 10 to 500 nm, more preferably 20 to 200 nm, as measured by the ellipsometric method in water.

The invention also relates to a functionalized polymer brush of random terpolymer of N-(2-hydroxypropyl) methacrylamide (HPMAA), carboxybetain methacrylamide (CBMAA) and sulfobetaine methacrylamide (SBMAA), having the structure II



wherein

S is a substrate having a surface suitable for binding of polymerization initiators;

R is a residue of a polymerization initiator selected from the group consisting of ATRP initiators, SET-LRP initiators and RAFT agents;

– is a covalent bond;

F is at least one functional entity covalently bound to the random terpolymer by an amide bond.

The present invention solves the above-described problem of loss of total surface electroneutrality in problematic hydrolytic reactions of residual active esters, which leads to reduced brush anti-fouling properties after binding of functional molecules. In the procedures known in the art, the hydrolysis of residual active esters, including using substances containing a carboxyl group, can regenerate carboxyl groups, but not completely, since the loss caused by the binding of the functional element is not compensated. The zwitterion thus replaced is also not structurally identical to the original zwitterion. It is also generally known that the electroneutrality of carboxybetaines is pH dependent due to changes in carboxyl group ionization while maintaining a permanent positive charge of the quaternary ammonium cation. The binding of a functional entity, which can be, for example, a large molecule with different domains and a large number of charges on its own, creates a substantially altered microenvironment on the surface, i.e. also a local pH, and thus affects the charge balance. The present invention solves this problem in a new way, by adjusting the equilibrium through adding the SBMAA monomer unit, which is a betaine with a permanently ionized sulfo group. The sulfo group does not participate in the reaction

of activating carboxyl groups with activating agents (e.g. EDC-NHS or other carboxyl activating agents known to the person skilled in the art), therefore a polySBMAA homopolymer could not be functionalized. Furthermore, a polySBMAA homopolymer does not have good anti-fouling properties. In poly(HPMAA-co-CBMAA-co-SBMAA), the functionalizability is ensured by the presence of CBMAA. The use of SBMAA in combination with HPMAA and CBMAA for the polymer brush has not been known so far. Surprisingly, the use of SBMAA is very advantageous and effective for overcoming the drawbacks of the prior art polymer brushes.

Within the above-mentioned range from 0.1 to 30 mol%, the SBMAA content in the random terpolymer may be optimized to cooperate with the functional entity to achieve the highest resistance to non-specific adsorption. This optimization can be performed by preparing several samples with different SBMAA contents within the described range, and selecting the appropriate SBMAA content according to the desired parameters.

The terpolymer of the present invention possesses a high resistance to non-specific adsorption of substances from biological media, and likewise the polymer brushes containing the said terpolymer possess high anti-fouling properties, even after the activation reaction (i.e., the active ester formation), binding of functional entity and deactivation.

The term "biological media" herein refers to body fluids, such as blood, cerebrospinal fluid, urine, saliva and ascitic fluid, but also to other media of biological origin, such as blood plasma and serum, cell lysates, tissue extracts, cell suspensions, media from biological production, drinking water, waste water and/or foodstuff.

The substrate S is a material that is coated with a functionalizable layer of terpolymer resistant to non-specific adsorption. The substrate is any material to the surface of which polymerization initiators can be covalently attached. Thus, suitable substrates include, in particular, materials containing reactive groups on the surface or inert materials coated with an anchoring layer adhering well to their surface and containing reactive groups for the attachment of an initiator, for example a layer of polydopamine prepared by autopolymerization on the surface of the material. The shape, dimensions, morphology and chemical nature of the substrate are not critical. The substrates may include planar or variously shaped objects, tubes, fibres, particles, membranes, microparticles, nanoparticles, porous materials. Materials of the substrate may include metals, silicon, silicate or aluminosilicate based materials (e.g. glass), polymers, inorganic materials - especially oxides of metals or non-metals, etc. In a preferred embodiment, the materials are in particular metals, silicon, oxides of metals or non-metals, silicates or

aluminosilicates. The substrate can be, for example, a surface of a sensor, a surface of a biosensor, or a sorbent, or a surface of a device or material used in healthcare.

The group R designates the residue of an initiator. To anchor the copolymer chain (for a grafting-from reaction), a polymerization initiator is first be attached to the substrate. Suitable initiators and suitable types of polymerization for grafting from the surface are known to the person skilled in the art, including ATRP (atom transfer radical polymerization) initiators, SET-LRP (single-electron transfer living radical polymerization) initiators or RAFT (reversible addition fragmentation transfer) polymerization reagents. The procedure for binding of the initiator to the substrate depends on the type of the substrate and the initiator, but its determination, as well as the determination of a suitable initiator for each substrate, is within the knowledge and ability of a person skilled in the art, without the need for further inventive efforts (a number of monographs, textbooks and review articles are available to the person skilled in the art, for example *Advanced Materials by Atom Transfer Radical Polymerization*, Krzysztof Matyjaszewski, Wiley Online Library, 2018).

F is a functional entity covalently attached by an amide bond to the polymer brush, more specifically to the residue of the carboxyl group of a CBMAA monomer unit. F is an entity containing an amino group, e.g. selected from proteins, peptides, antibodies, oligonucleotides, nucleic acids, DNA probes. F can be a biorecognition entity that specifically interacts with a target analyte, which may be, for example, a protein, a peptide, a nucleic acid, an oligonucleotide, or other organic or inorganic analytes.

The terpolymer poly(HPMAA-co-CBMAA-co-SBMAA) may be prepared by known techniques, e.g. by living radical polymerization methods. The terpolymer brush may be prepared by living radical polymerization from the surface of a substrate to form polymer brush chains end-tethered to the surface of the substrate. "Grafting to" methods can also be used, where an already synthesized polymer chain binds to the substrate.

Suitable polymerization methods for preparing the random terpolymer of the invention or a polymer brush containing the terpolymer, e.g. ATRP polymerization, SET-LRP polymerization, RAFT polymerization, their use for individual substrate types, the corresponding initiators and the corresponding reactive groups for initiator and substrate combinations are known from literature. Examples of combinations of initiators suitable for certain substrates are: 11-(trichlorosilyl)undecyl-2-bromo-2-methyl propanoate on glass and oxide-coated silicon; or  $\omega$ -mercaptoundecyl bromisobutyrate on gold; or an initiator bound to the surface of a substrate containing carboxyl groups which is prepared by incubation with a solution of  $\alpha$ -bromo-isobutyric acid, EDC and NHS; or 2-bromo-2-

methylpropanoyl bromide as an initiator for a substrate containing amino or hydroxyl groups on the surface, such as a polydopamine layer.

All monomers are methacrylamides of a similar type in terms of polymerization, have a similar polymerization rate constant, and the statistical nature of the polymerization is evidenced by the molar ratio of concentrations of SBMAA, HPMAA and CBMAA monomer units in terpolymers, identical to the polymerization batch composition.

The preparation of functionalized polymer brushes is performed by reacting the carboxyl groups of polycarboxybetaines (CBMAA units) in a polymer brush with activating agents, such as for example EDC (1-ethyl-3-(3-dimethylaminopropyl)-carbodiimide) and NHS (N-hydroxysuccinimide), to form active ester groups. The resulting active ester groups are further reacted with the amine group of a functional entity to form an amide covalent bond. The remaining unreacted active ester groups are then reacted with a deactivating agent, for example ethanolamine-O-sulphate and/or (2-aminoethoxy)acetic acid (amino-PEG2-acetic acid) and/or glycine. The use of ethanolamine-O-sulphate allows to optimize the overall charge of the surface.

The invention allows for universal anti-fouling treatment of various substrates containing reactive groups for the attachment of polymerization initiators. An anchoring interlayer, for example polydopamine, may be deposited on the surface of an inert substrate. The initiators cannot be bound to an inert substrate directly. The anchoring interlayer contains reactive groups for the attachment of initiators.

The present invention also relates to the use of the random terpolymer poly(HPMAA-co-CBMAA-co-SBMAA) for increasing the resistance of a surface to non-specific adsorption of substances from biological media (i.e., for increasing anti-fouling properties of a surface). In such use, the surface can be coated with the terpolymer poly(HPMAA-co-CBMAA-co-SBMAA), for example in the form of a coating or in the form of a polymer brush.

More specifically, the invention relates to the use of the random terpolymer poly(HPMAA-co-CBMAA-co-SBMAA) in the form of the terpolymer brush or a coating, or functionalized terpolymer brush, to achieve (substrate) surface resistance to undesired non-specific interaction with biological media components, especially with protein molecules and cells, and to achieve (substrate) surface resistance to adsorption/deposition of biological media components on the surface protected by the terpolymer.



The invention further includes the use of the functionalized terpolymer brush poly(HPMAA-co-CBMAA-co-SBMAA) for specific and selective interaction with a target analyte, such as a protein, a peptide, a nucleic acid, an oligonucleotide.

The present invention further encompasses sensors, in particular biosensors, for direct analyte detection or for multi-stage detection using added reagents, such as surface plasmon resonance (SPR) sensors, quartz crystal microbalance or fluorescent sensors that contain the polymer brush or the functionalized polymer brush according to the invention.

The present invention further includes membranes comprising the polymer brush or the functionalized terpolymer brush of the invention. The substrate is then typically a membrane, the layer of polymer chains being grafted onto the membrane surface. If the membrane is porous, the layer of polymer chains is grafted onto the surface of the pores.

The terms “polymer brush” and “terpolymer brush” in this chapter refer to a polymer brush consisting of the terpolymer poly(HPMAA-co-CBMAA-co-SBMAA).

#### Brief Description of Drawings

Figure 1 shows a typical IRRAS spectrum of the poly[HPMAA(70 mol%)-co-CBMAA(15 mol%)-co-SBMAA(15 mol%)] brush on gold. The characteristic absorption bands of the groups of individual components are marked: Am I and Am II for amide bands of the chain, -OH for the band of the hydroxyl group of HPMAA, -COO<sup>-</sup> for the band of the ionized carboxyl group of CBMAA, -SO<sub>3</sub><sup>-</sup> for the bands of the ionized sulfo group of SBMAA.

Figure 2 shows PM-IRRAS spectra of terpolymer prepared in solution by RAFT polymerization as described in Example 3.

Figure 3 is a response pattern of SPR sensor with a chip with gold surface coated with the polymer brush, according to Examples 4 and 5.

Figure 4 is a response pattern of SPR sensor upon detection of *E.coli* on the functionalized terpolymer brush, according to Example 6.

Figure 5: Detection of SARS-Cov-2 spiked in cell cultured medium using poly[HPMAA(77 mol %)-co-CBMAA (20 mol %)-co-SBMAA(3 mol %)] functionalized QCM platform with anti- SARS-Cov-2 antibodies (Example 8).

Figure 6: Detection of  $1 \times 10^5$  PFU/mL SARS-CoV-2 spiked in cultured cell medium using QCM sensor based on short peptide-functionalized poly[HPMAA(77 mol %)-co-CBMAA (20 mol %)-co-SBMAA(3

mol %)] surface (Example 9). The figure shows the detection response (black line) and blank response (red).

### Examples

#### Example 1: Preparation of a polymer brush on gold

A glass plate with a vapour-deposited gold layer was cleaned in a UV ozone generator for 10 minutes, then immediately rinsed with water and ethanol. The plate was then immersed in a 0.1 mM solution of  $\omega$ -mercaptoundecyl bromoisobutyrate initiator in ethanol for 48 hours at room temperature without exposure to light. The catalyst mixture was prepared in a Schlenk flask by dissolving CuCl (28 mg), CuCl<sub>2</sub> (8.4 mg) and Me<sub>4</sub>cyclam (96.8 mg) in degassed methanol (2 mL) under a nitrogen atmosphere and sonicated for 5 minutes until complete dissolution. In a second Schlenk flask, the monomers SBMAA (138 mg, 3 mol%), CBMAA (572 mg, 15 mol%) and HPMAA (1.847 mg, 82 mol%) were dissolved in degassed water (16.9 mL) and methanol (0.1 mL). Examples of additional batches for the preparation of surfaces with a different percentage of components are given in Table 1. After dissolution, the catalyst mixture was added to the monomer mixture under nitrogen. The homogeneous polymerization mixture was added to the reactor with a plate coated with initiator under nitrogen. The polymerization was carried out in the closed reactor for 2 hours at room temperature. The plate was then rinsed with water and stored in phosphate buffer (pH 7.4) at 4 °C before further use.

The chemical structure of the terpolymer brush was verified by infrared reflection absorption spectroscopy (PM-IRRAS). Figure 1 shows a typical IRRAS spectrum for one embodiment of the terpolymer brush.

Table 1: Selected examples of batches for the preparation of terpolymer with different content of individual monomers

Composition of polymerization batch [mol%]			Composition of polymerization batch [mg]		
HPMAA	CBMAA	SBMAA	HPMAA	CBMAA	SBMAA
84.5	15.0	0.5	1.903	572	23
82.0	15.0	3.0	1.847	572	138
80.0	15.0	5.0	1.802	572	230
75.0	15.0	10.0	1.689	572	460
70.0	15.0	15.0	1.576	572	690
55.0	15.0	30.0	1.239	572	1.379

### Example 2: Preparation of a polymer brush on glass

A glass plate was rinsed with acetone, sonicated for 20 minutes in 50% methanol at 20 °C and then sonicated for another 20 minutes in chloroform. The plate was then rinsed with water, air dried and cleaned for 4 minutes in a UV ozone generator. After cleaning, the plate was dehydrated for 1 hour at  $\geq 90$  °C in the presence of silica gel and immediately then immersed for 2 hours in a 3 mM solution of the initiator  $(\text{MeO})_3\text{-Si-(CH}_2\text{)}_{11}\text{-Br}$  in anhydrous n-heptane at room temperature. The plate was then rinsed with ethanol and water and placed in the reactor to polymerize. Another procedure for preparing the polymer brush is analogous to Example 1 above. The catalyst mixture was prepared in a Schlenk flask by dissolving CuCl (28 mg), CuCl<sub>2</sub> (8.4 mg) and Me<sub>4</sub>cyclam (96.8 mg) in degassed methanol (2 mL) under nitrogen atmosphere and sonicated for 5 minutes until complete dissolution. In a second Schlenk flask, the monomers SBMAA (138 mg, 3 mol%), CBMAA (572 mg, 15 mol%) and HPMAA (1,847 mg, 82 mol%) were dissolved in degassed water (16.9 mL) and methanol (0.1 mL). (Other examples of batches are the same as the examples of batches listed in Table 1). After dissolution, the catalyst mixture was added to the monomer mixture under nitrogen. The homogeneous polymerization mixture was added to the reactor with a plate with attached initiator under nitrogen. The polymerization was carried out in the closed reactor for 2 hours at room temperature. The plate was then rinsed with water and stored in phosphate buffer (pH 7.4) at 4 °C before further use.

### Example 3: Preparation of terpolymer in solution by RAFT polymerization

The terpolymer (pSBMAA 3 mol. %; pCBMAA 20 mol. %; pHPMAA 77 mol. %) in solution was prepared using modified RAFT (Reversible Addition Fragmentation Transfer) polymerization procedure described previously (C. Rodriguez-Emmenegger, B. V. K. J. Schmidt, Z. Sedlakova, V. Šubr, A. Bologna Alles, E. Brynda, C. Barner-Kowollik, *Macromolecular Rapid Communications* **2011**, 32, 958).

Briefly, monomers – *N*-(2-hydroxypropyl)methacrylamide (HPMAA; 344.0 mg; 77 mol. %), carboxybetaine methacrylamide (CBMAA; 151.2 mg; 20 mol. %) and sulfobetaine methacrylamide (SBMAA; 27.4 mg; 3 mol. %) – and initiator 4,4-azobis(4-cyanopentanoic acid) (0.504 mg; 0.45 mM) were dissolved in 4 ml of acetic acid buffer (0.27 M acetic acid and 0.73 M sodium acetate, pH 5.2) in a Schlenk flask. In a second glass vial, a solution of RAFT agent 4-cyano-4-(phenylcarbonothioylthio)pentanoic acid (100 mg; 5 mg/ml) in 20 ml of 0.05 M sodium hydroxide was prepared. Both freshly prepared solutions were mixed in the Schlenk flask in an ice bath and the mixture was purged with nitrogen and stirred for 1 hour. Then, the polymerization mixture was heated at 75 °C for 10 hours in an oil bath. The reaction was stopped via rapid cooling and exposure to air. The polymerization solution was then dialyzed against Milli-Q water for 72 hours using SpectraPor 3 membrane (MWCO: 3500 Da),

ultrapure water was changed several times. After the dialysis, the solution was freeze-dried to yield a solid product. The chemical structure of the terpolymer was verified by infrared spectroscopy. The infrared spectra contained characteristic bands of all components (amide:  $1642\text{ cm}^{-1}$ ,  $1528\text{ cm}^{-1}$ , carboxyl:  $1723\text{ cm}^{-1}$ ,  $1594\text{ cm}^{-1}$ , sulfo:  $1200\text{ cm}^{-1}$ ,  $1033\text{ cm}^{-1}$ ).

#### Example 4: Bacterial antibody binding

A poly[(HPMAA(80 mol%)-co-CBMAA(15 mol%)-co-SBMAA(5 mol%)] terpolymer brush was prepared on the gold layer of the chip according to Example 1. The chip was rinsed with water, inserted into the SPR sensor and carboxyl groups of CBMAA were activated for 20 minutes at a flow rate of  $10\text{ }\mu\text{L}/\text{min}$  with a solution of  $0.1\text{ M}$  NHS and  $0.5\text{ M}$  EDC in deionized water to the active ester. After activation, the level of sensor response for the surface in water was recorded.  $50\text{ }\mu\text{g}/\text{mL}$  of bacterial anti-Salmonella antibody was dissolved in borate buffer ( $10\text{ mM}$ , pH 8.5), infused into the microfluidic system of the SPR sensor at a rate of  $30\text{ }\mu\text{L}/\text{min}$  and covalently bound by reaction with the activated brush (20 minutes). After immobilization of the antibody, the level of sensor response in water was again recorded. The amount of bound antibody was determined from the difference between the sensor response in water before antibody injection and the response in water after immobilization was completed (Fig. 3, the 'immobilization level' corresponds to  $206\text{ ng}/\text{cm}^2$ ).

#### Example 5: Functionalization capacity and resistance to non-specific adsorption after binding of functional entities

According to Example 1, poly(HPMAA-co-CBMAA-co-SBMAA) terpolymer brushes were prepared containing (a)  $84.5\text{ mol}\%$  HPMAA,  $15\text{ mol}\%$  CBMAA,  $0.5\text{ mol}\%$  SBMAA, (b)  $82\text{ mol}\%$  HPMAA,  $15\text{ mol}\%$  CBMAA,  $3\text{ mol}\%$  SBMAA and (c)  $55\text{ mol}\%$  HPMAA,  $15\text{ mol}\%$  CBMAA,  $30\text{ mol}\%$  SBMAA on the gold layer. Furthermore, two already known reference antifouling surfaces were prepared, showing a high degree of resistance to non-specific bonds and at the same time sufficient functionalization capacity - a copolymer containing  $85\text{ mol}\%$  HPMAA and  $15\text{ mol}\%$  CBMAA (WO2016177354A3) and a polyCBAA homopolymer. The following is a procedure for the preparation of these polymers:

poly[HPMAA(85 mol %)-co-CBMAA(15 mol%)]

A glass plate with a vapour-deposited gold layer was cleaned in a UV ozone generator for 10 minutes, then immediately rinsed with water and ethanol. The plate was then immersed in a  $0.1\text{ mM}$  solution of  $\omega$ -mercaptoundecyl bromoisobutyrate initiator in ethanol for 48 hours at room temperature without exposure to light. The catalyst mixture was prepared in a Schlenk flask by dissolving  $\text{CuCl}$  ( $28\text{ mg}$ ),

$\text{CuCl}_2$  (8.4 mg) and  $\text{Me}_4\text{cyclam}$  (96.8 mg) in degassed methanol (2 mL) under a nitrogen atmosphere and sonicated for 5 minutes until complete dissolution. In a second Schlenk flask, the monomers CBMAA (572 mg, 15 mol%) and HPMAA (1,914 mg, 85 mol%) were dissolved in degassed water (16.9 mL) and methanol (0.1 mL). After dissolution, the catalyst mixture was added to the monomer mixture under nitrogen. The homogeneous polymerization mixture was added to the reactor with a plate coated with initiator under nitrogen. The polymerization was carried out in the closed reactor for 2 hours at room temperature. The plate was then rinsed with water and stored in phosphate buffer at 4 °C before further use.

#### polyCBAA

A glass plate with a vapour-deposited gold layer was cleaned in a UV ozone generator for 10 minutes, then immediately rinsed with water and ethanol. The plate was then immersed in a 0.1 mM solution of  $\omega$ -mercaptoundecyl bromoisobutyrate initiator in ethanol for 48 hours at room temperature without exposure to light. The catalyst mixture was prepared in a Schlenk flask by dissolving  $\text{CuCl}$  (28 mg),  $\text{CuCl}_2$  (8.4 mg) and  $\text{Me}_4\text{cyclam}$  (96.8 mg) in degassed methanol (2 mL) under a nitrogen atmosphere and sonicated for 5 minutes until complete dissolution. In a second Schlenk flask, the monomer CBMAA (3,590 mg) was dissolved in degassed water (16.9 mL) and methanol (0.1 mL). After dissolution, the catalyst mixture was added to the monomer mixture under nitrogen. The homogeneous polymerization mixture was added to the reactor with a plate coated with initiator under nitrogen. The polymerization was carried out in the closed reactor for 2 hours at room temperature. The plate was then rinsed with water and stored in phosphate buffer (pH 7.4) at 4 °C before further use.

The above-described polymer brushes were tested for resistance to non-specific adsorption: (a) activated and deactivated surface, (b) activated and functionalized surface after deactivation. The following procedure was analogous for all brushes. The chip with brush was rinsed with water, inserted into the SPR sensor and activated at a flow rate of 10  $\mu\text{L}/\text{min}$  for 20 minutes with a solution of 0.1M NHS and 0.5M EDC in deionized water. In case (a) the surface was further washed with borate buffer (10 mM, pH 8.5, flow rate 30  $\mu\text{L}/\text{min}$ ) for 25 minutes; in case (b) the surface was washed with borate buffer (10 mM, pH 8.5, flow rate 30  $\mu\text{L}/\text{min}$ ) containing a specific dissolved functional entity with primary amines for 25 min. The following entities were immobilized on the following surfaces:

poly[HPMAA(84.5 mol %)-co-CBMAA(15 mol %)-co-SBMAA(0.5 mol %)]: amino-terminal DNA oligonucleotide (4  $\mu\text{M}$  solution);

poly[HPMAA(82 mol %)-co-CBMAA(15 mol %)-co-SBMAA(3 mol %)]: anti-bacterial anti-Salmonella antibody (50  $\mu\text{g}/\text{mL}$  solution);

poly[HPMAA(55 mol %)-co-CBMAA(15 mol %)-co-SBMAA(30 mol %)]: poly L-lysine (50 µg/mL solution);

poly[HPMAA(85 mol %)-co-CBMAA(15 mol %)]: anti-bacterial anti-Salmonella antibody (50 µg/mL solution), or amino-terminal DNA oligonucleotide (4 µM solution), or poly L-lysine (50 µg/mL solution);

polyCBAA: anti-bacterial anti-Salmonella antibody (50 µg/mL solution), or amino-terminal DNA oligonucleotide (4 µM solution), or poly L-lysine (50 µg/mL solution).

Furthermore, in both cases (a) and (b), the same procedure was used for all surfaces. The brush was deactivated by reaction with 1M (2-aminoethoxy)acetic acid (30 min, flow rate 10 µL/min) and then incubated in PBS (10 mM phosphate buffer + 150 mM NaCl + 2.7 mM KCl, pH 7.4) for achieving equilibrium and constant sensor response. Then, 100% human blood plasma was injected at a rate of 30 µL/min at 25 °C for 10 minutes, followed by rinsing with PBS. After rinsing with PBS for 10 minutes, higher ionic strength PBS (10 mM phosphate buffer + 750 mM NaCl + 2.7 mM KCl, pH 7.4) was injected for 5 minutes to wash away the electrostatically adsorbed non-specific deposit, and finally the entire surface was relaxed again in PBS. The level of non-specific adsorption was determined from the difference between the sensor response in PBS before the blood plasma injection and 10 minutes after the end of the injection. The level of non-specific adsorption after washing in higher ionic strength PBS was determined from the difference of the sensor response in PBS before blood plasma injection and 10 minutes after the end of washing in higher ionic strength PBS. The results are shown in Figure 3, Table 2 and Table 3.

Figure 3 demonstrates that even at a concentration of 15 mol% CBMAA in the terpolymer, a sufficient amount of functional element (206 ng/cm<sup>2</sup> anti-Salmonella) binds to the surface, while achieving high resistance to non-specific adsorption - non-specific adsorption from undiluted human plasma was 0 ng/cm<sup>2</sup>.

Table 2 – Non-specific adsorption from undiluted blood plasma after activation and deactivation and activation/covalent binding of anti-Salmonella antibody and deactivation.

<b>Non-specific adsorption from undiluted blood plasma [ng/cm<sup>2</sup>]</b>			
	<b>poly[HPMAA(82 mol%)- co-CBMAA(15 mol%)- co-SBMAA(3 mol%)]</b>	<b>polyCBAA</b>	<b>poly[HPMAA(85 mol%)- co-CBMAA(15 mol%)]</b>
After activation / deactivation	8.1	66.1	20.8

After activation / deactivation and washing with higher ionic strength PBS	0	2.5	16.9
After activation / anti-Salmonella anchoring / deactivation	10.9	51.9	39.5
After activation / anti-Salmonella anchoring / deactivation and washing higher ionic strength PBS	4.5	8.5	40.9

Table 2 demonstrates the improved anti-fouling properties of the poly(HPMAA-co-CBMAA-co-SBMAA) terpolymer brush after activation and immobilization of functional elements compared to known anti-fouling carboxy-functional surfaces. At the same time, it shows a significantly lower level of non-specific adsorption even without the need to wash away the electrostatically adsorbed non-specific deposit.

Table 3 – Non-specific adsorption from undiluted blood plasma after activation and covalent attachment of positively (poly L-lysine) and negatively (amino-terminated DNA oligonucleotide) charged ligand under given functionalization conditions on terpolymer brushes with different molar proportions of individual monomer units.

<b>Non-specific adsorption from undiluted blood plasma [ng/cm<sup>2</sup>]</b>		
	<b>poly[HPMAA(84,5 mol%)-co-CBMAA(15 mol%)-co-SBMAA(0,5 mol%)]</b>	<b>poly[HPMAA(85 mol%)-co-CBMAA(15 mol%)]</b>
After activation / anchoring of amino-terminal DNA oligonucleotides / deactivation	1.7	4.1
After activation / anchoring of amino-terminated DNA oligonucleotides / deactivation and washing with higher ionic strength PBS	0	3.0
	<b>poly[HPMAA(55 mol%)-co-CBMAA(15 mol%)-co-SBMAA(30 mol%)]</b>	<b>poly[HPMAA(85 mol%)-co-CBMAA(15 mol%)]</b>
After activation / poly L-lysine anchoring / deactivation and washing with higher ionic strength PBS	6.0	11.7

Table 3 shows the advantage of tunability of the terpolymer brush composition over a wide range of sulfobetaine component content. For different ligands, the appropriate brush composition can be evaluated on the basis of the charge distribution so that after immobilization the surface remains as neutral as possible and thus resistant to non-specific adsorption. Thus, even lower levels of non-specific adsorption can be achieved than with known functionalizable anti-fouling surfaces without the sulfobetaine component.

#### Example 6: Biorecognition ability of terpolymer brush after binding of functional entities

According to Example 1, poly[HPMAA (75 mol%)-co-CBMAA (15 mol%)-co-SBMAA (10 mol%)] was prepared on the gold surface of the chip. The chip was inserted into the SPR sensor and functionalized with anti-*Escherichia coli* (*E. coli*) antibody, anti-*E.coli*, and with anti-carcinoembryonic antigen (CEA) antibody, anti-CEA, according to the procedure of Example 3. The latter antibody was used as a reference to show the specificity of *E. coli* detection. After functionalization, the remaining active esters were deactivated for 30 minutes by reaction with a solution of 1M (2-aminoethoxy)acetic acid (30 min, flow rate of 10  $\mu\text{L}/\text{min}$ ) and then the chip was allowed to stabilize in PBS (10 mM phosphate buffer + 150 mM NaCl + 2.7 mM KCl, pH 7.4). After stabilizing the sensor response, a solution of  $1 \times 10^7$  CFU/mL of inactivated *E. coli* in PBS (15 min, flow rate of 45  $\mu\text{L}/\text{min}$ ) was injected onto the chip. The chip was then rinsed again with PBS until the sensor response stabilized.

Figure 4 shows a record of the SPR sensor response. The response from the reference channel (black colour) in which anti-CEA antibody was immobilized was negligible against the specific response of the SPR sensor (red colour) in which anti-*E.coli* antibody was immobilized.

The polymer brushes in Examples 4, 5 and 6 were prepared in the thickness range of the random polymer layer from 80 to 100 nm (thickness was verified by ellipsometry and SPR in water).

#### Example 7

According to Example 1, the terpolymer brush with a composition of 81 mol% HPMAA, 15 mol% CBMAA, 4 mol% SBMAA was prepared on the gold surface of the chip. The chip was rinsed with water, inserted into the SPR sensor, and the carboxyl groups of CBMAA were activated for 20 minutes at a flow rate of 10  $\mu\text{L}/\text{min}$  with a solution of 0.5M EDC and 0.1M NHS in deionized water to form active ester. After activation, the level of sensor response for the surface in water was recorded. 50  $\mu\text{g}/\text{mL}$  of bacterial anti-*E.coli* antibody in borate buffer (10 mM, pH 8.5) was soaked in the microfluidic SPR sensor system at a flow rate of 30  $\mu\text{L}/\text{min}$  and immobilized with  $104 \pm 25$   $\text{ng}/\text{cm}^2$  of antibody.



Subsequently, the residual active esters were deactivated for 36 minutes with one of three deactivating agent solutions: (1) a solution of glycine (1M in deionized water, pH 7), or (2) a solution of (2-aminoethoxy)acetic acid (1M in deionized water, pH 7) and/or (3) a solution of ethanolamine-O-sulphate (0.9 M in deionized water, pH 8).

The surfaces thus prepared were further washed with PBS (10 mM phosphate buffer + 150 mM NaCl + 2.7 mM KCl, pH 7.4) for 10 minutes. Then, 100% human blood plasma was injected at a rate of 30  $\mu$ L/min at 25 °C for 10 minutes, followed by washing again with PBS. After washing with PBS for 10 minutes, higher ionic strength PBS (10 mM phosphate buffer + 750 mM NaCl + 2.7 mM KCl, pH 7.4) was injected for 5 minutes and finally the whole surface was relaxed again in PBS. The non-specific adsorption was determined from the difference in sensor response in PBS before blood plasma injection and 10 minutes after injection. The non-specific adsorption after washing with PBS with higher ionic strength was determined from the difference between the sensor response in PBS before the injection of blood plasma and 10 minutes after the end of injection with higher ionic strength PBS.

Table 4: Comparison of deactivation of residual active esters - non-specific adsorption from undiluted blood plasma after deactivation by two reference reagents used in the literature and a new reagent ethanolamine-O-sulphate

<b>Deactivating agent</b>	<b>Non-specific adsorption from 100% blood plasma (ng/cm<sup>2</sup>)</b>	<b>Non-specific adsorption from 100% blood plasma / washing with higher ionic strength PBS (ng/cm<sup>2</sup>)</b>
Glycine	20.3	13.7
(2-aminoethoxy)acetic acid	21.2	18.1
Ethanolamine-O-sulphate	16.6	6.0

Table 4 demonstrates the lower non-specific adsorption from the complex solution after deactivation of the functionalized terpolymer surface with ethanolamine-O-sulphate compared to reference already published methods and thus demonstrates the improved regeneration of anti-fouling properties after deactivation with ethanolamine-O-sulphate.

Example 8: QCM biosensor based on antibody-functionalized terpolymer brush for direct label-free detection of SARS-CoV-2 in complex biological media

To prepare *poly*[HPMAA(77 mol %)-co-CBMAA (20 mol %)-co-SBMAA(3 mol %)]-coated QCM crystals (QCM = quartz crystal microbalance), QCM crystals with a thin gold layer were cleaned in UV-

ozone cleaner for 10 minutes and subsequently rinsed with ultra-pure water and ethanol. Immediately after the cleaning, the crystals were immersed in an initiator solution of a 1 mM  $\omega$ -mercaptoundecyl bromoisobutyrate in ethanol to form a self-assembled monolayer (SAM) and were left in the solution for 3 days at room temperature in dark. Methanol and water were degassed via 6 freeze-pump-thaw cycles. The catalyst solution was prepared as follows: under the nitrogen atmosphere CuCl (151.9 mg), CuCl<sub>2</sub> (29.4 mg), and Me<sub>4</sub>Cyclam (338.8 mg) in a Schlenk tube were mixed with 7.1 mL of degassed methanol. The mixture was sonicated for 5 minutes to dissolve all solids. In a second Schlenk tube, monomers SBMAA (0.483 g, 3 mol %), CBMAA (2.667 g, 20 mol %), or HPMAA (6.069 g, 77 mol %) were dissolved in 13.3 mL degassed water and 46.1 mL degassed methanol and stirred. After the dissolution was completed, the catalyst solution was added to the monomer solution using a gastight syringe. The polymerization mixture was added into the reactor containing the substrates coated with the initiator SAM. The polymerization was carried out for 2 hours at room temperature. Finally, the samples were washed with ultra-pure water and stored in PBS at 6 °C until used.

Before the experiment, QCM crystal coated with *poly*[HPMAA(77 mol %)-co-CBMAA (20 mol %)-co-SBMAA(3 mol %)] was removed from storing solution, rinsed with ultrapure water, and mounted into QCM sensor with the microfluidic system. After, it was washed with PBS buffer for 5 minutes (a flow rate of 45  $\mu$ l/min) and ultrapure water for 5 minutes (45  $\mu$ l/min). Subsequently, brushes were activated with a freshly prepared solution of 0.1 M NHS and 0.5 M EDC for 20 minutes (7  $\mu$ l/min). Afterward, the coatings were washed for 3 minutes (60  $\mu$ l/min) with HEPES buffer (5 mM HEPES, pH 6). The 50  $\mu$ g/mL of the anti-SARS-Cov-2 (N-protein) antibody was diluted in HEPES buffer (5 mM HEPES, pH 7) and the solution was added and left to react with activated coating for 12 minutes (15  $\mu$ l/min). After, all coatings were rinsed again with HEPES buffer (5 mM HEPES, pH 6) for 10 minutes (30  $\mu$ l/min) and immersed in the deactivation solution of AEEA (1M aminoethoxy acetic acid, pH 7) for 25 minutes (7  $\mu$ l/min). After, the coatings were rinsed with PBS for 10 minutes (30  $\mu$ l/min) to create a baseline. Afterward, the SARS-Cov-2-spiked cell medium samples (ranging from 0 (blank) to  $1 \times 10^6$  PFU/mL) were added and let react for 12 minutes (30  $\mu$ l/min). Finally, all the coatings were rinsed with PBS buffer for 10 minutes (30  $\mu$ l/min). The concentration dependency of QCM sensor response is depicted in Figure 5.

Example 9: QCM biosensor based on peptide-functionalized terpolymer brush for direct detection of SARS-CoV-2 in complex biological medium

The QCM sensor coated with *poly*[HPMAA(77 mol %)-co-CBMAA (20 mol %)-co-SBMAA(3 mol %)] was prepared as described in Example 2.

Before the experiment, QCM crystal coated with *poly*[HPMAA(77 mol %)-co-CBMAA (20 mol %)-co-SBMAA(3 mol %)] was removed from storing solution, rinsed with ultrapure water, and mounted

into QCM sensor with the microfluidic system. After, it was washed with PBS buffer for 5 minutes (a flow rate of 45  $\mu\text{l}/\text{min}$ ) and ultrapure water for 5 minutes (45  $\mu\text{l}/\text{min}$ ). Subsequently, brushes were activated with a freshly prepared solution of 0.1 M NHS and 0.5 M EDC for 20 minutes (7  $\mu\text{l}/\text{min}$ ). Afterward, the coatings were washed for 3 minutes (60  $\mu\text{l}/\text{min}$ ) with HEPES buffer (5 mM HEPES, pH 6). The 50  $\mu\text{g}/\text{mL}$  of a short polyK-modified peptide sequence (GSGGSG-IIEEQAKTFLDKFNHEAEDLFYQS) with a high affinity to SARS-Cov-2 was diluted in HEPES buffer (5 mM HEPES, pH 7) and the solution was added and left to react with activated coating for 12 minutes (15  $\mu\text{l}/\text{min}$ ). After, all coatings were rinsed again with HEPES buffer (5 mM HEPES, pH 6) for 10 minutes (30  $\mu\text{l}/\text{min}$ ) and immersed in the deactivation solution of AEAA (1M aminoethoxy acetic acid, pH 7) for 25 minutes (7  $\mu\text{l}/\text{min}$ ). Then, the coatings were rinsed with PBS for 10 minutes (30  $\mu\text{l}/\text{min}$ ) to create a baseline. Afterwards, the  $1 \times 10^5$  PFU/mL SARS-Cov-2-spiked cell medium or pure unspiked cell medium (blank) sample was added and let react for 12 minutes (30  $\mu\text{l}/\text{min}$ ). Finally, all the coatings were rinsed with PBS buffer for 10 minutes (30  $\mu\text{l}/\text{min}$ ). The example of detection is depicted in Figure 6.

## Claims

1. Random terpolymer of N-(2-hydroxypropyl) methacrylamide, carboxybetaine methacrylamide and sulfobetaine methacrylamide.

2. The random terpolymer according to claim 1, containing:

- 0.1 mol % to 40 mol % of sulfobetaine methacrylamide;
- 0.1 mol % to 50 mol % of carboxybetaine methacrylamide; and
- N-(2-hydroxypropyl) methacrylamide forming balance to 100 mol %.

3. Polymer brush having structure I



wherein

S is a substrate having a surface suitable for binding of polymerization initiators;

R is a residue of a polymerization initiator selected from the group consisting of ATRP initiators, SET-LRP initiators and RAFT agents;

poly(HPMAA-co-CBMAA-co-SBMAA) is a random terpolymer according to claim 1 or 2;

– is a covalent bond.

4. Functionalized polymer brush having structure II



wherein

S is a substrate having a surface suitable for binding of polymerization initiators;

R is a residue of a polymerization initiator selected from the group consisting of ATRP initiators, SET-LRP initiators and RAFT agents;

poly(HPMAA-co-CBMAA-co-SBMAA) is a random terpolymer according to claim 1 or 2;

– is a covalent bond;

F is at least one functional entity covalently bound to the random terpolymer by amide bond formed between –NH- group of the functional entity and –C(O)- group of carboxybetaine methacrylamide.

5. The functionalized polymer brush according to claim 4, wherein the functional entity F is selected from the group consisting of proteins, antibodies, peptides, nucleic acids, oligonucleotides.

6. The polymer brush according to claim 3 or the functionalized polymer brush according to claim 4 or 5, wherein the thickness of layer of the random terpolymer in the polymer brush is 10 nm to 500 nm, preferably 20 nm to 300 nm, as measured by ellipsometric method in water.

7. A method for preparation of the functionalized polymer brush according to claim 4 or 5, comprising the steps of:

- subjecting the carboxybetaine carboxyl groups in a polymer brush to a reaction with activation agents for activation of the carboxyl groups to form active ester groups;
- subjecting the active ester groups to a reaction with amino group of the functional entity to form an amide covalent bond;
- subjecting the unreacted active ester groups to reaction with ethanolamine-O-sulphate and/or (2-aminoethoxy)acetic acid and/or glycine.

8. Use of the random terpolymer according to claim 1 or 2 for increasing the resistance of surfaces against non-specific adsorption of substances from biological media and/or against non-specific interactions with biological media components.

9. Use of the polymer brush according to claim 3 or the functionalized polymer brush according to claim 4 or 5 for increasing the resistance of substrate surface against non-specific adsorption of substances from biological media and/or against non-specific interactions with biological media components.

10. Use of the functionalized polymer brush according to claim 4 or 5 for specific and selective interactions with target analytes, wherein the target analytes are preferably selected from proteins, peptides, nucleic acids, oligonucleotides.

11. A sensor, characterized in that it comprises the polymer brush according to claim 3 or the functionalized polymer brush according to claim 4 or 5.

12. The sensor according to claim 11, which is selected from surface plasmon resonance sensors, quartz crystal microbalances and fluorescent sensors.

13. A membrane, characterized in that it comprises the polymer brush according to claim 3 or the functionalized polymer brush according to claim 4 or 5.

## Abstract

The present invention relates to a random terpolymer of N-(2-hydroxypropyl) methacrylamide, carboxybetaine methacrylamide and sulfobetaine methacrylamide, to a polymer brush and to a functionalized polymer brush containing this terpolymer.

The said random terpolymer increases the resistance of the substrate surface to non-specific adsorption of substances from biological media and/or to non-specific interaction with biological media components, and is suitable for use in the form of a polymer brush, for example in sensors or membranes.

Fig. 1

Fig. 2

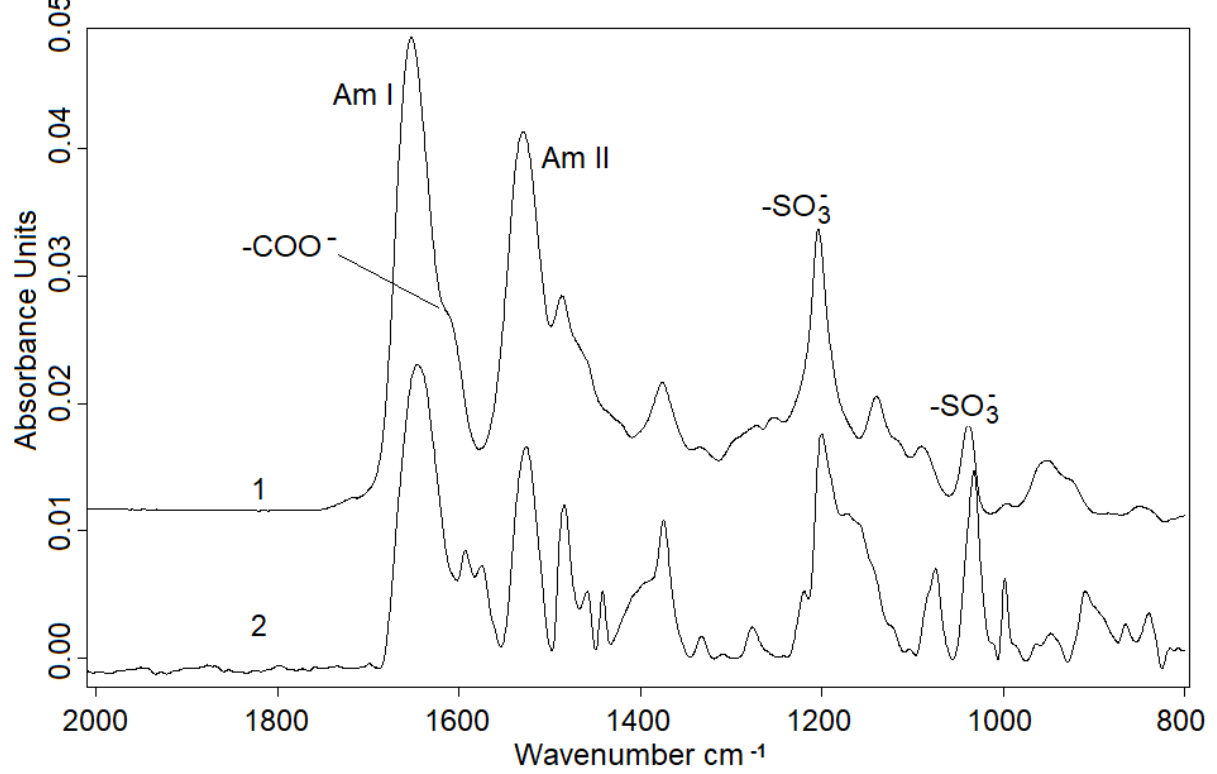


Fig.1: (1) FT IRRAS spectrum of terpolymer on gold. (2) FT IRRAS spectrum of terpolymer prepared by solution polymerization and evaporated on gold.

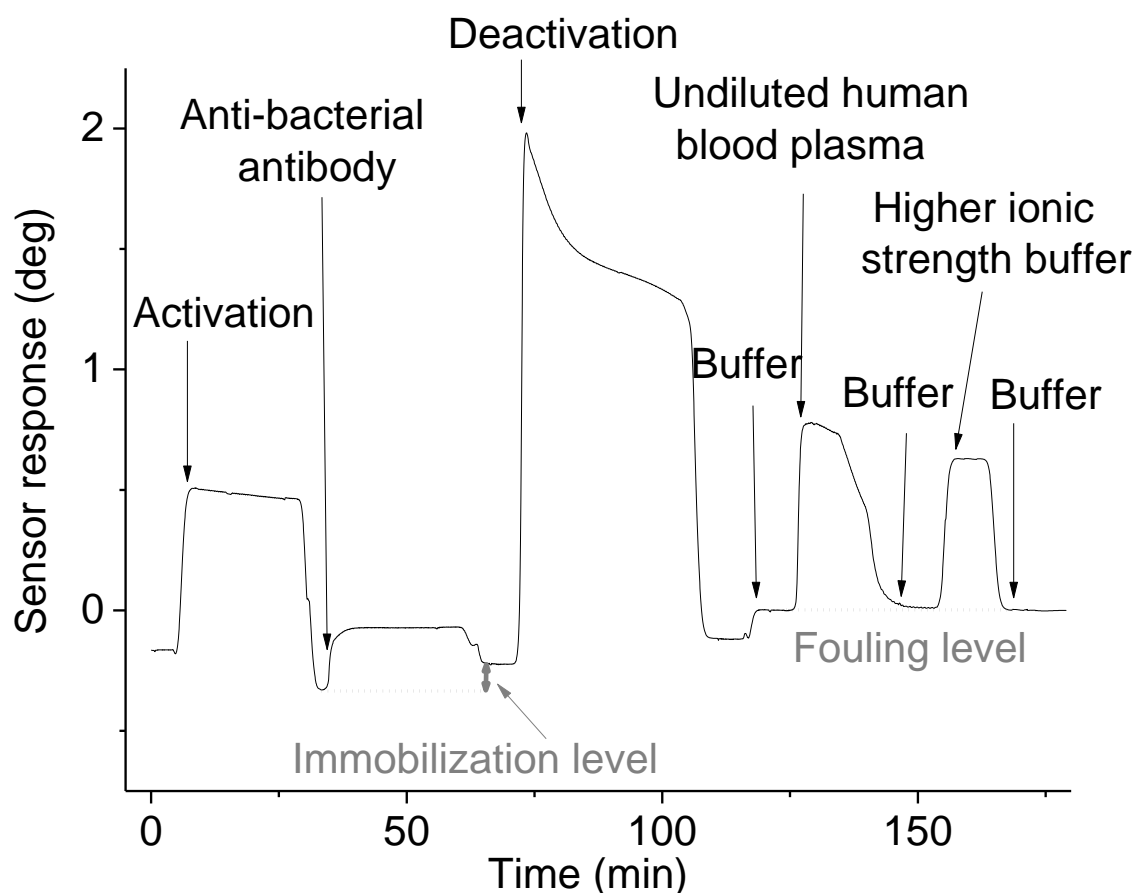


Fig. 3 Doplnit legendu a obrázek převést do angličtiny



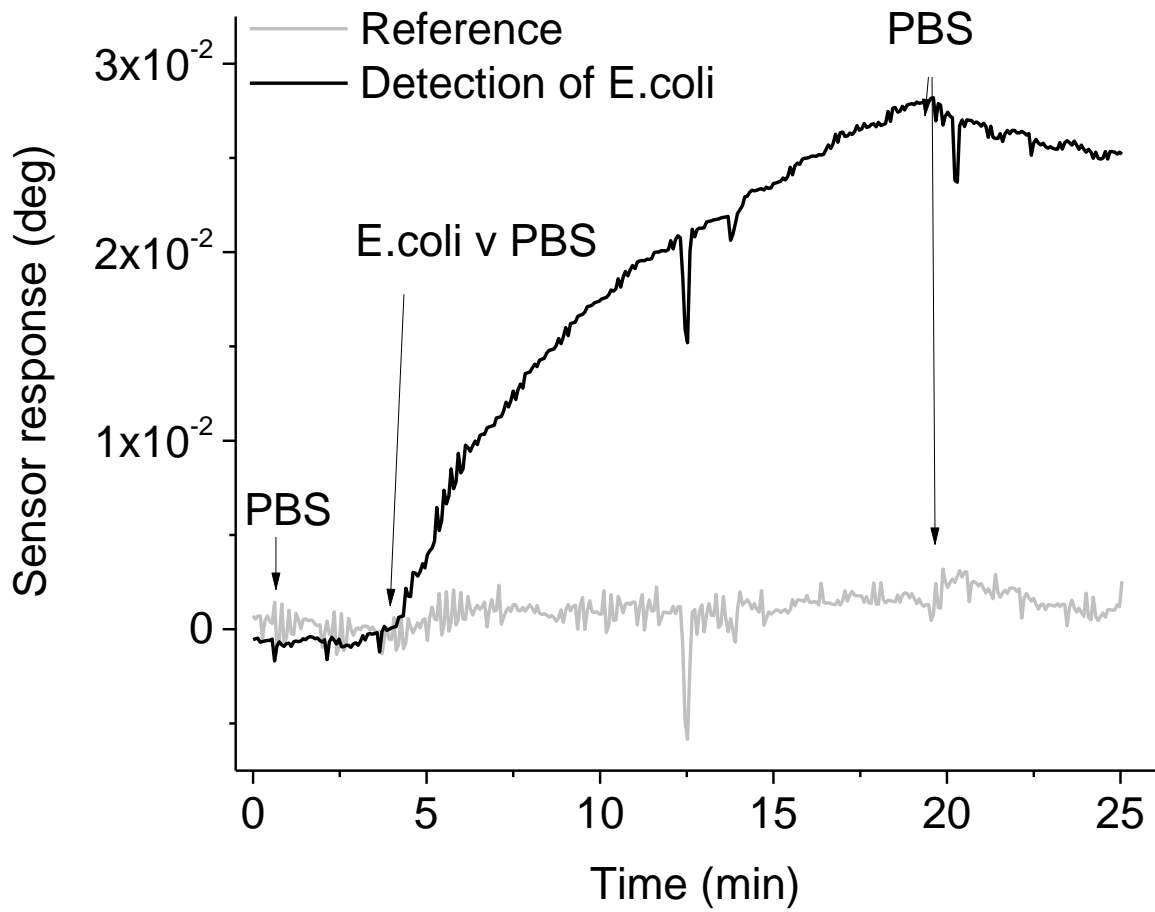


Fig. 4 Doplnit legendu a obrázek převést do angličtiny

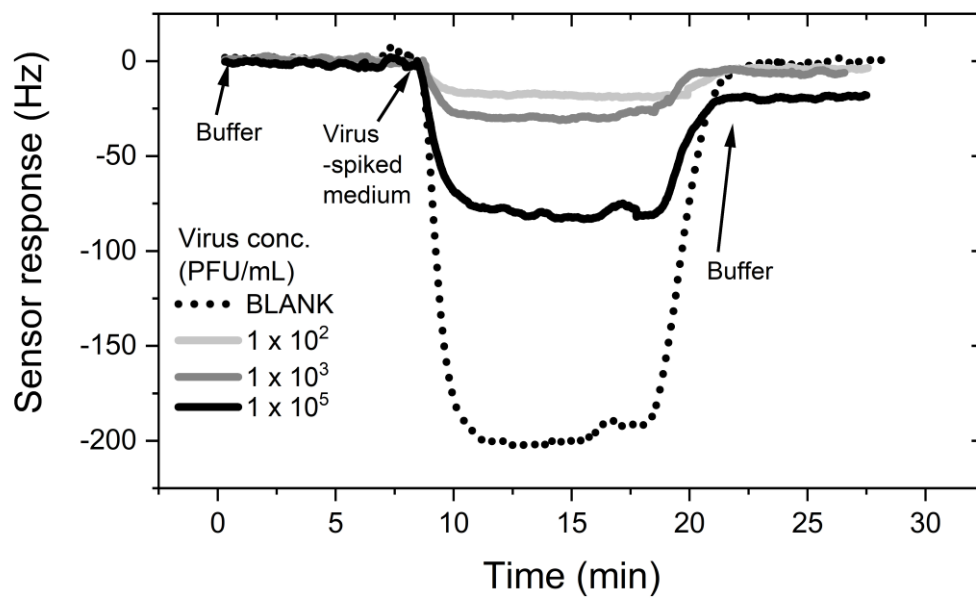


Fig. 5

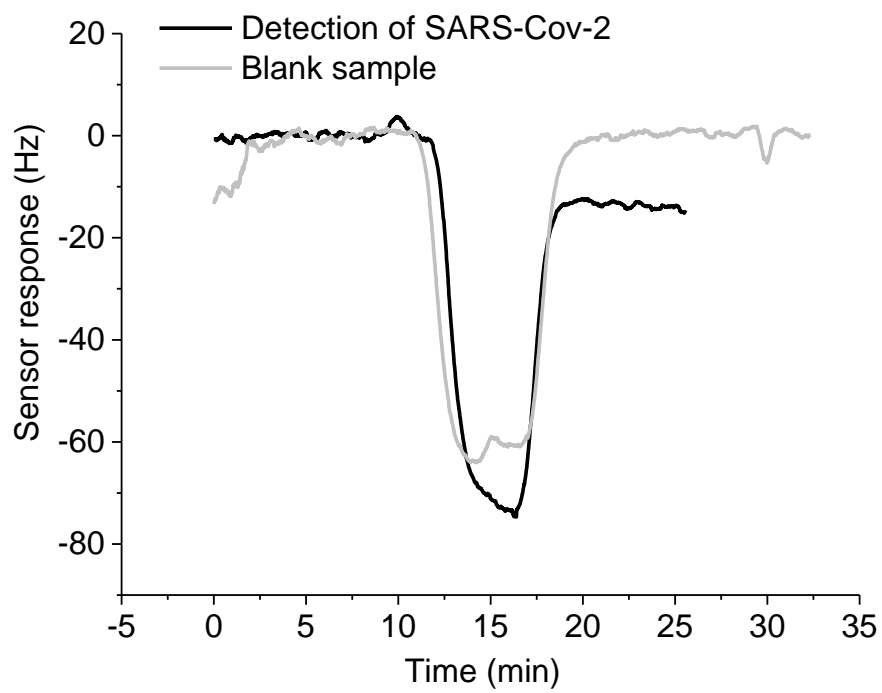


Fig. 6

# Appendix XVIII

Lísalová H., I. Víšová, P. Horák, M. Forinová, M. Vrabcová, A. Dejneka

**Biodetekční systém na bázi ultra-rezistentních funkčních polymerů  
pro rychlou detekci patogenních bakterií v potravinách**

Functional sample HL1/FZU/2019

**Biodetekční systém na bázi ultra-rezistentních funkčních polymerů pro rychlou detekci patogenních bakterií v potravinách**

**HL1/FZU/2019**

Hana Lísalová, Ivana Víšová, Petr Horák, Michala Forinová, Markéta Vrabcová, Alexandr Dejneka

Fyzikální ústav AV ČR, v.v.i.

Na Slovance 2

182 21 Praha 8

Česká republika

**Obsah:**

- 1 Úvod
- 2 Popis zařízení
- 3 Technická specifikace
- 4 Fotodokumentace

Autoři funkčního vzorku	Hana Lísalová, Ivana Víšová, Petr Horák, Michala Forinová, Markéta Vrabcová, Alexandr Dejneka
Pracoviště autorů	Fyzikální ústav AV ČR, v.v.i. Sekce optiky Oddělení optických a biofyzikálních systémů, Na Slovance 2 182 21 Praha 8 Česká republika
Země autorů	Česká republika
Název práce (funkčního vzorku)	Biodetekční systém na bázi ultra- rezistentních funkčních polymerů pro rychlou detekci patogenních bakterií v potravinách
Překlad názvu:	Biodetection system based on ultra-low fouling functional polymers for rapid detection of foodborne bacterial pathogens
Jazyk práce:	čeština
Stát vlast. výsledku	Česká republika
Rok vydání	2019



Druh výsledku	G <sub>f</sub> .vzorek – funkční vzorek
Interní id. kód výsledku přidělený tvůrcem:	HL1/FZU/2019
Ekonomické parametry výsledku	Funkční vzorek biodetekčního systému s potenciálem uplatnění na trhu v oblasti kontroly bezpečnosti potravin
Lokalizace výsledku:	Oddělení optických a biofyzikálních systémů, FZÚ AV ČR, v.v.i.
Technické parametry výsledku	Viz. kapitola 3
Název vlastníka výsledku	Fyzikální ústav AV ČR, v.v.i.
IČ vlastníka výsledku	68378271
Druh možnosti využití výsledku jiným subjektem:	A-Využití jiným subjektem podmíněné nabytím licence
Požadavek na licenční poplatek	A-poplatek požadován
Kategorie výsledku podle nákladů na jeho dosažení:	A-méně než 5 mil Kč
Číslo grantu:	TG02010056
Poskytovatel CEP:	Technologická agentura ČR
Země projektu:	Česká republika
Klíčové slovo AJ:	Low-fouling biochip, biosensor, bacterial pathogen, food safety
Anotace v jazyce práce:	Funkční vzorek laboratorního biodetekčního systému na bázi ultra-rezistentních funkčních polymerů byl vyvinut v reakci na aktuální potřeby trhu vyvinout technologii umožňující rychlou, citlivou a přesnou detekci bakteriálních patogenů v potravinách. Klíčovým prvkem systému na bázi „quartz crystal microbalance“ (QCM) je polymerní biočip se speciálními vlastnostmi kombinujícími vysokou schopnost navázání receptorů a rezistenci vůči nespecifickým vazbám látek přítomných v potravinách. Funkční vlastnosti vyvinuté technologie jsou demonstrovány pomocí citlivé detekce <i>Salmonella typhi</i>



	v homogenizovaném hamburgeru s detekčním limitem ~50 cfu/ml.
Překlad anotace AJ	A functional sample of the ultra-low fouling functional polymer-based bio-detection system was developed in response to current market needs to develop a technology that enables rapid, sensitive and accurate detection of bacterial pathogens in foods. A key element of the quartz crystal microbalance (QCM) system is a polymer biochip with optimized properties combining high receptor binding capacity and resistance to non-specific binding of substances present in foods. The functional properties of the developed technology are demonstrated by the sensitive detection of <i>Salmonella typhi</i> in a homogenized hamburger achieving a detection limit of ~ 50 cfu / ml.

## 1. Úvod

V dnešní době snadného a rychlého cestování a distribuce zboží po celém světě rapidně narůstá počet epidemií způsobených kontaminací potravin patogenními látkami, zejména bakteriálního a virového původu. Zvyšující se počet nálezů je způsoben jak nevhodným skladováním a nevhodnou úpravou potravin – ať už v konečných restauračních zařízeních či obchodech, tak nevhodnými podmínkami při dlouhých transpotech potravin z místa produkce na místo konzumace. S rostoucí poptávkou po dovozu potravin a potravinových surovin ze zemí s různou úrovní potravinové bezpečnosti a hygieny výrazně rostou kontaminační rizika pro obyvatelstva v cílových zemích. Např. CDC odhaduje, že každý rok každý šestý obyvatel v USA onemocní v důsledku konzumace kontaminovaných potravin a až 3000 z nich ročně zemřou [1, 2]. Mezi nejčastější patogeny způsobující taková onemocnění patří rozličné sérotypy *E. coli*, *Salmonella*, *Listeria*, nebo *Staphylococcus*. Z tohoto výčtu bakteriálních patogenů potravinové nákazy způsobené *Salmonellou* měly za následek více hospitalizací a úmrtí obyvatel v USA než jiné bakterie nalezené v potravinách a ročně si vyžádají léčebné náklady ve výši více než 365 milionů dolarů. Kontaminace byly nalezeny v řadě různých potravinových produktů, od zpracovaných potravin a polotovarů po zemědělské suroviny a v poslední době se problém týká i dalších nezemědělských produktů [3-5]. V České republice je situace obdobná. Např. zpráva o činnosti systému rychlého varování pro potraviny a krmiva (RASFF) v České republice za rok 2016 Státní veterinární zprávy (<https://www.svscr.cz/zivocisne-produkty/system-rychleho-varovani-pro>

potravin-a-krmiva-rasff) uvádí, že v roce 2016 byl největší počet nevyhovujících výrobků zaznamenán v kategorii maso a masné produkty, nejčastějším důvodem byla přítomnost patogenních mikroorganismů (zejména rod Salmonella). Hlavní město Praha, významné centrum cestovního ruchu i obchodu, které je zároveň vyhledávanou cílovou destinací migrace obyvatel z regionu a ze zahraničí za prací, je kontaminací (nejenom) potravin extrémně ohroženo.

Velikost epidemie a vážnost následků infekce způsobené konzumací kontaminovaných potravin patogenními látkami, např. bakteriálními patogeny, jsou přímo úměrné rychlosti odhalení zdroje nákazy a rychlosti nasazení adekvátní a účinné léčby. Proto je naprosto kritické co nejrychleji identifikovat konkrétní patogenní látku způsobující danou nákazu. Současné běžné metody identifikace a kvantifikace bakterií v potravinách využívají zejména zdoluhavé kultivační techniky příp. v kombinaci s genovými analýzami jako je metoda PCR. Identifikace patogenů tak představuje časově i experimentálně náročný proces vyžadující poměrně komplexní analýzu v certifikovaných laboratořích, což oddaluje zahájení rychlého a efektivního boje s nákazou. S potřebou rychlého a přesného odhalení patogenní látky v potravinách je spojena i tendence minimalizovat přípravu vzorků (například ředění, filtrování, ...) pro prováděné analýzy a odbourat nutnost transportu vzorků do certifikovaných laboratoří. Ideální by byla možnost provedení analýzy přímo v terénu v místě potřeby (např. v kontrolované provozovně, jídelně), čímž by se mohl výrazně ušetřit čas a náklady a minimalizovat následky nákazy.

V posledních letech je proto vynakládáno vysoké výzkumné úsilí celosvětově na vývoj rychlejších, citlivějších a nakonec i levnějších alternativních analytických metod, jako jsou biosenzory nebo biočipové analytické technologie, které by výše uvedené nedostatky pomohly vyřešit. Při podmínce minimalizace úpravy vzorku před analýzou na biočipu v biosenzoru však biosenzory naráží na zásadní problém a tím je nespecifická depozice nedetekovaných látek z analyzovaných komplexních biologických vzorků, včetně potravinových extraktů. Potravinový vzorek, např. homogenizovaný vzorek z teplého restauračního pokrmu, je velmi složitý systém, obsahující nejen cílovou detekovanou látku, ale především řádově vyšší koncentrace látek jiných – například přirozeně se vyskytujících složek sacharidů, tuků či proteinů. Tyto látky mají vrozenou vlastnost se „nespecificky“ vázat na libovolný povrch, tedy i na povrch biočipu. I relativně nízké depozity nespecifických látek na povrchy biočipů mohou vést k výraznému snížení citlivosti a reprodukovatelnosti detekčních metod a k navýšení pravděpodobnosti výskytů falešně pozitivních a falešně negativních výsledků. Tyto faktory výrazně snižují úspěšnost transferu nových biosenzorových technologií do rutinní praxe.

Tato nespecifická vazba je natolik zásadním a komplexním problémem, že i přes vývoj řady různých tzv. ultra-rezistentních materiálů, které mají schopnost bránit tvorbě nespecifických biologických depozitů, dodnes neexistuje komerčně dostupné řešení, které by si poradilo s detekcí patogenů přímo z neupravených (neředěných, nefiltrovaných) potravin či jiných komplexních biologických vzorků.



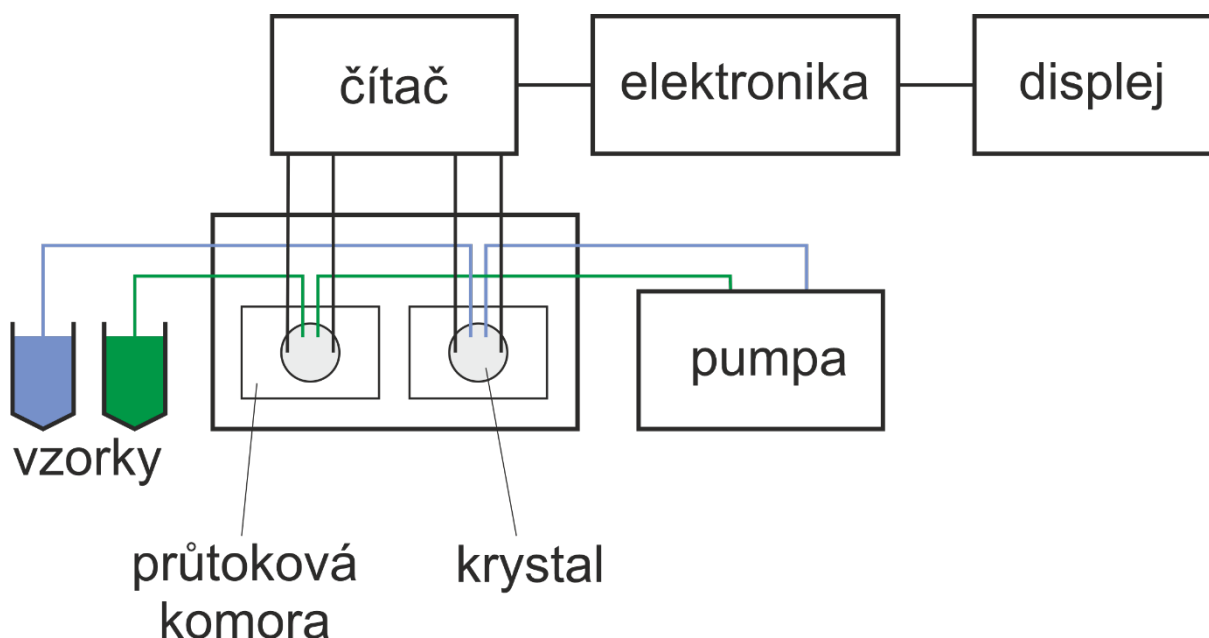


Vývoj funkčních povrchů, které v biologických médiích brání nespecifické tvorbě biologických depozitů a současně umožňují navázání bioaktivních látek zprostředkujících specifickou interakci povrchu s cílovými složkami biologického prostředí, je velmi důležitý pro řadu biotechnologických a lékařských aplikací, např. pro biočipové technologie, biosenzory, membrány a částice pro separaci a akumulaci biologických látek a buněk. I přes existenci řady různých typů ultra-rezistentních materiálů, jen u několika z nich byla dosud dostatečně prokázána schopnost uchovat odolnost proti nežádoucí biologické depozici při kontaktu s biologickými médii i po efektivním ukotvení biologicky aktivních látek. Taková kombinace vysoké odolnosti proti nespecifické depozici a dostatečná funkční kapacita byla v současné době prokázána u polymerních kartáčů obsahujících karboxybetainové funkční skupiny s navázanými bioaktivními látkami, např. u poly(karboxybetain akrylamidu) (polyCBAA). Předmětem řešení navrhovaného dílčího projektu je pokročilá charakterizace polyCBAA povrchů s navázanými bioaktivními látkami a pre-validace komerčního potenciálu pro použití v oblasti kontroly bezpečnosti potravin. V rámci realizace projektu budou za tímto účelem připraveny funkční polyCBAA povrchy s různými fyzikálně-chemickými vlastnostmi, např. tloušťkou nebo s různými bioaktivními látkami (protilátky, DNA proby) a bude charakterizována jejich odolnost vůči nespecifické depozici z různých potravinových médií a bioaktivita ve smyslu schopnost navázání cílové specifické látky v potravinách (modelových bakterií aj.).

## 2. Popis zařízení

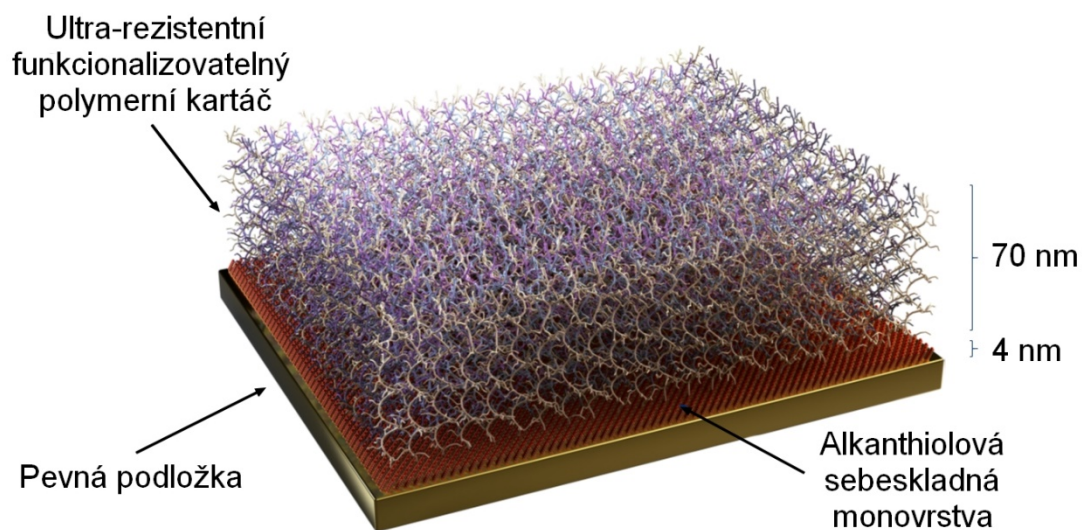
Funkční vzorek laboratorního biodetekčního systému se skládá z průtokové komory, do které se vkládá biočip s detekční vrstvou. Po vložení biočipu je tento připojen k elektronice, která sleduje změny ve frekvenci kmitání QCM senzoru (krystalu). Zhomogenizovaný vzorek analyzované potraviny se pomocí peristaltické pumpy přivede do kontaktu s QCM senzorem – biočipem s polymerní vrstvou a na základě změny frekvence kmitání je prováděna detekce cílové látky v reálném čase. Sestava s QCM senzorem je ovládána pomocí minipočítače Raspberry Pi s barevným dotykovým displejem a zároveň teplotně stabilizována pomocí Peltierova článku.

Popisované řešení používá dva měřicí kanály pro možnost detekovat dva nezávislé vzorky současně či odstínění interferencí z prostředí. Schéma měřicí sestavy QCM senzoru je zobrazeno na obrázku 1.



**Obr. č. 1** Schéma měřicí sestavy QCM senzoru

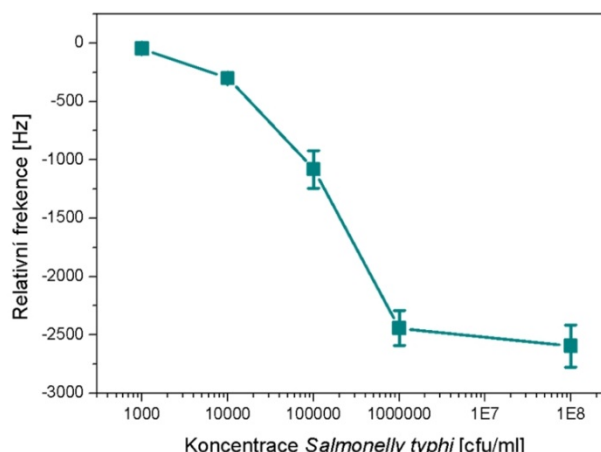
Klíčovým prvkem celého zařízení je biočip (povrch QCM senzoru) stávající se z polymerní vrstvy na bázi poly(CBAA). Byla vyvinuta metodika přípravy těchto vrstev na daných substrátech v laboratorních podmínkách na základě povrchově řízené radikálové polymerace, která umožňuje přípravu polymerních kartáčů o dostatečné povrchové hustotě polymerních řetězců. Pro dosažení cílových funkčních parametrů těchto vrstev byla metoda přípravy a funkcionalizace optimalizována z hlediska reakčních časů, koncentrace reagentů, typů rozpouštědel atd. Výsledné vrstvy polymerních kartáčů (obrázek 2) o tloušťce cca 70 nm ve vodě ideálně kombinují klíčové funkční vlastnosti, tj. rezistenci vůči nespecifickým vazbám a imobilizační kapacitu.



**Obr. č. 2** Schéma uspořádání biočipové vrstvy na bázi ultra-rezistentních polymerních kartáčů poly(CBAA) s optimalizovanými parametry.

Funkční vlastnosti biodetekčního systému na bázi ultra-rezistentních polymerních kartáčů s optimalizovanými vlastnostmi byly demonstrovány pomocí rychlé detekce *Salmonelly typhi* v homogenizovaném hamburgeru. Homogenizát z hamburgeru byl připraven pomocí standardní mikrobiologické procedury v homogenizátoru typu Stomacher (2 minuty homogenizace) a do takto připraveného homogenizátu byla injektována *Salmonella* o různé koncentraci bakterie. Detekce byla provedena na vyvinutém poly(CBAA) biočipu s kovalentně uchycenými protilátkami proti *Salmonelle typhi*. Detekční čas byl 15 minut, poté byl povrch promyt pufrům PBS s vysokou iontovou silou (750mM NaCl). Celkový čas detekce byl 20 minut. Výsledná kalibrační křivka senzoru a stanovený detekční limit jsou ukázány na obrázku č. 3.

**Detekční limit:**  
**50 cfu/ml**  
**v homogenizátu**  
**z hamburgeru**



**Obr. č. 3** Ukázka kalibrační křivky biodetekčního systému pro rychlou (do 20ti minut) detekci *Salmonella typhi* v homogenizovaném hamburgeru, na jejímž základě byl stanoven detekční limit 50 cfu/ml.

### 3. Technická specifikace laboratorního biodetekčního QCM systému

Princip měření: Jedná se o přesný křemenný mikrováhový senzor (quartz crystal microbalance, QCM) umožňující sledování změn rezonanční frekvence krystalu v reakci na změnu hmoty navázané na povrch krystalu v reálném čase. Spolu s využitím vyvinutých polymerních vrstev na površích výměnných biočipů celý systém tak představuje vysoce citlivý bezznačkový biosenzor reagující na malé změny hmotnosti v procesech probíhajících na povrchu senzoru.

Počet měřících kanálů: 2

Základní frekvence kmitání krystalu: 10 MHz

Rozměry biočipu (QCM krystalu): Ø14 mm

Rozměry zařízení (celé sestavy): cca 400 x 300 x 150 mm

Hmotnost: cca 2kg

Minimální objem analyzovaného vzorku: 50 ml

Rozsah měřících teplot: 15°C – 40°C

Typ zařízení transportující vzorek k povrchu biočipu: peristaltická pumpa

Průtoková rychlost: 0.01µl/min – 5ml/min



**FZU**

Fyzikální ústav  
Akademie věd  
České republiky

[www.fzu.cz](http://www.fzu.cz)

Materiál komponent fluidického systému: PMMA, PTFE, nerez

Citlivost měření

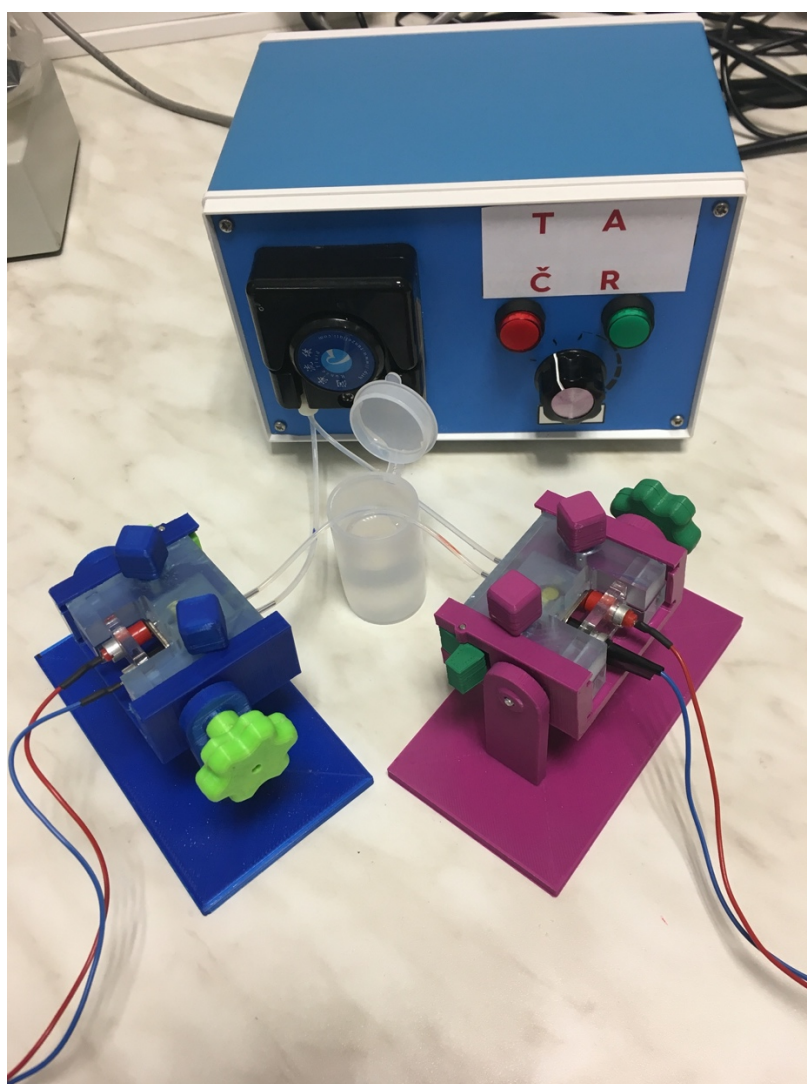
- Standardní citlivost na rezonanční frekvenci:  $\sim 2 \times 10^{-1}$  Hz

Operační systém: Raspbian (založeno na Debian Linuxu v.10)

Napájení

- Napájecí napětí: 220V AC 50Hz
- Příkon: 15W

#### 4. Fotodokumentace



Obr. č. 4 Detail měřící sestavy QCM senzoru



**FZU**

Fyzikální ústav  
Akademie věd  
České republiky

[www.fzu.cz](http://www.fzu.cz)



**Obr. č. 5** Ukázka měřící sestavy v temperovaném boxu

# Appendix XIX

Forinová M., A. Pilipenco, I. Víšová, P. Horák, M. Vrabcová, V. Hönig, M. Palus, J.  
Štěřba, A. Dejneka, H. Lísalová

**Funkční biočip s ultra-rezistentní polymerní vrstvou pro rychlou  
detekci viru SARS-CoV-2 pomocí metody QCM**

Functional sample HL1/FZU/2020



**Funkční biočip s ultra-rezistentní polymerní vrstvou pro rychlou detekci  
viru SARS-CoV-2 pomocí metody QCM**

**HL1/FZU/2020**

Michala Forinová, Alina Pilipenco, Ivana Víšová, Petr Horák, Markéta Vrabcová, Václav  
Hönig, Martin Palus, Ján Štěrba, Alexandr Dejneka, Hana Lísalová

Fyzikální ústav AV ČR, v.v.i.

Na Slovance 2

182 21 Praha 8

Česká republika

Obsah:

1. Úvod
2. Popis přípravy biočipu a technické parametry
3. Příklady využití funkčního biočipu pro detekci SARS-COV-2
4. Shrnutí

Autoři funkčního vzorku	Michala Forinová <sup>a</sup> , Alina Pilipenco <sup>a</sup> , Ivana Víšová <sup>a</sup> , Petr Horák <sup>a</sup> , Markéta Vrabcová <sup>a</sup> , Václav Hönig <sup>b,c</sup> , Martin Palus <sup>b,c</sup> , Ján Štěrba <sup>d</sup> , Alexandr Dejneka <sup>a</sup> , Hana Lísalová <sup>a</sup>
Pracoviště autorů	<sup>a</sup> Fyzikální ústav AV ČR, v. v. i. Na Slovance 1999/2 Praha 8 182 21 Česká republika  <sup>b</sup> Biologické centrum AV ČR, v.v.i. Parazitologický ústav Branišovská 1160/31 370 05 České Budějovice Česká republika  <sup>c</sup> Výzkumný ústav veterinárního lékařství, v.v.i., Hudcova 296/70 621 00 Brno Česká republika  <sup>d</sup> Jihočeská univerzita v Českých Budějovicích Přírodovědecká fakulta Branišovská 1645/31a 370 05 České Budějovice Česká republika
Země autorů	České republiky
Název práce (funkčního vzorku)	Funkční biočip s ultra-rezistentní polymerní vrstvou pro rychlou detekci viru SARS-CoV-2 pomocí metody QCM
Překlad názvu	Functional biochip based on ultra-low fouling polymer for rapid detection of SARS-COV-2 virus in crude biological fluids
Jazyk práce	čeština
Stát vlast. výsledku	Česká republika
Rok vydání	2020
Druh výsledku	Gf.vzorek – funkční vzorek
Interní id kód výsledku přidělený autorem	HL1/FZU/2020
Ekonomické parametry výsledku	Funkční biočip pro detekci SARS-CoV-2 s možností využití v oblasti bezpečnosti obyvatel a lékařské diagnostiky
Lokalizace výsledku	Oddělení optických a biofyzikálních systémů, FZU AV ČR, v. v. i.

Technické parametry výsledku	Viz kapitola 2
Název vlastníka výsledku	Fyzikální ústav AV ČR, v.v.i.
IČ vlastníka výsledku	68378271
Druh možností využití výsledku jiným subjektem	A – využití jiným subjektem podmíněné nabytím licence
Požadavek na licenční poplatek	A – poplatek požadován
Kategorie výsledku podle nákladů na jeho dosažení	A – méně než 5 mil. Kč
Číslo grantu	TN01000038
Poskytovatel CEP:	Technologická agentura ČR
Země projektu	Česká republika
Klíčová slova AJ	Antifouling, biochip, biosensor, COVID-19, SARS-CoV-2 detection
Anotace v jazyce práce	Funkční vzorek biočipu s ultra-rezistentní polymerní vrstvou byl vyvinut v reakci na aktuální celosvětovou pandemii onemocnění COVID-19. Ve spojení s metodou QCM funkční biočip nabízí rychlou a citlivou metodu detekce virových částic s minimálními nároky na přípravu vzorku. Důležitou součástí biočipu je unikátní polymerní vrstva, která kombinuje dvě klíčové vlastnosti: odolnost vůči nesespecifickým vazbám a vysokou schopnost vázat biorekogniční prvky. Funkčním biorekogničním prvkem je peptidová vrstva, přičemž struktura peptidu je navržena tak, aby peptid specificky rozpoznal a zachytil virové částice SARS-COV-2 z roztoku/média. Přítomnost a případně i koncentrace virových částic je vyhodnocena metodou křemenných mikrováh (z angl. <i>quartz crystal microbalance</i> - QCM). Výsledky prokázaly detekci částic v komplexním médiu s detekčním limitem $\sim 10^2$ PFU/ml. Vyvinutý funkční biočip může být adaptován i na jiné detekční metody.
Anotace v AJ	A functional sample of the biochip with antifouling polymer layer was developed in response to the current global COVID-19 pandemic. In conjunction with the QCM method, the functional biochip offers a fast and sensitive method for the detection of virus particles with minimal sample preparation requirements. An important component of the biochip is a unique polymer layer that combines two key desired properties: resistance to non-specific binding and high biorecognitive element loading capacity. The functional biorecognition element is a peptide layer. The peptide structure is designed so that the peptide specifically recognizes and captures SARS-COV-2 virus from the solution / medium. The presence and possible concentration of viral particles is evaluated by

	the method of quartz crystal microbalances (QCM). The results showed the detection of virus particles in a complex medium with a detection limit of $\sim 10^2$ pfu/ml. The developed functional biochip can be adapted to other detection methods.
--	---

## 1. Úvod

Pandemie onemocnění COVID-19 představuje velmi aktuální a palčivý globální problém ve světové populaci. Nový koronavirus 2019 (SARS-COV-2, z angl. *severe acute respiratory syndrome coronavirus 2*) způsobuje onemocnění respiračního aparátu, označované COVID-19. Epicentrum nákazy bylo lokalizováno v čínském Wuhanu a první případy byly zveřejněny v prosinci roku 2019. K 18. říjnu bylo v Evropě zaznamenáno 8 027 954 COVID-19 pozitivních jedinců a evidováno 256 540 úmrtí jedinců s COVID-19<sup>1</sup>. Dalekosáhlé jsou také sekundární důsledky, jako je selhání zdravotnických systémů a ekonomické ztráty, způsobené opatřeními ve snaze zabránit šíření pandemie („lockdown“ či omezení výroby a spotřeby), které v moderních dějinách nemají obdoby.

Možným řešením, kterým se zabývají mnohé vědecké skupiny a farmaceutické firmy, je vývoj očkovací protilátky. Část vakcín je ve fázi klinických hodnocení. Příkladem může být vakcína vyvíjená firmou AstraZeneca ve spolupráci s oxfordskou univerzitou nebo vakcína společnosti BioNTech ve spolupráci se společností Pfizer.

Časový horizont dostupnosti očkovacích látek a možné mutace viru vedou vědecké skupiny také k opačnému přístupu s cílem detekovat přítomnost virových částic v populaci, izolovat infikované jedince a zabránit tak včas dalšímu šíření nákazy. Nejčastěji užívanou metodou je detekce virové genomické RNA pomocí metody kvantitativní polymerázové řetězové reakce spojené s reverzní transkripcí v reálném čase (qRT-PCR). Tato metoda je výhodná z hlediska vysoké senzitivity, nevýhodou je však její časová náročnost, vysoká cena a potřeba speciálního vybavení a vyškoleného personálu.

Další možnosti pro detekci koronaviru představují antigenní testy, založené na detekci specifického antigenu (vybraného virového proteinu). Jejich výhodou je především rychlé provedení, relativně snadné použití a nízké finanční náklady. Některé z nich ovšem vykazují relativně nízkou specifitu a citlivost ve srovnání s qRT-PCR<sup>2</sup>. Ideální alternativní metodou k PCR by byla taková, která bude provedena v krátkém časovém rozmezí (< 15 minut) včetně přípravy vzorku, nevyžaduje vysoce vyškolenou obsluhu, transport vzorků do specializovaných laboratoří a nákladné vybavení. Ideálním řešením je analýza, jež může být provedena přímo v terénu, výhodou může být také možnost paralelní analýzy více vzorků současně a možnost opakovaného použití testu.

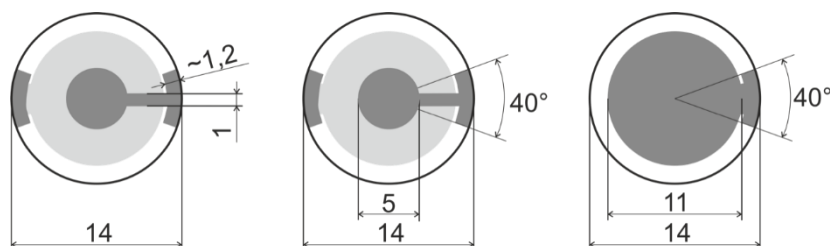
Možnou alternativu tak představují pokročilé biočipové technologie. Jedním z problémů, na které vývoj takovýchto nových analytických metod naráží, je nespecifická depozice látek z komplexních biologických vzorků (tzv. *fouling*). Ideální povrch biočipu by měl účelně odolávat těmto nespecifickým vazbám, zároveň však by měl být v dostatečné míře funkcionalizovatelný funkčním biorekogničním prvkem (v podobě například: protilátek, peptidů, DNA/RNA prób). Vrstva funkčních prvků pak slouží k rozpoznání a vazbě cílové detekované látky. Tyto vlastnosti byly nalezeny u povrchů, na které jsou navázány hydrofilní elektroneutrální polymerní kartáče, například ionogenní zwitteriontové s karboxybetainovou funkční skupinou, například: poly(karboxybetain akrylamid – pCBAA či poly(karboxybetain methalkrylát – pCBMA). Povrch může být tvořen pouze jedním typem monomeru či může docházet k jejich

kombinaci a tvorbě složitějších struktur, např. kopolymerů, nejčastěji statistických nebo blokových. Nicméně se ukazuje, že zachování vysoké míry rezistence povrchu po ukotvení bioreceptorů může být problematické a je potřeba dobře porozumět molekulárním mechanismům funkcionalizace a reaktivnímu chování polymerních řetězců na funkcionalizační procesy.

Prezentovaný funkční vzorek představuje biočip s funkčním povrchem, tvořený terpolymerním kartáčem poly(CBMAA-co-HPMAA-co-SBMAA), jehož postranní řetězce tvoří následující monomerní jednotky ve statistickém rozložení: karboxybetain methakrylamid (CBMAA), N-(2-hydroxypropyl) methakrylamid (HPMAA) a sulfobetain methakrylamid (SBMAA). Tento povrch je dále funkcionalizován pomocí aminové konjugační chemie peptidem, který selektivně rozpoznává a zachycuje SARS-CoV-2 protein. Výsledkem je vytvoření ultra-rezistentního biorekogničního povrchu pro detekci virových částic SARS-CoV-2 v komplexních biologických vzorcích. Je ověřena funkčnost biočipu pomocí analýzy vzorků obsahujících koncentrace infekčních částic SARS-CoV-2 v rozmezí  $1.3 \times 10^2 - 1.0 \times 10^4$  PFU/ml.

## 2. Popis přípravy biočipu a technické parametry

Funkční vzorek - biočip s terpolymerní funkční vrstvou s imobilizovaným peptidem pro detekci SARS-CoV-2. Základem biočipu je křemenný monitorovací krystal o průměru 14 mm, který je pokoven tenkou vrstvou zlata. Schéma substrátu pro metodu QCM, na jehož bázi byl připraven funkční biočip, je zobrazeno na obrázku 1.



**Obr. 1. Schéma substrátu (QCM krystalu), na jehož bázi je připraven funkční biočip.**

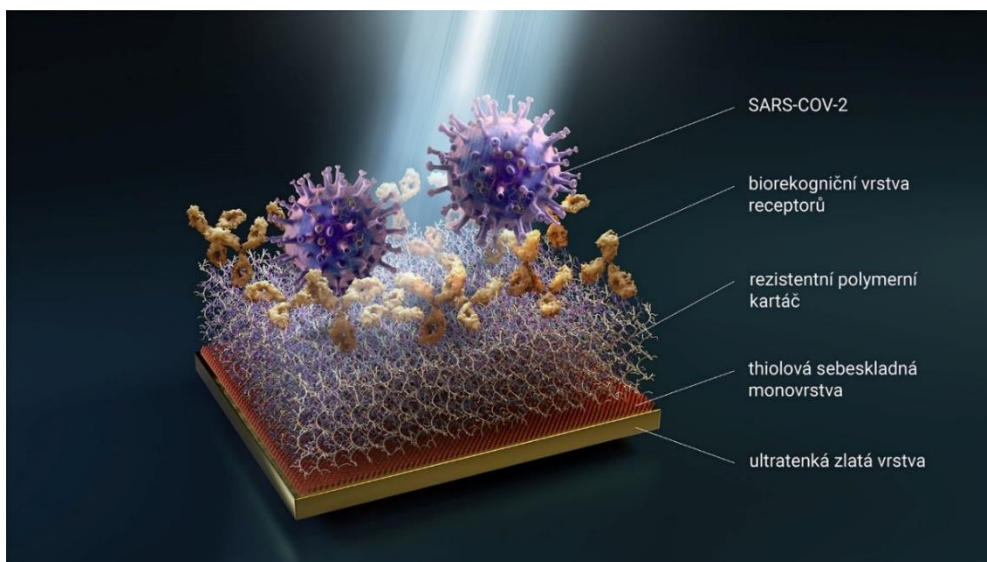
Funkční povrch na QCM krystalu se připravil následujícím způsobem: Nejprve je na zlatém povrchu pomocí kovalentní vazby vytvořena sebeskladná alkanthiolová monovrstva zakončená bromem, která slouží jako iniciátor pro syntézu polymerního kartáče. Pro daný biočip byl vytvořen terpolymer složený z N-(2-hydroxypropyl) methakrylamidu (HPMAA), karboxybetain methakrylamidu (CBMAA) a sulfobetain methakrylamidu (SBMAA): poly(CBMAA-co-HPMAA-co-SBMAA), v molárním zastoupení jednotlivých monomerů v polymeračním roztoku: 3 mol% SBMAA, 20 mol% CBMAA, 77 mol% HPMAA.

Poměr jednotlivých monomerů byl optimalizován pro danou aplikaci rychlé detekce SARS-CoV-2 v komplexních biologických médiích pomocí metody QCM. Polymerní řetězce jsou na povrchu biočipu syntetizovány pomocí iniciátoru radikálové polymerizace s přenosem atomu (ATRP). Zásadní inovací je zařazení monomerní jednotky SBMAA, betainu s trvale ionizovanou skupinou. Tato řeší problém ztráty elektroneutality povrchu po navázání funkčního prvku (v tomto případě peptidu). Funkcionalizace povrchu – navázání biorekogničního funkčního prvku: Na povrchu jsou nejprve zaktivovány karboxylové skupiny monomeru CBMAA pomocí NHS-EDC reagensů. Následně dojde k reakci aktivního esteru s aminoskupinou peptidu a jeho navázání za vzniku amidové vazby. Nezareagované aktivní estery jsou poté deaktivovány pomocí reakce s kyselinou (2-aminoethoxy)octovou.

Schéma výřezu funkčního vzorku biočipu je zobrazeno na obrázku 2. Biorekogniční molekulou může být v principu jakýkoliv peptid či protilátka, která specificky rozpoznává a zachycuje antigen viru SARS-CoV-2. V jednom z provedení funkčního vzorku biočipu byl vybrán peptid specificky rozpoznávající virový spike protein. Tento 23-merní peptidový fragment ACE2 PD  $\alpha$ 1 helix (*spike binding protein 1* - SBP1) doplněný poly lysinem pomocí glycin-serin linkeru byl dle standardního protokolu syntetizován v laboratoři Dr. Stephanopoulose v Arizona State University. Lysiny jsou zvoleny pro účinnější imobilizaci peptidu k polymeru. Je přitom známo, že koronavirus SARS-CoV-2 vstupuje do hostitelské buňky pomocí interakce jeho receptoru na povrchu buňky angiotenzin-konvertujícího enzym 2 (ACE2) a receptor-vázací domény (RBD) virového spike proteinu, který je zodpovědný za rekognici receptoru a fúzi membrán. V tomto provedení funkčního vzorku byla sekvence peptidu následující:

poly K – linker – SBP1

KKKKK-GSGGSG-IEEQAKTFLDKFNHEAEDLFYQS



**Obr. 2. Schématické zobrazení funkčního biočipu pro detekci SARS-COV-2.**

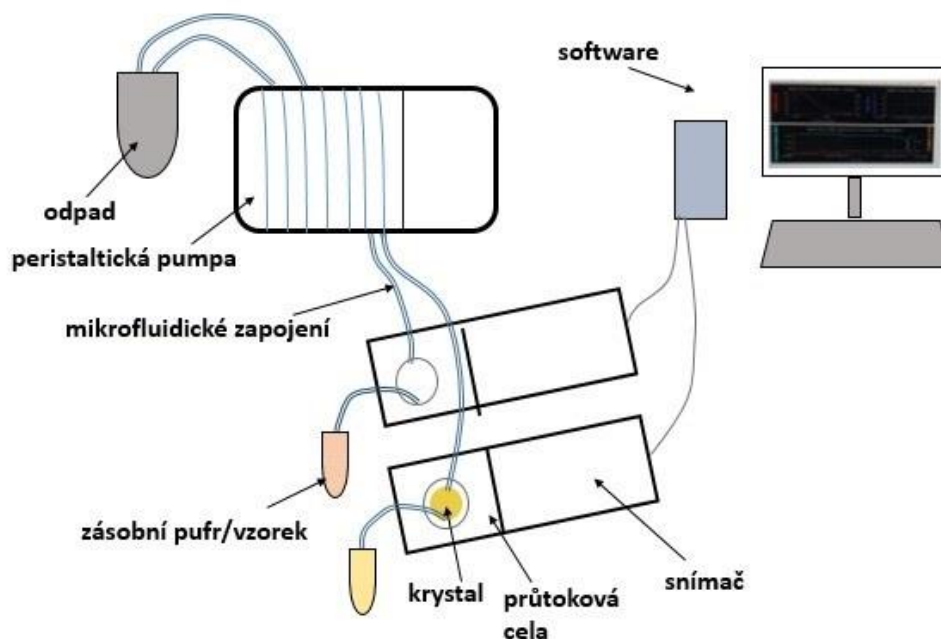
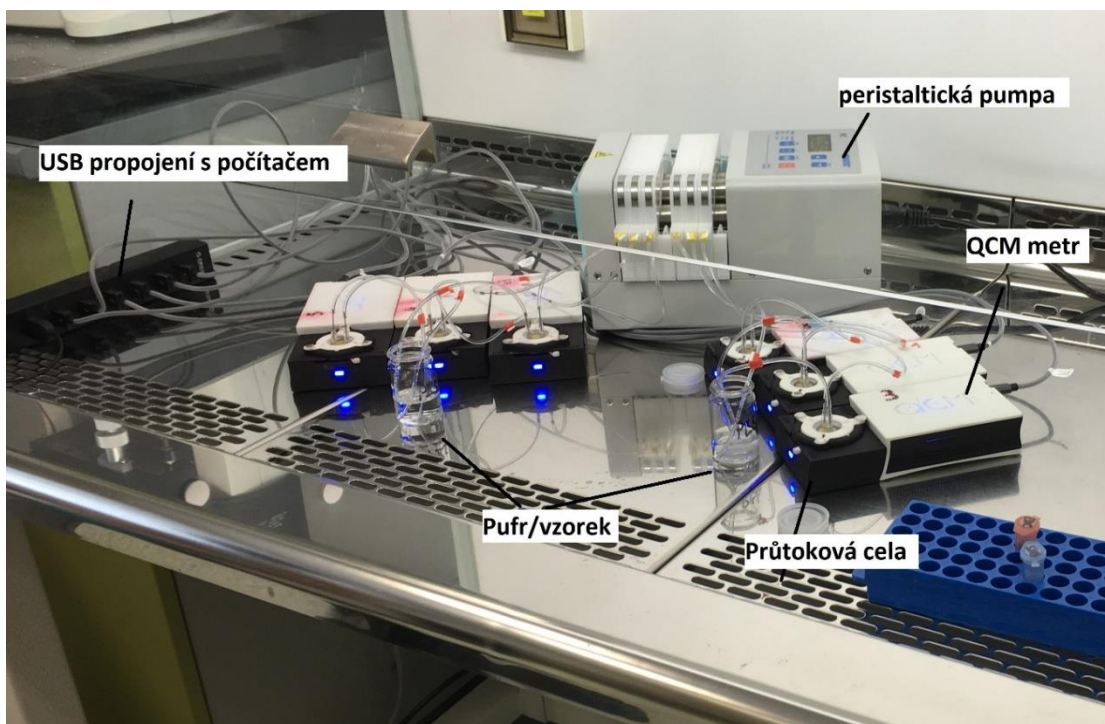
Technické parametry funkčního biočipu pro detekci SARS-CoV-2 pomocí metody QCM jsou sumarizovány v tabulce 1.

**Tabulka 1. Technické parametry funkčního biočipu.**

<b>Podložka</b>	<b>Rozměry</b>
Křemenný krystal	Diskovitý tvar, průměr: 14 mm, tloušťka: 0,2 mm
Adhezní vrstva Cr	Tloušťka: 2 nm
Vrstva zlata	Tloušťka: 100 nm
<b>Funkční prvky</b>	<b>Složení</b>
Terpolymerní vrstva	Složení: poly(CBMAA-co-HPMAA-co-SBMAA) (20 mol%-77 mol%-3 mol% <sup>-</sup> ) Tloušťka: 80 - 120 nm ve vodném roztoku
Biorekogniční peptid	Povrchová koncentrace: 50-100 ng/cm <sup>2</sup>

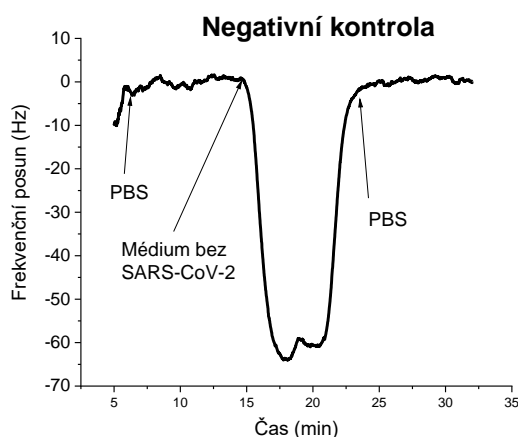
### 3. Příklady využití funkčního biočipu pro detekci SARS-COV-2

V jednom z provedení biočipu může analýza probíhat s použitím metody QCM. Základním stavebním kamenem QCM biosenzoru je tedy křemenný monitorovací krystal o průměru 14 mm, který je pokoven tenkou vrstvou zlata. Prezentovaný biočip je v tomto případě implementace umístěn do průtokové cely, kam je s použitím peristaltické pumpy přiváděna daná kapalina (pufr/vzorek) (Obrázek 3). Po celou dobu měření jsou pomocí softwaru v reálném čase zaznamenávány změny frekvence.

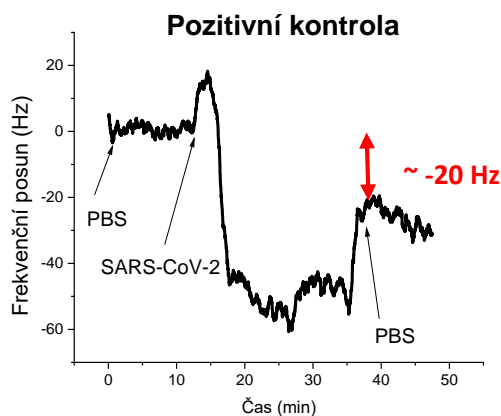


**Obr. 3. Fotografie QCM biosenzoru využívaného pro ověřování funkčních vlastností biočipu a schéma QCM senzoru.**

S pomocí tohoto biosenzoru byla provedena detekce virových částic v kultivačním médiu (popsáno níže). Rezistence funkcionalizovaného povrchu byla provedena pomocí negativní kontroly (srovnatelného média bez virových částic). Odezva senzoru při inkubaci funkcionalizovaného biočipu s negativní kontrolou byla nulová (Obrázek 4). Při detekční fázi, tj. inkubaci funkčního biočipu s pozitivní kontrolou, byla opakovaně změřena odezva  $\sim -20$  Hz pro koncentraci SARS-CoV-2 v médiu  $1 \times 10^4$  PFU/ml (Obrázek 5). Čas detekce byl v rozmezí 20 – 30 minut. Na obrázku 6 je zobrazena odezva senzoru pro různé koncentrace SARS-CoV-2 v biologickém médiu. Tyto odezvy naznačují potenciál biosenzoru i pro kvantitativní charakterizaci koncentrace virových antigenů v analyzovaném vzorku s detekčním limitem v řádu  $10^2$  PFU/ml.

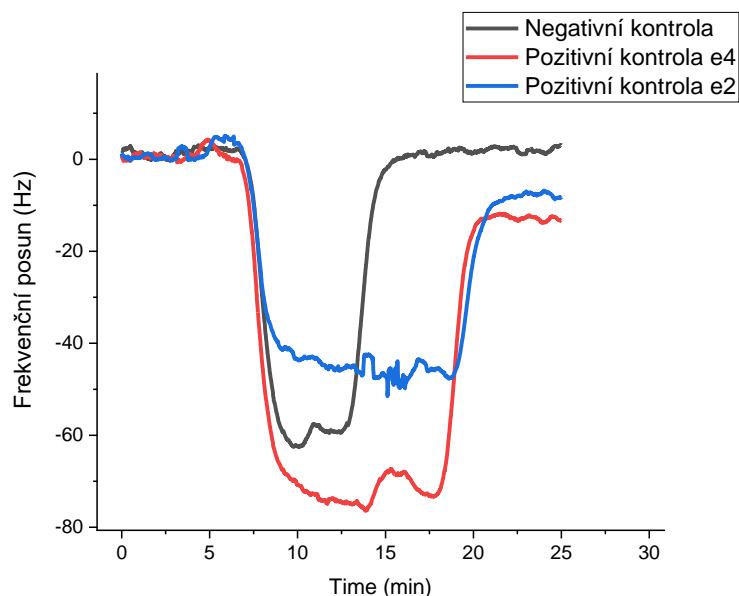


*Obr. 4. Ukázka odezvy senzoru na bázi funkčního biočipu při negativní kontrole.*



*Obr. 5. Ukázka odezvy senzoru na bázi funkčního biočipu při pozitivní kontrole.*





**Obr. 6. Ukázka odezvy sensoru při negativní kontrole a pozitivní kontrole (koncentrace  $\sim 10^2$  a  $\sim 10^4$  PFU/ml).**

Virová a buněčná kultura: Virové částice SARS-CoV-2 byly izolovány z klinických vzorků (Státního zdravotního ústavu, oddělení Centra epidemiologie a mikrobiologie, poskytnuté Dr. Janem Weberem, Institut organické chemie a biochemie, AV ČR v. v. i.). Vzorky byly až šestkrát pasážovány na buněčné kultuře Vero E6 (*African green monkey kidney cells*). Buňky byly kultivovány při 37 °C a 5% CO<sub>2</sub> v DMEM (Dulbecco's Modified Eagle Medium) médiu s nízkou koncentrací glukózy, doplněném 10% fetálním hovězím sérem, 1% L-glutaminem, 100 U/ml penicilinem, 100 ug/ml streptomycinem a 0,25 ug/ml amphotericinem B. Kvantifikace viru byla provedena metodou plakové titrace. Titr zásobní suspenze viru dosahoval 1,3 x 10<sup>4</sup> PFU/ml (plaque-forming units).

## 4. Shrnutí

Byl připraven funkční vzorek ultra-rezistentního terpolymerního povrchu s funkčním biorekogničním prvkem a s pomocí metody QCM byl ověřen jeho potenciál využití pro rychlou a citlivou detekci SARS-CoV-2 v komplexním biologickém médiu.

## Reference:

1. World Health Organization, *COVID-19 Weekly Epidemiological Update*. vol. September [https://www.who.int/docs/default-source/coronaviruse/situation-reports/20200921-weekly-epi-update-6.pdf?sfvrsn=d9cf9496\\_6](https://www.who.int/docs/default-source/coronaviruse/situation-reports/20200921-weekly-epi-update-6.pdf?sfvrsn=d9cf9496_6) (2020).
2. Společnost pro lékařskou mikrobiologii ČLS JEP, Laboratorní skupina COVID MZ ČR, *Přímá detekce SARS-CoV-2: detekce antigenu*. [https://koronavirus.mzcr.cz/wp-content/uploads/2020/09/Přímá-detekce-SARS-CoV-2-pomocí-antigenu\\_odborné-stanovisko.pdf](https://koronavirus.mzcr.cz/wp-content/uploads/2020/09/Přímá-detekce-SARS-CoV-2-pomocí-antigenu_odborné-stanovisko.pdf) (2020).